



COST is supported by the EU RTD Framework Programme and ESF provides the COST Office through an EC contract.

Proceedings of International Conference
Prague, 29 April 2011

Applications of Structural Fire Engineering



COST- the acronym for European **CO**operation in the field of **Scientific and Technical Research**- is the oldest and widest European intergovernmental network for cooperation in research. Established by the Ministerial Conference in November 1971, COST is presently used by the scientific communities of 35 European countries to cooperate in common research projects supported by national funds.

The funds provided by COST - less than 1% of the total value of the projects - support the COST cooperation networks, COST Actions, through which, with only around € 20 million per year, more than 30.000 European scientists are involved in research having a total value which exceeds € 2 billion per year. This is the financial worth of the European added value which COST achieves.

A bottom up approach (the initiative of launching a COST Action comes from the European scientists themselves), à la carte participation (only countries interested in the Action participate), equality of access (participation is open also to the scientific communities of countries not belonging to the European Union) and flexible structure (easy implementation and light management of the research initiatives) are the main characteristics of COST.

As precursor of advanced multidisciplinary research COST has a very important role for the realisation of the European Research Area (ERA) anticipating and complementing the activities of the Framework Programmes, constituting a ridge towards the scientific communities of emerging countries, increasing the mobility of researchers across Europe and fostering the establishment of Networks of Excellence in many key scientific domains such as: Biomedicine and Molecular Biosciences; Food and Agriculture; Forests, their Products and Services; Materials, Physics and Nanosciences; Chemistry and Molecular Sciences and Technologies; Earth System Science and Environmental Management; Information and Communication Technologies; Transport and Urban Development; Individuals, Society, Culture and Health. It covers basic and more applied research and also addresses issues of pre-normative nature or of societal importance.

**Proceedings of International Conference
Application of Structural Fire Engineering**
in Prague, 29 April 2011

The production of this publication was supported by COST, www.cost.esf.org.
COST Action TU0904

Integrated Fire Engineering and Response

Ed. Wald F., Horová K., Jirků J.

ISBN – 978-80-01-04798-9

Print Pražská technika , Czech Technical University in Prague

March 2011

250 copies, 465 pages

LIST OF CONTENTS

Preface	8
Burgess Ian, <i>United Kingdom</i>	
Session 1: Steel Structures	
Simplified method for temperature distribution in slim floor beams.....	11
Zaharia R., Duma D., Romania, Vassart O., Luxembourg, Gernay Th., Franssen J.M., <i>Belgium</i>	
Elastic buckling of steel columns under thermal gradient	17
Tsalikis C.T., Koltsakis E.K., Baniotopoulos C.C., <i>Greece</i>	
Adhesion at high temperature of FRP bars straight or bent at the end of concrete slabs.....	23
Nigro E., Cefarelli G., Bilotta A., Manfredi G., Cosenza E., <i>Italy</i>	
Mechanical properties of reinforcing bars heated up under steady stress conditions	31
Abramowicz M., Kisieliński R., Kowalski R., <i>Poland</i>	
Coupled structural-thermal calculations for restrained steel columns in fire.....	37
Kwaśniewski L., Balcerzak M., Poland, Ali F., <i>United Kingdom</i>	
Modelling creep in steel structures exposed to fire.....	43
Lee J., Gillie M., <i>United Kingdom</i>	
Fire modelling of axially-restrained tubular steel beams	49
Salem O., Hadjisophocleous G., Zalok E., <i>Canada</i>	
Material and creep behaviour of S460 in case of fire: Experimental investigation and analytical modelling.....	55
Schneider R., Lange J., <i>Germany</i>	
An approximation method for critical temperatures of steel members and horizontal displacements of columns	61
Hirashima T., Ikuta H., Hidani Y., <i>Japan</i>	
A simplified approach for predicting steel temperatures under design fires.....	67
Dwaikat M.M.S., Kodur V.K.R., <i>USA</i>	
Modelling of multiple localised fires and steel structural members response using the software Elefir-EN.....	73
Vila Real P., Couto C., Lopes N., <i>Portugal</i>	
Constitutive equations for structural steel subjected to fire: Some remarks	79
Korzen M., <i>Germany</i>	
Session 2: Concrete Structures	
Modelling of reinforced concrete frames in fire following an earthquake	87
Kadir Ab.M. A., Usmani A.S., Gillie M., <i>United Kingdom</i>	
Techniques for the evaluation of concrete structures after fire	92
Annerel E., Taerwe L., <i>Belgium</i>	
Thermal diffusivity of tensile cracked concrete	97
Ervine A., Gillie M., Stratford T.J., Pankaj P., <i>United Kingdom</i>	

Colour change of heated concrete: RGB colour histogram analysis as a method for fire damage assessment of concrete.....	103
Hager I., <i>Poland</i>	
Influence of transient strain on fire resistance of concrete elements.....	109
Lu L., Annerel E., Taerwe L., <i>Belgium</i> , Yuan Y., <i>China</i>	
A rational approach to fire resistance analysis of RC columns subjected to uniaxial/biaxial bending and axial restraint.....	115
Nguyen T.T., Tan K.H., <i>Singapore</i>	
Using opensees for an RC frame in fire.....	122
Zhang J., Usmani A., Jiang J., Jiang Y., Kotsovinos P. May I., <i>United Kingdom</i>	
Probabilistic analysis of concrete beams during fire	127
Van Coile R., Annerel E., Caspele R., Taerwe L., <i>Belgium</i>	
Shear strength of concrete at elevated temperature	133
Smith H.K.M., Reid E.R.E., Beatty A.A., Stratford T.J., Bisby L.A., <i>United Kingdom</i>	
Fire design of concrete and masonry structures: Software tools developed at the Czech Technical University in Prague	139
Štefan R., Procházka J., Beneš M., <i>Czech Republic</i>	
Study of slab fire resistance according to Eurocode using different computational methods.....	145
Čajka R., Matečková P., <i>Czech Republic</i>	
Axial restrain effects on fire resistance of statically indeterminate RC beams	149
Cvetkovska M., Todorov K., Lazarov L., <i>Macedonia</i>	
Numerical investigations of composite slab-beam floor systems exposed to ISO fire	155
Nguyen T.T., Tan K.H., <i>Singapore</i>	
Session 3: Composite Structures and Connections	
Analysis of steel–concrete composite beam with interlayer slip in fire conditions	165
Hozjan T., Kolšek J., Planinc I., Saje M., Srpčič S., <i>Slovenia</i>	
Fire safety engineering applied to composite steel-concrete buildings: Fire scenarios and structural behaviour	171
Nigro E., Ferraro A., Cefarelli G., <i>Italy</i>	
Munich fire test on membrane action of composite slabs in fire: Test results and recent findings	177
Stadler M., Mensinger M., Schaumann P., Sothmann J., <i>Germany</i>	
Influence of semi-rigid joint moment-rotation characteristics on the behaviour of composite steel-framed structures under fire conditions	183
Yuan Z., Tan K.H., <i>Singapore</i>	
Component-based element for endplate connections in fire.....	195
Dong G., Burgess I.W., Davison J.B., <i>United Kingdom</i>	
The fractural behaviour of steel welds at high temperature	201
Yu H., <i>China</i>	
Numerical analysis of HSS endplate connections at ambient and elevated temperatures.....	206
Qiang X., Bijlaard F., Kolstein H., Twilt L., <i>The Netherlands</i>	
Fracture simulation in a steel connection in fire: Simulation of a flush endplate connection at ambient and elevated temperatures including different methods for fracture simulation	213
Schaumann P., Kirsch T., <i>Germany</i>	

Thermomechanical nonlinear analysis: Finite element analysis of bolted steel connections using contact mechanics	219
Kalogeropoulos A., Drosopoulos G.A., Stavroulakis G.E., <i>Greece, Germany</i>	
A component-based model for fin-plate connections in fire	225
Taib M., Burgess I.W., <i>United Kingdom</i>	
Behaviour of heated composite joints: Preliminary numerical studies	231
Haremza C., Santiago A., Simões da Silva L., <i>Portugal</i>	

Session 4: Case Studies

A macroscopic finite element based computer model for evaluating the fire response of FRP-Strengthened Reinforced Concrete Beams	239
Ahmed A., Pakistan, Kodur V.K.R., <i>USA</i>	
Fire protection of steel structures using automatic water extinguishing system	246
Outinen J., <i>Finland</i>	
Role of CFD in the quantitative assessment of structural performance in fire scenarios	251
Gentili F., Grossi L., Bontempi F., <i>Italy</i>	
Evaluation of the fire resistance of the steel structure of a waste treatment plant using structural fire safety engineering	257
Vila Real P., Lopes N., <i>Portugal</i>	
Fire resistance of steel trusses with openees	263
Kotsovinos P., Usmani A., <i>United Kingdom</i>	
Temperature of steel columns exposed to localised fire	269
Sokol Z., <i>Czech Republic</i>	
Behaviour of frame columns in localised fires	275
Sun R., Burgess I., Huang Z., <i>United Kingdom</i>	
The role of active fire protection measures in a national fire safety concept in Germany	281
Klinzmann C., <i>Germany</i>	
Computational modelling for performance based fire engineering (PBFE)	287
Petrini F., Gkoumas K., <i>Italy</i>	
Loading-bearing capacity method for structural fire safety design – A case study	293
Du Yong D., Gou-qiang L., <i>China</i>	
RC frame exposed to fire after earthquake	299
Lazarov L., Todorov K., Cvetkovska M., <i>Macedonia</i>	

Session 5: Numerical Modelling

Adaptation of fea codes to simulate the heating and cooling process of timber structures exposed to fire: Mechanical behaviour	307
Hopkin D., El-Rimawi J., Silberschmidt V., Lennon T., <i>United Kingdom</i>	
Simulation of the structural behaviour of steel-framed buildings in fire	313
Gentili F., Giuliani L., <i>Italy</i>	
Numerical analysis of structures in fire using openees	319
Jiang J., Usmani A., Zhang J., Kotsovinos P., <i>United Kingdom</i>	
Development of heat transfer modelling capability in openees for structures in fire	324
Jiang Y., Usmani A., Welch S., <i>United Kingdom</i>	

A numerically derived modified conductivity model for softwood exposed to parametric design fires: Background, benchmarking and adaptation for cooling	331
Hopkin D., El-Rimawi J., Silberschmidt V., Lennon T., <i>United Kingdom</i>	
Travelling Fires in large compartments: Realistic fire dynamics for structural design.....	337
Rein G., Stern-Gottfried J., <i>United Kingdom</i>	
Application of a virtual resistance furnace: Fire resistance test simulation on a plasterboard membrane	343
Cayla F., Leborgne H., Joyeux D., <i>France</i>	
The impact of assumed fracture energy on the fire performance of timber beams: A numerical study.....	349
Hopkin D., El-Rimawi J., Silberschmidt V., Lennon T., <i>United Kingdom</i>	
Stochastic analysis of structures in fire by Monte Carlo simulation	355
Shi K., Guo Q., Jeffers A.E., <i>USA</i>	
Integrated numerical modelling in fire safety assessment: Current needs, challenges, potentiality and perspectives.....	361
Król P.A., <i>Poland</i>	
Numerical investigations of plasterboard separating elements subjected to fire.....	367
Tran H., Leborgne H., Zhao B., Millard A., <i>France</i>	
Fire simulation application in fire safety design for tunnel structures	373
Dudáček A., Bradáčová I., Kučera P., <i>Czech Republic</i>	
Fire analysis of RC precast segmental tunnels	379
Lilliu G., <i>The Netherlands</i> , Meda A., <i>Italy</i>	
Session 6: Fire Testing	
Prediction of temperature variation in an experimental building	387
Cheng X., <i>China</i> , Veljkovic M., Byström A., Iqbal N., Sandström J., Wickström U., <i>Sweden</i>	
Effective thermal conductivity of fire proof materials and the measuring method.....	393
Han J., Li G-Q., Lou G-B., <i>China</i>	
Fire load survey of commercial premises in Finland.....	400
Björkman J., Autio V., Ylihärsilä H., Grönberg P., Heinisuo M., <i>Finland</i>	
Systematisation of design fire loads in an integrated fire design system	405
Heinisuo M., Laasonen M., Outinen J., Hietaniemi J., <i>Finland</i>	
A structural fire engineering prediction for The Veselí fire test, 2011	411
Huang S-S., Burgess I., Davison B., <i>United Kingdom</i>	
Structural fire engineering in building renovation: Application of natural fire and heat transfer models to guarantee fire safety	417
Molkens T., <i>Belgium</i>	
Failure probability assessment for fire situation with a certain type of the network diagram: Example of application	423
Maślak M., <i>Poland</i>	
Application of fire safety engineering for open car parks in Italy.....	429
Nigro E., Ferraro A., Cefarelli G., Manfredi G. , Cosenza E., <i>Italy</i>	
Case studies of a new simplified natural fire model and safety concept for structural fire safety design	437

Zehfuss J., <i>Germany</i>	
Fire resistance of cast iron columns in Vinohrady brevery.....	443
Wald F., Dagefa M., <i>Czech Republic</i>	
Software application for estimation of fire resistance of the buildings construction.....	449
Vargovsky K., <i>Slovakia</i>	
The impact of flame retarded timber on Greek industries	456
Tsatsoulas D., <i>Greece</i>	
Author Index	463
Scientific and Organizing Committee	466

PREFACE

Structural fire engineering is a relatively new field for designers and building control authorities. However there is a growing acceptance that the fire-resistant design of buildings should be based on a logical analysis of their performance in the context of realistic fire scenarios, determined from an approach to safety which considers both the statistics of risk and the severity of possible outcomes. Research in this field has experienced very rapid growth since the mid-1990s, particularly in Europe, and there are now many examples of major structures for which structural fire engineering has been incorporated in the design process together with the more traditional fire safety concepts.

The papers published in this volume were presented at the second conference entitled *Applications of Structural Fire Engineering*, which was held at the Czech Technical University in Prague in April 2011. They cover topics across a wide range of research and advanced practice in structural fire engineering, and leading research groups in the field from Europe and world-wide are represented. A declared theme of the conference was the use of advanced modelling, and this is reflected in at least two thirds of the papers. The types of structural systems covered include steel, concrete, composite and timber framed buildings, as well as thermal modelling of fire scenarios. In order to gain acceptance with national and local fire regulation authorities, academic research findings must be used to develop both powerful computational tools and the simplified methods which are more accessible to non-specialists. The latter are particularly suitable for implementation in codes of practice; the structural Eurocodes have initiated this process by including simple, though performance-based, calculation procedures for fire resistance of structural elements which can be used either manually or in spreadsheets. These are necessarily restricted in scope, but mark a very significant psychological move away from the traditional prescriptive rules for fire protection which still dominate in design practice. Much of the work presented here is aimed at evaluating and enhancing these lower-level procedures. In the longer term it seems inevitable that fire-resistant design, particularly of large, complex buildings, will be based on thermo-structural “whole-structure” modelling in realistic fires. The development of components of these modelling tools is well represented in these articles. Although large-scale fire testing is extremely expensive, some testing at realistic scale continues, and these are providing invaluable evidence against which both the simplified and advanced computational approaches can be evaluated. The issue of robustness, or avoidance of disproportionate collapse as a result of discrete structural failures, is increasing in importance. The risks were amply illustrated by the progressive collapse of several buildings of the World Trade Center in New York in 2001 after multi-storey fires. It is clearly desirable that, in future, large buildings are designed so that failures due to unforeseen circumstances are arrested before a catastrophic sequence occurs.

This volume will be of interest both to active researchers and to those (such as regulatory authorities, fire safety engineers and structural designers) with an interest in the movement towards practical performance-based design of structures against fire.

Ian Burgess

Proceedings of International Conference
Applications of Structural Fire Engineering
Prague, 29 April 2011

Session 1

Steel Structures

SIMPLIFIED METHOD FOR TEMPERATURE DISTRIBUTION IN SLIM FLOOR BEAMS

R. Zaharia^a, D. Duma^a, O.Vassart^b, Th. Gernay^c, J.M. Franssen^c

^a Department of Steel Structures and Structural Mechanics, The “Politehnica” University of Timisoara, Romania

^b Research and Development, ArcelorMittal, Esch-sur-Alzette, Luxembourg

^c Department of Architecture, Geology, Environment & Constructions, University of Liege, Belgium

INTRODUCTION

In recent years, increasing interest has been shown throughout Europe in developing and designing Slim Floor systems in steel-framed buildings. The Slim Floor system is a fast, innovative and economical solution which combines prefabricated or casted concrete slabs with built-in steel beams, as shown in Fig. 1. The particular feature of this system is the special kind of girder with a bottom flange which is wider than the upper flange.

Using this arrangement, it is possible to fit the floor slabs directly onto the bottom flange plate of the beam, so that the two constituents thus make up the floor. Additional reinforcement may be provided above the bottom flange, in order to increase the resistance. The result is a reduced height of the slabs and a considerable degree of fire resistance, considering that the steel beam, excepting for the bottom flange, is integrated in the concrete slab.



Fig. 1 Slim Floor systems a) steel beam supporting a composite floor using steel sheeting
b) steel beam supporting prefabricated elements

To accompany the existing models of Slim Floor systems, ArcelorMittal (ArcelorMittal Commercial Sections) has developed three types of beams which utilize their products. As shown in Fig. 2, IFBs (Integrated Floor Beams) and SFBs (Slim Floor Beams) are built from hot-rolled profiles and welded steel plates. They feature a bottom flange plate which acts as a support for the floor slab. These beams are available for spans up to 8 m and for effective heights of 14 to 30 cm. The length of the bottom flange must guarantee a minimum support on both sides in accordance with the specific requirements of the slab manufacturer.

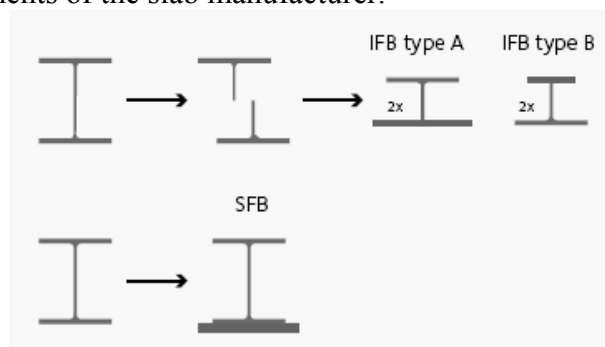


Fig. 2 ArcelorMittal beams for Slim Floor systems (ArcelorMittal Commercial Sections)

For the design of this type of floor, the composite action between the casted concrete and the steel beams is usually neglected in the calculation of the plastic design bending moment. The beams may be then calculated as steel elements and not as composite steel-concrete elements. On the other hand, due to the presence of the concrete, the temperatures in the steel beams are not uniform, and a

proper temperature distribution should be considered when calculating the fire resistance. The temperature distribution may be determined by a numerical analysis, using an appropriate program. Of course, this must be done for each particular situation, considering the dimensions of the steel beam inside the concrete and of the bottom flange exposed to fire on three sides.

In order to offer to the designer a tool to evaluate the temperatures in a Slim Floor system exposed to ISO fire, without the need of complex numerical simulations, a parametric study was done by the authors, based on numerical simulations using SAFIR program (Franssen, 2005). The aim was to propose a simplified method for the calculation of temperature in relevant points from the cross-section.

1 NUMERICAL MODEL

All the steel profiles presented in the brochure of ArcelorMittal for Slim Floor systems (ArcelorMittal Commercial Sections) were considered in the parametric study. The temperature on each cross-section was analysed with SAFIR and some formulas have been developed, function of different parameters.

For the thermal analysis, the material properties used in the numerical model (Fig. 3), are those of the Eurocodes for fire design (EN1992-1-2; EN1993-1-2) considering the upper limit of the thermal conductivity for concrete. The cross-section of the beams were exposed to ISO fire for 2 hours from bellow, the temperature in the top of the floor being considered 20°C.

Temperatures from relevant points of the cross-section were extracted from the numerical analysis, and the distance from the top of the bottom flange from which the temperatures are bellow 400° C was also monitored. For all cases, this distance was found on the height of the web, and consequently the temperature in the top plate never reaches 400°C (temperature at which it is considered that the yield strength of steel decreases at elevated temperatures) and the parametric study concentrated further on the temperature distribution on the bottom flange, web and concrete. Fig. 4 shows, as an example, the relevant points considered and the temperature distribution on the cross-section for a given case, after one hour of ISO fire exposure, by highlighting the 400°C limit.

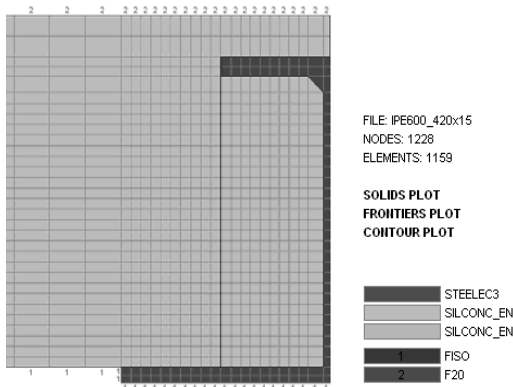


Fig. 3. Discretisation of the cross-section and exposure to fire

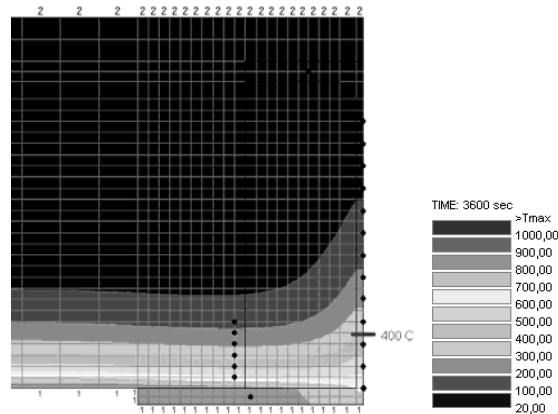


Fig. 4. The main analysed points on the cross-section

2 TEMPERATURE IN THE BOTTOM FLANGE

In a first approach, the temperature in the bottom plate was calculated using the simple approach presented in EN1993-1-2, table 4.2, considering the section factor $A_m/V = (b+2t)/(bt)$, for the flange exposed on three sides, with concrete floor above the upper flange. Some analyses emphasised that this approach leads to strongly conservative values of the load bearing capacity of the floor, calculated analytically, when compared to the load bearing capacity of the floor calculated numerically, using in the mechanical analysis the proper temperature distribution in the bottom flange. Therefore, in order to obtain conservatives values of the load bearing capacity but closer to reality, for the calculation of the temperature in the bottom plate, another method, was considered.

The temperature was monitored for the fire resistance demands of 30, 60, 90 and 120 minutes, in the point from the bottom plate shown in Fig. 4 (at a quarter of the length of the bottom flange). It was emphasized that this temperature depends essentially on the thickness of the bottom plate. Therefore, in order to derive simple formulas for the temperature evolution, the temperatures were represented as shown in Fig. 5, function of the thickness of the plate, for the different fire resistance demands. First and second order functions were found to fit better with the scatter, as Fig. 5 shows.

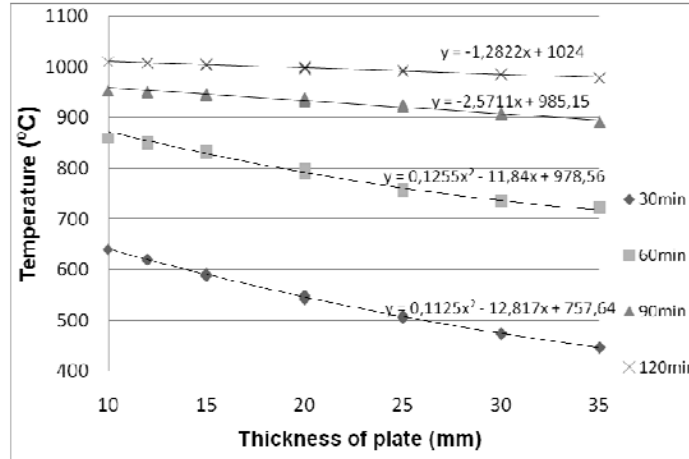


Fig.5. Temperature in bottom flange function of plate thickness

The following equation is proposed to determine the temperature in the bottom flange, in which T_i is in °C and the plate thickness t_{pl} is in mm:

$$T_i = A_i t_{pl}^2 + B_i t_{pl} + C_i \quad (1)$$

in which the coefficients A_i , B_i and C_i are given in Table 1. These coefficients represent the rounded values of the coefficients of the best-fit curves presented in Figure 5, in order to offer „cleanest” values for the designer.

Table 1. Coefficients for temperature calculation in the bottom flange

Time [min]	A_i	B_i	C_i
30	0.113	-12.50	760
60	0.130	-11.80	980
90	-	-2.60	990
120	-	-1.25	1025

3 TEMPERATURE IN THE WEB OF THE STEEL PROFILE

The temperature on the height of the web is almost not influenced by its thickness, but is strongly influenced by the distance from the bottom flange and, in a smaller amount, by the thickness of the bottom flange t_{pl} .

The temperatures were monitored for 30, 60, 90 and 120 minutes in the points from the web shown in Fig. 4. The temperatures were represented as shown in Figure 6, function of the distance from the top of the bottom plate, for the different fire resistance demands and for a given thickness of the bottom plate. Exponential functions were found to fit better with the scatter, as Fig. 6 shows.

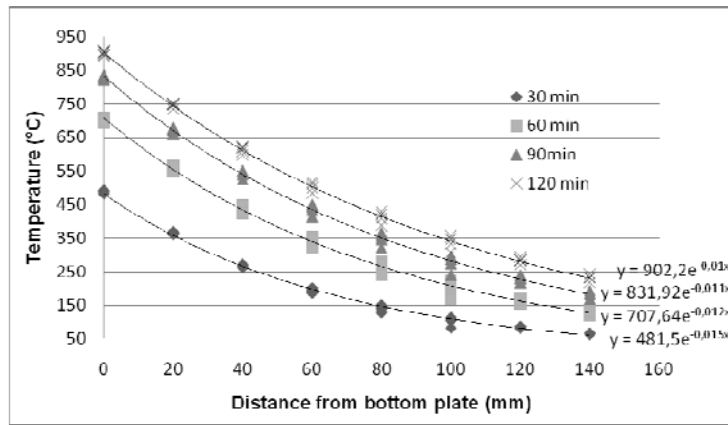


Fig. 6. Temperature in web function of height for bottom plate thickness of 12 mm

The following equation is proposed to determine the temperature in the web, in which T_w is in °C, the distance z along the height of the web measured from the top of the bottom flange is in cm and the plate thickness t_{pl} is in mm:

$$T_w = k_1 e^{k_2 z} \quad (2)$$

with $k_1 = A_w \ln(t_{pl}) + B_w$ $k_2 = C_w \ln(t_{pl}) + D_w$

in which the coefficients A_w , B_w , C_w and D_w are given in Table 2.

Table 2. Coefficients for temperature calculation in the web

Time [min]	A_w	B_w	C_w	D_w
30	-140.70	832.42	0.0317	-0.230
60	-103.80	968.60	0.0232	-0.182
90	-108.60	1146.70	0.0198	-0.154
120	-70.44	1124.40	0.0158	-0.134

4 TEMPERATURE IN THE REBARS ABOVE THE BOTTOM FLANGE

The temperature in the rebars above the bottom flange was considered equal to the temperature of the concrete. As in case of the web temperature, the temperature on the height of the concrete is strongly influenced by the distance from the bottom flange and, in a smaller amount, by the thickness of the bottom flange t_{pl} .

The temperature was monitored for 30, 60, 90 and 120 minutes in the points from the concrete above the bottom flange shown in Fig. 4, which are located in the zone of the possible positions of the rebars. As shown in Fig. 7, the temperatures were represented in a similar manner as for the web temperature distribution, function of the distance from the top of the bottom plate, for the different fire resistance criteria, for a given thickness of the bottom plate. Exponential functions similar to the ones for web temperature distribution were found for concrete.

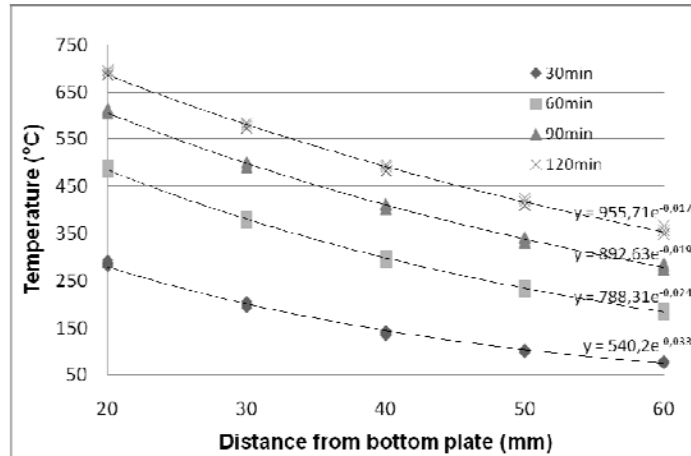


Fig. 7. Temperature in concrete function of height for bottom plate thickness of 12 mm

The following equation is proposed to determine the temperature in the concrete (rebars), in which T_c is in °C, the distance z measured from the top of the bottom flange is in cm and the plate thickness t_{pl} is in mm :

$$T_c = k_3 e^{k_4 z} \quad (3)$$

with $k_3 = A_c \ln(t_{pl}) + B_c$ $k_4 = C_c \ln(t_{pl}) + D_c$

in which the coefficients A_c , B_c , C_c and D_c are given in Table 3.

Table 3. Coefficients for temperature calculation in concrete (rebars)

Time [min]	A_c	B_c	C_c	D_c
30	-6.90	612.67	0.0009	-0.342
60	-4.06	834.64	-0.0005	-0.240
90	-2.71	970.63	-0.0005	-0.181
120	-1.37	1043.80	-0.0005	-0.150

5 CONCLUSIONS

The temperature distribution on the cross-sections of the composite Slim Floor beams subjected to ISO fire was investigated using numerical methods and some simple formulas have been developed for determining the values of temperatures in various points, by means of a parametric study. The temperatures were determined for the bottom flange and the web of the steel profile, and for the concrete, in the zone of the possible positions of the rebars.

Using these formulas, the load bearing capacity of the beams may be calculated, by means of a simple analytical approach, by considering each part of the cross-section that contributes to the load bearing capacity with the corresponding reduced resistance, function of the temperature.

ACKNOWLEDGEMENTS

This research was made in the frame of a diploma work, supervised in double coordination, within an ERASMUS project between the University of Liege, Belgium, and the „Politehnica” University of Timisoara, Romania.

REFERENCES

- ArcelorMittal Commercial Sections, Long Carbon Europe Sections and Merchant Bars, Slim Floor, An innovative concept for floors
- Duma D., Simple design method for the fire resistance of composite steel-concrete slim floor systems, T.F.E., Univ. de Liège (2010)
- EN 1992-1-2, Eurocode 2 – Design of concrete structures. Part 1-2. General rules – Structural Fire Design, CEN, Brussels, 2005

EN 1993-1-2, Eurocode 3 – Design of steel structures. Part 1-2. General rules – Structural Fire Design, CEN, Brussels, 2005

Franssen J.-M., SAFIR. A Thermal/Structural Program Modelling Structures under Fire, Engineering Journal, A.I.S.C., Vol 42, No. 3 (2005), 143-158, <http://hdl.handle.net/2268/2928>

PROFILARBED s.a., Groupe Arcelor, CENTRE DE RECHERCHES, Test au feu sur un Plancher type 'Slim Floor' EMPA/ETH Zurich, 1994, RPS Report No 24/95

ELASTIC BUCKLING OF STEEL COLUMNS UNDER THERMAL GRADIENT

Christos T. Tsalikis^a, Efthymios K. Koltsakis^b, Charalampos C. Baniotopoulos^c

^a Phd student, Institute of Metal Structures, Aristotle University of Thessaloniki, Greece

^b Asst. professor, Institute of Metal Structures, Aristotle University of Thessaloniki, Greece

^c Professor, Institute of Metal Structures, Aristotle University of Thessaloniki, Greece

INTRODUCTION

Breakout of fire in a steel building causes the progressive development of temperature fields in its members. Those members which are strictly inside the fire room quickly develop roughly uniform temperatures, while those bordering to the external environment sustain a clear thermal gradient over their cross-section. The behaviour of these members is governed by the development of flexural buckling conditions due to the thermal gradient, a matter that is going to be the focus of the present work. Thermal gradient causes the shift of the elastic neutral axis and, as a result, the generation of initial eccentricity, as the mechanical properties of the material depend on the imposed temperature field and taken to obey non-linear rules according to Eurocode 3. Hence, the problem of flexural buckling of a column under axial load without eccentricity transforms to a problem of elastic stability of a beam-column. On the other hand, the thermal gradient will cause different thermal elongation across the cross-section of the beam which will lead to the bowing of the column. The deflection of the column will be amplified due to second-order effects.

1 STATE OF THE ART

Extended research has been made on the behaviour of steel columns under fire conditions. Olawale and Plank (1988) studied the collapse analysis of steel columns in fire using the finite strip method. Burgess and Najjar (1993) studied the behaviour of a steel column under thermal gradient based on 'Perry-Robertson' principles and, later, proposed a nonlinear analysis of steel frames with the use of finite element method. Poh and Bennetts (1995) presented a general numerical analysis, incorporating residual or initial stresses and unloading-reloading of the member. Talamona et al. (1997) and Franssen et al. (1998) studied experimentally and numerically the behaviour of axially and eccentrically loaded columns and Franssen et al. (1995) proposed a simple model for the fire resistance of axially-loaded members according to Eurocode 3, based on numerical and experimental results. Usmani et al. (2001) commented on the importance of thermal effects and proposed basic principles for pin-ended members under uniform and non-uniform temperature distribution. Recently, Quiel and Garlock (2008) developed a close-form solution for perimeter columns under thermal gradients. Furthermore, a simple model, which concerns column under non-uniform temperature distribution along the member, was proposed by Tan et al. (2009). More recently, Dwaikat and Kodur (2010) developed another approach for evaluating plastic axial load and moment capacity curves for beam-columns under thermal gradients.

2 DESCRIPTION OF THE PROBLEM

2.1 Scope

This paper focuses on the behaviour of steel pin-ended columns under thermal gradients. Initially, it examines, separately, the effect of thermal gradient on the shift of the elastic neutral axis and, then, adds the thermal bowing of the member to investigate the combined behaviour. An IPE300 European cross-section will be used for the study of the above effects for several lengths in order to obtain the reduction of the maximum elastic axial load. The linear temperature gradient is imposed across the y-y axis, as shown in Fig. 1, which is also the major axis of flexural buckling. The

flexural buckling of the minor axis is not within the context of the present work since the influence of the thermal gradient is of main interest. As a result, it is assumed that it is properly restrained by the compartment elements.

2.2 Material

Eurocode 3 – Part 1.2 proposes the use of the usual stress-strain relationships multiplied by factors depending on the applied temperature. These factors affect the modulus of elasticity, the proportionality limit and the yield strength of the material; each one is inversely proportional to the imposed temperature. The shape of these functions is linear-elliptical-linear with the elliptical region depending on the proportionality limit. For the sake of simplicity, the bilinear laws was used with the yield strength factors reducing according to the modulus of elasticity ones. Furthermore, Eurocode gives the reduction factors through step functions. In order that continuous functions be obtained for the yield strength and the modulus of elasticity, curve fitting was applied:

$$\frac{E_{\theta}}{E_{20}} = \frac{f_{y,\theta}}{f_{y,20}} = 2,347 \sin(0,5275T + 2,6) + 0,193 \sin(7,803T - 1,438) \quad (1)$$

where $T = \theta/1000$ θ is the applied temperature in °C
 $f_{y,\theta}, f_{y,20}$ are the yield strength at the applied and ambient temperature respectively and
 E_{θ}, E_{20} are the modulus of elasticity at the applied and ambient temperature respectively

3 EVALUATION OF THE THERMAL GRADIENT EFFECT

At first, the influence of the thermal gradient will be examined. Assume a column without taking into consideration thermal stresses, residual stresses and initial eccentricities. The development of the temperature gradients will progressively move the elastic neutral axis to the ‘colder’ part of the cross-section. Given the planarity of the cross-section, according to Bernoulli-Navier hypothesis, the concept of the equivalent cross-section can be applied, as used for the composite sections (Burgess et al, 1994). The reduction of the modulus of elasticity is dependent on the imposed temperature, as seen in Eq. (1). The non-linear equation produces an arbitrary field of modulus of elasticity along the web of the cross-section. To overcome this obstacle and apply a constant E_{20} , the thickness of the web can be scaled according to the imposed temperature at each point of the cross-section, as shown in Fig. 1. The equivalent section will have a different centroid and reduced geometrical properties. Thus, the centroid:

$$Z_g = \frac{\int_0^H \int_0^{B_{eq}} z dy dz}{\int_0^H \int_0^{B_{eq}} dy dz} \quad (2)$$

where $B_{eq} = (E_{\theta}(\theta)/E_{20})B(z)$ the width of the equivalent section at a given z coordinate
 $\theta = (\Delta\theta/H)z + \theta_{min}$ the reference temperature at distance z from the extreme fiber

On the assumption of the absence of thermal expansion effects, the column behaves like a beam-column. The differential equation is given:

$$P(e + w(x)) = -EI_{eq} w''(x) \quad (3)$$

where e the distance between the mid-height of the cross section and the geometrical centroid
 P the applied force on the mid-height of the cross section

The maximum deflection of the column occurs at the mid-height of the total length. Based on the concept of maximum allowable stress, one can determine the secant formula for the equivalent cross-section:

$$\sigma_{y,\theta_{max}} = k_{E,max} P \left(\frac{1}{A_{eq}} + \frac{e}{I_{eq}} c \sec\left(\frac{l}{2} \sqrt{\frac{P}{EI_{eq}}}\right) \right) \quad (4)$$

where c is the distance from the centroid to the extreme fiber
 $k_{E,max}$ is the reduction coefficient of the modulus of elasticity for the maximum imposed temperature
 $\sigma_{y,\theta_{max}}$ is the yield stress for the maximum imposed temperature

The initial eccentricity and the reduction of the overall stiffness of the section affect adversely the stability behaviour of the column. The phenomenon is amplified for slender columns, where second-order effects are dominant. The concave side of the column at the mid-height coincides with the maximum temperature of the thermal gradient and the maximum lateral deflection of the member. At that position, the initial yield criterion is applicable. Following an iterative procedure, one can thus determine the maximum allowable mean stress as represented in Eq. (4).

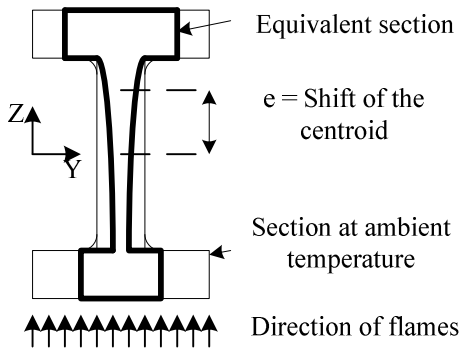


Fig. 1 Equivalent cross-section

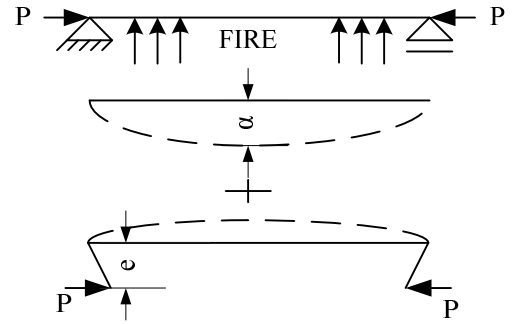


Fig. 2 Deflection due to thermal bowing and shift of the centroid

4 THERMAL BOWING

Consider a perfectly straight column. In normal conditions, the column is designed to resist the axial loads applied to it. In a sudden ignition of a local fire, column gradually loses its strength and stiffness. On the absence of axial restraints, the non-uniform temperature distribution will cause the thermal bowing effect. Column, apart from the thermal elongation, will deflect towards the heat source, as shown in Fig. 2. As a result, the concave side of the member will be that of lowest temperature. The increase of thermal elongation and thermal bowing, together with the relocation of the centroid grow simultaneously under the rise of the thermal gradient. Loading of the column pre-exists on it, but it is not necessary to study all the phenomena coupled. As ECCS (1985) advocates, it is the same either to raise the temperature under constant load or to raise the load under constant temperature in order to study the structural behaviour. Ignoring again for the sake of simplicity, the initial imperfections and the residual stresses, one can study the response of a column under fire situation in a similar way with that of normal conditions. Assume the initial imperfections that exist on real columns to be the thermal bowing effect on perfect columns. Moreover, to overcome the obstacle of non-uniform temperature distribution, the equivalent cross-section, as described previously, can be used to simulate the movement of the centroid and the loss of strength and stiffness of the real cross-section. Thus, the deflection of the equivalent column can be obtained:

$$w(x) = \frac{a_{\Delta\theta}}{1 - \frac{P}{P_{cr,eq}}} \sin\left(\frac{\pi x}{l}\right) - \frac{M_0}{2EI_{eq}} x(l-x) \quad (5)$$

where $a_{\Delta\theta}$ is the maximum deflection at the middle due to thermal bowing

P	is the applied force on the mid-height of the cross section
$P_{cr,eq}$	is the Euler buckling load of the equivalent cross section
M_0	is the edge-moment due to the shift of the centroid

Against this phenomenon, acts the shift of the centroid, as described above and represented at the second part of *Eq. (5)*. The edge moments, which depend on the slope of the thermal gradient, resist to the bowing of the member. Thus, the lateral deflection is being reduced by a constant-curvature equation and the net effect arises by the method of superposition. Following the same line for the determination of maximum allowable stress, initial yield is not clear. Columns of medium or high slenderness are highly possible to create the first yield at the middle of the length, where the maximum lateral deflection arises. At a cross-section level, the concave side is more susceptible to reach first the initial yield criterion with the convex side not to be underestimated due to the fact that the applied temperature there is larger. As far as the low-slenderness columns are concerned, the edges of the members are most apt to undergo the failure of the criterion on the high temperature side. *Eq. (5)* is valid for high slenderness ratios, where the curvature of the member has always the same sign. When the slenderness ratio reduces enough, then the shift of the centroid will be the dominant effect and the sign of the curvature will change. Consequently, the validity of the above equation is narrowed at medium and high slenderness ratios.

5 FEM VALIDATION

The analysis of the behaviour of the simply-supported steel column under the combined effect was validated for two certain cases with the general purpose finite element package ABAQUS. For the description of the material behaviour, both the mentioned bilinear laws and the true laws, that include the elastoplastic regions as given by Eurocode, are applied in order the deviation to be evaluated. The elements chosen for all members were 4-noded (reduced-integration) shell elements, designated as S4R in the ABAQUS element library. The out-of-plane deflection was restrained at the mid-height of the column. The end nodes were constrained to preserve the planarity of the cross-section. The analysis was performed in two steps. The first step imposes the thermal gradient and the second applies the axial load in an incremental manner. The solution is obtained through the standard analysis, which is implicitly based on static equilibrium. For algorithmical convergence purposes, the Arc-Length algorithm (Riks method) was adopted by the FE package. The Riks method is quite similar to the Newton-Raphson method, which is used mostly in nonlinear analyses, but it is more efficient if the tangent stiffness equals to zero.

6 RESULTS AND CONCLUSIONS

This paper focuses on two different approaches of the same problem. At the first approach, the beam-column equation was applied in order the effect of the shift of the centroid to be studied. Results show that the maximum allowable stresses are not far from the Euler buckling curves for the maximum temperature of the cross-section. The eccentricity that arises from the shift of the centroid cannot be studied independently. The initial deflection that arises from thermal bowing makes necessary the simultaneous behaviour of both phenomena. *Eq. (5)* adopts in his first term the function of an imperfect column's deflection and adds, in his second term, that of an edge-moment column. The resultant gives the total deflection of the column with a major limitation. The shift of the centroid should be always smaller than the lateral deflection of the column in order the equation to comply with the initial assumptions. As shown in Fig. 3, buckling curves approach the EC3 curve for the maximum temperature as thermal gradient raises. For small slopes of thermal gradients, buckling curves coincide with Euler curve. This unrealistic situation arises because of the initial assumption of perfect straight column. Furthermore, finite element analysis verifies the validity of this simple approach, as shown in Fig. 3, for a specific thermal gradient. On the contrary, the analysis of the finite element model with the application of the elastoplastic material laws, as proposed by Eurocode, gave more conservative results. This difference arises from the initial overestimation of the yield stress in the bilinear laws that applied to the elastic model. As mentioned before, the validity of this approach can be verified for medium and high slenderness

columns. Fig. 3 represents the discrepancy region between the analytical and FEA solution of low slenderness column. Initial eccentricity plays a dominant role at those slenderness ratios, which is a goal for further investigation. The principles presented here constitute a step towards generating the analytical tools necessary for use. With the appropriate determination of bilinear stress-strain laws and the addition of the other phenomena that govern a column even at ambient temperatures, this method can be used safely for the prediction of lower-bounds on the elastic buckling of medium and high slenderness columns.

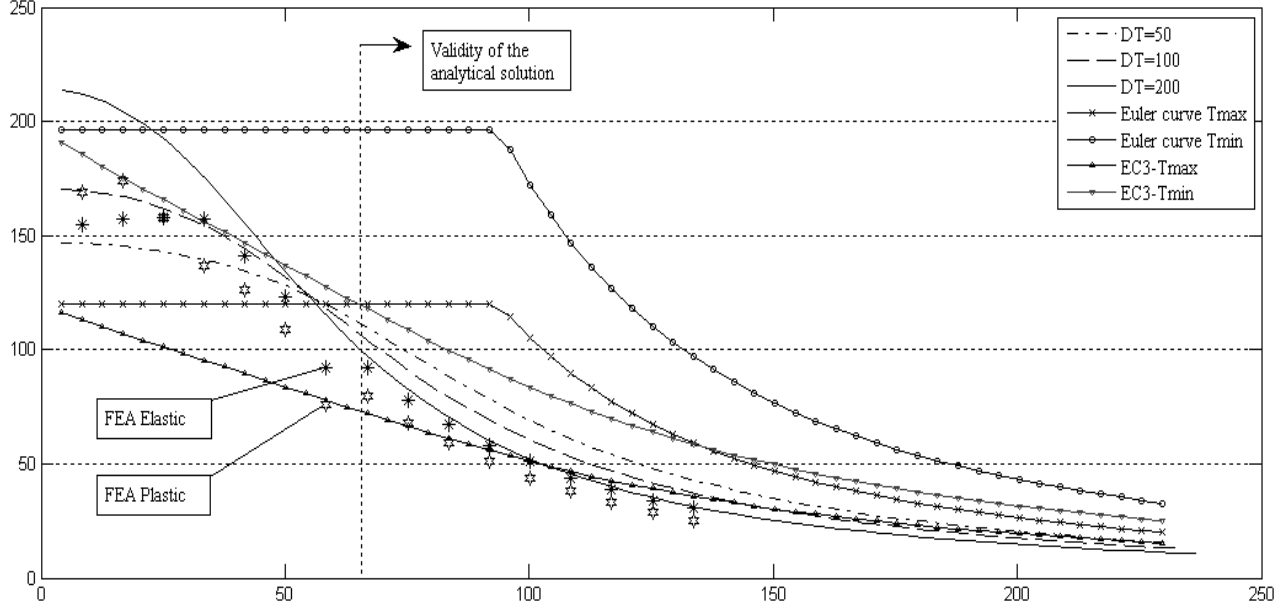


Fig. 3 Buckling curves for Tmax=500°C

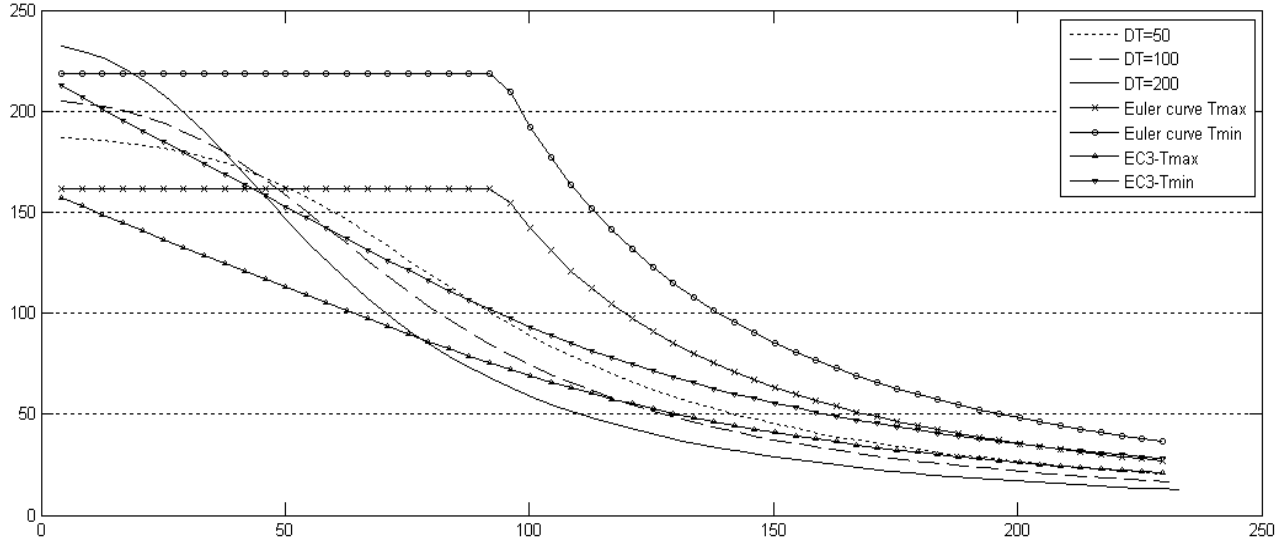


Fig. 4 Buckling curves for Tmax=400°C

REFERENCES

- Timoshenko S. P., Gere J. M., Theory of elastic stability, McGraw-Hill book company, 1961.
- European convection for constructional steelwork, Design manual on the European recommendations for the fire safety of steel structures, ECCS publication, 1985.
- Olawale A. O., Plank R. J., The collapse analysis of steel columns in fire using the finite strip method, International journal for numerical methods in engineering, 1988.
- Burgess I. W., Najjar S. R., A simple approach to the behaviour of steel columns in fire, J. of constructional steel research, 1994.
- Poh K. W., Bennetts I. D., Analysis of structural members under elevated temperature conditions, J. of structural engineering, 1995.
- Franseen J. M., Schleich J. B., Cajot L. G., A simple model for the fire resistance of axially-loaded members according to Eurocode 3, J. of constructional steel research, 1995.
- Talamona D., Franssen J. M., Schleich J. B., Kruppa J., Stability of steel columns in case of fire: Numerical modelling, J. of structural engineering, 1997.
- Franseen J. M., Talamona D., Kruppa J., Cajot L. G., Stability of steel columns in case of fire: Experimental evaluation, J. of structural engineering, 1998.
- Usmani A. S., Rotter J. M., Lamont S., Sanad A. M., Gillie M., Fundamental principles of structural behaviour under thermal effects, Fire safety journal, 2001.
- Quiel S. E., Garlock M. E.M., A closed-form analysis of perimeter member behaviour in a steel building frame subject to fire, Engineering structures, 2008.
- Tan K. H., Yuan W. F., Inelastic buckling of pin-ended steel columns under longitudinal non-uniform temperature distribution, J. of constructional steel research, 2009.
- Dwaikat M., Kodur V., A simplified approach for evaluating plastic axial and moment capacity curves for beam-columns with non-uniform thermal gradients, Engineering structures, 2010.
- Timoshenko S. P., Gere J. M., Theory of elastic stability, McGraw-Hill book company, 1961.
- Tsalikis C. T., Koltsakis E., Baniotopoulos C. C., Steel beam-column under thermal gradient, Proceedings of int. conference- Application of structural fire engineering, Prague 2009.
- Eurocode 3, Design of steel structures, Part 1-2, General rules- Structural fire design, EN1993-1-2, European committee for standardization, 2005.
- ABAQUS software, Dassault systemes Simulia corp., Providence, RI, USA.

ADHESION AT HIGH TEMPERATURE OF FRP BARS STRAIGHT OR BENT AT THE END OF CONCRETE SLABS

E. Nigro ^a, G. Cefarelli ^a, A. Bilotta ^a, G. Manfredi ^a, E. Cosenza ^a

^a University of Naples "Federico II", Department of Structural Engineering (D.I.ST.), Naples, Italy

INTRODUCTION

Nowadays several building codes (CAN/CSA 806-02, 2002; ACI 440.1R-04, 2003; CNR-DT203, 2006) are available for the design of concrete structures reinforced with Fiber Reinforced Polymers (FRP) bars in place of traditional steel reinforcement, even if few provisions and no calculation model taking account of fire condition are suggested. Only the Canadian code (CAN/CSA 806-02, 2002) provides a design procedure in fire situation based on the results of a parametric study conducted by Kodur and Baingo (1998). Consequently, FRP-Reinforced Concrete (FRP-RC) employment is mainly limited to applications, where fire resistance aspects are not particularly meaningful. Thus, in order to improve the confidence in the use of FRP-RC members in multi-story buildings, parking garages, and industrial structures, the performances of these materials in fire situations must be evaluated.

In the past authors tested six concrete slabs reinforced with GFRP bars by exposing them to heat in a furnace according to the time-temperature curve of ISO834 provided in EN 1363-1 (2001). The results of these tests are widely reported in Nigro et al. (2009a,b and 2010a,b). The tests were performed to evaluate their resistance and deformability in the fire situation by varying (a) external loads in the range of the service loads, (b) concrete cover in the range of usual values (30-50mm measured from extreme tension fiber to center of bar) and (c) bars anchoring length at the end of the concrete members, namely in the zone not directly exposed to fire (250-500mm). Three slabs characterized by concrete cover value equal to 51mm and anchoring length values in the slab unexposed zone equal to about 500mm, showed a better structural behavior in case of fire than three slabs characterized by concrete cover value equal to 32mm and anchoring length values equal to about 250mm. Hence, the importance of concrete cover in the zone directly exposed to fire for the protection provided to FRP bars, due to concrete low thermal conductivity was confirmed. Moreover, the anchoring length of the FRP bars in the zone of slab not directly exposed to fire at the end of the members was crucial to ensure slab resistance once, in the fire exposed zone of slab, the bars' temperature has achieved the glass transition value and the resin softening reduced the adhesion at the FRP-concrete interface. Based on such results, in the following sections are showed the results of three further fire tests recently carried out on three slabs reinforced with GFRP bars bent at the end of the member in order to make better the anchorage of the bars within the short zone not directly exposed to fire (i.e. 250mm). A comparison with the test results previously performed on six slabs will be also showed.

1. EXPERIMENTAL PROGRAM

The testing program (see Nigro et al., 2010a,b) involved the design and fabrication of nine full-scale concrete slabs reinforced with GFRP bars, without fire protection system. Table 1 shows the main geometrical properties of all of the nine slabs divided into three sets (namely Set I: S1,S2,S3, Set II: S4,S5,S6 and Set III: S7,S8,S9). The experimental investigation consisted of standard fire tests on the simply-supported slabs. Three slabs (S1, S2 and S3) were 3500mm long, 1250mm wide and 180mm thick; the concrete cover with reference to the bar centroid is 32mm. S4, S5, S6 slabs were 4000mm long, 1250mm wide and 180mm thick; the concrete cover values were 51mm. The slabs S7, S8 and S9 were identical to slabs S1, S2 and S3, respectively, except for the shape of the longitudinal bottom bars bent at the end (see Fig. 1). In order to avoid forming bar splice anchorages in the span of the slab, a single GFRP bar, whose length was that of the slab minus 20mm (i.e. twice the 10mm of concrete cover at each end of the slab), was employed for every slab.

Table 1 - Fire test main parameters for FRP reinforced concrete slabs.

Set	Slab	Length [mm]	Width [mm]	Thickness [mm]	Cover [mm]	Bottom bars (diameter/spacing) [mm]		Anchoring length [mm]	Bar shape
						longitudinal	transversal		
I	S1	3500	1250	180	32 ^(*)	Φ12/150	Φ12/200	250	Straight
	S2				26 ^(**)				
	S3								
II	S4	4000	1250	180	51 ^(*)	Φ12/125	Φ12/200	500	Straight
	S5				45 ^(**)				
	S6								
III	S7	3500	1250	180	32 ^(*)	Φ12/150	Φ12/200	250	Bent
	S8				26 ^(**)				
	S9								

(*) thickness of concrete cover measured from the bottom concrete surface to the centre of bar;

(**) distance from the bottom concrete surface to the nearest surface of reinforcement.

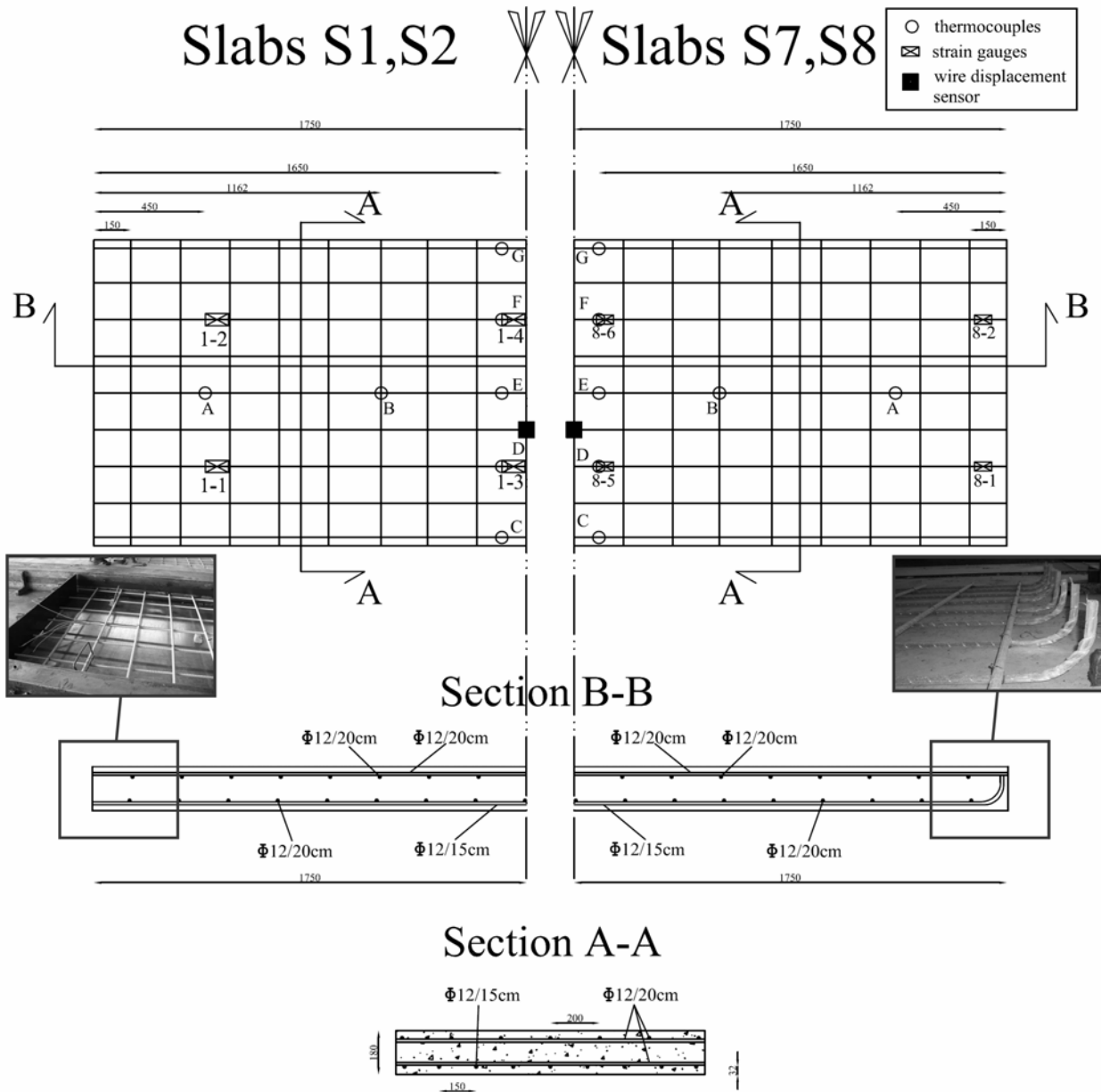


Fig. 1 – Geometrical details of slabs S1,S2,S7,S8 (dimensions in millimeters) - Detail of bars' end

The concrete was C35/45, according to European codes, and characterized by calcareous aggregate. For the GFRP reinforcement, E glass fibers and ortophtalic polyester resin was used by manufacture that provided FRPs. Tensile tests on FRP bars provided, in normal temperature condition, values of strength and Young modulus equal to 1000MPa and 50GPa respectively. The slabs were designed according to CNR-DT203 (2006) that provides design relationships to evaluate the bending moment resistance, M_{Rd} , at normal temperature. The design bending moment resistance of slabs was equal to $M_{Rd,1} \cong 65$ kNm except for slabs S3, S6, S9 for which $M_{Rd,2} \cong 46$ kNm. Further details regarding geometrical and mechanical properties of each slab are reported in Nigro et al 2010a.

Since the span between supports was 3200mm, the slabs 3500mm long (Set I and Set III) were external to furnace at each end for a length of 150mm, whereas the slabs 4000mm long (Set II) were external to furnace for a length of 400mm. A strip of about 100mm of rock wool was used to protect the steel supports from fire exposure. Therefore, the ends of each slab were not directly exposed to fire action for a length, namely anchoring length (see Table 1), of about 250mm for slabs of Set I and of Set III, and 500mm for slabs of Set II.

Slabs S1, S4 and S7 have not loaded during the fire exposure. Slabs S2, S5, S7 and S3, S6, S9 have been loaded with a predefined service load corresponding to about the 40% and 60%, respectively, of the ultimate bearing capacity of the slab in normal temperature design. The loads have been imposed, before and during fire exposure, by means of hydraulic jacks jointed to a steel frame. During the tests, the temperatures, at the top and bottom surface of the longitudinal bottom bar and within slab, and the deflection at midspan of each slab have been recorded (see Nigro et al., 2010a,b).

2. EXPERIMENTAL RESULTS

The displacements recorded at midspan of slabs S7, S8, S9 are plotted versus time in Figure 2a, in which also the average bars' temperature are plotted versus time. Moreover, in order to get a better comparison, the same data for slabs S1, S2, S3 and S4, S5, S6 are respectively reported in Figure 2b,c.

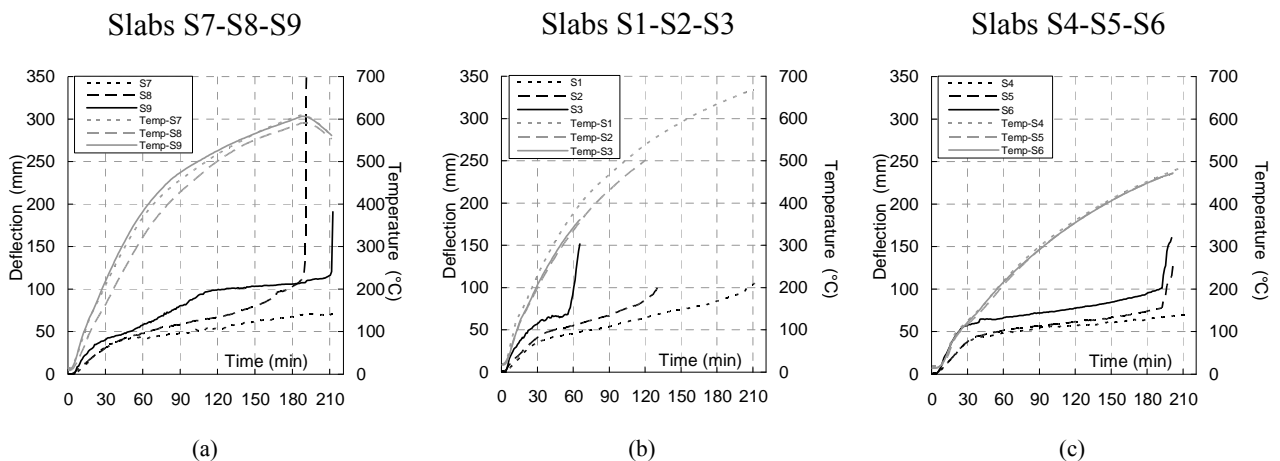


Figure 2 -- Displacements and Temperatures Vs time: (a) Slab S7-S8-S9, (b) slab S1-S2-S3, (c) slab S4-S5-S6

Hereafter, the deflection of slab X at time Y is indicated with the abbreviation $f_{X,Y}$. The slabs S8 and S9, stressed respectively at about 40% of $M_{Rd,1}$ and 60% of $M_{Rd,2}$, exceeded 180min of fire exposure and at fire exposure time equal to $t \approx 180$ min they attained very similar deflection values ($f_{S8,180} \approx 103$ mm and $f_{S9,180} \approx 106$ mm, respectively). Therefore the loads on the slabs were increased and the tests ended when the bending moment attained 45% of $M_{Rd,1}$ and 90% of $M_{Rd,2}$ for slabs S8 and S9 respectively. Unloaded slab S7, at 180 min attained a deflection $f_{S7,180} \approx 68$ mm; its residual resistance, evaluated after the slab cooling phase, when the temperature in the slab attained an average value equal to about 40°C, was about 60% of $M_{Rd,1}$.

In Table 2, for the first phase of the test (Stage 1, with constant load level), load level during fire tests, η_{fi} , and fire resistance time are compared for all slabs (Set I,II,III). It is clear that:

- the slabs S2, S3 (see Figure 2b) characterized by lower concrete cover and lengths of zone not directly exposed to fire (i.e. $c = 32\text{mm}$ and $L_{unexp} = 250\text{mm}$, respectively) showed a fire endurance equal to the 60 and 120 min depending on the load level;
- the slabs S5, S6 (see Figure 2c) with larger values of both c and L_{unexp} (i.e. 51mm and 500mm , respectively) attained a fire endurance larger than 180 min;
- the slabs S8, S9 (see Figure 2a) with low values of both c and L_{unexp} i.e. 51mm and 500mm , respectively) but characterized by bars with bent end attained the same fire endurance of slabs S5, S6 (i.e. 180 min) not depending on the load level.

Table 2 -- Load level during fire tests and fire resistance time (Stage 1); load level increasing at failure and failure mode (Stage 2)

Set	Slab	cover thickness c [mm]	un-exposed length L_{unexp} [mm]	Bar shape	STAGE 1		STAGE 2	
					load level during fire test	fire resistance time	load level at failure	failure mode
					η_{fi} [%]	T_e [min]	η_{fail} [%]	
	S1				10	180	55	
I	S2	32	250	Straight	40	120	50	Pull out
	S3				60	60	-	
	S4				10	180	100	
II	S5	51	500	Straight	40	180	85	Bar rupture
	S6				60	180	100	
	S7				10	180	60	
III	S8	32	250	Bent	40	180	45	Bar rupture
	S9				60	180	90	

All time-displacement curves of Figure 2 present a significant change of slope at about 30 min that corresponds to the change of slope characterizing the standard time-temperature curve of ISO 834 (EN 1363-1, 2001). This suggests that the trend of time-displacement curves depends mainly on the temperatures. In particular the mean of the temperatures recorded during fire tests at the top and bottom of the GFRP bars along longitudinal and transverse axis (fire exposed zone) of slabs S8 and S9 are shown in Figure 3a,b respectively. Moreover the mean of the temperature recorded through the 12 thermocouples embedded at the end of each slab are reported to show the temperatures in the zone of slabs which are not directly exposed to fire. As expected, the GFRP bars temperature values recorded under the bottom longitudinal bars in two slabs are significantly lower than those recorded in the furnace due to thermal inertia of concrete cover. Moreover the temperatures on the top of the bars are lower than those at the bottom of the bars due both to the different distance from exposed zone and to the low thermal conductivity of FRPs. It is meaningful to observe that the temperature recorded at the unexposed zone of slabs remained significantly low during the whole test and achieved a temperature almost equal to the glass transition temperature (i.e. 100°C) just after 180min of fire exposure. Thus during the fire exposure FRP bars were not particularly damaged in the unexposed zone, even if the increasing of temperature can influence the bond behavior of bars at concrete interface (Katz & Berman, 2000). By contrast after about 15 minutes FRP bars attained the glass transition temperature (i.e. 100°C) at the exposed zone of the slabs. Therefore, already in this initial phase of test the resin softening, due to temperatures attained in the bars, the adhesion at the FRP-concrete interface in the fire exposed zone of slab noticeably reduced (Katz & Berman, 2000). Hence, during the fire exposure the structural response depended mainly on the reinforcement anchorage at the fire unexposed end of the member. It is meaningful to observe that temperatures on the bars in the slab S9 were higher than those recorded in the slab S8: in particular, at 30 min the difference was equal to about 100°C and only after two hours the complete coincidence of the bars temperatures was obtained. Such differences were due to a not perfectly homogeneous heating in the oven compared to the ones recorded during the tests on the slabs S1-S6 (Nigro et al., 2010b).

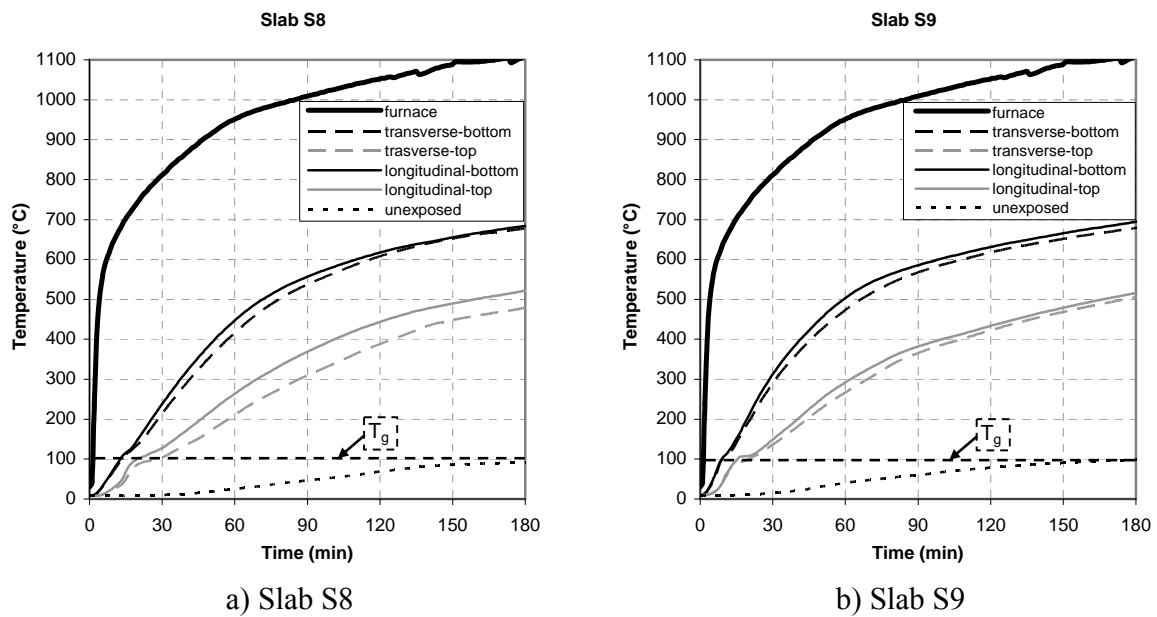


Figure 3 -- Temperatures in the bars during the fire test.

Moreover, based on the temperatures recorded and showed in Figure 3, in Figure 2 it is possible to observe that up to 60 min the slope of the curves decrease even if displacements increase. Since the load is constant the increase of displacement is probably due to the decreasing of Young modulus of bars owing also the deterioration of the fibers at high temperatures. Due to both higher temperatures and higher load level slab S9 a deflection greater than slab S8 up to 120 min of fire exposure (see Figure 2a) was attained when a temperature of about 600°C was recorded in the bars (see Figure 3). A sudden decrease of both stiffness and strength is highly probable for such high value of temperature. In particular for GFRP bars Wang & Kodur (2005) showed a sudden strength decrease of about 70% already at 500°C. Probably for this reason at 120 min the trend of the two curves reversed. The possibility that the bars of the slab S8, less loaded than slab S9, have undergone a rapid damage seems to be confirmed also by a jump in the displacement-time curve of slab S8 at about 165 min of fire exposure. Any way, as confirmed by the investigations on the slabs after the fire test showed below, the anchorage guaranteed by the bent ends of the bars seemed maintaining its effectiveness.

Finally, after 180min of fire exposure, the temperatures of the bars in slabs S8 and S9 achieved 700°C: in order to evaluate the resistance of the slabs after 3 hours of fire exposure the load was increased (until the failure attained at the load level η_{fail}). As showed in Table 2, at Stage 2, the slab S9 exhibited a resistance higher than slab S8 (90% of M_{Rd} vs 45% of M_{Rd}). The failure was essentially due to the strength of the bars; the number of bars of the slab S8 was higher than that of the slab S9 (9 and 6 respectively), hence the result seems strange. However, the nine bars of the slab S8 may be underwent to a higher loss of strength compared to the six 6 bars of the slab S9 because:

- the reduction of strength at high temperature can be sudden, but the temperature range in which this reduction is attained is not precisely defined.
- the cracking phenomenon may have caused preferential ways for the heat flow which may lead to a little local increasing of the bars' temperature and a local significant damaging of the bars.

Moreover, the comparison between the load levels attained at failure on slabs S7 and S8 clearly shows that the residual resistance of slab S7, loaded after cooling phase, is just slightly higher than the one of slabs S8, loaded after 180 minutes of fire exposure, in spite of the lower load level under fire condition and even if the slab S8 appeared particularly damaged during the fire exposure. Such a result is also showed by comparing the results of the tests on the slabs S1,S2 and S4,S5. Therefore the damage that GFRP bars undergo due to the high temperatures seems to be almost completely permanent and cooling

does not seem to allow a resistance recovery.

Figure 4 shows the slab S8 viewed from the furnace after the test. Near the midspan, through the larger crack, it is possible to examine the GFRP bars. The photo clearly shows the glass fibers of the longitudinal bars, broken and completely without resin. In order to examine the bond behavior of bars at the unexposed zone of slabs in which temperatures did not attain T_g , extensive investigations were performed by overturning slabs and picking the whole ends of slabs in the fire unexposed zone after tests. Such investigations confirmed integrity of the anchorage of the bars in the not directly exposed zone of slab (namely $L_{unexp} \approx 250\text{mm}$ – see Figure 5a) that, thanks to bars bent at the end, allowed bars pull out to be avoided by contrast to what was observed for the slabs S1,S2,S3 (see Figure 5b and Nigro et al., 2010a). Thus slabs S1, S2 and S3 failed when bars pulled out in the anchorage zone without the resistance of glass fibers in the fire exposed zone was attained. By contrast, the slabs S7, S8 and S9 failed as slabs S4, S5 and S6 when glass fibers attained their tensile strength. Based on such observations it is possible to look again at the test results reported in Table 2 in terms of fire endurance and resistance. The fire exposure time of slabs S6 and S9 was meaningfully higher than slab S3 due to the more efficient anchorage of the FRP bars in the unexposed zone of the slab. The comparison between the performances of slabs S5 and S8, when the load applied on the slabs increased, shows that a larger cover allowed bars strength decrease to be mitigated and slightly larger resistance to be obtained.

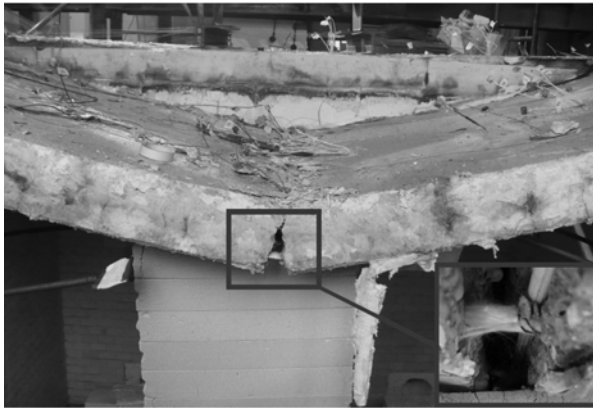
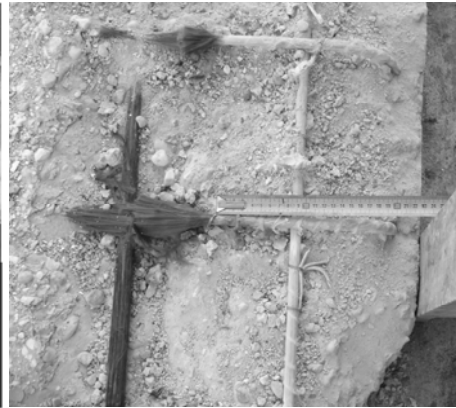


Figure 4 -- Slab S8 after failure



(a) Slab S9: zone not directly exposed to fire (b) Slab S1: lateral face

Figure 5 – Investigations after the fire tests at the end of the slabs: (a) bent bar and (b) straight bar.

3. REMARKS AND DISCUSSIONS

Experimental outcomes highlighted that the failure of the concrete slabs can be attained due to the rupture of the fibers in the middle of the member if a continuous reinforcement from side to side of the concrete element is used and zones not directly exposed to fire are guaranteed. These zones, near the supports, are necessary to ensure adequate anchorage of bars at the ends once in the fire exposed zone of slab the glass transition temperature is achieved and the resin softening reduces the adhesion at the FRP-concrete interface. Moreover it was shown that a large length of this anchoring zone which was not directly exposed to fire (i.e. 500mm) and adopted for straight bars can be reduced (i.e. 250mm) if the bars are bent at the end. By referring to the specific case of concrete slabs, it should be noted that the width of the beams on which slabs are placed are rarely lower than 250mm. Anyhow the bars cannot be overlapped in the area directly exposed to fire because the temperature attains so high values that the loss of adhesion at the concrete-FRP interface may occur and then the failure of structure could take place in a few time.

Therefore, if the bar anchorage allows the pull out of bars to be avoided the failure of slabs is attained due to very high temperatures, namely much higher than glass transition temperature T_g . The values of temperatures largely depend on the concrete cover that influences the temperatures in the bars during

fire whereas fire endurance depends on the fibers strength at high temperatures and consequently it may depend on the fiber types.

Therefore a simplified method to evaluate fire resistance of concrete slabs can leave out of consideration a detailed modeling of RC slabs and can mainly be based on the definition of the mechanical properties of bars at different temperatures. Moreover particular attention should be paid to high values of temperature for which sudden decrease of strength with high uncertainty are expected for bars.

4. CONCLUSIONS

Tests recently performed allowed to evaluate the resistance and the deformability of three GFRP bars reinforced slabs exposed to fire action according to the ISO 834 standard time–temperature curve. The slabs were characterized by concrete cover values equal to 32mm and anchoring length values in the slab unexposed zone equal to about 250mm. Moreover bars are characterized by bent ends.

Fire endurance of slabs and their deflections recorded during tests were showed in the paper:

- two slabs tested under different service loads achieved both 3 hours of fire endurance;
- one slab exposed to fire for 3 hours was loaded after the cooling phase showing a residual resistance not particularly higher than resistance assessed on similar slab suddenly after the 3 hours of fire exposure.

Fire endurance was compared with that assessed by means of same tests previously performed on other two groups of 3 slabs. In particular 3 slabs were identical excepting the shape of the bars at the end of the member, and 3 slabs were characterized by larger concrete cover (51mm) and anchoring length in the slab unexposed zone (500mm).

Comparisons showed that the anchorage obtained simply by bending bars at the end of member in a short zone (250mm) allowed to attain a good structural behavior in case of fire equivalent to that showed by slabs characterized by a large anchoring length (500mm). Moreover the concrete cover was confirmed particularly meaningful for the protection provided to FRP bars, allowing to delay the attainment of high temperature values in the bars. Experimental results, indeed, showed that the reduction of strength at high temperature can be sudden and the temperature range, this reduction is attained in, is not precisely defined.

Finally the cracking phenomenon may cause preferential ways for the heat flow which may lead to a little local increasing of the bars' temperature and a local significant damaging of the bars.

REFERENCES

- Abbasi A, Hogg PJ. (2006). Fire testing of concrete beams with fibre reinforced plastic rebar. *Composites Part A*, Elsevier 2006; Vol. 37, pp. 1142-1150.
- ACI (2003). *Guide for the Design and Construction of Concrete Reinforced with FRP Bars*. ACI 440.1R-04, American Concrete Institute, Farmington Hills, MI; 2003. 42pp.
- CNR (2006). *Guide for the design and constructions of concrete structures reinforced with Fiber Reinforced Polymer bar*. CNR-DT203/2006, Italian National Research Council, 2006.
- CSA (2002). *Design and construction of building components with fibre reinforced polymers*. CAN/CSA S806-02, Canadian Standards Association, Ottawa, ON; 2002. 210pp.
- Bisby, L.A., Kodur, V.K.R. (2007). Evaluating the fire endurance of concrete slabs reinforced with FRP bars: Considerations for a holistic approach. *Composites: Part B*; 38 (2007):547–558.
- Bisby LA, Green MF, Kodur VKR. (2005). Response to fire of concrete structures that incorporate FRP. *Prog Struct Eng Mater* 2005; 7(3):136–49.
- Blontrock H, Taerwe L, Matthys S (1999). Properties of Fiber Reinforced Plastics at Elevated Temperatures with Regard to Fire Resistance of Reinforced Concrete Members. In: *Proceedings of IV International Symposium on Fiber Reinforced Concrete Structures*, Baltimore, 1999.
- European committee for standardization (2001). EN 1363-1:2001. Fire resistance tests - General requirements. 2001.

- European committee for standardization (2004). EN 1992-1-2. Eurocode 2. Design of concrete structures – Part 1-2: General Rules – Structural Fire Design. March 2004.
- European committee for standardization (2002). EN1990. Eurocode 0. Basis of Structural Design. April 2002.
- European committee for standardization (2002). EN 1991-1-2 Eurocode 1. Actions on Structures – Part 1-2: General Actions – Actions on structures exposed to fire. November 2002
- Italian code (2008). NTC 2008. Norme Tecniche per le Costruzioni (in Italian). Supplemento Ordinario della Gazzetta Ufficiale della Repubblica Italiana del 4 febbraio 2008, n. 29.
- Katz A, Berman N (2000). Modeling the effect of high temperature on the bond of FRP reinforcing bars to concrete. *Cement & Concrete Composites*, Elsevier, Vol 22, pp. 433-443, 2000.
- Kodur V.K.R. and Baingo D (1998). Fire Resistance of FRP-Reinforced Concrete Slabs. Internal Report No. 178. Institute for Research in Construction, National Research Council Canada, 1998.
- Kodur VKR, Bisby LA, Foo S. (2005). Thermal behaviour of fire-exposed concrete slabs reinforced with fibre reinforced polymer bars. *ACI Struct J* 2005; 102(6):799–808.
- Nigro, E., Manfredi, G., Cosenza, E., Cefarelli, G., Bilotta, A. (2009a). Fire resistance of concrete slabs reinforced with FRP bars: theoretical models. *Proceedings of 9th International Symposium on Fiber Reinforced Polymer Reinforcement for Concrete Structures Sydney, Australia 2009*.
- Nigro, E., Manfredi, G., Cosenza, E., Cefarelli, G., Bilotta, A. (2009b). Fire resistance of concrete slabs reinforced with FRP bars: experimental investigation. *Proceedings of 9th International Symposium on Fiber Reinforced Polymer Reinforcement for Concrete Structures Sydney, Australia 2009*.
- Nigro E., Cefarelli G., Bilotta A., Manfredi G., Cosenza E. (2010a). Mechanical behavior of concrete slabs reinforced with FRP bars in case of fire: experimental investigation and numerical simulation. *3rd fib Int. Congress – Washington 2010*.
- Nigro E., Cefarelli G., Bilotta A., Manfredi G., Cosenza E. (2010b). Thermal behavior of concrete slabs reinforced with FRP bars in case of fire: experimental investigation and numerical simulation. *3rd fib Int. Congress – Washington 2010*.
- Sakashita M. (1997). Deflection of continuous fiber reinforced concrete beams subjected to loaded heating. *Proceedings of non-metallic (FRP) reinforcement for concrete structures*, vol. 58. Japan Concrete Institute; 1997, p. 51–8.
- Saafi M (2001). Design of FRP Reinforced Concrete Beams under Fire Conditions. *FRP Composites in Civil Engineering – Vol.II*, Elsevier, Alabama, USA, pp. 1235-1244, 2001.
- Tanano H, Masuda Y, Tomosawa F. (1999). Characteristics and Performances Evaluation Methods of Continuous Fiber Bars – State of the Art Studies on Fire Properties and Durability of Continuous Fiber Reinforced Concrete in Japan. In: *Proceedings of IV International Symposium on Fiber Reinforced Concrete Structures, Baltimore, 1999*.
- Wang Y.C., Kodur V. (2005). Variation of strength and stiffness of fibre reinforced polymer reinforcing bars with temperature. *Cement & Concrete Composites*, Elsevier, Vol 27, pp. 864-874, 2005.
- Weber A (2008). Fire-resistance tests on composite rebars. In: *Proceedings of CICE2008, Zurich, Switzerland, 2008*.

MECHANICAL PROPERTIES OF REINFORCING BARS HEATED UP UNDER STEADY STRESS CONDITIONS

Abramowicz Marian ^a, Kisieliński Rafał ^b, Kowalski Robert ^c

^a The Main School of Fire Service, Warsaw, Poland

^b Warsaw University of Technology, Faculty of Civil Engineering, Warsaw, Poland

^c Warsaw University of Technology, Faculty of Civil Engineering, Warsaw, Poland

INTRODUCTION

Proper knowledge of mechanical properties of reinforced steel, subjected to elevated temperature, is essential for correct prediction of load capacity as well as economical design of structural reinforced concrete elements within fire conditions, which can be obtained either by simplified engineering methods or by advanced computerized analyses. The most important mechanical properties of reinforced steel while subjected to high temperature are being commonly described by stress-strain relationship, a relationship that is the result of tensile test. When discussing the case of fire conditions, it would be necessary to determine the dependency of three variables: stress (σ), strain (ε) and temperature (θ). Such approach increases the number of possible configurations significantly, in regards to the correlation's experimental measurement. Testing specimens in presence of all three variable parameters could be difficult to achieve. As a result in practice two the most important ways of testing are usually used (Anderberg, 1988; Skowroński, 2004):

- at constant temperature (steady temperature state),
- at variable (increasing) temperature.

In the tests performed at constant temperature, the free thermal steel strain and creep elongations are usually not taken under consideration in the test results (Anderberg, 1988). Presuming, that the measurement of the elongation begins after stabilization of the elevated temperature within the specimen, and the load action is quite short, it is noticeable that during the test performed at constant temperature, the elongation occurring due to load action is measured. Free thermal steel strain should be added to obtained elongations, in order to procure the total strain. The test performed at constant high temperature does not resemble realistic conditions to which the structural elements are subjected during the real fire. However, the real fire conditions can be simulated during the tests performed at variable (increasing) temperature. Reinforcing bars of the real structural elements are stressed before the fire starts, which means that during the fire the bars are heated up while stressed. It is similar to tests, in which steel is subjected to variable, but constant at every single test, value of stress and heated, and the elongations are measured. During the tests conducted at variable (increasing) temperature it is possible to determine the total strain of reinforcement (Abramowicz et al, 2009). It should be mentioned, that the stress – strain relationship for tensioned reinforcement recommended in Eurocode EN 1992-1-2: 2004 is based on the test results performed at steady state temperature conditions (Anderberg, 1988).

The bars which are currently most frequently used for reinforced concrete structures, are produced in quenching and self-tempering process (Garbarz, 2002). Main principle behind the technology, designed at the turn of the 80s and 90s of the last century, is that the bar is cooled in three consecutive steps, after it has been removed from the last finishing stand. In the first step, the bar is shortly cooled in the cold water so that the outer layer is being quenched. Then, the bar is placed in the room – temperature air area. Such placement causes the tempering process in the quenched layer because the core is still hot, and is giving back the heat towards the surface. The third phase is the change of the core structure during the further cooling. The result of the process is non uniform microstructure with various mechanical properties (Fig. 1): the outer layer is tempered martensite, which is hard but brittle, the middle layer is formed of also hard and brittle bainite structures; however, it is significantly less harder than martensite, and the most inner part of the bar is composed of ferrite-pearlite structures, which are very mild (Garbarz, 2001; Hertz, 2006).

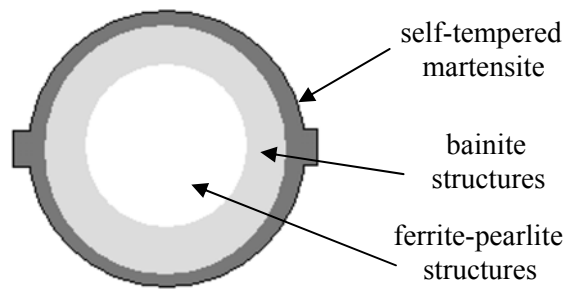


Fig. 1 The scheme of microstructure zones in the cross-section of bar produced in quenching and self-tempering process (Garbarz, 2001)

It is recommended in EN 10002-5: 1998 code, that mechanical properties of reinforcing steel should be tested on 5 mm, 10 mm or 20 mm diameter specimens turned from bars of bigger diameter. The recommendations may have come from the assumption embedded in the past, that the mechanical properties of reinforced steel were approximately the same in every point of the cross-section. Nowadays, it seems more adequate to perform tests directly on raw bars. It is speculated, that for bars with various diameters, the mechanical properties will not demonstrate the same reduction.

The paper shows the results of tests performed at variable (increasing) temperature, completed on raw bars, made of B500SP steel, manufactured in Poland using thermal strengthening technology.

1 EXPERIMENTAL STUDY

1.1 Testing arrangement

Testing was conducted using a hydraulic testing machine, onto which an electrically heated furnace was mounted. (Fig. 2). Both were electronically controlled. Tested bar passed through the furnace practically without touching it. The endings of specimen were fixed in specially prepared jaws. Only the middle part of tested bar was heated.

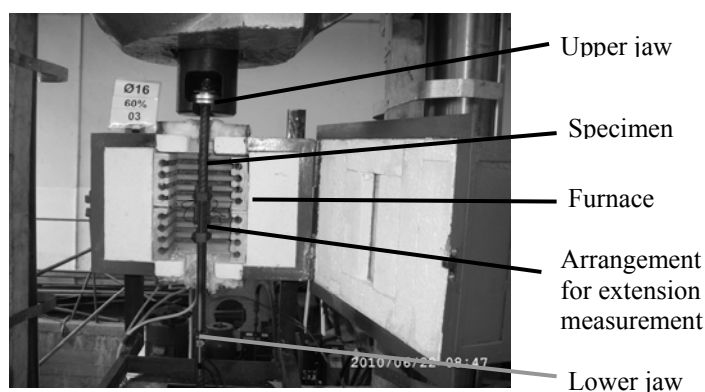


Fig. 2 Testing device

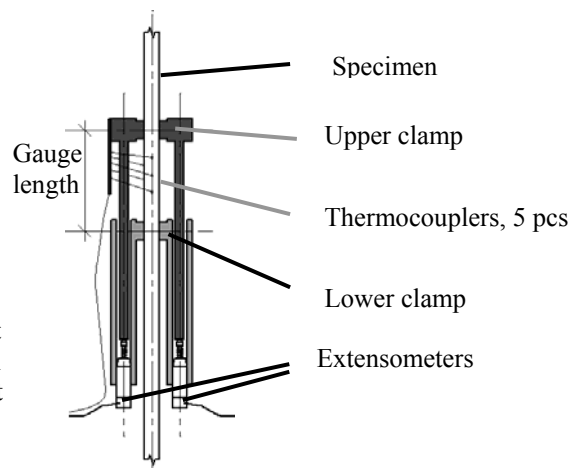


Fig. 3 Principle for extension measurement

Gauge length was 80 mm. It's elongation was measured with specially constructed device (Fig. 3). The device was made of two parts. The upper part was constructed of pair of rods connected together, made of WCL heat-resistant steel. The clamp that was fixing WCL rods, was attached to tested bar using four threaded pins. This arrangement created what was known as the upper point of gauge length. Rods in the upper part of the device had the ability to move in the lower part of the same device, that consisted of two pipes. Tested bar was connected to the lower part (second point of gauge length) in the same way as in the upper part. Extensometers were fixed, outside the furnace chamber, at the endings of pipes. Recorded outcome of the test was the total elongation

arising in the gauge length minus free thermal elongation of the device's upper part rods. The thermal elongation of WCL steel arised in the length equal to the gauge length of the specimen. The data pertaining to the thermal elongation of WCL heat resistant steel was derived experimentally, in the tests performed in dilatometer.

1.2 Specimens and test method

The tests were performed using 10, 12 and 16 mm diameter, made of B500SP steel, commonly used in Poland. The steel is produced by the application of QTB variant of thermal strengthening technology. The QTB is equivalent to TEMPCORE technology (Garbarz, 2001). B500SP steel satisfies the „C” class of plasticity according to EN 1992-1-1:2004. The value of yield strength claimed by the manufacturer is 500 MPa, and the tensile strength should vary between 575 and 675 MPa. Before testing in elevated temperature, tensile tests in room temperature were performed. Results of the tests and conclusions drawn from the results: levels of load used in the high temperature tests, are shown in Tab. 1.

Tab. 1 The results of B500SP steel tensile tests performed in room temperature and determined on the basis of it, values of load used in the high temperature tests.

Bar diameter, mm	Average yield strength, MPa	Average tensile strength, MPa	Assumed load values, MPa			
			% of average yield strength:			
			30	45	60	75
10	582.7	626.6	175	262	350	437
12	551.1	602.4	165	248	331	413
16	514.6	655.8	154	232	309	386

Specimens were stretched to the previously presumed load levels of: 0, 30, 45, 60 i 75% of average yield strength determined experimentally at room temperature (Tab. 1), and than, heated up under constant load until their break. The value of 10 °C/min heating rate was applied in all of the experiments; that is considered an approximate heating rate of main reinforcement ducts, which occurs in the RC elements during fire. Strain and temperature of each bar was recorded by a computer every 20 seconds. There were 5 tests performed for every load level and for every bar diameter. The total sum of 75 tests was performed (3 kind of bar diameter x 5 specimens x 5 load levels).

2 RESULTS AND DISCUSSION

The average strain-temperature relationships determined in the tests performed on loaded bars (black lines, filled markers) are shown in Fig. 3. In addition, the relationships based on assumptions of EN 1992-1-2 (grey lines, empty markers) are shown as well. All the dependences demonstrated here, take into consideration the sum of strain appearing due to load action and temperature dependent free thermal strain of steel.

The graph of free thermal strain of tested bars is shown on Fig. 4 (average results of test performed without load). In the temperature range up to 700 °C, close conformity to EN 1992-1-2 was achieved.

Taking into consideration Fig. 3, one should notice that in the stress levels of 30 and 45 % of average yield strength (f_{yk}), the strain curves are almost identical and consistent with curves based on EN 1992-1-2 assumptions. In the stress level of 60 and 75% f_{yk} the conformity is not of highest quality; however, in authors' opinion, it may be regarded as quite accurate. Practically speaking, there are no differences between strains.

In the range from the beginning of heating process to reaching a critical value of the temperature, at the stress level of 30 i 45% f_{yk} , the obtained relationships are linear, and at the stress level of 60 and 75% are close to linear. After reaching the critical value of temperature, there was an impetuous increase of strain, leading to the breaking of tested bar. The lower the load level, the higher the temperature in which the breaking process takes place.

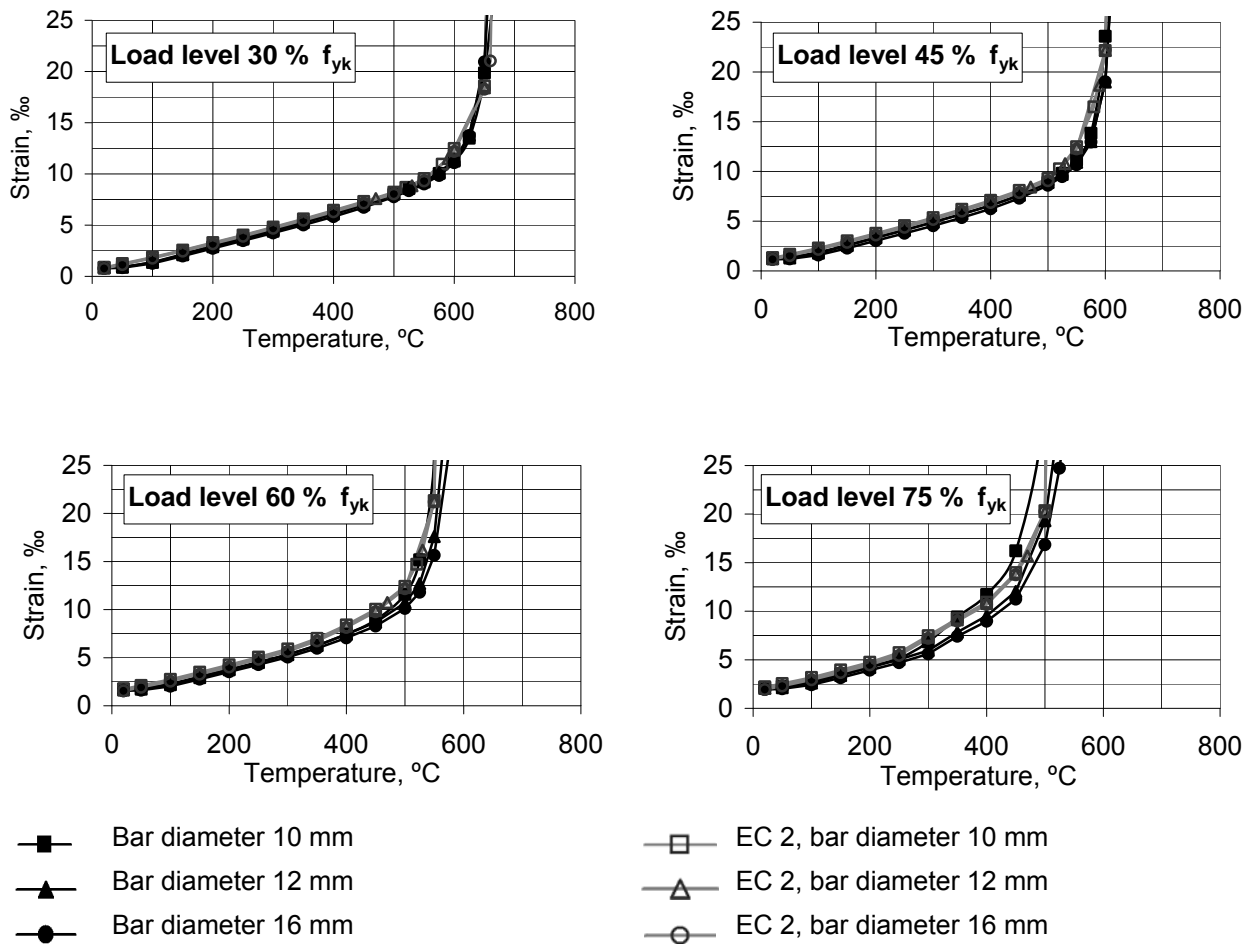


Fig. 3 Experimentally determined strain-temperature relationships

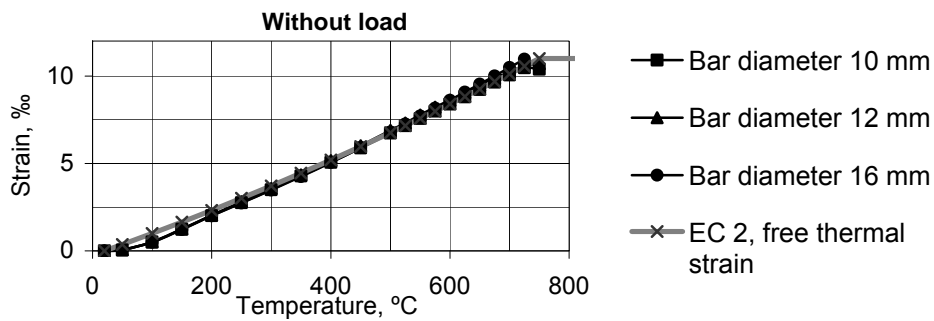


Fig. 4 Measured thermal elongation

The values of critical temperature, based on the test determined results shown in Fig. 3 are shown in Tab. 2. There were two separate temperatures: critical lower temperature ($\theta_{cr,lo}$), in which obtained relationship stops to be linear and critical upper temperature ($\theta_{cr,up}$), in which real destruction of specimen occurs.

Tab. 2 The values of critical temperatures estimated basing on test results shown in Fig. 3

Bar diameter, mm	Critical temperature, °C							
	% of average yield strength:							
	30		45		60		75	
	lower $\theta_{cr,lo}$	upper $\theta_{cr,up}$	lower $\theta_{cr,lo}$	upper $\theta_{cr,up}$	lower $\theta_{cr,lo}$	upper $\theta_{cr,up}$	lower $\theta_{cr,lo}$	upper $\theta_{cr,up}$
10	576	690	524	628	459	568	285	517
12	569	680	520	634	469	590	310	546
16	572	681	517	633	478	590	319	545
Medium	572	684	520	632	469	583	305	536

A graph presenting steel strength reduction factor ($k_{s,\theta} = f_{y,\theta}/f_{yk}$) prepared upon the average values of temperatures given in Tab. 1 is shown in Fig. 5. The values situated on vertical axis are the load levels applied in tests. On the horizontal axis, estimated values of lower and upper critical temperatures are situated. Test results was compared to the $k_{s,\theta}$ reduction factor relationships for strain values less and equal to or greater than 2%, recommended in EN 1992-1-2. In addition (Elghazouli et al., 2009) research results are shown.

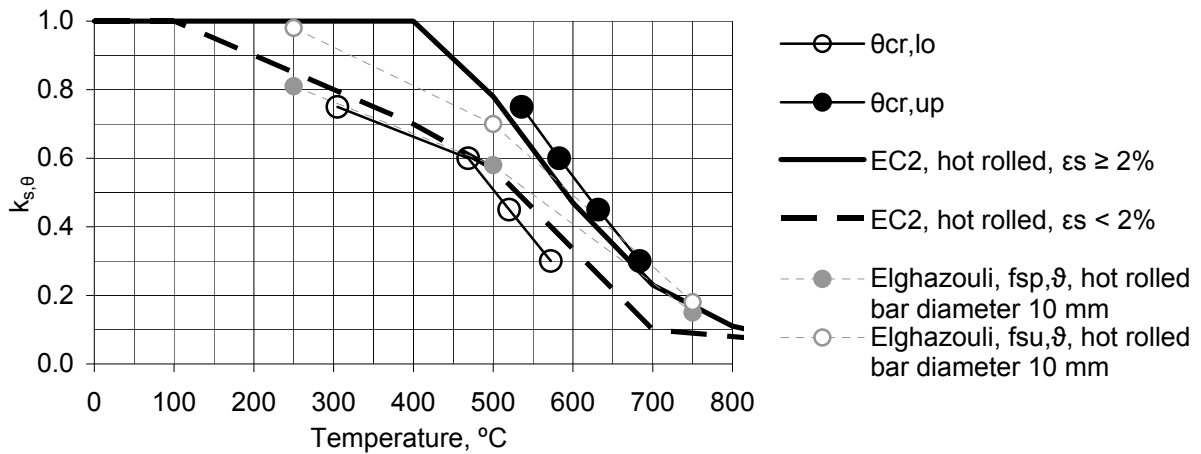


Fig. 5 Relative reduction of B500SP steel tensile strength in correspondence to temperature

The stress values in which braking of the bars may be expected, derived experimentally, based on the values of critical temperature ($\theta_{cr,up}$), are only slightly greater than values recommended in EN 1992-1-2. The stress values in which the strain-temperature relationships stop to be linear and impetuous increase of bar strain begins, experimentally specified, based on the the values of critical temperature ($\theta_{cr,lo}$), are only slightly lesser than the values recommended in EN 1992-1-2 for strain values limited to 2%. The test results (Elghazouli et al., 2009) of presently produced, similar in diameter bars, performed at constant temperature (steady temperature state) also indicate an accordance with EN 1992-1-2 curves.

Despite the fact, that the tests performed by authors were carried out at variable (increasing) temperature and recommendations of EN 1992-1-2 are based on tests carried out in steady (constant) temperature, the accordance of reduction factor for steel strength is quite accurate. It may be concluded that in case of heating reinforcement with heat rate about 10°C/min, the influence of heating time is not significant. While predicting the behaviour of reinforcement in bended RC elements in fire, it seems reasonable enough to take into consideration the sum of free thermal strain and the strain appearing due to load action.

4 CONCLUSIONS

The bars, which are currently most frequently used for reinforced concrete structures, are produced in a process, that results in various mechanical properties in several zones of bar cross-section. It

would be relevant to perform steel testing directly on bars, not on specimen turned from bars of bigger diameter.

In this paper, the results of tests performed on 10, 12 and 16 mm diameter bars, carried out in increasing temperature, with heating rate 10°C/min are shown. This type of testing simulates the conditions, to which the reinforcement of real, bended RC structural elements are subjected during the real fire..

The obtained strain-temperature relationships that range from the beginning of heating process to reaching a critical value of temperature, are close to linear. Afterwards, one may observe an impetuous increase of strain, leading to the breaking of tested bar.

The obtained strain-temperature relationships are accordant to the relationships found in the EN 1992-1-2 recommendations; despite the fact, that EN 1992-1-2 model assumptions are based on tests carried out in steady (constant) temperature.

Values of steel strength reduction factor also turned out to be accordant with the values determined using EN 1992-1-2 recommendations. It may be concluded, that while predicting a behaviour of thermal strengthened reinforcement in bended RC elements in fire, it seems justified enough, to take into consideration the sum of free thermal strain and the strain caused by stress.

REFERENCES

- Abramowicz M., Kowalski R.; Stress-strain relationship of reinforcing steel subjected to tension and high temperature. International Conference: Applications of Structural Fire Engineering, Prague 2009; Conf. Proc. p.134-139.
- Anderberg, Y.; Modelling Steel Behaviour. Fire Safety Journal, 13, 1988; p.17-26.
- Elghazouli A.Y., Cashell K.A., Izzuddin B.A.; Experimental evaluation of the mechanical properties of steel reinforcement at elevated temperature. Fire Safety Journal, 44, 2009; p.909-919.
- Garbarz B.; The progress in production and application of steel product used as reinforcing and prestressing bars (in polish). Metallurgy & Metallurgical Engineering News, 6, 2002; p. 236-245.
- Garbarz B.; Class 500 TECOR deformed rebars manufactured by Huta Ostrowiec S.A. using thermal strengthening technology (in polish). Transactions of the Institute for Ferrous Metallurgy 1, 2001; p. 21 – 37.
- Hertz K.D.; Quenched reinforcement exposed to fire. Magazine of Concrete Research, Vol.58, No. 1, 2006; p.43-48.
- Skowroński W.; Fire Safety of Metal Structures. PWN, Warsaw, Poland 2004.
- EN 1992-1-2: 2004: Eurocode 2: Design of concrete structures – Part 1-2: General rules - Structural fire design.
- EN 10002-5: 1991: Metallic materials – Tensile testing – Part 5: Method of testing at elevated temperature.

COUPLED STRUCTURAL-THERMAL CALCULATIONS FOR RESTRAINED STEEL COLUMNS IN FIRE

Lasław Kwaśniewski ^a, Faris Ali ^b, Marcin Balcerzak ^a

^a Warsaw University of Technology, Faculty of Civil Engineering, Warsaw, Poland

^b University of Ulster, School of The Built Environment, Jordanstown, Newrownabbey, United Kingdom

INTRODUCTION

Behaviour of structures in case of fire is usually strongly affected by primary and secondary thermal effects which can substantially reduce the structural robustness. For example in case of confined fires, adjacent structural elements having much lower temperatures, can impose both axial and rotational restrains. In such cases the thermal expansion can generate additional loading in axially and rotationally restrained columns. The prediction of this additional loading is difficult as it depends on temperature distribution in both the column and the restraints (connections). Another effect on column's buckling is due to the imperfections which are magnified in fire conditions especially when a column is subjected to non-uniform temperature distribution caused by a local fire, partial insulation or due to partially damaged fire protection.

The paper presents a study on numerical modeling of steel columns subjected to axial and rotational restraints and time dependent temperatures. The problem is investigated using nonlinear finite element simulations carried out using general purpose program LS-DYNA® (Hallquist, 2006). The coupled thermal – stress analyses were performed with mechanical integration time steps followed by thermal time steps where the heat transfer equations were solved and temperature field updated. Numerical predictions of structural response during heating are compared with published experimental data. As an example of validation, the experimental test presented by (Ali and O'Connor, 2001) has been selected. In this work the structural performance of steel columns is investigated using half scale specimens tested in fire under two values of rotational restraint and one value of axial restraint.

1 SELECTED EXPERIMENTAL FURNACE TESTS

The results of experimental investigation for steel columns 127x76UB13, performed at *The Fire Research Center, University of Ulster* in the collaboration with *The University of Sheffield*, presented by (Ali and O'Connor, 2001) were used. Half scale steel columns were tested in a furnace under different values of rotational and axial restraint, see Fig.1. For the chosen loading scenario the investigated members were first loaded to the level of approximately 205 kN and then heated. During the test, both axial forces and column expansion as well as lateral displacements in a mid-section were measured and recorded. Temperature was controlled and monitored by the set of thermocouples distributed uniformly at three levels of the furnace and two levels of the tested specimen. At each level of the column five thermocouples were used in the following arrangement: one attached to the center of the web and four attached to the column flanges. In the experiments (Ali and O'Connor, 2001) the axial and rotational restraints were applied through adjustable rubber pads and top and the bottom plates of the steel frame located outside the furnace, as shown in Fig. 1.

2 FE MODEL DEVELOPMENT

2.1 General assumptions

A numerical model of the selected steel specimen used in the experiment was developed, as shown in Fig. 2. Due to relatively small thicknesses of the component walls (i.e. flanges and web) a 3D shell model was used with heat transfer through the wall thickness neglected. Based on the average temperature profile recorded during the experiment, a time dependent temperature was applied to

the nodes representing the part of the column subjected to fire conditions. The heat transfer between the surroundings (interior of the furnace) and the beam was ignored. However, the heat transfer in the longitudinal direction (i.e. along the column's axis) was considered and was found important especially at the top and bottom of the column, close to the furnace walls (compare Section 2.4). The coupled thermal – stress analyses were performed with mechanical integration time steps followed by thermal time steps, where the heat transfer equations were solved and temperature field updated. During the first 100 seconds of simulation only the compressive loading of 205 kN is applied through a prescribed displacement of a rigid beam (see Fig. 2). Later, the displacement at the upper sides of rubber pads is fixed and the value of growing temperature is applied in accordance with the experimental recordings. The stiffness of the rubber pads of the elastic connecting plates (at the top and bottom) are set to produce assumed axial and rotational stiffness. Preliminary results obtained for simplified numerical models showed that although the mesh resolution is sufficient to properly capture the deformation caused by buckling there are clear quantitative discrepancies between the experimental data and the numerical results (Kwasniewski et al, 2010). Further investigation presented in this paper was focused on parametric study which indicated three important modeling parameters affecting numerical results: model description of material properties for the used grade of steel, geometrical imperfections, and longitudinal variation of the temperature in the column at the areas close to the furnace walls.

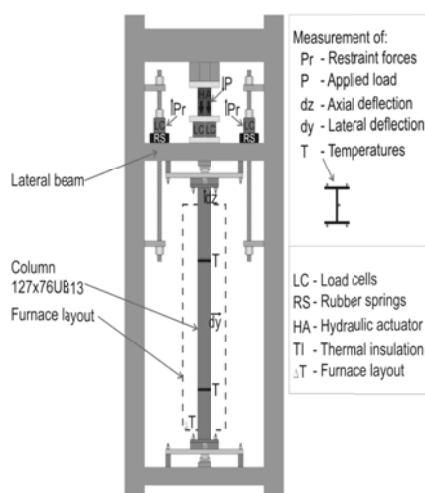


Fig. 1 Experimental test setup (Ali and O'Connor, 2001).

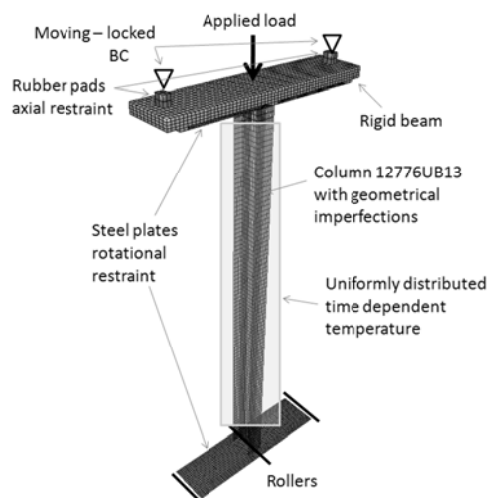


Fig. 2 FE model.

2.2 Material properties

Initially three temperature dependent material models were considered for the steel grade S275. The first material model applied nominal yield stress f_y without strain hardening ($f_u=f_y=275$ MPa). The second model took into consideration nominal yield stress and strain hardening approximated according to EN 1993-1-2 (Eurocode 3, 2005), ($f_y=275$ MPa, $f_u=1.25f_y$). Material parameters at ambient temperature for the third material model ($f_y=303$ MPa, $f_u=469$ MPa, $f_u=1.55f_y$), were based on the coupon tests presented in (Wald et al, 2004). The temperature dependence of stress strain relationships for all three cases was set based on formulae provided by (Eurocode 3, 2005) for carbon steel, see (Kwaśniewski et al, 2010) for more details. All the results presented below were calculated for the third material model, for $f_u=1.55f_y$.

2.3 Applied geometrical imperfections

It is well known that even small imperfections can significantly affect behavior of members axially loaded beyond the critical point. The actual imperfections, defined as the deviations from the ideal representation provided by an FE model, are not easily measured because they usually have many sources. Imperfections in steel columns can be due to variation of material properties, residual stresses, nonsymmetrical boundary conditions and loading, and imperfect geometry. Varied in time

and in space temperature fields caused by fires impose additional non-uniform displacements and strains, affecting initial geometry of the specimen.

In the FE model the most common technique is to introduce geometrical imperfections through prescribed perturbations of initial nodal positions. In this way a perfectly straight column is replaced by a slightly curved specimen. In many commercial programs imperfections are automatically generated through initial variations of nodal positions defined by a pattern giving space distribution and by amplitude defining maximum change of nodal coordinates. Herein prescribed harmonic perturbations were applied to the considered column. The effect of geometrical lateral imperfections of mid-span cross-section for four prescribed amplitudes: 0 mm (no imperfection) 1, 2, and 4 mm is shown in Figs 3 - 5.

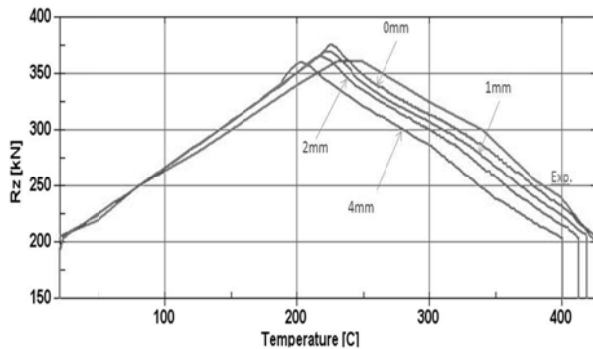


Fig. 3 Axial force vs. column temperature for different magnitudes of imperfections compared to experiment.

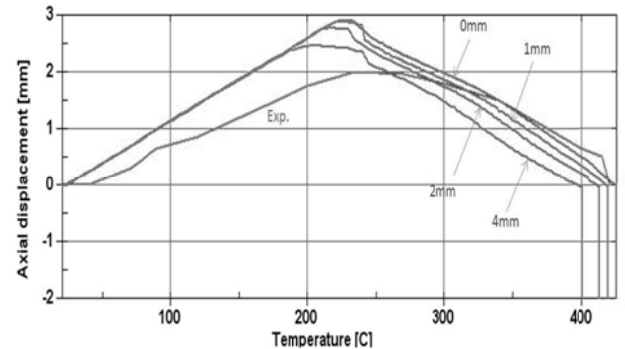


Fig. 4 Axial displacement vs. column temperature for different magnitudes of imperfections.

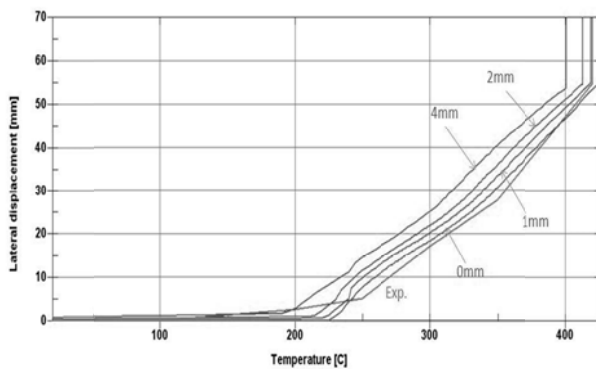


Fig. 5 Lateral displacement vs. column temperature for different magnitudes of imperfections compared to experiment.

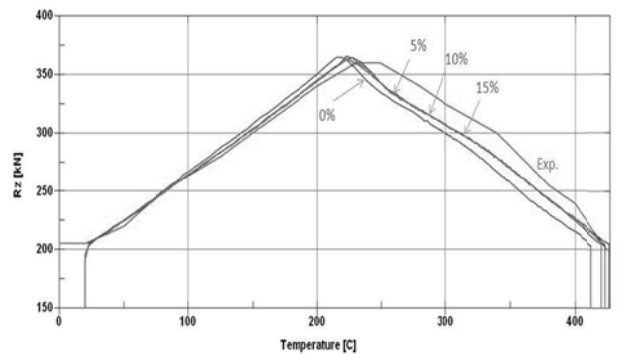


Fig. 6 Axial force vs. column temperature for varied temperature distribution - results for perturbation 2 mm.

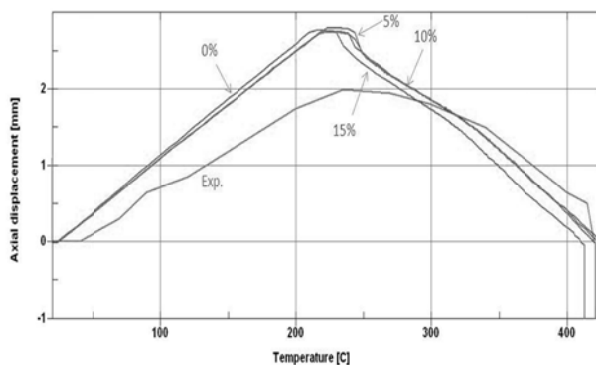


Fig. 7 Axial displacement vs. column temperature for varied temperature distribution - results for perturbation 2 mm.

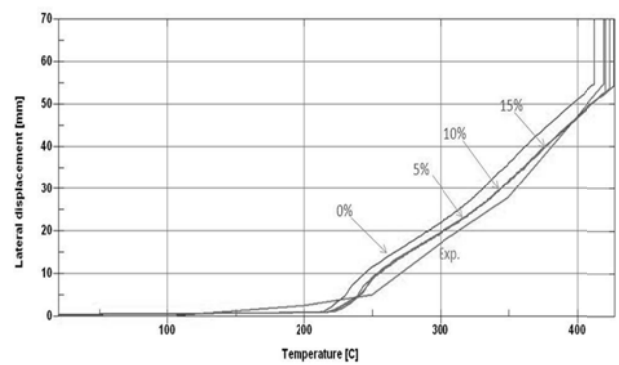


Fig. 8 Lateral displacement vs. column temperature for varied temperature distribution - results for perturbation 2 mm.

2.4 Reduction of heated column area

In the first modeling approach it was assumed that the whole volume of the column part placed inside the furnace, was subjected to the uniformly distributed in space and time dependent temperature field. Closer examination of photos showing the considered furnace experiments indicated that the bottom and top segments of the column, located near the furnace walls, were subjected to lower temperatures due to unavoidable heat transfer through the furnace openings. The next set of virtual tests was conducted for the third material model ($f_u=1.55f_y$), four magnitudes of imperfections and changed longitudinal distribution of temperature in the column. The original heated length of the column equal to 1750 mm was reduced here to 1460 mm. This central part of the column had been modeled to obtain the uniform distribution of prescribed time dependent temperature along its length, while the rest of the column was subjected to longitudinally varied temperatures, calculated from the heat transfer.

2.5 Variation of temperature along the length of the column

Another modification of numerical model taken into consideration is variation of column's temperature along its length. It is easy to predict that temperature distribution inside the furnace is not uniform, what is confirmed by comparison of temperature readings from 20 thermocouples located at: 300, 600, 1200, 1500 mm distance starting from the bottom of the column, (Ali and O'Connor, 2001). During the experiment temperature in the top half of the heated column is almost uniform, and the same situation is for the bottom half of the column. In the modified numerical model the applied prescribed temperature is varied between bottom and top halves of the column, and three values of relative difference in temperature are assumed: 5%, 10% and 15%. In the diagrams presented in Figs 6-8 the average value of temperature from two zones is taken as abscissa. Figs. 6-8 show comparison of numerical results for variable relative difference in temperature between the top and bottom halves of the column. The assumed variation of temperature along the length of the column improved the results in relation to the experimental ones, though difference between models with 5%, 10% and 15% of temperature variation is very small. For the next calculations 10% variation was applied as the most representative and closest to the experimental readings (Ali and O'Connor, 2001).

2.6 Variation of applied force

The next step in the FE model development is the modification of applied force. Originally the applied force was assumed to be constant during the heating phase although closer investigation indicated that its value was slightly changing during the experiment. The value of the applied axial force was measured during the experiment and this detailed data was used in the numerical modelling. Figs 9-11 present comparison between the results for the modified FE models and the previous model with assumed constant value of applied axial force. The comparison shows that the modification of the applied force improves the results in the reference to the experiment.

2.7 Modification of constraints

The axial constraints are generated in the tested specimen using rubber pads. With appropriate stiffness the rubber pads simulate interaction of the column with the adjacent structure due to axial elongation caused by change of temperature. Another step in the modification of the FE model was to apply discrete elements with nonlinear force-displacement relation according to the obtained experimental data. The results for the model with modified discrete constraints are presented in Figs 12-14.

2.8 Comparison for other test cases

In the next step a series of models were investigated for the variable loading levels, according to (Ali and O'Connor, 2001). All calculations were done for determined optimal modelling parameters i. e. the material model with $f_u=1.55f_y$ (see Section 2.2) harmonic nodal perturbation of 2 mm

(Section 3) and 10% difference in the temperature between the top and bottom halves of the column (Section 2.5).

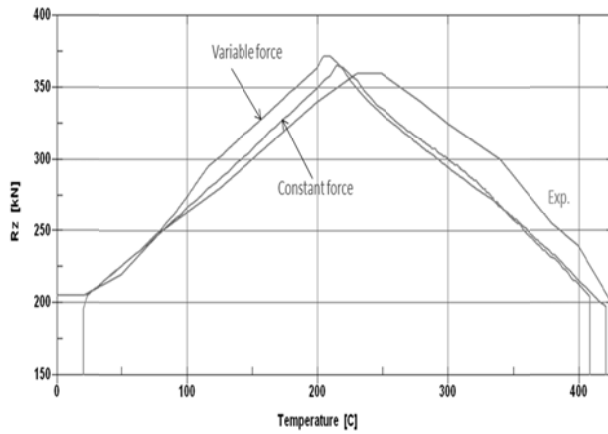


Fig. 9 Axial force vs. column temperature for constant and variable applied force - results for perturbation 2 mm.

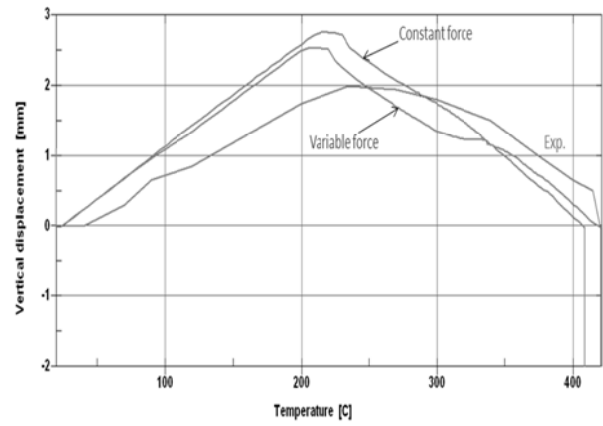


Fig. 10 Axial displacement vs. column temperature for constant and variable applied force - results for perturbation 2 mm.

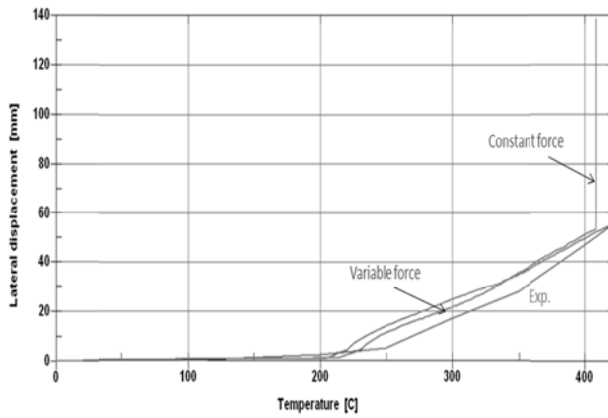


Fig. 11 Lateral displacement vs. column temperature for constant and variable applied force - results for different perturbation 2 mm.

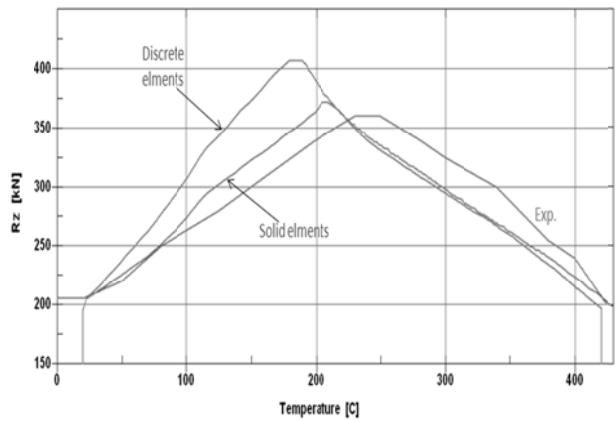


Fig. 12 Axial force vs. column temperature for standard and modified constraints - results for different perturbation 2 mm.

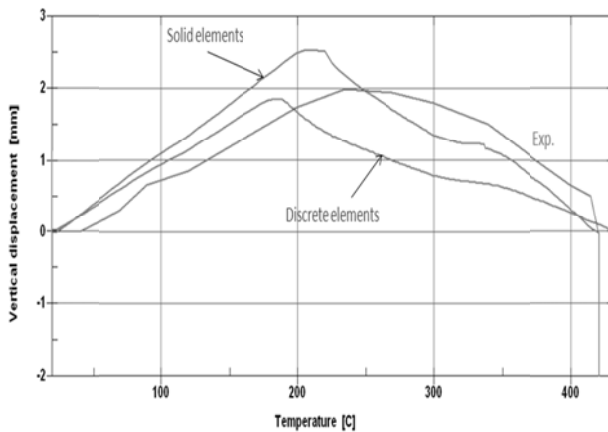


Fig. 13 Axial displacement vs. column temperature for standard and modified constraints - results for perturbation 2 mm.

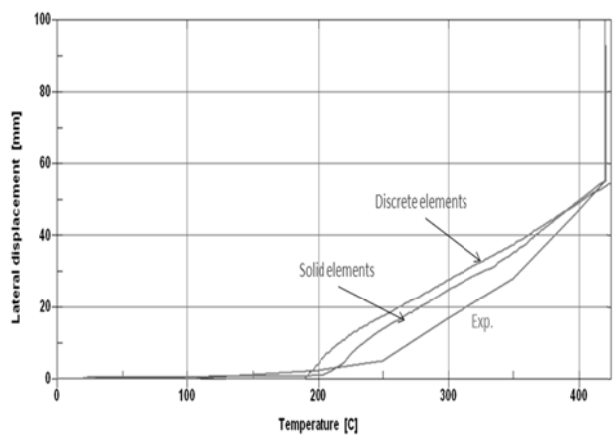


Fig. 14 Lateral displacement vs. column temperature for standard and modified constraints - results for perturbation 2 mm.

Tab. 1 Comparison of maximum generated forces

Column ref.	Loading level	Max. force generated in column [kN]	Calculated max. generated force in column
P3UB1	0	260	279
P3UB2	0.2	220	218
P3UB3	0.4	179	191
P3UB4	0.6	142	160
P3UB5	0.8	69	112

The maximum generated force in the column is selected as the representative result used for comparison with the experimental data. The generated force is calculated in a simplified way as a difference between the maximum recorded reaction and the value of prescribed force corresponding to the assumed loading level. Such comparison does not present real value of generated force due to the variation of the actual applied force during the execution of the experiment. The results, which are presented in Tab.1, show that almost for every analysed case the calculated value of generated force is bigger than the experimental one. The numerical results would be closer to the experimental ones if the variation of the applied loading is also considered.

3 SUMMARY

The paper summarizes a parametric study on FE modeling of axially and rotationally restrained steel columns subjected to furnace tests. The computer simulations were carried out using the coupled stress - thermal analysis implemented in the general purpose program LS-DYNA. The study was focused on improving prediction capabilities for the purpose of virtual testing. Common model calibration was replaced by experimental validation and extensive parametric study. The comparison of the numerical results and the experimental data was presented for the relationships between column's average temperature and axial force, axial displacement, and lateral displacement in the middle section. Three critical modeling characteristics were determined: material behavior, geometrical imperfections, and longitudinal variation of the column temperature. It was found that the postponed buckling occurring at higher furnace temperatures is due to nonuniform temperature distribution along the column, caused by heat transfer at the partially insulated furnace openings. The study shows how the modeling factors affect the numerical results without attempts to calibrate the FE model. In the authors' opinion it is not possible to correlate better numerical results with the existing experimental data without reducing model uncertainties (e.g. imperfection magnitudes and loading variation) through additional experiments and measurements.

REFERENCES

- Hallquist, J.O., LS-DYNA Keyword Manual. Livermore, Livermore Software Technology Corporation, 2006.
- Ali, F. and O'Connor, D., Structural performance of rotationally restrained steel columns in fire, *Fire Safety Journal*, 2001, 36, Issue 7, pp. 679-691.
- Kwasniewski, L., Krol, P.A., Lacki K., Numerical modeling of steel columns in fire, in: *Proceedings of COST Action C26 International Conference: Urban Habitat Constructions Under Catastrophic Events*, Naples, Italy, 16-18 September 2010.
- Wald F, da Silva LS, Moore D, Santiago A., Experimental behaviour of steel joints under natural fire, in: *ECCS - AISC Workshop*, 2004.
- CEN, European Committee for Standardization, EN 1993-1-2, Eurocode 3: Design of steel structures – Part 1-2: Structural fire design. Brussels, Belgium, 2005.

MODELLING CREEP IN STEEL STRUCTURES EXPOSED TO FIRE

James Lee ^a, Martin Gillie ^b

^a University of Edinburgh, BRE Centre for Fires Safety Engineering, Edinburgh, United Kingdom

^b University of Edinburgh, BRE Centre for Fire Safety Engineering, Edinburgh, United Kingdom

INTRODUCTION

The ability to model the behaviour of structures in fire conditions numerically has advanced rapidly in recent years with many complex phenomena now routinely represented. However, creep strains at elevated temperatures have been largely ignored to date. This is unfortunate because creep behaviour may significantly affect the time to failure of a heated structure and this time is crucial when egress is being considered. This paper examines the various analytical creep models available for metals and determines the appropriateness of each for inclusion in numerical models of creep. Numerical models are validated against experimental data from prestressed tendons typically used in post-tensioned concrete construction.

1 CREEP BEHAVIOUR

The most common type of creep in metals and that of most interest to the structural engineer, particularly at temperatures when fire is involved is power law creep [Gorash, 2008]. As the name suggests the rate of uniaxial creep straining shows a power law dependence on the deviatoric stress as shown in Eqn. 1. The value of the power exponent n , is dependent on the stress level typically ranging between 3 and 12. The use of the deviatoric stress represents the insensitivity of creep deformation on hydrostatic stresses. The parameter D , in Eqn. 1 represents the resistance against shearing of the metal. D is usually represented by terms including the shear modulus μ , at temperature T , (Eqn. 2) [Frost and Ashby, 1982], and a strain hardening parameter H (Eqn. 3) itself a function of accumulated creep strain. D may also include terms in any number of other evolving state variables S_i , which may affect the resistance of the metal to shearing. The shear modulus at room temperature (300K) is defined as μ_0 , and the melting point of the metal as T_M , in Kelvin. The values used in Eqn. 2 represent the shear modulus for steel. Eqn. 3 [Chaboche, 2008] represents the shear resistance due to strain hardening where as the strain evolves the resistance tends towards a steady state for appropriate values for m and k .

$$\dot{\varepsilon}^{cr} \propto \left(\frac{\sigma_{dev}}{D(\mu, H, S_i)} \right)^n \quad (1)$$

$$\mu = \mu_0 \left[1 - 1.09 \left(\frac{T - 300}{T_M} \right) \right] \quad \mu_0 = 8.1 \times 10^4 \text{ MPa} \quad (2)$$

$$H(\varepsilon^{cr}) = k(\varepsilon^{cr})^{1/m} \quad (3)$$

At stresses above around 10^{-3} times the shear modulus [Frost and Ashby, 1982] the power exponent in Eqn. 1 becomes increasingly high and the validity of the power law breaks down. In these cases the creep strain rate instead tends to follow an exponential dependence on the deviatoric stress (Eqn. 4). Creep at these stresses is known as power law breakdown creep.

$$\dot{\varepsilon}^{cr} \propto \exp \left(\frac{\sigma_{dev}}{D(\mu, H, S_i)} \right) \quad (4)$$

The temperature dependence of creep strain rate follows an Arrhenius relationship dependent on the activation energy of creep, Q_c , which is generally taken as that of self diffusion [Frost and Ashby, 1982; Gorash, 2008; Sherby and Weertman, 1979]. A full representation of power law and power

law breakdown creep in terms of stress and temperature T in Kelvin, where R , is the universal gas constant is thus.

$$\dot{\varepsilon}^{cr} \propto \left(\frac{\sigma_{dev}}{D(\mu, H, S_i)} \right)^n \exp\left(\frac{-Q_c}{RT} \right) \quad \sigma_{dev} \leq 10^{-3} \mu \quad (5)$$

$$\dot{\varepsilon}^{cr} \propto \exp\left(\frac{\sigma_{dev}}{D(\mu, H, S_i)} \right) \exp\left(\frac{-Q_c}{RT} \right) \quad \sigma_{dev} > 10^{-3} \mu \quad (6)$$

2 NUMERICAL MODELLING OF STRESS RELAXATION INCLUDING CREEP

Creep in prestressed steel tendons as used in Unbonded Post Tensioned (UPT) concrete slabs has become a concern in recent years when the slabs are exposed to fire. Although design codes specify minimum concrete cover to the tendons it is possible in extreme fire cases that sufficient temperatures may be reached at the points of minimum cover to activate creep. Anderberg [2008] has observed creep in prestressed steel tendons at temperatures down to 250°C. Of more concern is the case where concrete spalls directly exposing the tendon to fire. This is of greater concern than in the past as modern high strength concretes have showed an increased propensity to spall [Gales, 2009]. The lack of bonding of the tendon to the concrete removes any redundancy against local failure of the tendon therefore a local loss of prestress transfers to a global loss across the entire tendon span. Given that a single tendon often spans an entire floor over multiple bays this can be seen as a big issue. Although Eurocode 2 [CEN, 2004] states creep is implicitly accounted for within coded plastic stress strain curves it cannot account for time dependent straining. Therefore there is genuine concern that this data cannot account for the magnitude of the total inelastic strain accumulated over a given time or the creep strain rate which could strongly affect time to failure.

The mechanism of creep within a prestressed steel tendon at elevated temperature depends on the level of tensile stress the tendon experiences at a given time. The levels of prestress applied to concrete slabs in UPT construction via post-tensioning steel tendons is typically up to and in excess of 1000 MPa. Based on Eqn. 2 and assuming the transition stress between power law and power law breakdown creep to be around $10^{-3}\mu$ [Frost and Ashby, 1982], the transition stress at 250°C is 70 MPa. As thermal expansion cannot account for this level of relaxation prior to creep becoming active creep in prestressed steel tendons at elevated temperature must be described by a power law breakdown model (Eqn. 6).

Stress relaxation including the relaxation explicitly due to creep has been modelled in prestressed steel tendons within the commercial Finite Element Analysis (FEA) package ABAQUS and validated against test data by MacLean [2007]. MacLeans tests were performed by prestressing seven strand prestressing steel tendons 5400mm in length and approximately 13mm in diameter in a test bed to approximately 1000 MPa. A tube furnace was used in the centre of the bed to heat a 600mm length of the tendon this being 11% of the total tendon length. The heating protocol involved a temperature ramp phase at a heating rate of 10°C per minute to a given temperature followed by a 90 minute soak phase at this temperature before being allowed to cool naturally. The heating rate was chosen to correspond to the anticipated heating rate of a tendon within a concrete slab exposed to fire at a concrete cover of 20mm [MacLean, 2007]. Tests were carried out on tendons heating to 300°C, 400°C, 500°C and 700°C with prestress at the anchors recorded throughout the duration of the tests.

The element chosen to model the tendon was the continuum element C3D8T. This was chosen to allow contact on the radial surface of the tendon to be modelled for future incorporation into a full UPT concrete slab model. C3D8T elements also allow convective and radiative cooling from the radial surface of the tendon. In order to model creep with the aforementioned temperature distribution a coupled temperature displacement analysis has been used. In order to reduce computation half the tendon was modelled.

2.1 Creep models

Three different power law breakdown based creep models have been used to predict stress relaxation due to creep in prestressed steel tendons. The first is a standard power law breakdown model where the creep strain rate is modelled with an exponential stress dependence via a user defined subroutine in ABAQUS. The second uses an algorithm for transient creep commonly used in stand alone models [MacLean, 2007; Gales; 2009] developed by Harmathy [1967] also incorporated into ABAQUS via a user defined subroutine. During steady state creep this model reduces towards a standard power law breakdown model. The third tests the ABAQUS in-built hyperbolic sine model. As stresses rise above the transition stress this tends towards a standard power law breakdown exponential model whilst as stresses drop below the transition stress it tends to a power law representation. Further to this, a relaxation model using Eurocode 2 [CEN, 2004] plastic stress strain curve data, said to implicitly account for creep, has been used.

The power law breakdown algorithm used to represent uniaxial creep strain rate is shown in Eqn. 7. The constants were estimated from steady state regions of the experimental relaxation curves produced by MacLean [2007]. The normalising constants within the exponential, perhaps fortuitously, closely matched the inverse of the transition stress σ_0 , at given temperatures between power law and power law breakdown. The transition stress is taken as 10^{-3} times the shear modulus [Frost and Ashby, 1982] as shown in Eqn. 8. Therefore the deviatoric stress has been normalised against the transition stress which has a linear dependence on temperature modelled from Eqns. 2 and 8. Experimental curves show little evidence of strain hardening during the temperature ramp phase followed by rapid strain hardening when the temperature becomes constant. Given how rapidly steady state is then reached during the soak phase a strain hardening factor as in Eqn. 3 was not initially included in the model.

$$\dot{\varepsilon}^{cr} = 10^{13} \exp\left(\frac{\sigma_{dev}}{\sigma_0}\right) \exp\left(\frac{-Q_c}{RT}\right) \quad (7)$$

$$\sigma_0 = 10^{-3} \mu \quad (8)$$

Harmathy [1967] developed an equation for transient creep strain at elevated temperature and constant stress based around the Zener-Hollomon parameter, Z [Zener and Hollomon, 1944], a dimensionless creep constant $\varepsilon_{cr,0}$, and a combined temperature and time dependence known as temperature compensated time θ , (Eqn. 11). The Zener-Hollomon parameter has units of stress whilst temperature compensated time has units of time. The values of these parameters were determined through tests on grade 1725 prestressing steel by Harmathy and Stanzak [1970] and are shown in Eqns. 9 and 10. It should be noted how the Zener-Hollomon parameter closely resembles a power law breakdown creep strain rate model.

$$Z = 8.21 \times 10^{13} \exp(0.0145\sigma) \quad 172 < \sigma \leq 690 \text{ MPa} \quad (9)$$

$$\varepsilon_{cr,0} = 9.262 \times 10^{-5} \sigma^{0.67} \quad (10)$$

$$\theta = \int_0^t \exp\left(\frac{-Q_c}{RT}\right) dt \quad (11)$$

From these parameters Harmathy [1967] determined Eqn. 12 to predict transient creep strain reducing to a standard power law breakdown model at steady state based around the Zener-Hollomon parameter. Eqn.12 was differentiated with respect to time and then coded within a user defined subroutine for use in ABAQUS.

$$\varepsilon^{cr} = \frac{\varepsilon^{cr,0}}{\ln 2} \cosh^{-1}\left(2^{Z\theta/\varepsilon^{cr,0}}\right) \quad (12)$$

The general form of the ABAQUS in-built hyperbolic sine model is given in Eqn. 13 [ABAQUS Analysis Users Manual, v6.8]. Eqn. 7 was used as the basis in determining the constants used within this model. Taking the constant B to be the inverse of the transition stress σ_0 , Eqns. 7 and 13 are equivalent for deviatoric stresses far greater than the transition stress and similar even down to

values around 1.2 times the transition stress [Frost and Ashby, 1982]. In order to equate Eqns. 7 and 13 the power n is taken as 1 and the constant A taken as 2×10^{13} .

$$\dot{\epsilon}^{cr} = A \sinh^n(B\sigma_{dev}) \exp\left(\frac{-Q_c}{RT}\right) \quad (13)$$

In order to incorporate temperature dependence for the transition stress the constant B , must be tabulated against temperature. In the case of the in-built hyperbolic sine model this requires temperature to be tabulated as a field variable. To do this a user defined field subroutine is required to extract the temperature at each time increment and set it as a field variable. ABAQUS then uses interpolation to obtain non tabulated values of B , with temperature.

2.2 Validation of relaxation models including explicit creep representation

The following section shows attempts to validate the use of power law breakdown based creep models in modelling stress relaxation in prestressed steel tendons. The validity of using explicit creep models in predicting relaxation over Eurocode 2 [CEN, 2004] plastic stress strain data is also explored. Significantly, all three relaxation models where creep is explicitly included (Figs. 3, 4, and 5) display reasonable success in predicting both the overall magnitude of the relaxation and the time dependent relaxation during the temperature soak phase. This is not achieved when Eurocode 2 [CEN, 2004] plastic stress strain curve data is used in place of an explicit creep relaxation model (Fig. 6). Fig. 3 and Fig. 4 show that both the simple power law breakdown creep model (Eqn. 7) and Harmathy's [1967] transient creep model (Eqn. 12) predict the overall experimental relaxation data well. Though when Harmathy's [1967] equation is used (Fig. 4) there is an underestimation of stresses when the tendon is soaked at 500°C, generally a conservative model would be preferred. Where the ABAQUS in built hyperbolic sine creep model (Fig. 5) is used to represent the relaxation, the results are far more conservative but the error to the experimental relaxation is greater. It is likely however an adjustment in the constants used could improve this accuracy.

When Eurocode 2 [CEN, 2004] plastic stress strain curve data was used in place of an explicit creep model the predicted relaxation was significantly underestimated at temperatures between 400°C and 700°C (Fig. 6). The inability to account for time dependent relaxation (due to creep) accounts almost solely for the underestimate at 400°C, ultimately this makes a difference 100 MPa over a 90 minute period. As the temperature increases to 500°C the model also significantly underestimates the magnitude of the inelastic strains due to creep when compared to the test data the creep models. All models failed to complete at 700°C due to an inability to achieve convergence during implicit integration over the next time increment. In the relaxation cases using the ABAQUS in built hyperbolic sine creep model and the Eurocode 2 [CEN, 2004] plastic stress strain data (Figs. 4 and 5) this was due to rapid stress recovery immediately upon cooling. It is possible that softening the rate of cooling in the model which appears too rapid compared to the test data could allow convergence to be achieved in these cases. Where the power law breakdown creep model and Harmathy's [1967] creep strain equation were used in the relaxation models convergence to a implicit solution could not be achieved due to the highly transient nature of the relaxation at these points.

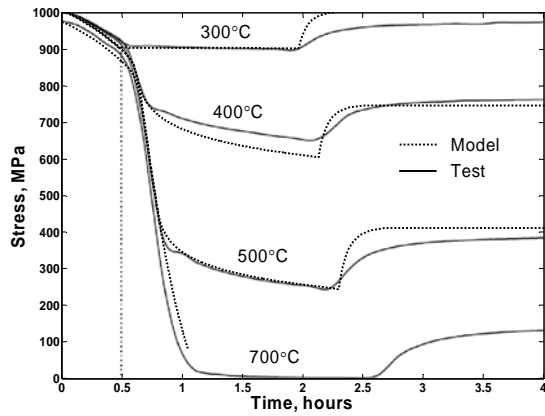


Fig. 3- Stress relaxation including a power law breakdown creep model

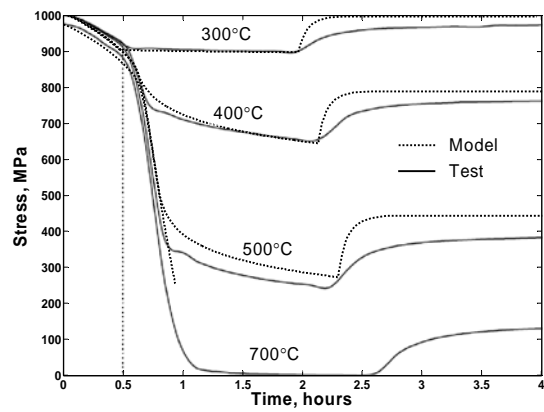


Fig. 4- Stress relaxation including the Harmathy [1967] creep equation

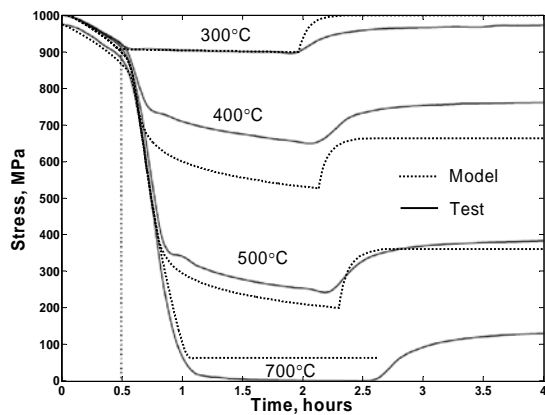


Fig. 5- Stress relaxation including the ABAQUS in-built hyperbolic sine creep model

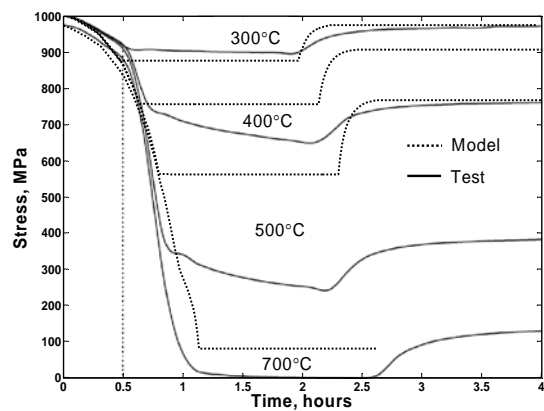


Fig. 6- Stress relaxation using Eurocode 2 [CEN, 2004] plastic stress strain curve data, no creep

3 CONCLUSION

Given the applicability and usefulness of commercial finite element modelling packages for modelling both isolated structural elements and larger scale structures it is desirable to be able to model creep within such software. This is highlighted in Fig. 6 where Eurocode 2 [CEN, 2004] plastic stress strain curves are clearly inadequate in accounting for stress relaxation due to creep between 400°C and 700°C in prestressed steel tendons. It should be noted however at temperatures below 400°C the Eurocode 2 [CEN, 2004] plasticity curves seem to do an adequate job. It is also likely only in extreme fire cases that structural steel would become exposed to temperatures greater than 400°C. The main issue in modelling creep numerically is indicated in Fig. 3 and Fig. 4. In both cases the models failed to complete when the soak temperature was set to 700°C due to an inability to achieve convergence during implicit time integration of the creep strain. This is a big issue in highly transient situations such as when strain hardening occurs rapidly. Therefore modelling creep in situations involving rapid temperature or stress changes and situations where strain hardening occurs rapidly will always be difficult. However, most situations in structural engineering involving creep do not have this degree of transience and it has been shown accurate modelling of creep strain rates can be achieved numerically across a wide temperature and stress range. In cases where it is desirable to include creep within a finite element model such as in unbonded post tensioned concrete slabs, the user defined subroutine option within ABAQUS is very powerful. It provides the versatility to code numerous representations for the uniaxial creep strain rate. An example of this is the use of Harmathy's [1967] equation within a subroutine to model the contribution of creep to stress relaxation in prestressed steel tendons (Fig. 4). This is a model commonly used to model

creep in stand alone models [Gales, 2009; MacLean, 2007]. Although ABAQUS has three in-built models the subroutine option provides versatility that the in built power law creep models in particular cannot provide. Although they may have their applicability at stresses below the transition stress between power law and power law breakdown. The in built hyperbolic sine creep model has the capability to model creep over a wider stress range and is particularly suited to higher stresses. Its versatility is enhanced by the use of the User Defined Field (USDFLD) subroutine allowing constants to be tabulated with respect to field variables such as temperature and accumulated strain.

REFERENCES

- ABAQUS, Inc., ABAQUS Analysis User's Manual, Version 6.8 d. Dassault Systèmes, 2008.
- Anderberg, Y., The Impact of Various Material Models on Structural Fire Behaviour Prediction. Fifth International Conference on Structures in Fire, Singapore, pp13, 2008.
- Chaboche, J. L., A Review of Some Plasticity and Viscoplasticity Constitutive Theories. International Journal of Plasticity, 24, 1642-1693, 2008.
- Frost, H. J. and Ashby, M. F., Deformation mechanism maps. Oxford: Pergamon press, 1982.
- Gales, J. A., Transient High Temperature Prestress Relaxation of Unbonded Prestressing Tendons For Use in Concrete Slabs. M.Sc thesis, Department of Civil Engineering, Queens University, Kingston, ON, Canada, 2009.
- Gorash, Y., Development of a Creep-Damage Model for Non-Isothermal Longterm Strength Analysis of High-Temperature Components Operating in a Wide Stress Range. Ph.D. Thesis, National Technical University, Kharkiv, Ukraine, 2008.
- Harmathy, T. Z., A Comprehensive Creep Model. Journal of Basic Engineering Transactions of the ASME, 89, 496-502, 1967.
- Harmathy, T. Z., and Stanzak, W. W., Elevated-Temperature Tensile and Creep Properties of Some Structural and Prestressing Steels. National Research Council of Canada. Division of Building Research, Ottawa, ON, 1970.
- MacLean, K., Post-Fire Assessment of Unbonded Post-Tensioned Concrete Slabs: Strand Deterioration and Prestress Loss. M.Sc thesis, Department of Civil Engineering, Queen's University, Kingston, ON, Canada, 2007
- Sherby, O. D., and Weertman, J., Diffusion-Controlled Dislocation Creep: A Defence. Acta Metallurgica, 27, 387-400, 1979.
- Zener, C., and Hollomon J., Effect of Strain Rate Upon Plastic Flow of Steel. Journal of Applied Physics, 15-22, 1944.

FIRE MODELLING OF AXIALLY-RESTRAINED TUBULAR STEEL BEAMS

Osama Salem, George Hadjisophocleous, and Ehab Zalok

Carleton University, Civil and Environmental Engineering Department, Ottawa, Canada

INTRODUCTION

There have been extensive research studies on the behaviour of different steel members and their connections at normal temperatures. Comparatively, less attention has been given to study the fire performance of steel members in general and steel connections in particular. This lack of research studies on steel connections at elevated temperatures is attributed to two main factors; first the complexity of the subject, second the high expenses of conducting the necessary fire-resistance tests for different types of steel connections. Moreover, and since steel connection behaviour at elevated temperature is greatly coupled with the behaviour of the connected members it is more efficient to carry out the fire-resistance tests of the steel members in assemblies (Liu et al, 2002 and Ding et al, 2007) rather than testing isolated steel members or isolated connections, which makes conducting such fire-resistance tests more complicated and much more expensive. All those factors encouraged many researchers to direct their efforts towards finite-element modelling of steel connections in fire, such as (Liu, 1996 and Yu et al, 2008).

Using unprotected structural steel members in buildings has increased considerably in recent years. According to the performance-based philosophy, this kind of application can be possible since structural steel members have inherent ability to resist fire. In this regard, a 3D finite-element model of unprotected axially-restrained tubular steel beams using ABAQUS software (2008) is presented in this paper. The finite-element model was validated against the experimental outputs of two large-scale fire-resistance tests that were conducted as part of a current research project at Carleton University, Ottawa, Canada. The research project was set up to experimentally and numerically investigate the impact of the end connections and axial restraint on the fire resistance of unprotected Hollow Structural Section (HSS) steel beams. Each HSS test beam was tested under applied transverse load that represents a beam load ratio of 0.5, and was axially restrained between two HSS steel columns. One type of beam-to-column steel connection, which is the extended end-plate moment connection, was tested in the presented two tests. In these tests, two different connection end plate thicknesses were examined, 12.7 mm and 19.0 mm. The outputs of the finite-element model showed good agreement with the experimental results.

1 EXPERIMENTAL TESTING

The experimental results that were used to validate the finite-element model presented in this paper are two large-scale fire-resistance tests that are part of a current research project at Carleton University, Ottawa, Canada. The test program of the research project consists of 10 large-scale steel-frame test assemblies with different extended end-plate connection configurations and different study parameters, such as end-plate thickness, degree of beam axial restraint, and level of fire protection. Eight of the ten steel-frame test assemblies were exposed to a standard fire without any fire protection except for the beams top flange that was fire-protected using 25 mm ceramic fibre strip to simulate the effect of the existence of a concrete slab on top of the steel beams. The remaining two test assemblies have the columns protected as well. Some of the experimental results that were used to validate the 3D finite-element model are presented in this paper. Not all experimental results of these two tests are shown here since the main objective of this paper is to focus on the finite-element model and especially on the fire performance of the axially-restrained tubular steel beams. Detailed experimental results for these two fire-resistance tests can be found in (Salem et al, 2010).

1.1 Test Facility

A new test furnace was constructed at Carleton University's Fire Laboratory to accommodate the testing of the ten steel-frame test assemblies of the current research project. The furnace is simply composed of a fire compartment of internal dimensions of 2700 x 2700 x 2200 mm high that is surrounded by a heavy steel loading structure, Fig. 1. The furnace has top, bottom, and side square openings to facilitate the insertion of the test elements, where the top openings are used to insert the test columns. The furnace walls are constructed of normal-weight concrete hollow blocks and are insulated from inside with 25 mm ceramic fibre blanket.

The furnace is equipped with two propane burner lines that are symmetrically placed in two sub chambers located at the bottom of the furnace in a position parallel to the test assembly. The propane burner lines are manually controlled to follow the CAN/ULC-S101-07 (2007) standard time-temperature curve. A flow measuring device is connected to the propane source pipe to monitor and control the delivered amount of propane during the fire-resistance tests. In order to monitor and control the temperature of the environment inside the furnace, six shielded K-type thermocouples, each within a 12.7 mm black iron pipe, are installed inside the furnace.

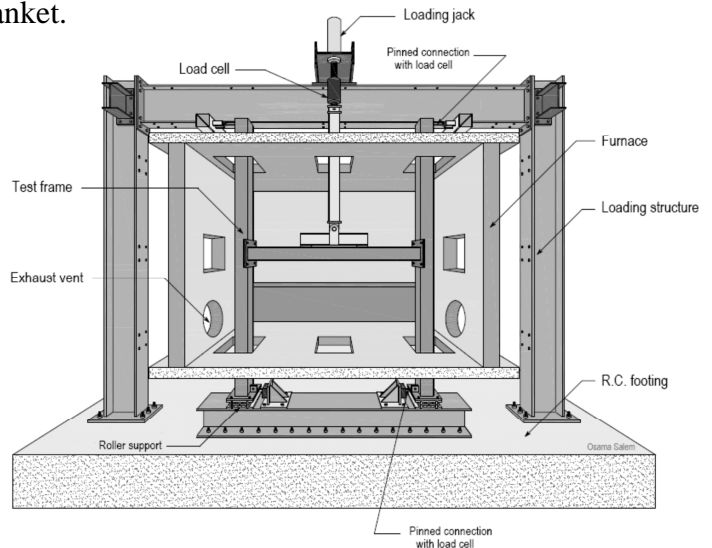


Fig. 1 A general test assembly inside the furnace

1.2 Test Assemblies Details

The two test assemblies presented in this paper were made of HSS steel members with hollow square section of 152 mm x 152 mm x 6.4 mm (6.0 in x 6.0 in x 0.25 in). The steel material that was used for all test assemblies components including all steel end plates is of grade (350W) as specified by CSA G40.20-04/G40.21-04 standards (2004). Each test assembly consisted of a 1950 mm beam that was connected at its ends to two 3200 mm columns by extended end-plate moment connections. Two different end plate thicknesses were tested, 12.7 mm (1/2 in) and 19.0 mm (3/4 in), in Tests 1 and 2, respectively. Each beam end plate was bolted to another end plate with the same thickness, either 12.7 mm or 19.0 mm, which was fillet-welded to one side of a tubular steel column. Four high strength bolts of ASTM A325 steel of 19.0 mm (3/4 in) diameter were used in each extended end-plate beam-to-column connection. The steel-frame test assemblies that are described in this paper can be found in typical industrial or commercial steel buildings. Details and dimensions of the test assemblies' beam-to-column connections are illustrated in Fig. 2.

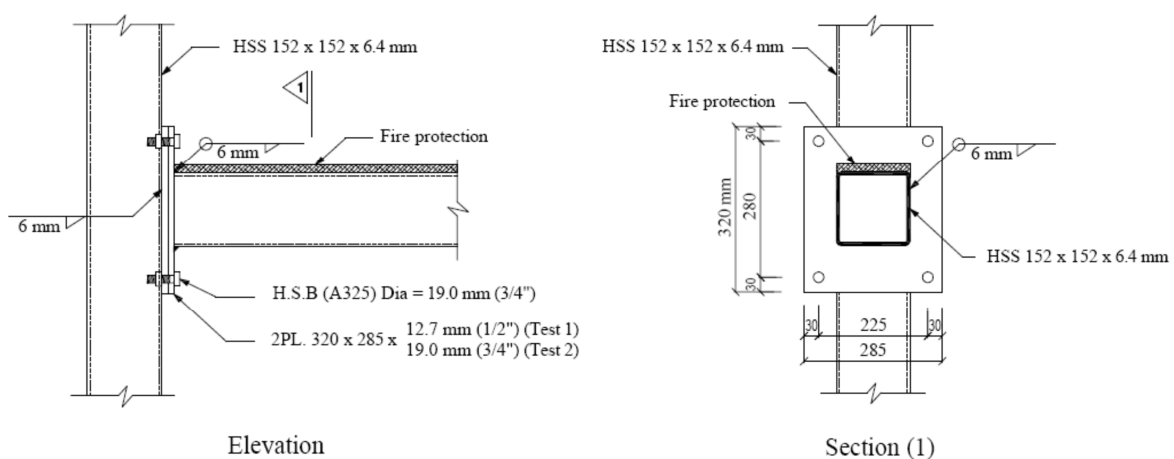


Fig. 2 Beam-to-column test connection details

1.3 Test Setup and Procedure

After installing the steel-frame test assembly inside the furnace, each test column was restrained at its top and bottom ends against in-plane and out-of-plane lateral displacements, while the top and bottom ends of the columns were rotationally unrestrained to avoid unnecessary moments at the columns' supports. To conform to CAN/ULC-S101-07 (2007), the vertical transverse load was gradually applied in four increments of 25% over two points on top of the test beam, where the full load was applied at least 30 min before the start of the fire-resistance test. The tests described in this paper were loaded with a transverse load of 110 kN representing a beam load ratio of 0.5. The beam load ratio is defined here as the ratio of the applied load during the fire-resistance test to the beam loading capacity calculated for simply supported beam end conditions at normal temperatures. Afterwards, the propane burners were turned on and the temperature inside the furnace was controlled to follow the CAN/ULC-S101-07 (2007) standard time-temperature curve. Throughout the fire-resistance tests, different measurements were taken in order to assess the structural behaviour of the test assemblies at elevated temperatures. Those measurements include: beam mid-span deflection, beam thrust force, connection moment capacity, and connection rotation. In order to measure the in-plane displacements of the different structural elements of each test assembly at elevated temperatures, 7 ceramic rods were installed inside the furnace and attached from the outside with a corresponding number of linear variable differential transducers (LVDTs). In Fig. 3, the displacement transducers denoted as LVDT 3 to LVDT 5 were utilized to record the steel beam vertical deflections, while other LVDTs were used to measure the horizontal displacements of the test columns at connection locations. The most important displacement is the beam mid-span deflection that was measured using LVDT 4. The beam mid-span deflection was used to identify when the failure criterion of the steel-frame test assemblies was exceeded indicating failure of the beam. Besides the installed LVDTs, the top and bottom supports of the column were equipped with special load measuring devices (pin load cells) to measure the horizontal reactions of the test columns. By knowing the column's top and bottom reaction forces, denoted R_T and R_B respectively, in Fig. 3, the connection hogging moment was calculated as the couple created by those reaction forces about the initial centreline of the test beam, where Eq. (1) was used to calculate the connection hogging moment (M_{hog}).

$$M_{hog} = R_T \cdot h_T + R_B \cdot h_B \quad (1)$$

Where R_T column top reaction, R_B column bottom reaction
 h_T vertical distance from the beam initial centre line to the column top reaction
 h_B vertical distance from the beam initial centre line to the column bottom reaction

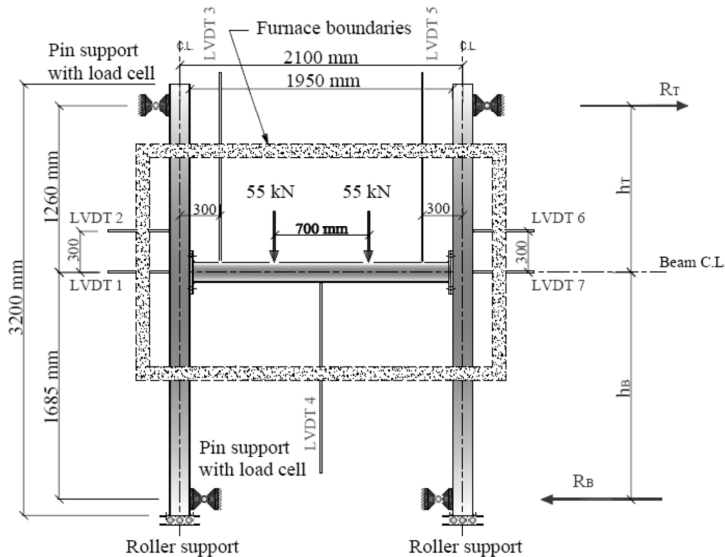


Fig. 3 Layout of a general test assembly inside the furnace

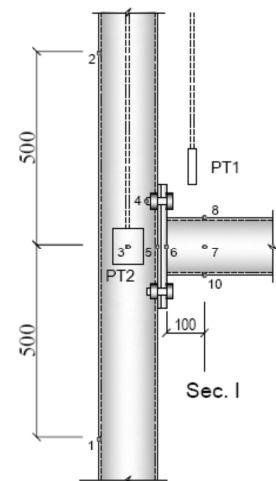


Fig. 4 Connection's thermocouples

For the thermal measurements, 22 ceramic-fibre insulated K-type thermocouples were welded to each test assembly at different locations. Three sections along the beam length, each with 4 thermocouples, were assigned to monitor the beam surface temperatures. For connection's temperatures, 6 of the 22 thermocouples were welded to different components of the beam-to-column connection including: the beam end plate, the top bolt, and the column sides, Fig. 4. In addition to the thermocouples, two plate thermometers were installed near one of the beam-to-column connections to measure the adiabatic surface temperature of the test assembly in order to be used in defining the thermal boundary condition in the finite-element model. All measurements were logged to a computer system every one second during the test.

2 FINITE-ELEMENT MODEL DESCRIPTION

A three-dimensional finite-element model was developed using ABAQUS software (2008) in order to study the fire behaviour of a tubular steel beam that is restrained between two steel columns with two extended end-plate moment connections. The four main parts of the beam-to-column connection; the beam, the end plates, the bolts, and the column were modelled using eight-node continuum hexahedral brick elements. These eight-node hexahedral brick elements (C3D8H in ABAQUS terminology) have the capability of representing large deformations and non-linearity of both geometry and material at elevated temperatures. For accurate modelling results, a fine mesh was used at the connection zone and at the beam's loading areas, where high stress and strain gradients are expected to occur. For the end plates' mesh, two elements through the 12.7 mm end plate were used, while three elements were used for the 19.0 mm end plate. Fig. 5 shows the details of the finite-element model.

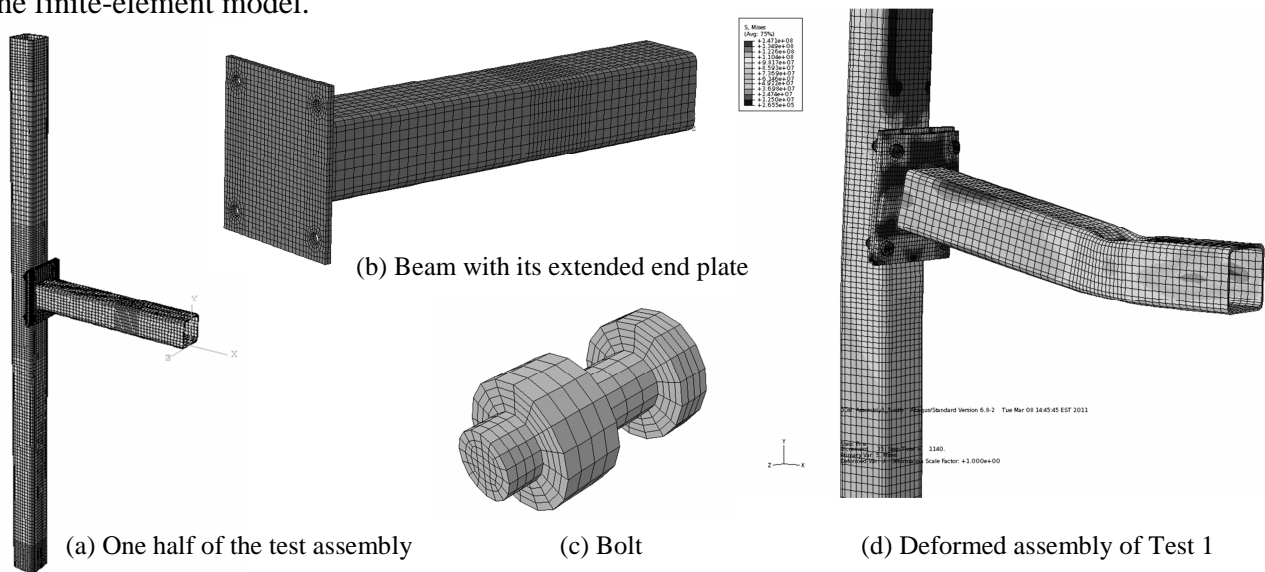


Fig. 5 Finite-element model details

2.1 Contact Interaction

Contact between all the connected components of the steel connection was modelled using surface-to-surface interaction command, with a small sliding option, in ABAQUS (2008). Contact pairs include; the bolt shanks-to-bolt holes, bolt heads-to-beam end plate, nuts-to-column connecting plate, and beam end plate-to-column connecting plate. The bolts were allowed to slip inside the 3 mm clearance holes of the beam end plate. Meanwhile, the bolts were tied to the column connecting plate, preventing the uncontrolled movement in the y-direction for the first analysis step, and then all bolts were freed of any restraints as contact was then already established.

2.2 Boundary Conditions

Due to the symmetry in the geometry of the steel-frame test assembly, only one quarter of the assembly was modelled. Therefore, all nodes existing in the planes of symmetry, planes x-y and y-z, Fig. 5(a), were restrained from moving in their respective perpendicular directions. In the loading

step of the finite-element model, a predefined concentrated pressure at a distance of 624 mm from the column face was modelled to simulate the applied transverse load. From the experimental results, it was noticed that there was a temperature gradient along the beam length and across its depth. Accordingly, heat transfer analysis was employed in the finite-element model, and the temperature distribution in the different parts of the finite-element model was checked against the corresponding experimental outputs before proceeding with the structural analysis in the finite-element model. The mechanical properties of steel at elevated temperatures were assumed to follow Eurocode 3 Part 1.2 (2005).

3 FINITE-ELEMENT MODEL VALIDATION

The experimental results of the two fire-resistance tests discussed were compared with the predictions of the finite-element model, where good agreement has been achieved in different measurements. For example, Figs. 6(a) and (b) illustrate a comparison of the beam-to-column connection deformations between the experimental results and the finite-element model predictions for Tests 1 and 2, respectively. As shown in Fig. 6(a), the high stresses that were developed due to the combination of the connection hogging moment and the beam axial thrust force of the connection of Test 1 led to early steel material softening in its weakest component and formed a plastic hinge in its thin beam end plate. That did not happen in Test 2, where minimal deformations occurred in its thicker plates and the plastic hinge was formed in the column just below the connection, as shown in Fig. 6(b).

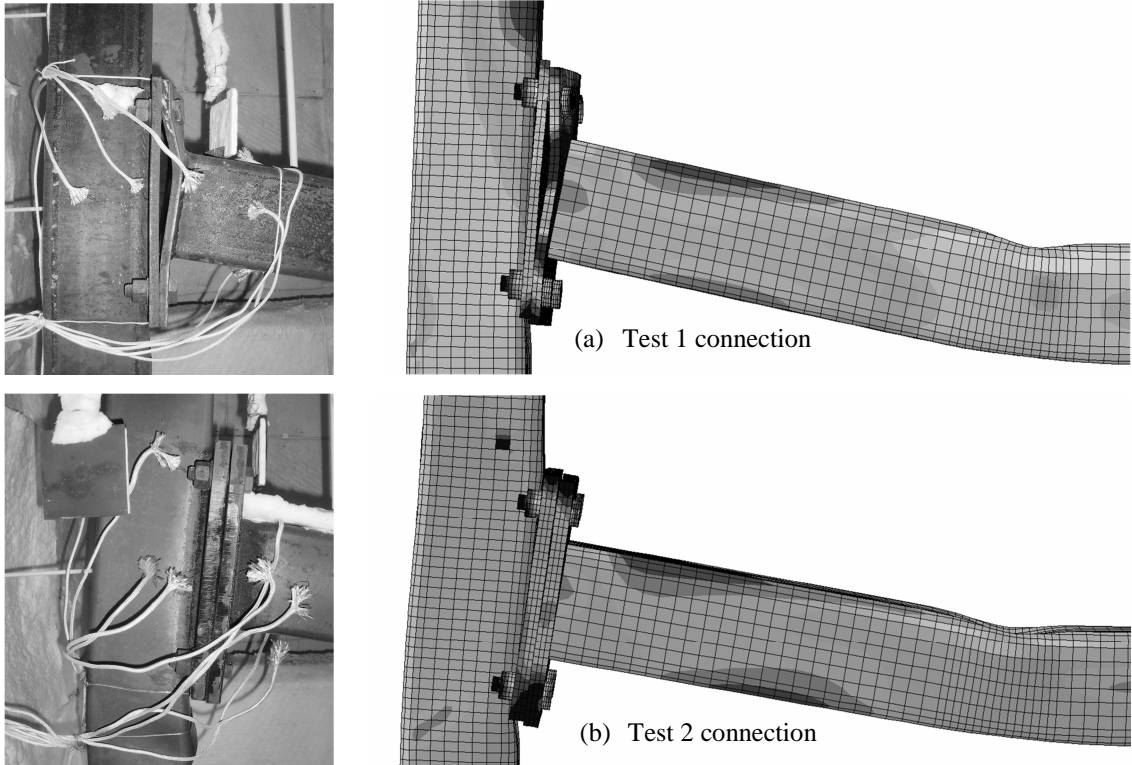


Fig. 6 Beam-to-column connections’ deformations after exposed to elevated temperatures

A comparison of the beam mid-span deflection between the experimental results and the finite-element model predictions for Test 1 and 2 is shown in Figs. 7(a) and (b). Very good agreement has been achieved between the experimental results and the model outputs for both beams up to a beam bottom flange temperature of about 650°C. Afterword, the finite-element model outputs became more conservative than the experimental results, where Test 1 beam reached its limiting deflection, which is about 100 mm calculated as span/20, at beam bottom flange temperature of about 715°C, while the finite-element model gave a prediction of about 680°C, Fig. 7(a). For Test 2 beam that reached its limiting deflection at beam bottom flange temperature of about 780°C, the model gave a prediction of about 740°C, Fig. 7(b).

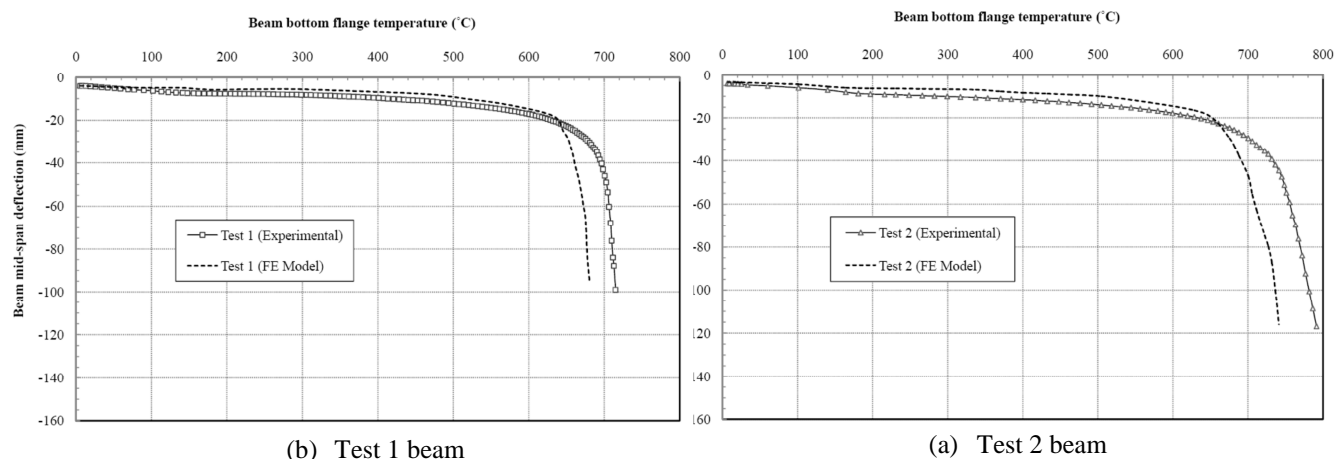


Fig. 7 Beam mid-span deflection with respect to beam bottom flange temperature of Tests 1 and 2

4 CONCLUSION

A 3D finite-element model of unprotected axially-restrained tubular steel beams was developed using ABAQUS software (2008). The finite-element model was validated against the experimental outputs of two large-scale fire-resistance tests that were conducted as part of a current research project at Carleton University, Ottawa, Canada. The comparisons demonstrated that the finite-element model simulated the experimental behaviour of the axially-restrained tubular steel beams at elevated temperature very well.

From both the experimental and the finite-element model results, it can be concluded that increasing the plates' thickness of the extended end-plate beam-to-column connection from 12.7 mm to 19.0 mm has increased the temperature of the connected steel beam at which failure occurred by about 65°C.

REFERENCES

- Liu T.C.H., Finite Element Modelling of Behaviours of Steel Beams and Connections in Fire, *Journal of Constructional Steel Research*, 36(3): 181-199, 1996.
- Liu T.C.H., Fahad M.K., Davies J.M., Experimental Investigation of Behaviour of Axially Restrained Steel Beams in Fire, *Journal of Constructional Steel Research*, 58: 1211-1230, 2002.
- Canadian Standard Association, CSA G40.20-04/G40.21-04, General Requirements for Rolled or Welded Structural Quality Steel, Rexdale, Ontario, Canada, 2004.
- European Committee for Standardization, ENV 1993-1-2, Eurocode 3, Part 1.2, Design of Steel Structures: Structural Fire Design, Brussels, Belgium, 2005.
- CAN/ULC-S101-07, Standard Methods of Fire Endurance Tests of Building Construction and Materials, Underwriters' Laboratories of Canada, Scarborough, Canada, 2007.
- Ding J., Wang Y.C, Experimental Study of Structural Fire Behaviour of Steel Beam to Concrete Filled Tubular Column Assemblies with Different Types of Joints, *Engineering Structures*, 29: 3485-3502, 2007.
- ABAQUS/Standard Users' Manual, Version 6.82, Hibbitt, Karlsson and Sorensen Inc., Pawtucket, Rhode Island, USA, 2008.
- Yu H., Burgess I.W., Davison J.B., Plank R.J., Numerical Simulation of Bolted Steel Connections in Fire Using Explicit Dynamic Analysis, *Journal of Constructional Steel Research*, 64: 515-525, 2008.
- Salem O., Hadjisophocleous G., Zalok E., Structural Performance of Extended End-plate Connections between Tubular Steel Members in Fire, *Proceedings of the 13th International Symposium on Tubular Structures*, The University of Hong Kong, Hong Kong, pp: 699-705, 2010.

MATERIAL AND CREEP BEHAVIOUR OF S460 IN CASE OF FIRE **Experimental Investigation and Analytical Modelling**

Regine Schneider^a, Jörg Lange^a

^a TU Darmstadt, Institute for Steel Structures and Materials Mechanics, Darmstadt, Germany

INTRODUCTION

The knowledge of the stress-strain relationships of structural steel at elevated temperatures is essential for the numerical modelling of the mechanical behaviour of steel structures in case of fire. In the Eurocode 3 Part 1-2 constitutive equations are given for structural steel at temperatures up to 1200 °C which are ready for the implementation in FE software. Following the Eurocode, these constitutive equations are uniformly valid for steel grades from S235 up to S460, although they are based on numerous test results predominantly obtained on steel grade S235. For the high strength fine-grained structural steel S460 only very few and widespread test results exist (Ruge / Winkelmann, 1980; ARBED-Récherches, 1991; Winter, 1998; Outinen et al., 2001; Lange / Wohlfeil, 2007) which deviate in parts considerably from the normative standard. This puts the validity of the constitutive equations given in EC3-1-2 into question for S460. Additionally, the creep behaviour under high temperatures has not yet been analysed for this type of steel.

Beyond the particular lack of knowledge concerning the high strength fine-grained structural steel S460, there is a general shortcoming in the design model of Eurocode 3 Part 1-2 concerning the consideration of time-dependent strain components. Creep strain becomes relevant for the behaviour of steel structures at elevated temperatures above approx. 400 °C. The constitutive equations of EC3-1-2 have been derived from transient tests and therefore creep is implicitly taken into account. But there is no possibility to allow for creep explicitly in fire design, considering the actual temperature profile of the structural member. With regard to the growing importance of Natural Fire Safety Concepts, where heating rates and therefore creep effects can be very different from those caused by a nominal fire according to the standard temperature-time curve, the implicit approach is not sufficient anymore.

This was the starting situation for an extended test programme at the Institute for Steel Structures and Materials Mechanics, mainly consisting of transient tests carried out at numerous commercial high strength fine-grained structural steels S460. In the first work package the constitutive equations for S460 under short-time high temperature were determined for the two delivery conditions N (normalized rolled) and M (thermomechanical rolled). In the next step, the time-dependent material behaviour at high temperatures was investigated by carrying out transient tests at different heating rates. An empirical creep law was derived from the results which is based on the concept of temperature-compensated time developed by Dorn, 1954 and Harmathy, 1967. Their creep law was refined and extended to the tertiary creep stage. By means of the newly developed creep law, creep can be taken into account explicitly and exclusively on the basis of transient test results. Its application allows for modelling the constitutive equations under consideration of the real time-temperature profile of the structural component.

This paper describes the experimental work and the obtained results and compares them to the actual state of standardization. It also responds to the creep law and its possible applications in modelling material behaviour. Furthermore, the results of simple non-linear limit load calculations are presented which were carried out using the derived constitutive equations for S460 and taking creep strain explicitly into account. The results demonstrate the influence of the material model on the structural behaviour in case of fire and put the constitutive equations given in EC3-1-2 into question, not only for S460, but due to the handling of creep generally for their application in Natural Fire Safety Concepts.

1 HIGH TEMPERATURE TESTS OF S460 SPECIMENS

1.1 Test Method and Experimental Setup

Stress-strain relationships at elevated temperatures can either be obtained in steady state or transient tests. Transient tests which are characterized by a constant load in combination with a defined heating process deliver more realistic results concerning the material behaviour in case of fire. Hence the transient test method was chosen for the experimental studies. Carrying out several tests at different load levels, the result of the transient tests is a set of temperature-strain curves. After elimination of the thermal strain ϵ_{th} , stress-strain relationships can be derived from these curves. Strictly speaking, the obtained stress-strain relationships are only valid for the particular heating rate chosen for the testing procedure. Furthermore, the included time-independent, load-dependent strain ϵ_{σ} and the creep strain ϵ_c cannot be separated from each other. Figures 1 and 2 show the experimental set-up and the shape of the standard test specimen. The tests were carried out in a furnace with three separately controlled heating zones. The gauge length of the extensometer was 15 mm. The temperature of the test specimen was determined by an additional thermocouple fastened to the specimen surface.

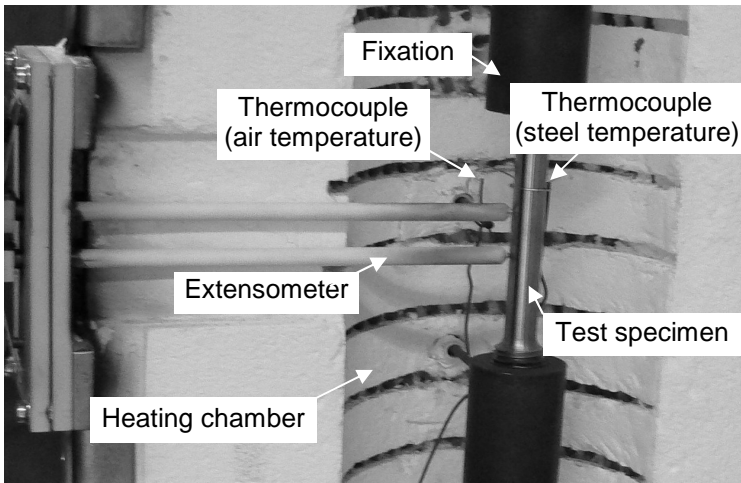


Figure 1. Testing device

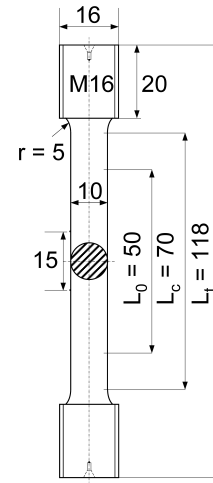


Figure 2. Test specimen [mm]

1.2 Test Materials and Test Programme

The investigated high strength fine-grained structural steels S460 are standardized in EN 10025 Parts 3 and 4 and differ in their delivery conditions (N - normalized rolled or M - thermomechanical rolled) as well as in their chemical composition. To assess the influence of these differences on the high temperature performance of S460, eight different materials were tested, see Table 1. Material “PM” is a thermomechanical rolled steel for pressure purposes according to EN 10028 Part 5.

All materials were tested under transient test conditions at a constant heating rate of 10 K/min and at ten different load levels between 25 and 500 N/mm². In addition, the thermal strain ϵ_{th} was determined for each material in an unstressed transient test. Materials M1, M2 and N2 were additionally tested in transient tests at constant heating rates between 3 and 30 K/min and at different load levels.

Tab. 1 Tested materials; Strength values in the rolling direction

Steel grade	S460M				P420M	S460N		
Abbreviation	M1	M2	M3	M4	PM	N1	N2	N3
Fabrication	ACC	ACC	ACC	QST				
Type of Product	Plate 25 mm	Plate 25 mm	Plate 58 mm	HEA 320	Plate 60 mm	Plate 60 mm	Plate 35 mm	IPE 550
R_{eH} (N/mm ²)	525	558	521	509	444	507	489	479
R_m (N/mm ²)	598	666	589	584	529	640	644	584

2 TEST RESULTS

2.1 Transient Tests with 10 K/min Heating Rate

Figures 3 and 4 show the temperature-dependent yield strength ($R_{t2,0}$) reduction compared to EC3-1-2 and the stress-strain relationships at 500 °C as constructed from the temperature-strain curves of the transient tests, both exemplarily for all materials of the delivery condition M. The results are related to the measured upper yield strength R_{eH} of the tested materials at room temperature, see Table 1.

The normalized rolled steels showed an inferior, but more homogeneous high temperature performance which was similar to the weakest thermomechanical rolled material.

It can be seen that at 500 °C several tested materials do not reach the specifications of EC3-1-2. This applies to the whole tested temperature range up to 800 °C. Comparing just the S460M steels, material M2 performs best. Compared to M1, M3 and M4, it has the highest total content of the microalloying elements niobium (Nb), vanadium (V) and titanium (Ti). These elements are important for the development of the fine-grained microstructure. The results show that a high content of certain alloying elements has, in combination with the thermomechanical rolling process, a positive influence on the high temperature performance of structural steel S460. The very favourable behaviour of the tested steel “PM” is caused by a high content of molybdenum (0.36 %) that increases the creep resistance by solid solution strengthening.

Based on the weakest thermomechanical and normalized rolled steel, the test results were described analytically by mathematical functions for both delivery conditions. Figures 5 and 6 show the test results approximated by an elliptical curve and straight lines, similar to the analytical model in EC3-1-2. It is obvious that the stress-strain relationships according to the Eurocode considerably overestimate the high temperature performance of S460 during the tests. The consequence is an overestimation of the bearing capacity of structural members made of S460 in fire design, see Chapter 4.

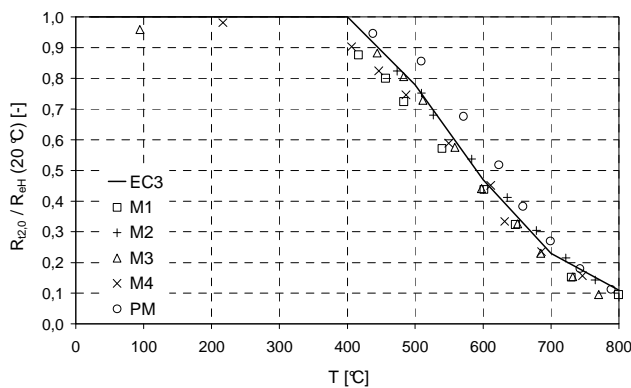


Figure 3. Yield strength reduction (M)

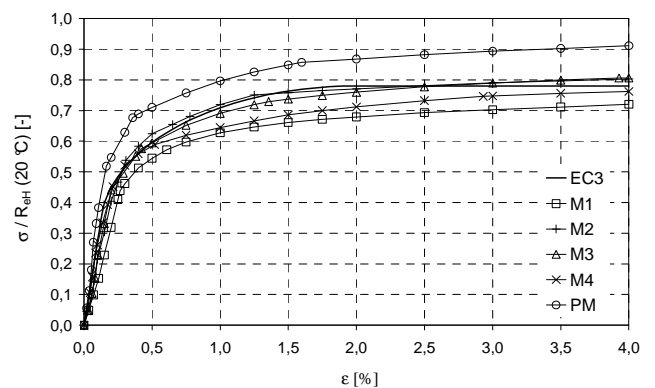


Figure 4. σ - ϵ -relationships at 500 °C (M)

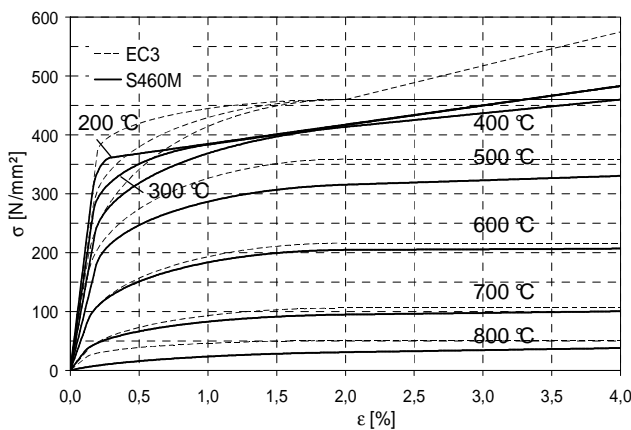


Figure 5. σ - ϵ -relationships 200 - 800 °C (M)

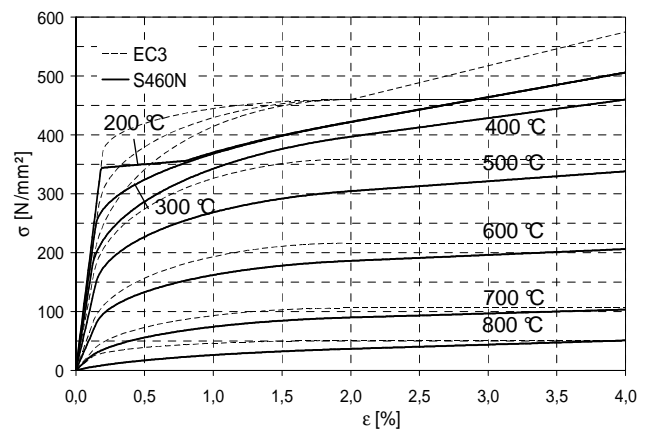


Figure 6. σ - ϵ -relationships 200 - 800 °C (N)

2.2 Transient Tests with Different Heating Rates

Fig. 7 shows the results of transient tests at a uniform stress level of 170 N/mm², but at different heating rates for material M1. With increasing heating rates, smaller strain values and higher failure temperatures can be observed because a smaller amount of creep is included in the test results. Regarding a certain temperature, the differences between the measured strain values of the various curves are only due to different amounts of creep strain ϵ_c . Hence creep behaviour of the material can be described by analysing the strain differences between the curves measured at different heating rates. This approach offers for the first time the possibility of taking the creep strain explicitly into account by performing exclusively transient tests.

3 DEVELOPMENT OF THE EMPIRICAL CREEP LAW AND APPLICATION

The objective was the quantification and analytical description of the creep strain ϵ_c as a function of time, stress and temperature. The evaluation of the test results was carried out using the concept of temperature-compensated time θ (see Dorn, 1954; Harmathy, 1967; Skowronski, 2004) because it is able to take continuously varying temperatures during the creep process into account without the application of laborious superposition rules, e.g. the strain hardening rule. The temperature-compensated time θ combines the two variables time and temperature and is defined in Eq. (1).

$$\theta = \int_0^t e^{\frac{-\Delta H}{RT}} dt \quad (1)$$

where

- ΔH Activation energy of creep [J/mol]
- R Gas constant [J/mol K]
- t Time [h]
- T Temperature [K]

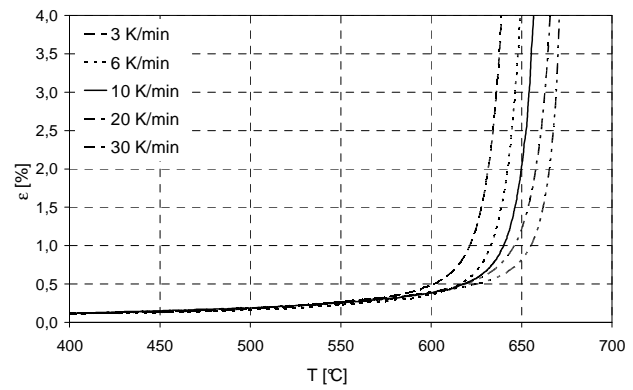


Figure 7. Temperature-strain curves, $\sigma = 170$ N/mm², material M1

The creep strain ϵ_c can be described by Eq. (2), where $B(\sigma)$ is a function only depending on the stress σ :

$$\epsilon_c = f(\sigma, \theta) = B(\sigma) \cdot \theta^n \quad (2)$$

By means of a two-step regression procedure, the exponent n and the stress-dependent function $B(\sigma)$ were determined. Analyses of the test data showed that a constant value of $n = 1/3$ as proposed by Skowronski, 2004 is not suitable for a proper description of the measured strain differences between the various temperature-strain curves because it does not comprise the ultimate creep stage before rupture (tertiary creep stage). A temperature dependency of the exponent n was already indicated by Cho / Findley, 1984. In excess of a pure temperature dependency, the exponent n was defined as a function of θ in the current research project. The creep law finally derived for material M1 is given in Eq. (3). For the materials M2 and N2 slightly deviant values for the constants were obtained.

$$\epsilon_c = B(\sigma) \cdot \theta^{a(\sigma)\theta + \frac{1}{3}} \quad (3)$$

$$B(\sigma) = \begin{cases} 803 \cdot \sigma & \text{if } \sigma < 0,08 f_{yk} \\ 15300 \cdot e^{0,01789 \cdot \sigma} & \text{if } \sigma \geq 0,08 f_{yk} \end{cases}$$

$$a(\sigma) = \begin{cases} -2,48 \cdot 10^6 \cdot \sigma^{4,586} & \text{if } \sigma < 0,4 f_{yk} \\ -1,8 \cdot 10^{13} \cdot e^{0,0442 \cdot \sigma} & \text{if } \sigma \geq 0,4 f_{yk} \end{cases}$$

The resulting ϵ_c - θ -relationship describes all phases of creep including the tertiary creep stage. It is shown in Fig. 8 for material M1, M2 and N2 in comparison to the shape of a creep law with $n = 1/3$.

For a defined heating process, leading to a certain maximum temperature, the expression θ has a constant value. This means that the formula for the creep strain occurring during this particular heating process is transformed into a function only depending on stress. This permits the elimination of the time-dependent strain proportions from the stress-strain relationships obtained in the transient tests. Furthermore, the stress-strain relations can be adapted to any heating process that a structural member might be subjected to in the course of a fire. The influence of creep on the stress-strain relationships for S460M (which have been derived from the transient tests with a heating rate of 10 K/min) is shown in Fig. 9 for heating rates from 2 to 50 K/min.

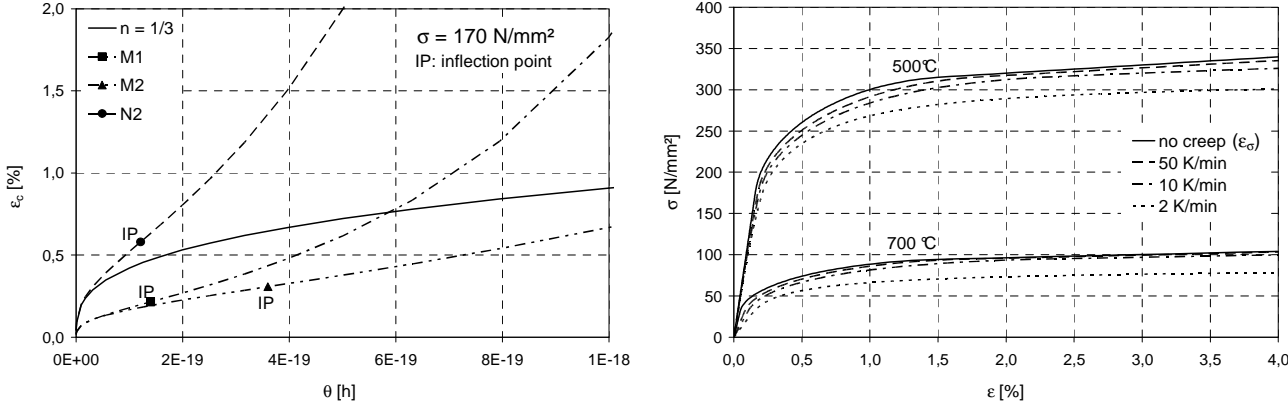


Figure 8. Empirical creep laws for M1, M2, N2 compared to the creep law with $n = 1/3$ Figure 9. Influence of creep on the stress-strain relationships for S460M

4 LOAD-CARRYING CAPACITY OF STRUCTURAL MEMBERS

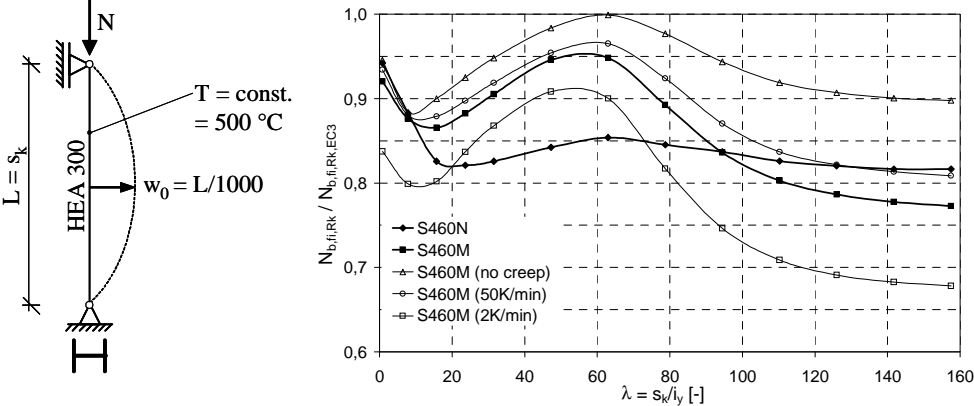


Figure 10. Ultimate loads of a column at 500 °C according to the test results, compared to EC3-1-2

The influence of the differences in the stress-strain relationships on the load-carrying capacity of structural members was investigated in nonlinear limit load calculations, using the frame analysis freeware programme Stab2D-NL. The results for a column with varying slenderness under central axial compression and initial bow imperfection at 500 °C are shown exemplarily in Fig. 10. The limit load $N_{b,fi,Rk}$ was calculated with the derived stress-strain relationships for S460M and S460N and related to the limit load $N_{b,fi,Rk,EC3}$ according to EC3-1-2. Additionally, the influence of creep according to the creep law given in Eq. (3) was examined for S460M. It can be seen that the load bearing capacity is severely affected by the material model used in the calculations and that the influence of creep is not negligible. This demonstrates the enormous importance of modelling the time-independent and time-dependent material behaviour correctly in the course of fire design. The observed undulation of the curves is due to the fact that, depending on λ , different parts of the constitutive equations are relevant for failure (slender column: $E_{0,T}$, compact column: $R_{t2,0,T}$).

5 SUMMARY

Various transient tests carried out at seven commercial high strength fine-grained structural steels S460 showed a better high temperature performance of the thermomechanical rolled steels compared to the normalized rolled ones. Nevertheless, several tested materials did not reach the specifications of EC3-1-2. Transient tests with different heating rates were evaluated and an empirical creep law based on the concept of temperature-compensated time was derived which comprises all stages of creep. It allows for the exact consideration of the creep strain - arising from any arbitrary heating process - in the stress-strain relationships. Nonlinear limit load calculations showed that the used material model and time-depending effects have a tremendous influence on the calculated bearing capacity and therefore on the fire resistance of structural members. The influence of creep grows in the course of the increasing application of Natural Fire Safety Concepts in performance-based design. The presented results emphasize that proper fire design is not possible without correct constitutive equations for the used materials and an adequate handling of creep strain.

Recommendations concerning the chemical composition and the fabrication process of S460 to improve the high temperature performance were developed by means of metallographic investigations. It could be shown that especially a high content of the microalloying elements (Nb, V, Ti) and a microstructure with distorted, irregular grains achieved by thermomechanical rolling and accelerated cooling (ACC, see Table 1) can improve the high temperature strength of S460.

REFERENCES

- EN 1993-1-2, Eurocode 3 – Design of steel structures, Part 1-2: General rules – Structural fire design, CEN, Brussels (Belgium), 2009.
- Ruge, J., Winkelmann, O., Verformungsverhalten von Bau-, Beton- und Spannstählen bei hohen Temperaturen, Sonderforschungsbereich 148 – Brandverhalten von Bauteilen – Teilprojekt B4, Arbeitsbericht für den Zeitraum 1978-1980, TU Braunschweig, Braunschweig (Germany), 1980.
- C.E.C. Agreement No 7210-SA/505, Practical design tools for unprotected steel columns submitted to ISO-Fire – Refao III, Final Report, Parts I-II-III. RPS Report No 11/91, ARBED-Récherches, Luxembourg, 1991.
- Winter, S., Untersuchungen zum Tragverhalten von Profilverbundstützen aus hochfestem Feinkornbaustahl StE 460 bei Normaltemperatur und im Brandfall, PhD Thesis, Technische Universität Darmstadt, Germany, 1998.
- Outinen, J., Kaitila, O., Mäkeläinen, P., High-Temperature Testing of Structural Steel and Modelling of Structures at Fire Temperatures, Report TKK-TER-23, HUT, Espoo (Finland), 2001.
- Lange, J., Wohlfeil, N., Untersuchungen zum Werkstoffverhalten des Feinkornbaustahls S460 unter erhöhten Temperaturen, Bautechnik 84(10), 711-720, 2007.
- EN 10025-3, Hot rolled products of structural steels, Part 3: Technical delivery conditions for normalized/normalized rolled weldable fine grain structural steels, CEN, Brussels (Belgium), 2004.
- EN 10025-4, Hot rolled products of structural steels, Part 4: Technical delivery conditions for thermomechanical rolled weldable fine grain structural steels, CEN, Brussels (Belgium), 2004.
- EN 10028-5, Flat products made of steels for pressure purposes, Part 5: Weldable fine grain steels, thermomechanically rolled, CEN, Brussels (Belgium), 2009.
- Dorn, J.E., Some Fundamental Experiments on High Temperature Creep, Journal of the Mechanics and Physics of Solids 3(2), 85-116, 1955.
- Harmathy, T.Z., A Comprehensive Creep Model, Journal of Basic Engineering 89, 496-502, 1967.
- Skowronski, W., Fire Safety of Metal Structures, Polish Scientific Publishers PWN, Warsaw (Poland), 2004.
- Cho, U.W., Findley, W.N., Creep and Creep Recovery of 2618-T61 Aluminium Under Variable Temperature, Journal of Applied Mechanics 51, 816-820, 1984.
- Stab2D-NL, Freeware from <http://www.u-pfeiffer.de/>, last quotation on March 1st 2011.

AN APPROXIMATION METHOD FOR CRITICAL TEMPERATURES OF STEEL MEMBERS AND HORIZONTAL DISPLACEMENTS OF COLUMNS

Takeo Hirashima ^a, Hiroko Ikuta ^b, Yuki Hidani ^a

^a Chiba University, Graduate school of Engineering, Chiba, Japan

^b NTT Facilities Inc, Tokyo, Japan

INTRODUCTION

It is important in structural fire safety design not only to ensure the load-bearing capacity of structures, but also to prevent the fire spreading, especially to upstairs compartments. When the performance of exterior elements subjected to load due to deformation of a frame is considered, the horizontal displacement of the tops of the outer columns is an important aspect. Computational analysis is often carried out to analyse the structural behaviour of frames in fire, but this is very labour-intensive. On the other hand, the development of displacements due to the thermal elongation of members of the steel frame may be predicted approximately by a manual process, considering the restraint provided by adjacent members [1, 2]. If a steel frame has the required ductility, the critical steel temperature can also be approximated on the basis of the theory of stability and simple plastic design [3, 4], because the thermal stress in the critical member disappears at the critical stage.

The purpose of this study is to discuss a manual approximation method for both the horizontal displacement at the tops of the outer columns and the critical temperatures of steel members in steel structures. The paper presents a comparison of the manual approximation of the structural behaviour of a steel frame exposed to fire with computational results.

1 COMPUTATIONAL ANALYSIS OF A STEEL FRAME

The computational analysis program used originates in a report by Becker and Bresler at the University of California Berkeley [5], and has been amended by Uesugi *et al.* at Chiba University [6 - 8]. This is a finite element analysis using Bernoulli-Euler beam elements, which is capable of modelling the three-dimensional behaviour of steel frames subjected to fire, and includes geometrical and material non-linearities.

The stress-strain curve of steel is represented by Richard's formulation [9]. Fig. 1 shows the stress-strain curves of a structural steel (design yield strength: 325 N/mm²) used in the program. The linear coefficient of thermal expansion α of steel [10] is given by

$$\alpha = (10.8 + 0.00338\theta) \times 10^{-6} \quad (1)$$

where θ is the steel temperature [°C].

A uniform temperature is applied to the steel members exposed to fire. Neither the creep of steel at elevated temperature or the effects of concrete floor slab are taken into consideration in this analysis. Figs. 2 and 3 show the framing plan and the elevation of the building for this case study. The structure is assumed to be an office building with 8 storeys, composed of Class 1 or Class 2 steel members which are designed against seismic loading [11]. The columns at the corners are square hollow sections, and the others are wide-flange H-sections. The design permanent load on a typical floor is 5.2kN/m². Fire is assumed to develop over the whole 4th floor, and the non-linear analysis is carried out on the 4th and 5th floors as a sub-frame. The effects of the stiffnesses and actions from adjacent members are taken into consideration using elastic interaction stiffnesses [7].

Figs. 4 and 5 show the deformation of the frame in fire. The deflection of columns is developed from the thermal elongations of the heated beams and restraint by the adjacent members. The deflection of the beams increases rapidly above 600°C; the deflected shape is asymmetric at 680°C, and the calculation fails to converge at 690°C. The collapse temperature may be above 690°C, but it is estimated in this computational analysis that critical temperature of the frame is 680°C.

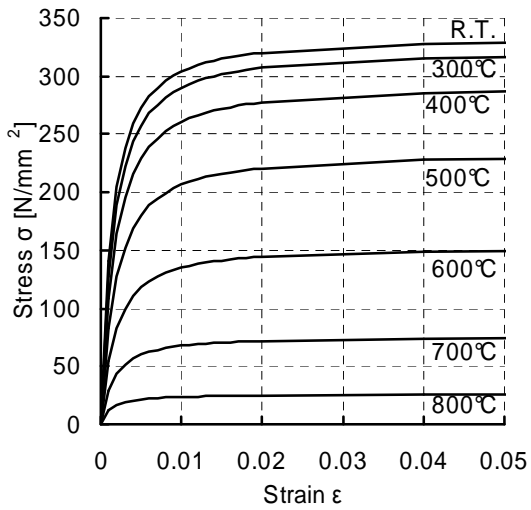


Fig. 1 Stress-strain curve of steel in the analysis

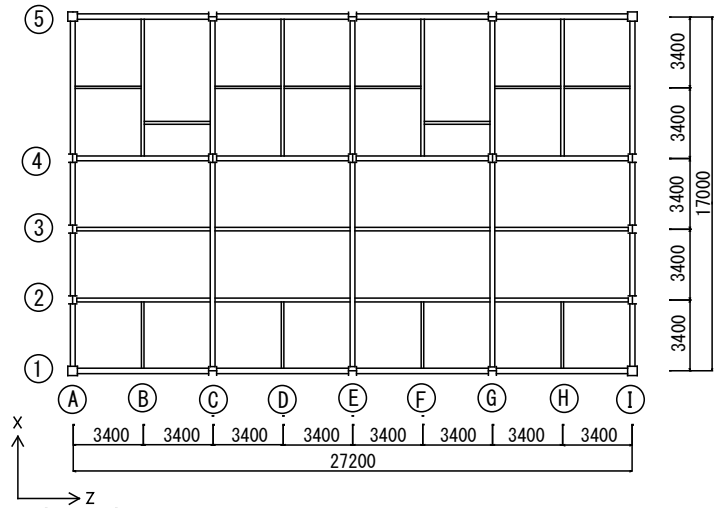


Fig. 2 Framing plan of a typical floor

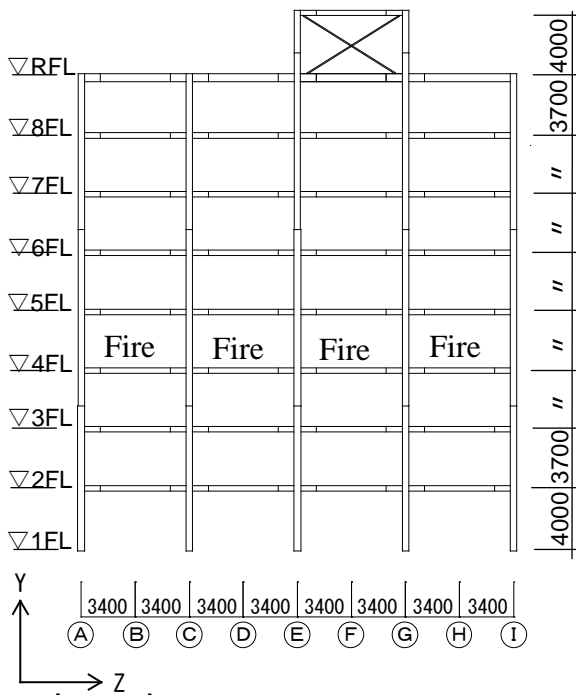


Fig. 3 Framing elevation

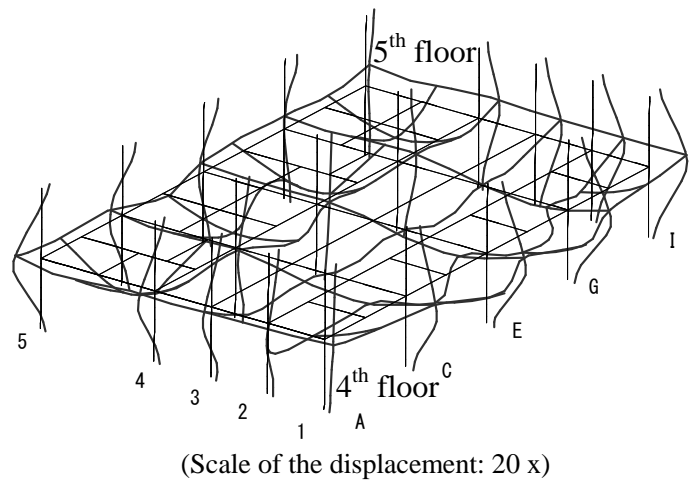


Fig. 4 Deformation of the sub-frame at steel temperature 600°C

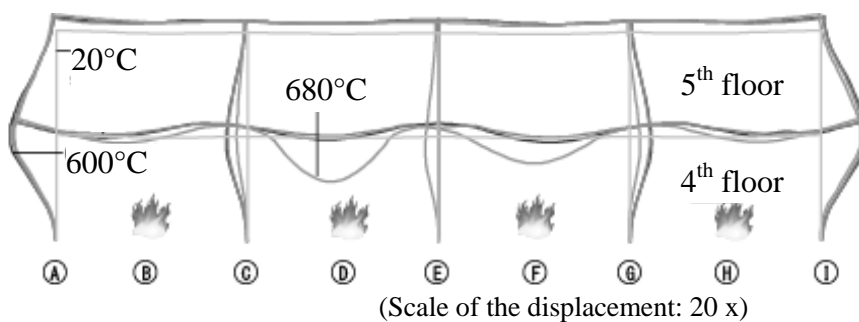


Fig. 5 Deformation of frame on gridline 4 in fire

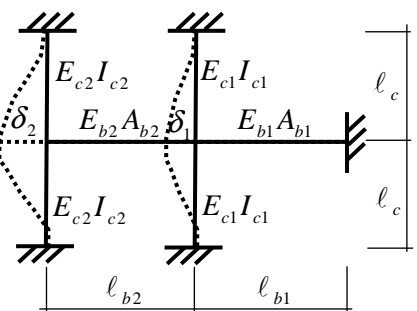


Fig.6 Simple modelling

2 HORIZONTAL DISPLACEMENT OF COLUMNS

Fig. 7 shows the joint translation angle of the outer columns. This is defined as the difference between the horizontal displacements at the top and bottom of the column divided by the floor height. The joint translation angle of the outer column in the frame on gridline 4 (Frame 4) from the computational analysis (legend “Comp. 4-A”) reaches 1/50 at 550°C. This may severely influence the performance in fire (e.g. local buckling at the ends of the columns, cracking in the fire protection materials, damage to spandrels, etc.) This value is greater for column 4-A than for 1-A because the bending stiffness of columns in Frame 4 is less than that in Frame 1 (see Fig. 2). Fig. 7 indicates that the joint translation angle of the outer columns is approximately proportional to the free expansion of the heated beams up to about 600°C, which corresponds to the temperature at which the deflections of the heated beams increase rapidly (see Fig. 9). This temperature range includes not only the elastic range but also the plastic range. Considering this result, the development of the horizontal displacements at the top of the outer columns can be approximated well with equations based on elastic thermal stress theory.

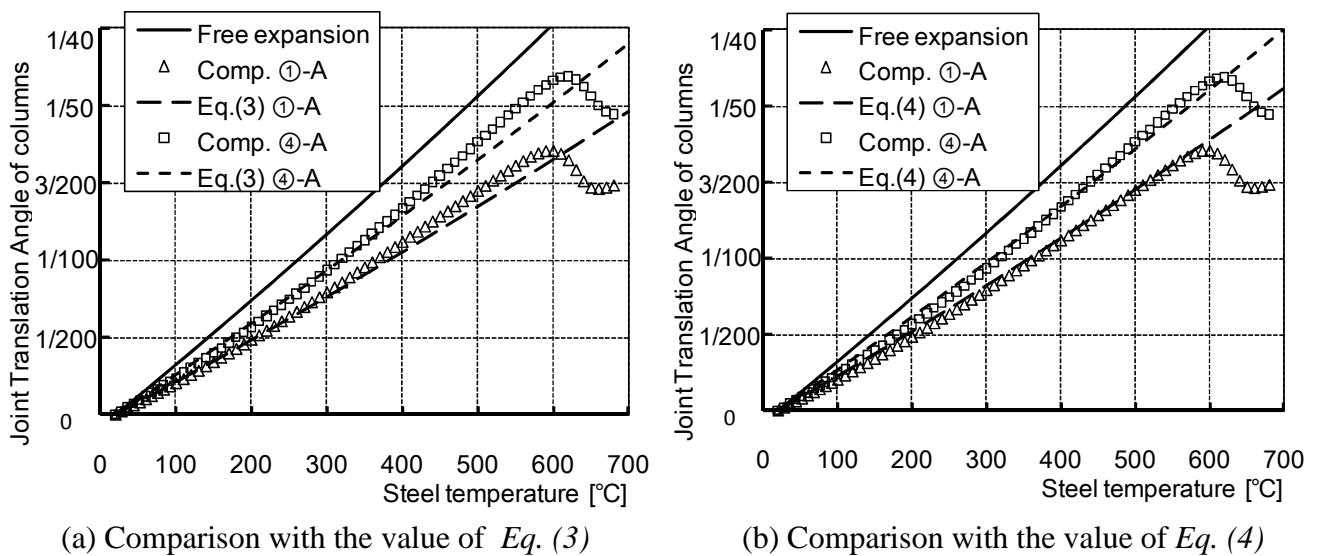


Fig. 7 Joint translation angle of the outer columns

The model of the frame exposed to a single-storey fire is simplified as shown in Fig. 6. The development of horizontal displacement at the top of the outer column $\delta_{1,2,\dots,n}$ can be calculated using *Eq. (2)*. In case of the simplified two-span frame shown in Fig. 6 the horizontal displacements δ_1 and δ_2 are given by *Eq. (3)*.

$$\begin{pmatrix} 1 & C_1 k_{c2} / k_{b1} & C_1 k_{c3} / k_{b1} & \cdots & C_1 k_{cn} / k_{b1} \\ -C_2 & 1 & C_2 k_{c3} / k_{b2} & \cdots & C_2 k_{cn} / k_{b2} \\ 0 & -C_3 & 1 & \cdots & C_3 k_{cn} / k_{b3} \\ 0 & 0 & \cdots & 1 & \cdots \\ 0 & 0 & 0 & -C_n & 1 \end{pmatrix} \begin{pmatrix} \delta_1 \\ \delta_2 \\ \delta_3 \\ \cdots \\ \delta_n \end{pmatrix} = \begin{pmatrix} C_1 \cdot \varepsilon_{b1}^{th} \cdot \ell_{b1} \\ C_2 \cdot \varepsilon_{b2}^{th} \cdot \ell_{b2} \\ C_3 \cdot \varepsilon_{b3}^{th} \cdot \ell_{b3} \\ \cdots \\ C_n \cdot \varepsilon_{bn}^{th} \cdot \ell_{bn} \end{pmatrix} \quad (2)$$

$$\delta_2 = C_2 (\delta_1 + \varepsilon_{b2}^{th} \cdot \ell_{b2}) \quad (3)$$

$$\delta_1 = \varepsilon_{b1}^{th} \frac{k_{b1} \cdot \ell_{b1} - C_2 \cdot k_{c2} \cdot \ell_{b2}}{k_{b1} + k_{c1} + C_2 \cdot k_{c2}} \quad \text{or} \quad \delta_1 = \varepsilon_{b1}^{th} \frac{C_1 \cdot k_{b1} \cdot \ell_{b1} - C_1 \cdot C_2 \cdot k_{c2} \cdot \ell_{b2}}{k_{b1} + C_1 \cdot C_2 \cdot k_{c2}}$$

where $\varepsilon_{b1,b2}^{th}$ thermal strain of the beam under free boundary conditions,

$\ell_{b1,b2}$ span of the beam [mm],

- $k_{b1,b2}$ axial stiffness of the beam at elevated temperature,
(i.e., $k_{b1} = E_{b1}A_{b1} / \ell_{b1}$, $k_{b2} = E_{b2}A_{b2} / \ell_{b2}$ [N/mm] (see Fig.6))
- $k_{c1,c2}$ sway stiffness of the column in bending at elevated temperature,
(i.e., $k_{c1} = 24E_{c1}I_{c1} / \ell_c^3$, $k_{c2} = 24E_{c2}I_{c2} / \ell_c^3$ [N/mm] (see Fig.6))
- $C_{1,2}$ restraint coefficient of the outer column against elongation of the heated beam.
(i.e., $C_1 = k_{b1} / (k_{b1} + k_{c1})$, $C_2 = k_{b2} / (k_{b2} + k_{c2})$)

As shown in Fig. 7(a), the value of Eq. (3) agrees with the result of the computational analysis within the elastic range (up to about 300°C). In the plastic range (above 300°C), the value of Eq. (3) falls below the computational analysis result because plastic hinges develop at the ends of the columns and the stiffnesses of the columns against bending decrease. Considering this result, Eq. (3) may be improved to the form

$$\delta_2 = C_2 \left(\delta_1 + \varepsilon_{b2}^{th} \cdot \ell_{b2} \right), \quad \delta_1 = \frac{k_{b1}}{k_{b1} + k_{c1} + k_{c2}} \varepsilon_{b1}^{th} \cdot \ell_{b1} \quad (4)$$

Values of δ_2 from Eq. (4) are greater than from Eq. (3). As shown in Fig. 7(b), the value from Eq. (4) approximates the maximum value well up to 600°C. Eq. (4) is also simpler than Eq. (3) for manual prediction. If Eq. (4) is valid, the horizontal displacements in the case of three or more spans may be given by Eq. (5).

$$\delta_n = C_n \left(\sum_{i=1}^{n-1} \delta_i + \varepsilon_{bn}^{th} \cdot \ell_{bn} \right), \quad \delta_k = \frac{k_{bk}}{k_{bk} + \sum_{i=k}^n k_{ci}} \varepsilon_{bk}^{th} \cdot \ell_{bk} \quad (5)$$

3 CRITICAL TEMPERATURES

This paper shows the comparison between the computational result, AIJ recommendation [3] values and Eurocode 3 [4] values for the critical temperature of the frame.

Fig. 8 shows the reduction factor for the effective yield strength of the steel. In the AIJ recommendation, the design effective yield strength of steel at elevated temperature is determined using a specified minimum value because of its variability. This computational analysis does not use the AIJ stress-strain curve of steel at elevated temperature. The modified value in Fig.8 refers to the stress at 2% strain in the stress-strain curves, and is similar to the Eurocode value.

Fig. 9 shows the deflection of beams in Frame 4 and in Frame C. The deflection of Beam C-E (between Frame C and Frame E) in Frame 4 is larger than that of Beam A-C above 600°C because the normal thermal stress of Beam C-E is larger than that of Beam A-C. The bending moment values due to permanent load are almost the same. Fig. 10 shows the resistances of both beams corresponding to the steel temperature and the effect of permanent load. The critical temperature is the temperature at the intersection of the resistance and the effect. The legend (“AIJ, mod. $k_{y,\theta}$ ”) means that the design buckling resistance moment of the beam is calculated according to the method of the AIJ recommendation [3] but the reduction factor for the yield strength of the steel is modified as shown in Fig. 8. In the case of a laterally unrestrained beam, the design plastic moment resistance about the minor axis is applied at the centre of the beam in consideration of lateral-torsional buckling. The design resistance given by AIJ is similar to the design buckling resistance moment from Eurocode 3. Both of the critical temperatures are between 670°C and 680°C. They approximately agree with results of computational analysis of the deflection behaviour of Beam C-E in Frame 4.

Fig.11 shows the variation of resistances of the Column 4-C due to the steel temperature and the effect of actions due to permanent load. The design buckling resistance of non-sway column given by AIJ is less than that of Eurocode between 200°C and 600°C, and is similar to that of Eurocode 3 above 600°C. The design buckling resistance of a column at elevated temperature in AIJ, as in ambient-temperature structural design, is determined taking account of imperfections.

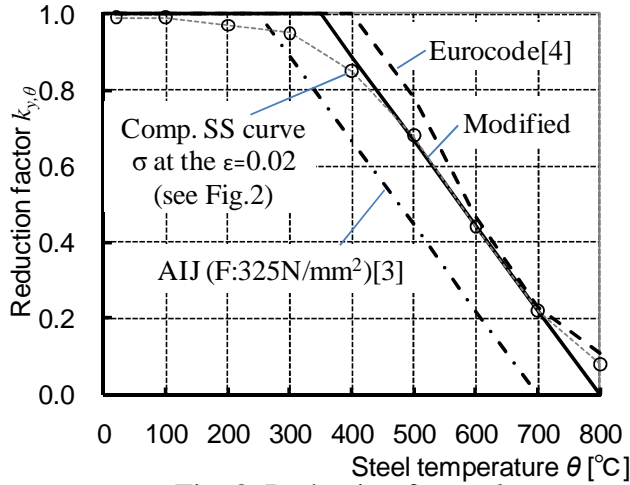


Fig. 8 Reduction factor $k_{y,\theta}$

(Notes of Fig. 8)

$k_{y,\theta}$: the reduction factor for the yield strength of steel at temperature θ

$$k_{y,\theta} = \begin{cases} 1 & \theta_{RT} \leq \theta \leq \theta_1 \\ 1 - \frac{\theta - \theta_1}{\theta_2 - \theta_1} & \theta_1 \leq \theta \leq \theta_2 \end{cases} \quad (6)$$

AIJ ($f_y=325\text{N/mm}^2$): $\theta_1 = 250$, $\theta_2 = 700$

AIJ ($f_y=235\text{N/mm}^2$): $\theta_1 = 300$, $\theta_2 = 750$

Modified $k_{y,\theta}$: $\theta_1 = 350$, $\theta_2 = 800$

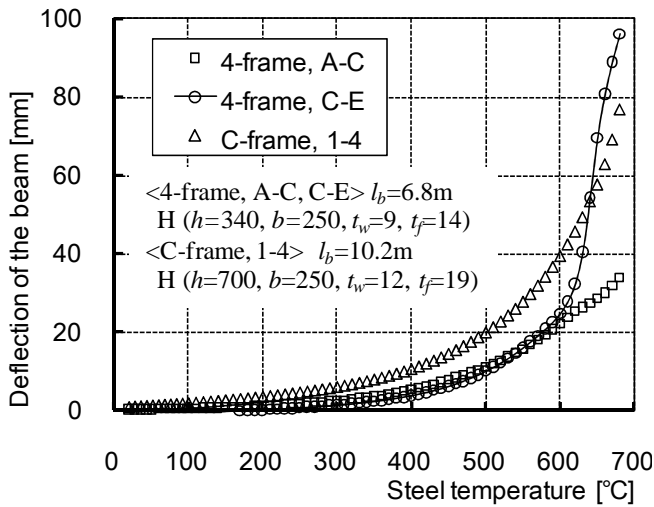


Fig. 9 Deflection of beams

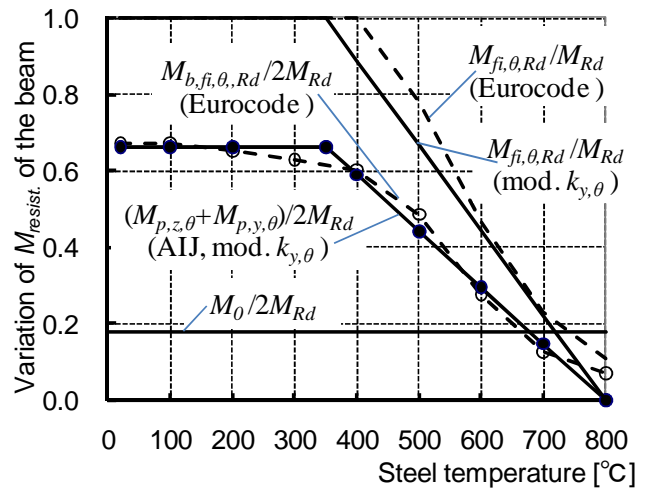


Fig. 10 Resistance of the beam (4-frame)

(Notes of Fig. 10)

M_{Rd} : design plastic moment resistance of the cross-section for an ambient temperature

$M_{fi,\theta,Rd}$: design moment resistance of the cross-section for a uniform temperature θ

$M_{b,fi,\theta,Rd}$: design buckling resistance moment for a uniform temperature θ ($\bar{\lambda}_{LT} = 0.642$)

$M_{p,z,\theta} = M_{Rd}$, $M_{p,y,\theta}$: design plastic moment resistance about the minor axis

M_0 : bending moment at mid-span of the beam under simple support condition due to permanent load

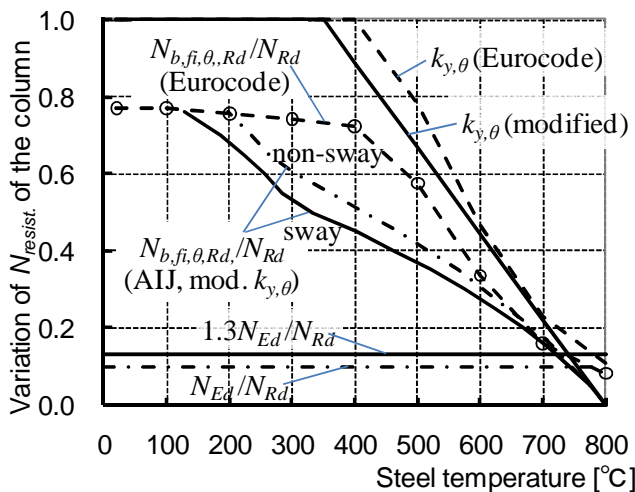


Fig. 11 Critical temperature of the column (4-C)

(Notes of Fig. 11)

N_{Rd} : design plastic resistance to normal force of the cross-section at ambient temperature

N_{Ed} : design normal force

$N_{b,fi,\theta,Rd}$: design buckling resistance at temp. θ

H-section: $h=414$, $b=405$, $t_w=18$, $t_f=28$,

Length of the column: $\ell = 3700$

The non-dimensional slenderness at ambient

Temperature, sway: $\bar{\lambda} = 0.638$,

non-sway: $\bar{\lambda} = 0.455$ ($\ell_e = \ell$)

The design buckling resistance is less than the buckling resistance based on tangent modulus theory. In case of a sway frame (i.e. a frame which has no bracing) with all its columns heated in a fire floor, 130% of the design normal force is imposed on the columns. The critical temperature of the column according to the method of AIJ is about 720°C. In this case study, the result of the computational analysis does not give the critical temperatures of columns.

4 CONCLUSIONS

This paper presents a manual approximation method for the horizontal displacement at the top of a steel column due to thermal elongation of heated steel beams in fire. In this case study, the manual approximation result for the horizontal displacements of the columns agrees well with the computational results. Calculation of the critical temperatures of frames in fire is also discussed, comparing AIJ recommendation values and Eurocode values. In this case study, the design resistance of the beam according to AIJ is similar to the design buckling resistance moment of Eurocode 3, and both approximately agree with computational analysis results.

This is only a single case study. Future work will study more cases and will consider the effects of concrete floor slabs and non-uniform temperature distributions in the cross-sections of steel members on the deflection behaviour of steel frames in fire.

REFERENCES

- D. J. Johns, Thermal stress analyses, 1965
- H. Saito, "Behavior of End Restrained steel members under fire", Bulletin of the Fire Prevention on Society of Japan, Vol. 15, No. 1, 1966 (in Japanese)
- Architectural Institute of Japan, "Recommendation for fire resistant design of steel structures", 1st edition 1999, 2nd edition 2008 (in Japanese)
- Eurocode 3: Design of steel structures Part 1-2: General rules - Structural fire design, BS EN 1993-1.2, 2005
- Becker, J., Bresler, B., FIRES-RC--- A Computer Program for the Fire Response of Structure --- Reinforced Concrete Frames, Report No. UCB FRG74-3, University of California Berkeley, July 1974
- H. Saito, H. Uesugi, M. Yamaguchi, and A. Kodaira, Thermal Stress and Deformation of Steel Structures of High Rise Buildings in Fire, Fire Safety Science -- Proceedings of the Second International Symposium, International Association for Fire Safety Science, 1988, pp. 719-728.
- H. Lin and H. Uesugi, Three Dimensional Analysis Method of High Rise Structure Exposed to Compartment Fire (Part 1. The Formulation of Restraint Force and Adjacent Displacement for Local Sub-structure), Journal of Structural Engineering, Vol.44B, Architectural Institute of Japan, 1998, pp. 1-8 (in Japanese)
- Y. Li, H. Lin, T. Hirashima, H. Uesugi, T. Wakamatsu, An Analytical Method of Deflection Behavior Concerning Three-dimensional Steel Frame Exposed to Fire which takes Account of the Thermal Expansion of a Floor Slab, International Journal for Fire Science and Technology, Vol.24, No.4, Center for Fire Science and Technology, Tokyo University of Science, 2005, pp. 211-236
- Richard, R.M and Abbott, B.J., "Versatile Elastic-Plastic Stress-Strain Formula", EM4 Technical Note, 1975, pp. 511-515
- Tasnim, U. and Charles, G.C., Effects of Elevated Temperature on Structural Members, Journal of the Structural Division, ASCE, Vol. 101, No. ST 7, 1975
- The Japan Iron and Steel Federation, Koukouzou-sekkeiensyu 4th edition, 2003 (in Japanese)

A SIMPLIFIED APPROACH FOR PREDICTING STEEL TEMPERATURES UNDER DESIGN FIRES

M.M.S Dwaikat ^a, V.K.R. Kodur ^b

^a Research Associate, Dep. of Civil and Environmental Engineering, Michigan State University, East Lansing, MI. USA

^b Professor, Dep. of Civil and Environmental Engineering, Michigan State University, East Lansing, MI. USA

INTRODUCTION

For evaluating fire resistance of a steel structural member an accurate assessment of cross sectional temperatures is required. Any discrepancy in cross sectional temperatures could lead to an incorrect sectional size of the structural member or an increase/decrease in the thickness of the required fire protection levels (Buchanan 2002, Purkiss 2007, Silva 2005). Therefore, proper evaluation of steel temperature as a function of fire exposure time is the most important step in structural fire engineering, which focuses at assessing the performance of structural members under fire conditions (Franssen et al. 2009).

In fire resistance calculations, the development of temperature profile in a cross section as a function of time is referred to as thermal analysis and is generally carried out using complex numerical models that are based on either finite element or finite difference methods (Buchanan 2002). These approaches, though provide accurate results, may not be attractive or practical because detailed numerical modeling of thermal analysis is quite complex, requires trained skills and large number of input parameters, such as temperature-dependent thermal properties and boundary conditions. Also, results from such numerical analysis are generally sensitive to numerical parameters needed for the solver subroutines, such as time increment and element mesh size (Buchanan 2002, Franssen et al. 2009).

Other simpler methods for calculating steel temperature include “spreadsheet method” that is based on one-dimensional finite difference techniques, and “best-fit method” that is based on statistical regression (Buchanan 2002). While the accuracy of spread sheet method is dependent on the selected time increment, the accuracy of the best-fit method is bounded within the range 400-600°C. The limitations can be ascribed to the fact that the spreadsheet method is a simplified one-dimensional finite difference incremental solution. Also, the best-fit method, for instance, was derived for calculating average steel temperature in proximity to the critical temperature of steel, which corresponds to 50% strength loss (yield strength) in steel. Thus, the temperature predicted by best-fit method may not be reliable at temperatures beyond roughly $\pm 25\%$ of critical temperature of steel which is 538°C (Buchanan 2002). In addition, the best-fit method is applicable for standard fire exposures only and cannot be used for design fire exposures.

Therefore, there is a need for a simple yet sufficiently reliable approach for evaluating temperatures in a steel cross section. Such simple method can facilitate reliable assessment of cross-sectional steel temperature without the need for using complex algorithms that are sensitive to various input parameters.

1 HEAT TRANSFER EQUATION

1.1 Governing Equations

The governing partial differential equation for heat transfer within the cross section of a structural member (beam, column, etc) can be written as (Purkiss 2007):

$$\rho c \frac{dT}{dt} = \nabla \cdot (k \nabla T) \quad (1)$$

where k = conductivity matrix, ρc = heat capacity, T = temperature, t = time, and ∇ = is the spatial gradient operator.

At the fire-member (e.g. beam) interface, heat is transferred through radiation and convection. The heat flux on the boundary due to convection and radiation can be given by the following equation:

$$q_b = (h_{con} + h_{rad})(T - T_f) \quad (2)$$

where h_{rad} and h_{con} are the radiative and convective heat transfer coefficients, and are defined as:

$$h_{rad} = \sigma \varepsilon (T^2 + T_f^2)(T + T_f) \quad (3)$$

T_f = temperature of the atmosphere surrounding the boundary (in this case it is the fire temperature), σ = Stefan-Boltzmann constant = 5.67×10^{-8} (W/m²·°K⁴), and

ε = emissivity factor and it is related to the “visibility” of the surface to the fire.

Generally, Eqs. (1 and 2) are simplified into one dimensional problem and then finite difference method is applied for solving the simplified equation. The accuracy of such solution is highly dependent on the size of the time increment; in addition, the analysis is complex and requires intensive use of spreadsheets calculations.

To overcome the above drawbacks and limitations in the current approaches, a simplified equation for predicting temperature in steel sections is derived. In order to simplify the partial differential equation (1), the following assumptions are made (Dwaikat 2010): Steel temperature (due to the high conductivity of steel) has a uniform distribution, leading to $\nabla^2 T = 0$, the radiation problem can be approximately described as an equivalent convection problem, and temperature in insulation material is assumed to be equal to an average of steel and fire temperatures, i.e. $(T_s + T_f)/m$, where $m = 2$ for linear variation of temperature across the insulation material.

Based on the assumptions listed above, Eq. (1) can be reduced to the following one dimensional differential equation:

$$\frac{dT_s}{dt} = \frac{\left(\frac{F_p}{A_s}\right)(T_f - T_s)}{c_s \rho_s \left(1/h_{con} + t_p/k_p\right) \left(1 + \frac{c_p \rho_p}{c_s \rho_s} \frac{F_p t_p}{A_s m}\right)} - \frac{dT_f/dt}{\left(1 + \frac{c_s \rho_s}{c_p \rho_p} \frac{A_s m}{F_p t_p}\right)} \quad (4)$$

where h_{con} is the convective heat transfer coefficient, $c_s \rho_s$ and $c_p \rho_p$ are the heat capacity of steel and insulation, respectively, k_p is conductivity of the insulation material, A_s is the cross sectional area of steel section, t_p is the thickness of protection, and F_p is the heated perimeter of the section.

1.2 Exposure to Standard Fire

For evaluating fire resistance of structural members, standard time-temperature curves as specified in ISO 834 (1975) and ASTM E119 (2008) are used. The time-temperature curves of these standard fires can be obtained through the following relations:

$$\text{ASTM E119: } T_f = 20 + 750 \left(1 - \exp\left(-3.79553\sqrt{t/60}\right)\right) + 170.41\sqrt{t/60} \quad (5a)$$

$$\text{ISO 834: } T_f = 20 + 345 \log(8t + 1) \quad (5b)$$

where T_f is fire temperature (in °C) as a function of time t (in minutes). In order to obtain a simplified solution for Eq. (4), the fire time-temperature curve of a standard fire (T_f) is fitted by a power function of the form: $T_f = at^n$. For ISO 834 standard fire $a = 469.9$ and $n = 0.1677$ ($R^2 = 0.995$), and for ASTM E119 standard fire $a = 496.5$ and $n = 0.1478$ ($R^2 = 0.989$).

If we assume that the temperature in steel has the following form:

$$T_s(t) = T_f \left(1 - e^{-st}\right) \quad (6)$$

where s is a correlation coefficient, then by substituting Eq. (6) into Eq. (4), dividing by T_f , substituting $\frac{dT_f/dt}{T_f} = \frac{n}{t}$, multiplying by e^{st} , substituting $e^{st} = 1 + st$ (for $st < 1$), and neglecting small

terms ($\ll 1.0$) we obtain:

$$s = \frac{\left(\frac{F_p}{A_s} \right)}{c_s \rho_s \left(\frac{1}{h + t_p} / k_p \right) \left(1 + \frac{c_p \rho_p F_p t_p}{c_s \rho_s A_s m} \right) (n+1)} \quad (7)$$

Using s from Eq. (7), Eq. (6) can be used to predict steel temperature at any time step, without the need for incrementing time steps. Equation (6) can be applied in one step (no time-steps needed) and this is an advantage over one-dimensional finite difference equations (such as those specified in the Eurocode 2005), whose accuracy is dependent on the size of time increment used.

1.3 Exposure to Design Fire

While the temperature in a standard fire continues to increase indefinitely, the design (parametric) fire simulates a decay phase after reaching a maximum temperature ($T_{f,max}$). A typical design fire can be represented by a parametric fire curve as specified in Eurocode 1 (EC1 2002). Figure 1 (a) illustrates the characteristics of a typical parametric fire scenario.

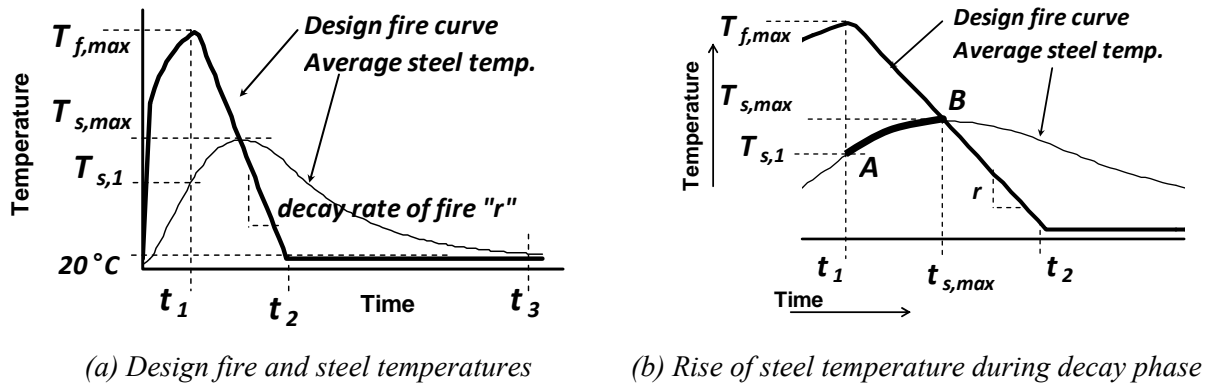


Fig. 1: Characteristics of typical parametric “design” fire exposure

The heating phase of a design fire is specified parametrically in Eurocode 1 in terms of the factor Γ according to the following equation (EC1 2002):

$$T_f = 1325(1 - 0.324 \exp(-0.2t\Gamma) - 0.204 \exp(-1.7t\Gamma) - 0.472 \exp(-19t\Gamma)) \quad (8)$$

where t in Eq. (8) is the time in hours. The factor Γ is dependent on the ventilation characteristics and thermal inertia of fire compartment. For $\Gamma = 1.0$, the heating phase of a parametric fire represents the ISO 834 standard fire. When $\Gamma > 1.0$, the temperature of the growth phase of the parametric fire is higher than the fire temperature of ISO 834 fire curve, and the opposite is true when $\Gamma < 1.0$.

Heating phase of a design fire can also be fitted using a power function (i.e. $T_f = at^n$). For instance, for a parametric fire with $\Gamma = 0.5$, $a = 312$ and $n = 0.229$ ($R^2 = 0.95$), while for parametric fire with $\Gamma = 1.5$, $a = 474$ and $n = 0.176$ ($R^2 = 0.97$). Steel temperature during the heating phase of a design fire can then be computed using Eq. (6).

The decay phase of a design fire starts at $t = t_1$, as shown in Fig. 2. In the parametric fires specified by the Eurocode (EC1 2002) the decay phase is always linear with a decay rate “ r ” that is dependent on the duration of growth phase t_1 , as shown in Fig. 1(b). If the rise in steel temperature after t_1 (the segment **AB** in Fig. 1(b)) is represented by a quadratic function, and if we assume that the maximum steel temperature occurs on the same decay curve of the fire (i.e. point **B** is on the fire curve), then the equation for the average steel temperature between t_1 and $t_{s,max}$ can be written as:

$$T_s = \alpha t^2 + \beta t + \gamma \quad (9)$$

where α , β , and γ are orientation coefficients. In order to estimate the maximum temperature in steel ($T_{s,max}$) the following boundary conditions for Eq. (9) are utilized:

- at point **A** ($t = t_l$): $T_s = T_{s,l}$ (using Eq. (11) at $t = t_l$), and $dT_s/dt = \text{slope from Eq. (11) at } t = t_l$,
- and at point **B** ($t = t_{s,max}$): $T_s = T_f$, and $dT_s/dt = 0$.

By applying the above four boundary conditions on Eq. (9) and solving for $t_{s,max}$ and $T_{s,max}$ we obtain:

$$t_{s,max} = t_l \left(1 + \frac{T_{f,max} - T_{s,l}}{\frac{1}{2}T_{s,l} + rt_l} \right) \quad (10)$$

$$T_{s,max} = \frac{T_{f,max} + 2t_l r}{1 + 2t_l r / T_{s,l}} \quad (11)$$

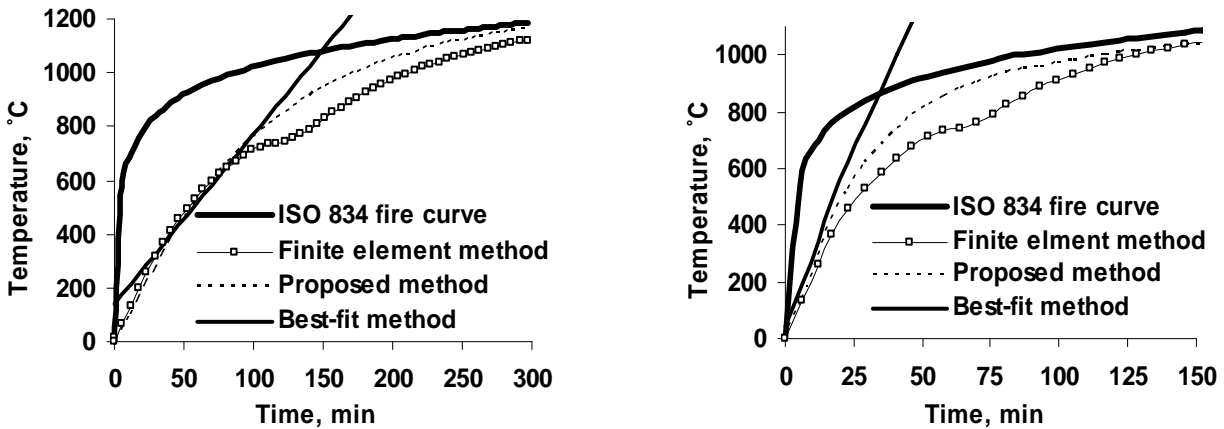
As it will be shown through comparison to rigorous finite element analysis, the last two simple equations give a good approximation for both the maximum temperature attained in steel beam during exposure to a design fire scenario and for the corresponding time of attaining that maximum average steel temperature.

2 NUMERICAL ANALYSIS

In order to verify the validity, predictions from the proposed equations are compared with results from rigorous finite element analysis. The finite element model for thermal analysis is developed using ANSYS (2007). In the thermal analysis, solid plane elements were used to discretize the cross section and the boundary conditions simulated both radiation and convection that would result in a fire exposure. The high temperature thermal properties of steel were based on the Eurocode while the thermal properties of the insulation were based on experimental results (Dwaikat and Kodur 2011a,b,c). The details of the finite element modeling and validation can be found elsewhere (Dwaikat 2010, Dwaikat and Kodur 2011a,b,c).

3 VERIFICATION OF THE PROPOSED EQUATIONS

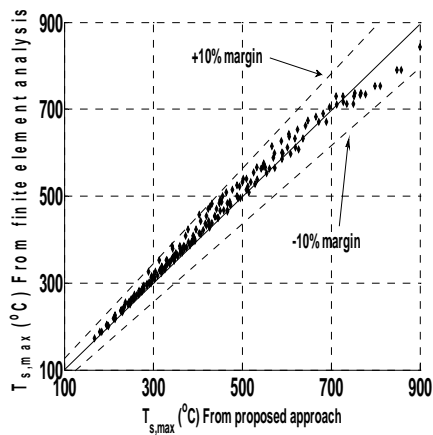
The validity of the approach is established by comparing predicted temperatures against data from fire tests and against results from finite element analysis generated via ANSYS. Fig. 2 shows a sample of comparison for protected ($t_p \neq 0$) and unprotected ($t_p = 0$) steel section. In addition, predictions from the proposed method are also compared with the temperatures predicted by “best-fit” method. Fig. 3 shows that maximum steel temperature and the corresponding time as predicted by the proposed approach and by finite element analysis for different steel sections exposed to different design fire scenarios. The comparisons shown in Fig. 2 and 3 indicate that the proposed equations are capable of predicting the temperature in steel section exposed to different fire scenarios. The simplicity of the proposed method makes it attractive for use in design situations.



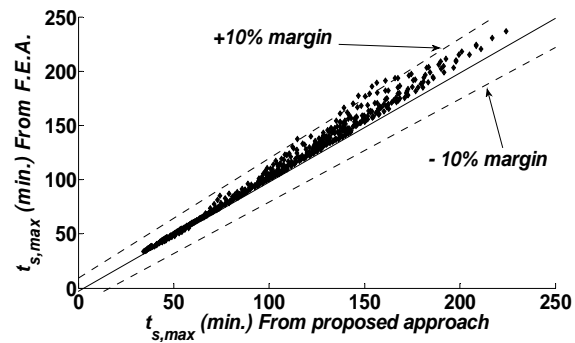
(a) Protected steel section

(b) Unprotected steel section

Fig. 2: Steel temperature obtained by the proposed approach to those obtained using different methods



(a) Maximum steel temperature



(b) Time for reaching maximum steel temperature

Fig. 3: Comparing predictions from proposed equations and from finite element analysis for $T_{s,max}$ and $t_{s,max}$

4 CONCLUSIONS

Based on the results presented in this paper, the following conclusions can be drawn:

- The current approaches for evaluating steel temperature in fire exposed sections are either complex (finite element or finite difference) or simplistic with limited validity (best-fit method).
- A new approach is proposed for evaluating temperature in steel sections exposed to standard or design fire scenarios, and is applicable for protected or unprotected steel sections.
- The proposed approach, derived based on heat transfer principles, is capable of estimating steel temperature for the whole section or in parts of the section, which enables predicting fire induced thermal gradient in section exposed to fire from 1, 2, 3, or 4 sides.
- The proposed approach gives better estimates of temperature than the best-fit method for the entire range of fire exposure time.
- The simplicity and wide range of applicability of the proposed approach makes it attractive for application in practical design situations.

5 ACKNOWLEDGEMENTS

The authors wish to acknowledge the support of National Science Foundation (through Award# CMMI 0652292 and CMMI 0757900). Any opinions, findings, conclusions, or recommendations expressed in this paper are those of the authors and do not necessarily reflect the views of the sponsors.

REFERENCES

- ANSYS, “ANSYS multiphysics”, version 11.0 SP1 ANSYS Inc., 2007
- ASTM E119, “Standard methods of fire test of building construction and materials,” American Society for Testing and Materials, West Conshohocken, PA, USA, 2008
- Buchanan, A.H. “Structural design for fire safety”, John Wiley & Sons Ltd., Chichester, England, 2002
- Dwaikat, M.M.S. and Kodur, V.K.R. “A performance-based methodology for fire design of restrained steel beams”, Journal of Constructional Steel Research, 67(3), pp. 510-524, 2011
- Dwaikat, M.M.S. and Kodur, V.K.R. “An Engineering Approach for Predicting Fire Response of Restrained Steel Beams”, in Press, Journal of Engineering Mechanics, ASCE, 2011b
- Dwaikat, M.M.S. and Kodur, V.K.R. “Strength Design Criteria for Steel Beam-Columns with Fire Induced Thermal Gradients”, in Press, Engineering Journal, AISC, 2011a

- Dwaikat, M.M.S., "Response of restrained steel beam subjected to fire induced thermal gradients," Ph.D. Thesis, Michigan State University, East Lansing, MI, USA, 2010
- EC1, "EN 1991-1-2: Actions on structures. Part 1-2: General actions - Actions on structures exposed to fire", European Committee for Standardization, Brussels, Belgium, 2002
- EC3, "EN 1993-1-2: Design of steel structures. Part 1-2: General rules - Structural fire design", European Committee for Standardization, Brussels, Belgium, 2005
- Franssen, J.M., Kodur, V.K.R. and Zaharia, R. "Designing steel structures for fire safety", Taylor & Francis Group, London, UK, 2009
- ISO 834, "Fire resistance tests – elements of building construction", International Organization for Standardization", 1975
- Purkiss, J. A. "Fire safety engineering design of structures", 2nd Ed., Butterworth-Heinemann, Linacre House, Jordan Hill, Oxford OX2 8DP, UK, 2007
- Silva, V. P. "Determination of the steel fire protection material thickness by an analytical process—a simple derivation", Engineering Structures, 27, pp. 2036–2043, 2005

MODELLING OF MULTIPLE LOCALISED FIRES AND STEEL STRUCTURAL MEMBERS RESPONSE USING THE SOFTWARE ELEFIR-EN

Paulo Vila Real ^a, Carlos Couto ^b, Nuno Lopes ^c

^a Professor, University of Aveiro, LABEST - Department of Civil Engineering, Portugal

^b Research student, University of Aveiro - Department of Civil Engineering, Portugal

^c Assistant professor, University of Aveiro, LABEST - Department of Civil Engineering, Portugal

INTRODUCTION

With the recent approval of the Eurocodes, it became possible for structural engineers to consider physical based thermal actions and to do performance based design, instead of using prescriptive rules based on nominal fire curves. This opens the door to the use of much more realistic characterization of the fire scenarios and consequently allowing for more cost effective structures without compromising their safety in case of fire.

Guidance paper L (concerning the Construction Products Directive - 89/106/EEC) that gives information on the “Application and use of Eurocodes”, states that one of the aims and benefits of the Eurocode programme is that it allows common design aids and software to be developed for use in all Member States. The software Elefir-EN (Vila Real, P. and Franssen, J. M., 2010; Franssen, J. M. and Vila Real, P., 2010) that is in line with this statement was used in this work to model the thermal response of the steel beams of a closed car park subjected to a multiple localised fire according to Annex C of Part 1-2 of Eurocode 1. The software allows for the calculation of the critical temperature of the steel members and subsequent evaluation of the thickness of the fire protection material necessary to fulfil the required fire resistance.

The main objective of this work is not to check the fire resistance of a real car park but to show the capabilities of the new software Elefir-EN concerning the modelling of multiple localised fires due to simultaneously burning of cars.

1 CHARACTERIZATION OF THE FIRE

According the European Project “Demonstration of real fire tests in car parks and high buildings” (European Commission, 2001) the classification of cars based on its calorific potential is given in Tab. 1. These results were obtained using the calorimetric hood to collect all smokes, combustion products and pollutants emitted during the combustion of real car burning. From the tests several experimental curves of the Rate of Heat Release (RHR) function of the time were obtained and simplified curves were proposed and validated.

Tab. 1 Classification of cars

Type	Category 1	Category 2	Category 3	Category 4	Category 5
Peugeot	106	306	406	605	806
Renault	Twingo-Clio	Mégane	Laguna	Safrane	Espace
Citroen	Saxo	ZX	Xantia	XM	Evasion
Ford	Fiesta	Escort	Mondeo	Scorpio	Galaxy
Opel	Corsa	Astra	Vectra	Omega	Frontera
Fiat	Punto	Bravo	Tempra	Croma	Ulysse
Wolkswagen	Polo	Golf	Passat	-	Sharan
Energy	6000 MJ	7500 MJ	9500 MJ	1200 MJ	

Fig. 1 shows the simplified RHR curve for a class 3 car fire. The referred project also suggests curves for the same type of cars that start burning with a delay of 12 and 24 minutes. In Fig. 2 these curves are shown and a fourth curve for of a car that starts to burn with a delay of 36 minutes has been added.

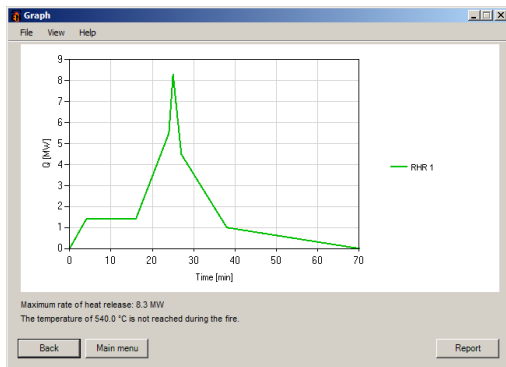


Fig. 1 Rate of heat release of a single class3 car fire

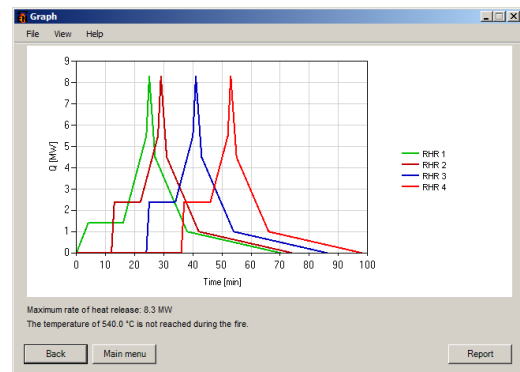


Fig. 2 Rate of heat release of a single class 3 car fire with a delay of 12 minutes

Tab. 2 gives the values of the rate of heat release as a function of time of each car with time delay of 12 minutes.

Tab. 2 Values of the rate of heat release of four burning class 3-cars

Time (min)	1 st Car	Time (min)	2 nd Car	Time (min)	3 rd Car	Time (min)	4 th Car
0	0	12	0	24	0	36	0
4	1.4	13	2.4	25	2.4	37	2.4
16	1.4	22	2.4	34	2.4	46	2.4
24	5.5	28	5.5	40	5.5	52	5.5
25	8.3	29	8.3	41	8.3	53	8.3
27	4.5	31	4.5	43	4.5	55	4.5
38	1	42	1	54	1	66	1
70	0	74	0	86	0	98	0

1.1 Fire scenarios

In this work, five fire scenarios, as shown in Fig. 3, have been considered according to the Rate of Heat Release of a class 3 car (see Tab. 1):

- i) Fire scenario 1: One car burning below the beam at mid-span;
- ii) Fire scenario 2: Three cars of class 3 in a normal parking bay with an ignition time delay for each car of 12 minutes;
- iii) Fire scenario 3: Four cars of class 3 in a normal parking bay with an ignition time delay for each car of 12 minutes It will be shown that the burning of the fourth car does not affect the maximum temperature of the beam;
- iv) Fire scenario 4: Three cars of class 3 in a normal parking bay with an ignition time delay for each car of 12 minutes;
- v) Fire scenario 5: Four cars of class 3 in a normal parking bay with an ignition time delay for each car of 12 minutes.

In Fig.3 it is shown also the sequence of ignition of the different fire scenarios considered.

The temperature of the beam was evaluated using the program Elefir-EN at the mid-span section and with the rate of heat release of the Fig.1 for Fire Scenario 1 and at the extremity of the beam and considering the rate of heat release of the Fig.2 in the remaining fire scenarios.

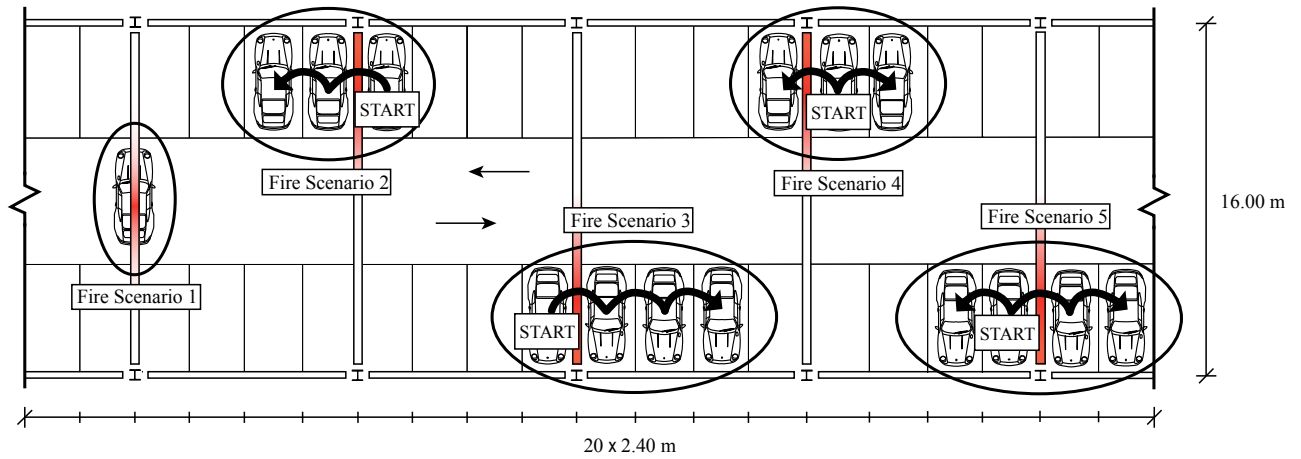


Fig. 3 Fire scenarios and sequence of ignition

1.2 Localised fires

Annex C of part 1.2 of Eurocode 1 gives two models for the temperature development in case of a localised fire. Which one has to be used depends on the vertical length of the flame L_f given by the following Eq. (1):

$$L_f = -1.02D + 0.0148Q^{2/5} \quad [\text{m}] \quad (1)$$

where D is the diameter of the fire and Q the rate of heat release.

Fig. 4, taken from Annex C of part 1.2 of Eurocode 1, shows the length of the flame when the fire source is on the floor level and the flame does not impact the ceiling.

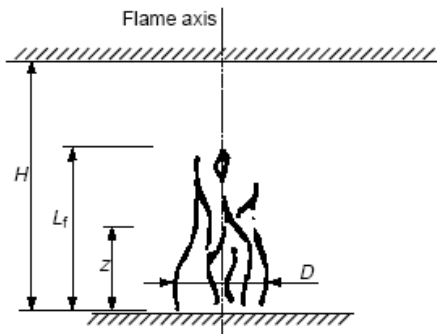


Fig. 4 Localised fire not impacting the ceiling

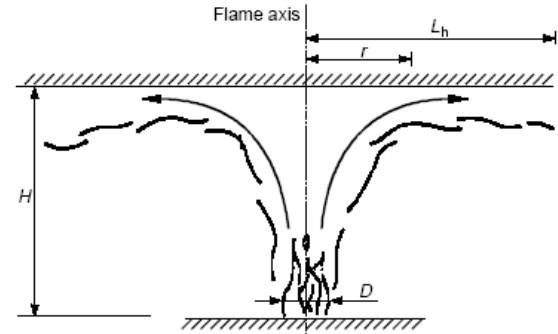


Fig. 5 Localised fire impacting the ceiling

When the flame does not impact the ceiling, Eurocode 1, based on the Heskestad method gives Eq. (2) for evaluating the temperature development $\theta_z(t)$ that depends on the diameter of the fire D , the rate of heat release Q and the height z along the flame axis from the position of the source.

$$\theta_{(z)} = 20 + 0.25Q_c^{2/3} (z - z_0)^{-5/3} \leq 900 \quad [^\circ\text{C}] \quad (2)$$

When the flame is impacting the ceiling ($L_f \geq H$; see Fig. 5) the Eurocode 1 based on the Hasemi method, gives the heat flux \dot{h} [W/m²] received by the fire exposed unit surface area at the level of the ceiling (see Eq. (3)) as:

$$\begin{aligned} \dot{h} &= 100\,000 & \text{if } y &\leq 0.30 \\ \dot{h} &= 136\,300 - 121\,000y & \text{if } 0.30 < y < 1.0 \\ \dot{h} &= 15\,000y^{-3.7} & \text{if } y &\geq 1.0 \end{aligned} \quad [\text{W/m}^2] \quad (3)$$

This heat flux depends on the diameter of the fire D , the rate of heat release Q , the distance between the fire source and the ceiling H and the horizontal distance between the vertical axis of the fire and

the point along the ceiling where the flux is calculated, as shown in Fig. 5. According to the Eurocode 1 this model can not be used in situation where the diameter of the fire source D is bigger than 10 meters and the rate of heat release of the fire Q is bigger than 50 MW.

The method gives heat flux \dot{h} [W/m²] received by the fire exposed unit surface area and the net heat flux \dot{h}_{net} , has to be calculated by

$$\dot{h}_{net} = \dot{h} - \alpha_c \cdot (\theta_m - 20) - \Phi \cdot \epsilon_f \cdot \epsilon_m \cdot 5.67 \times 10^{-8} \cdot [(\theta_m + 273)^4 - 293^4] \quad [\text{W/m}^2] \quad (4)$$

In case of several separate localised fires, Eq. (3) may be used in order to obtain the different individual heat fluxes $\dot{h}_1, \dot{h}_2, \dot{h}_3$. etc., received by the fire exposed unit surface area at the level of the ceiling. The total heat flux may be taken as:

$$\dot{h}_{tot} = \dot{h}_1 + \dot{h}_2 + \dot{h}_3 + \dots \leq 100000 \quad [\text{W/m}^2] \quad (5)$$

2 TEMPERATURE IN STEEL MEMBERS SUBJECTED TO LOCALISED FIRES

EN 1993-1-2 gives two different equations for calculating the temperature of steel members subjected to fire, depending on whether the members are protected or not. The procedures that are used to evaluate the temperature in the case of localised fires are presented in this section.

2.1 Unprotected steel members

EN 1993-1-2 provides a simple equation for calculating the thermal response of unprotected steel members. Assuming an equivalent uniform temperature distribution throughout the cross-section, the increase in temperature $\Delta\theta_{a,t}$ in an unprotected steel member during a time interval Δt is given by:

$$\Delta\theta_{a,t} = k_{sh} \frac{A_m/V}{c_a \rho_a} \dot{h}_{net,d} \Delta t \quad [^\circ\text{C}] \quad (6)$$

where the meaning of the variables can be found in the Eurocode.

For unprotected sections, the heat flux used in Eq. (6) is the sum of a convective part and a radiative part, $\dot{h}_{net,d} = \dot{h}_{net,c} + \dot{h}_{net,r}$. This heat flux is easily calculated if the gas temperature, θ_g , is known.

For localised fires not impinging the ceiling, the gas temperature is given by Eq. (2). In the case where the localised fire impinges on the ceiling, the heat flux is given by Eq. (3), and this can be directly used in Eq. (6) for calculating the temperature in unprotected steel members.

2.2 Protected steel members

EN 1993-1-2 provides a simple design method to evaluate the temperature development of steel members insulated with fire protection materials. Assuming uniform temperature distribution, the temperature increase $\Delta\theta_{a,t}$ of an insulated steel member during a time interval Δt , is given by

$$\Delta\theta_{a,t} = \frac{\lambda_p A_p / V}{d_p c_a \rho_a} \frac{(\theta_{g,t} - \theta_{a,t})}{(1 + \phi/3)} \Delta t - (e^{\phi/10} - 1) \Delta\theta_{g,t} \quad [^\circ\text{C}] \quad (7)$$

the variables being defined in the Eurocode. This equation is only based on the gas temperature. For localised fires not impinging the ceiling, the gas temperature is given by Eq. (2) and the development of the steel temperature is calculated from Eq. (7). However, Eq. (7) can not be applied directly in the case of a fire impinging the ceiling, because the effect of the fire is given as an impinging flux, see Eq. (3). A procedure has to be established to transform the impinging heat flux into an equivalent gas temperature. Cadorin et al. (2003) suggests deducing a fictitious temperature that has the same effect on steel elements as the heat flux calculated with this method. This is the temperature of a steel profile with a very high massivity factor. This steel profile has a temperature which is very close to the gas temperature. This procedure is used in the program Elefir-EN. The program first evaluates the gas temperature as the temperature of a fictitious unprotected steel profile with very high section factor ($A_m/V = 10000 \text{ m}^{-1}$ is adopted) using Eq. (6)

and the net heat flux given by Eq. (4). After evaluating the gas temperature, the temperature of the protected steel profile is then calculated using Eq. (7).

3 TEMPERATURES OF THE BEAM

The program Elefir-EN first evaluates the length of the flame to decide which method has to be used (Heskestad or Hasemi). In the case of multiple localised fires only the fires in which the flame impacts the ceiling are considered and the others are ignored. Fig. 6 shows the flame length development during the fire, considering that the diameter of the cars is $D = 3.9$ m and the height of the compartment is $H = 2.7$ m.

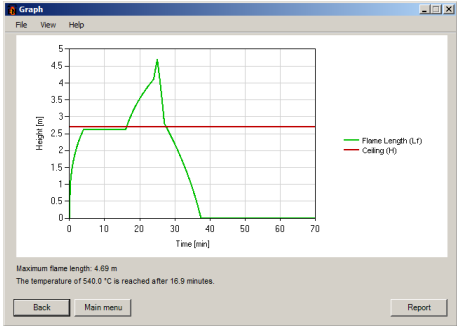
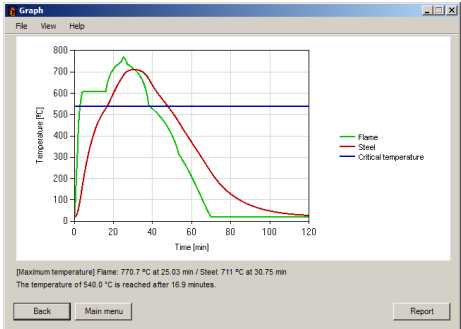
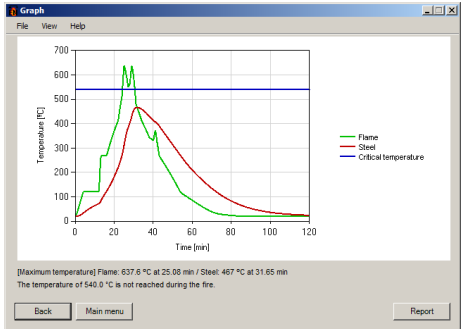


Fig. 6 Flame length development for a single burning car

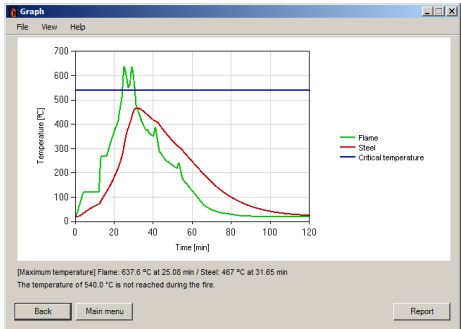
Fig. 7 shows the gas temperature and the temperature of the main beam, supposing that it is made of IPE 500, the critical temperature is 540 °C , the diameter of the cars is $D = 3.9$ m and the height of the compartment is $H = 2.7$ m.



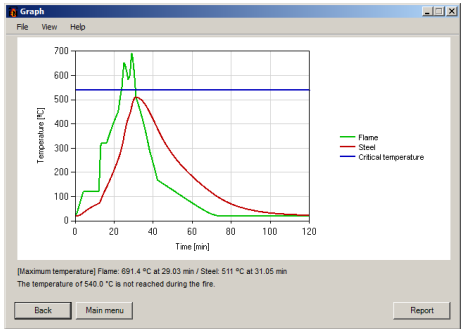
a)



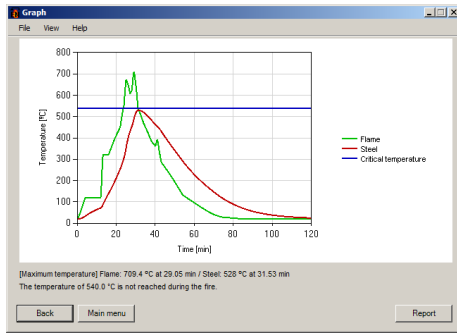
b)



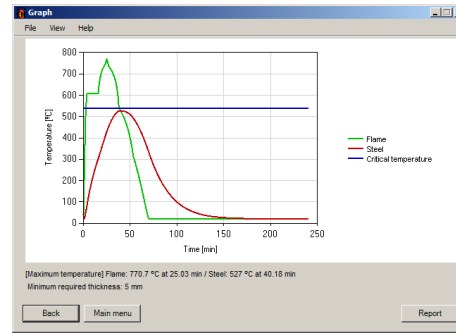
c)



d)



e)



f)

Fig. 7 Temperature development. a) Scenario 1; b) Scenario 2; c) Scenario 3 d) Scenario 4; e) Scenario 5; f) Scenario 1 with the beam protected

Tab. 3 shows the maximum temperature obtained for the main beam in all the fire scenarios. From that table it can be concluded that, due to the scenario 1 the main beams should be protected so that the temperature doesn't reach the assumed critical temperature of 540 °C during the complete duration of the fire including the decay phase or during a required period of time. If the load-bearing function is required during the complete duration of the fire, the program Elefir-EN gives, for example, a need of 5 mm of sprayed vermiculite cement on the contour of the beam (see Fig. 7 f)).

Tab. 3 Maximum temperatures of the main beam

	Scenario 1	Scenario 2	Scenario 3	Scenario 4	Scenario 5
$\theta_{a,max}$ [°C]	710.9	466.7	466.7	510.9	528.5

4 CONCLUSION

This paper has shown the capability of the software Elefir-EN for dealing with several separate localised fires. The software is an essential tool for structural engineers in the design office, enabling quick and accurate calculations to be produced, reducing design time and the probability of errors in the application of the equations.

REFERENCES

- Cadorin, J.-F., Compartment Fire Models for Structural Engineering, Thèse de doctorat, University of Liege, Belgium, 2003.
- CEN, EN 1991-1-2, Eurocode 1 – Actions on structures – Part 1-2: General actions – Actions on structures exposed to fire, Belgium, 2002.
- CEN, EN 1993-1-2, Eurocode 3 – Design of steel structures – Part 1-2: General rules – Structural fire design, Belgium, 2005.
- EUROPEAN COMMISSION, “Demonstration of real fire tests in car parks and high buildings”, Contract n° 7215 PP 025, 1 July 1998 to 20 June 2001.
- EUROPEAN COMMISSION, Guidance paper L (concerning the Construction Products Directive - 89/106/EEC) - Application and use of Eurocodes, Brussels, 27 November 2007.
- Franssen, J. M., Vila Real, P. – Fire Design of steel structures, ECCS ed and Ernst & Sohn ed., 2010.
- Vila Real, P., Franssen, J. M. – Elefir-EN V1.2.3 (2010), Software for fire design of steel structural members according the Eurocode 3. <http://elefiren.web.ua.pt>.

CONSTITUTIVE EQUATIONS FOR STRUCTURAL STEEL SUBJECTED TO FIRE Some Remarks

Manfred Korzen ^a

^a BAM Federal Institute for Materials Research and Testing, Division 7.3 Fire Engineering, Berlin, Germany

INTRODUCTION

Although identified on the basis of so-called instationary creep-tests the constitutive model of Eurocode 3 (EN 1993-1-2, 2010) – hereinafter referred to as EC3 – represents a non-linear rate-independent relationship between stress and mechanical strain. I.e. the experimentally observed phenomenon of creep at constant stress but linear time varying temperature is described only through the temperature dependence of the material parameters characterizing the EC3 constitutive model. As a consequence some important phenomena cannot properly be described: E.g. creep or relaxation at constant temperature, creep or relaxation at non-monotonic temperature rates or sensitivity of the instationary creep process on the temperature rate.

1 CONSTITUTIVE EQUATION AND TESTING MACHINE AS AN OPERATOR

We attack our task to find a convenient constitutive equation for steel subjected to fire from the standpoint of the experimenter using a servocontrolled material testing system (s. Fig. 1), i.e. the material as well as the model is looked upon as an operator (Krempel, 1974). These operators map a time-dependent input (loading function) into a corresponding time-dependent output (response function). We limit our attention to uniaxial stress cases with macroscopically homogeneous states of stress σ and infinitesimal strain ε . According to this terminology a classical strain-controlled tension test at strain rate $\dot{\varepsilon}^*$ and temperature θ^* is defined by two loading functions: (i) $\varepsilon(\tau) = \dot{\varepsilon}^* \tau$ and (ii) $\theta(\tau) = \theta^* = const.$ and one response function $\sigma(t)$. We neglect any heating due to dissipation. The experimental input-output relationship, which is realized through the servocontrolled testing machine including the device for heating of the specimen, corresponds to a mathematical operator (Onat, 1972), i.e.

$$\sigma(t) = \underset{0 \leq \tau \leq t}{F} (\varepsilon(\tau), \theta(\tau)). \quad (1)$$

The symbol F defines an operator, which assigns with every $\varepsilon(\tau)$ and $\theta(\tau)$ on $[0, t]$ a $\sigma(t)$. It is a challenging task for the experimenter to identify the properties of this operator, which represents the material and is referred to as a constitutive equation. It is important to note that this equation is never obtained directly because in an experiment it is only possible to obtain a response function. Therefore, a constitutive equation must be constructed in such a way that it gives for a certain input the corresponding output like the tested material.

2 EC3 MODEL

The constitutive equation of EC3, i.e.

$$\sigma = f(\varepsilon^m, \theta) \quad (2)$$

defines a one-dimensional non-linear algebraic relation between σ , infinitesimal mechanical strain ε^{mech} and temperature θ . It looks like a non-linear thermo-elastic constitutive model (s. Fig. 2) and insofar as a special case of eq. (1). Therefore by definition eq. (2) is rate-independent, i.e. the

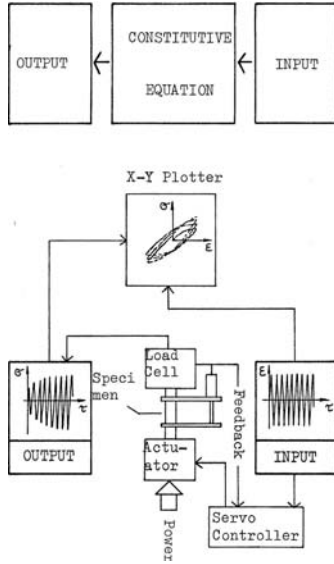


Fig. 1 Constitutive Equation and Material as an Operator (figure below after Morrow, 1965)

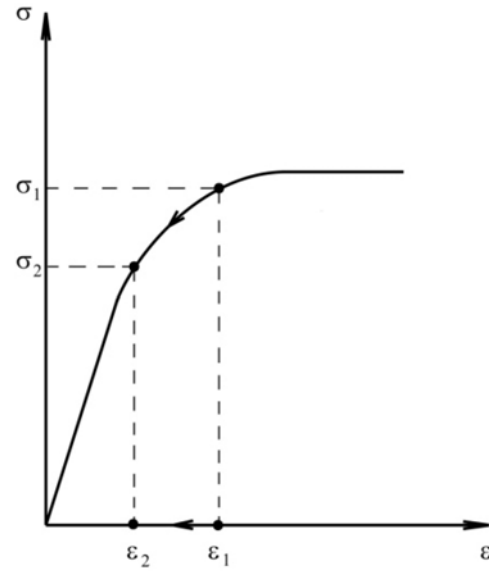


Fig. 2 Non-Linear Elastic Behavior

material response does not depend on the rate of loading. Another point of view is achieved through the well known fact, that the experimental basis of eq. (2) are so-called instationary creep tests. Those type of tests are characterized through loading functions L_σ and L_θ of type

$$L_\sigma(\tau) = \sigma^* = const., \quad (3)$$

$$L_\theta(\tau) = \dot{\theta}^* \tau. \quad (4)$$

I.e. the specimen is loaded up to $\sigma = \sigma^*$ and then at this stress level heated up with a temperature rate of $\dot{\theta}^*$. The response functions for N tests at N stress levels look like

$$\varepsilon_1(t) = g_1(\sigma = \sigma_1^* = const., \theta(t) = \dot{\theta}^* t) \quad (5.1)$$

⋮

$$\varepsilon_N(t) = g_N(\sigma = \sigma_N^* = const., \theta(t) = \dot{\theta}^* t). \quad (5.N)$$

Each response function depends on the stress level and on the temperature rate. We achieve at eq. (2) assuming that σ^* and $\dot{\theta}^*$ are no longer parameters but variables and inverting eq. (5) to give

$$\sigma = f(\varepsilon, \theta) \quad (6)$$

and after subtracting the thermal strain

$$\sigma = f(\varepsilon^m, \theta). \quad (2)$$

I.e. the stress-strain relationship of EC3 is derived through the usage of response functions as constitutive equations. Keeping that in mind a more precise characterization of eq. (1) would be that it gives the necessary constant stresses to reach a given mechanical strain ε^{mech} at a heating rate of $\dot{\theta}^*$. Especially, the phenomenon of creep at constant temperature and the influence of the temperature rate on creep cannot be described through eq. (2).

3 CONCEPT OF A CONSTITUTIVE MODEL

Due to the shortcomings of the EC3 stress-strain relationship we are looking for a more appropriate constitutive equation especially with concern to the experimental phenomenon of classical as well as instationary creep. Our model is based on the very classical three-parameter solid of viscoelasticity (Flügge, 1975). Only two main modifications are introduced: (i) the strain ε is replaced by the mechanical strain ε^{mech} and (ii) the static stress σ^{stat} , i.e. the stress response for

slow motions, is no longer a linear function – as in linear viscoelasticity – but a rate-independent functional of the deformation variable so that we have finally

$$\dot{\sigma} = -\frac{1}{\lambda(\theta, \sigma - \sigma^{stat})} [\sigma - \sigma^{stat}] + E_0(\theta) \dot{\varepsilon}^{mech}, \sigma(0) = 0 \quad (7)$$

$$\dot{\sigma}^{stat} = g(\theta, \text{sign}(\dot{\varepsilon}^{mech}), \varepsilon^m, \sigma^{stat}) \dot{\varepsilon}^{mech}, \sigma^{stat}(0) = 0 \quad (8)$$

with

$$g(\cdot) := E_e(\theta) \frac{\beta(\theta) E_e(\theta) - \text{sign}(\dot{\varepsilon}^{mech}) [\sigma^{stat} - E_p(\theta) \varepsilon^{mech}]}{\beta(\theta) E_e(\theta) - \kappa(\theta) \text{sign}(\dot{\varepsilon}^{mech}) [\sigma^{stat} - E_p(\theta) \varepsilon^{mech}]} \quad (9)$$

$$\varepsilon^{mech} := \varepsilon - \alpha(\theta) [\theta - \theta_0] \quad (10)$$

where $(\cdot)^{\bullet}$ denotes the material time derivative. Round brackets are symbols for “function of” whereas square brackets are used in the algebraic sense. Eqs. (7) and (8) (s. Fig. 3) define a system of non-linear non-autonomous ordinary differential equations of type

$$\dot{y} = \underline{h}(y(t), t), y(0) = y_0 \quad (11)$$

with initial conditions for σ and σ^{stat} . Eq. (11) may be stiff in certain regions (Hairer et al., 2002). Eq. (8) (s. Fig. 4) defines implicitly the aforementioned rate-independent functional for the static stress σ^{stat} (Valanis, 1980). In contrast to classical constitutive equations of elasto-plasticity eq. (8) is defined without a yield surface and corresponding loading conditions. Eqs. (7) and (8) belong to the class of so-called *unified theories* which do not separate plastic and creep strains, and represent inelastic deformation by a set of equations, employing a number of internal variables. In our case one internal variable is used and corresponds to σ^{stat} .

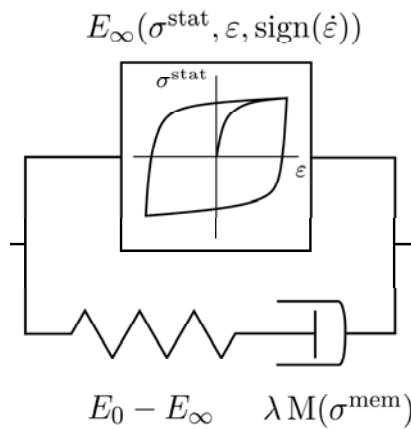


Fig. 3 Spring-dashpot model of proposed constitutive equation

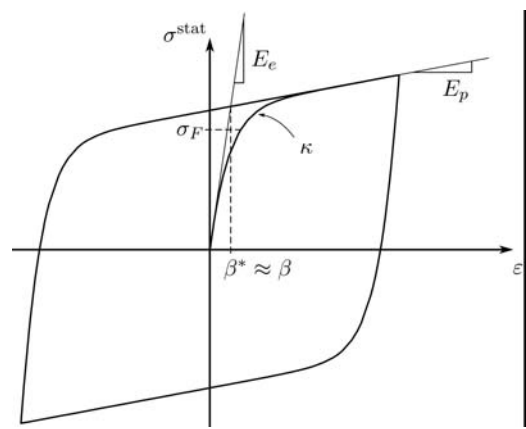


Fig. 4 Stress-strain diagram of static stress with temperature dependent material parameters

In the asymptotic limiting case of *fast loadings* ($\dot{\sigma} \rightarrow \infty$, $\dot{\varepsilon}^{mech} \rightarrow \infty$) eq. (7) reduces to

$$\dot{\sigma} = E_0(\theta) \dot{\varepsilon}^{mech}, \quad (12)$$

i.e. a linear elastic response with the temperature dependent spontaneous Young's modulus $E_0(\theta)$.

The limiting case of *slow loadings* ($\dot{\sigma} \rightarrow 0$, $\dot{\varepsilon}^{mech} \rightarrow 0$) yields

$$\sigma = \sigma^{stat}, \quad (13)$$

i.e. a hysteretic response (s. Fig. 4), which is represented by the static stress σ^{stat} . Beside this qualitative analysis numerical simulations are realized with the software package *RAUDAU* (Hairer, 1996).

4 STRESS AND TEMPERATURE CONTROLLED INPUT FUNCTION - CREEP

In order to simulate creep, i.e. to define stress and temperature as input functions in the terminology of chapter 2, we have to arrange the constitutive equations in the following form:

$$\dot{\varepsilon}^{mech} = \frac{\sigma - \sigma^{stat}}{\lambda(\theta, \sigma - \sigma^{stat}) E_0(\theta)} + \frac{\dot{\sigma}}{E_0(\theta)}, \varepsilon^{mech}(0) = 0 \quad (14)$$

$$\dot{\sigma}^{stat} = g(\theta, \text{sign}(\dot{\varepsilon}^{mech}), \varepsilon^m, \sigma^{stat}) \dot{\varepsilon}^{mech}, \sigma^{stat}(0) = 0 \quad (15)$$

Assuming that the material parameters relaxation time λ , spontaneous Young's modulus E_0 as well as the parameters κ , β , E_e and E_p of the static stress are identified as functions of temperature we can use the constitutive model as an operator to run simulations for different inputs of stress and temperature. As an example we run some simulations for the case of instationary creep. The material responses in Fig. 5 demonstrate the sensitivity of the creep response to temperature rate. In Fig. 6 it can be observed what happens if the temperature switches from one value to the other in comparison with the corresponding behaviour at constant temperature rate. The simulated material responses represented in both figures looks plausible but are in contrast to the EC3 model behaviour which does not show any sensitivity to temperature rate.

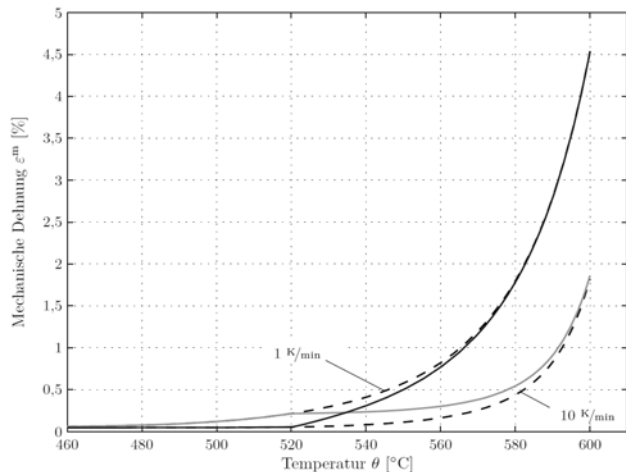
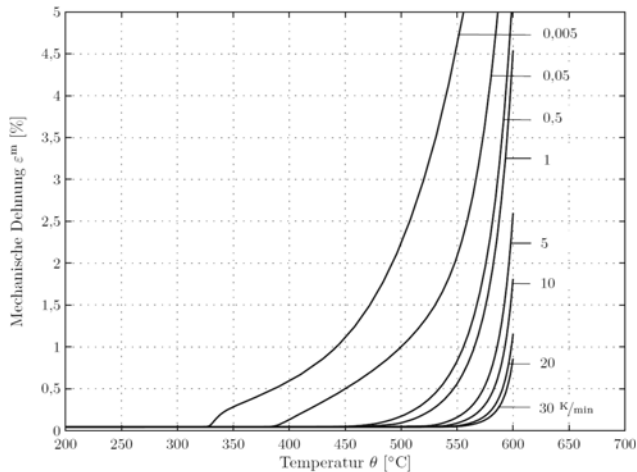


Fig. 5 $\varepsilon^{mech}(t)$ at $\sigma^* = 100$ MPa and different $\dot{\theta}^*$

Fig. 6 $\varepsilon^{mech}(t)$ at $\sigma^* = 100$ MPa and different $\dot{\theta}^*$ with jumps in $\dot{\theta}^*$

5 COMPARISON BETWEEN MODEL AND EXPERIMENT

In order to make a quantitative comparison between the proposed model and experiment we executed a special transient creep test with a specimen of S235 steel. In contrast to the classical heating with a ramp of constant temperature rate we realized it with a triangle temperature-time pattern. The heating was realized through high-frequency inductive coils, which normally are used for so-called TMF (thermo-mechanical fatigue) tests. The strain was measured with a special clip-on extensometer directly attached to the surface of the specimen.

The experimental results as well as the data of the numerical simulation are presented in Fig. 7. The bottom figure demonstrates the extraordinary precise realization of the temperature input function together with the input function for the simulation. The top figure visualizes the measured total strain (\bullet) together with the simulated thermal strain (top), total strain (middle) and mechanical strain (bottom). The correlation between model and experiment is quite good.

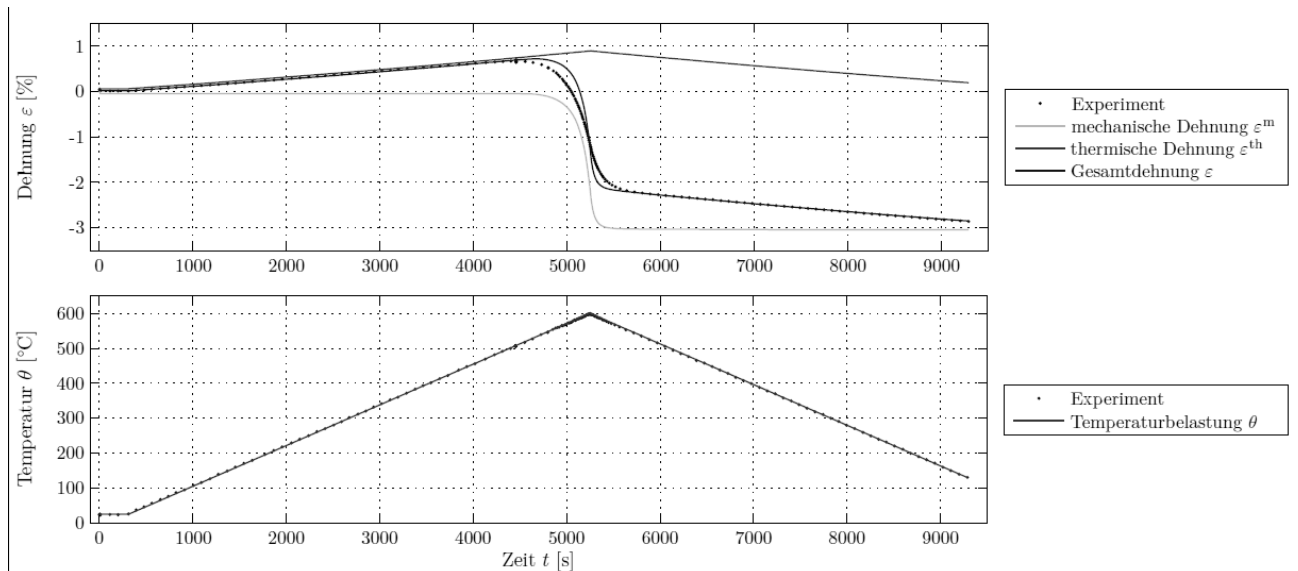


Fig. 7 Input (temperature) and output (strain) of non-monotonic transient creep test at $\sigma^* = 100$ MPa and $|\dot{\theta}^*| = 7$ K/min, \bullet : experimental data

6 SUMMARY AND ACKNOWLEDGEMENT

After introducing the operator point of view on material and constitutive equation the EC3 model has been discussed together with its shortcomings. An alternative constitutive equation approach within the operator terminology was presented together with its basic capabilities. Finally the behaviour of the proposed model was compared with the results of a challenging experiment related to transient creep, and demonstrated a quite good correlation.

The author is very grateful to Le Trung Nguyen who has done all simulations.

REFERENCES

- EN 1993-1-2, Eurocode 3: Design of steel structures – Part 1.2: General rules- fire design, CEN (Comité Européen de Normalisation), Brussels, Belgium, 2010)
- Flügge W., Viscoelasticity, Berlin, 1975.
- Hairer E. Wanner G., Solving ordinary differential equations II, Berlin, 2002.
- Hairer, E., RADAU5, Université de Genève, 1996.
- Krempf, E., Cyclic Creep – An Interpretative Literature Survey, Welding Research Council Bulletin, No. 175, 1974, 63-123.
- Morrow J., Cyclic plastic strain energy and fatigue of metals, ASTM STP No. 378, 1965, 45-87.
- Onat E.T., Fardshisheh F.; Representation of creep of metals, Oak Ridge National Laboratory, Oak Ridge, Tennessee, U.S.A., Report ORNL-4783, 1972.
- Valanis K.C., Fundamental consequences of a new intrinsic time measure. Plasticity as a limit of the endochronic theory, Archives of Mechanics **32** (1980) 171-191.

MODELLING OF REINFORCED CONCRETE FRAMES IN FIRE FOLLOWING AN EARTHQUAKE

Ab.Kadir M A^a, A.S Usmani^b, M. Gillie^c

^aPhD student, School of Engineering, The University of Edinburgh, Edinburgh EH9 3JF, United Kingdom

^bProfessor, School of Engineering, The University of Edinburgh, Edinburgh EH9 3JF, United Kingdom

^cLecturer, School of Engineering, The University of Edinburgh, Edinburgh EH9 3JF, United Kingdom

INTRODUCTION

Earthquakes are natural hazards which occur in seismic areas and can cause devastating damage in urban infrastructure and facilities. Sometimes earthquake events are followed by fires which may cause more damage than the earthquake itself. Essentially, seismic design codes are relevant for designing a structure for an expected level earthquake and do not consider fire safety. In general, these two events are considered to occur separately.

A large number of post-earthquake building fires result in the collapse of the buildings. As a result of earthquake damage the fire resistance of a structure may be significantly impaired. In their study of the 1906 San Francisco earthquake and the 1923 Tokyo earthquake (Scawtorn e.al,2005) have shown that about 80% of the building damage was due to the fires following the earthquake rather than the earthquake itself. This may pose a serious threat to the structural integrity and be detrimental to the life safety of the occupants and rescue workers. Hence, it is prudent to consider such scenarios in the design of buildings constructed in seismic zones (Mousavi et al. 2008). Consequently, understanding the performance and response of structures in a fire following an earthquake is important at the design stage.

The aim of this study is to model a number of experiments being conducted on 2D reinforced concrete frames exposed to fire following simulated cyclic pushover. Increasing cyclic displacements are applied at the slab level in a pushover analysis to simulate the damage to the structure as a result of an earthquake.

1 REINFORCED CONCRETE FRAME MODELLING

A number of preliminary analyses were carried out on a 2D finite element model of the frame to determine its capacity under lateral pushover and its behaviours under cyclic loads. Based on the results, from the preliminary analyses, increasing cyclic displacements was applied to the frame as a second loading step (after applying all gravity loading in the first step). The columns and beam cross-sections were then exposed to temperature distributions obtained from a heat transfer analysis also carried out in the preliminary stage.

The temperature distributions were the result of radiative heat fluxes from a one hour compartment fire applied to the internal surfaced of the frame.

A computational analysis for this study was performed using ABAQUS. The reinforced concrete frame consisted of four columns supporting four beams and a slab on top floor and four beams at plinth level. The frame was modelled as a 2D frame with beam elements assigned for columns, beams and slab. Truss elements were used to model reinforcement bars. The frame model is shown in Figure 1. The total height of the frame is 6.0m with the distance between the plinth and top beams being roughly 3m. The cross section of the columns is 300mm x 300mm and that of the beams is 230mm x 230mm. Slabs thickness is 120mm. In order to reduce computational time the slab was modelled as apart of the overall

beam cross section in 2D. Eight steel bars of 20 mm diameter were used for the columns and six steel bars of 16 mm diameter were used for beam (3 each on the top and bottom). Node and element numbering of the model was as shown in Figure 2 and Figure 3.

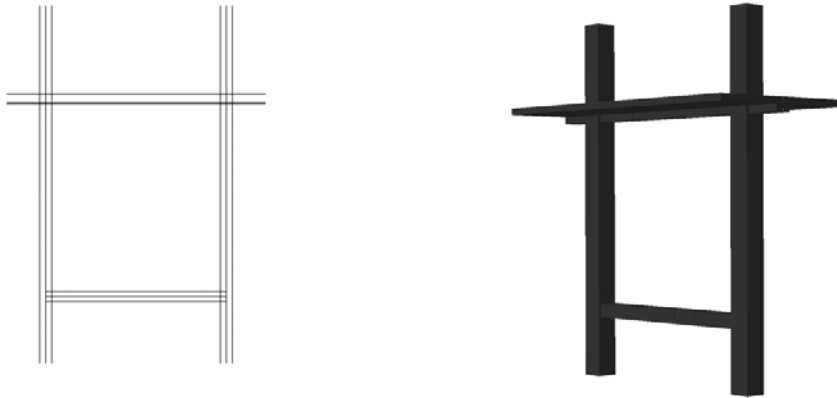


Fig. 1 2D The Analytical model

Temperature dependent material properties for concrete and steel were assigned according to the Euro Code 2. Concrete strength of 34MPa and steel strength 415 MPa was used. Permanent loads of 100kN on each column and 2.3kN/m² on the slab are applied. This load was constant throughout the analysis. Due to loading and unloading cycles on the frame, degradation of strength of the concrete and reinforcing bars was considered. Therefore, the concrete damaged plasticity was used in the analysis.

In the thermo-mechanical analysis, temperatures were assigned at the integration points of the elements at node locations. Five temperatures were assigned to the beam and three node temperatures to the column. The temperature exposures were assumed to occur only between the plinth beams and the top beam slab. The compartment temperatures were increased from 20°C to 1000°C in 5 minutes and maintained for another 55 minutes, as in Figure 4.

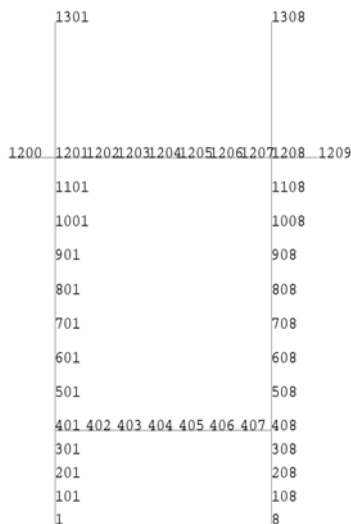


Fig. 2 Node Numbering

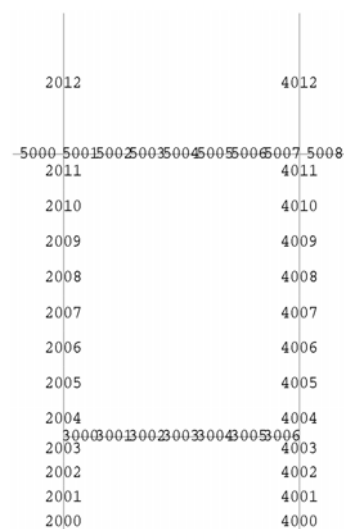


Fig. 3 Element Numbering

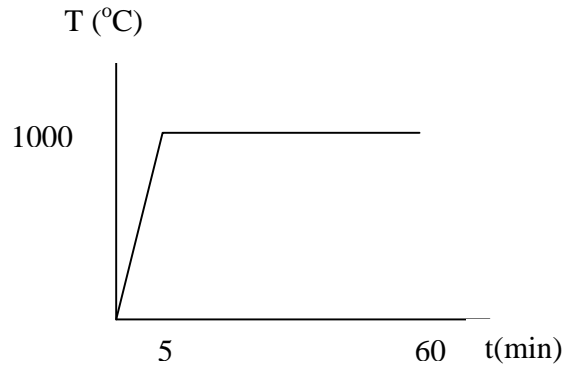


Fig. 4 Temperature Amplitude

2 PERFORMANCE OF RC FRAME

An analysis was performed to get an overview of the capacity of the frame. Figure 5 shows the hysteresis curve after a 7 cycle displacement load was applied at the slab level of the frame. Displacement was also observed at the slab level (node number 1208). The maximum base shear is around 300kN corresponding to a displacement of the frame of approximately 90mm. Three further cases were studied. A maximum displacement of 100mm was applied over 4 cycles for case I, 70% of this for case II and 30% for case III.

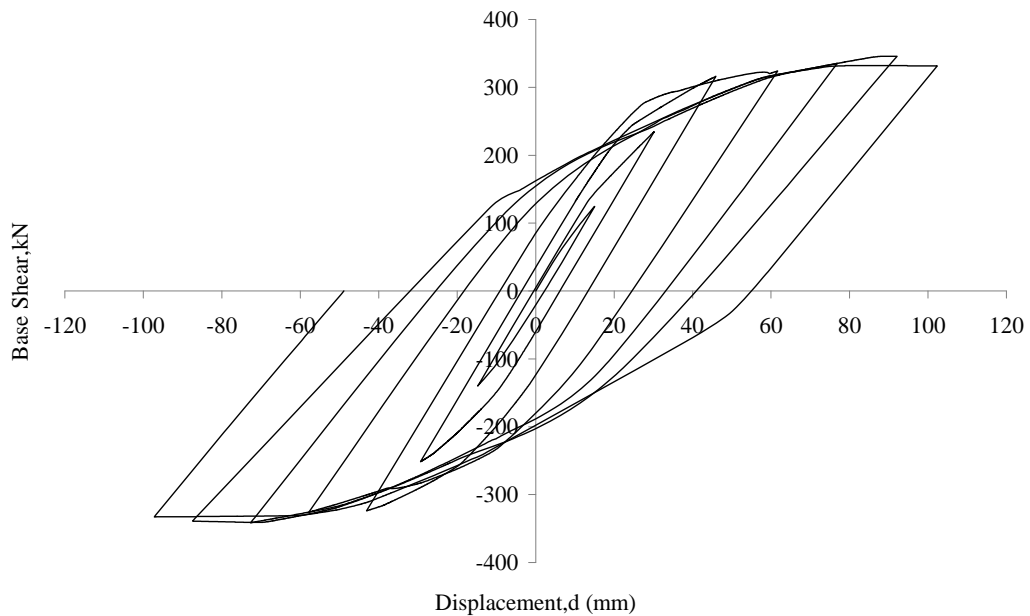


Fig. 5 Hysteresis Curve

Figure 6 illustrates the displacement history for the three cases. The results in this figures show that there are residual displacements after when the base shear is brought to zero at the end of the loading

cycles. The residual displacements are seen to increase with increasing magnitudes of the applied cyclic displacements.

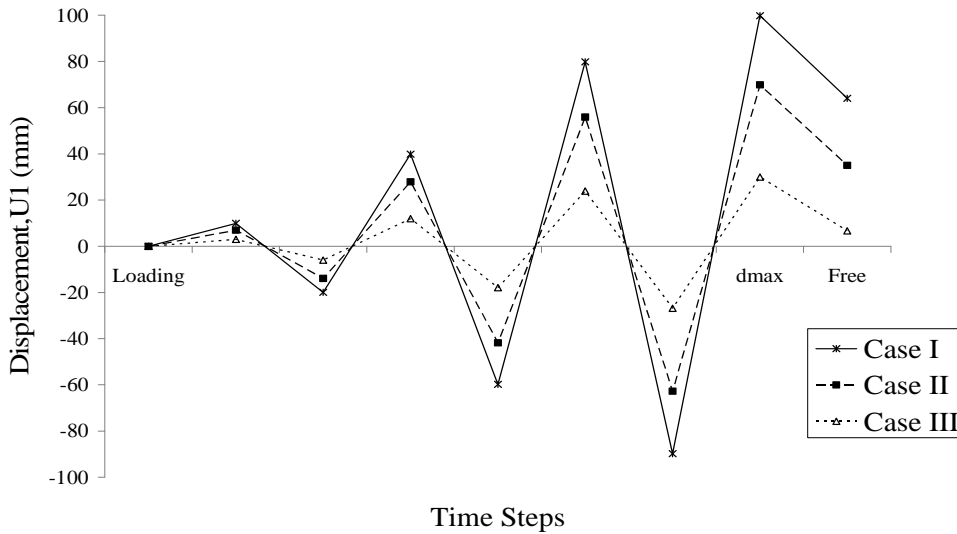


Fig. 6 Displacement history

Figure 7 shows the displacement history when after the frame is subjected to heating for all the three cases. The frame appears to stiffen under the heating and the residual displacements seem to recover. The reaction forced of the frame for the cases was observed in this study as shown in Figure 8.

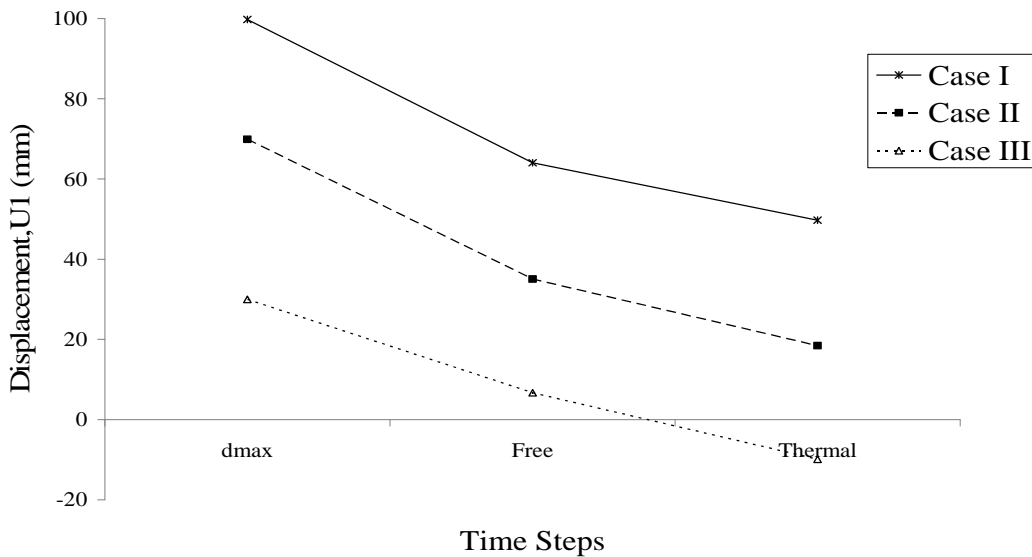


Fig. 7 Displacement of the frame after the temperature applied

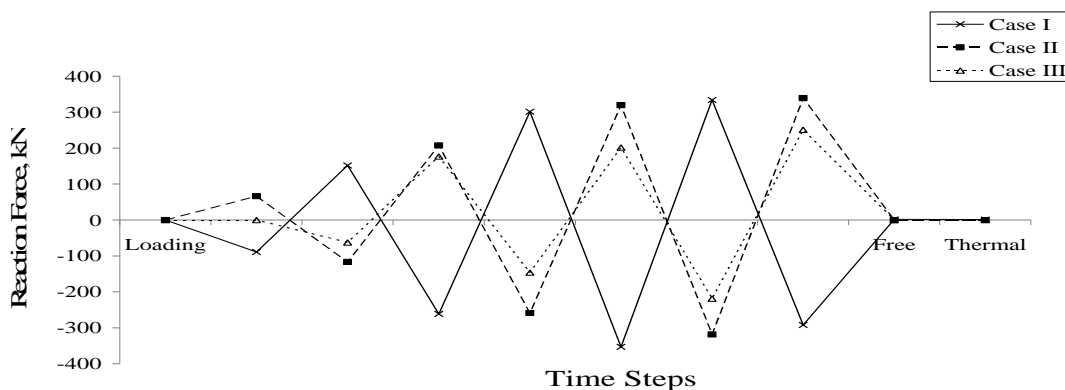


Fig. 8 Reaction force of the frame for the three cases

3 COMPARISONS

The eventual aim of this work is to compare the computational results with the test results on real frame currently being carried out at IIT Roorkee in India.. Both the model development and the tests are currently incomplete and full finding will be reported in future papers.

4 CONCLUSION

This study was carried out to model a number of experiments being conducted on 2D reinforced concrete frame exposed to the fire following simulated cyclic pushover. The computational analysis shows there is a reduction in the residual displacement of the frame after heating. Further studies need to be implemented to compare the computational analysis with the test results.

5 ACKNOWLEDGEMENTS

This study has been funded by Universiti Teknologi Malaysia. We would like to thank all members in the UK-India Education and Research Initiative (UKIERI) project group which has contributed the data.

REFERENCES

Abaqus: Abaqus Analysis User's Manual. Providence, Dassault Systemes Simula Corp,2008
 EN1992-1-2. Eurocode 2: Design of concrete Structures-Part 1-2: General Action-Actions on Structures Exposed to Fire, 1999.
 Mousavi, S. Bagchi, A. Kodur, V.K.R. Post-Earthquake Fire Hazard to Building structures, Canadian Journal of Civil Engineering, 35: 689-698, 2008
 Scawthon, C., Eidinger J.M. and Schiff, A.J., editors, Fire Following Earthquake, ASCE Publications, 2005.

TECHNIQUES FOR THE EVALUATION OF CONCRETE STRUCTURES AFTER FIRE

Emmanuel Annerel^a, Luc Taerwe^b

^aGhent University, Faculty of Engineering and Architecture, Department of Structural Engineering,

^bMagnel Laboratory for Concrete Research, Ghent, Belgium

INTRODUCTION

During a fire, concrete structures behave in most cases very well (Taerwe, 2008). It could therefore be of economic interest to repair the damaged structures, as costs for demolition and rebuilding can be avoided and the building can be reused faster. Different assessment techniques are possible to detect the internal damage (Annerel, 2009).

This paper studies the application of the Schmidt Rebound Hammer and colorimetry as tool to assess the fire damage of concrete structures. Firstly, experimental data is acquired under laboratory conditions on small specimens. Secondly, this information is used to evaluate the damage of a case study consisting of a girder exposed to a real fire. Both techniques show to be very useful in evaluating the fire damage and can provide the necessary information for a calculation of the residual load bearing capacity.

1 CONCRETE MIX

In this paper a traditional vibrated concrete with siliceous aggregates and ordinary Portland cement (TC) is studied. For 1 m³, it is composed of 640 kg sand, 525 kg gravel 2-8 mm, 700 kg gravel 8-16 mm, 350 kg cement and 165 liter water. Cubes with size 150 mm are cast and cured for 4 weeks in an air-conditioned room (RH >90%, 20±1°C), after which they are stored at 60% RH and 20±1°C for drying until further testing. The mean compressive strength at 28 days is 56.5 N/mm².

2 COLORIMETRY

At an age of 3 months, cores are drilled out of the cubes, sawn in 6 discs, polished and dried till testing time for at least two weeks at 60°C. Since this was repeated for another cube cast at a later time, a total of 24 discs were obtained. Two discs (belonging to different mixes) were heated without mechanical load at a heating rate of 30°C/min to the target temperature (till 1160°C), which was kept constant for 1h. The discs were slowly cooled in the oven, after which they were immediately tested for colour.

The colour is measured with an X-rite SP60 spectrophotometer according to the CIE Lab-colour space. In this colour system 'L*' is the lightness with values between 0 (black) and 100 (white), while 'a*' is spread between magenta (positive values) and green (negative values) and 'b*' is positioned between yellow (positive values) and blue (negative values). The coarse aggregates were masked with black ink to minimize the effect of the colourful aggregates. During heating the colour describes a path in the a*b*-colour space (Fig. 1), changing from grey at 20°C to red-pink at 300-600°C, to whitish grey at 600-900°C and buff at 900-1000°C.

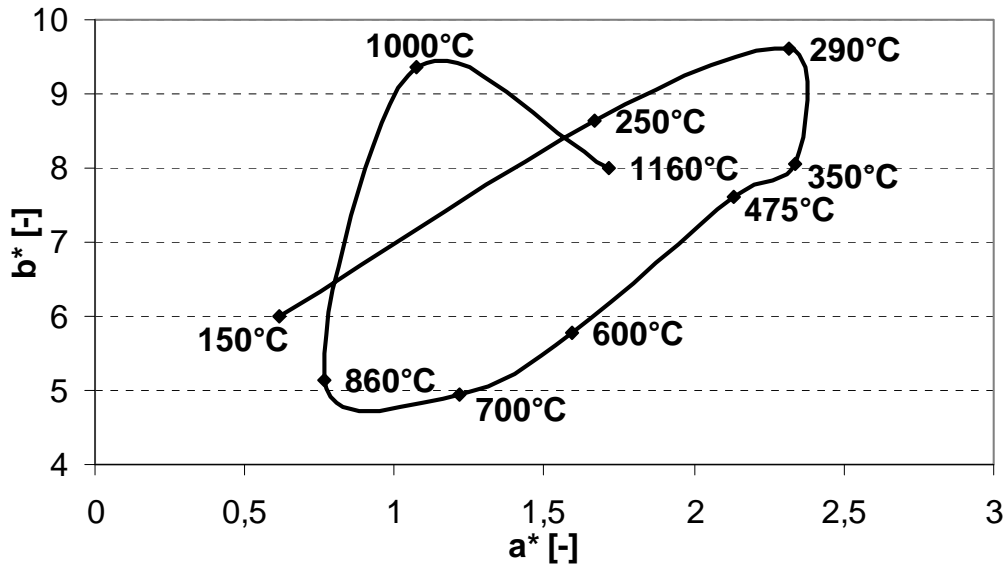


Fig. 1: Colour evolution of traditional concrete with masked aggregates

Similar colour paths can be found from cores drilled out of a heavily heated structure and cut in discs parallel to the fire exposed surface. Comparing the shape of these paths with Fig. 1 results in the detection of different isotherms, such as $\sim 300^{\circ}\text{C}$, $\sim 600^{\circ}\text{C}$, $\sim 800^{\circ}\text{C}$, $\sim 1000^{\circ}\text{C}$. On the other hand, the core can also be sawn in halves along its longitudinal axis. Study of the colour changes along this longitudinal axis would only result in the detection of the 300°C isotherm, since the temperature gradient is steep at the surface layers. Based on the found isotherms, the residual load bearing capacity can be calculated with the methods given in EN 1992-1-2:2004.

3 SCHMIDT REBOUND HAMMER

The influence of the temperature and storage conditions after fire are tested on half TC cubes heated till uniform temperatures of up to 600°C . The specimens are allowed to cool slowly in the furnace, after which they were stored for 28 days in water or in air (60% R.H., $20 \pm 1^{\circ}\text{C}$). Fig. 2 depicts the relative rebound index (RRI) tested immediately after cooling (0d) and after 28 days of storage, as well as the compressive strength loss measured on an additional series of heated cubes. RRI is calculated as the percentage of the rebound belonging to a target temperature after a storage period (RI_T) divided by the rebound of an unheated reference sample at the beginning of the storage period ($\text{RI}_{20^{\circ}\text{C}}$).

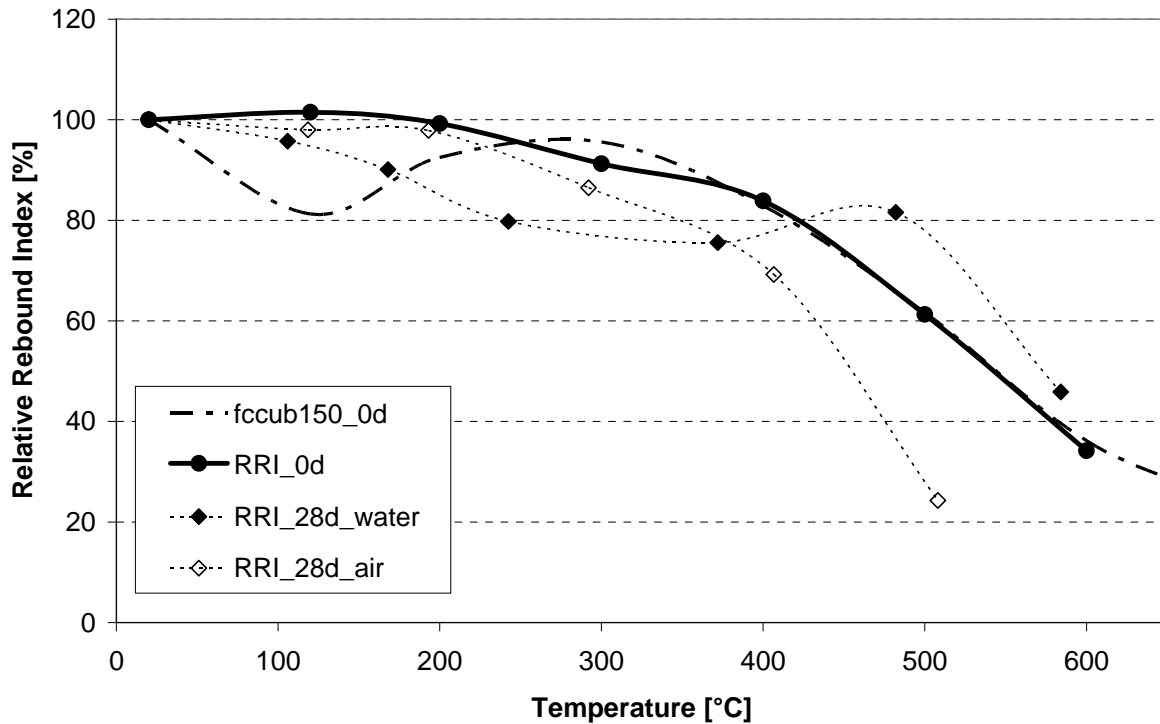


Fig. 2: Decrease of Rebound Index as function of temperature and storage conditions for traditional siliceous concrete

It appears that the results at 0 days after heating are close to EN 1992-1-2:2004 and the compressive strength decay of TC cubes (except for the strength drop at about 100°C). Differences in the evolution of the surface hardness between storage in water and in air are clearly visible. Below 400°C, a higher loss of Rebound Index is noticed for storage in water than in air. On the other hand, beyond 400°C, the surface hardness recovers strongly for specimens stored in water and a further decay is found for air storage. Due to atmospheric effects such as rain and sun, measurements on in-situ structures will be between the extremes as given on the graph.

Based on these results, the following criteria are formulated for the interpretation of the relative rebound index ($RI_T/RI_{20^\circ C}$):

- $RI_T/RI_{20^\circ C} \geq 0.85$: concrete element is superficially damaged only
- $0.85 \geq RI_T/RI_{20^\circ C}$: concrete element should be further investigated

The Schmidt Rebound Hammer can be used as a valuable tool to have a first attempt of the fire damage of concrete elements. Due to its penetration depth of about 30 mm, the degradation of the concrete cover is tested. This degradation is strongly related to the remaining load bearing capacity, since it protects the reinforcement from heating.

4 CASE STUDY: FIRE DAMAGE OF A GIRDER FROM AN INDUSTRIAL HALL

4.1 Description

In 2010 an industrial hall in Belgium consisting of pretensioned roof girders with a span length of 21 meters has burnt out. The fire started in the archive located at a mezzanine, just beneath the girders.

Fig. 3 shows the damage to one of the roof girders. Considering the colour change of the concrete surface, the surface temperature must have been around 900-1000°C. The roof consists of a composite concrete-steel slab, which has bent towards the fire. The concrete of the girder has spalled over a few centimetres. However, the strands are still covered with concrete and were not directly exposed to the fire. Therefore, it is investigated to which extent the fire damaged has

reached the reinforcement. This information is necessary for a calculation of the residual load bearing capacity of the girder.

The concrete cover of a reference girder is 36-40 mm for the stirrups and 45-50 mm for the strands when measured from the side faces. From the bottom, the cover is 39-40 mm for the strands.



Fig. 3 Fire damage of roof girder

4.2 Results Schmidt Rebound Hammer

Surface hardness readings are performed along the length of the girder, as presented in Tab. 1. Locations 1 and 2 are situated at half span length and in the zone with severe fire damage, while location 3 is at 2.5 m of the supports and approximately 4 m from the fire. The relative rebound index is calculated by means of the measurement of a reference girder found in the neighbouring construction with similar properties. It is clear that the fire has influenced the surface hardness ($RI_T/RI_{20^\circ C} < 0.85$) at locations 1 and 2, while location 3 is not affected.

Tab. 1 Schmidt Rebound Hammer measurements

Test location		Direction of measurement	Average	Standard deviation	$RI_T/RI_{20^\circ C}$ [-]
Reference girder	web	side	45.6	2.0	1.00
	flange	side	44.3	2.5	1.00
	flange	bottom	50.9	1.0	1.00
Location 1	web	side 1	36.8	1.8	0.81
	web	side 2	41.2	1.1	0.90
	flange	side 1	30.8	2.3	0.70
	flange	bottom	44.8	1.1	0.88
Location 2	web	side 2	38.0	1.4	0.83
	flange	side 2	30.0	5.7	0.59
	flange	bottom	39.6	1.7	0.78
Location 3	web	side 1	41.0	2.4	0.90
	flange	side 2	44.6	1.3	0.98
	flange	bottom	47.8	4.1	0.94

4.3 Results colorimetry

To know the depth of the fire damage inside the concrete, a core is drilled through the web of the exposed girder in the heavily damaged zone. The core has been exposed to fire from both sides. Damage is observed with the naked eye till a depth of 12 mm from one side and 10 mm from the other side. Based on these findings, the zone between 50 and 70 mm is assumed to be not affected by the heat and is taken as reference. From recordings with the spectrophotometer, a fire damaged zone of 25 mm from the first side and 13 mm from the other side can be detected (Fig. 4). The

values near to the surface can be related to temperatures of about 300-600°C (based on Fig. 1). These depths of fire damage are below the measured concrete cover thicknesses. Therefore, the reinforcement has not been heated to critical temperatures and the load bearing capacity of the girder should be adequate.

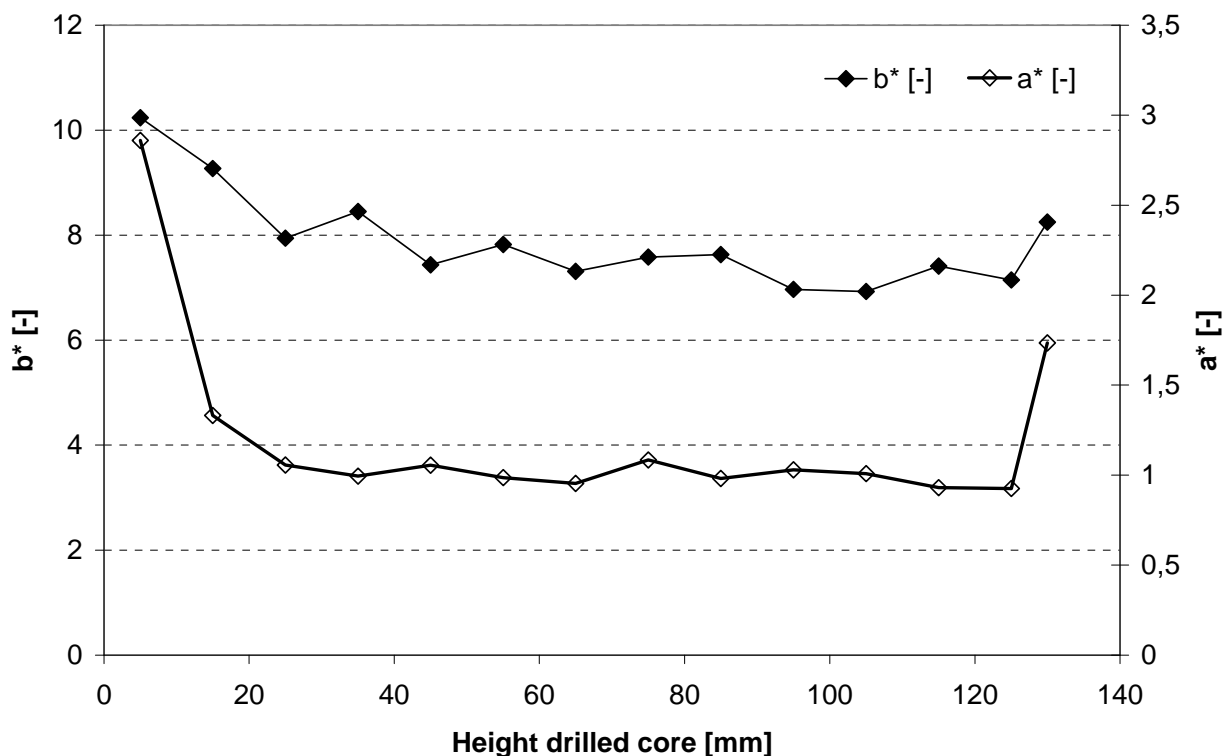


Fig. 4: Development of a^* and b^* over the body of the girder

5 CONCLUSIONS

- With increasing temperature, the concrete colour describes a colour path in the a^*b^* colour space.
- Experimental laboratory work results in a critical relative rebound index of 0.85 for siliceous concrete.
- Both techniques proved to be useful to detect the extent of fire damage of a concrete girder exposed to a natural fire.
- Although a pretensioned girder was exposed to high temperatures, the remaining bearing capacity is assumed to be sufficient since the strands are not heated.

6 ACKNOWLEDGEMENT

The authors would like to thank the Fund for Scientific Research in Flanders (FWO) for the financial support through the research grant “Damage assessment and estimation of the residual strength of concrete members after exposure to fire”.

REFERENCES

- Taerwe L., Annerel E., Loading test on a retrofitted pretensioned concrete girder after fire, Proceedings of the 2nd International Conference on Concrete Repair, Rehabilitation, and Retrofitting (ICRRR), Alexander, M. et al. (Eds.), CRC Press, Cape Town, 2008.
- Annerel E., Taerwe L., Revealing the temperature history in concrete after fire exposure by microscopic analysis, Cement and Concrete Research, vol. 39, Issue 12, 2009.

THERMAL DIFFUSIVITY OF TENSILE CRACKED CONCRETE

Adam Ervine ^a, Dr. M. Gillie ^a, Dr. T.J. Stratford ^a, Dr. P. Pankaj ^a

^a University of Edinburgh, School of Civil, Edinburgh, UK

1 INTRODUCTION

Safety and economic considerations dictate that structures are built to resist extreme events, such as a major earthquake or fire, without collapse but some structural damage may be allowed. However, in seismic regions, a fire following an earthquake is considered to be a major threat due to the risk of ignition of damaged gas and/or fuel services. The fire resistance such as the concrete cover of the structure may be compromised during the earthquake period; hence the effect of a subsequent fire will be amplified and may lead to collapse of the structure.

This study examines the effect of tensile cracking on the thermal properties of reinforced concrete. Concrete beams in four-point bending are heated on their tensile faces. A comparison is made between the thermal response when the beam is undamaged, and subject to minor or major damage. Whilst the thermal conductivity of concrete is well documented, most available data relates to concrete that is undamaged. There are many scenarios (e.g. analysis of structures subject to fire following earthquake) in which knowledge of the conductivity of damaged concrete may be important. This is because the conductivity of damaged concrete may be significantly different to that of undamaged concrete and could lead to earlier structural failure in fire. The experiments detailed in this paper were designed to establish if tensile cracking resulting from damage alters the effective thermal diffusivity ($k/\rho c$) of concrete to a degree that can not be neglected in analyses of fire affected structures. Three hypotheses are considered,

1.1 Hypothesis I

Tensile cracking affects the thermal diffusivity of concrete so that heat transfer is more rapid, hence the reinforcement layers will experience high temperatures more quickly than in an intact section. This would cause the steel to be subjected to localised heating and elongation which could lead to failure of a member or structure more quickly than an undamaged structure.

1.1 Hypothesis II

Tensile cracking affects the thermal diffusivity of concrete so that heat transfer is less rapid, hence the reinforcement layers will experience high temperatures later in a fire than an intact section. This could cause structures to perform better than an undamaged structure..

1.1 Hypothesis III

Tensile cracking does not significantly affect the thermal diffusivity of concrete. The reinforcement layers will experience similar temperatures in a similar time to those experienced by an intact section. This would mean that the effects of tensile cracking on thermal diffusivity are negligible and do not need to be accounted for in analyses or design.

2 PREVIOUS WORK

There has been research into the thermal properties of concrete and how they vary with temperature. Similarly, there has been work on the cracking of concrete and reinforced concrete in tension. However, these research themes have yet to be fully combined to determine the thermal properties of cracked reinforced concrete.

Kong *et al* (2007), and Beeby and Scott (2005) studied the behaviour of average tensile crack width with respect to the tensile stress within reinforcement. However the stresses and strains considered all fell into the elastic region of the reinforcement which corresponds to very small crack widths (of the order of 1×10^{-1} mm). It would be inappropriate to extrapolate this information to situations where concrete members are damaged because in such cases the reinforcement steel may have yielded and cracks reached widths in the order of 1 e^1 mm or greater.

Vejmelková *et al* (2009) studied the effects of cracks on the hygric and thermal characteristics of concrete and obtained data suggesting the conductivity of cracked concrete decreases due to the increased porosity of the material and only increases with an increase in moisture content. They suggested that the air within cracks acts as an insulator and hence hinders the propagation of heat through the structure. A significant limitation of this work is the fact that the crack dimensions were not reported so the results cannot be combined with Kong *et al*'s work to find a relationship between crack width and conductivity. Furthermore, plain, not reinforced concrete was used so application of the results to real structures would be difficult in any case.

Thus, work aimed at determining the thermal properties of crack damaged reinforced concrete is very limited. The work that has been undertaken has either been with un-reinforced concrete or within the elastic range of the reinforcement. The inclusion of reinforcement in the concrete during an experiment that considers cracking is vital because the reinforcement drastically alters the cracking pattern and crack propagation through a section. During extreme events such as earthquakes and blast it is unreasonable to assume that the reinforcement remains within its elastic range as these extreme events will cause larger cracks to form in the concrete. The larger the cracks within the concrete cover the more influential the buoyancy effects within these cracks become. The air within the cracks may no longer act as an insulator as Vejmelková *et al* suggest but may effectively allow the heat to instantaneously penetrate the concrete to the reinforcement level.

3 EXPERIMENTAL DESCRIPTION

An experimental programme was undertaken to establish which of the three hypotheses detailed in the introduction is most representative of reality. To do this beams in four point bending were heated on their tensile faces and rate of heat transfer measured for different crack widths. The beams used were doubly reinforced 35MPa (nominal) concrete with dimensions of $90 \times 160 \times 870$ mm. The reinforcement was 10Φ mm 460MPa steel. Concrete cover was 20mm on all sides with the exception of the tensile face which had a cover of 40mm. Increased cover on the tensile face was designed to induce larger tensile cracks which would be representative of beams of larger, more realistic dimensions. The beams were then loaded vertically upwards as shown in Fig. 1, either to failure or to the required deflection depending on the stage of the experiment (see Tab. 1). Heating was applied from above via a radiant gas panel.

Loads were recorded from load cells that sat under the loading jacks and deflections from gauges at mid-span and other key locations. Load and deflection data was recorded at 2s intervals. Strain fields within the area of zero shear were recorded using image correlation by taking photographs of both sides of the beam at 5s intervals and processing these with a program developed by Bisby, Take and Caspary. Temperatures in the beam during both the heating and cooling phases were recorded using a large number of thermocouples within the heated section of the beam, with the highest density being in the tensile concrete cover. Full details of the apparatus are shown in Fig. 1 to Fig. 3.

Beams were tested with various heating and loading arrangements as detailed in Table 1. Critical to the test programme was comparing the heat-transfer in the beams when they were damaged to different degrees. The behaviour of beams with "minor" and "major" damage was compared. To allow damage levels to be defined, two beams were loaded without heating and their load-deflection behaviour recorded. Minor damage was defined as the crack width that occurred when an unheated beam was loaded to point at which it ceased to behave linearly. Major damage was defined as the crack width that occurred when an unheated beam was loaded to its ultimate load. Crack widths of these magnitudes were maintained during the thermal tests by controlling the deflections of the beams.

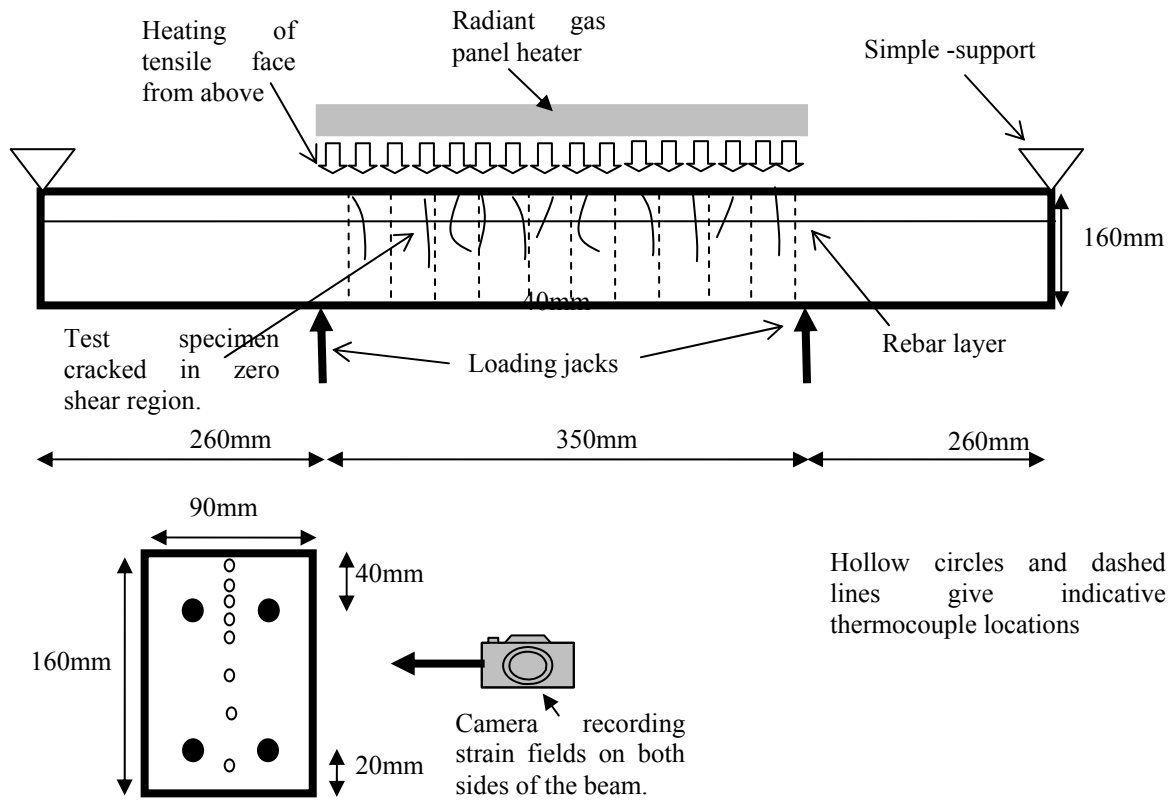


Fig. 1 Experimental setup showing side view of loaded beam and a typical cross-section.



Fig. 2 Loading set-up

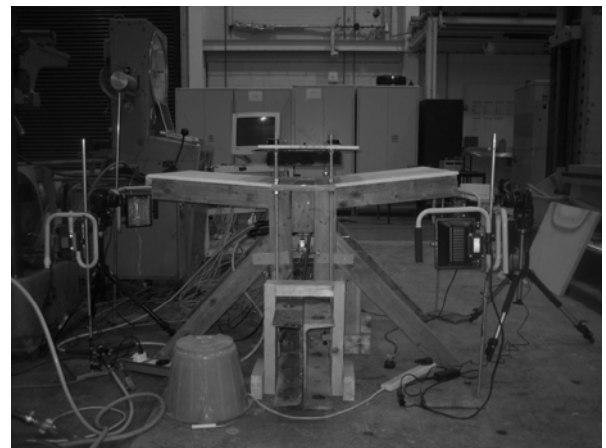


Fig. 3 General thermo-mechanical set-up

Table. 1 Loading permutations examined during the test programme.

Permutation	Thermo-couples	Loading Phase	Heating Phase	Aim
1	-	√	-	Load incrementally to failure to determine crack widths and distribution as function of load
2	-	√	-	Repeat of permutation 1
3	√	√	√	To determine effect of minor damage on thermal behaviour.
4	√	√	√	To determine effect of minor damage on thermal behaviour.

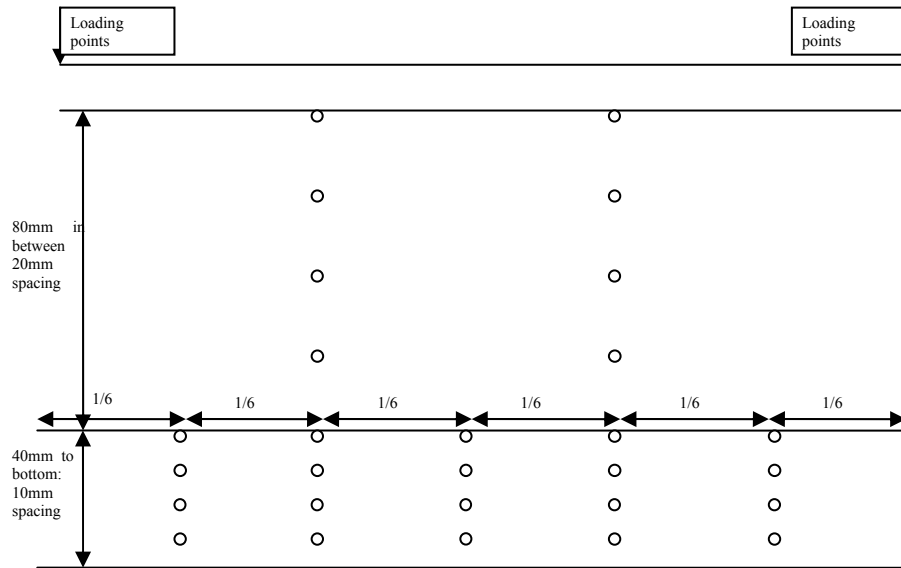


Fig. 4 Placement of thermo-couples

As the investigation is to determine if tensile cracking has any effect on the thermal diffusivity the majority of the thermo-couples were placed within the concrete cover on the tensile side of the beam. This can be seen in Fig. 4.

3 EXPERIMENTAL RESULTS

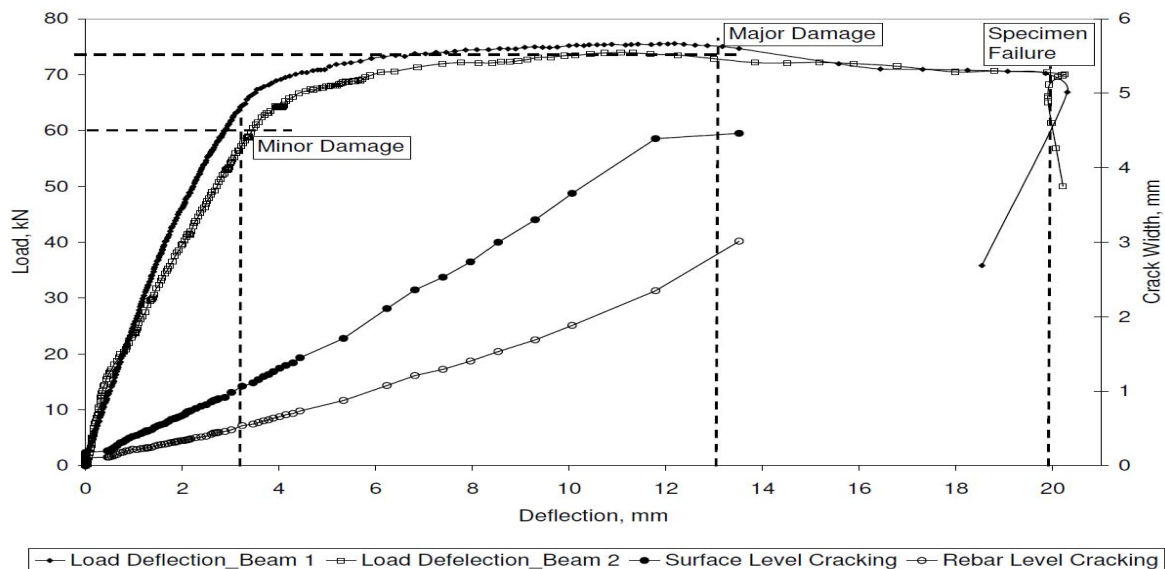


Fig. 5 Load versus deflection (left axis); Crack width versus Deflection (right axis)

3.1 Definition of Damage

From Fig. 5 it can be seen that the beams subject to purely mechanical load behaved similarly. Transition from elastic to plastic behaviour occurred at approximately 60kN with a mid-span deflection of 3.5mm and the ultimate load was approximately 75kN (approximately 1.3 times the design load). These results therefore can be used as measures of minor and major damage states in terms of crack widths. The label "minor damage" will be defined as a state that occurs under reasonable serviceability loads; whilst "major damage" will be defined to occur some way into the plastic region. Therefore, the minor damage state will be set to experience loads in the region of 60kN and a mid-span deflections of 3mm; whereas the major damage state will be set to experience loads in the region of 74kN and a mid-span deflection of 12.5mm. Images of these states can be seen in Figs 6 and 7.

Table. 2 – Damage State Summary

	Minor Damage	Major Damage
Load, kN	60	74
Mid-span Deflection, mm	3	12.5
Average Surface Crack Width, mm	0.75	3
Average Rebar Level Crack Width, mm	0.4	1.5

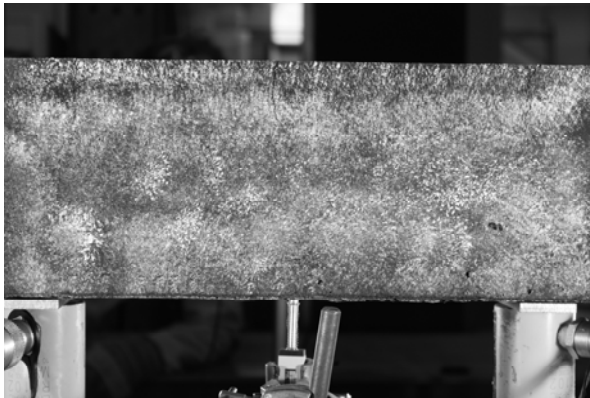


Fig. 6 Minor damage image

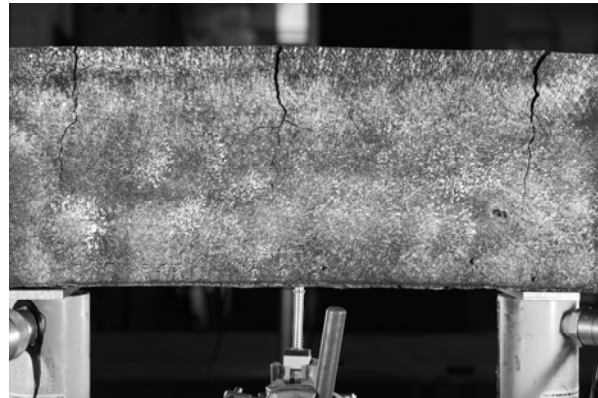


Fig. 7 Major damage image

3.2 Thermal Results

Figs. 8 and 9 show the curves from averaged thermocouple temperatures at depths of 10mm to 40mm (i.e. level of tensile reinforcement). In both figures there is a clear change in gradient at about 100°C for all curves. This is caused by the latent heat required to evaporate the moisture from the concrete during heating. Throughout the heating phase differences are seen between the damaged and undamaged cases whilst during cooling the differences are no longer present. The differences are largest for the case of major damage (Fig. 9) and also at greater depths. The recorded differences in temperatures between the damaged and undamaged cases remain small at all times (a peak difference of about 10% occurs for major damage at around 2000s and 40mm depth).

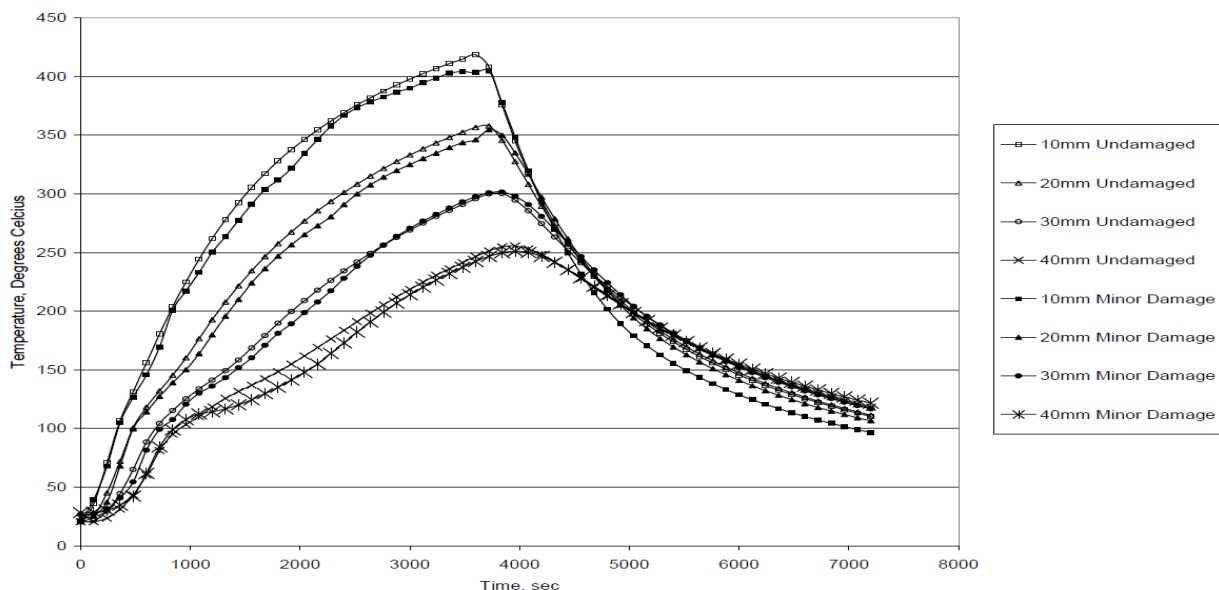


Fig. 8 Comparison of thermal profiles for minor and major damaged sections

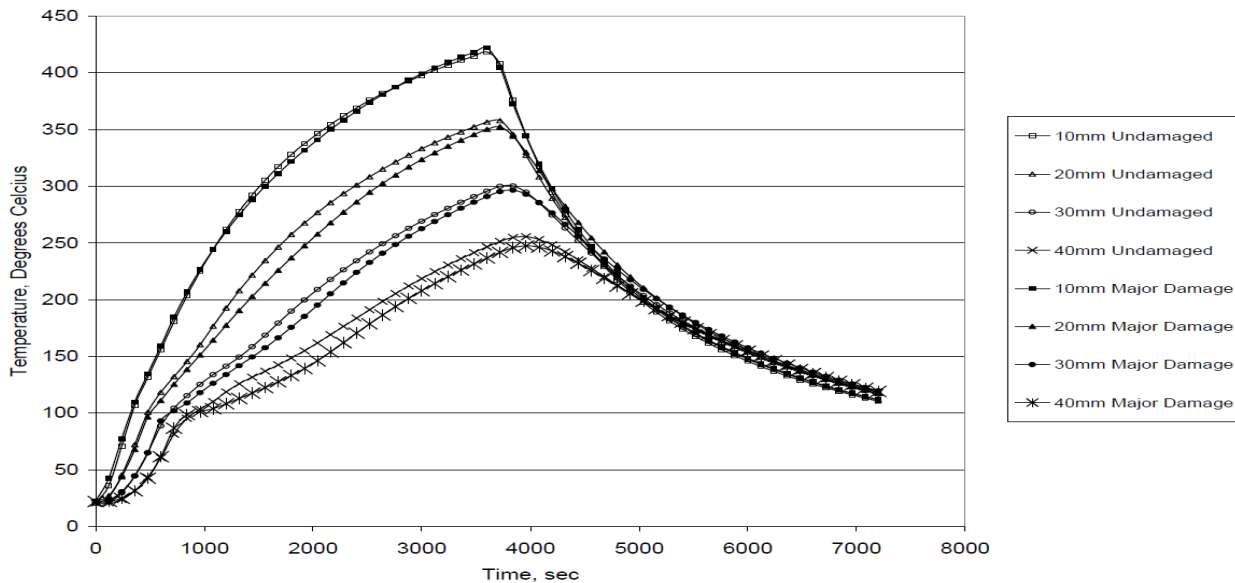


Fig. 9 Comparison of thermal profiles for minor and major damaged sections

4 CONCLUSIONS

The main conclusion of this work is that there is no significant increase or decrease in the thermal diffusivity of concrete with tensile cracking where the cracks are up to the order of 10^1 mm at the heated surface. Therefore hypothesis III, as defined in the introduction, can be broadly accepted whilst hypotheses I and II are rejected. This conclusion is significant because it implies that in calculations, thermal material properties do not need to be made a function of strain or crack width for the conditions covered within this investigation. This information is particularly relevant for numerical simulations. Performing thermal then mechanical analyses of heated structures sequentially, as is typically undertaken currently, remains a valid approach. It remains the case that fully coupled thermal-mechanical analyses, which involve substantially more complex numerical solutions, are not necessary for structural calculations even when significant tensile damage is induced in the structure.

REFERENCES

- Vejmelková, E., Padevět, P. and Černý, R., Effects of cracks on hygric and thermal characteristics of concrete, Ernst & Sohn (2009)
- Beeby, A.W. and Scott R.H., Cracking and deformations of axially reinforced members subjected to pure tension, Magazine of Concrete Research, (2005), 57, No.10, December 611-621
- Kong, K.L., Beeby, A.W., Forth, J.P. and Scott R.H., Cracking and tension zone behaviour of RC flexural members, Structures and Buildings 160 Issue SB3 (22/03/2007), 165-172
- Bisby, L., Take, A.W. and Caspary, A., Quantifying Strain Variation in FRP Confined Concrete using Digital Image Correlation: Proof-of-Concept and Initial results, Department Civil Engineering, Queen's University, Canada

COLOUR CHANGE OF HEATED CONCRETE

RGB colour histogram analysis as a method for fire damage assessment of concrete

Izabela Hager^a

^a Cracow University of Technology, Faculty of Civil Engineering, Cracow, Poland

INTRODUCTION

The assessment of fire damage to concrete structures usually starts with a visual evaluation, which consists of observing the presence of changes caused by heat exposure. In order to simplify this task, a four-degree classification of damage to beams, columns and slabs (LCPC, 2005, The Concrete Society, 2008) has been developed, which includes the usual repair methods for each class of damage. The condition of members is classified through the assessment of the following parameters: the presence of soot and smoke deposits; the colour change of concrete; concrete flaking or spalling; the presence of cracks and microcracks; the degree to which reinforcing steel is exposed; and possible visible deformation to the structure (excessive deflection of beams and lateral distortion of columns). Most of the in situ techniques used to assess the condition of concrete after being exposed to fire are well-known methods, widely used to check the properties of concrete in structures. In case of fire damage, laboratory techniques are also frequently used to assess concrete integrity. These tests require the sampling of material and laboratory testing. The tests carried out on concrete core samples are designed to determine the residual mechanical properties of the damaged concrete (direct method) or else to estimate the temperature to which the concrete was exposed during the fire (indirect methods). Such tests include resonance frequency method, ultrasound method, DTA, TGA, X-ray diffraction, scanning microscopy, thermoluminescence, chemical or petrographic analyses or colourimetry.

1 COLOURIMETRY APPLICATION

Colourimetry is an indirect method that uses the fact that when concrete is heated, its colour changes. Colour changes caused by temperature within construction concrete are easy to identify by means of visual comparison with concrete unaffected by high temperature. However colour change is not directly related to changes in the mechanical and physical properties of concrete, but provides an indicator of the temperature achieved by the concrete during fire. Temperature data can be used for a quantitative estimation of properties such as the compressive strength or modulus of elasticity when the $f_c(T)$, and $E(T)$ relationship are identified.

The existing technique of a rough estimation of the temperature to which concrete was subjected involves an inherently subjective visual colour analysis. It is generally agreed (Short et al, 2001) that when heated up to between 300 °C and 600 °C concrete will turn red, between 600 °C and 900 °C it will turn whitish-grey, and heating to between 900 °C and 1000 °C gives the concrete a buff colour. The most pronounced changes in colour occur in concretes made from silicate aggregates which become red or pink when heated to between 300 °C and 600 °C The red colouration in the temperature range is caused by the oxidation of mineral components with iron compounds (oxides or hydroxides, etc.).

In order to describe concrete colour changes in a precise manner, a variety of colour description techniques are used (Short et al., 2001, Luo, Lin, 2007, Annerel, Taerwe, 2009, Felicetti, 2004).

In the tests conducted by Faure and Hemond described in (LCPC n°62, 2005), a spectrophotometer was used directly on the surface of concrete samples. The method used by Short (Short et al., 2001) consisted of observing samples through a polarising microscope equipped with a colour analysing software package. The technique proposed by Felicetti (Felicetti, 2004) employs a general purpose digital camera for taking pictures and analysing the colour changes of the concrete depending on the temperature reached. The latter method, however, requires consistent lighting, which is not easy to

achieve. A light tent is required, and the white balance of the camera has to be adjusted. Recently, the author proposed a technique in which a flatbed scanner (Hager, 2010) is used to obtain constant lighting conditions while pictures of concrete samples are taken. No expensive measurement equipment and/or colour analysis computer software is necessary to perform these measurements. In this method, pictures taken with a general-purpose scanner (HP Scanjet G2410) are analysed using an image analysis software package, in this case Scion Image (version 4.0.3, Scion Corporation ©, USA). The Scion package is a freeware tool created to facilitate digital image analysis within the medical sector. In terms of the method proposed for concrete analysis, a digital image is split into three RGB (Red Green Blue) colour components – red, green and blue – then presented as a histogram using counts of pixel intensity. The results of the histogram show colour distribution in unheated concrete and in concrete heated across a temperature range from 100 °C to 1000 °C. Histograms from laboratory-heated concrete provide a scale which is then used to determine the temperature actually reached by concrete in a structure. This is done by comparing the scale images with the images of cored samples taken from the structure. The method offers a simple and inexpensive way of identifying the areas or depth of the concrete affected by fire temperature.

In general, two different approaches can be used when using colour analysis to assess the condition of concrete after a fire. First, the external surface of the element can be examined; this involves the observation of an element's outer walls – in particular, the cement paste. By examining the extent of change of the element's surface colour, the impact of the temperature can be assessed. However this method is not feasible if the surface has been affected by smoke or covered with soot. The other option is to observe the surface with visible aggregates. This is the engaged, cored, or spalled surface of the element. The observation consists of examining the surface with exposed aggregate grains or a cut surface produced as a result of coring or sawing. These processes reveal aggregate grains that, during heating, often significantly change into more intense red or pink colours. This change is more pronounced and easier to distinguish than the change of the cement paste.

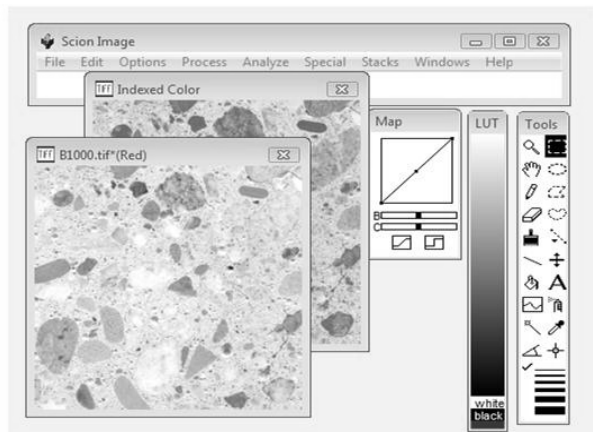


Fig. 1 Scion Image environment.

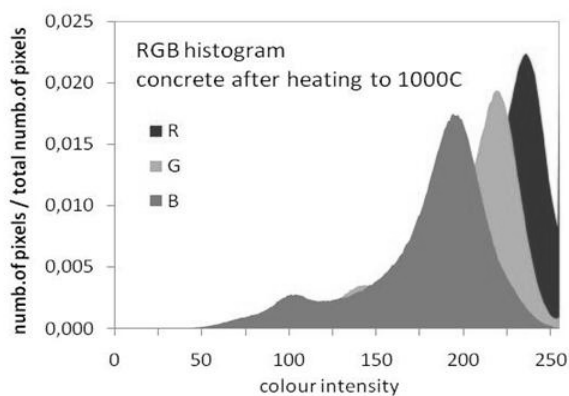


Fig. 2 RGB normalized histogram.

2 SOFTWARE DESCRIPTION

The Scion Image package v. 4.0.3, (Scion Corporation ©, USA) is an image processing and analysis program. It can acquire, display, edit, enhance, analyze and animate images. It reads and writes TIFF and BMP files, providing compatibility with many other applications, including programs for scanning, processing, editing, publishing and analyzing images. It supports many standard image-processing functions, including contrast enhancement, density profiling, smoothing, sharpening, edge detection, median filtering, etc. Scion Image for Windows can be used to measure user-defined regions of interest for an element including its area, centroid, perimeter, etc. It also performs automated particle analysis and provides tools for measuring path lengths and angles. Results can be printed, exported to text files, or copied to the program's clipboard. It supports multiple windows and eight levels of magnification.

All editing, filtering, and measurement functions operate at any level of magnification and can be undone. Scion Image manipulates, displays and analyses images. Images are two-dimensional arrays of pixels (picture elements). All pixels are represented by Red Green Blue values ranging from 0 to 255. The software environment is presented on Fig. 1.

3 MATERIALS AND TESTING PROCEDURE

The tested materials were on ordinary (OC) and high performance (HPC) concretes, mortars and cement pastes. Both concretes consisted of the cement type CEM II/A-V 42.5R, water and natural riverbed aggregates: sand 0-2 mm; gravel 2-8 mm and 8-16 mm. The mix composition of concretes is given in Table 1. The mortars and cement pastes were confectioned with the same cement and w/c (water/cement) ratio than concretes.

Tab. 1 Concretes mix proportions

	Unit	OC	HPC
cement CEM II/A - V 42,5 R	kg/m ³	322	478
water	dm ³ /m ³	193	129
w/c	-	0,6	0,27
sand 0 - 2 mm	kg/m ³	623	
gravel 2 - 8 mm	kg/m ³	660	
gravel 8 - 16 mm	kg/m ³	550	

The colour change observation was performed on the surfaces of the sample concretes, mortars and cement pastes. The samples were heated in an electric furnace with a constant heating rate of 1°C/min to reach subsequent temperatures of T =100, 200, 300, 400, 500, 600, 700, 800, 900 and 1000 °C. After cooling digital images were taken from the sample surfaces with scanner.

A general-purpose flatbed scanner (HP Scanjet G2410) was used. The pictures were taken with a pixel density resolution of 600 ppi. The images were then exported as TIFF raster files into the Scion Image software described above. It features an option to export the results in a text file for further processing. The testing was based on the RGB colour model because of its widespread use in digital equipment (scanners and computer screens). The RGB model is of the additive type, where adding the RGB components produces colours.

The digital images of samples surfaces were decomposed into RGB components using Scion Image. The frequencies of occurrence of red, green and blue pixel components were presented as frequency histograms. The RGB model assumes intensity levels ranging from 0 to 255 that are shown on the horizontal axis where black equals 0, and white 255. On the vertical axis the numbers of pixels of a certain intensity in an image are presented.

The testing involved a normalisation process where the values corresponding to the number of pixels with a specified intensity were divided by the total number of pixels in a given image (Fig.2). Histogram normalisation makes comparison of images with different pixel counts possible. Additionally, the process produces functions that have properties of the probability density function (Hager, 2010). Histograms can be used to generate a number of parameters defining the properties of this function, including the maximum and standard deviation values, curtosis, etc. Differences between these parameters reflect different properties of the image histogram and allow for comparisons.

4 RESULTS

The results of the testing of the impact of heating temperature on the colour change of ordinary and high performance concretes, mortars and cement pastes are presented in Fig.3.

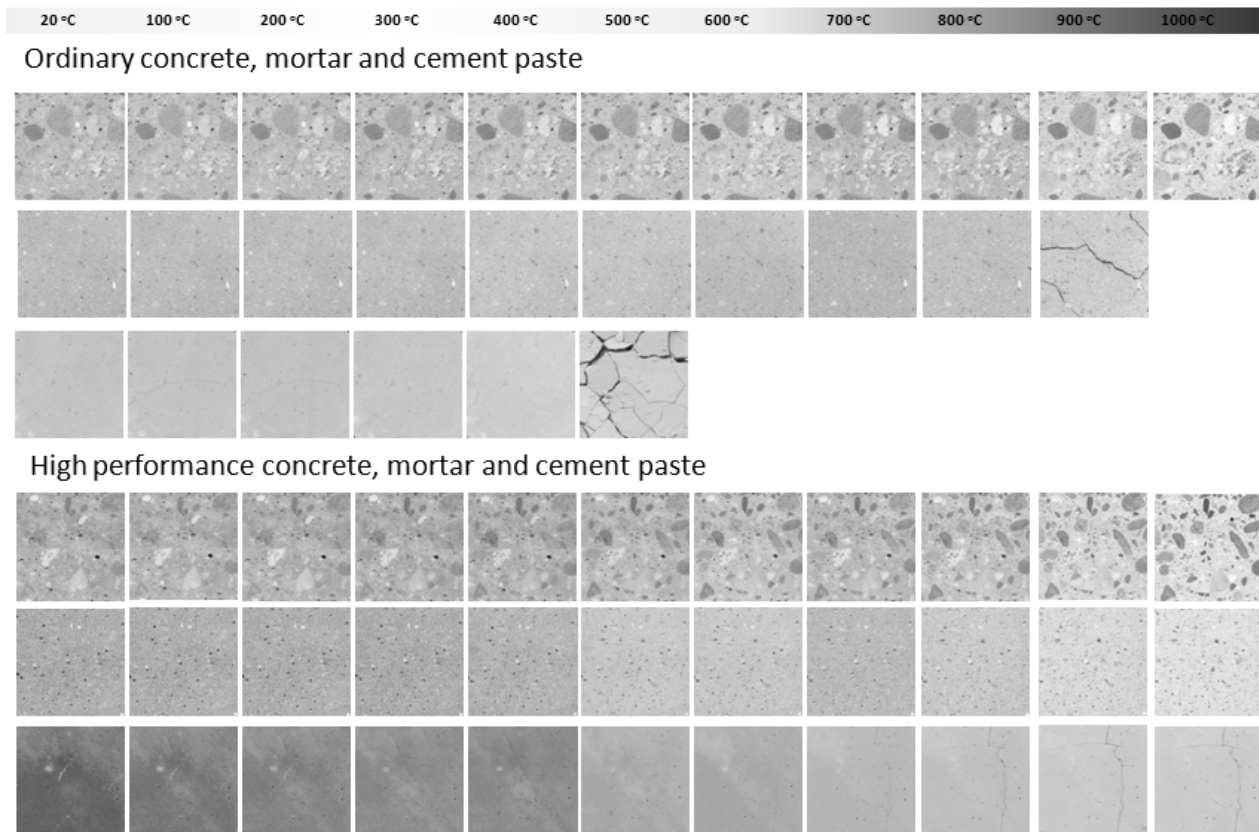


Fig. 3 Colour change of ordinary and high performance concretes, mortars and cement pastes heated to temperature ranging from 100 to 1000 °C.

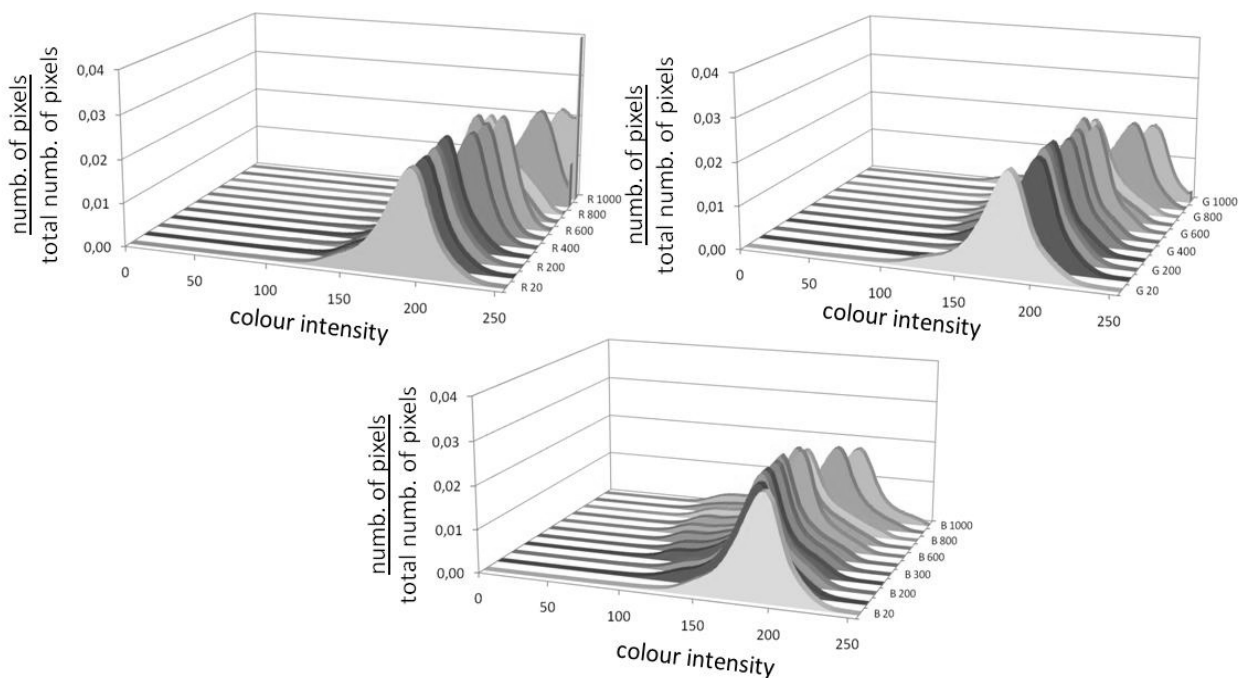


Fig. 4 A comparison of normalised histograms of the red, green and blue component intensity values obtained for an ordinary concrete samples in the range of temperatures from 20 to 1000 °C.

As an example, for ordinary concrete the normalised histograms of the red, green and blue components (Fig. 4) are presented as a function of heating temperature.

Colour changes observed as a result of heating were mainly caused by water evaporation and dehydration of cement paste and chemical reactions in the mineral components of the aggregate. The most intense colour change was observed in components containing minerals including iron (jarosyite, goethite). As temperature rises, aggregates and components containing calcium carbonate CaCO_3 go through the process of calcination and their colour is dominated by pale shades of white and grey.

The samples of concretes used in this study were also tested in compression in order to determine a relationship between the strength parameters of the material concerned and the temperature of exposition. To this end samples in the form of a 15 cm cube were heated at a rate of $0,5^\circ\text{C}/\text{min}$. to reach the target temperatures of 200, 400, 600 and 800 °C. Once the temperature was reached the samples were heated for five more hours to stabilise the temperature across the section. The samples were then cooled down to 20 °C and tested in compression. The chart on Fig. 5. shows the residual compressive strength of tested HPC and OC concretes.

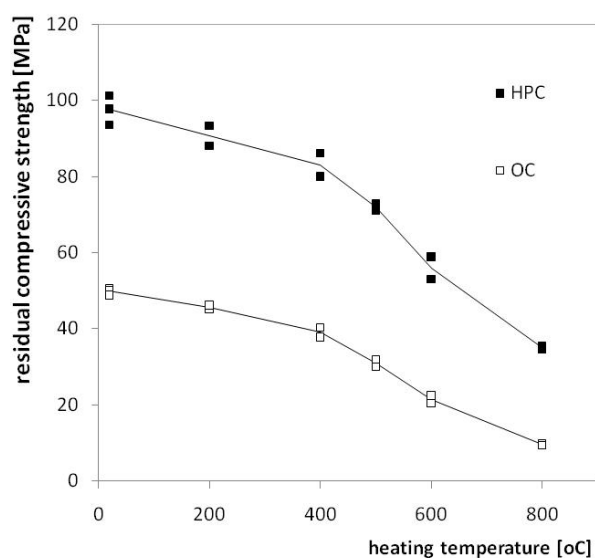


Fig. 5 Residual compressive strength of a) ordinary concrete, b) high performance concrete as a function of temperature.

5 SUMMARY AND ACKNOWLEDGMENT

During a real fire, temperatures within a concrete section do not generally reach equilibrium values. A thermal gradient is established where the temperature of the outside layers is drastically increased, while the temperatures of the inner concrete may be relatively low. The method described in the paper is the useful technique for estimating the maximal exposition temperature of concrete subjected to fire by using an analysis of the colour image. A scanner seems to be a useful and simple tool for making digital images of samples/cores resulting in guaranteed consistent lighting conditions. The scanner requires no special preparation of the samples. A similar degree of usefulness and simplicity was established with regard to the colour analysis using the RGB model and the readily available software package Scion Image. A calibration scale was produced by taking images of concrete samples heated to temperatures across the 100 - 1000 °C range. The scale can be used to estimate the exposition temperature of concrete in structures subjected to a real fire. In practice, several techniques should be combined in order to obtain a sufficiently complete and accurate picture of the damage to the concrete member in question.

The study was supported in part by the Polish Ministry of Higher Education Grant N N506 045040.

REFERENCES

- LCPC n°62, Présentation des techniques de diagnostic de l'état d'un béton soumis à un incendie, Laboratoire Central des Ponts et Chaussées, Paris, France, 2005, p. 114.
- Assessment, Design and Repair of Fire-Damaged Concrete Structures, Technical Report No.68, The Concrete Society, London, United Kingdom, 2008, p.80.
- Hager I., The Application of RGB Histogram Analysis of Colour Images as a Method of Assessing the Condition of Concrete in Structures After Fire, Proceedings 6th International Conference on Structures in Fire SiF'10, Michigan State University, East Lansing, United States of America, 2-4 of June of 2010, ed.: Venkatesh Kodur, Jean-Marc Franssen
- Hager, I., Methods for assessing the state of concrete in fire damaged structures, Cement Lime Concrete, July / August 2009, nr 4, p. 167-178.
- Annerel E., Taerwe L., Revealing the temperature history in concrete after fire exposure by microscopic analysis, Cement and Concrete Research 39 (2009)
- Felicetti, R. Digital camera colorimetry for the assessment of fire-damaged concrete, in: P.G. Gambarova, R. Felicetti, A. Meda, P. Riva, Proceedings of the Workshop: Fire Design of Concrete Structures: What now? What next? fib Task Group 4.3 'Fire Design of Concrete Structures', Milan, 2004, pp. 211–220.
- Luo H. L., Lin D.F. Study the surface color sewage sludge mortar at high temperature, Construction and Building Materials 21 (2007), p 90-97
- Short N. R., Purkiss J. A., Guise S. E., Assessment of fire damaged concrete using colour image analysis, Construction and Building Materials, Vol. 15 (2001) p. 9-15.

INFLUENCE OF TRANSIENT STRAIN ON FIRE RESISTANCE OF CONCRETE ELEMENTS

Limin Lu ^a, Emmanuel Annerel ^a, Luc Taerwe ^a, Yong Yuan ^b

^a Ghent University, Faculty of Engineering and Architecture, Department of Structural Engineering, Ghent, Belgium

^b Tongji University, Department of Civil Engineering, Shanghai, China

INTRODUCTION

Reinforced concrete (RC) elements generally have good fire-resistance ability. Knowledge of the temperature dependant material properties of concrete and steel bars is important for understanding of the fire-response of a RC structure. At high temperatures, the total strain of concrete is for a large extent influenced by load dependent strains, the so called transient strain and creep strain. Although these types of strain are not considered in simplified calculation procedures of concrete elements exposed to fire as provided in EN 1992-1-2, they may be of major importance for the development of deformation during heating (Sebastjan Bratina, 2006; Paolo Riva, 2002).

Based on the mechanical properties of concrete and steel bars at elevated temperatures as given in literature (EN 1992-1-2, Jin, Tao 2009), a numerical model which includes transient strain and creep strain is proposed. The computational procedure consists of a coupled thermo-mechanical analysis, including the development of the temperature, the deflection and ultimate bending moment. The proposed approach is validated by experimental data from fire tests executed on simply supported slabs exposed to an ISO 834 fire load. The influence of transient strain is analyzed by comparing the calculating results.

1 NUMERICAL MODEL

1.1 General

The proposed method is based on an average stiffness method to analyze reinforced concrete elements subject to bending. The numerical process is performed in three steps: 1) thermal calculation; 2) mechanical properties of the cross section and 3) structural analysis.

The RC element is divided into a number of small segments along its length (Fig.1). The mid-section of each segment represents the behavior of the whole segment. Firstly, the thermal field of the cross sections is analyzed at each time step and then material properties are adjusted according to the obtained temperatures. Secondly, the stiffness of each segment is generated by sectional stress strain analysis using the changing properties of concrete and steel bars. The ultimate bearing moment can also be generated during this process. Thirdly, average stiffness of the element will be induced based on the conclusions of sectional analysis, and the deflections can be calculated by structural analysis.



Fig.1. RC element and layout of segments

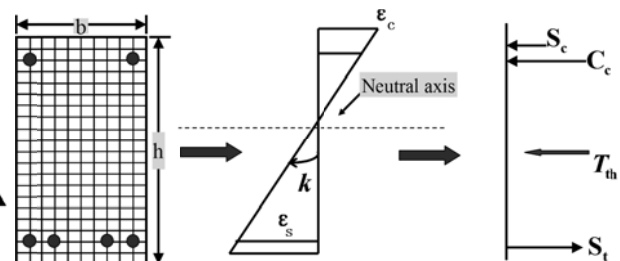


Fig.2. Section and strain relationship

1.2 High temperature properties of concrete and steel bars

The temperature field at each time step within the element is calculated by finite element method. As the heating conditions along the element are assumed to be identical, the temperature field of the

element can be simplified into a 2D problem. Steel bars are neglected as they don't significantly influence the temperature distribution in the cross section. The thermal conduction coefficient and the specific heat of concrete are taken according to EN 1992-1-2 (EC2). Generally, beams are assumed to be heated from three sides and slabs only from the bottom. The temperature calculation is carried out by means of the finite element package DIANA.

(1) High temperature properties of concrete

According to EC2, the total strain of concrete ε_{mc} at a higher temperature T is a sum of four parts: mechanical strain ε_{σ} , thermal strain ε_{th} , transient strain ε_{tr} and creep strain ε_{cr} , as shown by equation (1).

$$\varepsilon_{mc} = \varepsilon_{\sigma}(\sigma, T) + \varepsilon_{th}(T) + \varepsilon_{tr}(\sigma_0, T) + \varepsilon_{cr}(\sigma_0, T, t) \quad (1)$$

Thermal strain is a function of temperature only, mechanical and transient strain are determined by both the temperature and initial stress and the creep depends on all three basic. These properties can be well approximated by the equations (2), (3) and (4) (Jin Tao, 2009). The stress-strain relationship of concrete at high temperature is given by equation (5).

$$\varepsilon_{th} = \begin{cases} -1.8 \times 10^{-4} + 9 \times 10^{-6} T + 2.3 \times 10^{-11} T^3 & \text{for } 20^{\circ}\text{C} \leq T \leq 700^{\circ}\text{C} \\ 14 \times 10^{-3} & \text{for } 700^{\circ}\text{C} \leq T \leq 1200^{\circ}\text{C} \end{cases} \quad (2)$$

$$\varepsilon_{tr}(\theta, \sigma) = \frac{\sigma}{f_c} (-2.64 \times 10^{-13} T^4 + 2.93 \times 10^{-10} T^3 - 9.46 \times 10^{-8} T^2 - 5.79 \times 10^{-6} T + 0.00027) \quad (3)$$

$$\varepsilon_{cr} = \frac{\sigma}{f_c} \times (43.11 e^{-0.00477T} + 123.21) \left(\frac{t}{10800} \right)^{0.3} \times 10^{-6} \quad (4)$$

$$\sigma_c = \begin{cases} f_c^T \left[a \left(\frac{\varepsilon_{\sigma}}{\varepsilon_p^T} \right) + (3-2a) \left(\frac{\varepsilon_{\sigma}}{\varepsilon_p^T} \right)^2 + (a-2) \left(\frac{\varepsilon_{\sigma}}{\varepsilon_p^T} \right)^3 \right] & 0 \leq \varepsilon_{\sigma} \leq \varepsilon_p^T \\ \frac{f_c^T (\varepsilon_{\sigma} / \varepsilon_p^T)}{b(\varepsilon_{\sigma} / \varepsilon_p^T - 1)^2 + \varepsilon_{\sigma} / \varepsilon_p^T} & \varepsilon_{\sigma} \leq \varepsilon_p^T \end{cases} \quad (5)$$

where σ initial stress of concrete ;
 a, b coefficients;
 ε_p^T elastic limit strain at high temperature;
 f_c, f_c^T compressive strength of concrete at ambient and high temperature;
 t, T time and temperature.

(2) High Temperature properties of steel

Similar to concrete, the total strain of steel bars contains three parts: mechanical strain $\varepsilon_{s,\sigma}$, thermal strain $\varepsilon_{s,th}$ and creep strain $\varepsilon_{s,cr}$. as shown by expression (6). Thermal strain of steel can be calculated with reference to the length at 20°C, by equation (7). Compared to the thermal and mechanical strain, creep strain of steel is quite small, and is neglected in the calculation. The stress-strain relationship of steel bars can be expressed by equation (8).

$$\varepsilon_{ms} = \varepsilon_{s,\sigma}(\sigma, T) + \varepsilon_{s,th}(T) + \varepsilon_{s,cr}(\sigma, T, t) \quad (6)$$

$$\varepsilon_{s,th} = \begin{cases} -2.416 \times 10^{-4} + 1.2 \times 10^{-5} T + 0.4 \times 10^{-8} T^2 & \text{for } 20^{\circ}\text{C} \leq T \leq 750^{\circ}\text{C} \\ 11 \times 10^{-3} & \text{for } 750^{\circ}\text{C} < T \leq 860^{\circ}\text{C} \\ -6.2 \times 10^{-3} + 2 \times 10^{-5} T & \text{for } 860^{\circ}\text{C} < T \leq 1200^{\circ}\text{C} \end{cases} \quad (7)$$

$$\sigma_s = \begin{cases} \varepsilon E_s^T & 0 \leq \varepsilon \leq \varepsilon_{sp}^T \\ f_{sp}^T - c + (b/a)[a^2 - (\varepsilon_{sy}^T - \varepsilon)^2]^{0.5} & \varepsilon_{sp}^T \leq \varepsilon \leq \varepsilon_{sy}^T \\ f_{sy}^T & \varepsilon_{sy}^T \leq \varepsilon \leq \varepsilon_{st}^T \\ f_{sy}^T [1 - (\varepsilon - \varepsilon_{st}^T) / (\varepsilon_{su}^T - \varepsilon_{st}^T)] & \varepsilon_{st}^T \leq \varepsilon \leq \varepsilon_{su}^T \end{cases} \quad (8)$$

where

$$\begin{aligned} e_{sp}^T &= f_{sp}^T / E_s^T; e_{sy}^T = 0.02; e_{st}^T = 0.15; e_{su}^T = 0.20; \\ a &= (e_{sy}^T - e_{sp}^T)(e_{sy}^T - e_{sp}^T + c / E_s^T); b = c(e_{sy}^T - e_{sp}^T)E_s^T + c^2; \\ c &= (f_{sy}^T - f_{sp}^T)^2 / [(e_{sy}^T - e_{sp}^T)E_s^T - 2(f_{sy}^T - f_{sp}^T)]; \\ E_s^T &\text{ is young's modulus of steel at } T; \\ f_{sp}^T &\text{ is yield strength of steel at } T; \\ f_{sy}^T &\text{ is ultimate strength of steel at } T; \end{aligned}$$

1.2 Mechanical properties of the cross-section

At each time step, a moment-curvature relationship (M-k) can be generated by sectional analysis (Fig.2). The mechanical analysis is based on the following assumptions mentioned in (Kodur, V.K.R, 2008):

- (1) Plane sections remain plane after bending;
- (2) Bond slip between steel bars and concrete is neglected;
- (3) Spalling of concrete is neglected;
- (4) For bending elements, shear deformations are not considered.

Firstly, the rectangular section with dimension $b \times h$ is set into a coordination system, with the bottom line of the section coinciding with the X-coordinate and left line of the section coinciding with the Y-coordinate. Then the section is divided into $m \times n$ small units (Fig.2), the area of each unit being $\frac{b}{m} \times \frac{h}{n}$. The location of each unit in this system can be expressed as (x_i, y_i) .

According to the plane section assumption, a linear relationship exists for the concrete strains and steel bar strains. The total strain of the upper most units is remarked as ε_{mc0} , and then the total strain of other concrete units and the total strain of the steel units can be computed by the following expressions:

$$\varepsilon_{mc} = \varepsilon_{mc0} - k(h - y_i) \quad (9)$$

$$\varepsilon_{ms} = k(h - \alpha_s) - \varepsilon_{mc0} \quad (10)$$

where $\varepsilon_{mc}, \varepsilon_{ms}$ the total strain of concrete units and steel bars;

y_i Y-coordinate location of unit i ($i = 1, 2, 3, \dots$);

k curvature;

α_s thickness of the concrete cover of steel bars.

The mechanical strain of concrete and steel units can be generated by substituting $\varepsilon_{mc}, \varepsilon_{ms}$ expressed by (9) and (10) into equation (1) and (2). With the mechanical strain of concrete units and steel units, stress of each unit is determined by solving equations (5) and (8). Once the stresses of concrete units and steel units are known, the force of them in high temperature can be computed by equation (11) and (12).

$$S_R = \sum_{i=1}^{n_s} A_{si} \sigma_s \quad (11)$$

$$C = \int \sigma_c dA = \sum_{i=1}^m \sum_{j=1}^n \sigma_c(T_{i,j}, \varepsilon_{\sigma}) \quad (12)$$

where C, S_R the resulting force of concrete and steel stresses;

A_{si} the area of one steel bar;

Based on the compatibility criterion and a convergence criterion, an iterative process of curvature k is carried out to make a balance between C and S_R . The iterative process will end at a balanced state and the moment of this state can be expressed by equation (13) where y_c is the effective center of concrete. Through this process, moment-curvature curves at each time step will be generated, and the average stiffness of each segment can be computed by equation (14).

$$M = C(y_c - \alpha_s) = S_R(y_c - \alpha_s) \quad (13)$$

$$EI(t, l_i) = M(t, l_i) / k(t, l_i) \quad (14)$$

1.3 Structural analysis

The next step is nonlinear structural analysis using the calculation results of the cross section. To obtain the deflection of the bending element at any time step under a given load, the global stiffness matrix and related nodal loads should first be analyzed. The deflection of the structure can be determined by equation (15).

$$[K_g][u] = [P] \quad (15)$$

where $[K_g]$ the global stiffness matrix of the elements;

$[u]$ the deformation matrix of all the segments nodes;

$[P]$ the relative nodal load matrix.

Thus, for each time step, after thermal computing, sectional analysis and structural analysis, the ultimate bearing moment and the deflection of the RC element under a given fire curve will be generated.

2 TEST VALIDATION

The proposed numerical model is validated by the fire test results reported by Minne R et al, (1979).

2.1 Slab tests

Simply supported slabs, measuring $1900 \times 150 \times 4900$ mm, were positioned in a steel frame and loaded by means of two hydraulic jacks situated at $1/4$ th of the effective span which measured 4.5 m. The slabs are one-way spanning, designed for a service live load of $3kN/m^2$ and an admissible steel stress of $240N/mm^2$. Table 1 presents the total applied load during heating and the properties of siliceous aggregates concrete before heating. Table 2 shows the reinforcement properties. For each group of slabs, differences can be found in the number of reinforcing bars and the concrete cover on the main reinforcement. During the fire tests, the temperature at the main reinforcement depth and the deflection at mid-span were measured.

Tab.1. Applied load and concrete material properties

	Applied force [kN]	f_c [N/mm ²]	f_{ct} [N/mm ²]	E_c [N/mm ²]	ρ [kg/m ³]
G1	14.5	53.4	4.62	45200	2420
G2	15.7	54.6	4.63	38100	2400
G3	14.6	53.8	5.45	39800	2393

Tab.2. Reinforcement properties before heating.

	Longitudinal reinforcement			Transversal reinforcement	Concrete cover [mm]
	f_s N/mm ²	$\epsilon_{failure}$ [%]			
G1	504	17.7	15 x Ø10	26 x Ø 6	15
G2	504	17.7	17 x Ø10	26 x Ø 6	25
G3	504	17.7	18 x Ø10	26 x Ø 6	35

2.2 Results and conclusions

The obtained deformation of slab G1, G2 and G3 measured during test as well as the calculation results without transient creep strain considered are shown in figure 3. The mid-span deflection curves calculated with and without transient strain are compared in figure4.

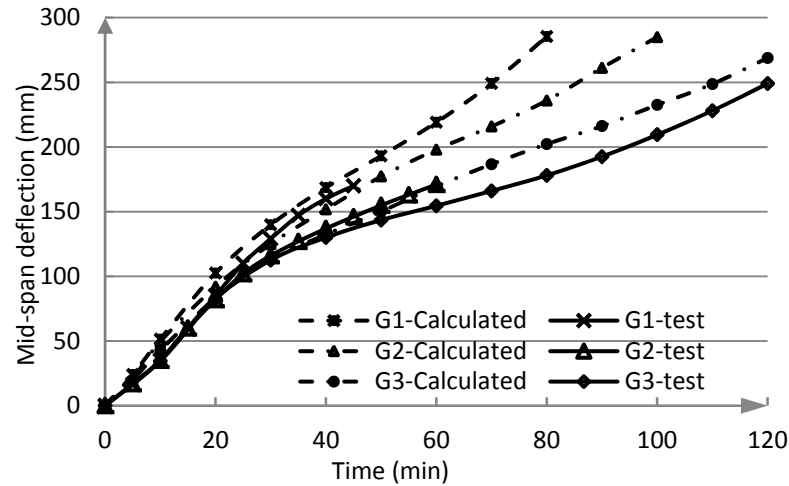


Fig.3 Mid-span deflections of G1, G2 and G3 (transient strain not considered)

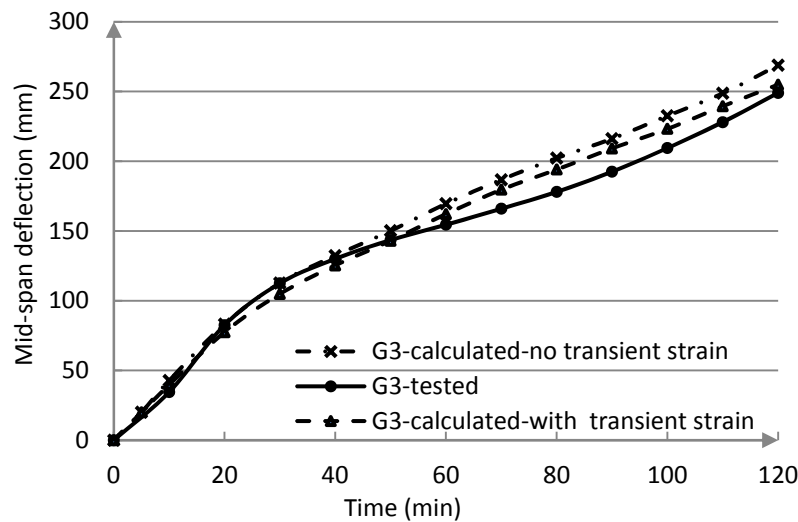


Fig.4 Mid-span deflections of G3 with and without transient strain

From Fig.3 and Fig.4, the following conclusions can be derived:

- (1) G1 and G2 failed after 60 min heating in the test, and G3 last until 2hrs. As the slabs are heated from the tensile side, the ultimate bearing capacity of the elements is decided by steel bars, so the thickness of the concrete cover is essential for the fire-resistance of the structures.
- (2) The numerical results and the test results are very close and have similar trend. After 30 min, the numerical results are higher than the tested ones, but the differences are acceptable.

(3) Fig.4 indicates that the calculation became more accurate when transient strain is considered. Without it, the deflections will be overestimated. However, for slabs this influence is small and can be neglect in the future design.

3 ACKNOWLEDGMENT

The author would like to thank the China Scholarship Council for the financial support through her PhD study.

REFERENCES

- Eurocode 2: Design of concrete structures-Part 1.2: General rules-Structural fire design, EN1992-1-2, 2004.
- Fib Bulletin 38: Fire Design of Concrete Structures—Materials, Structures, and Modeling, 2007.
- Kodur, V.K.R., Dwaikat, M.B, Flexural Response of Reinforced Concrete Beams Exposed to Fire. *Structural Concrete*, 2008, 1(9):45-54.
- Minne R, Vandamme M., Fire Resistance of Reinforced Concrete Slabs, Laboratory for Fuel Technology and Heat Transfer, Ghent University, 1979.
- Paolo Riva. Parametric Study on the Behavior of RC Beams and Frames under Fire Conditions. *fib Guidelines for the Structural Design of Concrete Buildings Exposed to Fire*. 2002.
- Sebastjan Bratina, Saje M., Igor Planinc, The effects of Different Strain Contributions on the Response of RC Beams in Fire. *Engineering Structures*, 2006, 29: 418–430.
- Tao Jin. Experimental Investigation on Strength and Deformation of Self-compacting Concrete at Elevated Temperature. PhD Thesis, Tongji University and Ghent University, China and Belgium, 2009.

A RATIONAL APPROACH TO FIRE RESISTANCE ANALYSIS OF RC COLUMNS SUBJECTED TO UNIAXIAL/BIAXIAL BENDING AND AXIAL RESTRAINT

Truong Thang Nguyen^a, Kang Hai Tan^a

^a Nanyang Technological University, School of Civil and Environmental Engineering, Singapore

INTRODUCTION

Although great efforts have been made in studying the behaviour of reinforced concrete (RC) columns under fire conditions (Lie et al, 1991, 1993; Dotreppe et al, 1999; Tang, 2001; Kodur et al, 2004; Bratina et al, 2005), there is still a need of more sophisticated analytical models for fire resistance analysis of those subjected to practical conditions such as uniaxial and biaxial bending as well as presence of adjacent unheated structural elements. So far, the issue has been discussed by Tan and Yao (2003, 2004) who proposed an indirect approach using separate analyses conducted on two principal cross-sectional bending planes of rectangular columns. Raut et al (2010) proposed an approach for modelling fire response of RC columns under biaxial bending. Fire resistance predictions obtained from the proposed numerical model were compared with those in code provisions. These comparisons indicated that current codes and standards neglect the effect of either uniaxial or biaxial bending and may not yield reliable fire resistance predictions. However, there was no published paper on validation of columns under biaxial bending, since the reported fire tests reported were confined to uniaxially-loaded specimens.

This paper introduces an approach of direct sectional analysis for RC columns subjected to either uniaxial or biaxial bending combined with axial restraint under fire conditions. By incorporating the results of thermal and structural analyses obtained from SAFIR software (Franssen, 2005), in which Eurocode nonlinear material models at elevated temperatures were adopted, temperature-dependent load resistance of columns can be determined at incremental time steps with an arbitrary position of the inclined neutral axis. The failure time can be captured with the most possible failure criterion, i.e. when the applied load reaches either buckling or ultimate capacity of the column at that temperature. Effects of axial restraint and non-standard fires are also considered in the model. A computer program was developed so that experimental data of thirty-nine fire tests conducted at universities of Braunschweig (Hass, 1986) and Nanyang Technological University in 2010 were used to validate the accuracy of the proposed approach.

1 BEHAVIOUR OF RC COLUMNS AT ELEVATED TEMPERATURES

Some aspects of behaviour of axially-restrained RC columns at elevated temperatures are briefly demonstrated in Fig. 1. They include regression of interaction diagram due to deterioration of material strength and stiffness (Fig. 1(a)), non-uniform distribution of strain/stress/strength on the column cross section (Fig. 1(b)), and occurrence of thermal-induced axial force (Fig. 1(c)).

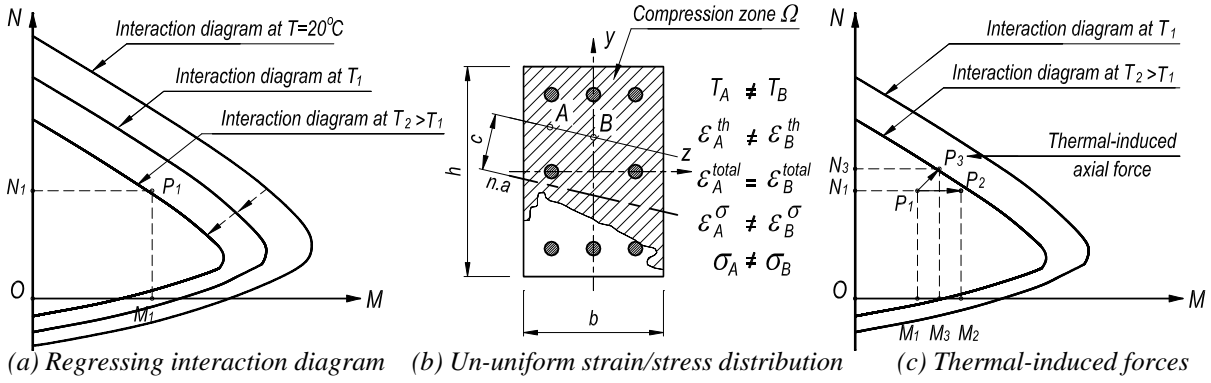


Fig. 1 RC Column behaviour at elevated temperatures

2 SECTIONAL ANALYSIS AT ELEVATED TEMPERATURES

2.1 Assumptions

These assumptions are adopted in the analysis: (1) Cross-section remains plane after bending and normal to the centroidal axis; (2) Total strains in concrete and reinforcing steel at the same level are equal; (3) Stresses in concrete and reinforcing steel can be computed from strains based on corresponding elevated-temperature stress-strain curves for these materials; (4) Tensile strength of concrete in fire conditions is neglected in the calculations; (5) At a certain temperature, concrete is assumed to have failed when the maximum stress-induced compressive strain reaches the maximum limit; (6) Lateral-torsional buckling of columns is neglected in the analysis; (7) Effect of shear deformations is very small and negligible, and (8) Only rectangular columns are addressed.

2.2 Principles of Analysis

Consider a uniaxially-loaded column designed at room temperature to sustain a set of ultimate loads (N_1, M_1). As shown in Fig. 2(a), point $P_1 (N_1, M_1)$ is located on the column interaction diagram at ambient condition. Since fires are considered as accidental events, it is regulated that at fire limit state, only the effect of service loads are considered. Hence, at the beginning of the fire, the column is subjected to an axial load N_2 determined by multiplying the ultimate load N_1 by a reduction factor η_{fi} . Point I represents axial load N_2 and the corresponding moment M_2 .

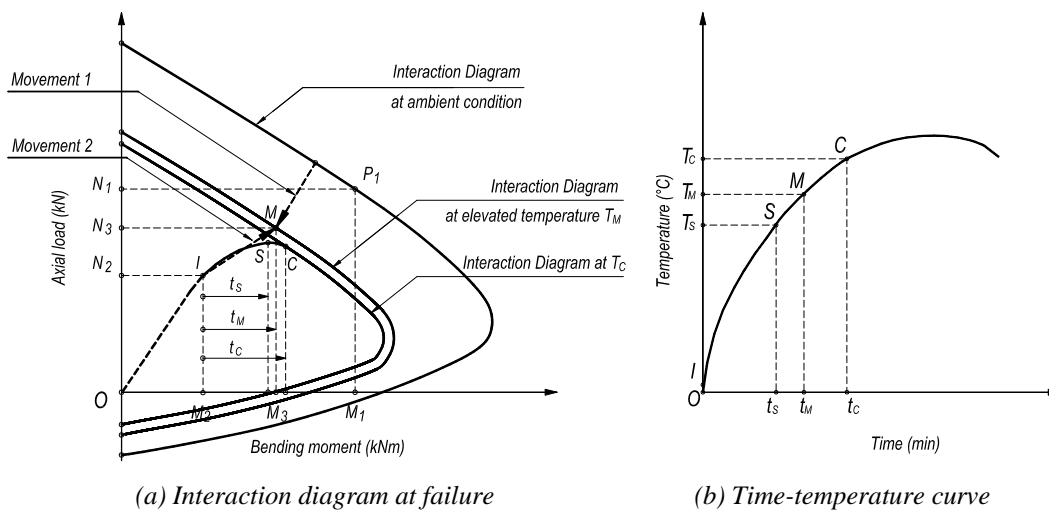


Fig. 2 Principles of analysis

In fire conditions, there are two movements acting in opposite directions in Fig. 2(a). The first inward movement is the regression of interaction diagram as temperature rises. Due to axial restraint, axial force in the column increases resulting in the second outward movement. For

biaxially-loaded columns with temperature-dependent interaction surfaces, these two movements occur in three-dimensional space. If the column is stocky or the load eccentricity is small, material failure occurs after a period of time t_M when the load path and ultimate load capacity at temperature T_M coincide at point M (N_3, M_3). As shown in Fig. 2(b), t_M is the period of time to reach temperature T_M . The terms t_M and T_M can be referred to as the material failure time and failure temperature, respectively. If the column is of either high slenderness or high load eccentricity, due to deterioration of material stiffness as temperature rises, the column may lose its stability at point S where the derivation $\partial M/\partial N$ approaches infinity before becoming negative and a run-away trend occurs in the column mid-height lateral deflection. Then this column is deemed to have failed in stability mode before ultimate load capacity is reached. The terms t_S and T_S respectively represent the buckling time and buckling temperature. Combined failure mode is identified if after the column buckles, the load path and regressing interaction diagram coincide at point C. The terms t_C and T_C respectively represent the critical time and critical temperature.

2.3 Proposed Approach of Sectional Analysis

Consider a rectangular column subjected to an axial load N with eccentricities e_y and e_z corresponding to the respective bending moments $M_z=Ne_y$ and $M_y=Ne_z$. As shown in Fig. 3(c), the maximum compressive stress occurs at point B at the North-East corner of the cross-section. The position of a general neutral axis can be identified by two key parameters, namely, inclined angle β and distance from point B represented by the length c_n of line BG perpendicular to the neutral axis. Based on the neutral axis position, distributions of strain components can be further analyzed.

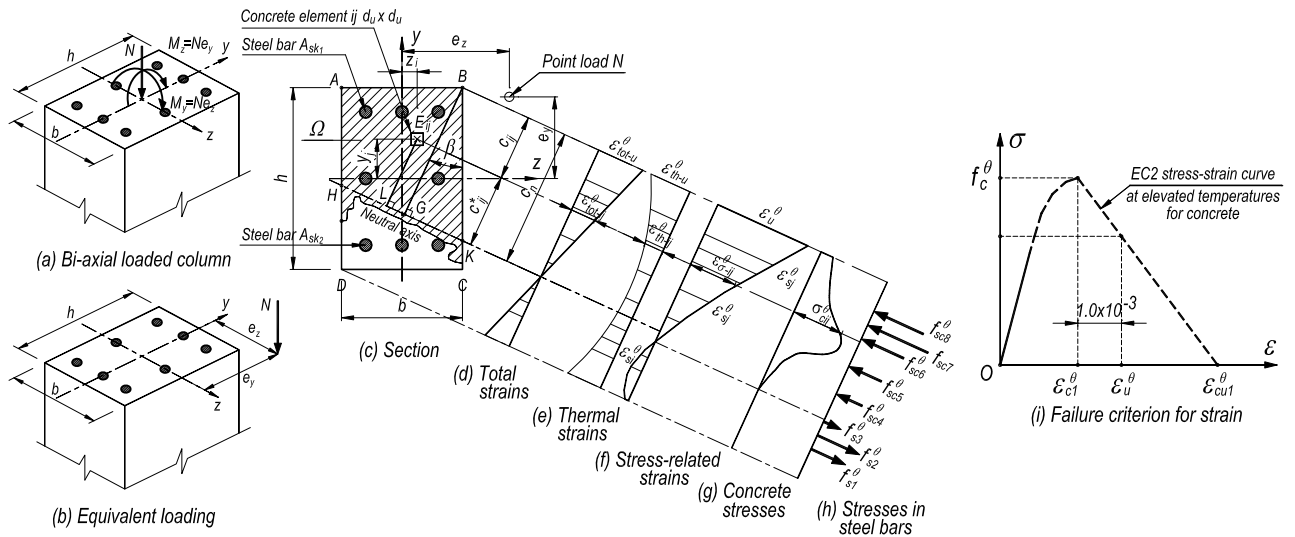


Fig. 3 Direct sectional analysis at elevated temperatures

Sectional analysis at elevated-temperature is more complicated than that at ambient condition due to: (1) The ABHK zone of total softening-strains limited by the neutral axis is no longer rectangular. It can be triangular, trapezoidal, or pentagonal; (2) Compression zone Ω is different from ABHK zone due to the presence of thermal and transient strains, and (3) Distribution of compressive stresses in compression zone is non-uniform due to different temperature distribution profiles across the column cross-section. Therefore, the method of equivalent rectangular stress block cannot be used in this analysis. An approach is proposed in this paper to determine load resistances contributed by concrete and reinforcing steel bars by integrating compressive and tensile stresses over the whole cross-section of the column.

In this direct sectional analysis of the Eurocode-based approach, ultimate values of total strain $\varepsilon_{tot-u}^\theta$ and stress-induced strain ε_u^θ at point B (Figs. 3(c), (d)) are proposed as shown in Tab. 1.

Tab. 1 Strain failure criterion

Concrete temperature (°C)	$\varepsilon_{c1}^{\theta} \times 10^{-3}$	$\varepsilon_{cul}^{\theta} \times 10^{-3}$	$\varepsilon_u^{\theta} \times 10^{-3}$	Siliceous aggregates		Calcareous aggregates	
				$\varepsilon_{th}^{\theta} \times 10^{-3}$	$\varepsilon_{tot-u}^{\theta} \times 10^{-3}$	$\varepsilon_{th}^{\theta} \times 10^{-3}$	$\varepsilon_{tot-u}^{\theta} \times 10^{-3}$
20	2.5	20.0	3.5	-0.000	3.500	-0.000	3.500
100	4.0	22.5	5.0	-0.743	4.257	-0.494	4.506
200	5.5	25.0	6.5	-1.804	4.696	-1.192	5.308
300	7.0	27.5	8.0	-3.141	4.859	-2.058	5.942
400	10.0	30.0	11.0	-4.892	6.108	-3.176	7.824
500	15.0	32.5	16.0	-7.195	8.805	-4.630	11.370
600	25.0	35.0	26.0	-10.188	15.812	-6.504	19.496
700	25.0	37.5	26.0	-14.009	11.991	-8.882	17.118
800	25.0	40.0	26.0	-14.000	12.000	-11.848	14.152
900	25.0	42.5	26.0	-14.000	12.000	-12.000	14.000
1000	25.0	45.0	26.0	-14.000	12.000	-12.000	14.000
≥1100	25.0	47.5	26.0	-14.000	12.000	-12.000	14.000

In Tab. 1, the temperature-dependent terms $\varepsilon_{c1}^{\theta}$, $\varepsilon_{cul}^{\theta}$ and $\varepsilon_{th}^{\theta}$ are respectively the strain corresponding to the compressive strength, ultimate strain, and thermal strain specified in EC2 Part 1-2 (Eurocode, 2004b). Yao (2003) proposed that neither $\varepsilon_{c1}^{\theta}$ nor $\varepsilon_{cul}^{\theta}$ can be used as the strain failure criterion since the former marks the beginning of strain softening while the latter represents the end. Hence, the ultimate stress-induced strain ε_u^{θ} is determined by adding an amount of 1.0×10^{-3} to the respective yield strain $\varepsilon_{c1}^{\theta}$ (Fig. 3(i)). This additional value is adopted based on the ambient condition in which ε_u^{θ} is 3.5×10^{-3} and $\varepsilon_{c1}^{\theta}$ is 2.5×10^{-3} . It is also satisfied that ε_u^{θ} always lies in between $\varepsilon_{c1}^{\theta}$ and $\varepsilon_{cul}^{\theta}$ in this proposed determination. In Tab.1, linear interpolation can be applied to calculate strain criterion at any temperature.

Once ε_u^{θ} is obtained, the direct sectional analysis can be conducted to obtain the temperature-dependent load resistance of the column:

$$N_{Rd}^{\theta} = \sum_{ij} \sigma_{cij}^{\theta} d_u^2 + \sum_{k_1} A_{sk_1} (f_{sck_1}^{\theta} - \sigma_{ck_1}^{\theta}) + \sum_{k_2} A_{sk_2} f_{sk_2}^{\theta} \quad (1)$$

$$M_{Rdy}^{\theta} = \sum_{ij} \sigma_{cij}^{\theta} d_u^2 z_i + \sum_{k_1} A_{sk_1} (f_{sck_1}^{\theta} - \sigma_{ck_1}^{\theta}) z_{k_1} + \sum_{k_2} A_{sk_2} f_{sk_2}^{\theta} z_{k_2} \quad (2)$$

$$M_{Rdz}^{\theta} = \sum_{ij} \sigma_{cij}^{\theta} d_u^2 y_j + \sum_{k_1} A_{sk_1} (f_{sck_1}^{\theta} - \sigma_{ck_1}^{\theta}) y_{k_1} + \sum_{k_2} A_{sk_2} f_{sk_2}^{\theta} y_{k_2} \quad (3)$$

where sub-indexes i and j represent concrete elements in compression zone; k_1 and k_2 denote steel bars located in compression and tension zones, respectively. The term d_u is dimension of the basic square concrete element E_{ij} ; A_{ski} represents cross-sectional area of the reinforcing bar at position k_i ; Stress σ_{cij}^{θ} of the concrete element E_{ij} at position (z_i, y_j) can be determined based on values of T_{ij} , $\varepsilon_{\sigma-ij}^{\theta}$, and the EC2 material model of concrete at elevated temperatures.

In the proposed model, since the inclined neutral axis can be directly determined, the convergence criteria of material failure would be simpler as they are expressed in a direct manner:

$$\text{If } N_{Ed}^{\theta} = N_{Rd}^{\theta} \text{ then } M_{Edy}^{\theta} = M_{Rdy}^{\theta} \text{ or } M_{Edz}^{\theta} = M_{Rdz}^{\theta} \quad (4)$$

The terms M_{Rdy}^{θ} , M_{Rdz}^{θ} in Eq. (4) are the real moment resistances about principal axes of the column cross-section. In Fig. 4, dashed curves $AP'_yC'_yD'_y$ and $AP'_zC'_zD'_z$, which are the intersections between the 3-D interaction surface and two vertical planes, represent the physical meanings of M_{Rdy}^{θ} and M_{Rdz}^{θ} , respectively.

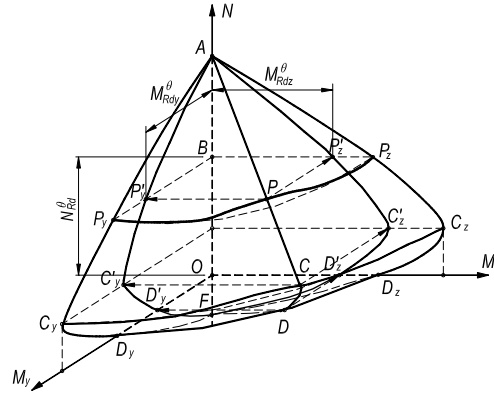


Fig. 4 Interaction surface at temperature θ

2.4 Proposed Computer Program

Based on the elevated-temperature direct sectional analysis introduced in Section 2.3, a computer program named FRRC was proposed. The basic principle applied in the program is to locate an inclined neutral axis throughout the cross-section by iterations. Three loops of iteration are involved: (1) Time steps; (2) Variation of angle β of the inclined neutral axis, and (3) Distance c_n from the neutral axis to the most-compressive corner of the cross-section.

As time progresses, nonlinear elevated-temperature mechanical properties can be determined through associated subroutines of the program. Sectional analysis can be conducted for any arbitrary neutral axis position. Potential failures can be checked following the convergence criteria shown in Section 2.3. The time step at which the program converges is identified as failure time.

3 CASE STUDIES

3.1 Case Study 1

Case study 1 was carried out based on test results of thirty-three RC columns subjected to fire conducted by Hass (1986). Details and test conditions of some typical specimens are shown in Tab. 2. The columns were subjected to either pure compression or uniaxial bending without any axial restraint. Standard fire curve ISO 834 was applied for all the fire tests.

Tab. 2 Case study 1 - Details of test specimens

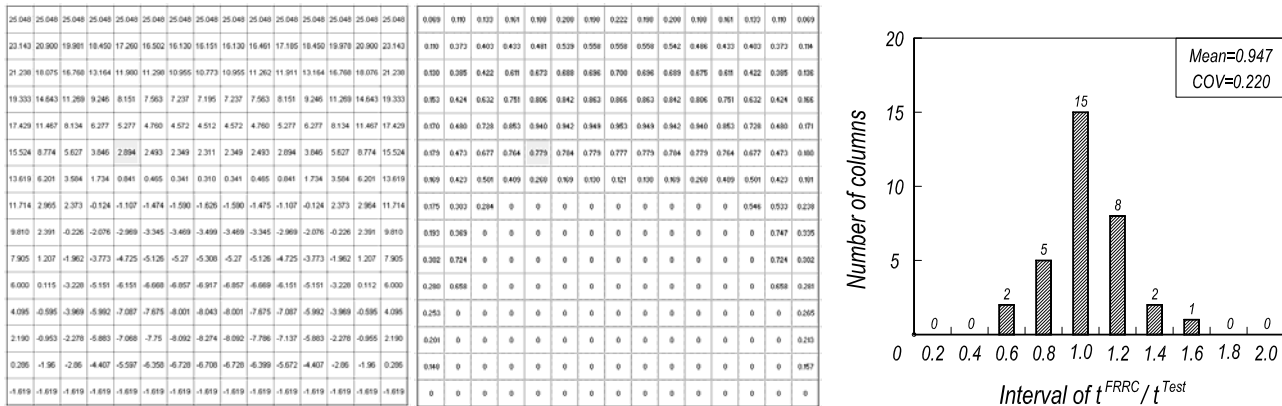
No.	Ref.	b (mm)	H (mm)	Rebar (mm)	L (m)	f'_c (MPa)	f_y (MPa)	End Cond.	d' (mm)	e (mm)	N_{app} (kN)	t^{Test} (min)
1	1	300	300	6 Φ 20	3.76	24.1	487	p-p	38	30	710	86
2	2	300	300	6 Φ 20	3.76	24.1	487	p-p	38	0	930	84
33	41	300	300	6 Φ 20	4.70	31.5	526	p-p	38	150	465	50

Analysis results obtained from the proposed analytical approach and the associated computer program are shown in Tab. 3. The terms N_{Rd} and M_{Rd} are axial load and moment capacities of the columns at ambient condition, respectively. The term η_{fi} is the reduction factor, which is the ratio between the applied load N_{app} and the ambient resistance N_{Rd} . Failure time t^{FRRC} and other detailed descriptions of the column at failure including angle β of the inclined neutral axis, depth of neutral axis c_n , and contributions of concrete (N_{Rdc}^θ , M_{Rdc}^θ) and reinforcing steel bars (N_{Rds}^θ , M_{Rds}^θ) to the column load resistance, were determined by the FRRC program.

Tab. 3 Case study 1 – Analysis results of test specimens

No.	Ref.	N_{Rd} (kN)	M_{Rd} (kNm)	η_{fi}	N_{Rdc}^{θ} (kN)	N_{Rds}^{θ} (kN)	M_{Rdc}^{θ} (kNm)	M_{Rds}^{θ} (kNm)	β (rad)	c_n (mm)	t^{FRRC} (min)
1	1	1669.2	96.8	0.517	485.2	229.6	27.8	25.3	0	126	85
2	2	2132.6	62.5	0.436	666.0	348.6	21.1	18.8	0	150	82
33	41	690.6	150.5	0.673	658.2	-31.3	52.6	68.4	0	120	45

The strain and stress distributions in concrete given by the program are shown in Figs. 5(a) and 5(b), respectively. Comparison between the proposed analysis results and experimental data in terms of failure time is shown in Fig. 5(c). Statistical analysis shows a mean agreement of 0.947 and a COV of 0.220. It can be seen in this case study that when the Eurocode elevated-temperature material properties are incorporated, the proposed approach gives good agreement and conservative prediction of the fire resistance for axially- and uniaxially-loaded RC columns without axial restraint, compared to the test results.



(a) Concrete stress-related strain

(b) Concrete stress

(c) Statistical analysis

Fig. 5 Case study 1

3.2 Case Study 2

In this case study, results of six axially-restrained column specimens tested at Nanyang Technological University in 2010 are used to validate the proposed approach. All the columns had identical 300 mm square cross-section and 3.3 m length. They were cast from the same batch of concrete with mean cylinder strength of 55 MPa. Reinforcing bars of 6T20 with 550 MPa yield strength were typically designed for the six specimens. In the tests, three specimens were uniaxially-loaded with eccentricities of 25, 40 and 60 mm and another three were loaded in biaxial bending with corresponding eccentricities of (25, 25), (40, 40) and (60, 60mm). As calculated from Tab. 4, the average ratio between the predicted and tested failure times (t^{FRRC}/t^{Test}) is 1.099. Hence, the proposed approach overestimates the fire resistance of axially-restrained columns.

Tab. 4 Case study 2 – Test and analysis results of failure time

Col.	C1-3		C1-4		C1-5		C2-1		C2-2		C2-3	
	t^{Test}	t^{FRRC}										
F. time (min)	166	190	211	190	159	196	182	194	189	202	176	208
Ratio	1.145		0.900		1.232		1.065		1.069		1.182	

4 SUMMARY AND ACKNOWLEDGMENT

In the proposed rational analytical computer-based approach, effects of uniaxial and biaxial bending as well as axial restrained were considered in a direct sectional analysis. Good agreement in the failure time between the proposed approach and experimental data can be obtained for either axially-

restrained or unrestrained column subjected to eccentric load which is either uniaxial or biaxial bending. More conservative results were observed in the case of columns without axial restraint.

This research was funded by grant M47030016 A*STAR and supported by manpower research account MINDEF-NTU/JPP/FY05/14.

REFERENCES

- Lie, T. T., Celikkol, B., Method to Calculate the Fire Resistance of Circular Reinforced Concrete Columns, *Materials Journal*, 88(1), 84-91, 1991.
- Lie, T. T., Chabot, M., Evaluation of the Fire Resistance of Compression Members Using Mathematical Models, *Fire Safety Journal*, 20(2), 135-149, 1993.
- Dotreppe, J. -C., Franssen, J. -M., Vanderzeypen, Y., Calculation Method for Design of Reinforced Concrete Columns under Fire Conditions, *ACI Structural Journal*, 96(1), 9-18, 1999.
- Kodur, V. K. R., Wang, T. C., Cheng, F. P., Predicting the Fire Resistance Behaviour of High Strength Concrete Columns, *Cement and Concrete Composites*, 26(2), 141-153, 2004.
- Bratina, S., Cas, B., Saje, M., Planinc, I., Numerical Modelling of Behaviour of Reinforced Concrete Columns in Fire and Comparison with Eurocode 2, *International Journal of Solids and Structures*, 42(21-22), 5715-5733, 2005.
- Raut, N., Kodur, V. K. R., Modelling of Fire Response of Reinforced Concrete Columns under Biaxial Bending, *Proceedings of the Sixth International Conference SiF*, 206-215, USA, 2010.
- Tang, C. Y., An Iterative Formula for Fire Resistance of Columns, *Mater Thesis*, Nanyang Technological University, Singapore, 2001.
- Tan, K. H., Yao, Y., Fire Resistance of Four-Face Heated Reinforced Concrete Columns, *Journal of Structural Engineering*, 129(9), 1220-1229, 2003.
- Tan, K. H., Yao, Y., Fire Resistance Reinforced Concrete Columns Subjected to 1-, 2-, and 3-Face Heating, *Journal of Structural Engineering*, 130(11), 1820-1828, 2004.
- Hass, R., *Practical Rules for the Design of Reinforced Concrete and Composite Columns Submitted to Fire*, Institute fur Baustoffe, Massivbau und brandschutz der Technichen Universita Braunschweigo, 1986.
- Frassen, J. M., SAFIR. A Thermal/Structural Program Modelling Structures under Fire, *Engineering Journal*, A.I.S.C., 42, 3: 143-158, 2005.
- Eurocode EN 1991-1-1:2004, *Design of Concrete Structures – Part 1-1: General Rules and Rules for Buildings*, 2004a.
- Eurocode EN 1991-1-2:2004, *Design of Concrete Structures – Part 1-2: General Rules, Structural Fire Design*, 2004b.

USING OPENSEES FOR AN RC FRAME IN FIRE

Jian Zhang^a, *Asif Usmani^b, Jian Jiang^b, Yaqiang Jiang^b, Panagiotis Kotsovinos^b and Ian May^a

^a School of Built Environment, Heriot-Watt University, Edinburgh EH14 4AS, United Kingdom

^b School of Engineering, The University of Edinburgh, Edinburgh EH9 3JF, United Kingdom

INTRODUCTION

With increasing urbanisation and industrialisation earthquakes represent an ever greater risk to life, livelihoods and to the sustainability of society's rapid development. In built-up areas, especially major cities with tall buildings and extensive gas mains, this risk is compounded by post earthquake fires. In fact, losses resulting from fires developing soon after the earthquake may be comparable to those resulting from the shaking (EQE International, 1995). The risk is certainly increased by the hampering of fire response due to the extreme traffic congestion, collapsed houses and buildings, rubble in the streets, the concomitance of multiple fires and the possible difficulties in water supply soon after the earthquake (Buchanan, 2001).

To develop a comprehensive earthquake and fire research programme based on exploiting the complementary strengths of the collaborating institutions, a project funded by UKIERI is currently underway. Objectives of this project may be stated as: a) Developing a detailed understanding of the mechanics of the response of earthquake damaged structures (primarily reinforced concrete frames) subjected to fire (through small and large scale testing and developing computational models); b) Developing mathematical models for determining the reliability of structural components and structures subjected to compound seismic and fire loading, which account for the uncertainties associated with the loading and damage estimation, to enable realistic quantification of performance.

To model the experiment, a software named OpenSees has been developed so that it could be used to perform thermo-mechanical analyses. OpenSees is an open source object oriented software framework developed at UC Berkeley and currently supported by PEER and Nees. OpenSees has so far been focussed on providing an advanced computational tool for analysing the non-linear response of structural frames subjected to seismic excitations (Usmani et al, 2010). A key feature of OpenSees is the interchangeability of components and the ability to integrate existing libraries and new components into the framework (not just new element classes) without the need to change the existing code (Mazzoni et al, 2007). However one of the limitations of OpenSees is that thermal analysis can not be carried out by it up to date. In order to overcome this flaw so that it can be used to model the experiment of UKIERI, some new classes have been added into OpenSees and the some thermal analysis has been performed. The compared results show an acceptable agreement between theory, OpenSees, Abaqus.

1 NEWLY ADDED OPENSEES CLASSES

As mentioned above, there is not much work to do to let the OpenSees "recognize" a new class, and this advantage can be shown by the progress of introducing thermal action to the elastic beam-column element. A new derived class of *ElementalLoad*, called *Beam2dThermalAction* or *Beam3dThermalAction*, and a new member function of elastic beam-column element were all required to add into OpenSees to perform the linear analysis of elastic element in thermal loading.

It is more complicated to perform a thermal analysis to the nonlinear beam-column element. *Material* and *SectionForceDeformation* classes' information has to be passed to the element class while carrying out the nonlinear analysis, and all of these classes must be temperature related. Fig. 1 above shows the new classes that have been implemented within the existing framework (the original OpenSees classes are identified by the greyed boxes).

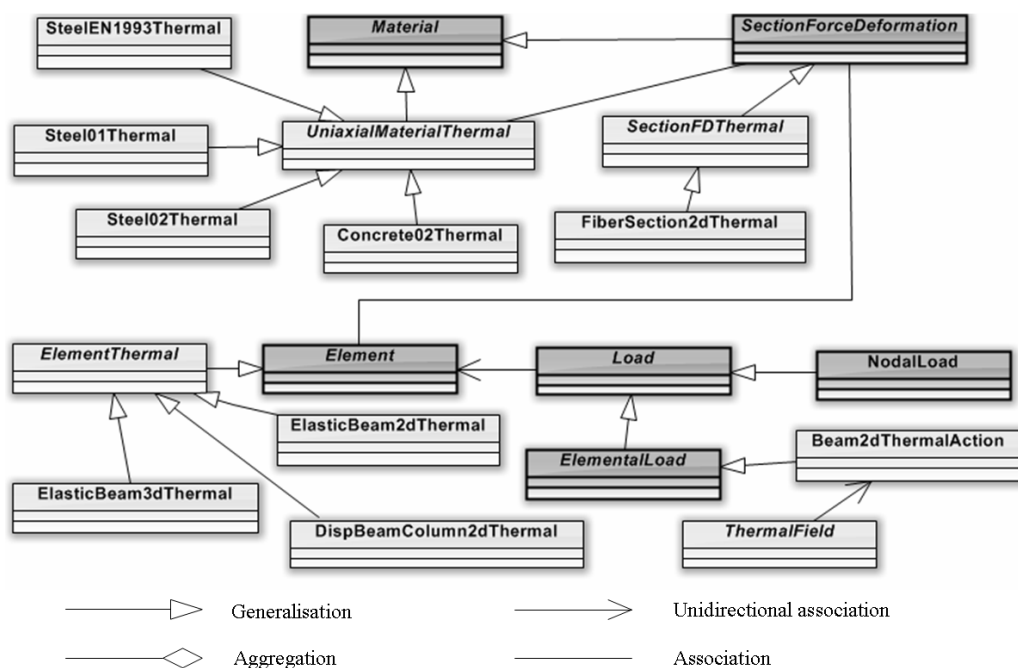


Fig. 1 New classes introduced to the current OpenSees framework for performing thermo-mechanical analyses

2 A BENCHMARK TEST FOR ELASTIC BEAM-COLUMN ELEMENT

A series of benchmark problems have been used to test the new thermo-mechanical code in OpenSees. For instance one was to predict the mid-span deflection, end rotation and axial force in an elastic beam (Young's Modulus $E = 10\text{GPa}$, area of cross section $A = 9 \times 10^4 \text{mm}^2$) under udl and thermal loading ($T_{\text{top}} = 20\text{C}$, $T_{\text{bottom}} = 800\text{C}$, thermal expansion coefficient $\alpha = 12 \times 10^6 / \text{C}$) both ends of which are restrained in translation (Fig. 2), however the rotations are free. Analytical, OpenSees and ABAQUS solutions are shown in Table 1, all of which are in agreement.

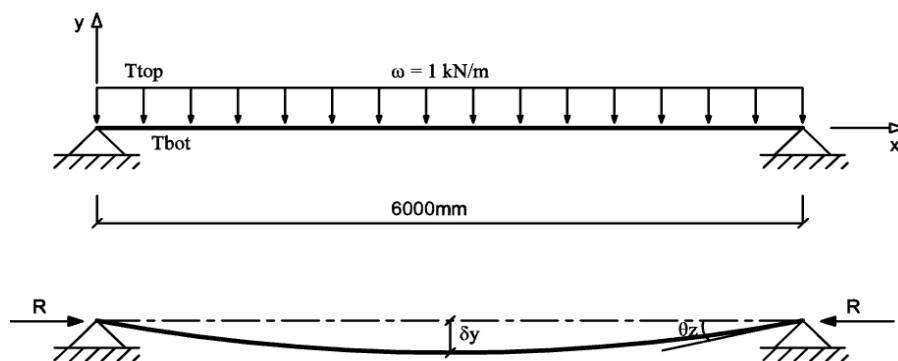


Fig. 2 An end-restrained elastic beam under udl and thermal loading

Table 1 compared results among analytical, OpenSees and ABAQUS

	udl			thermal			udl and thermal		
	analytical	OpenSees	ABAQUS	analytical	OpenSees	ABAQUS	analytical	OpenSees	ABAQUS
$\delta y(\text{mm})$	2.5	2.5	2.51	140.678	140.4	140.4	143.178	142.9	142.91
$\theta z(\text{rad})$	0.133	0.133	0.133	0.936	0.936	0.936	0.0949	0.0949	0.0949
$R(\text{kN})$	0	0	0	4212	4212	4120	4212	4212	4120

3 MODELLING OF AN TEST FRAME

An RC frame is being tested in India under simulated earthquake damage and a subsequent fire. To predict the behaviour of the frame, a two dimension frame model has been analysed. The model was at first subjected to a gradually increased cycle of lateral displacements after loading the columns and the slab/beams with gravity loads. The complete analysis was carried out over a number of steps. In the first step the frame was subjected to increasing quasi-static cyclic displacements as shown in Figure 3. Displacement control was used for the analysis with node 1 (see Figure 4) regarded as the control point with a maximum displacement of approximately 200mm.

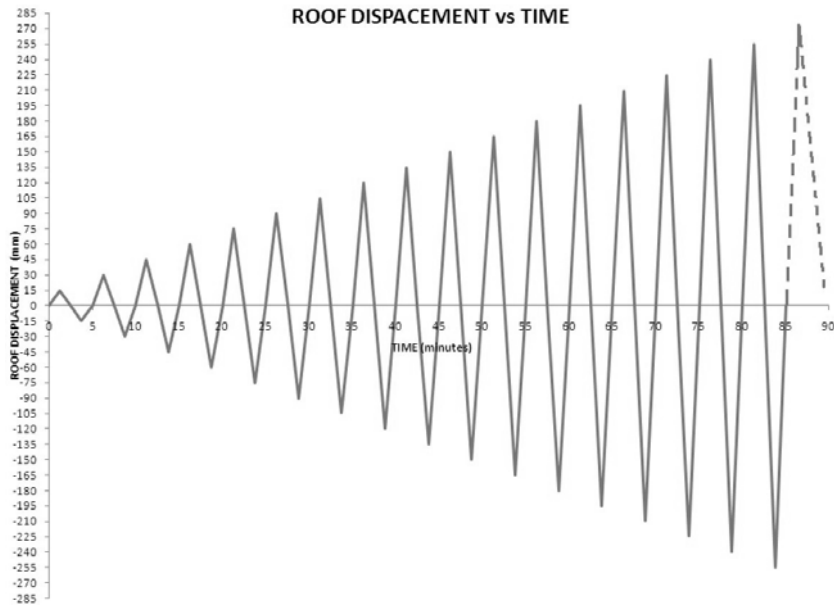


Fig.3. Frame model and the displacement – force curve of control node 1

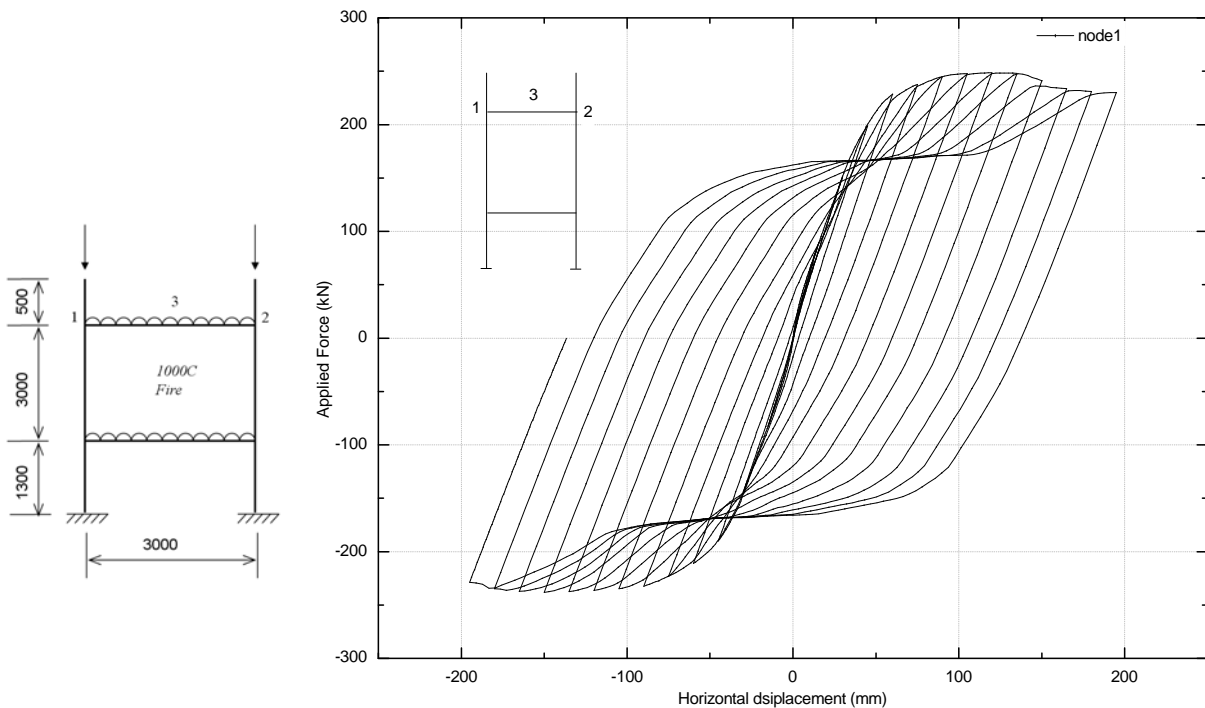
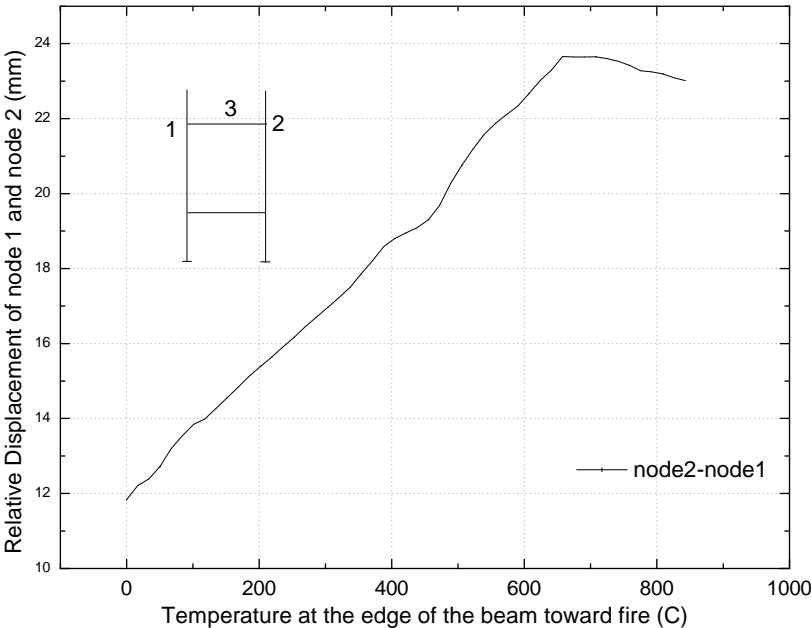
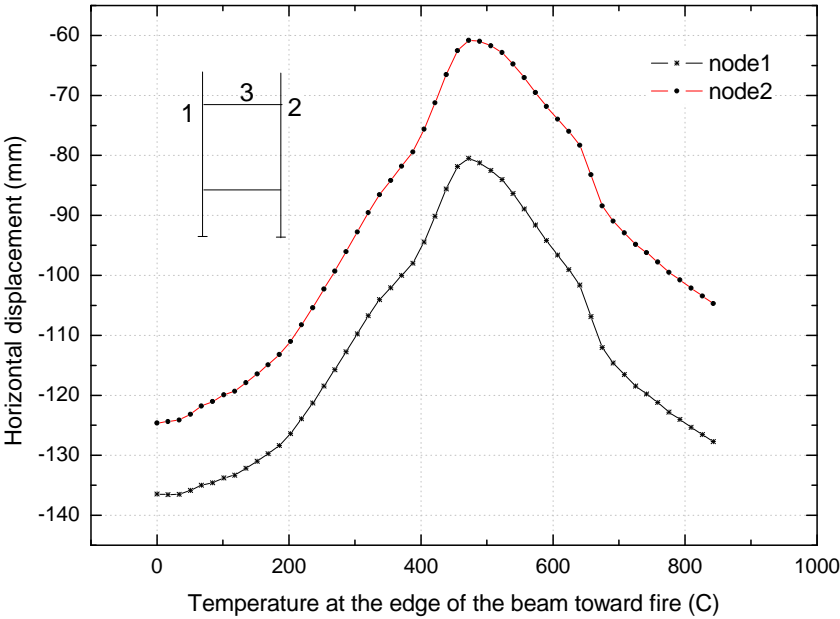


Fig.4. Frame model and the displacement – force curve of control node 1

The Figure 4 shows the complete force-displacement plot node 1. The plot shows that the analysis was carried until maximum displacements of just under 200mm were reached on both sides. The displacement was then reduced until the force at the control point become zero, leaving a permanent residual displacement of approximately 130mm. The displacement corresponding to zero force was obtained from an earlier analysis.

After the damage inducing cyclic displacement step, the frame was subjected to a 1000°C constant fire lasting 3600 seconds. An interesting feature of the behaviour was that the frame seemed to “stiffen” because of the fire. The absolute displacement of node 1 decreased from around -140mm to -80mm under fire until the maximum (exposed face) temperature of the beam reached 450°C, and then it dropped to around -130mm at the end of the heating (Fig. 5). The deflection at the midspan of the upper beam is also shown in Fig. 5 which shows relatively low values as the current model lumps the slab and beam sections together to form the beam. The test results are still awaited, however it is expected that the slab will produce greater deflections after the fire than possible with this 2D model



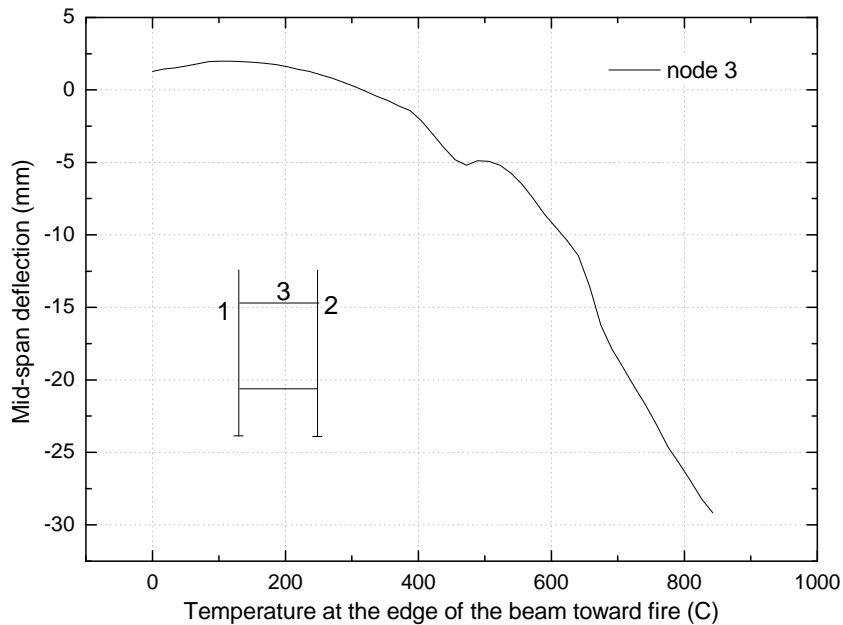


Fig.5. Displacements of node 1, 2 and 3

After the damage inducing cyclic displacement step, the frame was subjected to a 1000°C constant fire lasting 3600 seconds. An interesting feature of the behaviour was that the frame seemed to “stiffen” because of the fire. The absolute displacement of node 1 decreased from around -140mm to -80mm under fire until the maximum (exposed face) temperature of the beam reached 450°C, and then it dropped to around -130mm at the end of the heating. The relative displacement of node 1 and node 3 increased steadily before the temperature reached 650°C, following by a slight drop after that (Fig. 5). The possible reason is that the elongation of the upper beam was affected by two factors – axial thermal elongation and deflection of the beam. The relative displacement of the two nodes increased while axial thermal elongation had a greater effect, otherwise it would decrease. The deflection at the midspan of the upper beam is also shown in Fig. 5 which shows relatively low values as the current model lumps the slab and beam sections together to form the beam. The test results are still awaited, however it is expected that the slab will produce greater deflections after the fire than possible with this 2D model

4 CONCLUSION

A fully nonlinear 2D thermo-mechanical frame analysis capability has been added to OpenSees and had been tested against a number of benchmark problems to ensure that it is working correctly. It has also been combined with the native nonlinear static analysis capability in OpenSees to model damaged frames subjected to fire. Open source codes offer an excellent opportunity for researchers to collaborate across geographical boundaries and build a truly international community to solve engineering problems that are of common concern. This work is a small contribution to the OpenSees movement and considerable further development is in train. Future developments will include full 3D thermo-mechanical analyses for frames by further developing OpenSees beam and shell elements.

REFERENCES

- EQE International. The January 17, 1995 Kobe earthquake—an EQE summary report. April, 1995..
- Buchanan AH. Structural design for fire safety. Chichester, England: Wiley; 2001.
- A. Usmani, J. Zhang, J. Jiang, Y. Jiang, P. Kotsovinos, J. Zhang And I. May. Using OpenSees for structures in fire. 6th International Conference on Structures In Fire, 2010.
- S. Mazzoni, F. Mckenna, et al, OpenSees Command Language Manual, 2007.

PROBABILISTIC ANALYSIS OF CONCRETE BEAMS DURING FIRE

Ruben Van Coile ^a, Emmanuel Annerel ^a, Robby Caspeeel ^a, Luc Taerwe ^a

^a Ghent University, Department of Structural Engineering, Magnel Laboratory for Concrete Research, Ghent, Belgium

INTRODUCTION

In this paper a simple computational tool is presented, which provides insight in the time and temperature dependent reliability of concrete beams during fire. The uncertainty of basic variables is taken into account through Monte Carlo simulations, resulting in a quantification of the uncertainty regarding the bending moment capacity during fire and the corresponding evolution of the safety level. The results of these full-probabilistic simulations are compared with the semi-probabilistic calculation methods as specified in EN 1992-1-2 (CEN, 2004a).

1 MODEL CONCEPTS

The goal of this paper is to quantify the evolution of the structural safety of concrete beams subjected to bending during fire. Due to the changing temperature distribution over the concrete cross-section, the limit state function for bending during fire cannot be formulated analytically. Hence, a computational tool was developed in order to calculate the structural response of concrete members during fire iteratively and to enable a full-probabilistic analysis of this structural response.

1.1 Deterministic analysis

A basic deterministic model is developed in EXCEL, calculating the bending moment capacity for a concrete beam at t minutes of exposure to the ISO 834 fire curve. The beam is assumed to be exposed to fire from three sides (bottom and side faces). The temperature distribution in a cross-section is calculated by the finite element program DIANA and used as input for the EXCEL model.

The bending moment capacity ($M_{R,fi,t}$) is calculated in the ultimate limit state and by the assumptions of the classical linear-elastic structural analysis according to EN 1992-1-1 (CEN, 2004b). Stresses introduced by internal thermal restraint are not considered in this model.

The effects of fire on the material properties of both concrete and reinforcing steel are considered through a temperature dependent function. This kind of simplification corresponds to the methodology followed in EN 1992-1-2. The actual evaluation of the local temperatures θ_i in the concrete cross-section and the corresponding local material properties is performed in discrete square elements measuring 5 mm x 5mm. This type of discretization is visualized in Fig. 1, with ϵ_i the local strain in the ultimate bending limit state, equal for all i at the same vertical distance from the beam bottom. For each discrete concrete segment, the reduction factors of EN 1992-1-2 on the material properties are applied. The model allows to implement alternative definitions of the reduction factors.

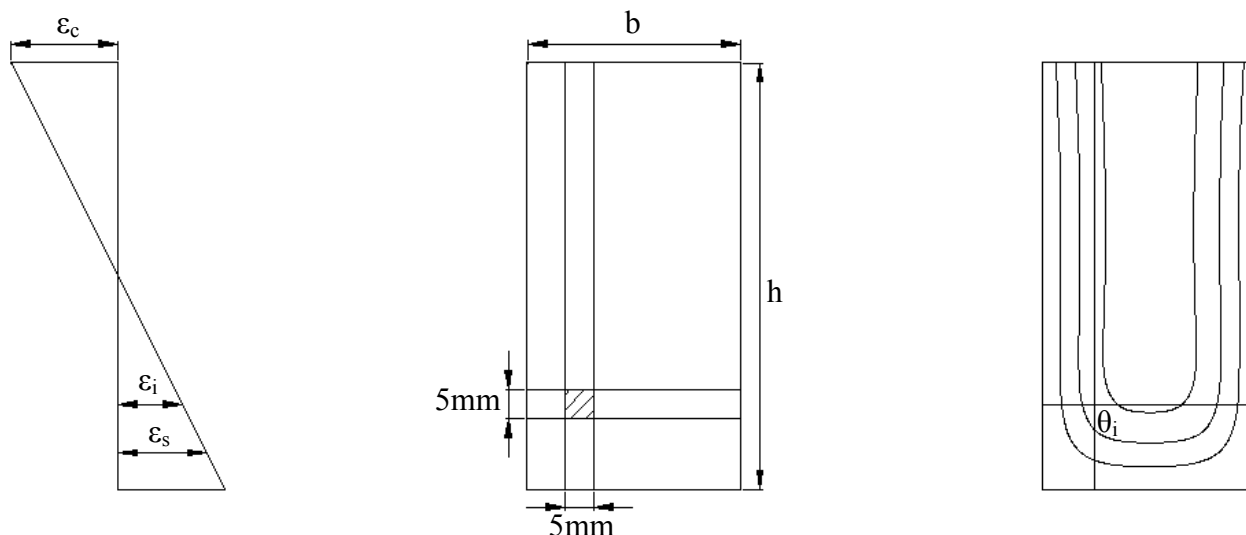


Fig. 1: Discretization of beam cross
(concrete beam (center), temperature distribution (right), distribution of strains (left))

1.2 Modelling of variables

In order to evaluate the uncertainty of the bending moment capacity during fire and to calculate the safety level, the uncertainties with respect to the basic variables must be incorporated in the model through their respective probability distribution functions. This modeling of uncertain variables is implemented independently from the deterministic analysis described above, and can therefore easily be modified. This procedure results in a high degree of flexibility and allows for the incorporation of updated information when this is available. The distributional characteristics considered in this paper are based on (Holický and Sýkora, 2010) and the applicable distribution types are presented in Tab. 1. All stochastic variables are considered independent. If more specific information is available with respect to the correlation between specific variables, the developed model can be further adjusted.

Tab. 1: Stochastic variables in full-probabilistic model

Symbol	Name	Distribution
h	beam height	Normal
b	beam width	Normal
$f_c(20^\circ\text{C})$	20°C concrete compressive strength	Lognormal
$f_y(20^\circ\text{C})$	20°C yield strength reinforcement	Lognormal
$E_c(20^\circ\text{C})$	20°C concrete modulus of elasticity	Lognormal
A_s	reinforcement section	Normal
c	concrete cover	beta $[0; 3c_{\text{nominal}}]$ (*)
χ	model uncertainty	Lognormal

(*) a beta distribution with the same characteristics as described in (Holický and Sýkora, 2010), but defined over the range $[c_{\text{nominal}}-5; c_{\text{nominal}}+5]$ would be more suitable in the opinion of the authors of this paper

Additionally, in order to take the uncertainty regarding the reduction of the mechanical properties at high temperatures into account, a temperature-dependent normal distribution is proposed for the reduction factors for both the concrete compressive strength and the reinforcement yield strength. Both normal distributions are characterized by a mean value equal to the nominal reduction factor of EN 1992-1-2 and a standard deviation based on laboratory tests (Annerel, 2010). For the compressive concrete strength, the standard deviation of the reduction factor is assumed to be 0 at 20°C and 0.045 at 700°C. Linear interpolation is used for intermediate values. For the mechanical reinforcement properties, a similar assumption is made, with a standard deviation of 0.065 at

600°C. The concept is illustrated in Fig. 2 where the 5%, 50% and 95% fractiles of the reduction variable $f_c(\theta)/f_c(20^\circ\text{C})$ are visualized. It is important to note that this uncertainty in reduction factor is additional to the uncertainty on the material characteristics at ambient temperature (20°C). Similarly, Fig. 3 visualizes the 5%, 50% and 95% fractiles of the reduction variable $f_y(\theta)/f_y(20^\circ\text{C})$. No spalling is taken into account, although this could be implemented through a probabilistic degradation function for the concrete cover c .

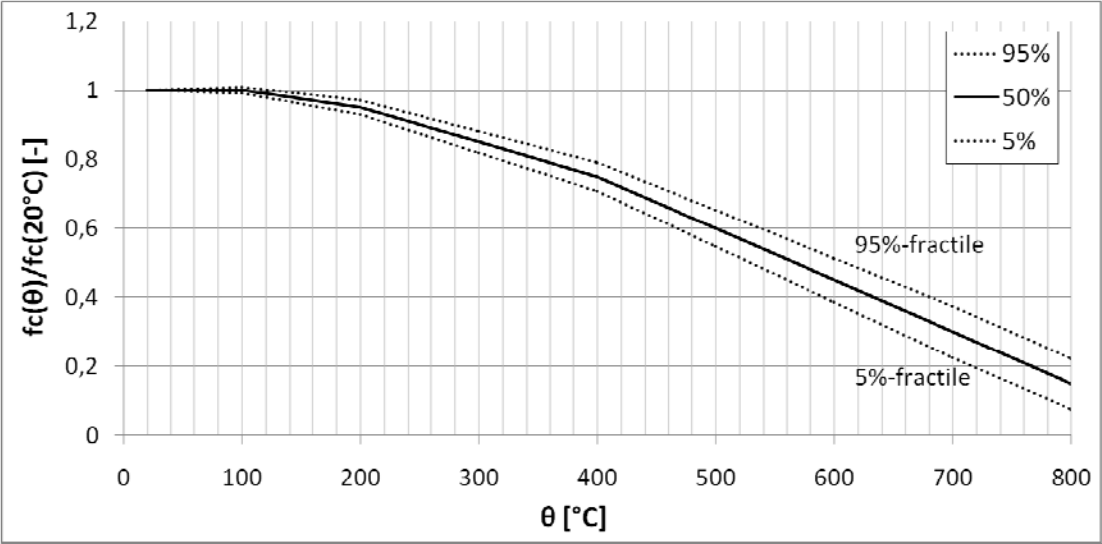


Fig. 2: 5%, 50% and 95% fractiles of reduction factor $f_y(\theta)/f_y(20^\circ\text{C})$

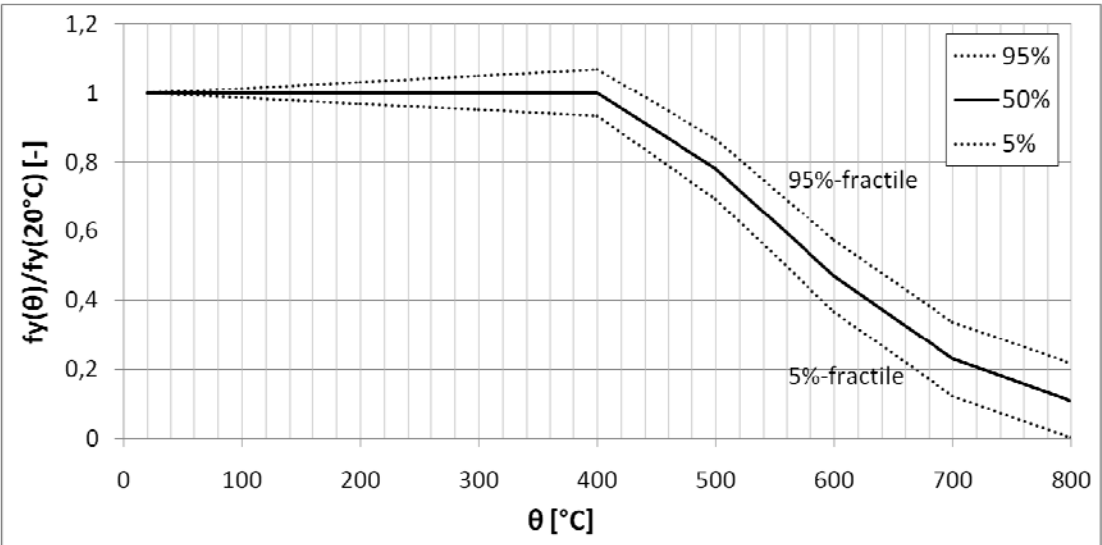


Fig. 3: 5%, 50% and 95% fractiles of reduction factor $f_c(\theta)/f_c(20^\circ\text{C})$

1.3 Uncertainty propagation: crude Monte Carlo simulations

The properties of each beam are characterized by a vector \underline{X}_i of randomly generated values of the variables described above. 10000 vectors \underline{X}_i are generated. For all of these realizations the bending moment capacity during fire is evaluated by the described deterministic analysis. The results of these calculations are analyzed statistically, resulting in an expected value and standard deviation of the bending moment capacity of the concrete beam exposed to fire. This type of analysis by repeated random sampling of the parameter space is generally referred to as Monte Carlo sampling.

2 INTERPRETATION OF MODEL RESULTS

Traditionally, EN 1992-1-2 defines the fire resistance time t_R through equation (2), with $M_{Rd,fi,t}$ the design value of the bending moment capacity and $M_{Ed,fi,t}$ the design value of the bending moment induced by the design loads.

$$M_{Rd,fi,t} \geq M_{Ed,fi,t} \quad \text{for } t \leq t_R \quad (2)$$

$M_{Ed,fi}$ is considered to be constant, thus without consideration of indirect thermal actions, i.e. $M_{Ed,fi,t} \equiv M_{Ed,fi}$. A method for evaluating the safety level of a concrete beam during fire is proposed by equations (3) and (4).

$$P_{f,1} = P[M_{R,fi,t} < M_{Ed,fi}] = \Phi(-\beta_1) \quad (3)$$

$$P_{f,2} = P[M_{R,fi,t} < M_{Rd,fi,t}] = \Phi(-\alpha_R \beta_2) = \Phi(-\beta_2) \quad \text{where } \alpha_R = 1 \text{ as } \sigma_E < 0.16\sigma_R \quad (4)$$

Both equations compare the results of the Monte Carlo simulations for the bending moment capacity with the design values of the semi-probabilistic calculation method of EN 1992-1-2. Equation (3) allows for an evaluation of the structural fire resistance, but is dependent on the variable load. On the other hand, as elaborated in (Gulvanessian et al, 2002), equation (4) allows to evaluate the intrinsic safety of the design value of the bending moment capacity of the beam configuration, i.e. β_2 indicates which fractile of the bending moment distribution corresponds to the design value given by the Eurocodes. According to Eurocode 0 (CEN, 2002), the sensitivity factor α_R can be assumed equal to 1 for this case since $\sigma_E/\sigma_R < 0.16$. This result is based on additional Monte Carlo simulations in which the standard deviation of the design value of the bending moment induced by the design loads was simulated and compared to the simulated standard deviation of the bending moment capacity. The stochastic characteristics for the design loads are based on (Holický and Sýkora, 2010).

Although β_1 and β_2 are not the conventional definitions of the safety index β and consider only the stochastic nature of the resistance effect, both equations allow to investigate the influence of the basic variables on the safety level. Since the main objective of this study is to compare the safety level of different configurations and to analyze the effect of basic stochastic assumptions on the evolution of the safety level, the deviation from the classical definition is acceptable. Furthermore, since α_R can be assumed equal to 1, at the fire resistance time t_R equations (3) and (4) are equal, as shown mathematically by equation (5). As such, the fire resistance time of the beam can be approximated by the intersection of the β_1 and β_2 curves.

$$\Phi(-\beta_{1,t_R}) = P[M_{R,fi,t_R} < M_{Ed,fi}] = P[M_{R,fi,t_R} < M_{Rd,fi,t_R}] = \Phi(-\alpha_R \beta_{2,t_R}) = \Phi(-\beta_{2,t_R}) \quad (5)$$

Finally, both equations (3) and (4) can be evaluated by using the frequentist interpretation of probability.

3 APPLICATION EXAMPLE

As an application example, simulation results are presented for the concrete beam presented in Table 2. The distribution parameters for the random variables considered are given in Tab. 3, based on (Holický and Sýkora, 2010). According to the ‘table method’ of (CEN, 2004a) the characteristics of the example beam correspond to a fire resistance of 90 min ($a = 40$ mm, $a_{sd} = 50$ mm, $b_{min} = 300$ mm) when the beam is simply supported. In accordance with the calculation methodology of EN 1992-1-1 (CEN, 2004b) the example beam has a design value of 358 kNm for the bending moment capacity at ambient temperature.

Table 2: Configuration example concrete beam

Symbol	Characteristic	Unit	Nominal Value
h	beam height	mm	600
b	beam width	mm	300
$f_{ck}(20^{\circ}\text{C})$	20°C characteristic compressive strength	MPa	40
$f_{yk}(20^{\circ}\text{C})$	20°C characteristic yield strength	MPa	500
$E_c(20^{\circ}\text{C})$	20°C concrete modulus of elasticity	GPa	34.5
$E_s(20^{\circ}\text{C})$	20°C steel modulus of elasticity	GPa	200
c_1	bottom concrete cover	mm	30
\emptyset_1	bottom reinforcement diameter	mm	20
$\#_1$	number of bottom reinforcement bars	-	5
s_1	spacing bottom reinforcement bars	mm	50
c_2	top concrete cover	mm	30
\emptyset_2	top reinforcement diameter	mm	20
$\#_2$	number of top reinforcement bars	-	5
s_2	spacing top reinforcement bars	mm	50
χ	model uncertainty	-	1.2

Tab. 3: Stochastic models for variables

Symbol	Variable	Distribution type	Mean μ	Standard deviation σ
h	beam height	normal	600 mm	5 mm
b	beam width	normal	300 mm	5 mm
$f_c(20^{\circ}\text{C})$	20°C concrete compressive strength	lognormal	45.4 MPa	2.7 MPa
$f_y(20^{\circ}\text{C})$	20°C steel yield strength	lognormal	581 MPa	41 MPa
$E_c(20^{\circ}\text{C})$	20°C concrete modulus of elasticity	lognormal	34.5 GPa	5.2 GPa
$c_{1,2}$	concrete cover	β [0; $3c_{\text{nominal}}$]	30 mm	2 mm
χ	model uncertainty	lognormal	1.2	0.15

Simulation results for the example beam are presented in Fig. 4. The curves in Fig. 4 are normalized according to the 50% fractile of the bending moment capacity ($M_{R,fi,t,50}$) at the start of the fire (i.e. at ambient temperature). The intersection of the design value of the bending moment capacity and the design value of the bending moment induced by the design loads is situated at approximately 83 minutes of exposure.

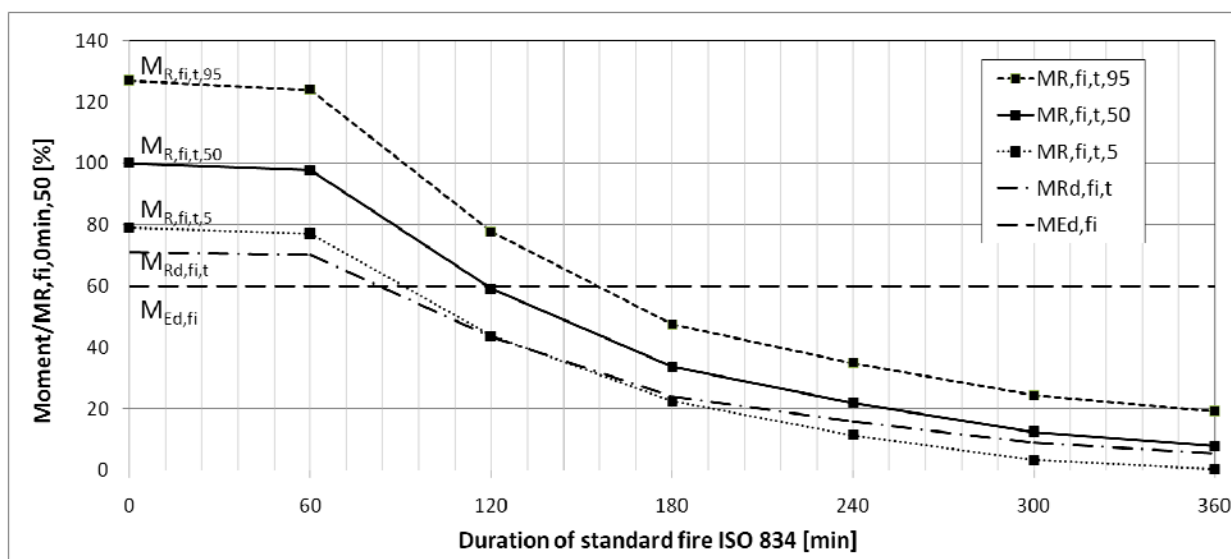


Fig. 4: Model results for example beam ($M_{R,fi,t,50} = 583$ kNm)

The calculated safety indices β_1 and β_2 according to equation (3) and (4) are visualized in Fig. 5. The intersection of both curves corresponds to a fire resistance of 80 min. While the decrease of β_1 indicates the increasing probability of structural failure, the decrease of β_2 corresponds to an increasing probability that the design value of the bending moment capacity ($M_{Rd,fi,t}$) overestimates the actual bending moment capacity ($M_{R,fi,t}$) of the example beam. The latter can be explained by the uncertainty related to the reduction of material properties at elevated temperatures and the uncertainty of the reinforcement temperature (i.e. the concrete cover). These elements are not explicitly taken into account by the semi-probabilistic design methods in the Eurocode (CEN, 2004a).

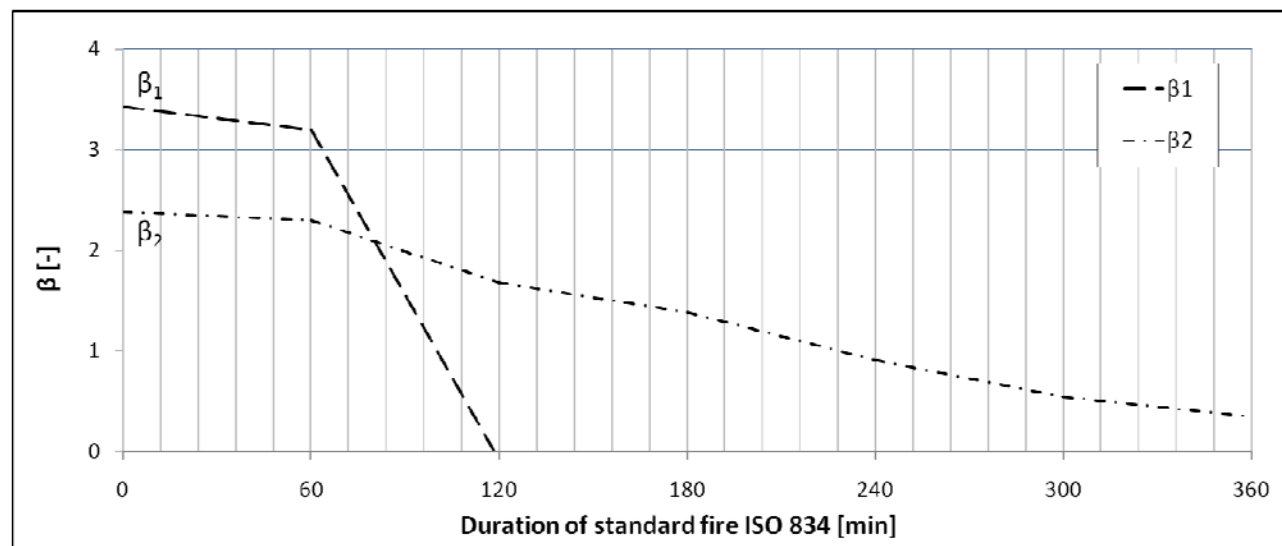


Fig. 5: β_1 and β_2 for example beam configuration

By altering the beam configuration the simulated fire resistance time can be increased. Simulations indicate that an increase of the concrete cover is particularly efficient, while increasing the concrete compressive strength has less impact.

4 CONCLUSIONS

- A full-probabilistic model is developed for analyzing the safety level of concrete beams
- Based on the probabilistic analysis of a beam the fire resistance time was found to be smaller than tabulated by EN 1992-1-2 (CEN, 2004a).
- The fire resistance of a beam can be increased by altering the beam configuration, or by decreasing the uncertainty on e.g. the concrete cover through sampling and testing.

REFERENCES

- Gulvanessian H, Calgaro JA, Holický M. Designers' guide to EN 1990: Eurocode 0: basis of structural design. London: Thomas Telford; 2002
- CEN. Eurocode 0: Basis of structural design. European Standard EN 1990; 2002
- CEN. Eurocode 2: Design of concrete structures: Part 1-2: Structural fire design, European Standard EN 1992-1-2; 2004a
- CEN. Eurocode 2: Design of concrete structures: Part 1-1: General rules and rules for buildings, European Standard EN 1992-1-1; 2004b
- Annerel E, Taerwe L. Evolution of the strains of traditional and self-compacting concrete during and after fire. Mater. Struct. 2010; Online First
- Holícký M, Sýkora M. Stochastic models in analysis of structural reliability, Proceedings of the International Symposium on Stochastic Models in Reliability Engineering, Life Sciences and Operation Management, Beer Sheva, Israel; 2010

SHEAR STRENGTH OF CONCRETE AT ELEVATED TEMPERATURE

Holly K. M. Smith ^a, Emma R. E. Reid ^a, Andrew A. Beatty ^a, Tim J. Stratford ^a, Luke A. Bisby ^a

^a BRE Centre for Fire Safety Engineering, The School of Engineering, The University of Edinburgh, Edinburgh, UK

INTRODUCTION

Performance based methods for designing concrete structures in fire have focused to date upon the flexural performance of beam and slab elements and large displacement mechanisms for sustained load capacity at high temperature. Shear failure has received little attention, but there is a growing awareness that shear can govern the failure of concrete structures in fire, for example in punching shear (Bamonte *et al.*, 2009) or as a consequence of restrained thermal expansion (Faria *et al.*, 2010).

Shear is carried in reinforced concrete through the interaction of (Regan, 1993)

- compressive force paths within the concrete;
- tensile crack bridging by the reinforcing steel (relying upon concrete-steel bond);
- dowel action in the reinforcing steel; and
- friction across cracked surfaces due to aggregate interlock.

Modelling the complex interplay of these shear-carrying mechanisms is notoriously difficult, even at ambient temperatures. Accurate finite element modelling requires a very detailed representation of the load carrying phenomena and their constitutive responses (Kotsovos & Pavlović, 1995). Whilst we have understanding of how (for example) the compressive strength of concrete and the tensile strength of steel are affected by elevated temperature (e.g. Khoury, 2000; Zhang *et al.*, 2000), there is currently insufficient elevated temperature understanding of the shear mechanisms and their interaction to allow reliable finite element modelling of concrete in shear in fire.

This paper describes an investigation of the effect of elevated temperature upon the shear performance of concrete. It is a first step in determining detailed constitutive information that can be used in modelling and design.

1 EXPERIMENTAL PROGRAMME

A series of shear blocks were constructed and tested, which are shown in Fig. 1. These were similar in concept to the shear blocks tested by Mattock (Mattock & Hawkins, 1972), but a modified geometry was adopted, based upon that used by Ali *et al.* (2008).

Shear blocks are designed to load a reinforced concrete section in pure shear, and hence fail along by cracking along the central shear plane (Fig. 1). The behaviour of this crack is characterised by aggregate interlock action and reinforcement bridging, and is particularly relevant to the shear failure of columns where aggregate interlock is mobilised due to the confinement provided by the axial force in the column.

The shear blocks were heated so as to expose the concrete to temperatures that are known to affect the properties of concrete. Residual strength tests were conducted on the specimens after cooling. (The second phase of these tests will involve strength tests whilst at elevated temperature).

1.1 Specimen Construction and Conditioning

Sixteen shear block specimens were cast. The specimens had dimensions 100×160×320mm, which was governed by the physical size and the thermal mass that could be effectively heated. The specimens were reinforced with 6 mm diameter smooth steel bars with an ambient yield strength of 415 MPa (Fig. 2). Four pieces of reinforcement crossed the shear failure plane, with additional reinforcement to provide anchorage and to prevent failure of the concrete away from the shear plane.

The concrete was provided by a local readymix supplier, with a maximum aggregate size of 10mm, an ambient compressive strength of $f_c = 29$ MPa (based upon cube tests), and an ambient tensile strength of $f_t = 1.8$ MPa (based upon split-cylinder tests).

After removal from the moulds, the specimens were cured in a water tank for one week, followed by seven weeks in a low humidity environment, controlled by a dehumidifier. To reduce the moisture content of the specimens and hence minimise the likelihood of spalling, the specimens were pre-dried at 90°C for seven days. Two standard 100mm cylinder specimens were cast for each shear block, and these were conditioned in the same way.

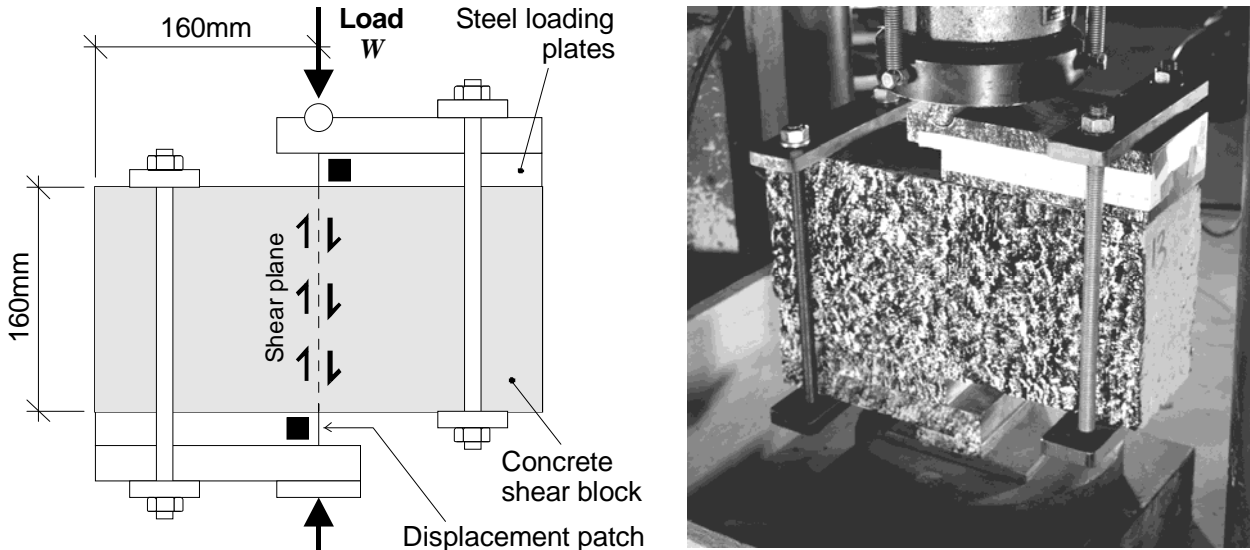


Fig.1 Overview of the shear block test arrangement

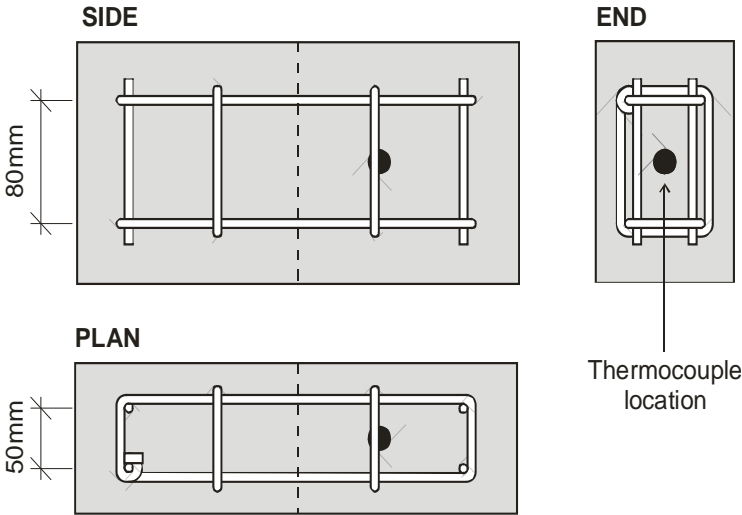


Fig.2 Details of the shear block reinforcement

1.2 Heating regime

The specimens were heated in an electric furnace, which could accommodate one shear block and two cylinders at a time. They were heated to temperatures of 112°C, 188°C, 390°C, 475°C and 622°C, as shown in Tab. 1. Another set of specimens was unheated (17°C).

Tab. 1 Specimen Test Programme and Key Results

Specimen ID	Heating duration [mins]	Target internal temperature [°C]	Achieved peak internal temperature [°C]	Compressive concrete strength [N/mm ²]	Tensile concrete strength [N/mm ²]	Shear failure load [kN]	Shear failure stress [N/mm ²]	Frictional shear stress [N/mm ²]
17-1	-	17	17.2	25.1	4.1	100.5	6.3	-
17-2			17.0			93.7	5.9	-
17-3			17.1			110.5	6.9	3.5
17-4			17.5			119.2	7.5	2.6
112-1	120	112	102.7	26.9	3.7	103.5	6.5	2.9
112-2			109.2			97.5	6.1	3.9
112-3			122.6			102.0	6.4	2.7
188-1	120	188	178.1	27.8	3.9	93.0	5.8	2.4
188-2			191.2			88.5	5.5	3.6
188-3			196.1			106.3	6.6	3.3
390-1	120	390	379.9	19.3	2.5	91.0	5.7	1.9
390-2			399.8			95.0	5.9	3.3
475-1	120	475	464.1	17.5	2.2	79.8	5.0	-
475-2			486.5			81.8	5.1	1.5
622-1	165	622	619.9	12.6	1.8	71.8	4.5	1.8
622-2			624.4			67.9	4.2	1.8

A thermocouple was placed at the centre of the shear block (Fig. 2) to record the internal temperature, and a second thermocouple was used to record the furnace temperature. The furnace was used to heat the specimens as quickly as possible, with an oven temperature increase rate in the range 5 and 15°C/min. After the initial heating, the furnace was controlled manually to achieve the required temperature inside the concrete. All specimens were heated for 2 hours, except for those at the highest temperature, for which it was necessary to increase the heating duration to 2 ¾ hours.

After heating, the specimens were left in the furnace to cool, and then each specimen was left for seven days before its strength was determined.

1.3 Strength tests

Steel loading plates were added to the shear block to force shear failure, as shown in Fig. 1. The specimens were loaded using a hydraulic universal test machine at an initial rate of 20 kN/min, with the applied load recorded using a load cell.

Digital image correlation was used to obtain the specimen displacements from a sequence of 21 megapixel photographs taken at a frequency of 0.2 Hz. The specimens were painted with a high-contrast speckle pattern prior to testing, and a bespoke image-processing algorithm was used to track the motion of selected patches of the speckle pattern from image to image (Bisby & Take, 2009). Digital image correlation was chosen rather than a traditional displacement measurement technique because it allows the positions at which displacements are measured to be selected after the test; allows relative displacements to be measured within the concrete (hence avoiding the effects of local crushing at the supports); allows both the shear displacement and crack opening displacement to be measured across the cracked surface; and allows any variations in displacement along the crack surface to be observed. The resolution of digital image correlation for this application was in the order of 0.006 mm

A cylinder compression and split-cylinder tension test (conducted to EN 12390) accompanied each shear block test.

2 EXPERIMENTAL RESULTS

Tab.1 provides a summary of the key experimental results.

2.1 Heating regime

Fig. 3 shows the temperatures recorded within the concrete shear blocks and the corresponding temperatures in the furnace. The peak temperatures within each specimen are given in Tab. 1.

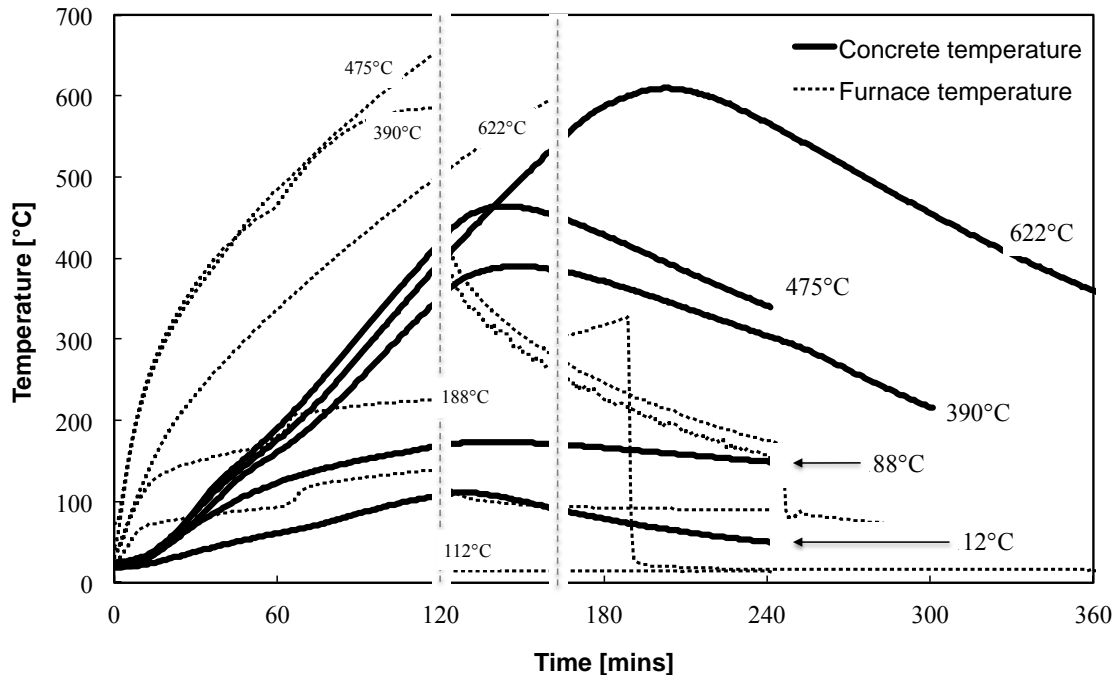


Fig. 3 Recorded temperatures in the furnace and within the concrete blocks

2.2 Strength variation with temperature

Fig. 4 plots the variation in compressive and tensile strengths of the concrete that were obtained from the cylinders that were heated at the same time as the shear blocks. For clarity, these have been normalised by the ambient temperature strength of the concrete, and the average strength variation with temperature is shown. The reduction in concrete strength with temperature is as expected, but it should be noted that some of the specimens suffered from poor compaction.

Fig. 4 also plots the variation in the shear strength of the shear blocks with temperature. The shear strength follows a similar trend to the concrete strength variation. However, the reduction in shear strength is less pronounced at high temperatures, because it is dependent upon the strengths of both the concrete and steel.

2.3 Load-displacement and crack opening width responses

Fig. 5 shows the load versus shear displacement measured across the crack. For clarity, one load-displacement response has been plotted for each temperature; these were chosen to be a good representation of the full set of results; other responses were similar.

The load-deflection response of the shear blocks has an initial peak load, at which point the shear crack fully forms and the shear capacity drops to a frictional value that is governed by aggregate interlock, confinement by the reinforcement, and reinforcement dowel action. The initial stiffness and the peak strength of the specimen reduced with temperature, whereas the displacement corresponding to the peak strength increased with temperature.

The post-peak frictional shear strength was also affected by temperature, with two clear groups apparent: the lowest three temperatures carried a frictional shear of 50 kN; the highest three temperatures carried a frictional shear of 25 kN. At the three lower temperatures, diagonal tension cracks initially formed at an angle to shear plane, which coalesced into a single shear crack. The reinforcement sheared across the crack, and caused some separation of the cover concrete.

At the three higher temperatures, the straight shear crack formed immediately. Cover concrete bursting was far more extensive, and this allowed the reinforcement to debond and reduced confinement of the shear crack. The aggregate could also be heard to “snap” during the higher temperature residual tests. Consequently, the performance of the shear blocks was governed by a combination of the residual strength of the concrete, the residual strength of the reinforcement and the complex interaction between the two.

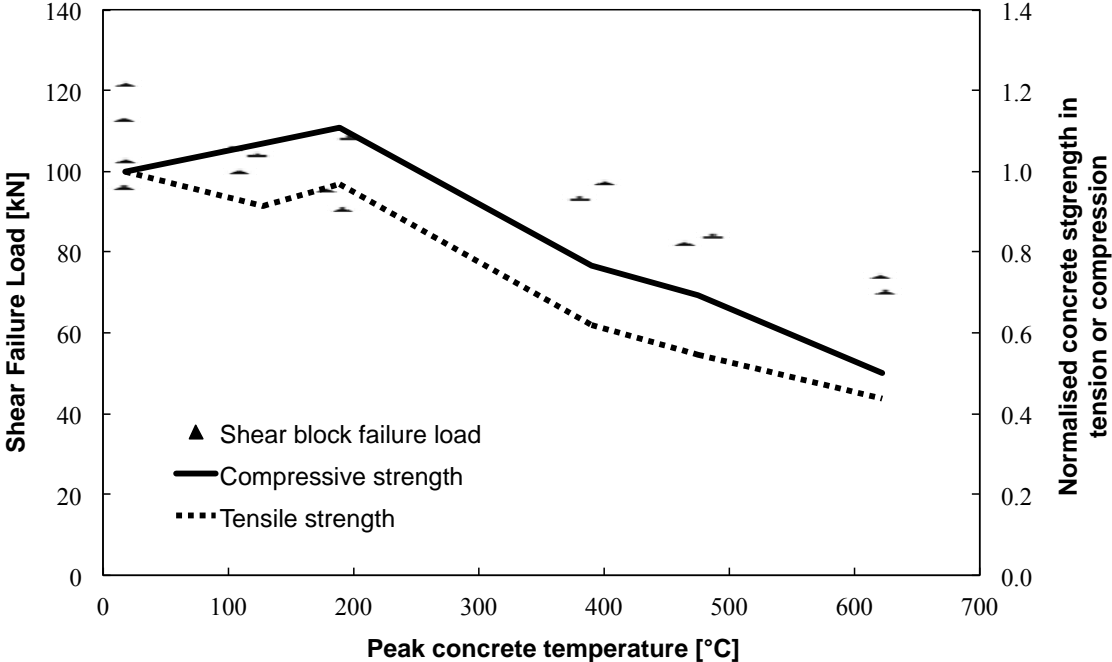


Fig. 4 The effect of temperature upon the residual strength of the shear block, and upon the residual compressive and tensile strengths of the concrete.

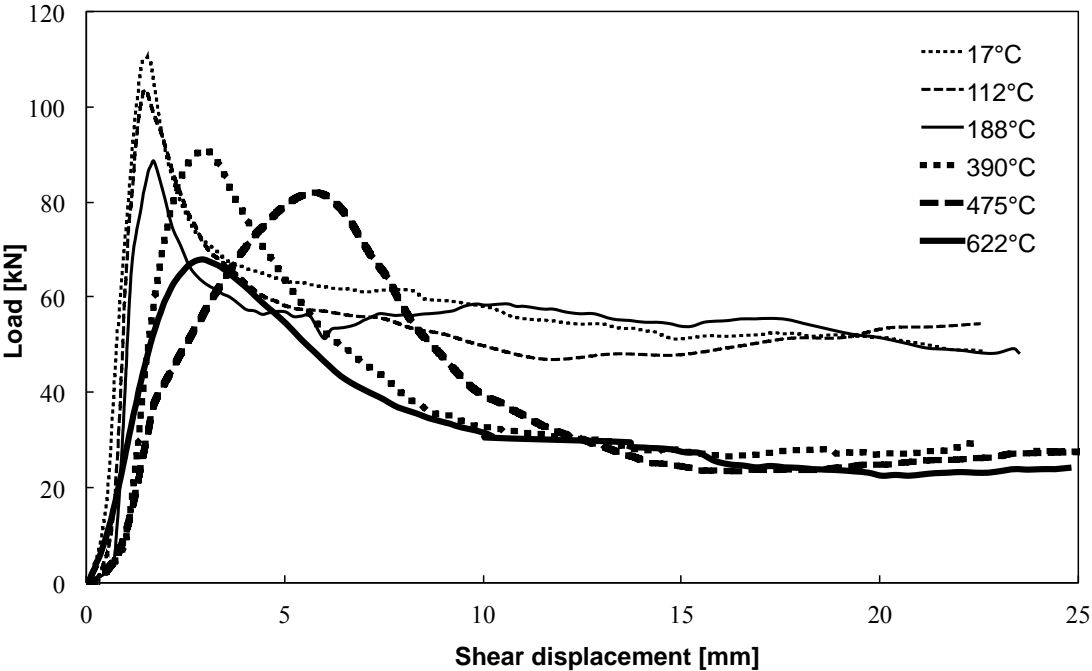


Fig. 5 The effect of temperature on the residual load-displacement response of the shear blocks

Digital image correlation was used to determine the crack opening widths that developed as the load was applied, and these are plotted in Fig. 6. Again, the response is split into two groups, with the three higher temperatures characterised by larger crack opening displacements, even prior to the peak load being reached.

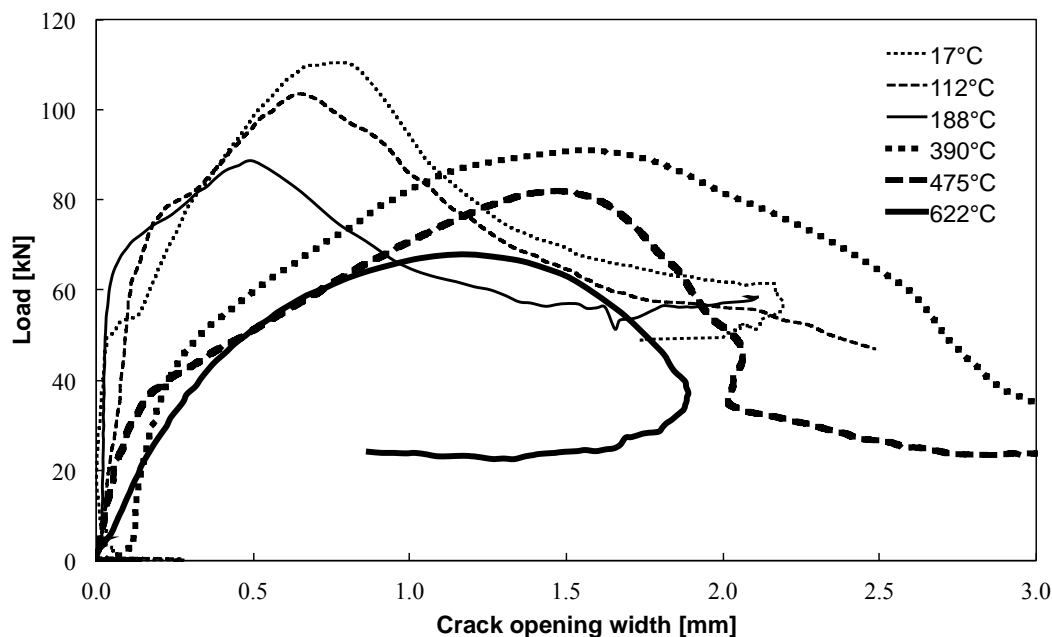


Fig. 6 The effect of temperature on crack opening width development.

3 SUMMARY

The results presented in this paper demonstrate that the residual shear strength of reinforced concrete is affected by the temperature to which it has been exposed. The reduction in shear performance depends upon the interaction of the concrete and the reinforcing steel. For example, the tests have shown that concrete exposed to high temperatures suffers from increased cover separation (due to the reduced tensile strength), which allows greater reinforcement debonding and hence less confinement, which in turn mobilise less aggregate interlock shear.

REFERENCES

- Ali, M., Oehlers, D., & Griffith, M. (2008). Shear transfer across cracks in FRP strengthened RC members. *Journal of Composites for Construction*, 12(4):416-424.
- Bamonte P., Felicetti R., Gambarova P.G. (2009). Punching shear in fire-damaged reinforced concrete slabs. *American Concrete Institute*, 265:345-366.
- Bisby, L. A., Take, W. A. (2009). Strain Localizations in FRP Confined Concrete: New Insights. *Proceedings of the ICE - Structures and Buildings*, 162(5):301-309.
- Faria R., Xavier H.F., Real P.V. (2010). Simplified procedure for shear failure assessment of RC framed structures exposed to fire. *Structures in Fire – Proceedings of the 6th international conference*, Michigan, 197-205.
- Khoury, G. (2000). Effect of fire on concrete and concrete structures. *Progress in Structural Engineering and Materials*, 2(4):429-447.
- Kotsovos M.D. & Pavlović M.N. (1995) *Structural concrete – Finite-element analysis for limit-state design*. Thomas Telford Ltd., London.
- Mattock, A., & Hawkins, N. (1972). Shear Transfer in Reinforced Concrete - Recent Research. *PCI Journal*, (March-April):55-75.
- Regan P.E. (1993). Research on shear: a benefit to humanity or a waste of time? *The Structural Engineer*, 71(19):337-347.
- Zhang B., Bicanic N., Pearce C.J., Balabanic G. (2000), Assessment of toughness of concrete subject to elevated temperatures from complete load-displacement curve - part II: experimental investigations. *ACI Materials Journal*, 97(5):556-566.

FIRE DESIGN OF CONCRETE AND MASONRY STRUCTURES **Software Tools Developed at the Czech Technical University in Prague**

Radek Štefan ^a, Jaroslav Procházka ^a, Michal Beneš ^a

^a Czech Technical University in Prague, Faculty of Civil Engineering, Prague, Czech Republic

INTRODUCTION

During the last few years, scientific and professional community has focused on developing effective software tools to fire design of structures. In many cases, utilization of an appropriate software tool is the only way (except fire tests) to assess a real behaviour of a structure under fire conditions. On the other hand, when designing simple and commonly used structures or structural members, the usage of software tools is not necessary. However, in these cases, it also may lead to significant time saving.

In this paper, brief information about software tools to fire design of concrete and masonry structures developed at the Czech Technical University in Prague are summarised. Section 1 present computer program *TempAnalysis* (Štefan, Procházka, 2009), which is intended for thermal analysis of rectangular cross-sections exposed to fire. In Section 2, software *HygroThermAnalysis* (Štefan, Beneš, 2010) is briefly described. This software can be used to hygro-thermal analysis of concrete cross-sections under fire conditions. Moreover, using this software, it is also possible to predict concrete surface spalling. Section 3 describes software package *FiDeS* (Štefan, 2010), destined for fire design of concrete and masonry structures according to Eurocodes. The presented software tools have been developed in MATLAB (2008) environment. They are available for free on web site <http://concrete.fsv.cvut.cz/~stefan/research.htm>.

1 TempAnalysis SOFTWARE

1.1 Software description

TempAnalysis software (Štefan, Procházka, 2009) is intended for thermal analysis of rectangular cross-sections exposed to fire. Using this program, it is possible to solve one-dimensional (slabs, walls) and two-dimensional (beams, columns) heat transfer problem. The program consists of two parts: pre-processor for input data and post-processor for display of results. The pre-processor dialog window is shown in Fig. 1. Material properties (density, thermal conductivity and heat capacity) of an analysed cross-section can be assumed as linear (i.e. temperature independent) or non-linear (i.e. temperature dependent). For concrete, material model defined by EN 1992-1-2 (2004) is preset in the program. An analysed cross-section can be protected by insulation on the fire-exposed sides. In this case, the thickness of the protective layer and its material properties shall be defined. A design fire scenario is represented either by the standard temperature-time curve ISO 834 or, alternatively, by the parametric curve according to EN 1991-1-2 (2002). For a one-dimensional problem, one-sided or two-sided fire exposure can be set. For a two-dimensional problem, two-, three- or four-sided fire exposure can be chosen.

Heat transfer model included in the program is described in detail in (Štefan, Procházka, 2010c). The space discretization of the governing equations is carried out using a finite element method. The time discretization is performed using a semi-implicit difference scheme. In the previous version of the *TempAnalysis* software, a two-dimensional problem has been based on a simplified approach proposed by Hertz (2006), which consists in two separate one-dimensional solutions in x - and y -direction, see (Procházka, Štefan, 2009; Štefan, Procházka, 2010c). In the current version, a two-dimensional problem can be solved either using the simplified approach mentioned above or, alternatively, with the use of the two-dimensional finite element method with bilinear quadrilateral finite elements, for comparison see Fig. 4.

In the post-processor part of the program, it is possible to display a value of temperature of any point of the analysed cross-section and to plot a resulting temperature profile or temperature field, see Fig. 2–3.

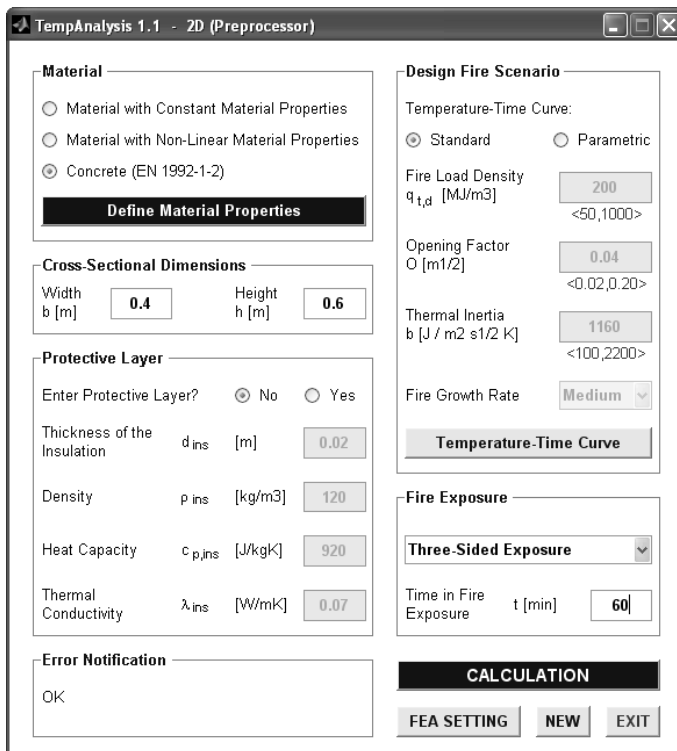


Fig. 1 Pre-processor dialog window

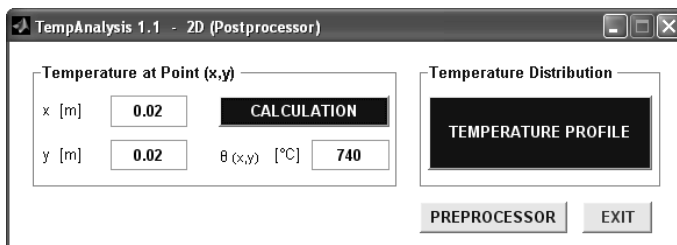


Fig. 2 Post-processor dialog window

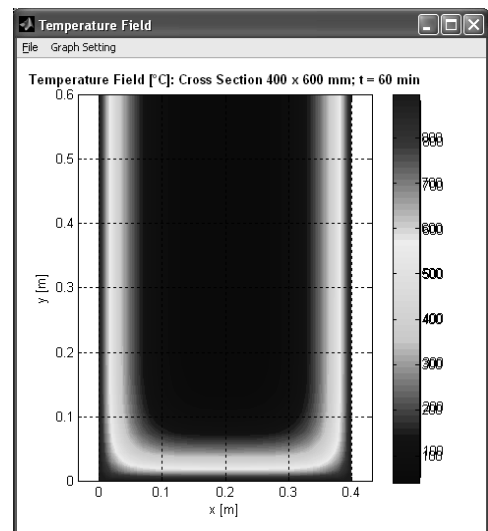
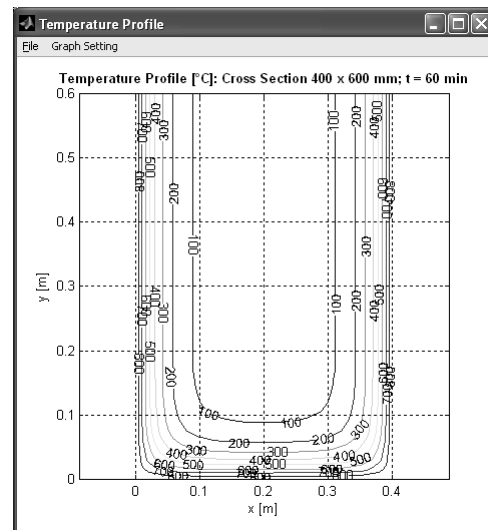


Fig. 3 Temperature profile/field

1.1 Software validation

A validity of the *TempAnalysis* software has been assessed by comparing the results obtained by the software with the corresponding data given by Eurocodes and by literature. Fig. 4 shows the temperature profiles of a concrete cross-section $400 \times 400 \text{ mm}^2$ subjected to standard fire (ISO 834, four-sided exposure) for 60 minutes. It is obvious that when using the simplified procedure for the two-dimensional problem (two separate one-dimensional solutions), the results given by the *TempAnalysis* software are a little bit different from the standard profiles given by EN 1992-1-2 (2004). Nevertheless, for practical design, this accuracy seems to be sufficient. On the other hand, when using the two-dimensional finite element method, the results obtained by finite element analysis (FEA) are in accordance with the standard profiles.

For illustration, comparison of calculated temperatures with the measured data provided by (Haksever, Anderberg, 1981) appears in Fig. 5. A scheme of the analysed cross-section is shown in Fig. 6. For the FEA, material properties of concrete have been taken from EN 1992-1-2 (2004) assuming the values listed in Table 1. Regarding the uncertainties in the input data, an accordance of the calculated temperatures with the measured data can be evaluated as fully sufficient.

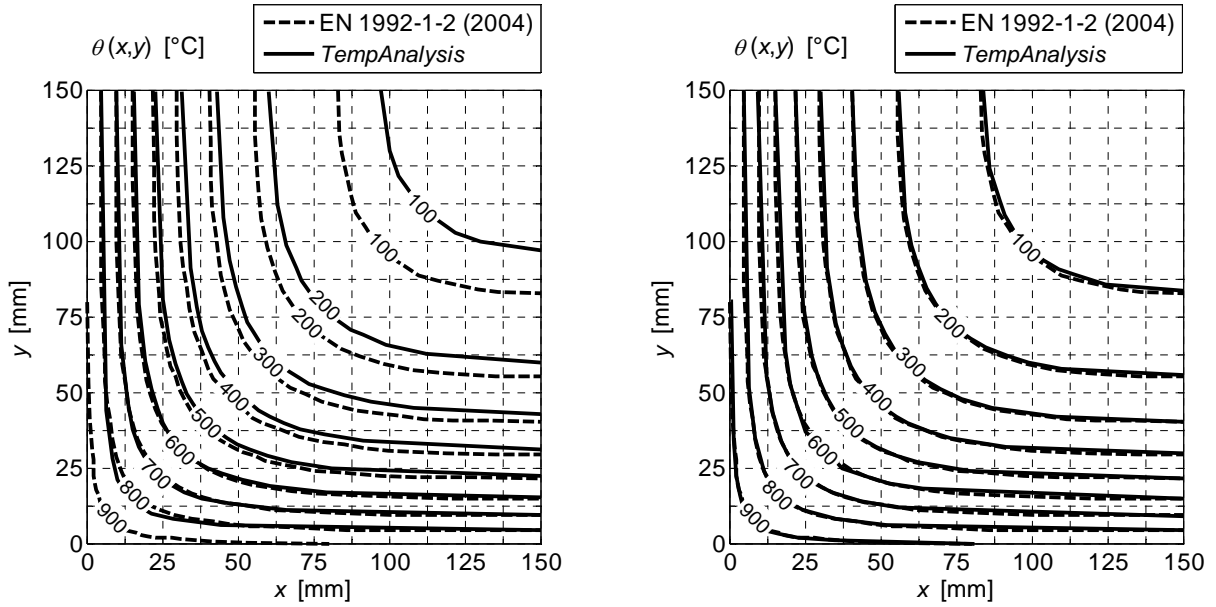


Fig. 4 Comparison of temperature profiles obtained by *TempAnalysis* software using a simplified algorithm (left) or using two-dimensional finite element method (right) with the temperature profiles given by EN 1992-1-2 (2004)

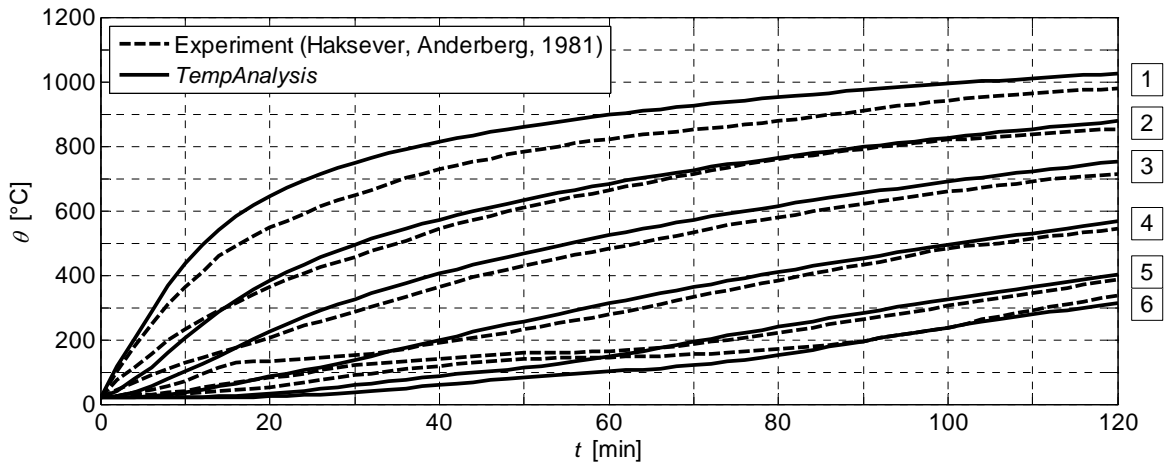


Fig. 5 Comparison of temperature profiles obtained by *TempAnalysis* software using two-dimensional finite element method with the measured data given by (Haksever, Anderberg, 1981)

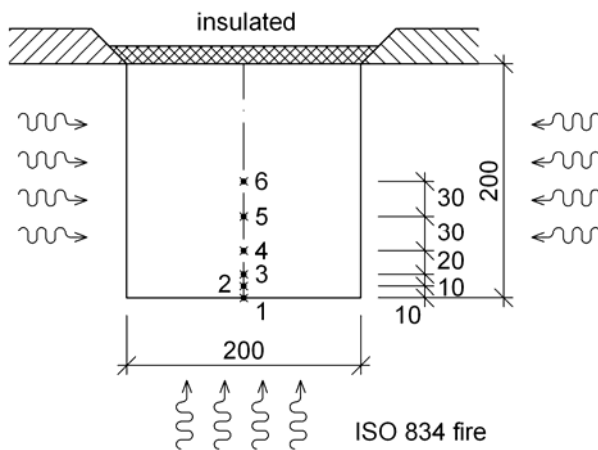


Fig. 6 Scheme of the analysed cross-section (Haksever, Anderberg, 1981)

Table 1 Parameters used in FEA

Parameter	Value	Unit
α_c	25	$\text{W m}^{-2} \text{K}^{-1}$
Φ	1	-
ε_s	0.7	-
ε_f	1	-
σ	$5.67 \cdot 10^{-8}$	$\text{W m}^{-2} \text{K}^{-4}$
$\rho(20)$	2400	kg m^{-3}
u	3	% of weight
λ	Lower limit	

2 HygroThermAnalysis SOFTWARE

HygroThermAnalysis software (Štefan, Beneš, 2010) is intended for hygro-thermal analysis of concrete rectangular cross-sections exposed to fire. Using this program, it is possible to solve one-dimensional (slabs, walls) and two-dimensional (beams, columns) heat and moisture transfer problem. The program consists of two parts: pre-processor for input data and post-processor for display of results. The pre-processor dialog window is shown in Fig. 7.

Heat and moisture transfer model included in the program is based on Bažant-Thonguthai (1978) model and it is described in (Beneš, Štefan, 2010; Beneš et al., 2011). The space discretization of the governing equations is carried out using a finite element method. The time discretization is performed using a semi-implicit difference scheme.

In the post-processor part of the program, it is possible to display values of temperature, water content and pore pressure at any point of the analysed cross-section and to plot resulting temperature, pore pressure and water content distributions, as shown in Fig. 8. Using a heuristic engineering criterion (see Beneš et al., 2011), spatial distribution of the spalling damage can be predicted by the program, see Fig. 9.

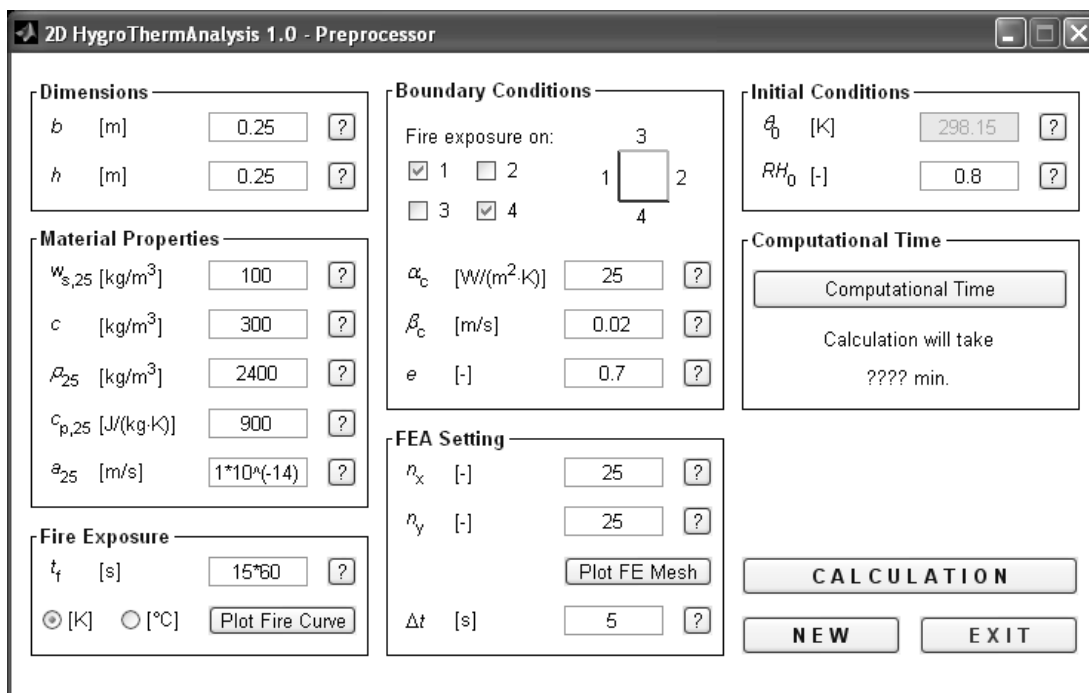


Fig. 7 *HygroThermAnalysis* – pre-processor dialog window

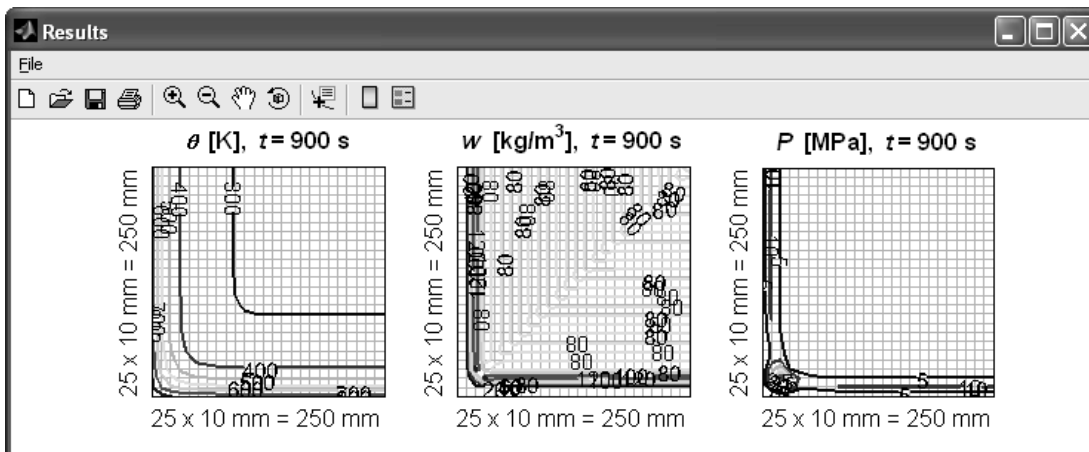


Fig. 8 *HygroThermAnalysis* – distribution of temperature, water content and pore pressure

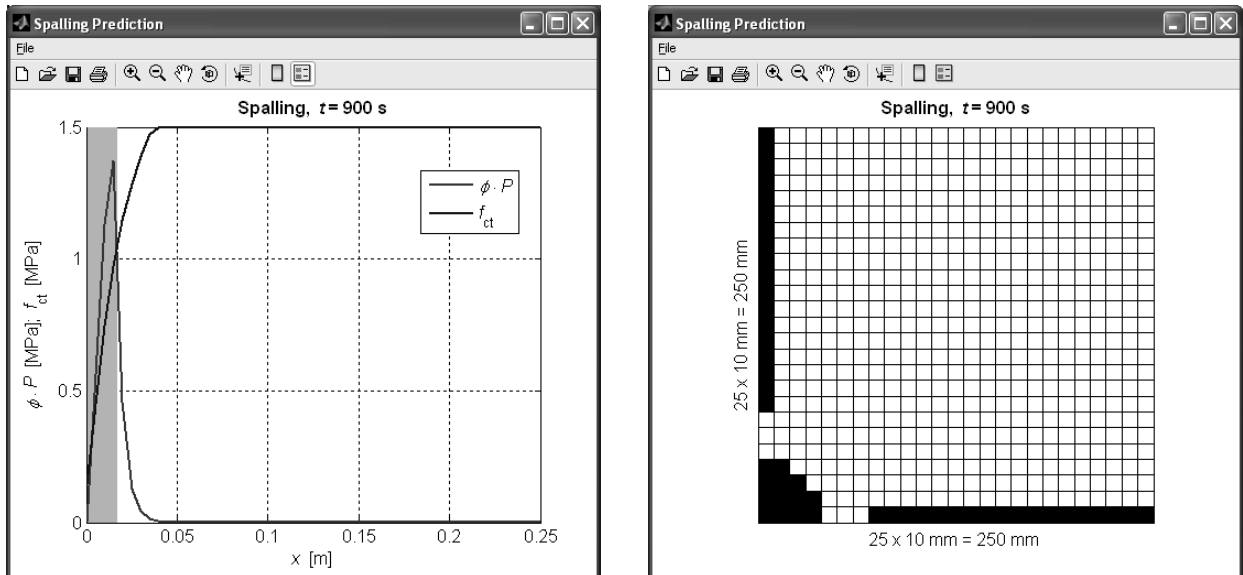


Fig. 9 *HygroThermAnalysis* – prediction of spalling of concrete wall (left) and column (right)

3 FiDeS SOFTWARE PACKAGE

FiDeS (Štefan, 2010) – **Fire Design Software** is a software package to fire design of concrete and masonry structures according to Eurocodes. This package consists of five computer programs: (i) computer program to temperature analysis of a fire compartment according to EN 1991-1-2 (2002); (ii) computer program to temperature analysis of a cross-section exposed to fire; (iii) computer program to fire design of concrete structural members according the tabulated data given by EN 1992-1-2 (2004); (iv) computer program to fire design of concrete structural members using the simplified calculation methods given by EN 1992-1-2 (2004); and (v) computer program to fire design of masonry structural members according the tabulated data given by EN 1996-1-2 (2005). In the actual version of the *FiDeS* software, the user interface is only in Czech. However, the English version is currently being prepared, see Fig. 10. More information about this software can be found in (Štefan, R., Procházka, J., 2010a, 2010b; Wald et al., 2011).

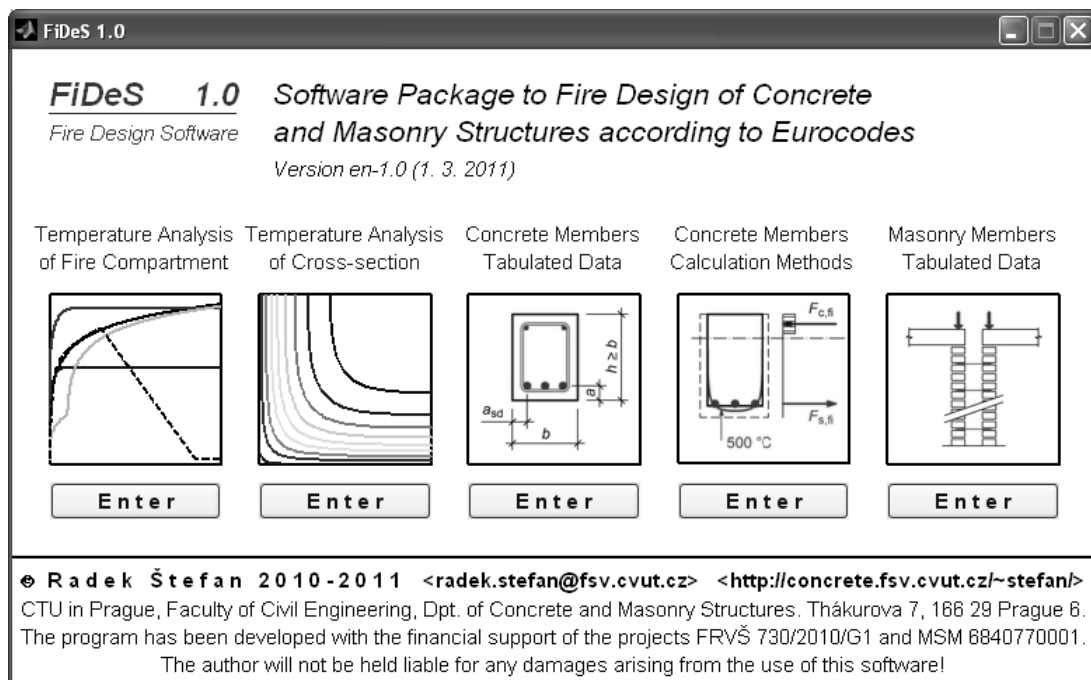


Fig. 10 *FiDeS* – main dialog window

4 SUMMARY AND ACKNOWLEDGMENT

In the present paper, software tools to fire design of concrete and masonry structures developed at the Czech Technical University in Prague have been briefly described.

This outcome has been achieved with the financial support of the Ministry of Education, Youth and Sports of the Czech Republic, project No. MSM6840770001 (the first and the second author) and project CIDEAS No. 1M0579 (the third author). Additional support from the grant Reg. No. OHK1-041/11 “Modelling of concrete structures during fire” (the first and the third author) provided by the Grant Agency of the CTU in Prague is greatly acknowledged.

REFERENCES

- Bažant, Z. P., Thonguthai, W (1978), Pore Pressure and Drying of Concrete at High Temperature. *J. Eng. Mech. Div.* 104 (1978), 1059–1079.
- Beneš, M., Štefan, R. (2010), Surface spalling of concrete structures during fire, *Stavební obzor* (submitted 2010). (in Czech).
- Beneš, M. et al. (2011), Analysis of coupled transport phenomena in concrete at elevated temperatures, *Appl. Math. Comput.* (accepted 2011), DOI: 10.1016/j.amc.2011.02.064.
- EN 1991-1-2 (2002), Eurocode 1: Actions on structures – Part 1-2: General actions – Actions on structures exposed to fire, CEN, Brussels.
- EN 1992-1-2 (2004), Eurocode 2: Design of concrete structures – Part 1-2: General rules – Structural fire design, CEN, Brussels.
- EN 1996-1-2 (2005), Eurocode 6: Design of masonry structures – Part 1-2: General rules – Structural fire design, CEN, Brussels.
- Haksever, A., Anderberg, Y. (1981), Comparison between measured and computed structural response of some reinforced concrete columns in fire. *Fire Saf J* 4, 1981, pp. 293-297.
- Hertz, K. (2006), Users Guide for the Program ConTemp.exe [online], Kgs. Lyngby: DTU, Institute of Building Structures, 2006. URL: <http://www.byg.dtu.dk/English/Research/Software.aspx>
- MATLAB (2008) [computer program]. Version 7.6.0.324 (R2008a). USA, The MathWorks, 2008.
- Procházka, J., Štefan, R. (2009), Temperature Distribution through a Cross-Section Exposed to Fire, In *Concrete and Concrete Structures*, Žilina: Žilinská univerzita, Stavebná fakulta, 2009, p. 277-284. ISBN 978-80-554-0100-3.
- Štefan, R. (2010), FiDeS – Software Package for Fire Design of Concrete and Masonry Structures according to Eurocodes [software online]. Prague: CTU in Prague, Faculty of Civil Engineering, 2010. (in Czech) URL: <http://concrete.fsv.cvut.cz/~stefan/>
- Štefan, R., Beneš, M. (2010), HygroThermAnalysis [software online]. Prague: CTU in Prague, Faculty of Civil Engineering, 2010. URL: <http://concrete.fsv.cvut.cz/~stefan/>
- Štefan, R., Procházka, J. (2009), TempAnalysis – Computer Program for Temperature Analysis of Cross Sections Exposed to Fire [software online]. Prague: CTU in Prague, Faculty of Civil Engineering, 2009. URL: <http://concrete.fsv.cvut.cz/~stefan/>
- Štefan, R., Procházka, J. (2010a), Computer Program for Assessment of Fire Resistance of Concrete Beams and Slabs Using Tabulated Data Given by EN 1992-1-2, In *Betonárske dni 2010: Zborník prednášok*, Bratislava: STU, 2010, s. 253-256. ISBN 978-80-8076-089-2. (in Czech).
- Štefan, R., Procházka, J. (2010b), Computer Program for Assessment of Fire Resistance of Concrete Columns and Walls Using Tabulated Data Given by EN 1992-1-2, In *Betonárské dni 2010*, Praha: ČBS ČSSI, 2010, s. 461-463. ISBN 978-80-87158-28-9. (in Czech).
- Štefan, R., Procházka, J. (2010c), Program for Determination of Temperatures in Concrete Rectangular Cross Sections Exposed to Fire, *Stavební obzor*, 2010, roč. 19, č. 9, s. 274-278. ISSN 1210-4027. (in Czech).
- Wald F. et al. (2011), Software Tools to Structural Fire Design, Prague: CTU in Prague, Faculty of Civil Engineering, 2011. ISBN 978-80-01-04746-0.

STUDY OF SLAB FIRE RESISTANCE ACCORDING TO EUROCODE

Using different computational methods

Radim Čajka^a, Pavlína Matečková^a

^a VSB-TU Ostrava, Faculty of Civil Engineering, Ostrava, Czech Republic

INTRODUCTION

Eurocode 1992-1-2 includes the following alternative design methods: detailing according to tabulated data, simplified calculating method for specific types of members and general calculating method for simulating the behavior of structural members, parts of structure or the entire structure. For determining the fire resistance of reinforced concrete slab structure the tabulated data and the simplified calculating method are used. Temperature distribution in concrete cross-section is determined using FEM analysis (ANSYS) and numerical solution (Nonstac) of differential equation of heat transfer. Calculated temperatures are compared with temperature profiles given in annex A. Structural response of slab cross-section is determined using “500°C” isotherm method.

1 HEAT EXPOSURE

1.1 Study example and input data

In the paper study example of slab cross-section with thickness 200 mm is analysed. The slab is reinforced with profile 10/100 mm, concrete cover is 25 mm, distance between the reinforcement centre of gravity and exposed side of the slab is 30 mm. Slab is made of concrete C20/25 and steel B420B.

Thermal properties of concrete are assumed as temperature dependant according to Eurocode 2 (2006). Heat conductivity is given with upper (1) and lower (2) limit value.

$$\lambda_c = 2.0 - 0.2451(\theta/100) + 0.0107(\theta/100)^2 \quad (1)$$

$$\lambda_c = 1.36 - 0.136(\theta/100) + 0.0057(\theta/100)^2 \quad (2)$$

Basic value of concrete specific heat is 900 (J/kgK). With increasing temperature concrete specific heat grows to the value 1100 (J/kgK).

According to P ENV version of Eurocode 2 (1998) it is recommended to use the value 2300 kg/m³, without the temperature dependence. According to Eurocode 2 (2006) the density is given as a function of temperature, as the density is influenced with water evaporation, but without the recommended value for the initial density. The common concrete density is given also in Eurocode 1, part 1-1 (2004) with the value 2400 kg/m³, reinforced concrete 2500 kg/m³. Reinforcement in the concrete cross-section influences the final density but as the reinforcement is placed locally it could not influence significantly the result temperature distribution. Therefore in this study example the density is supposed with value 2300 kg/m³ and 2400 kg/m³.

Temperature in burning space is supposed according to standard time temperature curve, heat transfer goes on partly with convection and partly with radiation. Temperature on unexposed side is supposed constant. Appropriate parameters of heat transfer are given explicitly in Eurocode 1, part 1-2 (2004).

1.2 Temperature profiles

The easiest way to appoint the temperatures in cross-section exposed to standard fire is to use temperature profiles in Annex A of Eurocode 2. As for the slab structures, the temperature profile is given only for the thickness 200 mm. Particular temperatures in reinforcement are compared with calculated temperatures in the Fig. 1.

1.3 FEM analysis

The FEM analysis is provided using ANsys computer program. In the Table 1 there are sequenced temperatures in reinforcement for different input data. Temperature profiles in concrete slab respond well with the values calculated for time dependant material properties, with the initial density 2400 kg/m^3 , and initial coefficient of heat conductivity 2.0 J/kg.K according to (2). Temperatures in reinforcement are compared in the Fig.1.

Tab. 1 Temperatures in reinforcement – Ansys

	temperature dependent			constant		
λ	2.0	1.36	2.0	2.0	1.36	2.0
density	2400	2400	2300	2400	2400	2300
Time	Temp.	Temp.	Temp.	Temp.	Temp.	Temp.
min	°C	°C	°C	°C	°C	°C
0	20	20	20	20	20	20
30	271	245	277	370	332	367
60	423	402	430	574	533	574
90	517	502	524	687	647	689
120	585	575	592	765	726	767

1.4 Numerical analysis - Nonstac

Numerical analysis is provided using Nonstac computer program, (Čajka, 2010). Though the temperature distribution in cross-section in case of fire is generally three dimensional in many cases one dimensional temperature distribution satisfies with sufficient accuracy. Nonstac computer program solves numerically Fourier differential equation of one dimensional heat transfer using Runge-Kutta method (Nevřiva, 1975) and it is possible to input time dependant thermal properties of material and heat transfer due to convection and radiation. Thermal material properties have to be input as linear or quadratic function and therefore the thermal properties have to be input as regression polynomial. In the Table 2 there are sequenced temperatures in reinforcement for different input data.

Tab. 2 Temperatures in reinforcement – Nonstac

	temperature dependent		constant		
λ	2.0	1.36	2.0	1.36	2.0
density	2400	2400	2400	2400	2300
Time	Temp.	Temp.	Temp.	Temp.	Temp.
min	°C	°C	°C	°C	°C
0	20	20	20	20	20
30	331	291	370	332	340
60	504	465	574	533	540
90	604	569	687	647	654
120	670	643	765	726	732

Considering the temperature independent values of thermal material properties the result temperatures in reinforcement calculated using ANsys and Nonstac software respond together. Considering the temperature dependant values of thermal material properties the temperatures calculated using Nonstac software are higher than temperatures calculated using ANsys software. One of the reasons could be the fact that thermal properties are input as regression polynomial. The temperatures are compared in the Figure 1.

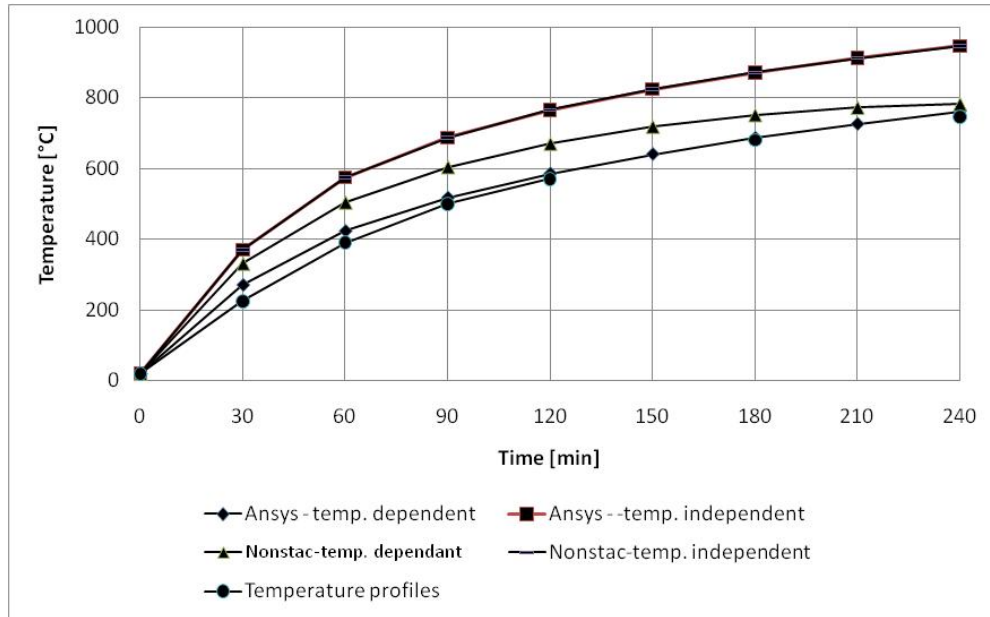


Fig. 1: Comparing the temperature in reinforcement

2 STRUCTURAL RESPONSE AND FIRERESISTANCE

2.1 Action effect

In this study example bending moment from action effect for permanent design situation is $m_{Ed} \cong m_{Rd} = 46$ kNm/m.

Reducing coefficient for accidental situation in case of fire is in the interim approximately 0.4 to 0.7. In the simplified analysis it is possible to use 0.7 on the safe side, then $m_{Ed,fi} = \eta_{fi} \cdot m_{Ed} = 0.7 \times 46 = 32$ kNm/m.

2.2 Fireresistance

The simple way to appoint the fire resistance is to use the tables in the chapter 5 Eurocode 2 (2006). In the Table 5.8. in Eurocode 2 (2006) it is possible to settle the fireresistance 90 minutes.

In the Table 3 there are sequenced load bearing capacities in case of fire for the time 90 minutes, temperature in reinforcement is supposed according to temperature profiles and calculated using Nonstac and Ansys software, thermal material properties are considered as temperature dependant.

Tab. 3 Bending moment load bearing capacity – time 90 minutes

			Profiles	Ansys	Ansys	Nonstac
Heat conductivity - temp. dep.	λ	kJ/kg.K		2.0	2.0	2.0
Density - temperature dep.	ρ	kg/m ³		2400	2300	2400
Temperature in reinforcement	θ_R	°C	500	517	524	604
Steel strength	$f_{yd,fi}$	Mpa	328	305	232	193
Bending moment - capacity	$m_{Rd,fi}$	kNm/m	42	39	30	25
Bending moment - action effect	$m_{Ed,fi}$	kNm/m	32	32	32	32
Assessment			OK	OK	X	X

It is obvious that appointing the temperature in reinforcement according the temperature profiles and consequent fireresistance corresponds with the table fireresistance.

Temperature in reinforcement according to temperature profiles respond well with the temperatures calculated using ANsys software for the initial density 2400 kg/m³, and initial coefficient of heat

conductivity 2.0 J/kg.K . Criterion R for bending moment load bearing capacity is fulfilled for time 90 minutes.

Considering the initial density 2300 kg/m³ the temperatures in reinforcement are higher and criterion R for bending moment bearing capacity for time 90 minutes is not fulfilled.

Temperature in reinforcement calculated using Nonstac software are higher than using Ansys software and the fireresistance for time 90 minutes for criterion R-bearing capacity is not fulfilled.

3 SUMMARY

In the paper the study example of reinforced concrete slab is analyzed. Temperature in reinforcement is settled using temperature profiles and Ansys and Nonstac software. Input data for thermal analysis are not given strictly, in the paper there are compared temperatures in reinforcement for different input data using different computational methods and particular software. Numerical solution of differential equation of heat transfer is provided using FEM analysis and Ansys software and Runge-Kutta method and Nonstac software. Considering temperature independent thermal properties the result temperatures correspond together. Considering the temperature dependant thermal properties the result temperatures calculated using Nonstac software are higher than using ANsys software. One of the reasons could be the fact that thermal properties are input as regression polynomial.

Table fireresistance of analyzed slab is 90 minutes. In this time the bending moment load bearing capacity is settled for different calculated temperatures in reinforcement. As the simplified method is more advanced then detailing according to tabulated data, it is expected that resulting fire resistance of slab structure using simplified calculating methods gives more favorable values than detailing according to tabulated data. This study would like to point out that in some cases design according to tabulated data is more favorable than simplified method.

4 ACKNOWLEDGMENT

This outcome has been achieved with the financial support of the Ministry of Education, Youth and Sports of the Czech Republic, project No. 1M0579, within activities of the CIDEAS research centre.

REFERENCES

- CSN EN 1991-1-1: Eurocode 1: Actions on structures - Part 1-1: General actions - Densities, self-weight, imposed loads for buildings, Prague 2004
- CSN EN 1991-1-2: Eurocode 1: Actions on structures - Part 1-2: General actions - Actions on structures exposed to fire, Prague 2004
- CSN EN 1992-1-2: Eurocode 2: Design of concrete structures - Part 1-2: General rules - Structural fire design, Prague 2006
- CSN PENV 1992-1-2: Design of concrete structures - Part 1-2: General rules - Structural fire design, Prague 1998
- Čajka, R.: Software Nonstac, registration number AR-SW-2010-02, output of project Rheological sliding joint with thermo-controlled viscoelastic properties No. FR-TI2/746. Ostrava 2010
- Nevřiva, P.: Simulation of regulating systems on computer. SNTL Prague 1975. In Czech.

AXIAL RESTRAIN EFFECTS ON FIRE RESISTANCE OF STATICALLY INDETERMINATE RC BEAMS

Meri Cvetkovska ^a, Koce Todorov ^a, Ljupco Lazarov ^a

^a University “Ss. Cyril and Methodius”, Faculty of Civil Engineering, Skopje, Macedonia

INTRODUCTION

Fire resistance is a measure of the ability of a building element to resist a fire. It's determination in case of structural systems is a complex nonlinear problem in which the strength and the stiffness of the elements as well as the inner forces are continuously modified. Mainly, several groups of nonlinearity sources can be identified: nonlinear distribution of temperature through the element thickness, temperature-dependent material properties (thermal and mechanical), nonlinear boundary conditions and nonlinearity due to reaching strength capacity.

In reinforced concrete structures the connections between columns and beams are usually constructed as relatively rigid, which means that interaction between these elements exists when they are exposed to external influences of different nature. In case of fire loading, applied only to one part of the structure, the high thermal expansion may produce high axial forces in the heated elements by the surrounding unheated elements. In some cases these forces can have either positive or negative influence on the fire resistance of the considered elements.

In this paper three different support conditions, such as: pin-pin, pin-fixed and fully fixed are used to model beams with various level of axial restraint. The beams are exposed to the ISO-fire curve. The numerically obtained results are presented and on the basis of these results it can be observed that the augmented axial spring stiffness increases the induced axial forces, as well as the fire resistance of elements.

1 SUPPORT CONDITIONS OF STRUCTURAL BEAM ELEMENTS

Reinforced concrete beams as a part of space frame structural systems are axially restraint elements. The level of axial restraint depend on many factors, such as: type of structural system, dimensions of surrounding elements (beams and columns), their lengths, type of connections, characteristics of used structural materials, etc. At the beginning of fire loading, axial restrains are maximal. During the time, as a result of high temperatures and nonlinear temperature distribution in the cross sections of the heated elements, modulus of elasticity of steel and concrete decreases, internal forces are redistributed and additional cracks appear. These initiate decrease of columns and beams stiffness and reduction of axial restraint effects (Daniela, 2004 and Mostafaei et al., 2009).

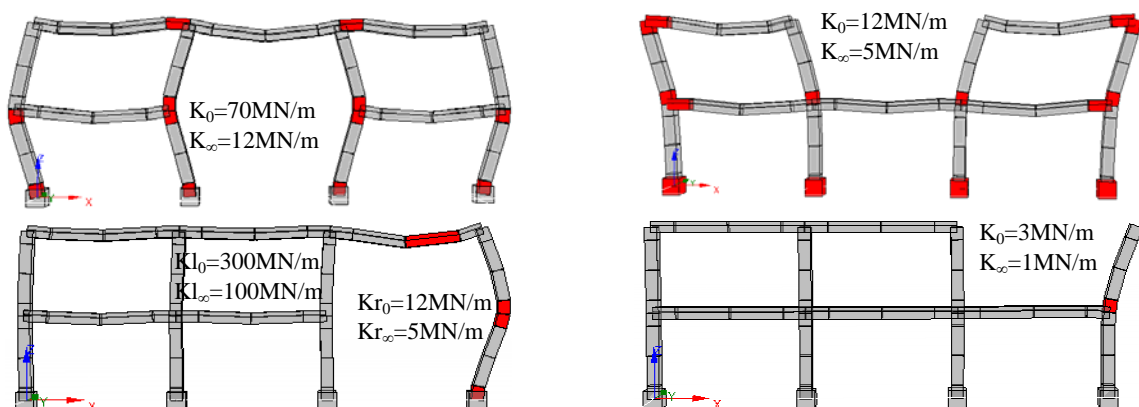


Fig. 1 Influence of structural system on the beam axial stiffness restrain

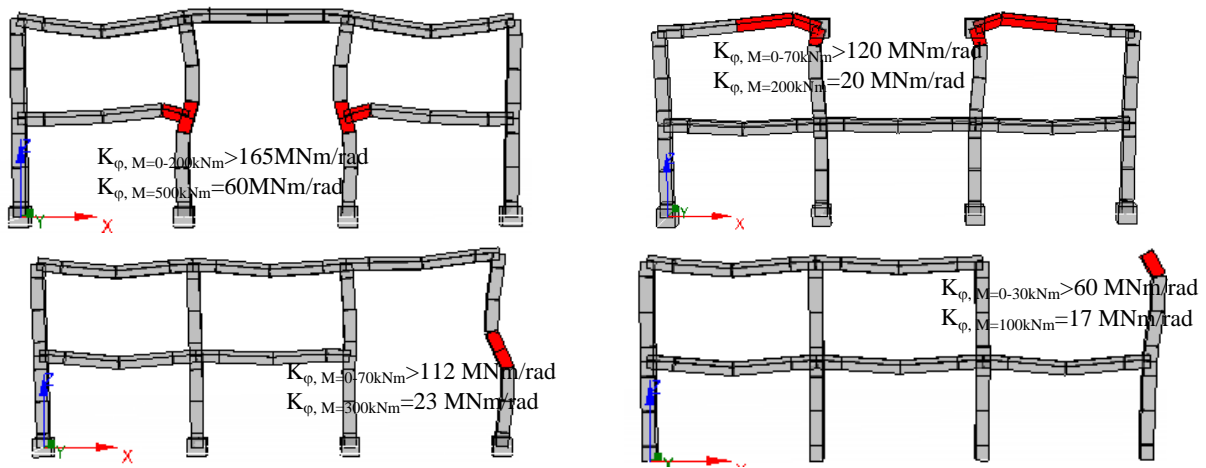


Fig. 2 Influence of structural system on the beam rotational stiffness restraint

If we want to analyse the beam behaviour as a separate unit, isolated from the structure, the appropriate time dependent boundary conditions should be applied to the beam ends. Selected results for the boundary conditions for different positions of the beam element as a part of a 3 bay, 2 story frame are presented on Fig.1 and Fig.2. The frame geometry is: 3.0m story height and 5.0m bay span. All columns and beams are of size 40/40cm. Axial and rotational stiffness dependence of the beam element position and the nodes displacements (axial translation and rotation) are presented on Fig.3.

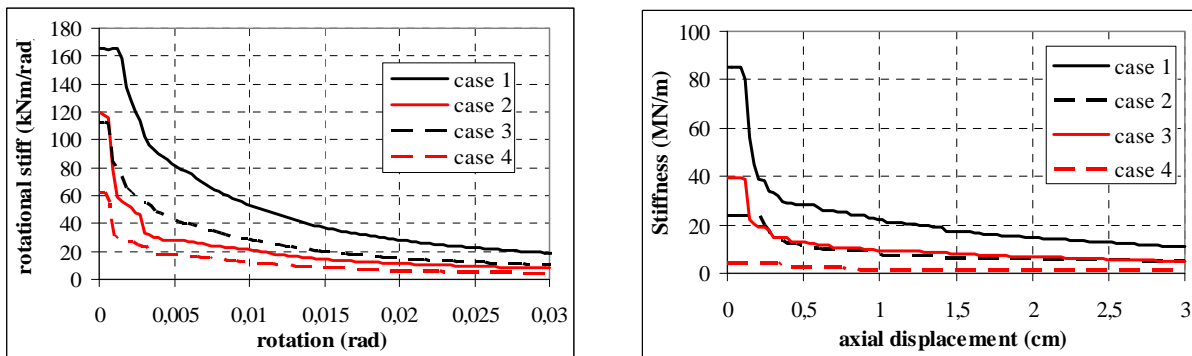


Fig.3 Rotational and axial stiffness dependence of node displacements

2 COUPLED THERMAL – STRESS ANALYSIS

Today, as a result of many years of investigations, there are three basic methods for determining the fire resistance of structural elements and their assemblies. The oldest method is the performance of a fire test of loaded elements, in compliance with the national regulations and standards, or comparison of the elements with the results from already performed tests on similar or identical elements. The second method implies the use of empirical formulae that are based on the results from performed fire tests and holds for a certain combination of: structure, material and protective coating. The third method, based on the principles of structural mechanics and theory of heat transfer, represents an analytically elaborated approach to design elements with a predefined fire resistance. Generally, numerical analysis of the whole structure in case of fire proofs that the structure, or its elements, loaded by a defined load and exposed to thermal effects, satisfies certain functional requirements, expressed through the ultimate state for bearing capacity and usability. Verification of the numerically achieved results usually is based on comparison with the experimental results from the fire tests performed on the same or similar elements (Cvetkovska et al., 2009 and Ellingwood et al., 1991).

To define the fire resistance of structures as assemblies of structural elements, experimental investigations of models are almost impossible. Spreading the temperature field in time domain is

practically impossible to be simulated on a model of small proportions. Hence, model investigations can hardly be accepted due to the high cost. For the last twenty years, particular importance has therefore been given to the analytical definition of the problem.

The program FIRE (Cvetkovska, 2002) carries out the nonlinear transient heat flow analysis (modulus FIRE-T) and nonlinear stress-strain response associated with fire (modulus FIRE-S). The solution technique used in FIRE is a finite element method coupled with time step integration. The modulus FIRE-S takes in to accounts the dimensional changes caused by temperature differences, changes in mechanical properties of materials with changes in temperature, degradation of sections by cracking and/or crushing and acceleration of shrinkage and creep with an increase of temperature.

The effect of creep at elevated temperatures in the program FIRE is included by the temperature dependent stress-strain relationships for concrete and steel, recommended in EC2. The model proposed is capable of predicting the fire resistance of reinforced concrete structural elements with a satisfactory accuracy.

3 AXIAL RESTRAIN EFFECTS ON FIRE RESISTANCE OF BEAMS

In order to investigate the influence of axial stiffness restraint on the fire resistance of reinforced concrete beams, few numerical parametric analyses are performed. The beam and the cross section geometry, as well as reinforcement details are presented on Fig. 4 and Fig. 5. The beam is analysed as one span beam with different end boundary conditions (pin-pin, pin-fixed and fixed-fixed). In the first case the beam is fixed on the both sides and the uniform load is 45 KN/m'. For the second case fixed-pin boundary conditions are used and the uniform load is 28 KN/m'. For the third case pin-pin boundary conditions are used and the uniform load is 15 KN/m'. For all three cases the reinforcement is taken in such a way that the stresses in steel bars due to nominal load q are approximately 60% of the yield strength, for the negative moment reinforcement, and 45%, for the positive moment reinforcement. The variable stiffness in axial direction is achieved by spring element at one end of the beam. The spring stiffness is varied from $K=0$ MN/m to $K=\infty$.

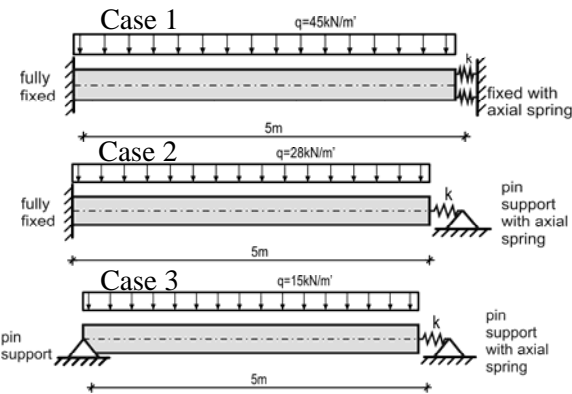


Fig. 4 Beam geometry and variable support conditions

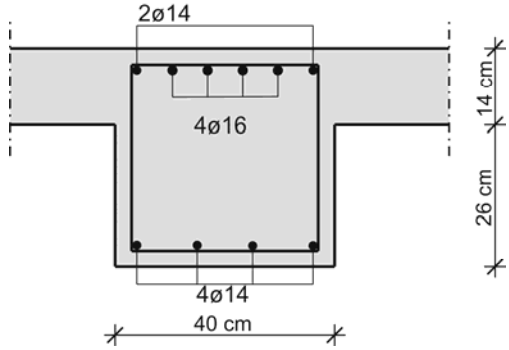


Fig. 5 Cross section geometry and reinforcing details at the fixed support, for Case 1

The fire induced axial forces in case of restrained axial displacements by springs with different stiffness are presented on Fig.6 and Fig. 7. The moment redistribution, caused by the non-uniform temperature field in the cross section of the beam exposed to fire from the bottom side, results in increase of negative moment at the supports and decrease of positive moment at the mid-span. In Case 1 the fixed boundary conditions enable redistribution of moments on both sides that results in lower values of the induced axial forces than in Case 2, where the redistribution is enabled only at the fixed support. For that reason in Case 3 the induced axial forces have highest values, but only if the axial spring stiffness is less than 7 MN/m (Fig. 9). The maximal values of the induced axial force as a function of the axial spring stiffness are presented on Fig.8 and Fig. 9.

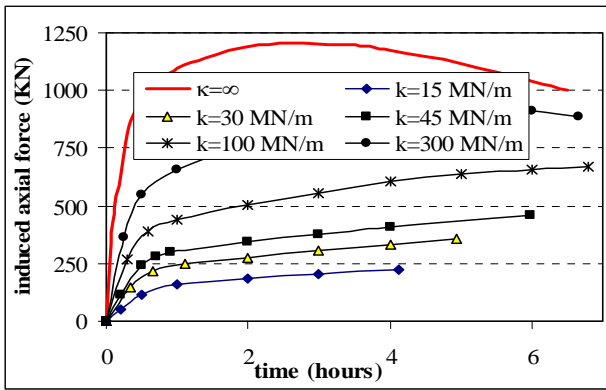


Fig. 6 Fire induced axial force for different spring stiffness in Case 1 (fixed-fixed ends)

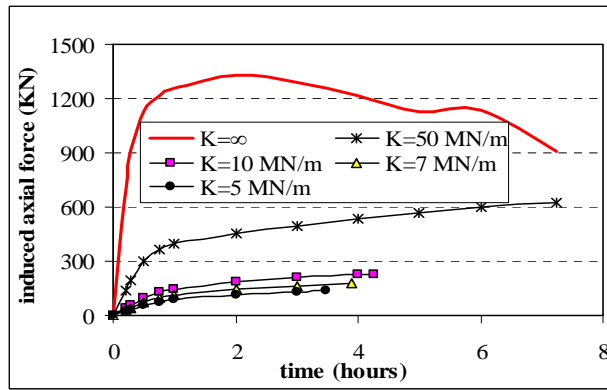


Fig. 7 Fire induced axial force for different spring stiffness in Case 2 (pin-fixed ends)

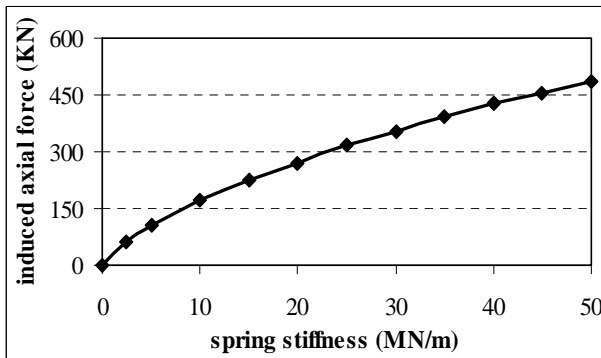


Fig. 8 Max. induced axial force dependence of spring stiffness for Case 1

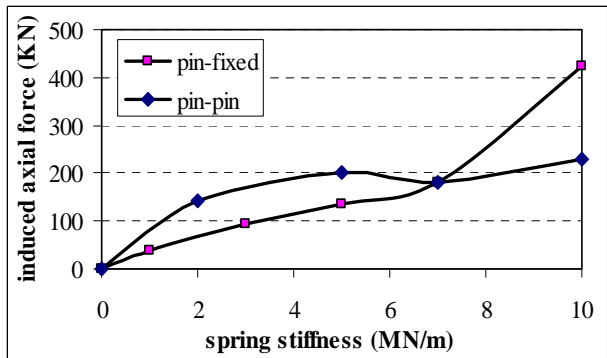


Fig. 9 Max. induced axial force dependence of spring stiffness for Case 2 and Case 3

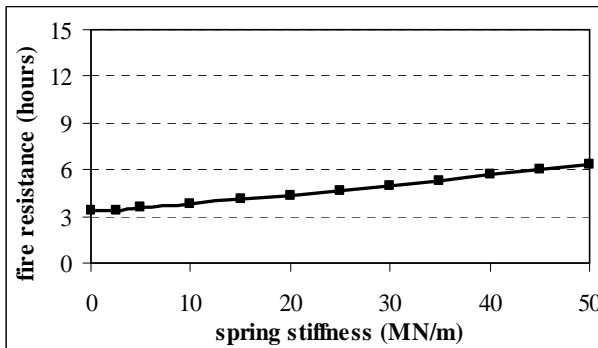


Fig. 10 Axial spring stiffness influence on the fire resistance of the beam in Case 1

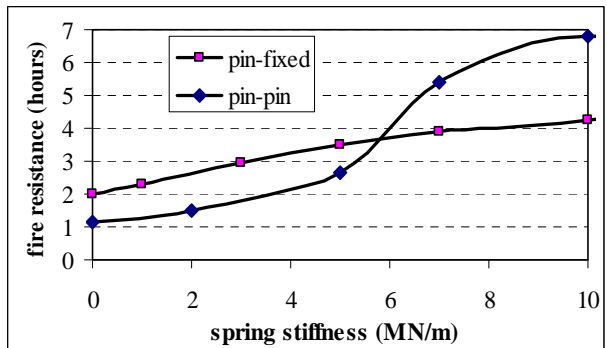


Fig. 11 Axial spring stiffness influence on the fire resistance of the beam in Case 2 and Case 3

The induced axial force acts as a prestressing force and delays the moment when yielding of the top reinforcement will occur, so it has a positive effect on the fire resistance of the beam. It has a positive effect on the bottom reinforcement, too. In the case without axial restraint, as a result of the moment redistribution, the positive moment at the mid-span decreases, but the stresses in the bottom reinforcement are still high and close to the yield strength for the current temperature. If the restraint exists the induced axial force decreases the stresses of the positive moment. The augmented axial spring stiffness increases the induced axial force, as well as the fire resistance of the beam (Fig. 10 and Fig.11) and in the same time decreases the longitudinal displacement at the end of the beam (Fig. 12 and Fig. 13). If, in Case 1, the spring stiffness was increased over 50 MN/m the positive effect on the fire resistance of the beam is negligible, therefore results are presented only for the lower values. In Case 2 and Case 3 the positive effect is negligible for spring stiffness higher than 10 MN/m.

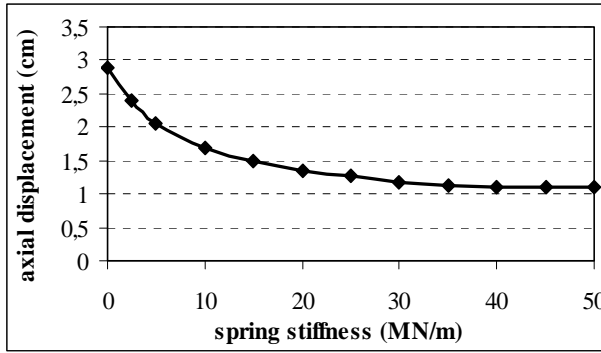


Fig. 12 Axial spring stiffness influence on the support displacement for Case 1

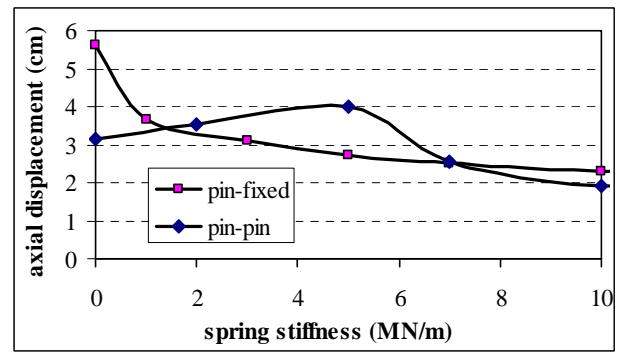


Fig. 13 Axial spring stiffness influence on the support displacement for Case 2 and Case 3

4 FIRE RESISTANCE OF A BEAM AS A PART OF A STRUCTURE

As it was previously mentioned, to define the fire resistance of a beam as a separate unite, isolated from the structure, the appropriate time dependent boundary conditions should be applied to the beam ends.

For example, if we want to analyse the fire scenario when the fire is in the first story middle span by separating the beam from the structure, the appropriate boundary conditions have to be defined according to the values presented on Fig. 1 and Fig.3 - case 1. For that purpose the expected values for the axial displacements of the nodes should be adequately considered. According to the values presented on Fig. 2-case 1, the rotational stiffness should be defined. The axial stiffness restrain at each node varies from $K_1=40$ MN/m (Fig. 3, case 1), in the moment when the structure is loaded only by uniform load q , to $K_1=20$ MN/m (or $K_1=10$ MN/m only on one side), after 1 hour fire action. Because the surrounding elements are not fire exposed, the rotational stiffness during the fire action is almost constant on both sides and should be taken with the initial value of 850MNm/rad. The cross section geometry, as well as reinforcement details for the current beam are the same as for the beam presented on Fig. 4, case 1 and Fig. 5.

A satisfactory accuracy is achieved by comparing the results obtained by analysing the beam as a separate element (fire scenario FS1) with the results obtained by analysing the whole structure (fire scenario FS2). For both cases the results are presented in Tab. 1. The real behavior of the beam (as a part of the whole structure) is presented on Fig. 14.

According to the results presented on Fig. 10, the fire resistance of the same beam with the same loading conditions and the same final axial stiffness of the spring ($K_1=10$ MN/m only on one side), but with a different rotational stiffness ($K_3=\infty$ on both sides) is $t=3.83$ hours. In case when the beam is treated as a separate element (FS1, Tab. 1) the fire resistance is 3.75 hours. The real fire resistance of the whole structure is $t=3.45$ hours.

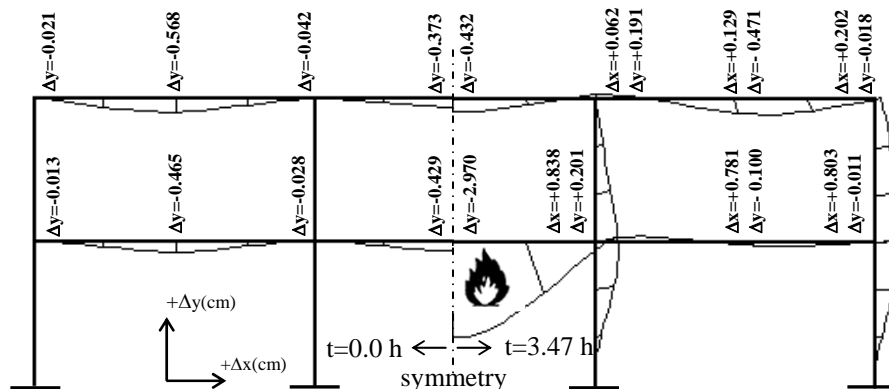


Fig.14 Deformation history of the frame exposed to fire in the first story middle bay

The final results for the displacements in axial direction (Fig. 12, $\Delta x=1.69\text{cm}=2*0.845\text{cm}$) and for the vertical displacement at mid-span ($\Delta y=3.42\text{cm}$) at the moment of failure are almost the same, but little higher than in fire scenario 1 (FS1). The reason is the assumed constant value for the axial spring stiffness and the difference in the assumed rotational stiffness. In this case the rotational stiffness has a small effect on the final results, but for an another fire scenario it should be considered adequately.

Tab. 1 Fire resistance of a beam as a separate element and as a part of a structure

	fire scenario	axial displacement on one side Δx (cm)	vertical deflection in the middle Δy (cm)	negative moment M_1 (KNm)	moment at the middle of spam, M_2 (KNm)	induced axial force N (KN)
t=0.0	FS1	0	0.413	-100.57	39.16	0
	FS2	0	0.429	-101.55	38.17	0
t=1.0	FS1	-0.572	1.301	-164.6	-25.40	-114
	FS2	-0.584	1.344	-165.6	-26.27	-128
t=2.0	FS1	-0.700	2.087	-152.66	-14.00	-139
	FS2	-0.707	2.171	-152.40	-13.01	-140
t=3.47	FS1	-0.805	2.966	-136.36	1.90	161
	FS2	-0.838	2.970	-136.3	2.57	147
t=3.75	FS1	-0.827	3.213	-132.6	5.05	166

5 CONCLUSIONS

According to the results, complete or even partial restraints of end supports displacements in axial direction dramatically change, for better, the fire resistance of this type of structures. This is mainly attributed to the axial force induced due to the support restraints. Generally speaking, the axial compression force increases the fire resistance of the structure.

Since a physical testing program for investigating the response of a large variety of structural elements under differing restraint, loading, and fire conditions is impractical and expensive, analytical studies supported by the results of physical experiments could efficiently provide the data needed to resolve questions related to the design of structures for fire safety.

REFERENCES

- Cvetkovska M., Nonlinear stress strain behaviour of RC elements and RC frames exposed to fire, PhD. Thesis, University Ss.Cyril and Methodius – Skopje, R. Macedonia, 2002.
- Cvetkovska M., Trpevski S., Ivanisevic N, Nonlinear Finite Element Analysis of RC Beams Subjected to Fire, 33rd IABSE Symposium (International Association for Bridge and Structural Engineering), Bangkok, Thailand, 2009.
- Daniela B., The Effect of Support Conditions on the Fire Resistance of a Reinforced Concrete Beam, Fire Engineering Research Report 04/5, 2004.
- Ellingwood B., Lin T.D., Flexure and shear behavior of concrete beams during fires, Journal of the Structural Engineering, Vol.117 No.2, 1991.
- Mostafaei H., Mannarino J., A Performance -based approach for fire-resistance test of reinforced concrete columns, IRC-RR-287, 2009.

NUMERICAL INVESTIGATIONS OF COMPOSITE SLAB-BEAM FLOOR SYSTEMS EXPOSED TO ISO FIRE

Tuan Trung Nguyen^a, Kang Hai Tan^a

^a Nanyang Technological University, School of Civil and Environmental Engineering, Singapore

INTRODUCTION

Due to Basingstoke and Broadgate fire incidents, composite slabs consisting of steel beams and lightly reinforced concrete slabs with steel decking showed remarkable resilience by mobilizing tensile membrane action (TMA) at large displacements. The conditions necessary for the mobilisation of TMA are two-way bending of the slab and vertical support along all four edges. Over past 20 years, a number of research works on TMA of composite slabs in fire have been conducted. Almost all the previous studies utilise the assumption of continuous vertical restraint at all times during a fire. However, at elevated temperatures the edge beams will deform, and will experience large deflections. Therefore, further research studies are necessary to consider the effects of slab-beam interactions on the development of TMA in slabs. Parameters such as perimeter beam deflections, effect of stiffness and strength of fire-protected boundary beams as well as different slab configurations will be studied.

This paper presents finite element (FE) investigations on the behaviour of composite slab-beam systems under fire conditions. A simplified FE model is developed using ABAQUS because of its capabilities for static loading, thermal analysis, and a robust concrete material model. The model is first validated against published test data. A parametric study is then undertaken using this validated model. The investigated parameters are: stiffness of perimeter beams and aspect ratios of slab panels.

1 VERIFICATION OF NUMERICAL MODELLING

1.1 Solution Strategy

Structures in fire are generally subjected to large deformations. An accurate simulation of this behaviour usually meets with numerical convergence difficulty. To overcome this, an explicit dynamic solver is adopted because it uses consistent large-deformation theory. Furthermore, compared to standard static analysis, the explicit dynamic solver allows pre-processing and provides an easy solution procedure (Hongxia et al. 2008).

To simulate accurately the behaviour of a structure in a fire, knowledge of the temperature distributions within heated structural members is essential. *Sequentially coupled thermal-stress analysis procedure* is used because the thermal fields are the driving forces for the stress analysis but the thermal solution does not depend on the stress solution. Therefore, the numerical models will consist of two different parts, one for heat transfer analysis and the other for structural analysis. *Concrete damaged plasticity model* is adopted since it is a fairly robust concrete model which defines the biaxial and uniaxial material behaviour subjected to generally monotonic loading through a variety of input parameters. In the following simulations, reinforcement is modelled by using the rebar layer technique. In this approach, the effects associated with the rebar/concrete interface, such as bond slip and dowel action, are modelled approximately by introducing 'tension stiffening' into concrete modelling to simulate load transfer across cracks through rebar.

Thermal and mechanical properties of concrete and steel at elevated temperatures specified in Eurocode 4 are adopted in this study. However, it is necessary to convert material data from engineering stress-strain curves in Eurocode to true stress-strain relationships, especially for large deformation problems, where strain localisation in reinforcing bars plays a significant role in the behaviour of reinforced concrete structures. The following equation can be used (ABAQUS 2009):

$$\sigma = S(1+e) \quad ; \quad \varepsilon = \ln(1+e) \quad (1)$$

where S and e represent engineering stress and engineering strain, respectively.

1.2 Thermal Model

The temperature distribution within all heated members is determined from the thermal analysis of a 1-D model based on heated cross sections. It means that the analysis assumes that temperatures only vary across the thickness and do not vary in the horizontal direction. The recorded temperatures at different positions of the composite slab from the Fracof test (Zhao et al. 2008) are adopted for this validation. In this test, the total depth of the composite slab was 155 mm and it was exposed to the ISO fire condition from below. More details of the test are presented in Section 1.3. Material properties for thermal analysis, i.e. specific heat and conductivity, can be found in Palm (1994).

Thermal analysis is performed by discretizing the cross section with DC2D8 element (8-node quadratic heat transfer quadrilateral). Reinforcing bars are not included in the thermal analysis and are assumed not to affect the temperature distribution in the cross section. The temperatures of the reinforcing bars are assumed to be equal to those of the concrete at the same level in the cross section. The effect of concrete cracks on thermal distribution is also ignored.

Fig. 1 shows a typical temperature distribution across the slab thickness. The recorded temperature at the heated surface is used as input data. Comparisons of temperature distribution between FE simulation and experimental results are conducted for the mid-depth and unheated surfaces (Fig. 2). It can be observed that the simulation matches very closely the recorded temperatures.

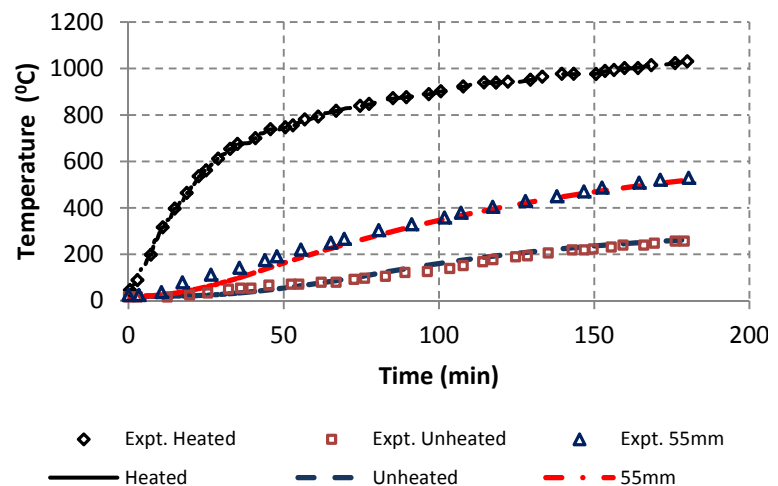
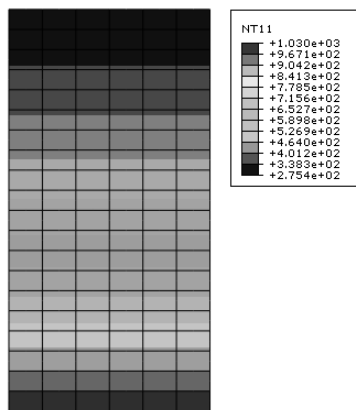


Fig. 1 Shell temperature distribution

Fig. 2 Temperature comparison

1.3 Slab-Beam System Model

To verify the validity of the slab-beam model, the Fracof fire test conducted in France (Zhao et al. 2008) is adopted here for comparison purpose. In this test, a single slab panel with two unprotected intermediate beams was tested under exposure to a 120 minute ISO 834 Standard fire. The slab, representative of a corner compartment, had a long span of 8.74m and a short span of 6.66m. It consisted of four equally-spaced IPE 300 secondary beams spanning in the longer direction and two IPE 400 primary beams in the shorter direction. The slab/beam system was supported by four HEB 260 steel columns using simple connections. Total depth of the slab was 155mm with COFRAPLUS 60 decking. To simulate continuity across two adjacent edges of the slab, reinforcing steel mesh (7mm diameter bars at 1500mm centres, placed 50mm below the top of the slab) was welded to two additional steel beams. All perimeter beams and columns were fire-protected, while intermediate beams and the composite slab were left unprotected. The slab resisted a uniform load of 3.84kN/m^2 , representative of imposed load at the fire limit state.

A simplified model is proposed, taking account of steel beams, concrete slab and reinforcing mesh. Assuming that the contribution of the steel decking on the load-carrying capacity of the slab is insignificant, the 150mm thick concrete slab is modelled as a flat slab, representative of the effective depth of the composite slab. The layers of reinforcing bars in the slab are treated as being smeared uniformly across the concrete shell element.

The model considers the slab as an isolated slab panel, vertically supported at the column positions. The vertical support along the slab edges is provided by the protected perimeter beams. Rotational restraints along two adjacent edges are used to simulate the slab continuity across these edges.

Shell element type S4R is used to discretize the beams and the slab. The top flange of the steel beams and parts of the slab above these beams are tied together using *surface-based contact interactions*. To avoid an overlap between the two reference surfaces, an offset between two tied surfaces is adopted.

To simulate transient heating, the FE simulation comprises two steps: (1) apply mechanical loading; (2) apply heating. The recorded temperatures are used as input data, based on which the mechanical behaviour is obtained.

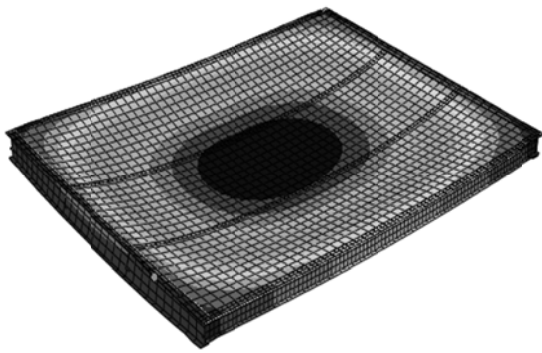


Fig. 3 Deformed shape

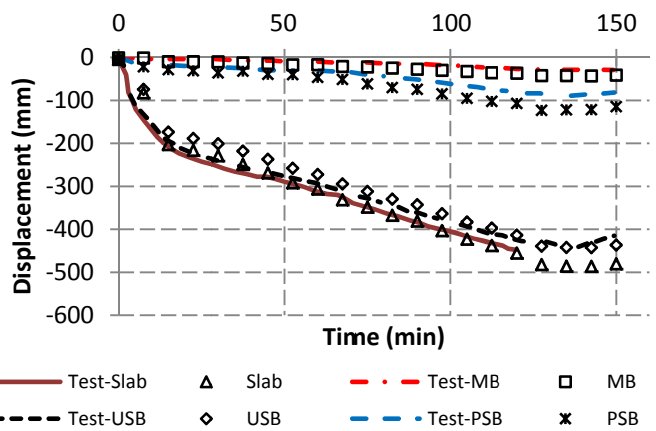


Fig. 4 Comparison of the results

A comparison of the central vertical displacements of the members between the numerical predictions and actual test results is shown in Fig. 4. It can be seen that the numerical results follow closely the experimental curves.

2 PARAMETRIC STUDY

2.1 Introduction

Given the reasonably good agreement between the numerical model and the experimental data for both structural and thermal responses, the above FE model shows the capability to simulate the behaviour of composite slab-beam systems in fire. Therefore, this model is adopted for parametric study.

Considering the size of the electrical furnace in the experimental programme, it is decided to test small-scale specimens. The investigated prototype slab panel is an interior 9m x 9m panel. In the parametric study, the slab obtained by scaling down to 1/4 of the panel is chosen as the control specimen (Figs. 5 & 6). The control slab is uniformly loaded with a predefined load level of 0.6 with a value of 19.20kN/m². This load level is defined as the applied load divided by the yield-line load at ambient temperature (P_{test}/P_{yield}). After being loaded up to the desirable load level, the slab is heated from the bottom.

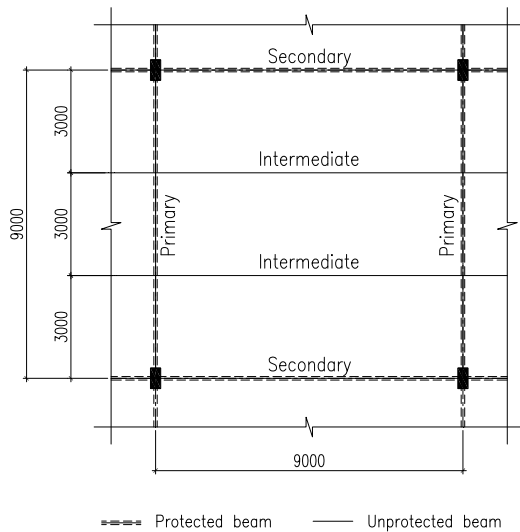


Fig. 5 Prototype interior slab panel

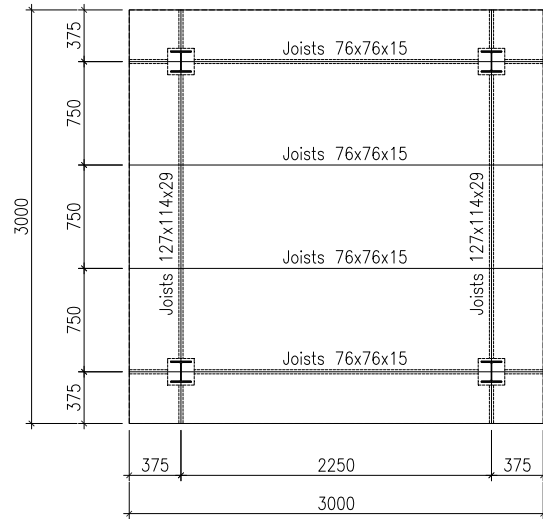


Fig. 6 Control slab

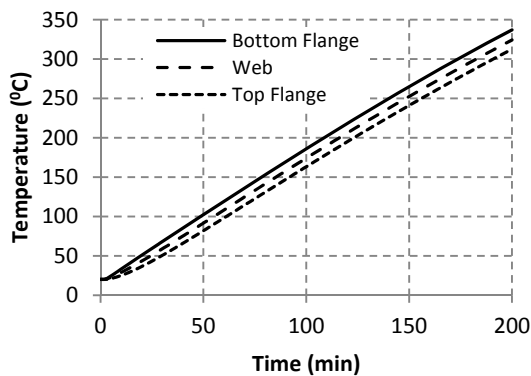
It is worth noting that the steel decking is not modelled in the simulations in recognition of debonding of steel decking under fire conditions, resulting in no contribution to the load-carrying capacity of the slab at the limit state.

2.2 Heat transfer analyses

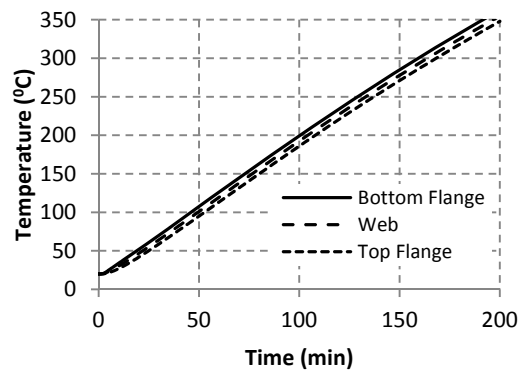
Under fire conditions, the mechanical behaviour is adversely affected by temperatures. Therefore, a series of thermal analyses have to be conducted to ascertain the temperature distributions for the control model before embarking on structural analysis. Using the validated model in Section 1.2, thermal analyses are performed for the 50mm concrete slab, the 127x114x29-joists protected main beam (MB), the 76x76x15-joists protected secondary beam (PSB) and the 76x76x15-joists unprotected secondary beam (USB). It is assumed that the slab is exposed to the ISO 834 fire curve from the bottom, while the beams are exposed to the same fire curve from three sides.

In ABAQUS, to conduct thermal analysis for protected steel beams, the protective material is defined as one independent part attached to the beam section through a surface-based contact interaction. *Gap conductance* is adopted and specified as a function of clearance that is incorporated through contact property assignment. Thermal boundary conditions are simulated by defining prescribed temperatures at particular points.

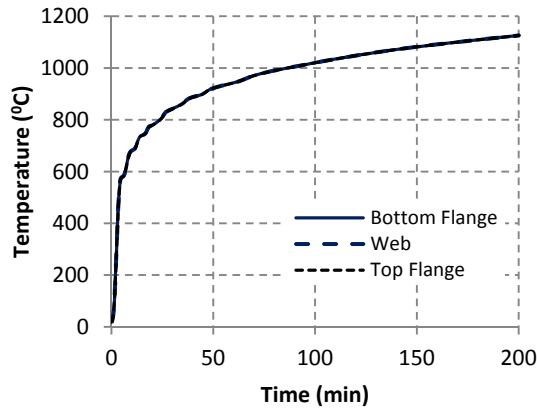
Fig. 7 shows the variation of temperatures within the cross sections of the main and secondary beams and the slab. Based on these temperatures as input data, the mechanical behaviour of the model can be obtained.



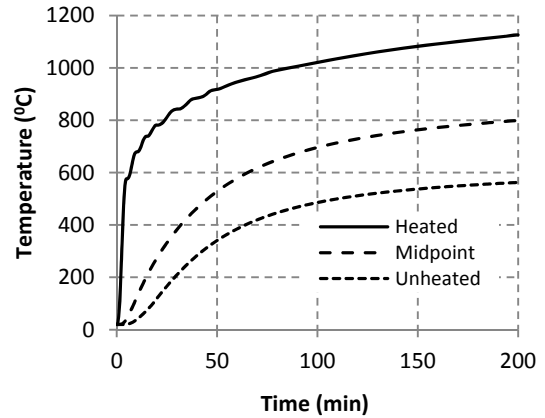
a) Protected main beam (MB)



b) Protected secondary beam (PSB)



c) Unprotected intermediate beam (USB)



d) Slab

Fig. 7 Simulation of heat transfer analyses

2.3 Effect of stiffness of perimeter beams

To investigate the effect on stiffness of perimeter beams on the development of TMA in the slab, four cases are analysed with different sizes of beams for one slab configuration as shown in Tab. 1.

Tab. 1 Case studies for stiffness of perimeter beams

Case study	Denote	MB	SB	I_y - MB	I_y - SB	Note
4	ST0	Joists 127x114x29	Joists 76x76x15	I_1	-	No intermediate beam
5	ST1	Joists 127x114x29	Joists 76x76x15	I_1	I_2	Control model
6	ST2	Joists 127x114x29	Joists 89x89x19	I_1	$2I_2$	
7	ST3	Joists 152x127x37	Joists 76x76x15	$2I_1$	I_2	

Fig. 8 compares the midspan vertical deflection of the slabs. It can be seen that slab ST0 without intermediate beams has a similar deflection trend to those models with intermediate beams, but with significantly greater deflection. It can also be observed that as stiffness of the edge beams increases, failure of the slab occurs later with a smaller deflection. Increasing the stiffness of protected secondary beams has a greater beneficial effect on the slab deflection than increasing the stiffness of primary beams. Increasing the stiffness of primary beams only has the effect on the slab deflection when it has undergone $2.9d$ (d : effective depth of slab).

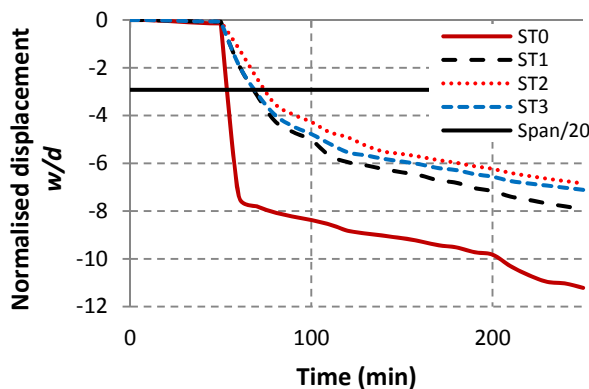


Fig. 8 Midspan vertical slab deflection with different stiffness of perimeter beams

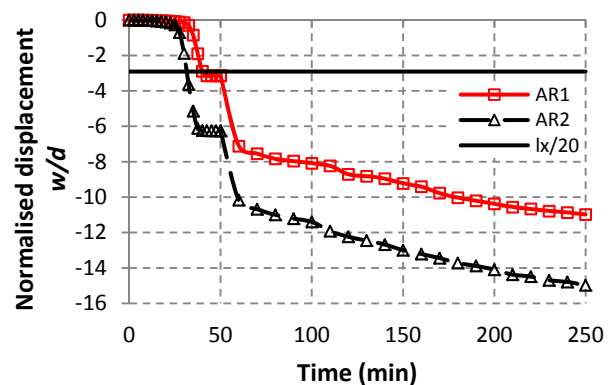
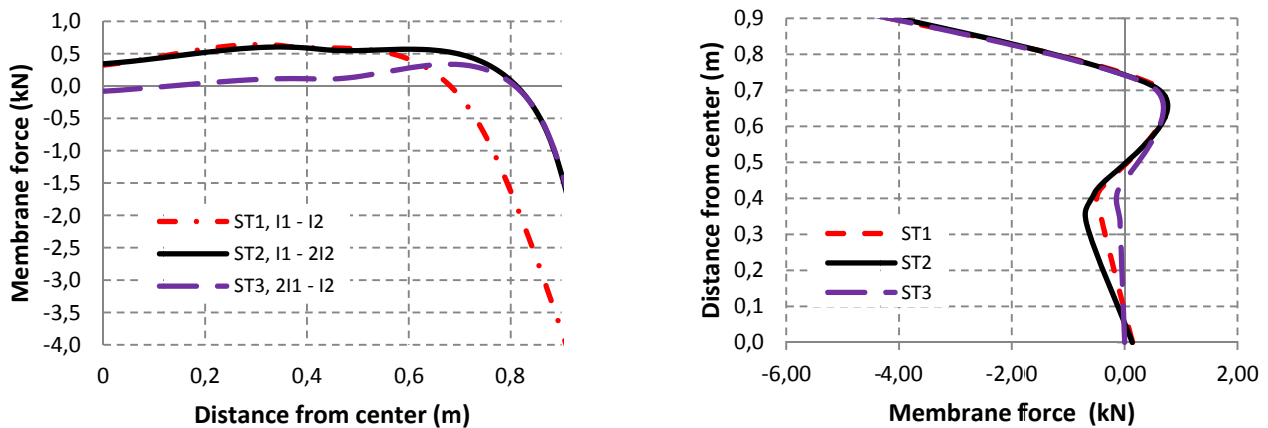


Fig. 11 Midspan vertical deflection of the slabs with different aspect ratios

A comparison of the distribution of membrane forces across the slab thickness at midspan at a slab deflection of $6.8d$ for three cases is shown in Fig. 9. In this figure, positive values indicate tensile forces and negative values compressive forces. As can be seen, in slab ST2, greater tensile

membrane forces are mobilized compared to slab ST1. However, at this deflection, slab ST3 provides less tensile membrane forces than slabs ST1 and ST2. Due to T-beam action, parts of the slab above the beams are still in compression. Therefore, estimating the enhancement of the slab load-carrying capacity due to TMA without considering the presence of the perimeter beams may not be accurate. It is obvious that the in-plane membrane mechanism comprises a compressive ring of concrete around the slab perimeter and tensile membrane action in the central region of the slab. Based on the strains of both concrete and reinforcement, the predicted failure modes are given in Fig. 10. The slab may fail by fracture of reinforcing rebars over the unprotected secondary beams, or by failure of the compressive ring at the corners. If the intermediate beams are over-stiff, a different failure mode may occur. As can be seen in Fig. 9(b), in slab ST2, part of the slab is still in compression. This shows that as stiffness of secondary beams increases, it seems to be more difficult to mobilize TMA in both directions, resulting in possible formation of plastic hinges in the perimeter beams, i.e. folding mechanism (Abu et al. 2010).



a) Along Y axis (parallel to secondary beam) b) Along X axis (parallel to main beam)

Fig. 9 Distribution of membrane forces at the slab deflection of 6.8d

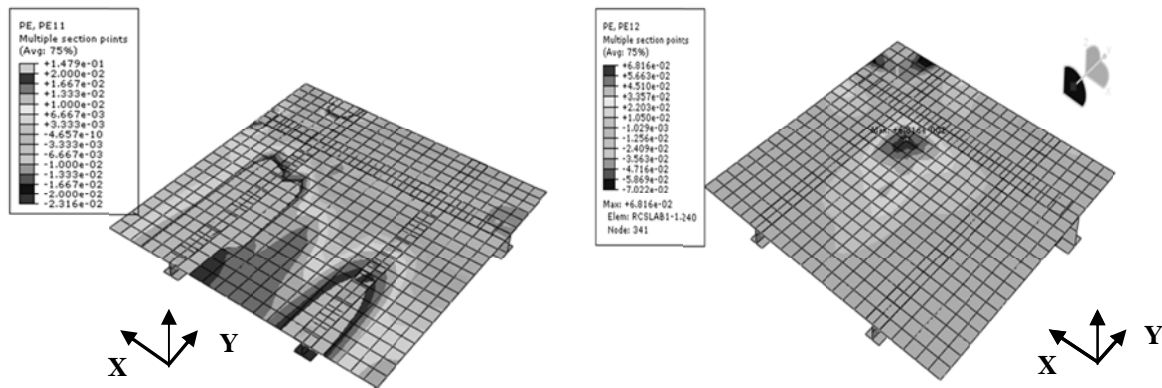


Fig. 10 Predicted failure modes

2.4 Effect of aspect ratios of slabs

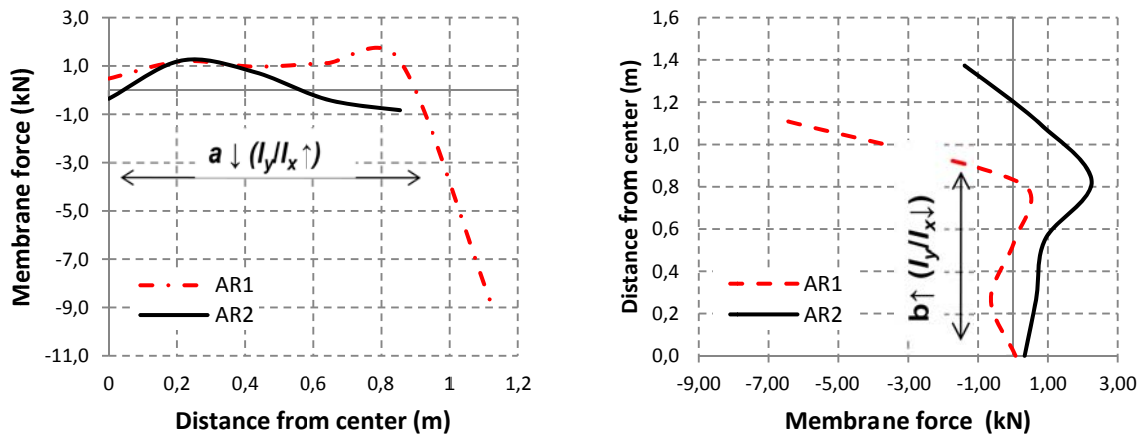
In this section, two different slab geometries are analysed to investigate the effect of aspect ratio of slabs on the development of TMA. To clearly delineate this effect from the others, isolated panels without intermediate beams (IB) are adopted for analysis. For both cases, the slab is 50mm thick with the same size of perimeter beams.

Fig. 11 compares the midspan vertical deflection of the slabs. The span/20 criterion is also indicated. As can be seen, during the first 20 minutes, the slabs have a similar rate of deflection. After 20 minutes, the deflection of slab AR2 increases at a faster rate than that of slab AR1. Slab AR2 reaches the deflection limit of 112mm, just after 31 minutes at the loading phase.

Tab. 2 Case studies for aspect ratio of slabs

Case study	Denote	l_x (m)	l_y (m)	Aspect ratio	Note
8	AR1	2.25	2.25	1.0	No IB
9	AR2	2.25	3.375	1.5	No IB

The distribution of membrane forces across the midspan sections at the slab deflection of $10d$ is plotted in Fig. 12. It can be observed that as the aspect ratio increases, the behaviour of two-way spanning slabs approaches that of one-way slabs. Thus, less tensile membrane force is mobilised. It is worth noting that since the temperatures of the protected perimeter beams are still low, these beams can maintain strength and stiffness in fire. Therefore, in the vicinity of the perimeter beams, there is significant compressive membrane force.



a) Along X axis (parallel to shorter span) b) Along Y axis (parallel to longer span)

Fig. 12 Distribution of membrane forces at the slab deflection of $10d$

3 CONCLUSIONS

In this paper, numerical simulations were used to investigate the behaviour of composite slab-beam systems under fire conditions. It is demonstrated that the FE model gives reasonable accuracy compared to test results, providing an efficient, economical and yet accurate tool to study the membrane behaviour of composite slab-beam systems in fire. From the parametric study, it can be concluded that: (1) Unprotected intermediate beams can reduce slab deflection and increase the fire resistance of composite slab-beam systems; (2) At the same large deflection of the slab, if the secondary beams have greater stiffness the slab can generate greater tensile membrane force compared to the control model; (3) As the aspect ratio of two-way RC slabs increases, less tensile membrane force is mobilised; (4) Failure modes of composite slab-beam systems may be different from those of composite slabs.

Currently, an experimental programme conducted on $1/4$ scale models of composite slab-beam systems under fire conditions is being prepared in NTU to study the behaviour experimentally.

ACKNOWLEDGMENT

The work presented in this paper is supported by the research funding from Agency for Science, Technology and Research (A*STAR). Their financial support is gratefully acknowledged.

REFERENCES

- Abu, A. K., V. Ramanitarivo, et al. (2010). Collapse Mechanisms of Composite Slab Panels in Fire. Sixth International Conference on Structures in Fire (SiF'10).
- Hongxia, Y., I. W. Burgess, et al. (2008). "Numerical simulation of bolted steel connections in fire using explicit dynamic analysis." *Journal of Constructional Steel Research* **64**: 515-525.
- Palm, J. (1994). "Temperature analysis using ABAQUS." *Fire Technology* **30**(3): 291-303.
- Zhao, B., M. Roosefid, et al. (2008). Full scale test of a steel and concrete composite floor exposed to ISO fire SiF'08, Singapore, NTU.

Proceedings of International Conference
Applications of Structural Fire Engineering
Prague, 29 April 2011

Session 3

Composite Structures and Connections

ANALYSIS OF STEEL–CONCRETE COMPOSITE BEAM WITH INTERLAYER SLIP IN FIRE CONDITIONS

Tomaž Hozjan^a, Jerneja Kolšek^b, Igor Planinc^a, Miran Saje^a and Stanislav Srpčič^a

^a University of Ljubljana, Faculty of Civil and Geodetic Engineering, Ljubljana, Slovenia

^b Kraški Zidar d.d., Sežana, Slovenia

INTRODUCTION

Steel–concrete composite beams are often employed in office and industrial buildings for fast and economic erection. Most usually they comprise a steel girder and a reinforced concrete slab interconnected by shear connectors. The number of shear connectors largely determines whether the composite cross-section behaves as compact or partially connected. In any cases, the deformation of the beam causes some relative tangential displacement (slip) between the steel girder and the concrete slab. While usually being very small, slip can have a substantial effect on the overall ductility of the beam, which indicates that it should be taken into account in the analysis (Ranzi et al, 2007). This seems to be particularly true when analysing behaviour of composite beams subject to extreme conditions including fire.

Mathematical modelling of behaviour of a steel–concrete composite beam during fire is a demanding problem. It appears, however, that the problem can be solved with a sufficient accuracy, if it is divided in two independent uncoupled processes, each to be solved separately. The first process consists of determining the spatial and time distributions of temperature and pore pressure in the steel–concrete composite beam. The second process describes the mechanical response; there the temperature and pore pressure distributions serve as a loading to result in the mechanical response of the slab subjected to the simultaneous action of mechanical and fire loads (Hozjan, 2009).

There is a number of mathematical models available to determine the temperature field in the composite concrete–trapezoidal steel plate slab. The growth of temperature in concrete triggers an increase of pore pressure and induces the moisture transport through the heated concrete such that moisture travels from the moist section to a dry one or condenses. The model by Tenchev et al. (2001) is implemented in the present work. It represents a substantially modified model previously proposed by Bažant et al. (1997) and is now considered to be rather complete for the analysis of concrete structures in fire. It is represented by a system of coupled transient differential equations, describing heat and mass transfer and pore pressure development. We note that the Tenchev model is only one among a few recent mathematical models of moisture and heat transfer in concrete at elevated temperatures proposed in literature.

There are various models for describing a mechanical response of a steel–concrete composite beam subject to simultaneous action of mechanical and fire loads. Most of them employ the finite element methods. Their precision largely depends on a proper modelling of the interaction between the reinforced concrete slab and the trapezoidal steel plate, the applied material models of concrete, reinforcement and steel plate at elevated temperatures, and the corresponding models of temperature and viscous strains of steel, creep of concrete and transient strains of concrete. The problems are often computationally so demanding that the analysis must be limited to 2D.

In this paper we present a new numerical model for the analysis of steel–concrete composite beams exposed to fire. The model consists of two successive steps. For the description of slow transient phenomena involving heat and mass transport and the pore pressure increase in concrete, a somewhat modified thermo-hydro-chemical model of Tenchev is employed (Tenchev et al, 2001). For the determination of mechanical response of the steel–concrete composite slab during fire numerical model with the following assumptions is used: (i) the layers of a steel–concrete composite slab are described with Reissner's kinematically exact model of the beam, (ii) the slip can occur at the interface between the layers but no transverse separation between them is possible,

(iii) an additive split of strains, where thermal, mechanical and viscous strains of steel at elevated temperatures, along with creep of concrete and transient strains of concrete are considered, (iv) strain-based finite elements are employed. In the numerical example that follows, we test the accuracy of the present numerical model by comparing the results of our model with the data of experimental data (Wainman et al, 1988) and the numerical results of Huang et al. (1999).

1 FIRE ANALYSIS OF STEEL–CONCRETE COMPOSITE BEAM

1.1 First step of the fire analysis

Development of gas temperature in the fire compartment depends on many parameters and is therefore both a complex task to do and unreliable. For this reason engineers use simplified parametric temperature–time curves instead, which provide relationships between gas temperature in a compartment and time for a number of standardized situations (Ma et al, 2000). Once the variation of the surrounding gas temperature in the compartment has been defined, heat and mass transfer in the composite beam can be performed.

1.1.1 Heat and mass transport in composite beam

A coupled heat and moisture transfer in concrete exposed to fire can be mathematically described with a system of differential equations consisting of mass conservation equations for each phase of concrete and the energy conservation equation (Thenchev et al, 2001) as follows:

Water conservation:

$$\frac{\partial \bar{\rho}_L}{\partial t} = -\nabla \mathbf{J}_L - \dot{E}_L + \frac{\partial \bar{\rho}_D}{\partial t} \quad (1)$$

Water vapour conservation:

$$\frac{\partial (\varepsilon_G \bar{\rho}_V)}{\partial t} = -\nabla \mathbf{J}_V + \dot{E}_L \quad (2)$$

Air conservation:

$$\frac{\partial (\varepsilon_G \bar{\rho}_A)}{\partial t} = -\nabla \mathbf{J}_A \quad (3)$$

Energy conservation:

$$(\underline{\rho C}) \frac{\partial T}{\partial t} = -\nabla \cdot (-k \nabla T) - (\underline{\rho C v}) \cdot \nabla T - \lambda_E \dot{E}_L - \lambda_D \frac{\partial \bar{\rho}_D}{\partial t} \quad (4)$$

In Eqs. (1)–(4) ρ_i is the density of a phase i , \mathbf{J}_i is the mass flux of each phase (L is free water, V is water vapour and A is dry air) per unit volume of gaseous material, $\varepsilon_G \bar{\rho}_V$ and $\varepsilon_G \bar{\rho}_A$ are mass concentrations of air and water vapour per unit volume concrete, \dot{E}_L is the rate of evaporation of free water (including desorption), t is time. In Eq. (4) $\underline{\rho C}$ is heat capacity of concrete, k is thermal conductivity of concrete, $\underline{\rho C v}$ relates to the energy transferred by fluid flow, λ_E is the specific heat of evaporation, λ_D is specific heat of dehydration and T is the absolute temperature. As in the model proposed by Tenchev et al. (2001), we here assume that the liquid pressure is equal to the gas pressure, $P_G = P_L$. This causes the capillary pressure, P_C , to be equal to zero, which is physically true only at a full saturation of pores with liquid water. It is also assumed that air and water vapour behave as an ideal gas and $\bar{\rho}_L$ of free water is determined with the help of sorption curves defined by Bažant et al. (2001).

By summing Eqs. (1) and (2) we end up with three partial differential equations. The solution is obtained numerically with the finite element method, where the primary unknowns of the problem

are temperature T , pore pressure P_G and water vapour content ρ_v . For a detailed description of the problem and its numerical formulation, see Tenchev et al. (2001).

1.2 Second step of the fire analysis

Once the temperature variation in time and space has been obtained, we may start the second step of the fire analysis where we determine the stress-strain state of steel–concrete composite slab. We find the solution in an incremental way.

We divide the time of the duration of fire into time intervals $[t^{i-1}, t^i]$, and determine iteratively the stress and strain state at each time t^i . The layers of the steel–concrete slab are modelled by Reissner's geometrically exact beam theory (Reissner, 1972), but with the effect of shear deformations being neglected.

We consider an initially straight, planar, two-layer steel–concrete slab of undeformed length L . The steel–concrete slab is subjected to a conservative, time independent load, and a time-dependent growth of temperature; for further details a reader is referred to Hozjan (2009).

The related governing equations are:

Kinematic equations:

$$1 + u^{j'} - (1 + \varepsilon^j) \cos \varphi = 0, \quad j = a, b \quad (5)$$

$$w' + (1 + \varepsilon^a) \sin \varphi = 0 \quad (6)$$

$$\varphi - \kappa = 0 \quad (7)$$

Equilibrium equations:

$$R_x^{j'} + q_x^j + p_x = 0, \quad j = a, b \quad (8)$$

$$R_z' + q_z = 0 \quad (9)$$

$$M' - M_c' = 0 \quad (10)$$

$$Q^a (1 + \varepsilon^a) - M_c^a - m_y = 0 \quad (11)$$

$$M^b = M - M^a \quad (12)$$

$$R_z^b = R_z - R_z^a \quad (13)$$

$$N^j = R_x^j \cos \varphi - R_z^j \sin \varphi, \quad j = a, b \quad (14)$$

$$Q^j = R_x^j \sin \varphi + R_z^j \cos \varphi, \quad j = a, b \quad (15)$$

Constitutive equations:

$$N^j - N_c^j = 0, \quad j = a, b \quad (16)$$

$$M^a - M_c^a = 0 \quad (17)$$

Constraining equations:

$$\Delta' = \varepsilon^a - \varepsilon^b \quad (18)$$

$$p_x^a - p_x^b = 0 \quad (19)$$

$$p_z^a - p_z^b = 0 \quad (20)$$

$$\left[\frac{M_c^{a'} + m_y^a}{(1 + \varepsilon^a)} \right]' = R_x^{a'} \sin \varphi^a + R_z^{a'} \cos \varphi^a + N^a \kappa^a \quad (21)$$

$$p_t = G(x, \Delta, T, \sigma, \dots) \quad (22)$$

$$x^* = x + \Delta \quad (23)$$

where $(\square)'$ denotes the derivatives with respect to x and index j denotes the particular layer of the composite beam (a and b). Variable u^j is the component of a displacement vector and φ^j is the rotation angle at the reference axis. w is the lateral displacement and φ is the rotation at the

At the contact between steel and concrete, the heat flux is taken to be permitted but the moisture flux is prevented due to the impervious steel surface and the perfect contact, resulting in the zero gradient of pore pressure and vapour content. Consequently, vapour cannot escape through the boundary between steel and concrete. The remaining data are: density of concrete 2400 kg/m³, density of cement 300 kg/m³, initial temperature 20°C, initial pore pressure 0.1MPa, initial water vapour content 0.013 kg/m³, water vapour content on boundary 0104 kg/m³, initial porosity of concrete 0.15, initial permeability of concrete 1·10⁻¹⁶ and initial free water amount 10 kg/m³.

The distribution of temperature over the cross-section of the composite beam at 10, 30 and 60 min is presented in Fig. 2a. As expected the results show that the rate of increase in temperature of the steel beam is much higher than that of the concrete slab. This is due to a higher thermal conductivity and lower specific heat of steel. We may also notice that the temperature in the top flange and in the upper part of the web of the steel profile is lower compared to the bottom part. This is due to the heat flow from the steel beam to the less hot concrete slab.

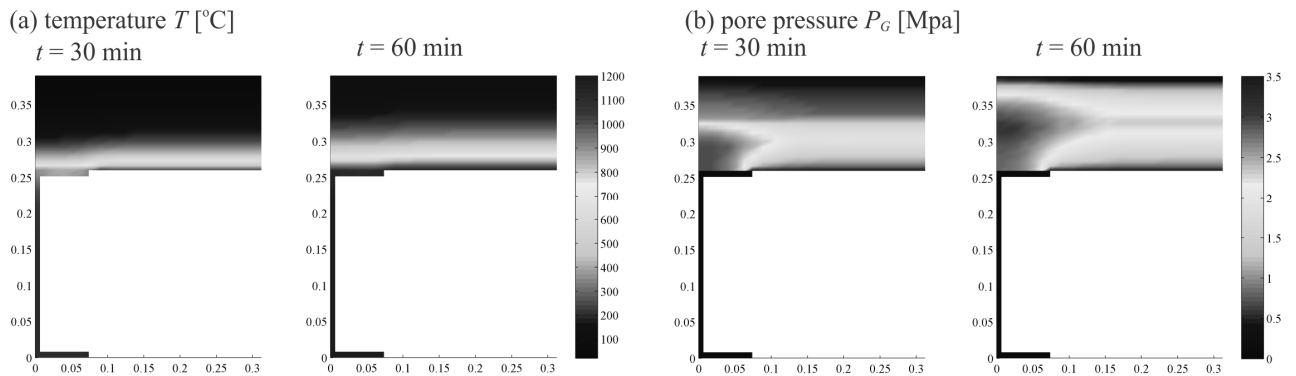


Fig. 2 (a) Distribution of temperature over the cross-section at 30 and 60 min. (b) Distribution of pore pressure over the cross-section at 30 and 60 min.

Fig. 2b shows the distributions of pore pressure over the cross-section at significant instants. As observed from the figures, the increase of pore pressure is largest at the contact between the steel beam and the concrete slab. After 60 min of fire have passed, the increased pore pressure zone spreads between the steel-concrete contact and the increased free water front. The zone of the high pore pressures extends with the increase of temperature and tends to spread over the whole concrete section. We can notice that the high pore pressure in concrete is also due to the impervious steel-concrete contact. Since the pore pressure on the area near the bottom of concrete deck, which is not in contact with the flange of the steel beam, is substantially smaller than the pore pressure over the area where the steel flange and the concrete deck are in contact.

2.2 Mechanical analysis of composite beam exposed to fire ISO 834

Fig. 3 shows the increase of the midspan deflection with temperature of the bottom flange for cases S1 and S2. The present numerical results are compared with the experimental data (Wainmann et al, 1988) and with the numerical results (Huang et al, 1999). It is clear that the agreement with both the experimental and the numerical data is good. In both cases, S1 and S2, failure of the composite beam as predicted by the present formulation takes place due to failure of the composite cross-section. Prior to failure, a material instability was observed in the concrete part of the cross-section, yielding shortly after to the material instability of the composite cross-section. As observed from Fig. 3, the rapid increase of the midspan deflection starts at about 700°C (case S1) and 650°C (case S2), leading to the failure of the critical cross-section. As already mentioned, failure temperatures agree well with those in experiment which are roughly 780°C and 670°C in cases S1 and S2, respectively. The computed critical deflections also agree well with the measured ones.

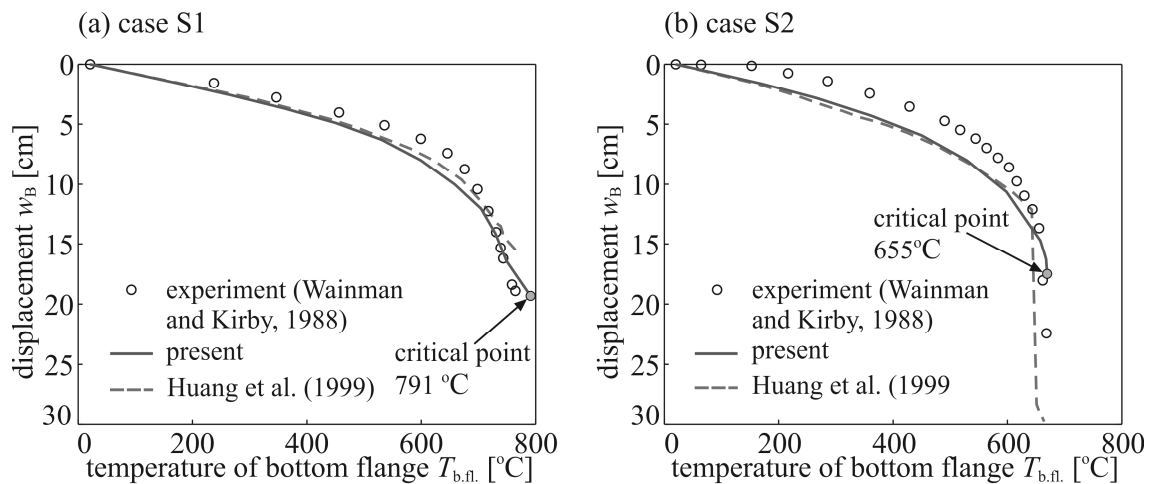


Fig 3. The variation of the midspan deflection with temperature. (a) case S1; (b) case S2.

3 ACKNOWLEDGMENT

The work of J. Kolšek was partly financially supported by the European Union, European Social Fund. The support is gratefully acknowledged.

4 SUMMARY

We presented the numerical model for the fire analysis of planar composite beam structures. The temperature field in concrete was determined with a coupled model of slow transient phenomena involving heat and mass transport and pore pressure increase in concrete. For the mechanical analysis, the strain-based non-linear beam finite element was used. The model considers both the kinematical and material non-linearity. The slip between the concrete slab and the steel sheet is allowed, while the delamination is neglected. The numerical example shows that the present beam formulation is appropriate for the thermo-mechanical analysis of frame-like structures, as it is accurate and robust.

REFERENCES

- Bažant Z.P., Kaplan M.F., Concrete at high temperatures: material properties and mathematical models, Longman, Harlow, 1996.
- Hozjan T., Nonlinear analysis of composite planar structures exposed to fire, University of Ljubljana, Faculty of Civil and Geodetic Engineering, Doctoral thesis (in Slovene), 2009.
- Huang Z., Burgess I.W., Plank R.J., The influence of shear connectors on the behaviour of composite steel-framed buildings in fire, *J. Const. Steel Res*, 51(3):219–237, 1999.
- Ma, Z.C., Makelainen P., Parametric temperature-time curves of medium compartment fires for structural design. *Fire Saf. J.*, 34(4):361–375, 2001.
- Reissner E., On one-dimensional finite-strain beam theory: The plane problem, *Journal of Applied Mathematics and Physics (ZAMP)*, 23, 795–804, 1972.
- Ranzi G., Bradford M.A., Direct stiffness analysis of a composite beam-column element with partial interaction, *Comp. Struct.*, 85(15–16):1206–1214, 2007.
- Tanchev R.T., Li L.Y., Purkiss J.A., Finite element analysis of coupled heat and moisture transfer in concrete, subjected to fire, *Num. Heat Transfer Part A*, 39(7):685–710, 2001.
- Wainman D.E., Kirby B.R., Compendium of UK standard fire test data, unprotected structural steel–1., Ref. No. RS/RSC/S10328/1/87/B, Rotherham (UK): Swinden Laboratories, British Steel Corporation, 1988.

FIRE SAFETY ENGINEERING APPLIED TO COMPOSITE STEEL- CONCRETE BUILDINGS: FIRE SCENARIOS AND STRUCTURAL BEHAVIOUR

Emidio Nigro^a, Anna Ferraro^a, Giuseppe Cefarelli^a,

^a University of Naples FedericoII, Department of Structural Engineering (D.I.ST.), Naples, Italy

INTRODUCTION

The structural analysis carried out in non-linear field (mechanical and geometrical) and full scale tests (BRE, 2004) show that the behaviour of structures subjected to fire is influenced not only by thermal degradation of materials, but also by further multiplicity of factors, such as the constraint conditions, structural redundancy, stiffness and ductility of the members of the structure, and loading paths. No less important are the fire scenarios and their severity, the spread of flames, the growth rate and the ventilation factor of the compartment (which influences the types of fire).

The Fire Safety Engineering (performance-based approach) allows, through the definition of specific fire scenarios and the application of advanced computational models, to take into account in an accurate way the temperature distribution within the elements and the mechanical and geometric nonlinear structural response in the fire situation. Therefore, the current Italian (D.M.16-02-2007; D.M.09-03-2007; D.M.09-05-2007; D.M.14-01-2008) and European (EN 1991-1-2; EN 1994-1-2) codes for fire structural design allow both prescriptive and performance-based approaches (Fig 1).

In this section we describe the global fire analysis of composite steel-concrete frames belonging to an office building. The considered frame presents a 24 meters overall length consisting of three equal spans and a 14 meters height consisting of four levels. The frame belongs to a three-dimensional structure with a square plant and bracing in the direction perpendicular to the frame studied: Fig. 2 shows a carpentry type and geometric characteristics of the considered frame.

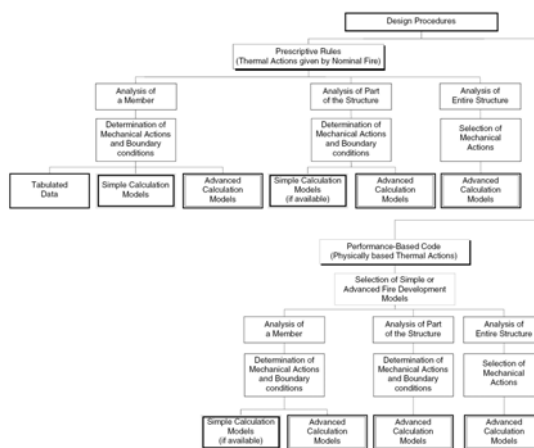


Fig. 1 Fire design methods according to the Eurocodes.

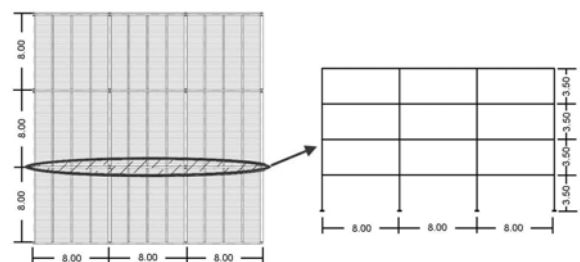


Fig. 2 Carpentry type and geometric characteristics.

The columns are arranged with the axis of maximum inertia within to the plane of the frame. Beam-to-column connections ensure the rigidity of the nodes and they are assumed to be able to withstand the forces for a time at least equal to the time of fire resistance of elements transmitting the forces. The building was designed and checked under normal conditions for all load combinations required by the Italian Technical Standards for Construction (D.M.14-01-2008). After the analysis in normal situation, it was performed a design in fire situation by the tabular method proposed by EN 1994-1-2. It is useful to underline that the new Italian Technical Code is largely inspired to Eurocodes.

The seismic design of the frame was done in low ductility class and according to the capacity design criteria required by the Italian Code (D.M.14-01-2008).

The composite steel-concrete floor consists of a profiled steel sheeting Siscofloor 5/75/720 bond with concrete slab thickness of 75 mm, for a total height of the slab of 150 mm. Moreover, there is a longitudinal reinforcement $\phi 10/25\text{cm}$ in the concrete slab for the limitation of crack width. The secondary beam is composite with steel beam HE140B connected to the slab with headed stud connectors. The design of structures for earthquake resistance was conducted with reference to seismic zones 2 according to the Italian Code. The columns of the frame designed are partially encased with HE500B steel profile. The beams are composed by a HE260B steel profile and a composite slab 15 cm thick. The seismic design of the columns is mainly regulated by the damage limitation state, therefore they result oversized with respect to the ultimate limit state. In particular, for the ultimate limit state, the beams have a load level in hogging bending moment close to unity, in each case. In order to have a standard fire resistance of 45 minutes (R45), based on the tabular data suggested in EN1994-1-2, the composite beam was also designed as partially encased with 16 cm^2 of reinforcement in the concrete between the flange. Moreover, the partially encased composite columns have a standard fire resistance of 45 minutes.

The design vertical loads on the structure were determined according to the Italian Code (D.M.14-01-2008), which classifies the fire as an exceptional action. Therefore, the mechanical actions to be considered for fire design situation were defined by the exceptional load combination *Eq. (1)*:

$$F_d = A_d + G_{k1} + G_{k2} + \sum_{i=1}^n \psi_{2i} \cdot Q_{ki} \quad (1)$$

The characteristic value of variable load, Q_{k1} , was defined for the specific use of the office areas. Each floor can be considered as a compartment. The compartment is open space and it has a plant area of 576m^2 , 12 windows width 5.0m and height 1.50m. The enclosure is made by material with density 2000 kg/m^3 , specific heat 1113 J/kgK and thermal conductivity 1.04 W/mK .

The specific fire load (D.M.09-03-2007) is defined as the total heat potential of all combustible materials that are placed in the fire compartment with reference to the gross area of the compartment, adjusted by parameters corresponding to the participation in the combustion of the several materials. The fire load is an index of fire hazard: the more is the fire load, the more is the severity of an fire. In the case study the fire load density is assumed equal to $q_f = 655\text{ MJ/m}^2$. It's corresponding to the 95% fractile of the fire load Gumbel statistical distribution (see Nigro et al, 2009). The design fire load density is calculated using the following equation *Eq. (2)*:

$$q_{f,d} = \delta_{q1} \cdot \delta_{q2} \cdot \delta_n \cdot q_f = 600\text{ MJ/m}^2 \quad (2)$$

where $\delta_{q1}=1.0$ factor taking into account the fire activation risk due to the size of the compartment;

$\delta_{q2}=1.0$ factor taking into account the fire activation risk due to the type of occupancy;

$\delta_n=0.765$ factor taking into account the different active fire fighting measures i .

These factors are defined according to Italian code (D.M.09-03-2007).

The fire analysis were carried out exposing the structure both to standard time-temperature fire curve (see Nigro et al, 2008; 2009; 2010b) and to natural time-temperature fire curves (see Nigro et al, 2011), i.e. localised fire (pre-flashover fire simulated by Hasemi's method) or generalised fire (post-flashover fire simulated by parametric curve). The structural fire analyses were performed with an advanced structural model, which allows taking into account the nonlinear behaviour of materials and structure, and the effects of constrained thermal deformation.

The structural analysis was conducted by analyzing a representative plane frame. Both thermal and mechanical analyses were conducted using the nonlinear program SAFIR2007, developed at the University of Liege (see Franssen, 2008).

1 FIRE ANALYSES

The possible types of natural fire are both localised fires and generalised fires. The first can be dangerous for some structural members, the second can be dangerous for all structural elements

1.1 Fire Scenario 1.

In order to understand the structural behaviour, it is analyzed the generalized fire scenario 1 (black curves in Fig. 6 and in Fig. 7). As a consequence of the heating the structural members begin to expand. The thermal elongation of the beam is constrained by the lateral stiffness of the columns and therefore the heated beams are subjected to compressive axial forces (Fig. 7). Moreover, an increment of the hogging bending moments is produced by the thermal bowing.

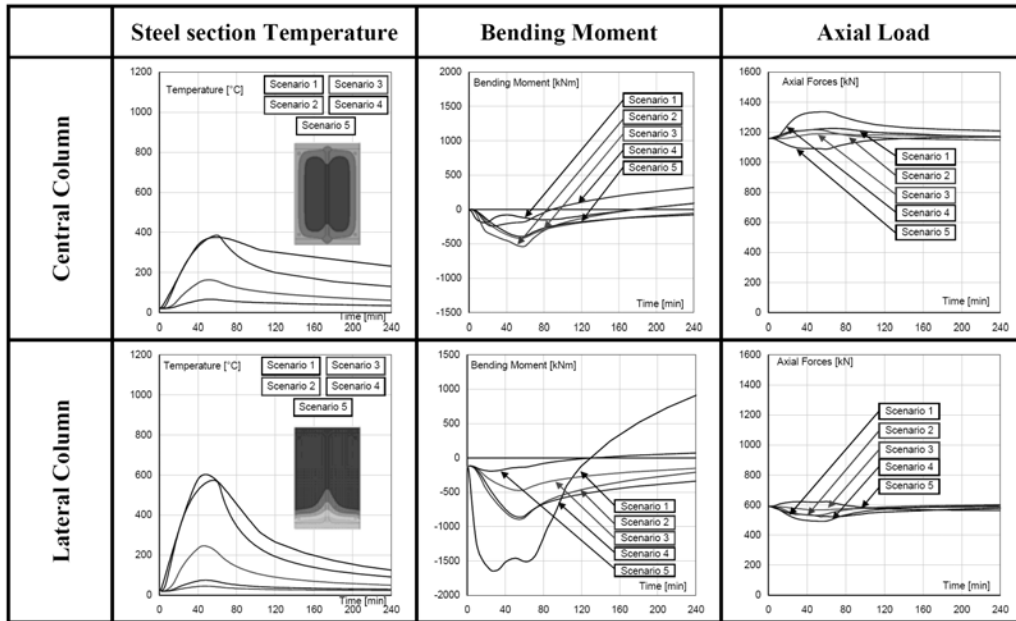


Fig. 6 Evolution of temperatures and stresses in the columns.

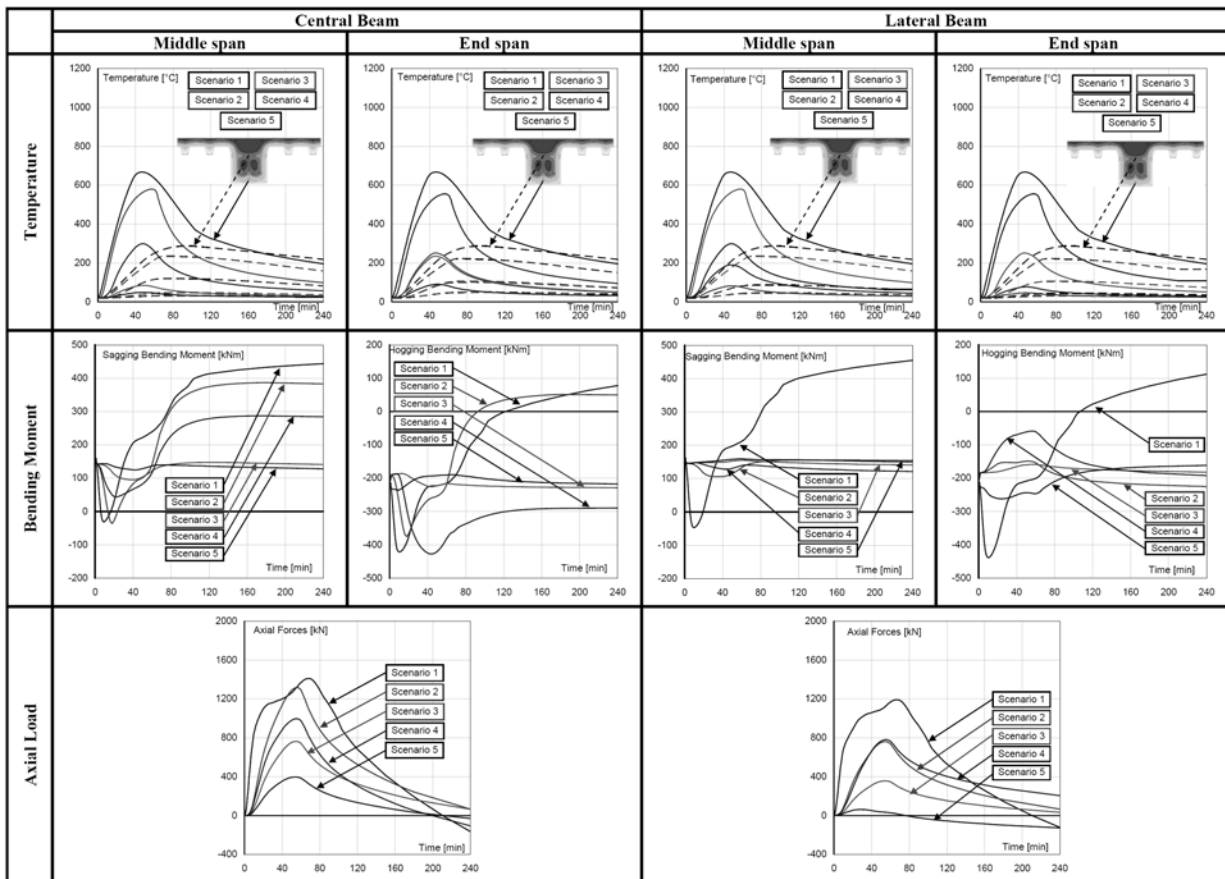


Fig. 7 Evolution of temperatures and stresses in beams.

The bending moment diagram and the corresponding deformed shape at different fire exposure time are reported in Fig. 8. The lateral columns, heated on a single side, show an increase of the bending moment due to both the beam thermal bowing and the P- Δ effects. The lateral columns, heated on a single side, show an increase of the bending moment due to both the beam thermal bowing and the P- Δ effects. The axial force of the internal columns, heated on all sides, increases; in fact, the columns thermal elongation is constrained by the shear stiffness of the beams. After about 50 minutes of fire exposure the cooling of the structural members begins (Fig. 6 and in Fig. 7), with consequent thermal bowing opposite to that of the heating phase; such curvature is able to reverse the trend both of the bending moment and the displacement of the beams (Fig. 7). The structure does not return to the same initial conditions after the fire exposure; in fact, during the heating and cooling phase plastic deformations occur at the ends of the structural members, as shown by the diagrams of bending moments during the fire exposure time (Fig. 7) and the residual strains at the end of the cooling phase (Fig. 8).

1.2 Fire Scenario 2.

The previous remarks can be done for each other scenarios. The deformed shape and the corresponding bending moment diagram at different time of exposure to fire scenario 2 are reported in Fig. 9. This case is interesting because, as can be seen from Fig. 6 and in Fig. 7 (red curves), after the fire exposure the beam is stressed by sagging bending moments over the entire central span and it has plastic hinges at its ends. However, the residual strains after fire exposure of the members not directly exposed to fire are smaller than the ones of fire scenario 1; even the bending moment diagrams of these members are slightly different from the ones at the beginning of fire.

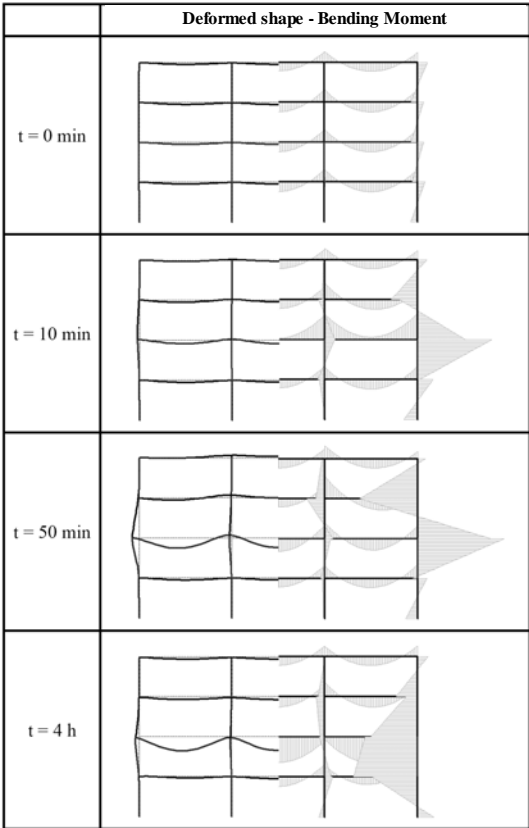


Fig. 8 Deformed shape and bending moment (Fire Scenario 1).

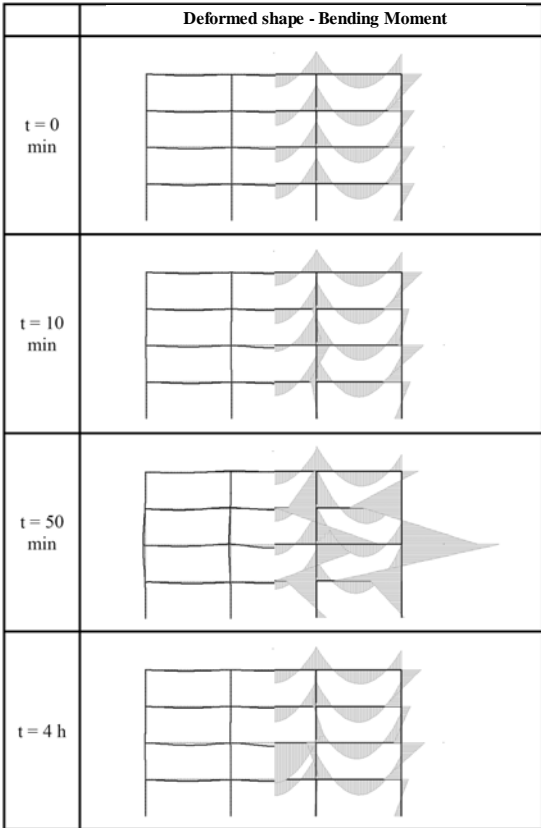


Fig. 9 Deformed shape and bending moment (Fire Scenario 2).

2 CONCLUSIONS

The Fire Safety Engineering (performance approach) allows, through the definition of specific fire scenarios and the application of advanced computational models, to estimate the structural response in the fire situation. In Italy, the fire safety building regulations are basically prescriptive; however, the performance based design and advanced calculation methods may be applied either in the lack of prescriptive rules or in the case of “derogation” with respect to prescriptive rules.

The central stage in Fire Safety Engineering process is the correct identification of fire scenarios. In this paper many different fire scenarios have been considered. In particular the structural behaviour for natural fires has been evaluated considering generalised and localised fire conditions.

For the case study, the obtained results show first of all that the level of indirect actions caused by constrained thermal expansions is more significant for generalised fire scenarios (i.e. fires involving large compartments) which can lead to possible failure of columns.

Moreover, a natural fire, differently from a standard fire, is characterized by a heating phase and a cooling phase. During the heating fire exposure the structural behaviour is non-linear and plastic strains can be achieved in the structural members; for this reason, the structure during the cooling phase is different from the initial structure. Therefore, after the cooling phase the stresses and the forces in the structural element can be different from the ones before the fire exposure. The stresses and forces induced by constrained thermal deformations may cause structural collapse; however, they cannot fully controlled by the prescriptive approach, as this approach is based on the assumption of a standard fire curve which increases unrealistically

REFERENCES

- BRE, Results and Observations from full-scale fire test at BRE. Cardington 2004.
- Ministry of Interior (Italian Government) 16 February 2007. Classificazione di resistenza al fuoco di prodotti ed elementi costruttivi di opere da costruzione, GU n. 74 del 29 marzo 2007
- Ministry of Interior (Italian Government) 9 March 2007. Prestazioni di resistenza al fuoco delle costruzioni nelle attività soggette al controllo del Corpo nazionale dei vigili del fuoco, GU n. 74 del 29 marzo 2007.
- Ministry of Interior (Italian Government) 9 May 2007. Direttive per l’attuazione dell’approccio ingegneristico alla sicurezza antincendio, GU n. 117 del 22 maggio 2007.
- Ministry of Infrastructure and Transport (Italian Government) 2008. Technical Code for the Constructions. G.U. n. 29 of 14 January 2008.
- EN 1991-1-2. Eurocode 1. Actions on structures - Part 1-2: General actions - actions on structures exposed to fire, November 2002.
- EN 1994-1-2. Eurocode 4. Design of Composite Steel and Concrete Structures - Part 1-2: General rules - Structural fire design, August 2005.
- Franssen J.M., (2008) - User Manual for SAFIR2007a: A Computer Program for Analysis of Structures Submitted to the Fire, University of Liege, Belgium, January.
- Nigro E., Ferraro A., Cefarelli G., Structural fire analysis of composite steel-concrete frames (in Italian). *Costruzioni Metalliche* n. 6: 49-62, 2008.
- Nigro E., Pustorino S., Cefarelli G., Princi P., Progettazione di strutture in acciaio e composte acciaio-calcestruzzo in caso di incendio (in Italian), Ed. Hoepli, Milano, 2009.
- Nigro E., Ferraro A., Cefarelli G., Member, substructure and global structural fire analyses of steel-concrete composite frames. International Conference on Urban Habitat Constructions under Catastrophic Events. Naples, September 16-18, 2010a.
- Nigro E. Ferraro A., Cefarelli G., Application of FSE approach to the structural fire safety assessment of steel-concrete composite structures. International Conference on Urban Habitat Constructions under Catastrophic Events. Naples, September 16-18, 2010b.
- Nigro E., Ferraro A., Cefarelli G., Fire Safety Engineering Approach Applied to Structures. (in Italian). In press on *Costruzioni Metalliche* n. 1, 2011.

MUNICH FIRE TESTS ON MEMBRANE ACTION OF COMPOSITE SLABS IN FIRE – TEST RESULTS AND RECENT FINDINGS

Martin Stadler ^a, Martin Mensinger ^b, Peter Schaumann ^c, Jörg Sothmann ^c

^a Technische Universität München, Chair for Metal Structures, Munich, Germany, Member of TUM Graduate School

^b Technische Universität München, Chair for Metal Structures, Munich, Germany

^c Leibniz Universität Hannover, Institute for Steel Construction, Hannover, Germany

INTRODUCTION

Composite beam slab systems show a very good behaviour in case of fire. Due to large deformations membrane forces are activated inside the slab and wider spans can be bridged. Secondary beams are not necessary at elevated temperatures and can be left unprotected. In several European countries research projects were carried out to analyse this phenomenon. In Great Britain and Switzerland membrane action is already used to design slab systems in fire. To enable such design rules in Germany further investigations are required. Available design methods need to be adapted to German design rules and some remaining issues have to be clarified. For this reason the research project “Nutzung der Membranwirkung von Verbundträger-Decken-Systemen im Brandfall” (Utilisation of membrane action for design of composite beam-slab-systems in fire) was initiated by the authors.

Main objective of the project is to understand the behaviour of intermediate beams between two slab panels. Large rotations lead to huge cracks in the concrete chord above the edge beams. That may reduce the load bearing capacity of these beams. Two large scale fire tests have been performed in Munich (Fig. 1 and Fig. 2) to analyse this issue, to calibrate numerical models and to validate analytical assumptions. Test results and latest findings of the project are presented in this paper.



Fig. 1 First Munich fire test



Fig. 2 Second Munich fire test

1 TEST ARRANGEMENT

The test arrangements should represent office buildings and similar multi storey structures. The specimens both consisted of two slab panels with overall dimensions of 5.0 m by 12.5 m (Fig. 3 and Fig. 4). They were supported by hot rolled I-beams and six reinforced concrete columns. The columns were not part of the investigation. All edge beams were protected with intumescent coating for a fire resistance of 60 minutes. The secondary beams were left unprotected. Two tests with slightly different arrangements have been performed. Only the orientation of the secondary beams, the flooring system and the intumescent coating system has been varied. The first specimen was built with a lattice girder precast slab and the second one with a profiled steel sheeting composite slab. The cross sections and reinforcement amount have been designed for an office building at

ambient temperature according to EN 1994-1-1. The utilization factors S_d/R_d were chosen very close to 100% to avoid structural integrity based on oversizing.

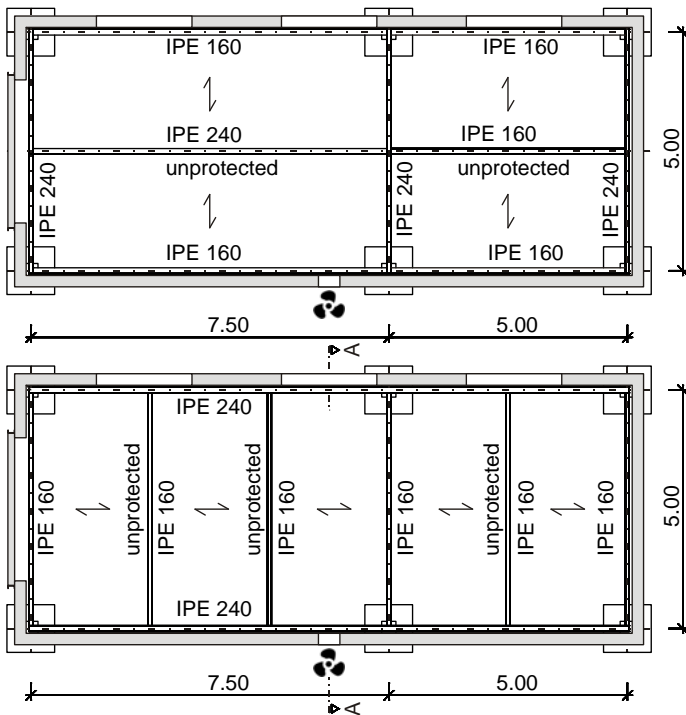


Fig. 3 Plan view of test 1 (above) and 2 (below)

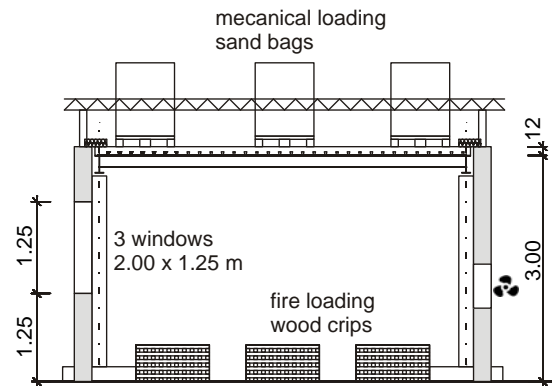


Fig. 4 Section A-A

The fire exposure of the slabs was intended to follow as close as possible the ISO 834 fire curve. The edge beams also have been inside the furnace to be able to deform freely and to investigate the influence of the edge beams on membrane action. The loading should be representative for office buildings. To ensure these boundary conditions a 3.0 m high temporary furnace was built by aerated concrete bricks. Sandbags were placed on top of the slab to simulate a uniform distributed load of 2.1 kN/m². Wood cribs consisting of 4.9 m³ spruce timber constituted the fire load. Three windows in one wall provided natural ventilation and a fan was installed in the opposite wall to readjust the ventilation.

2 TEST RESULTS

2.1 Test 1

At the first test with the lattice girder precast slab the gas temperatures exceeded 1000°C. Due to slightly non-uniform temperature distribution the maximum average gas temperature was about 900°C after 40 minutes (Fig. 5). The longer secondary beam heated up to 900°C the shorter beam even up to 950°C. The temperature in the edge beams remained below 500°C. Partially the intumescent coating detached from the lower flange. Therefore the lower flange of the intermediate beam reached almost gas temperature. The upper flange and the web stayed cooler than 500°C. The larger panel reached a maximum deformation of 260 mm after 60 minutes and the shorter panel about 200 mm. After 19 minutes a huge crack appeared in the smaller panel close to the intermediate beam (Fig. 6). The upper reinforcement layer ruptured completely in this crack and smoke passed through the gap. The slab did not collapse during the whole test but it lost its integrity (criterion “E”).

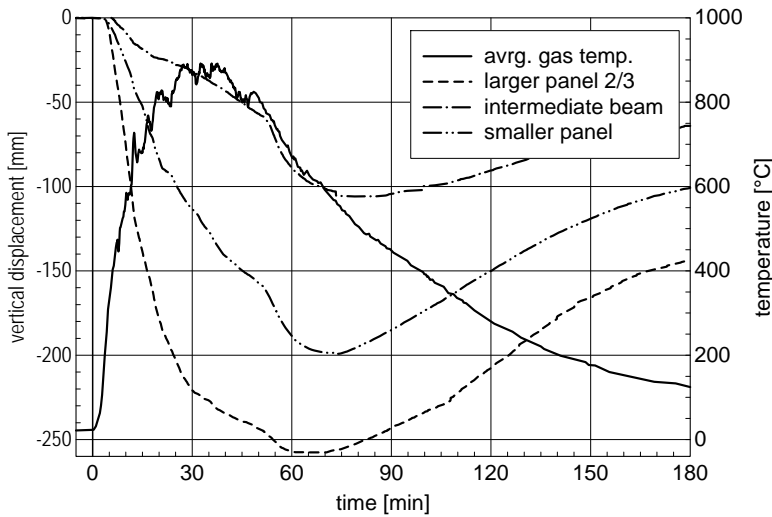


Fig. 5 Gas temperature and displacements first test



Fig. 6 Crack above intermediate beam first test

2.2 Test 2

The second test showed a very good behaviour of the composite slab during the whole experiment. The gas temperatures reached their maximum of more than 900°C after 40 minutes. The unprotected secondary beams reached over 800°C and the protected edge beams remained below 350°C. A maximum temperature of about 500°C was measured in the intermediate beam. The larger panel deformed vertically more than 250 mm and the smaller panel about 190 mm after 60 minutes (Fig. 7). The intermediate beam achieved the same deformation as the smaller panel after three hours. A large crack appeared above the intermediate beam (Fig. 8). However, all three criterions (REI) for fire resistance were kept during the whole test.

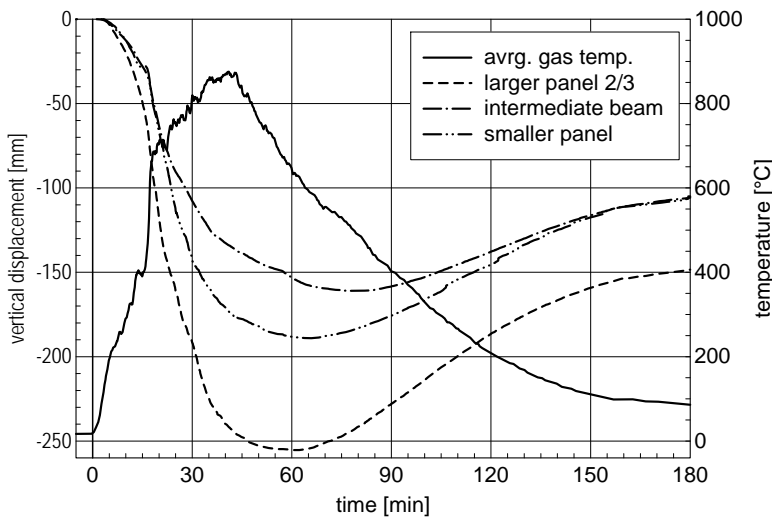


Fig. 7 Gas temperature and displacements second test



Fig. 8 Crack above intermediate beam second test

3 FIRE SIMULATION

In order to dimension the ventilation conditions the zone-model based software OZone developed by the University of Liege was used. The predicted temperature-time-curve matches the test data closely (Fig. 9). However, some differences occurred between measured and predicted temperature-

time-curve mainly caused by the humidity of the wood. The humidity considerably influences the combustion heat of fuel (c.h.o.f.) of the wood. The predicted curve was computed with the OZone default value for a c.h.o.f. of 17.5 MJ/kg. At the first test the wood had a measured humidity of 11.2%. This humidity leads to a reduced c.h.o.f. of 16.3 MJ/kg. With this reduction the simulated curve is very close to the measured curve in the heating phase. Only the cooling phase differs from the test data (Fig. 9).

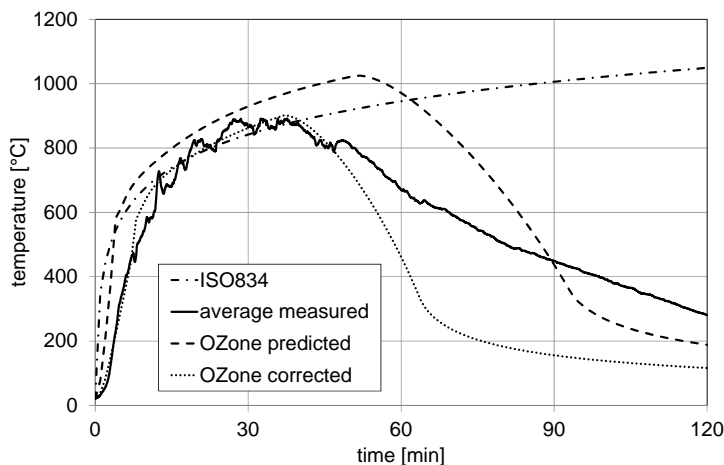


Fig. 9 Comparison of simulated and measured gas temperatures

4 EDGE BEAM BEHAVIOUR

The load bearing mechanism of the slab-beam-system is very complex. It will be discussed in the context of the first test. Assuming the slab has rigid vertical support and no edge beams the typical membrane force distribution occurs (Fig. 10). In each panel tensile membrane forces appear in the centre of the panel and a compression ring around the perimeter. This force distribution was described in former works and simplified design methods are based on it (e.g. Newman et al, 2000). But the forces change considerably when taking the edge beams into account (Fig. 11). A compression ring does not exist anymore. The edge beams elongate due to thermal expansion. This elongation is restrained by the slab and leads to compression in the beams and tension in the slab. In the model with rigid support the highest compression stresses in the concrete arise in the middle of the longer edge and the highest tensile forces occur in the middle of the slab in longitudinal direction. Whereas by including the edge beams the highest concrete compression emerges diagonal at the corners and considerable tensile forces occur above the intermediate beam.

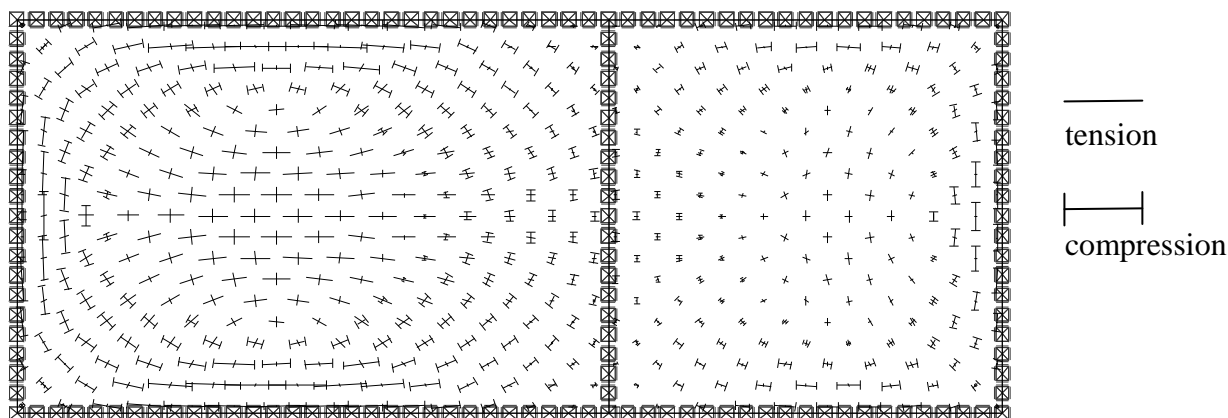


Fig. 10 Membrane forces, slab with rigid support

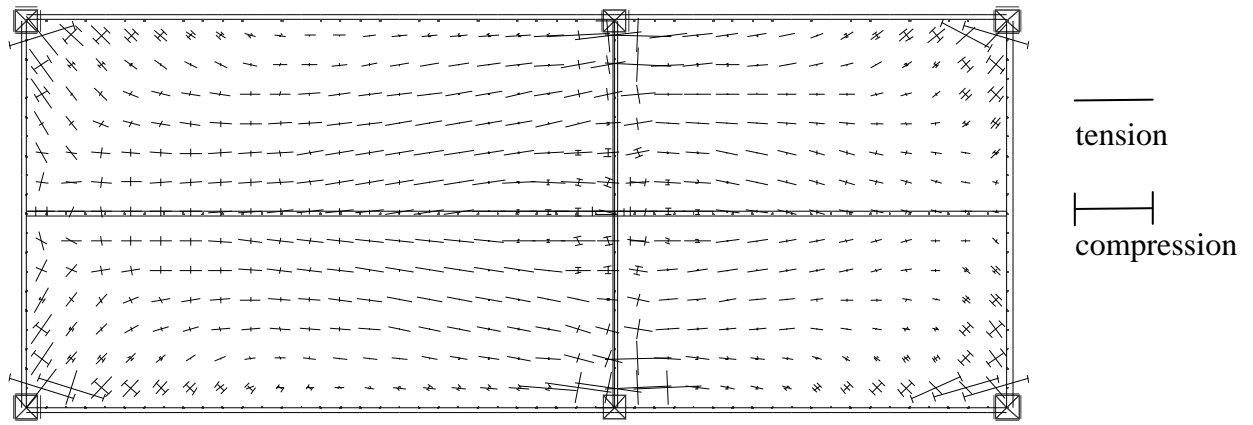


Fig. 11 Membrane forces, slab supported by edge beams

The tensile forces in the reinforcement above the intermediate beam are mainly caused by the hogging moment. This can be shown by considering the stresses in the top layer of the slab (Fig. 12a). Material nonlinearities reduce these stresses but even a bending hinge above the intermediate beam is not sufficient. The tensile forces are reduced but do not disappear (Fig. 12b). A possible explanation is that the slab acts like a three times supported cable in longitudinal direction. During the test all this led to cracking of the concrete above the intermediate beam, yielding and finally even to rupture of the reinforcement in the crack. With the ruptured reinforcement in the tension-zone the slab was not able to bear shear forces anymore and a huge shear crack was formed close to the intermediate beam. After that all the constraint forces have been removed and the slab again got into equilibrium with a different force distribution (Fig. 12c). To prevent this kind of failure further research is necessary.

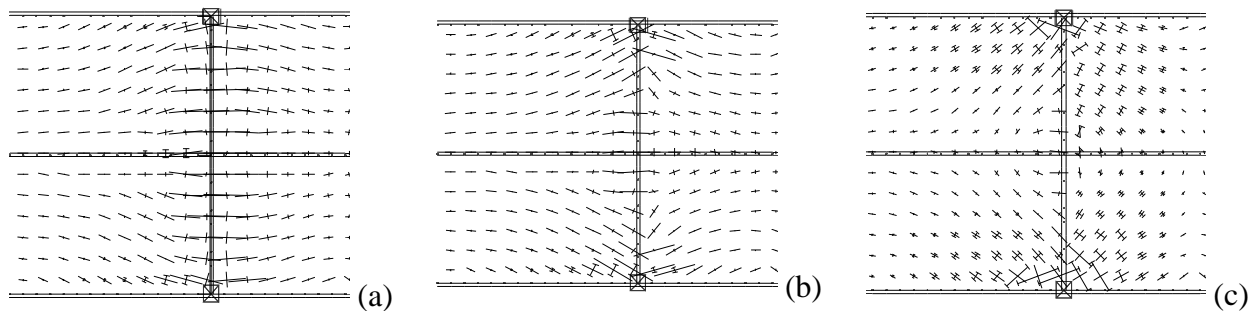


Fig. 12 Principal stresses top layer of slab, continuous (a) hinge (b) ruptured reinforcement (c)

5 SUMMARY

An on-going research project shall enable the use of membrane action for fire design of composite slabs in Germany. Within this project two large scale fire tests have been performed in Munich in 2010. The tests confirmed that membrane forces enhance the load bearing capacity considerably. In the test with the lattice girder precast slab a huge crack occurred above the intermediate beam. The slab lost its integrity and smoke streamed out of the crack. The provided explanation of the authors is that the reinforcement above the intermediate beam yielded due to the hogging moment and tensile membrane forces. No reinforcement was available anymore to transfer shear forces, a huge crack opened close to the intermediate beam and the reinforcement ruptured in the crack. Further research work is necessary to identify the parameters that induce this kind of failure and to develop design rules to avoid it in future.

6 ACKNOWLEDGEMENT

The authors would like to thank the sponsors of the project. Special thanks go to the German steel construction association DASt, the German ministry of economy and technology represented by the AiF and the construction company Max Bögl that enabled with big effort the assembly of the tests. Further supporters of the projects are: ArcelorMittal, Montana Bausysteme, Rütgers Organics, Sika, Xella, Hilti, stahl + verbundbau, Köco and HBM.

Das IGF-Vorhaben 16142 N der Forschungsvereinigung Deutscher Ausschuß für Stahlbau e.V. – DASt, Sohnstraße 65, 40237 Düsseldorf wurde über die AiF im Rahmen des Programms zur Förderung der industriellen Gemeinschaftsforschung und –entwicklung (IGF) vom Bundesministerium für Wirtschaft und Technologie aufgrund eines Beschlusses des Deutschen Bundestages gefördert.

(The IGF-research project 16142 N of the research association “Deutscher Ausschuß für Stahlbau e.V. – DASt, Sohnstr. 65, 40237 Düsseldorf” was supported via the AiF within the framework of the programme to support the cooperative industrial research and development (IGF) from the federal ministry of economy and technology due to a resolution of the German Bundestag.)

REFERENCES

- Abu A. K., Burgess I. W., Plank R. J.: Slab panel vertical support and tensile membrane action in fire. In: *Steel and Composite Structures* 8 (2008), pp. 217–230
- Abu A. K.: Behaviour of Composite Floor Systems in Fire. University of Sheffield, Department of Civil & Structural Engineering, Diss. 2009
- Bailey C. G.: Membrane action of slab / beam composite floor systems in fire. In: *Engineering Structures* 26 (2004), pp. 1691-1703
- Mensinger M., Schaumann P., Stadler M., Sothmann J.: Membranwirkung von Verbunddecken bei Brand – Stand der Technik. In: *Stahlbau* 79 (2010), Nr. 4, pp. 298–305
- Newman G. M., Robinson J. T., Bailey C. G.: Fire safe design: A new approach to multi-storey steel-framed buildings, Steel Construction Institute, Ascot 2000 (SCI publication 288)
- Tesar C. N.: Zum Tragverhalten von Verbunddeckensystemen im Brandfall, Diss. Zürich: vdf Hochsch.-Verl. an der ETH (IBK-Bericht, 309) (2008)

INFLUENCE OF SEMI-RIGID JOINT MOMENT-ROTATION CHARACTERISTICS ON THE BEHAVIOUR OF COMPOSITE STEEL-FRAMED STRUCTURES UNDER FIRE CONDITIONS

Zhen Yuan^a, Kang Hai Tan^a

^aNanyang Technological University., School of Civil and Environmental Engineering, Singapore

ABSTRACT

This paper presents the results of a numerical study to illustrate the advantages of incorporating the actual behaviour of semi-rigid joints in the analyses of composite steel-framed structures under fire conditions using ABAQUS. To overcome the lack of a reliable and economical method to obtain the moment-rotation characteristics of composite joints under fire conditions, the authors have developed a new component-based mechanical model with inclusion of a new component model to represent the RC slab in tension. The predicted moment-rotation characteristics of joints were input as a 'spring' macro-element into the finite element analysis. Two representative sub-frames with and without axial restraint were analysed respectively to investigate qualitatively the influence of axial restraint on the sub-frame behaviour. In multi-span steel-framed structures with more than three spans, significant axial restraints to heated sub-structures often arise from adjacent unheated structures under fire conditions, due to structural continuity and redundancy. By comparing the beam behaviour within the two sub-frames, the significant influence of axial restraint can be illustrated. Parameters affecting the beam behaviour at elevated temperatures such as the beam-end boundary condition, load ratio and effect of axial restraint were also investigated. From the discussion of analytical results, it is shown that incorporating the semi-rigid joint characteristics in the analysis can greatly improve the beam performance at elevated temperatures.

1 INTRODUCTION

The main objective of this paper is to develop a more in-depth understanding of the behaviour of full-scale steel-framed structures incorporating composite beam-to-column joint characteristics under fire conditions, which can lead to a more rational analysis of composite steel-framed structures for the fire limit state. Current design of composite steel-framed structures in fire has been developed from the single member behaviour under standard fire conditions. This approach is widely considered to be too conservative since it generally leads to excessive fire protection to be applied to steel members. This is because a number of aspects of structural behaviour in fire, such as global and local failure of structures, restraint to thermal expansion imposed by surrounding structures, and force redistribution in highly redundant structures, cannot be replicated in isolated member tests.

Full-scale fire tests on a composite steel-framed structure such as Cardington tests (Moore and Lennon, 1997) provided first-hand observations of the frame behaviour under natural fire loads but it is very difficult to obtain detailed measurements, or to quantify various parameters that control the frame behaviour. Realistic scaled sub-frame fire tests are also few and usually simulate the transient-temperature conditions in fire tests. Hence, it is useful to develop numerical models to study the behaviour of steel-framed structures subjected to fire. Some researchers have developed 3-D numerical models of steel sub-frames under fire conditions (Liew et al., 1998; Tan et al., 2002; Liu, 2006; Santiago et al., 2008). However, the elevated-temperature moment-rotation behaviour of beam-to-column joints was often assumed to follow either a rigid-plastic or an elastic-plastic relationship, due to the lack of a reliable and economical method to obtain the moment-rotation ($M-\phi$) characteristics of composite beam-to-column joints. To overcome this constraint, the authors have developed a new mechanical model with inclusion of a new component model to represent the

RC slab in tension. The new mechanical model can generate accurate $M-\phi$ characteristics of composite beam-to-column joints at elevated temperatures (Yuan, 2010).

In this paper the authors present the numerical results to illustrate the benefits and advantages of incorporating the actual behaviour of semi-rigid joints in the analysis of composite steel-framed structures under fire conditions using ABAQUS. Only the heating phase up to failure was analysed while the cooling phase was not included. This is due to a number of challenges, such as the lack of material constitutive data during the cooling phase and the much more computationally challenging problems of fracture and strain localisation in concrete slab.

A total of three parameters were investigated, which include beam-end boundary conditions (pinned, semi-rigid and rigid joints), the load ratio, and the axial restraint. Two representative sub-frames with and without axial restraint were analysed respectively to investigate *qualitatively* the influence of axial restraint on the sub-frame behaviour.

2 THE NEW MECHANICAL MODEL FOR COMPOSITE JOINTS

Based on the principles of the component method, the authors have developed a new component-based mechanical model for a composite steel top-and-seat-and-web (TSW) angle joint (Yuan, 2010) shown in Fig. 1. A major innovative feature of this model is the inclusion of a new joint component to represent an RC slab in tension. Each joint component is idealised as a ‘spring’ with certain stiffness and strength characteristics. The rotation centre of the joint under symmetric hogging moments is located at the point O in Fig. 1, which is the intersection of the centreline of the seat angle plate and the column flange.

The joint components include RC slab in tension (rcst), RC slab in longitudinal shear (rls), shear studs in shear (sts), column web in compression (cwc), column web in tension (cwt), column flange in bending (cfb), bolts in tension (bt), top angle in bending (tab), bolt in shear (bs), top angle in tension (tat), top angle in bearing (tabb), beam flange in bearing (bfbb), web angle in bending (wab), beam web in bearing (bwbb), web angle in bearing (wabb), beam web in tension (bwt), column web in shear (cws), seat angle in bearing (sabb), beam flange in compression (bfc) and seat angle in compression (sac). The general concept is to assemble the respective force-displacement relationship of each row of components to obtain the overall moment-rotation behaviour of the joint. The joint rotation for an applied moment is calculated based on the principle of equilibrium, compatibility and components force-displacement relationship at all rows of components. The complexities of the calculation process result from the interactions among different constitutive relationships and non-linearities of each row of components. However, the proposed joint model can be implemented through the Excel spreadsheet.

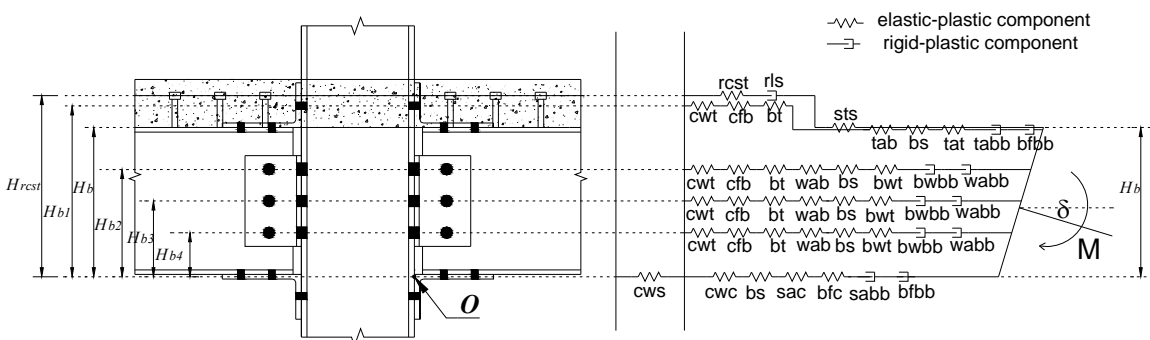


Fig. 1 New component-based mechanical model for a composite steel TSW angle joint

2.1 Initial rotational stiffness

Calculation of the initial rotational stiffness requires the input of initial stiffness of each component and the position of each component in the joint itself. The behaviour of each component is defined through either an elastic-plastic or a rigid-plastic spring. The former assumes that initial

deformations are reasonably linear with applied load until plastic deformation occurs, while the latter assumes that initial deformations are negligible until plasticity creeps in. The component-based mechanical model can be simplified by the procedure shown in Fig. 2. Using the proposed spring model shown in Fig. 2 the force equilibrium conditions give rise to Eq. (1):

$$F_r = F_s; F_r + F_{b1} + F_{b2} + F_{b3} + F_{b4} = F_c \quad (1)$$

where F_r is the tension force in the RC slab and F_{bi} ($i = 1,2,3,4$) is the respective tension force in each row of springs, respectively. F_s is the shear force in shear studs and F_c represents the compressive force in the column web.

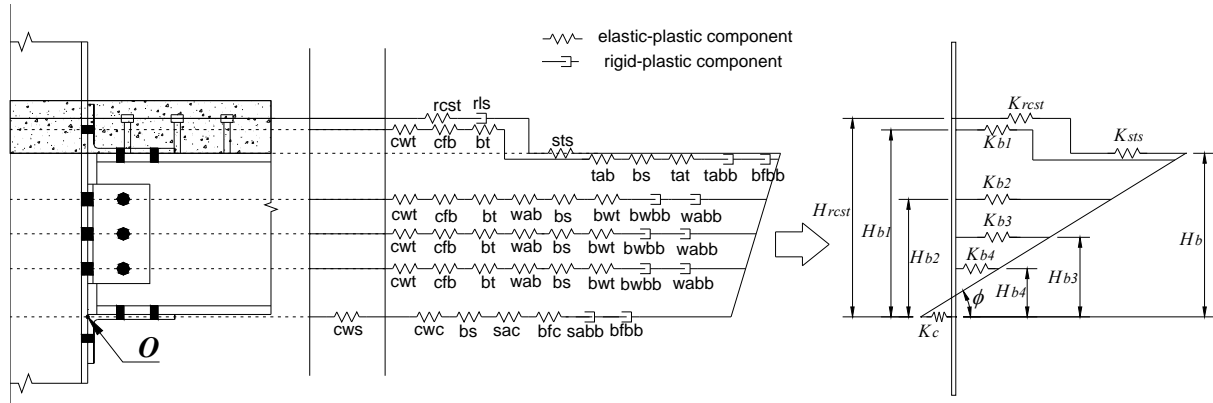


Fig. 2 Simplification process of the mechanical model into the spring model

From Hook's law the elongation of each row of spring is calculated as

$$F_r = K_r \Delta_r; F_{bi} = K_{bi} \Delta_{bi}, i = (1,2,3,4); F_s = K_s \Delta_s \quad (2)$$

where K and Δ are the stiffness and elongation of the respective row of springs.

The compatibility equilibrium gives rise to

$$\frac{\Delta_r + \Delta_s + \Delta_c}{H_b} = \frac{\Delta_{bi} + \Delta_c}{H_{bi}} = \phi \quad (3)$$

where H_b is the beam depth and H_{bi} ($i = 1,2,3,4$) is the distance from each row of springs to the centreline of the seat angle plate in contact with the beam bottom flange.

After solving the algebraic equations, the forces in each row of springs can be obtained. Since at the initial stage of loading the internal tensile forces are low, all the components' behaviour is elastic. Therefore, the moment is calculated using forces in reinforcement and each row of springs in this case through Eq. (4).

$$M = F_r H_r + F_{b1} H_{b1} + F_{b2} H_{b2} + F_{b3} H_{b3} + F_{b4} H_{b4} \quad (4)$$

where M is the moment and H_r is the distance from rebar centre to the centre line of bottom seat angle plate in contact with the beam bottom flange. Hence, the initial rotational stiffness $K_{\phi,i}$ is equal to M/ϕ .

2.2 Moment Capacity

The joint moment capacity $M_{j,Rd}$ can be calculated from Eq. (5) by summing up the product of tension or compression capacity of each row of components and the distance between each row of components to the centreline of seat angle.

$$M_{j,Rd} = F_{r,Rd} H_r + F_{b1,Rd} H_{b1} + F_{b2,Rd} H_{b2} + F_{b3,Rd} H_{b3} + F_{b4,Rd} H_{b4} \quad (5)$$

where $F_{r,Rd}$ and $F_{bi,Rd}$ ($i = 1,2,3,4$) are the tension capacity of the RC slab and of each row of components, respectively. The tension/compression capacity of each row of springs is limited by the minimum strength of its constituent components, and individual row capacity when considering the failure mechanism involving a group of rows of springs. Moreover, it is obvious that the total capacity of any combination of rows of springs shall not exceed the aggregate sum of individual rows of components.

2.3 Influence of strain hardening

Strain-hardening behaviour of each component after reaching plastic capacity is important for correctly predicting the full-range moment-rotation curve of the joint and its ultimate moment capacity. To account for strain-hardening of steel, Faella et al. (2000) proposed a simple method without a significant increase in the computational effort. Fig. 3 shows a typical quadric-linear moment-rotation relation of a component, where f_y is the yield strength and f_u is the ultimate strength, E_h is the strain hardening modulus and k_ϕ is the initial rotational stiffness. This approach was adopted in the proposed mechanical model.

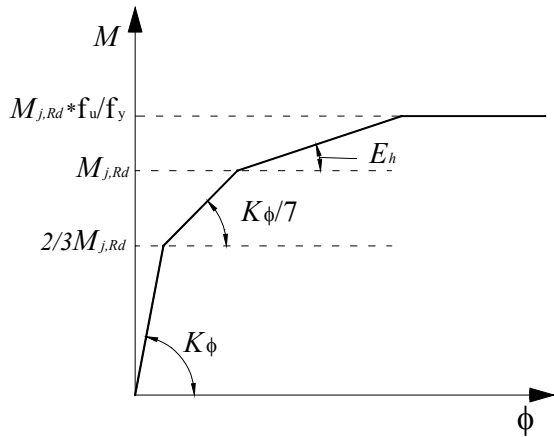


Fig. 3 A typical quadric-linear moment-rotation relationship of a row of components

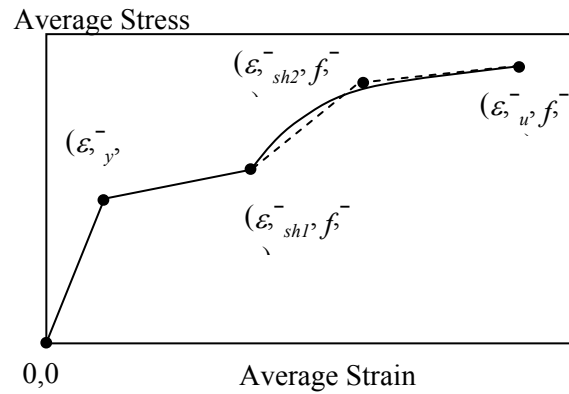


Fig. 4 The tri-segmental model and the multi-linear model of embedded reinforcing bars

2.4 The proposed new joint component of the RC slab in tension

The tension-elongation behaviour of the RC slab is highly non-linear due to tensile cracks and progressive bonding failures between embedded reinforcing bars and cracked concrete. To derive the tension-elongation relationship of the RC slab, two fundamental definitions need to be defined: (i) the space-averaged stress-strain relationship and (ii) the effective length of the RC slab in tension. This was achieved by utilising the individual constitutive models of cracked concrete and embedded rebar which were derived semi-theoretically and validated experimentally by Maekawa et al. (2003). Some minor modifications were applied to account for the important differences between the actual RC slab behaviour and the assumptions of Maekawa's model.

2.4.1 Space-averaged stress-strain relationship of an RC slab in tension

Although the localised stress and strain distribution within the cracked concrete and the steel bars are not uniform across the tensile cracks, this non-uniformity can be explicitly incorporated into structural analysis through averaging the stress and strain spatially along the full length of an RC element (Maekawa et al., 2003). Based on the micro-bond analysis, the space-averaged stress-strain response of an embedded rebar was found to fit well using a tri-segmental model proposed by Maekawa et al. (2003), as shown in Fig. 4. The first segment is linear up to the average yield point $(\epsilon_{y,y}^-, f_{y,y}^-)$, which represents the elastic range of reinforcement. The second segment is still linear and is connected to the average strain-hardening point $(\epsilon_{sh1,y}^-, f_{y1,y}^-)$, while the last segment is an

exponential curve, similar in form to the strain-hardening part of bare bars, up to the average ultimate stress and strain ($\bar{\epsilon}_u, \bar{f}_u$). The exponential part of the curve is simplified and replaced with a bi-linear curve with an additional strain-hardening point ($\bar{\epsilon}_{sh2}, \bar{f}_{y2}$) as shown in Fig. 4. The details of this stress-strain model can be found in Chapter 11 of Nonlinear Mechanics of Reinforced Concrete (Maekawa et al., 2003) and is not discussed here.

For modelling of concrete, the average tensile stress-strain relation proposed by Okamura and Maekawa (1991) can be expressed by Eq. (6), where f_t is the tensile strength of concrete, ϵ_{tu} is the tensile cracking strain equal to 0.02% and c is the coefficient equal to 0.4 for deformed bars.

$$\frac{\sigma_t}{f_t} = \left(\frac{\epsilon_{tu}}{\epsilon} \right)^c \quad (6)$$

Thus, the averaged tensile stress-strain relationship of an RC slab with a few major cracks can be obtained by superimposing the individual constitutive stress-strain model of the embedded steel bars and the cracked concrete slab together. If the average elongation of the RC slab is known and therefore the average strain is calculated, the total tensile force across the section of the RC slab can be computed.

2.4.2. Effective length of an RC slab in tension

To define the effective length, two distinct stages of behaviour are considered: before and after the occurrence of the first major tensile crack. The strain development along an embedded steel bar in a pull-out test before the occurrence of the first major crack is presented in Fig. 5(a) (Maekawa et al., 2003). It was observed that the strain at the stressed end increases proportionally with the applied load. On the other unstressed end, the strain is apparently always zero. From experimental measurements and numerical analysis (Maekawa et al., 2003), when the first major crack occurs, the rebar tensile strain generally lies between 0.0001 and 0.0003. At this strain, the length of the RC element that has developed significant strain is limited to a length of approximately twice the rebar diameter from the stressed end (Fig. 5(a)), while tensile strains at other locations are almost zero. To be conservative, the average strain of an RC slab is defined as 0.0001 at the occurrence of the first major crack. Hence, the effective length of the RC slab before the first major crack occurs is defined as two times the rebar diameter.

After the first major crack has occurred, the reinforcing bars over this major crack will experience an abrupt increase in localised strain because they will carry all the tensile forces. Consequentially, this will cause the strain development to progress quickly along the steel bars (Maekawa et al., 2003). Soon after that, the second and third major tensile cracks will occur. Tensile strain will develop to the full length of the RC element as illustrated in Fig. 5(b). The overall strain distribution is approximately a triangular shape (Fig. 5(a) and Fig. 5(b)). Assuming an RC slab has the same strain as the loaded end for the whole of its effective length, the effective length of the RC slab in tension is approximately equal to half of its full length (l_{full}). Therefore, the effective length (l_e) of an RC slab in tension is

$$l_e = 2 \times \text{the diameter of rebar} \quad \text{before the first major crack occurs} \quad (7)$$

$$l_e = 0.5 \times l_{full} \quad \text{after the first major crack has occurred} \quad (8)$$

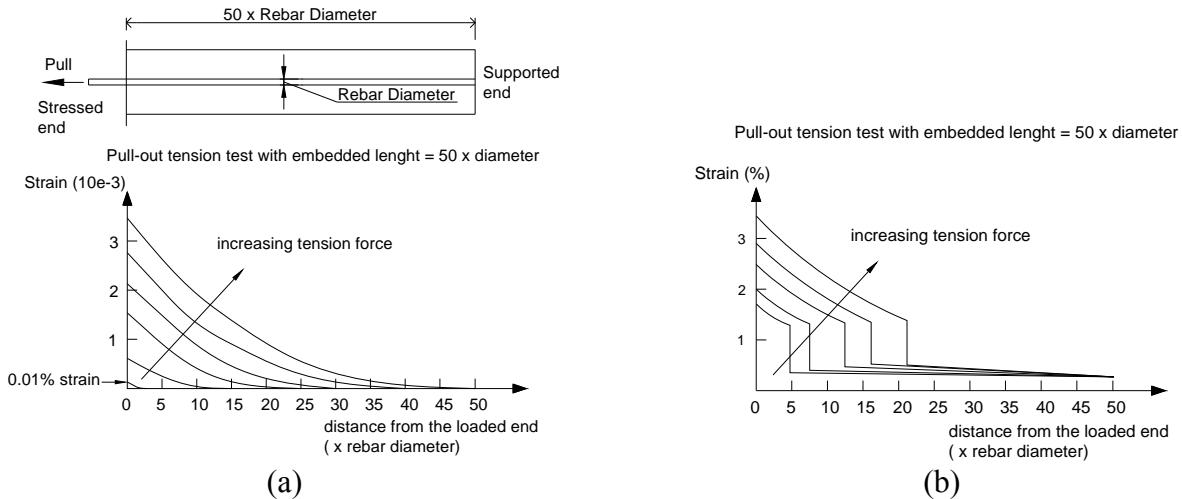


Fig. 5 Strain distributions of embedded steel bars in a pull-out tension specimen before and after the occurrence of the first major tensile crack

After obtaining the space-averaged stress-strain relationship and the effective length of an RC element in tension, the tension-elongation relationship can be derived from Hook's law. Before the occurrence of the first major tensile crack, for an elongation, the average stress of the embedded rebar and the cracked concrete can be calculated from the average strain equal to the elongation/the effective length (twice the rebar diameter). The tension forces in the rebar and the cracked concrete can be calculated from the product of the average stress and the cross-sectional area of the rebar and the cracked concrete, respectively. The total tension force across the section of the RC element is the sum of the tension forces in the rebar and in the cracked concrete, respectively. Hence, the tension-elongation relationship of the RC element in tension can be derived. After the first major tensile crack has occurred, the effective length of the RC element will be changed to half of the full length under tension. The same approach before the occurrence of the first major tensile crack of is used to derive the tension-elongation relationship.

2.4.3. Modifications of the stress-strain models

It should be noted that the aforementioned stress-strain model for the embedded rebar and the cracked concrete was mainly verified against the pull-out tests of a single reinforcing bar from RC stubs. Hence, successful application assumes that tensile strain of all bars should be fairly uniform across the RC element section. However, for the RC slab subject to induced tension forces from a hogging moment, a variation of tensile strains and stress in the rebar across the section does exist (Gil and Bayo, 2008). The reinforcing bars near the column stub will develop higher tensile strains and hence fracture earlier than the reinforcing bars further away from the stub. Moreover, shear studs have an influence on the average stress-strain characteristic of the RC slab. Unfortunately, there is no test data on an RC slab in tension with embedded shear studs. Therefore, the actual behaviour of this element requires further test results.

In the absence of any experimental data for verification, it is recommended to adopt a conservative limit to define the ultimate tensile strength of an RC element. After a parametric study, it is found that the second strain-hardening stress (f_{y2}^-) (see Fig. 4(b)) is about 95% of the averaged ultimate stress (f_u^-), irrespective of the post-yield behaviour of bare bars, reinforcement ratios and concrete strengths. Hence, it is postulated that *the second strain-hardening stress (f_{y2}^-) is adopted as the characteristic ultimate strength for embedded reinforcement in the RC element in tension.*

2.5 Validation of the new mechanical model

As can be seen in Tab. 1, the new mechanical model yields accurate and consistent predictions of the $M-\phi$ behaviour of composite steel TSW angle joints at various elevated temperatures (Yuan, 2010).

Tab. 1 Summary of the test results and the analytical evaluations

Elevated Temperature Test										
Joint	BFC Temp.	$M_{u,test}$	$M_{u,pred}$	$M_{u,test}/$	Failure Mode		$K_{i,test}$	$K_{i,pred}$	$K_{i,test}/$	
Specimen	(°C)	(kNm)	(kNm)	$M_{u,pred}$	Test	Predicted	(kNm/rad)	(kNm/rad)	$K_{i,pred}$	
C1-T1	434	201	202	0.995	A	A	141644	59606	2.376	
C1-T2	569	138	133	1.038	B	B	25415	21073	1.206	
C2-T1	633	165	150	1.100	B	B	21259	19632	1.083	
C2-T2	646	150	139	1.079	B	B	17436	21098	0.826	
C2-T3	491	211	208	1.014	B	B	85714	57163	1.499	
C3-T1	651	207	214	0.967	C	C	43490	26866	1.619	
C3-T2	551	278	263	1.057	C	C	53894	24039	2.242	
C3-T3	424	338	326	1.037	D	D	86458	60262	1.435	
Ambient Temperature Test										
C1-A1	26	215	225	0.956	D,A	D	37588	41690	0.902	
C1-A2	26	154	133	1.155	B	B	40372	41708	0.968	
C2-A1	26	269	256	1.051	B	B	104600	63591	1.645	
C2-A2	26	279	253	1.103	B	B	61646	63591	0.969	
C3-A1	26	286	273	1.048	B	B	81970	84025	0.976	
C3-A2	26	278	275	1.011	B	B	65450	84154	0.778	
				Mean	1.044				Mean	1.323
				SD	0.054				SD	0.508

Note: A = Local yielding/buckling of beam flange in compression; B = Longitudinal shear splitting of RC slab; C = Local buckling of column web in compression; D = Yielding of main reinforcement bars; BFC = Beam flange in compression.

3 LOAD RATIO

For steel beams, the concept of load ratio R (BSI, 2003) is defined as the load or moment carried at the time of a fire to the moment capacity at 20°C (BS5950 Part 8). The load ratio R should be taken as the greater of:

$$R = \frac{M_f}{M_c} \quad \text{or} \quad R = \frac{mM_f}{M_b} \quad (6.1)$$

where M_f is the applied moment at the fire limit state, M_b is the buckling moment resistance (lateral torsional), M_c is bending moment resistance, and m is the equivalent uniform moment factor.

In all analyses the steel beams are uniformly loaded with a load ratio of 0.6 to represent typical full service loading, as recommended in BS5950 Part 8. In practice, the design of steel beams usually neglects the moment resistance of the beam-to-column joint, so the applied loads are the same for the pinned, semi-rigid and rigid joint cases.

4 FAILURE TEMPERATURE

The term ‘failure temperature’ is defined as the temperature at which the mid-span deflection of the middle beam reaches span/20, as recommended in BS 476: Part 21 (BSI, 1987). A limiting temperature of 1000°C was imposed due to excessive deflection of the central beam beyond this temperature. It should be recognised that the concept of ‘failure temperature’ is adopted only as a basis for comparing fire resistance performance. In actual fire conditions this criterion does not necessarily correspond to failure of structures.

5 A REPRESENTATIVE SUB-FRAME

A representative sub-frame is designed from a fire scenario in a braced steel-framed building, as illustrated in Fig. 6(a). The fire outbreak was confined to a middle compartment of a steel framed structure, where the middle beam is directly heated by the fire. Fig. 2(a) shows that the end-span beams do not provide any axial restraint to the middle beam. One the other hand, if the end-span beams provide significant axial restraint to the middle beam, then the axial restraint to the middle beam should be considered in the analysis.

The loading arrangement is shown in Fig. 6(a). Numerical studies conducted by El-Rimawi (1989) concluded that the results of sub-frame analysis are reasonably representative of the full-scale frame tests under fire conditions. Temperature distributions are shown in Fig. 6(b). The end-span beams, the upper columns and the beam-to-column joints outside the fire compartment were assumed to remain at 20°C. The middle beam temperature (1.0T) was assumed to be uniform across the beam section and along the entire beam length in the analysis. The lower columns were assumed to be thermally insulated and sustained only 0.5T. Temperature of the beam bottom flange within the joint zone was assumed to be 0.7T, as suggested by Lawson (1990). In addition, the temperature distributions within the joint were assumed to follow the observations in the isolated joint tests in Tab. 2 (Yuan, 2010).

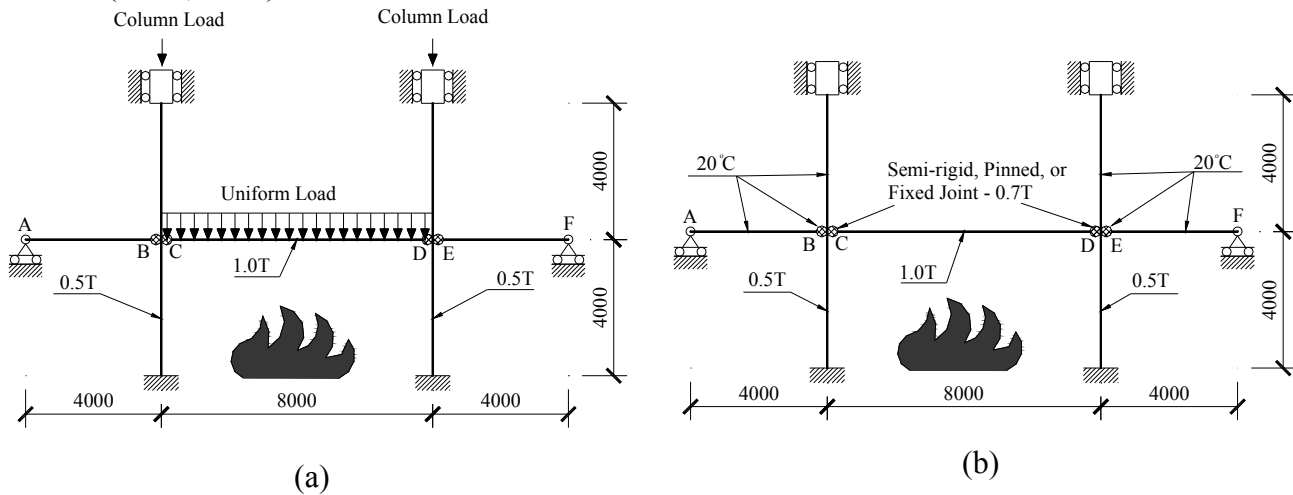


Fig. 6 A representative sub-frame model and typical loading for a steel-framed structure without axial restraint

Tab. 2 Summary of the temperature profiles for eight joint specimens

Relative temperature to the beam bottom flange temperature	C1-T1	C1-T2	C2-T1	C2-T2	C2-T3	C3-T1	C3-T2	C3-T3	Average
Beam top flange	0.70	0.80	0.83	0.82	0.79	0.88	0.86	0.83	0.82
Beam mid-height web	0.97	0.99	0.99	0.99	0.99	0.98	0.99	1.00	0.99
Beam bottom flange	1.00	1.00	1.00	1.00	1.00	1.00	1.00	1.00	1.00
Central web angle	0.84	0.95	0.97	0.96	0.98	1.01	1.03	1.04	0.97
Seat angle	0.99	1.00	0.96	1.00	1.01	0.98	0.98	1.02	0.99
Top angle	0.70	0.81	0.79	0.78	0.71	0.77	0.76	0.70	0.75
Column Flange (near seat angle)	0.88	0.93	0.95	0.96	1.00	0.97	1.01	1.06	0.97
Column Flange (near top angle)	0.79	0.84	0.84	0.85	0.79	0.84	0.85	0.75	0.82
Column web in compression at seat angle	0.82	0.94	0.96	0.97	1.03	0.97	1.02	1.04	0.97
Reinforcement bar	0.27	0.21	0.27	0.24	0.25	0.23	0.25	0.26	0.25
Shear stud	0.41	0.57	0.52	0.50	0.48	0.44	0.48	0.43	0.48
Concrete slab at directly above top flange	0.47	0.51	0.49	0.50	0.47	0.49	0.44	0.42	0.47
Concrete slab at 50mm above top flange	0.34	0.33	0.31	0.33	0.30	0.29	0.24	0.29	0.30
Concrete slab at 100 mm above top flange	0.31	0.21	0.24	0.24	0.24	0.21	0.21	0.24	0.24
Furnace temperature	1.38	1.32	1.30	1.38	1.43	1.41	1.54	1.63	1.42

Nominal material properties were adopted for modelling steel beams, columns, reinforcement and the slab in the analysis. All beams and columns were assumed to be of Grade S355 steel. The RC slab thickness was assumed to be 130mm. The effective width of the RC slab was defined as one quarter of the interior longitudinal span (the effective width=2.0m), as specified in EC4 Part 1.1

(CEN, 2004). The same effective width was assumed for the end-span slabs for consistency. The slab reinforcement was 10T10 located at 100mm above the slab soffit. The nominal yield strength of reinforcement was 460N/mm² with C40 ($f_{cu} = 40 \text{ N/mm}^2$) as the concrete grade. Poisson's Ratio of 0.2 was adopted for concrete and 0.3 for structural steel and reinforcement. For the concrete slab in the hogging moment region, the maximum tensile strength of concrete was defined as 10% of its maximum compressive strength. Elevated-temperature material properties of concrete and steel were defined according to EC2 Part 1.2 (CEN, 2005) and EC3 Part 1.2 (CEN, 2005).

A half model of the representative sub-frame was analysed using ABAQUS (2008) to reduce the running time. In the finite element model, two-noded beam elements were used to model the beams and the columns. Four-noded thick shell elements were employed to model the slab. The beam elements were offset from the slab elements by using pre-set options in ABAQUS. Spring elements were used to simulate the moment-rotation curves of semi-rigid joints. Concrete damaged plasticity with tension stiffening material model was utilised to include concrete tension stiffening effect.

5.1 Influence of boundary conditions

The mid-span deflection of the middle beam was obtained for incorporating rigid, semi-rigid and pinned joint characteristics, respectively. This was achieved by idealising the beam-to-column joints at B, C, D and E in Fig. 6(a) with respective moment-rotation characteristics of rigid, semi-rigid and pinned joints. The 'rigid' joint assumed no relative rotation between the beam ends and the columns, while the 'pinned' joint assumed zero strength and stiffness. On the other hand, the beam-end joints at A and F were idealised as roller supports, allowing horizontal movements.

The semi-rigid joint characteristics were represented by utilising joint C1 configuration shown in Fig. 7. Based on the new mechanical model, the predicted ultimate moment resistance $M_{j,u}$ of joint C1 at ambient temperature is 227kNm. Meanwhile, the sagging moment capacity of the composite beam ($M_{b,Rd}$) is 345kNm according to EC4 Part 1.1. The joint moment-rotation characteristics at different temperatures were obtained from analytical predictions by the mechanical model, as shown in Fig. 8.

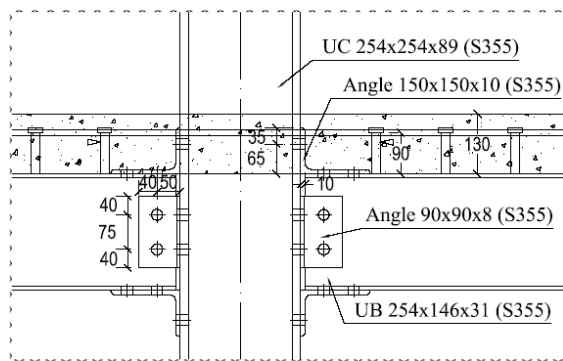


Fig. 7 Configuration details of joint C1

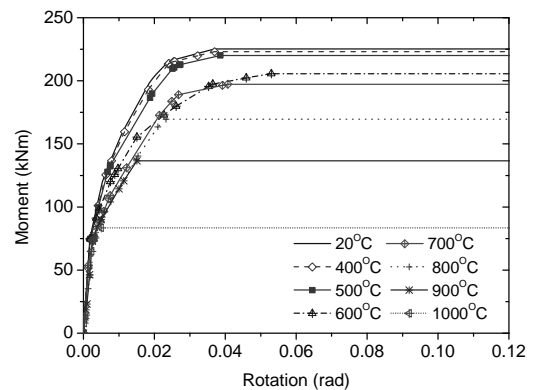


Fig. 8 Analytical moment-rotation relationships of joint C1

A load ratio of 0.6 is applied to the middle beam, which is equivalent to a uniform load of 25.9kN/m. The middle beam behaviour incorporating C1 joint characteristics is shown in Fig. 9, together with 'fully-rigid' and 'fully-pinned' joint characteristics. The middle beam deflection is very small for temperatures up to 400°C and 700°C for pinned and rigid joint cases, respectively. A further increase in temperature causes a progressive increase in middle beam deflection until it reaches 1/20 of beam span at the 'failure temperatures' of 670°C and 830°C for pinned and rigid joints, respectively. Thus, the failure temperature of the beam with rigid joints is nearly 160°C higher than those with pinned joints.

The middle beam response with semi-rigid joint C1 is close to that with rigid joints. The failure temperature is 810°C, which is 140°C higher than the beam with pinned ends. It is clear that incorporating semi-rigid joint characteristics greatly enhances the beam performance and increases

the failure temperature. Firstly, the stiffness of semi-rigid joints at the beam ends can significantly reduce the mid-span deflection. Secondly, the hogging moment resistance of the joint can help to redistribute excessive mid-span sagging moment to the two beam ends, compared with pinned-end case.

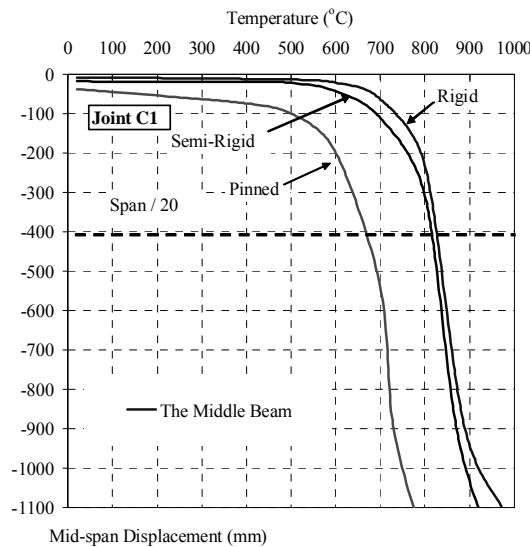


Fig. 9 Middle beam behaviour incorporating C1 joint characteristics

5.2 Influence of load ratio

In an actual multi-storey building, load levels may vary due to changes in building functions. Hence, the effect of the load ratio on the beam response under fire conditions was studied.

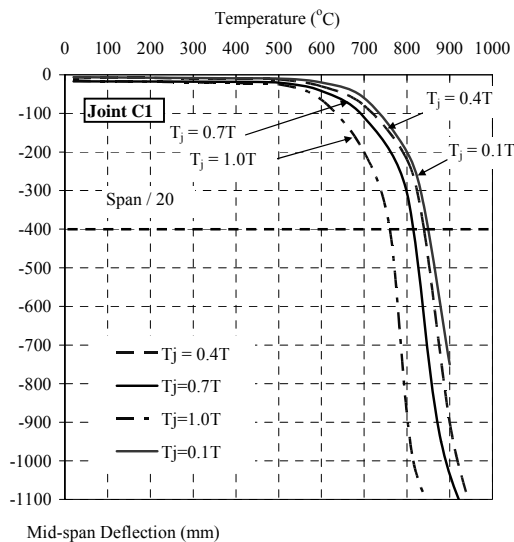


Fig. 10 Influence of joint temperature on the middle beam response

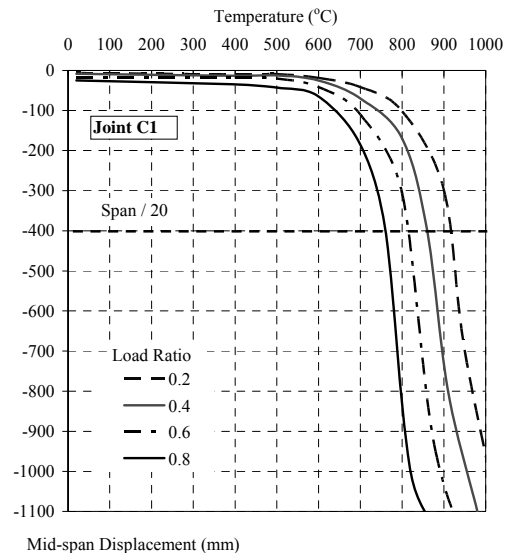


Fig. 11 Influence of the load ratio on the middle beam response

The middle beam behaviour incorporating joint C1 characteristics (semi-rigid joint) for nominal load ratios ranging from 0.2 to 0.8 are shown in Fig. 11. It is observed that the failure temperature decreases significantly in an almost linear manner when the load ratio increases. At a load ratio of 0.2, the failure temperature of the beam exceeds 920°C, but at a load ratio of 0.8, the beam failure temperature is reduced to 760°C. There is little change in the failure temperature of the beam up to a load ratio of 0.2.

5.3. Influence of axial restraint

The following study investigates *qualitatively* the influence of axial restraint on the middle beam response at elevated temperatures. If a multi-span steel structure has more than 3 spans and is subjected to a natural fire load, the fire design of the middle beam should consider the influence of structural restraint provided by unheated adjacent structures. At the heating stage, the middle beam will tend to elongate due to thermal expansion. Significant axial restraint induced at the heating stage will result in an increase in the mid-span deflection due to non-uniform heating and compression force induced in the beam at this stage. In the analyses, the beam-end joints at A and F in Fig. 6(a) were idealised as fixed supports, not allowing any movements or rotations.

To simplify the modelling process, it was assumed that the beam was uniformly heated across the section and along its axis so that there was no additional beam deflection due to thermal-bowing effect. The middle beam behaviour incorporating C1 joint characteristics analyses with and without axial restraint is compared in Fig. 12, together with three types of joint characteristics making six analyses.

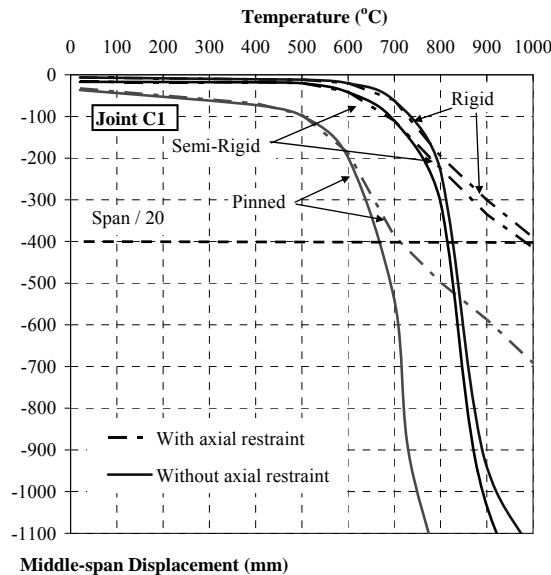


Fig. 12 Influence of axial restraint on the middle beam response incorporating joint C1 characteristics

It is observed that the influence of axial restraint on the maximum mid-span deflection is not very obvious when the middle beam deflection is less than 100mm at temperatures up to 700°C, beyond which the rate of mid-span deflection reduces quickly with increasing temperatures due to catenary action. At large beam deflections (approximately $L/40$), catenary action kicks in and helps the beam to resist applied load. Thereafter, the rate of beam deflection is reduced significantly at high temperatures (Fig. 12), compared with the beam without axial restraint. A further increase in temperature causes a progressive increase in the middle beam until it reaches $1/20$ of beam span at ‘failure temperatures’ of 710°C and 1010°C for pinned and rigid joints, respectively (Fig. 12), which are higher than the respective 660°C and 830°C for the middle beam without axial restraint. It can be seen that the middle beam deflections with axial restraint are consistently less than those without axial restraint (Fig. 12).

6. CONCLUSIONS

A numerical study was carried out to illustrate the advantages of incorporating semi-rigid joint characteristics in the analysis of steel-framed structures under fire conditions using ABAQUS. A total of five parameters affecting the beam behaviour at elevated temperatures were investigated, including the beam-end boundary condition, the load ratio and the influence of axial restraint. The numerical results show that incorporating semi-rigid joint characteristics in sub-frame analyses

greatly enhance the beam behaviour under fire conditions. Besides, the inclusion of axial restraint in sub-frame analyses leads to significant improvements in the middle beam behaviour within multi-span steel-framed structures with more than three spans.

REFERENCES

- ABAQUS Version 6.8. Analysis User's Manual. Simulia, U.S.A., 2008.
- Al-Jabri, K. S. The Behaviour of steel and composite Beam-Column Connections in fire, Ph.D. Thesis, University of Sheffield, U.K., 1999.
- British Standards Institution (BSI), "BS5950 Structural Use of Steelwork in Building - Part 8: Code of practice for fire Resistance Design", BS 5950 Part 8, U.K., 2003.
- British Standards Institution (BSI), "Fire Tests on Building Materials and Structures: Methods for Determination of the Fire resistance of Load-bearing Elements of Construction", BS 476 Part 21, U.K., 1997.
- El-Rimawi, J. A., "The Behaviour of Flexural Member under Fire Conditions", Ph.D. Thesis, University of Sheffield, U.K., 1989.
- European Committee for Standardization (CEN), "Eurocode 4: Design of Composite Steel and Concrete Structures, Part 1.1: General rules and rules for buildings", EN 1994-1-1, Brussels, Belgium., 2004.
- European Committee for Standardization (CEN), "Eurocode 2: Design of Concrete Structures, Part 1.2: General Rules – Structural Fire Design", EN 1992-1-2, Brussels, Belgium., 2005.
- European Committee for Standardization (CEN), "Eurocode 3: Design of Steel Structures, Part 1.2: General Rules – Structural Fire Design", EN 1993-1-2, Brussels, Belgium., 2005.
- Lawson, R. M. (1990), "Behaviour of Steel Beam-to-column Connections in Fire", *The Structural Engineer*, Vol. 68, No.14, pp. 263-271, 1990.
- Liew, J. Y. R., Tang, L.K., Halmass Tore and Choo, Y. S. Advanced analysis for the assessment of steel frames in fire. *Journal of constructional research steel*, Vol. 47, pp. 19-45, 1998.
- Liu, T. C. H. Fire resistance of unprotected steel beams with moment connections. *Journal of constructional research steel*, Vol. 62, pp. 1165-1170, 2006.
- Moore, D. B. and Lennon, T. (1997), "Fire engineering design of steel structures", *Progress in Structural Engineering and Materials*, Vol. 1, No. 1, pp. 4-9., 1997.
- Santiago, A., Simões da Silva, L., Vila Real, P. and Veljkovic, M. Numerical study of a steel sub-frame in fire. *Computers and structures*. Vol. 86, pp. 1619 – 1632, 2008.
- Tan K. H., Ting S. K. and Huang Z. F. (2002), Visco-Elasto-Plastic Analysis of Steel Frames in Fire, *Journal of Structural Engineering*, Vol. 128, No. 1, pg. 105-114, 2002.
- Yuan Z., "The Behaviour of Composite Top-and-Seat-and-Web Angle Joints at Elevated Temperatures", Ph.D. Thesis, Nanyang Technological University, Singapore, 2011.

COMPONENT-BASED ELEMENT FOR ENDPLATE CONNECTIONS IN FIRE

G. Dong, I. W. Burgess and J. B. Davison

Department of Civil and Structural Engineering, The University of Sheffield, Sheffield S1 3JD, UK

INTRODUCTION

This paper describes the development of a component-based finite element to model endplate joints between beams and columns in steel structures under fire conditions. Observations from the full scale fire tests at Cardington and collapse of buildings at the World Trade Centre in 2001 have raised concerns that joints are potentially the weakest parts of a structure (Burgess, 2007). When designing a steel building, the joints are always assumed to transfer shear reactions, and in some cases beam end-moments. In fact, due to the combination of thermal and mechanical effects caused by heating, the resultant forces on joints (in addition to shear) vary from pure moment, to moment and compression, and eventually to almost pure tension.

The Component Method is a practical approach initially proposed by Tschemmernegg *et al* (1987) for ambient-temperature conditions and now included in EC 3 Part 1-8 (CEN, 2005). This element is compatible with the EC3 Part 1-8 design method. A joint is divided into a collection of key components, whose behaviour is characterised as that of nonlinear springs. Its essential properties, including temperature variation, physical connection details and unloading characteristics, are taken into account in assigning properties to its components. Therefore, individual components are capable of dealing with loading-unloading-reloading cycles, and changing temperatures. Rigid links are used to connect the components in order to represent the whole joint, which enables the element to tackle the interaction of internal forces.

1 DEVELOPMENT OF THE COMPONENT-BASED ELEMENT

The development of the component-based element is divided into three basic steps:

- Step1: identification of the active components.
- Step2: specification of the component characteristics.
- Step3: assembly of the active joint components.

1.1 Identification of the active components

Active components are those which either contribute to the deformation of a joint or limit its strength (Block, 2006). EC3 Part 1-8 (Table 6.1) lists the basic components for endplate connections. Figure 1 (Spyrou, 2002) shows the general zones of structural action within the connection for which components will be assembled to create this component-based element.

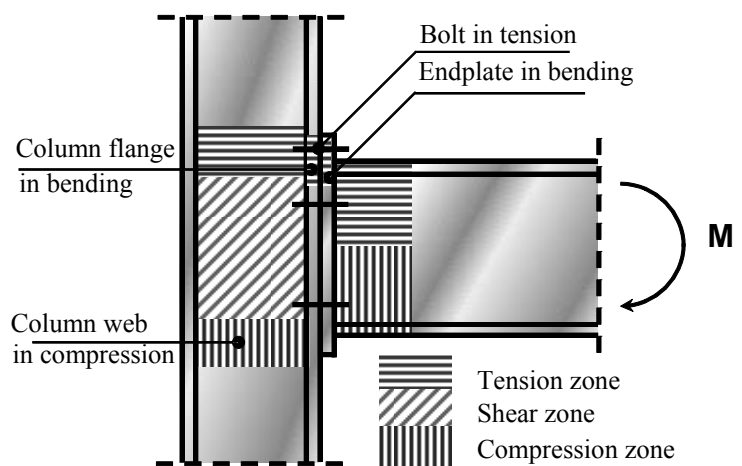


Fig. 1 Active component in COMPFIRE joints (Spyrou, 2002).

1.2 Specification of the component characteristics

In order to cover the fire case, each component's behaviour must be analysed at elevated temperatures (using F.E. studies and/or experiments) and then described with a simplified analytical model. The component's performance in fire can then be modelled.

1.2.1 Typical tension/compression component Force/Displacement curve

In the present version of the connection element, the component behaviour (Figures 2 and 3) is based on a set of derivations from earlier studies (Hu *et al.*, 2007 and Yu *et al.*, 2009), and these will be characterised in the next version. Each component has an ‘ultimate strength’, at which its maximum resistance occurs. Beyond the ultimate strength, the component is considered as ‘fractured’, and stops working structurally. Practically, a compression component ‘fracture’ cannot occur, and the ultimate point is where the compression component buckles or its deformation is too large to be acceptable. In order to consider the component’s behaviour at elevated temperature, reduction factors and ductility factors (Figures 4, 5 and 6) are temporarily introduced in the current version i.e. reducing the ambient temperature resistance and ductility for temperature effects. .

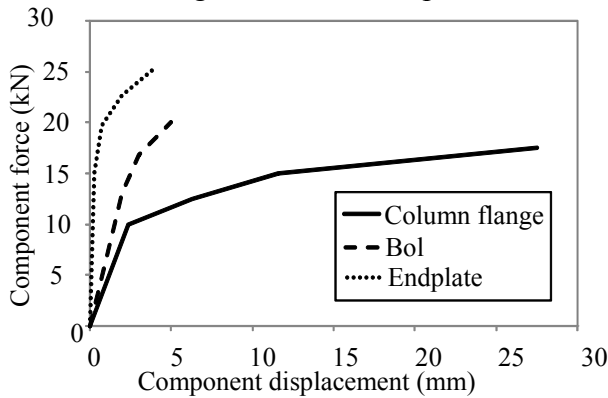


Fig 2 Tension component behavior at 20 °C

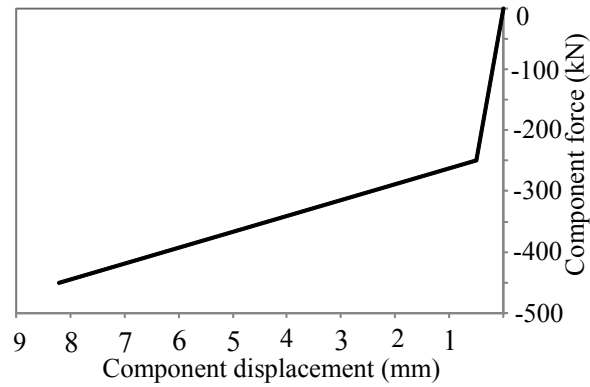


Fig 3 Compression Component behavior at 20 °C

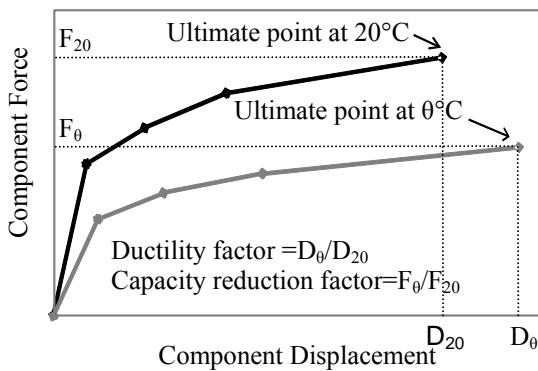


Fig 4 Definition of the ductility factor/reduction factor

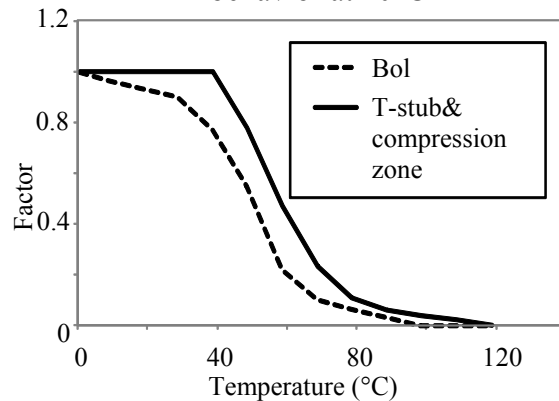


Fig 5 Component capacity reduction factor

1.2.2 Unloading of components

When a component carries a large enough force, the material maybe strained into the inelastic region, and the component will then have irreversible deformation (‘residual deformation’) when its force is removed. To date, the classic Massing rule has been employed to deal with this ‘memory effect’. In the Massing rule, the unloading curve is the original loading curve doubled in scale and rotated by 180°. If the initial loading curve (Block, 2006) is represented by

$$D = f(F) \quad (1)$$

then the unloading curve can be described as

$$\frac{(D_A - D)}{2} = f\left(\frac{F_A - F}{2}\right) \quad (2)$$

Where intersection point (D_A, F_A) in (Fig 7) are respectively the displacement and the force at which unloading occurred.

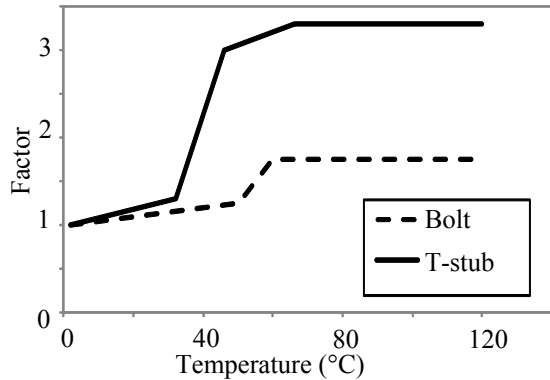


Fig 6 Ductility factor for tension component

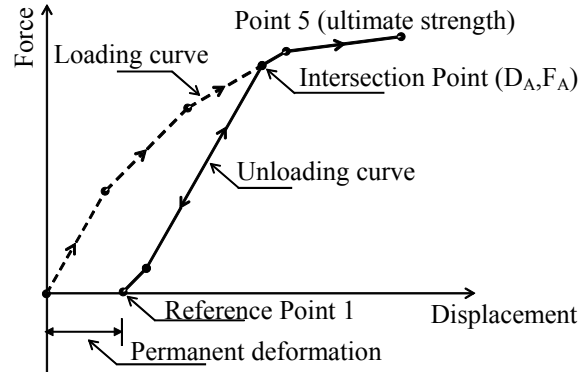


Fig 7 Typical loading/unloading curve

When a component is heated in a fire, its temperature changes continuously and the F/D curve is temperature-dependent. The component's permanent deformation is assumed not to change when only the temperature changes.

1.3 Assembly of active joint components.

Figure 8 shows a typical layout of the endplate connection component assembly. The connection element has 2 nodes, 1 and 2, to connect to the beam and column respectively and internally consists of 5 tension spring (bolt) rows and 2 compression spring rows. The components for vertical shear are not considered at present, but will be developed later.

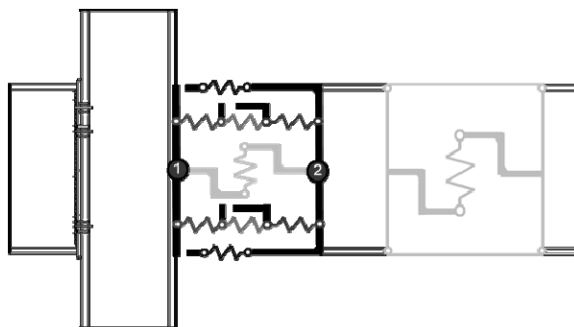


Fig 8 Component assembly for endplate connections

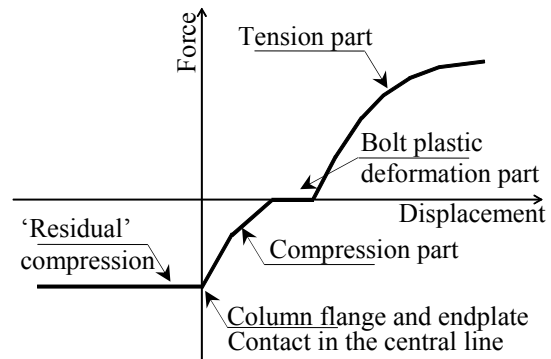


Fig 9 Typical tension bolt row F/D curve

A tension bolt row is characterised by an effective spring composed of a group of springs in series, representing the endplate in bending, a bolt in tension and the column flange in bending. Maximum resistance is defined by the weakest spring.

A typical Force/Displacement (F/D) curve for a tension bolt row consists of four parts (Figure 9): the 'tension part', 'bolt plastic deformation part', 'compression part' and 'residual compression part'. The 'tension part' shows the three components under tension. The 'compression part' represents the state in which the plastically deformed endplate and column flange are pushed back until their centres come into contact. The 'bolt plastic deformation part' represents the stage between the 'tension' and 'compression' parts, at which the applied tension reduces to zero, and the deformed endplate and column flange have not yet come into contact. As the bolt-in-tension component does not work under compression, its stiffness is zero during the 'bolt plastic

deformation' part. The 'residual compression' part is based on the assumption that the tension bolt row can transfer a certain amount of compression force. However, as the parts of the connection represented by the compression spring group are much stiffer than this, the compression spring group will transfer most of the compression force.

2 RESULTS

The current version of the component-based element has been successfully incorporated into a nonlinear global structural analysis program *Vulcan* (Huang, 2004). In order to test the element, an

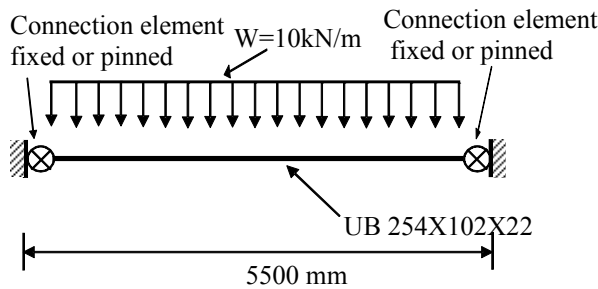


Fig 10 Isolated beam with connection elements

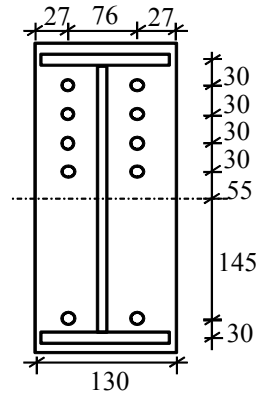


Fig 11 Analysed endplate connections

isolated beam, with connection elements at its ends, and with complete axial restraint beyond these, was designed (Figure 10). The beam section is 254x102UKB22. Endplate thickness is 12mm and the steel grade is S275. No out-of-plane deflection is allowed. The joint (Figure 11) is designed to test the connection element's full capacity for 5 tension bolt rows. The joint data are hard-coded in the current version of the connection element.

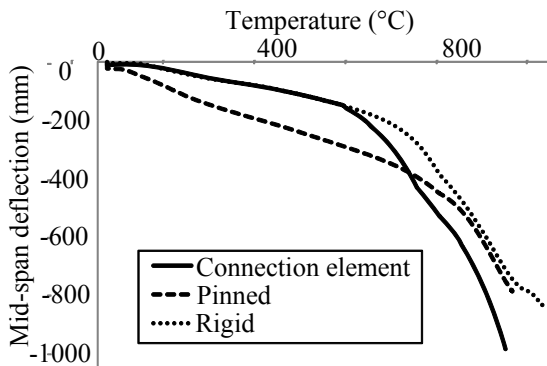


Fig 12 Beam mid-span deflections

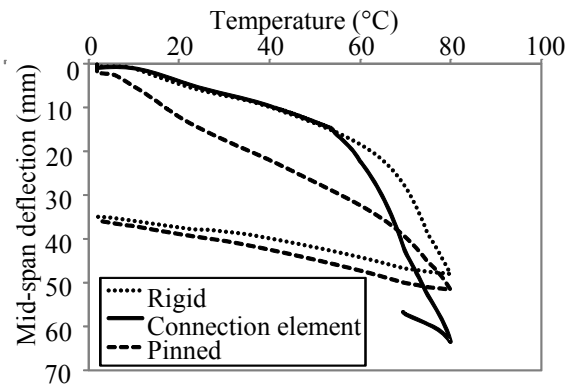


Fig 13 Beam deflection with cooling from 800°C

It can be seen from Figure 12 that at high temperatures (above 800°C) the deflections of the rigid and pinned connections become very close, when the beam is in its catenary stage and under nearly pure tension. It is also noticeable that the deflection of the beam with the connection elements lies initially between those of the beams with rigid and pinned connections. Above 685°C, the beam with the connection elements has a larger deflection than either of the rigid or pinned cases. This is because catenary action causes a net shortening of the distance between the beam ends which is greater than the thermal expansion, and the residue of this net shortening can be accommodated by extension of the bolt rows.

Figure 13 shows that the connection element is capable of modelling the cooling behaviour of

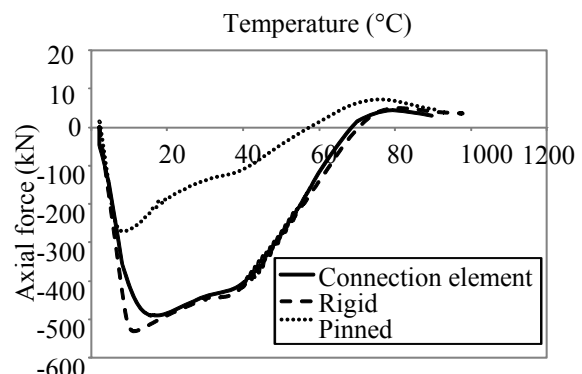


Fig 14 Axial force in connection

connections. The calculation has stopped due to fracture of the bolt in the first tension bolt row.

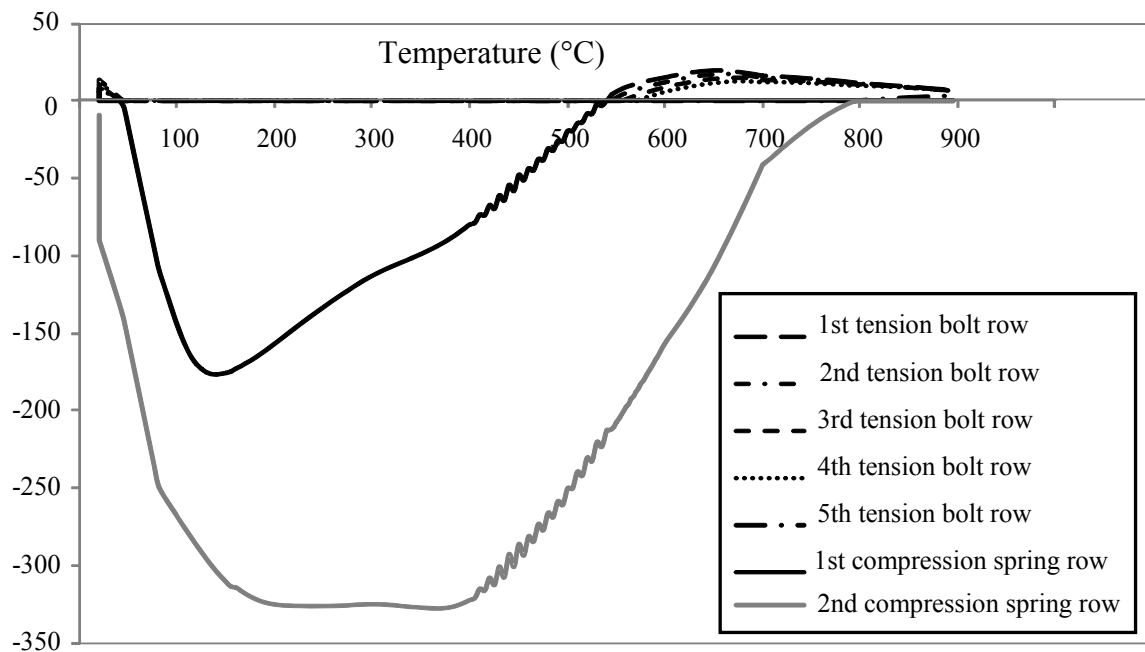


Fig 15 Component force

Figures 14 and 15 show how the connection element deals with the combination of forces in the joint when the beam is heated. In the initial stage, the top 4 tension bolt rows and the bottom (2nd) compression spring row work to resist the beam end rotation due to the applied load. After the beam is heated it starts to expand, and the connection is subjected to a combination of compression and bending, at which stage all the top 4 tension bolt rows are gradually ‘switched off’ as the tension force in the top of the section is offset by the thermal expansion. Once all the tension bolt rows have temporarily stopped working, the top compression spring row starts to work together with the bottom compression spring row, and the whole section is under compression. With the temperature increasing further, the beam’s deflection increases sharply, and the top 4 tension bolt rows progressively replace the top compression spring row in resisting the combination of compression force and moment. Above 600°C, the beam progressively develops catenary tension and reduces its bending action. Eventually all 5 tension bolt rows are working and both of the compression spring rows are ‘switched off’.

3 CONCLUSION

This connection element can be used in modelling of the behaviour of steel structures in fire, and has now been very largely validated. It will contribute to the accurate prediction of the behaviour of buildings in fire scenarios, including the ductility and failure of connections, allowing progressive collapse sequences to be traced, and facilitating global performance-based design against fire. Further component development and parametric studies are currently underway which will enable a more refined analysis tool to be used in structural modelling.

5 ACKNOWLEDGEMENT

The research leading to these results has received funding from the European Community's Research Fund for Coal and Steel (RFCS) under *grant agreement* n° RFSR-CT-2009-00021.

REFERENCES

- Block F.M. (2006), “Development of a component-based finite element for steel beam-to-column connections at elevated temperatures”, PhD Thesis, University of Sheffield
- Block, F.M., Davison, J.B., Burgess, I.W. and Plank, R.J. (2007), ‘The Development of a Component-Based Connection Element for Endplate Connections in Fire’, *Fire Safety Journal*, 42 (2007) pp 498–506.
- Burgess I.W. (2007), 'Connection Modelling in Fire', Proc. COST C26 Workshop "Urban Habitat Constructions under Catastrophic Events", Prague, (2007) pp 25-34.
- CEN (2005), “EC3: Design of steel structures, Part 1.8: Design of Joints”, European Committee for Standardization, Document BS EN1993-1-8:2005.
- Hu, Y, Davison JB, Burgess IW and Plank RJ (2007), ‘Comparative study of the behaviour of BS 4190 and BS EN ISO 4014 bolts in fire’. The 3rd International Conference on Steel and Composite Structures (ICSC07). Manchester. July, pp 587-592. ISBN 978-0-415-45141-3.
- Huang, Z., Burgess, I.W. and Plank, R.J. (2004), ‘3D Modelling of Beam-Columns with General Cross-Sections in Fire’, Paper S6-5, Third International Workshop on Structures in Fire, Ottawa, Canada, (May 2004) pp 323-334.
- Spyrou S. (2006), “Development of a component-based model of steel beam-to-column joints at elevated temperatures”, PhD Thesis, University of Sheffield
- Yu, H.X., Burgess, I.W., Davison, J.B. and Plank, R.J. (2009), 'Development of a Yield-Line Model for Endplate Connections in Fire', *J. Construct. Steel Research*, 65 (6), (2009) pp1279-1289.
- Tschemmernegg, F., Tautschnig, A., Klein, H., Braun, Ch. And Humer, Ch. (1987), “Zur Nachgiebigkeit von Rahmenknoten – Teil 1” (Semi-rigid joints of frame structures Vol. 1– in German), *Stahlbau* 56, Heft 10, pp299-306.

THE FRACTURAL BEHAVIOUR OF STEEL WELDS AT HIGH TEMPERATURE

Hongxia Yu ^a

^a Dept. of Civil Engineering, Tsinghua University, Beijing, China

INTRODUCTION

The stiffness and strength of steel degrade with the increase of temperature quickly, which makes the behavior of steel constructions in fire hazards a major concern. To evaluate the stability of steel constructions in fire, the properties of structural steel at elevated temperatures have been extensively investigated (Kirby and Preston, 1988; Cooke, 1988). However, latest researches show that connections, rather than structural members such as beams or columns, are generally the weakest link in the structure. Fig. 1 shows a picture of connection failure in a full-scale structural fire test (Newman et al, 2004). Tearing of the endplate from the connected beam web can be clearly observed. Connections are the key elements to hold the structural members together and failure of which could quite possibly initiate the progressive collapse of the whole structure as demonstrated by the collapse of the WTC towers (NIST, 2008). Therefore, design connections with sufficient robustness have been internationally recognized to be important to prevent inappropriate collapse of structures when subjected to accidental loads.

In a set of experiments designed to investigate the robustness of connections at high temperature, failure of welds have been widely observed to occur to the locations where flexible or flush endplate connections were welded to the beam web similar to that shown in Fig. 1 (Hu et al, 2008; Yu et al, 2011). Weld fracture at elevated temperatures are also observed for other structural members such as the concrete filled tubular column shown in Fig. 2. Contrary to the widely observed failure of welds in fire situation, little research has been performed on the behavior of structural welds at high temperature. Therefore, a set of experiments were designed to study the ultimate tensile resistance and fractural behavior of the two most common structural welds at various temperatures. The test results are reported in this paper.



Fig. 1 Fracture of a Partial depth endplate connection



Fig. 2 Fracture of the weld in a concrete filled steel tubular column fire test

1 TEST ARRANGEMENT

A total of 54 specimens were tested in two groups. The first group used Q235 steel with E43 electrode and the second group used Q345 steel with E50 electrode. For each group, 27 tests were performed for 9 temperatures including 20°C and 100°C-800°C. For each temperature, three tests were performed to ensure the reliability of the results. The specimens were designed as two tapered steel bars welded together in the smaller ends as shown in Fig. 3a. The width at the smaller ends is 6mm and at the bigger ends is 20mm. The thickness of the specimen is 20mm uniform along the whole length. The finished specimen takes the shape as shown in Fig. 3b. By visual observation, the welding is clean and uniform with no obvious imperfections. The width of the weld is from 10-12mm and the thickness of the weld in the narrowest position is 7-8mm.

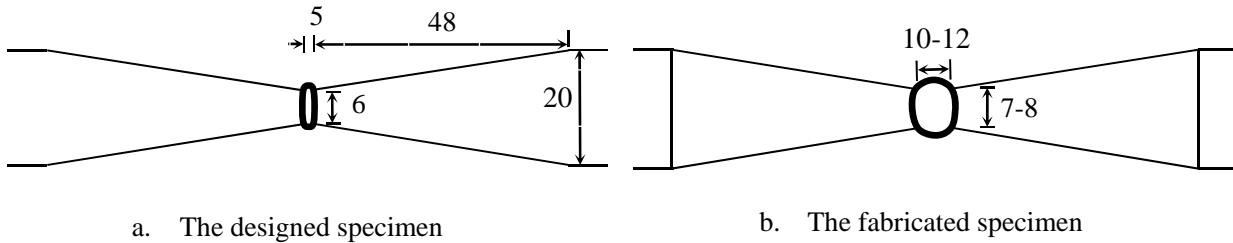


Fig. 3 Design and fabrication of the specimen

2 TEST RESULTS

2.1 Tensile Strength

The ultimate resistances of the two groups of tests are shown in Table 1. A graphical view of the results is shown in Fig. 4. It can be seen from the figure that the three results agree with each other very well for each temperature, especially when the temperatures are above 400°C, which means the specimens were fabricated satisfactorily and the possibility of strong influence from the imperfections in the welds can be cleared.

Both groups show the rule that the tensile resistances reduce slightly at 100°C, then start to increase until 300°C. At 400°C, the resistances are nearly the same with those at 20°C. And from 400°C upwards, the resistances reduces quickly. If all the resistances are divided by their average resistances at ambient temperature, the strength reduction factor can be obtained for these welds. Strength reduction factors for welds at elevated temperatures are also proposed by EC3: Part 1.2 (CEN, 2005). A comparison of the test results against the code proposal is shown in Fig. 5. It can be seen that the tested strength reduction factors follow that of the EC3 curve very well in the medium range of 500°C to 600°C. Below that, the test results show a slight increase of the resistance at around 300°C and above that, the failure resistance is 50%-100%h higher than the code proposal.

Comparison of the weld strength reduction factor against the strength reduction factor for steel gives useful information regarding which of them will be more vulnerable to failure at high temperatures. Therefore, the strength reduction factor for hot-rolled steel according to a Chinese fire safety design code (CECS, 2006) is also shown in Fig. 5. It can be seen that the weld strength is slightly lower than the steel strength at 500°C and 600°C. At higher temperatures, they are very close to each other. In general, welds have similar strength reduction factors to that of hot-rolled steel. Since the strengths of weld and steel degrade at similar rates, weld failure in fire should not become a special concern.

Tab. 1 The ultimate resistances of the specimens

Temperature [°C]	Q235 with E43 [kN]			Q345 with E50 [kN]		
	(1)	(2)	(3)	(1)	(2)	(3)
20	84	85.1	84.8	99.2	100	97.9
100	79.15	79.75	81.85	93.7	92.2	102.1
200	85.15	95.5	96.5	98.1	99.8	92.6
300	101.8	100.8	97	107.2	104	111.4
400	87.4	87.1	82.2	98.2	102.7	100
500	50.9	49.45	47.4	70.2	69.25	70.15
600	29	28.55	34.3	41.85	41.95	42.6
700	17.15	16.8	16.9	21.5	27	21.35
800	12.45	14.95	13.1	16.7	15.7	16.8

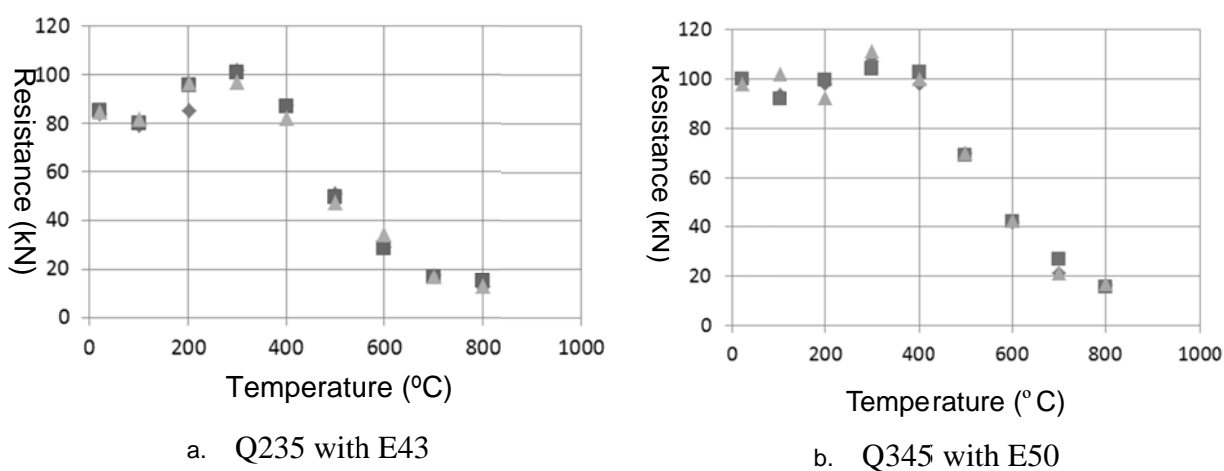


Fig. 4 Reduction of the weld resistances with temperature

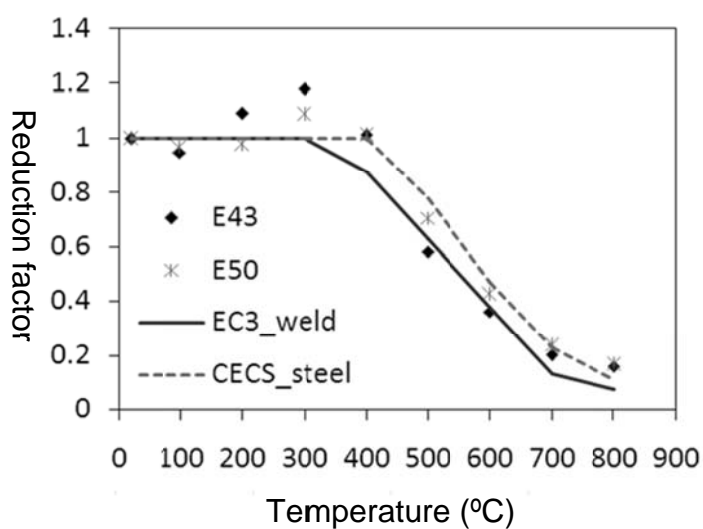


Fig. 5 Reduction of the weld strength in comparison with steel

2.2 Failure Mode

Several typical failure modes can be identified from the test results. They are shear fracture within the weld, irregular fracture within the weld, shear fracture at the interface and tensile failure at the interface as shown in Fig.6. When the temperature is from 20°C to 400°C, the failure mode could be any one among failure modes a, b and c and different failure modes do not seem to have a clear influence on the failure resistances. When the temperature is 500°C and above, the failure mode is conformably mode d, i.e. the tensile failure at the interface between the weld and the steel with obvious necking of the failed section.

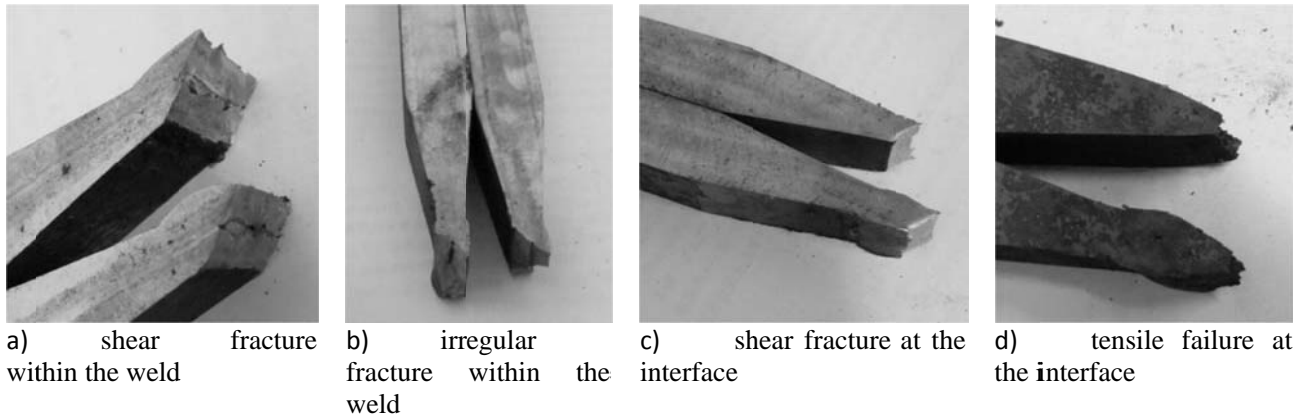


Fig. 6 The failure modes

Associated with different failure modes, the force-displacement relationships of these specimens show distinct characteristics. When the temperature is from 20°C to 400°C, the force increases with the displacement until the peak point and dropped suddenly to zero with a brittle fracture of the specimen. When the temperature is 500°C and above, the force increases gradually to the peak point and reduces slowly to zero with further increase of the displacement. Therefore, at high temperature, the specimens generally show much better ductility.

3 CONCLUSIONS

This paper reports a set of test results on structural steel welds at elevated temperatures. The purpose of the test was to investigate the ultimate resistance and failure modes of steel welds at various temperatures and provide guidance for the fire safety design of structural steel connections. The test results show that the ultimate resistances of the welds reduce with the increase of temperature after 400°C. The resistance degradation rate is similar to that of hot-rolled steel. Therefore, no special consideration seems to be necessary for the failure of steel welding. However, when the temperature is from 20°C to 400°C, the welds show brittle fracture at small deformations, which could have explained the observation of weld cracks in connection fire tests. At temperatures above that, welded region behaves extremely well in terms of both strength and ductility.

ACKNOWLEDGEMENTS

This work was financially supported by the Fund for Returned Oversea Scholars to Start Research by the Ministry of Education (20091021043).

REFERENCE

- Kirby B.R. and Preston R.R., High temperature properties of hot-rolled, structural steels for use in fire engineering design studies, *Fire safety journal* Vol.13, p. 27-37, 1988.
- Cooke G.M.E., An introduction to the mechanical properties of structural steel at elevated temperatures, *Fire safety journal*, Vol.13, p.45-54, 1988.
- Newman G.M., Robinson J.T., Bailey C.G., *Fire Safety Design: A New Approach to Multi-Storey Steel-Framed Buildings*. The Steel Construction Institute, 2004.
- NIST, Final Report on the Collapse of the World Trade Center Building 7- Draft for Public comment. USA, National Institute of Standards and Technology, 2008.
- Hu Y., Davison J.B., Burgess I.W. and Plank R.J., Experimental Study on Flexible Endplate Connections in Fire, *Proc. 5th European Conf. Steel Structures*, Graz, Austria, p.1007-1012, 2008.
- Yu H.X., Burgess I.W., Davison J.B. and Plank R.J., Experimental and Numerical Investigations of the Behaviour of Flush Endplate Connections at Elevated Temperatures, *J. Struct. Eng., ASCE*, V137, No 1, p.80-87, 2011.
- CEN (European Committee for Standardization), BS EN 1993-1-2, Eurocode 3: design of steel structures, Part 1.2: General rules- structural fire design. British Standards Institution, UK, 2005.
- CECS, DG/TJ08-008-2000 Technical code for fire safety of steel structures in buildings (in Chinese), China Engineering Construction Standard, 2006.

NUMERICAL ANALYSIS OF HSS ENDPLATE CONNECTIONS AT AMBIENT AND ELEVATED TEMPERATURES

Xuhong Qiang^a, Frans Bijlaard^a, Henk Kolstein^a, Leen Twilt^b

^a Faculty of Civil Engineering and Geosciences, Delft University of Technology, 2600GA Delft, the Netherlands

^b Formerly: Center for fire research of Institute TNO for Building and Construction Research, Delft, the Netherlands

INTRODUCTION

In Europe, endplate connections are typical beam-to-column connections for low-rise steel buildings erected using welding at workshops and bolting in situ. The simplicity and economy associated with their fabrication make the connections popular for steel structures.

Rules for the prediction of strength and stiffness of endplate connections at ambient temperature have been included in design codes, such as Eurocode3 Part1-8 (CEN 2005), but they are mainly based on mild steel connections. Girao Coelho and Bijlaard (Girao Coelho and Bijlaard 2007) have found that the high strength steel (HSS) S690 endplate connections satisfy the design provisions for resistance and achieve reasonable rotation demands at ambient temperature. However, no quantitative guidance on HSS endplate connections in fire condition is available.

Recent research on bolted connections has revealed that bolts failure becomes critical at elevated temperatures, although the design for ambient temperature assumes more ductile failure (Burgess 2009, Yu et al. 2008, Yu et al. 2009a, and Yu et al. 2009b). I.e. mild steel bolted connections are relatively brittle at elevated temperatures. So, making bolted connections more ductile at elevated temperatures is a significant mission for structural engineers, in order to improve the robustness of steel connections in fire condition.

In order to enhance fire safety of endplate connections, a numerical research has been conducted, combining HSS endplate with mild steel beam and column. In this paper, the numerical modelling of HSS endplate connections is compared with that of mild steel endplate connections, to gain essential understanding and quantification on how HSS endplate connections behave at ambient and elevated temperatures. The accuracy of this numerical model is validated against the results of tests conducted by Yu et al. on mild steel flush endplate connections (Burgess 2009, Yu et al. 2008, and Yu et al. 2009b). Moreover, a parametric study on the effects of endplate thicknesses is conducted, and an achievement is obtained for improving the ductility of endplate connections at elevated temperatures.

1 TESTS IN UNIVERSITY OF SHEFFIELD

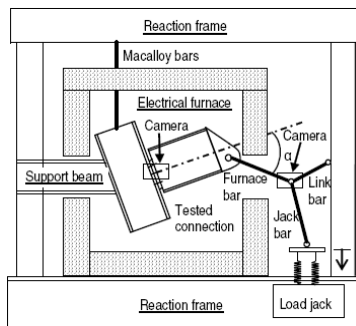


Fig.1 Test setup

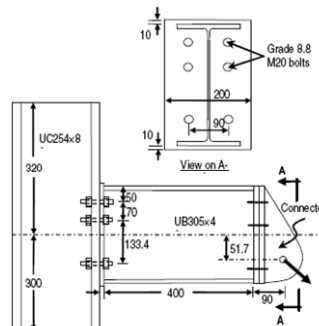


Fig.2 Typical flush endplate connection specimen

From 2005 to 2008, the Universities of Sheffield and Manchester conducted a joint research project with the aim of investigating capacity and ductility of steel connections at elevated temperatures (Yu et

al. 2008, Burgess 2009). A test setup was adopted in which four types of connections were subjected to a combination of tension and shear forces. In order to illustrate the experimental behaviour of mild steel endplate connections at ambient and elevated temperatures, only the tests on flush endplate connections are used herein.

A detailed description of the test setup and test measurements was given by Yu previously (Yu et al. 2008). The tests were performed in an electrical furnace, as shown in Fig.1. Fig.2 shows the details of a typical flush endplate connection in tests. In all cases, a UC254×89 section made of S355 was used for the column, and the beam section was UB305×165×40 made of S275.

2 FINITE ELEMENT ANALYSIS METHOD

The finite element software ABAQUS is used to simulate the behaviour of endplate connections both at ambient and elevated temperatures.

2.1 Geometric Details and Element Type

The details of all connections' components used in FEM are exactly the same with those of the test specimens. Because the geometric details, load, temperature distribution and boundary conditions are symmetric, half of the endplate connection is modelled, to shorten computing time. The FE components are shown in Fig.3, including bolt shank, nut, washer, endplate, beam and column. The bolt holes are modelled 2mm larger than the bolt shank diameter, and the hexagon bolt heads are modelled as cylinders for simplicity. The whole connection is modelled using C3D8I element, because of its excellence in simulating contact interactions, non-linear material properties and stress concentrations.

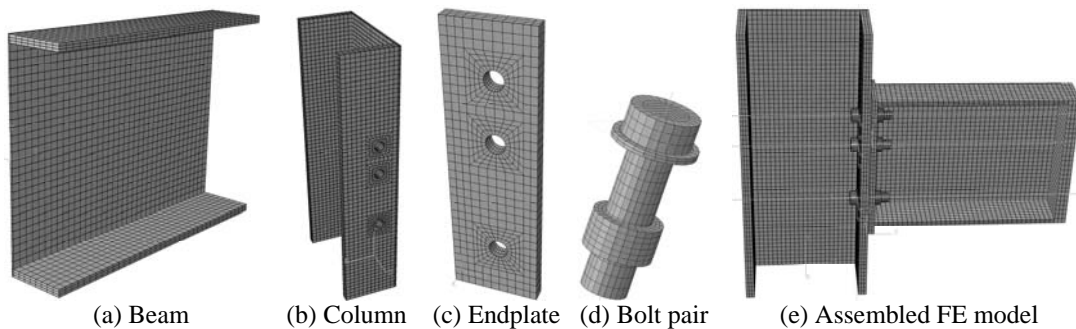


Fig.3 FE model and its mesh generation

2.2 Contact Interaction

To handle contact interaction problem, the whole analysis process comprises 6 analysis steps. In the first step, the bolts, the washers and the endplate are restrained of all direction freedoms temporarily, and then a very small pretension is applied to every bolt for restraining the bolt pairs temporarily. The temperature field for all components is 20°C. In the second step, the bolts, washers and the endplate are freed of any temporary restraint. In the third step, the actual magnitude of pretension is applied to every bolt. In the fourth step, the length of every bolt is fixed. In the fifth step, the temperature field for all components is modified to a preselected temperature. (For the analysis at ambient temperature, the temperature field is kept constant.) In the sixth step, an equivalent surface traction converted from the actual inclined force with its preselected initial load angle is applied to the end of the beam. The first four steps help contact interactions to be established smoothly, which is effective to decrease calculation time and eliminate errors.

Surface-to-surface contact, with a small sliding option, is used for all contact surfaces to fully transfer the load. The contact pairs in the endplate connection comprise the washers-to-column flange, column

flange-to-endplate, endplate-to-nuts. And the washer is tied to bolt head in each bolt pair for simplicity and the nuts are tied to the corresponding bolt shanks.

2.3 Material Properties

In this FE modelling, the material properties of mild steels (including S275 and S355) and bolt pairs are the same with those reported by the University of Sheffield (Hu et al. 2008, Renner 2005, and Yu et al. 2009a). The material properties of S690 at elevated temperatures reported by Chen and Young (Chen and Young 2006) are used for HSS.

2.4 Loads and Welds

An additional endplate is modelled at the other end of beam, for applying surface traction, as shown in Fig.3 (e). The initial load angles used in tests are also taken into consideration when applying surface traction. The magnitude of pretension for each bolt is 224kN, to agree with the average reported in the experimental investigation (Yu et al. 2008 and Yu et al. 2009b). The welds between endplate and beam are modelled by tie restraint instead of solid modelling, in order to simplify the model.

3 VALIDATIONS AGAINST EXPERIMENTAL RESULTS

3.1 Ambient Temperature

In Yu et al.'s tests, at ambient temperature experimental results on 10mm S275 endplate with initial load angle of 55 degree (10E55RS275) and 8mm S275 endplate with initial load angle of 35 degree (8E35RS275) are available. So, the corresponding numerical modellings are conducted, using ABAQUS/Standard, based on the above-mentioned FE analysis method.

The force-connection rotation curves for both specimens are shown in Fig.4. It can be seen that the FEM simulations and Yu et al.'s test results are in good agreement. For the two specimens, the maximal discrepancies between numerical simulations and experimental data are both about 10%, and both appear in the converting stage between linear and non-linear performances. It can be concluded that the numerical modelling described here can simulate the response of endplate connections at ambient temperature with reasonable accuracy.

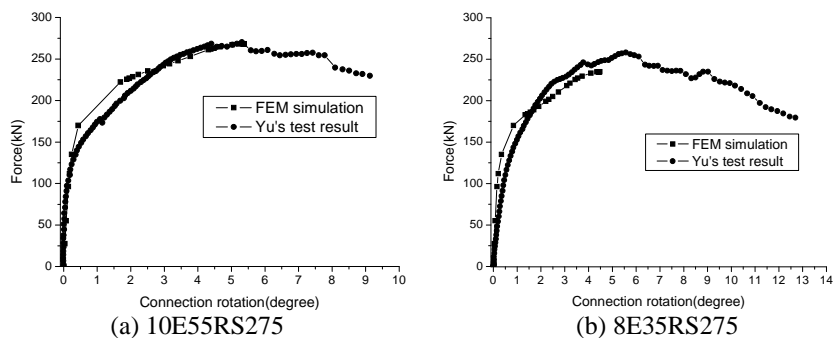


Fig.4 Force-rotation curves of connections at ambient temperature

3.2 Elevated Temperatures

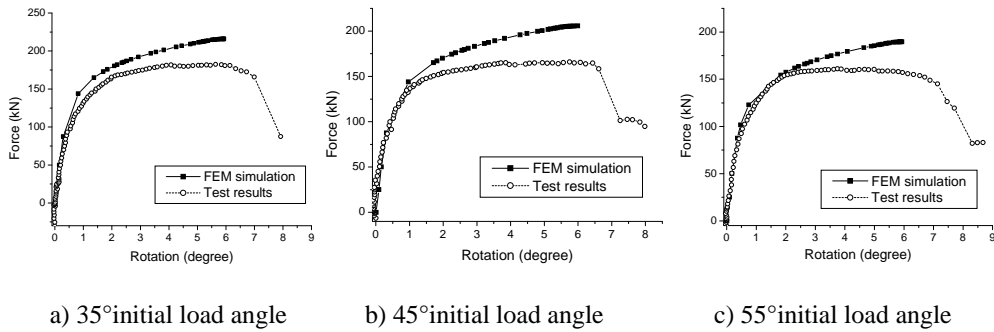


Fig.5 Force-rotation comparisons of 10mmS275 at 450°C

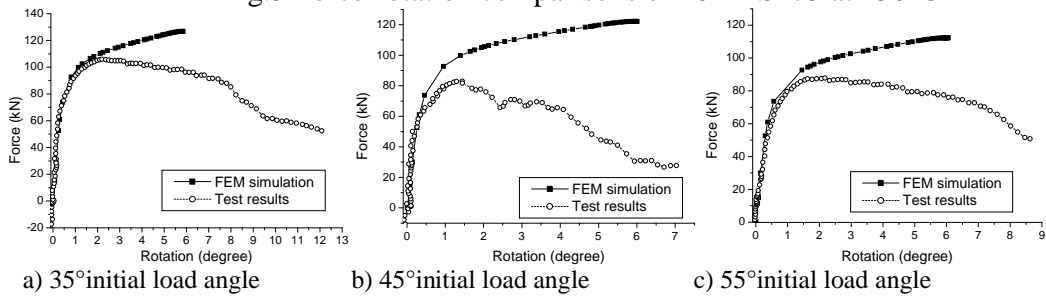


Fig.6 Force-rotation comparisons of 10mmS275 at 550°C

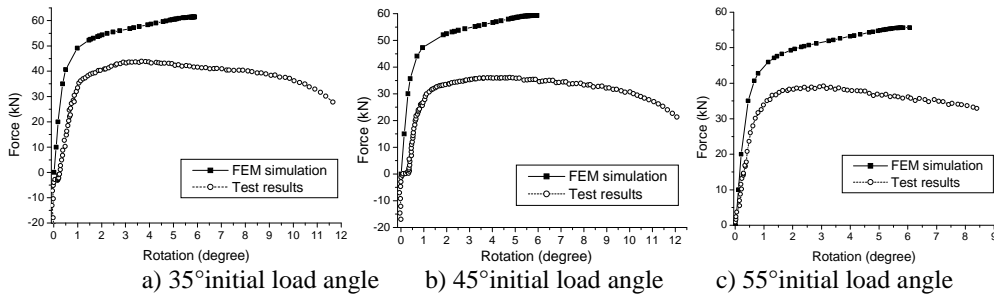


Fig.7 Force-rotation comparisons of 10mmS275 at 650°C

In Yu et al.'s fire tests, the connection specimens (10mmS275 endplate connections) have been heated to three preselected elevated temperatures (450°C, 550°C and 650°C) and then loaded till failure occurred. For each elevated temperature, the specimens were tested with three initial load angles (35, 45 and 55degree). The corresponding numerical modellings are conducted and shown in Fig.5-7.

For the initial liner stage of the force-rotation curves obtained by FEM simulations, they are in good agreement with Yu et al.'s test results at 450°C and 550°C. But at 650°C the strength of the connections obtained from FEM are much higher than test data. This is because in tests the connections are loaded at a very slow deflection rate (i.e. the specimens are loaded till failure in about 120 min) and at constant temperature, but there are no such material properties of S275 corresponding to so slow steady-state conditions available. So the material property used in FEM can not exactly reflect its actual behaviour in tests, especially at very high temperatures, such as 650°C. Moreover, at very high temperatures, creep effects will have a significant influence, especially when the specimens are heated very slowly. However, in the FE analysis creep has not been taken into account, leading to an overestimation of strength and stiffness of the connections. For these reasons the tests at 650°C will be excluded from the following FE analysis, and the numerical analysis below 650°C is acceptable to simulate or predict the behaviour of endplate connections at corresponding elevated temperatures.

4 NUMERICAL PREDICTION OF HSS ENDPLATE CONNECTIONS

4.1 Same Thick Endplates in Connections

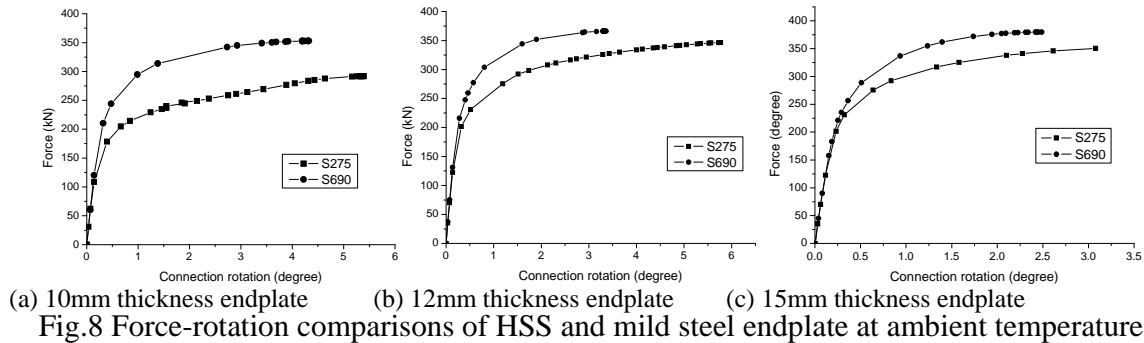


Fig.8 Force-rotation comparisons of HSS and mild steel endplate at ambient temperature

The force-rotation capacities of HSS endplate connections at ambient temperature and at elevated temperatures are compared with that of mild steel ones, with the same endplate thickness. The results for initial load angle of 45 degree at ambient temperature are illustrated in Fig.8. And the comparison of HSS endplate and mild steel endplate for 10mm thickness with initial load angle of 55 degree at 450°C and 550°C are illustrated in Fig.9.

As we predict, it is found that at ambient temperature the load-bearing capacities of HSS endplate connections are higher than that of mild steel connections using the same thick endplates, but the ductility of the former is worse. So using the same thick HSS endplate in connections to take place of mild steel endplate at ambient temperature is proved not effective to improve ductility.

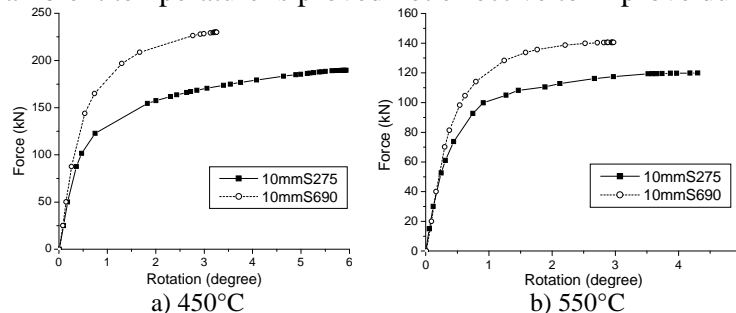


Fig.9 Comparisons of HSS endplate and mild steel endplate connections at elevated temperatures

Similar to that at ambient temperature, it is found that at elevated temperatures the load-bearing capacities of HSS endplate connections are also stronger than mild steel endplate connections with the same endplate thickness, but the ductility of the former is worse. It is obvious that using the same thick HSS endplate instead of mild steel endplate in connections is not effective to improve the ductility of endplate connections at elevated temperatures.

4.2 Parametric Study on Endplate Thickness

To predict thickness effect of endplate on strength and ductility of connections, a parametric study both at ambient temperature and at elevated temperatures is conducted using the proposed FE model. The parameter concerned, i.e. thickness of endplate, is varied.

4.2.1 Ambient Temperature

The obtained force-rotation capacities of HSS S690 endplate connections with various endplate thicknesses at ambient temperature are compared with that of mild steel S275 endplate connections, as shown in Fig.10 a.

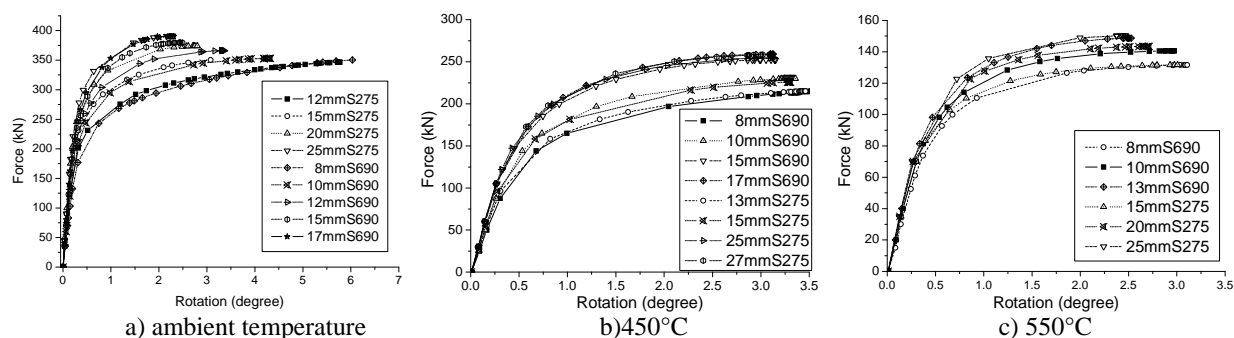


Fig.10 Effects of endplate thicknesses at ambient and elevated temperatures

It can be seen that the 8mm thick S690 endplate connection (8mmS690) is as strong as the 12mm thick S275 endplate connection (12mmS275), but the former is more ductile. Similar conclusions can be drawn for the other comparison pairs: 10mmS690-15mmS275, 12mmS690-20mmS275 and 17mmS690-25mmS275.

These conclusions demonstrate that at ambient temperature the connection with a thin HSS endplate enhances its ductility and simultaneously achieves the same resistance as that with a thick mild steel one. This is positive for improving the ductility of endplate connections at ambient temperature, and also indicates a beneficial research idea for enhancing the ductility of endplate connections at elevated temperatures.

4.2.2 Elevated Temperatures

At the same elevated temperature (i.e. 450°C and 550°C), the simulated force-rotation capacities of various thicknesses of HSS endplate connections are compared with that of mild steel endplate connections, as shown in Fig.10 b and c. A similar conclusion can be drawn with that at ambient temperature: at elevated temperatures, a thinner HSS endplate provides the same load-bearing capacity as that of a mild steel endplate connection, and enhances the ductility of the connection by various percentages. This achievement is positive for improving the fire-resistance design of endplate connections at elevated temperatures.

5 CONCLUSION

This paper reports on a numerical analysis method of endplate connections using ABAQUS/Standard, in order to predict the performances of HSS endplate connections at ambient temperature and at elevated temperatures. This analysis may be used as a basis for investigating how HSS endplate connections behave not only in normal condition but also in fire condition.

The challenge of modelling contact interactions is solved successfully by FEM, considering material and geometric non-linear effects. The FE modelling is verified appropriate to simulate mild steel endplate connections at ambient and elevated temperatures with reasonable accuracy. Based on this, the performances of HSS endplate connections at ambient temperature and at elevated temperatures are further analyzed and compared with that of mild steel one.

It is found that a thinner HSS endplate can enhance the ductility of connection both at ambient temperature and at elevated temperatures, and simultaneously achieve almost the same load-bearing capacity with a mild steel endplate connection. This FE model may be used for further investigation of improving the behaviour of HSS endplate connections in fire conditions.

By the present modelling method, the critical locations of endplate connections can be identified, but the occurrence of component failure cannot be predicted. To improve the capability of this numerical simulation, solid modelling of welds taking into account fracture features is necessary in future works.

REFERENCE

- Burgess, I.W. (2009), "The Robustness of Steel Connections in Fire", Proceeding of ASCCS 2009, Leeds, 103-114.
- Chen, J. and Young, B. (2006), "Behaviour of High Strength Structural Steel at Elevated Temperatures", Journal of Structural Engineering, 1948-1954.
- European Committee for Standardization (CEN)(2005), BS EN 1993-1-8, Eurocode3: Design of steel structures, Part 1-8: Design of joints. British Standards Institution.
- Girao Coelho, A.M. and Bijlaard, F.S.K. (2007), "Experimental behaviour of high strength steel end-plate connections", Journal of Constructional Steel Research, **63**, 1228–1240.
- Hu, Y., Burgess, I.W., Davison, J.B., and Plank, R.J. (2008), "Modelling of flexible endplate connections in fire using cohesive elements", Proceeding of Structures in Fire Workshop, Singapore.
- Renner, A. (2005), "The effect of strain-rate on the elevated-temperature behaviour of structural steel", Research dissertation. UK: University of Sheffield.
- Yu, H., Burgess, I.W. Davison, J.B., and Plank, R.J. (2008), "Experimental Investigation of the Behaviour of Flush Endplate Connections in Fire", Proceeding of Structures in Fire Workshop, Singapore.
- Yu, H., Burgess, I.W. Davison, J.B., and Plank, R.J. (2009 a), "Tying Capacity of Web Cleat Connections in Fire. Part 1: Test and Finite Element Simulation", Engineering Structures, **31** (3), 651-663.
- Yu, H., Burgess, I.W., Davison, J.B. and Plank, R.J. (2009 b), "Development of a Yield-Line Model for Endplate Connections in Fire", Journal of Constructional Steel Research, **65** (6), 1279-1289.

FRACTURE SIMULATION IN A STEEL CONNECTION IN FIRE

Simulation of a flush endplate connection at ambient and elevated temperatures including different methods for fracture simulation

Peter Schaumann^a, Thomas Kirsch^a

^a Leibniz University Hannover, Institute for Steel Construction, Hannover, Germany

INTRODUCTION

Actual developments in numerical simulations of the structural behaviour in fire situation are focussed on taking into consideration the interaction of all structural members in a global numerical approach. Therefore it is necessary to model the load bearing behaviour of connections in detail. In this paper a detailed 3D numerical model of a bolted steel endplate connection taking into account nonlinearities, e.g. temperature dependent material, is presented. The simulation is validated by experimental tests conducted at the University of Sheffield in 2008. During some of the experimental tests, large deformations and fractures occurred. These phenomena are simulated with the numerical model as well.

1 STATE OF THE ART

Since the first study of connection behaviour (Wilson et al, 1917), investigations in joints were traditionally based on experiments. The finite element method was used to simulate connection behaviour since 1974, when Krishnamurthy developed a two-dimensional FE-Model to simulate an endplate connection (Krishnamurthy, 1974). While experimental and numerical investigations at ambient temperatures have been conducted in a large number, tests at elevated temperatures are rather seldom. The reason for this might be that studying connection behaviour at elevated temperatures is costly because a number of tests at different temperatures are needed to develop a moment-rotation-temperature curve. However, elevated temperature tests on beam-to-column-connections have been carried out by (Kruppa, 1976), (Wang et al, 2007) and (Schaumann et al, 2008) for example. Further high temperature tests on different connections in fire, taking into account tensional forces caused by catenary action of adjacent beams, have been performed by Yu and will be used for this investigation. Results have been published for different connection types in (Yu et al, 2007), (Yu et al, 2008a), and (Yu et al, 2009), to mention but a few.

In addition, numerical investigations have been conducted for some elevated temperature tests. For example in (Sarraj et al, 2007) a numerical model of fin plate connections has been developed. In (Yu et al, 2008b) a simulation of a steel connection using explicit analysis was presented. The explicit equation solver algorithm was found to be an alternative to the standard algorithm especially if large deformations occur. In (Hu et al, 2008) a flexible endplate connection in fire using an explicit dynamic analysis was presented. To simulate a tensile fracture of the beam web, cohesive elements were included to the analysis.

2 METHODS

In this paper, a numerical simulation of a joint at ambient and elevated temperatures is presented. The numerical calculation has been conducted using the FE-software Abaqus. Both, the implicit (Abaqus/Standard) and the explicit solver algorithm (Abaqus/Explicit) have been applied to the analysis.

A shear fracture in the endplate, which occurred during some of the tests, was simulated using two different methods. The first method was the use of cohesive elements located where shear failure occurred in the test. The second method was a fracture strain criterion for ductile materials. This algorithm is able to reduce the stiffness of elements and delete them during the analysis.

3 PARAMETER OF EXPERIMENTS AND NUMERICAL SIMULATION

3.1 Test Setup and Geometry of the Connection

During 2007 and 2008 the University of Sheffield carried out a wide range of experimental tests within different steel connections, different temperatures and a different load angle α (c.f. Fig. 1). The test setup, geometrical details and material properties of this test have been published in (Yu et al, 2008a) in detail and will be described shortly. The general test assembly is shown in Fig. 1.

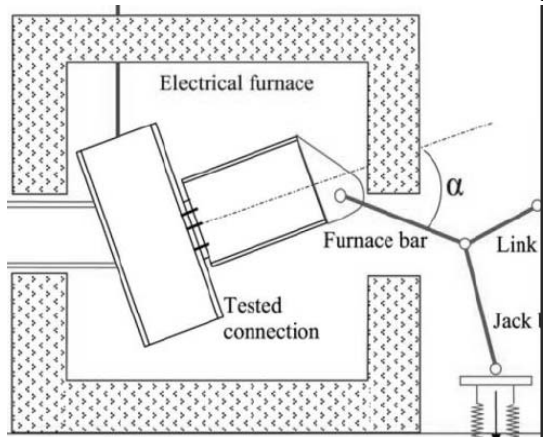


Fig. 1 Scheme of test setup (Yu et al, 2008a)

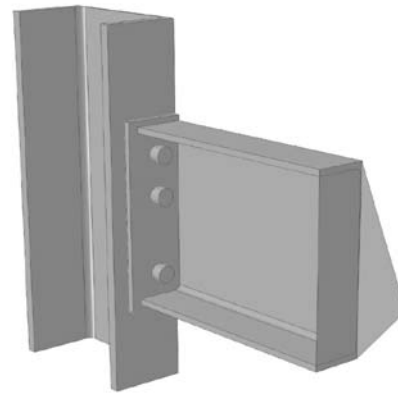


Fig. 2 Numerical model of flush endplate connection (including symmetry)

The distance controlled load is induced by a jack through a construction of three steel struts, which are connected by hinges. Due to this construction, the load angle α (c.f. Fig 1) is variable. For the numerical simulation, tests with an initial load angle of $\alpha=55^\circ$ have been used. It has to be taken into account that the load angle is changing during the test for the reason of the jack movement and the joint rotation.

The investigated connection consists of a flush endplate of dimensions 325x200x10 and is connected to the column by six M20 grade 8.8 bolts. The connection detail can be found in Fig. 2. The beam cross section is UB 305x165x40 and the column cross section is UC 254x89. The numerical model has been created as half-geometry taking into account the connection symmetry to reduce computing time.

3.2 Material Properties

The beam and the endplate are made of S275 grade steel. As described in (Yu et al, 2009) for one of the tests, a standard tensile test specimen has been cut from the beam flange to determine the material properties at ambient temperatures. The Young's Modulus is $E=176,350 \text{ N/mm}^2$, the yield stress is $f_y=356 \text{ N/mm}^2$ and the ultimate tensile stress is $f_u=502 \text{ N/mm}^2$. As there were no tests available for the endplate and the column, the material parameters have been adopted.

There were no tests to gain material properties at elevated temperatures. For this reason investigations of (Renner, 2005), which have been conducted with tensile specimen at different steady-state temperatures and different strain rates, were used to extrapolate the data. Material properties according to the Eurocodes have not been used as those properties are developed for transient temperatures. The material properties used in the numerical model are shown in Fig. 3.

According to bolt behaviour, three bolts have been tested at ambient temperatures. An average tensile force of 224 kN and a Young's Modulus of $206,009 \text{ N/mm}^2$ were determined (c.f. (Yu et al, 2009)). There is no data available to determine the stress strain relationship for bolts at steady-state elevated temperatures. For this reason the relationship has been determined by equations from (Eurocode 3, 2010). Reduction factors for yield stress according to (Hu et al, 2007) have been used. The stress-strain-relationship used for the bolts is shown in Fig. 4.

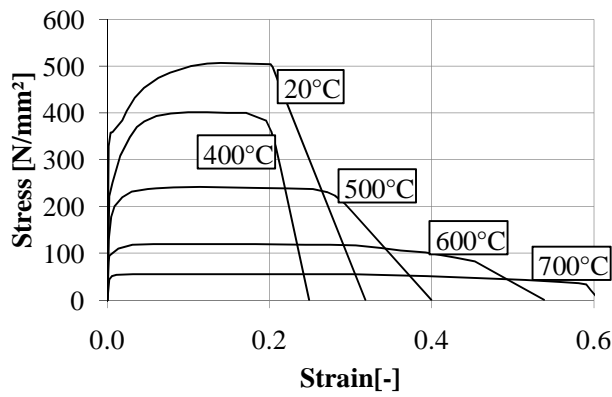


Fig. 3 Stress-strain-relationship for structural steel in numerical model

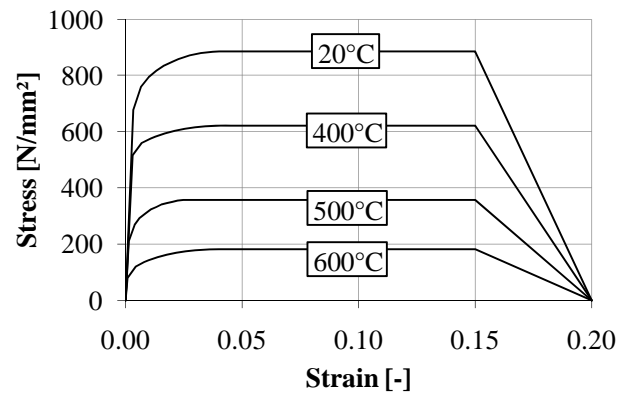


Fig. 4 Stress-strain-relationship for bolts in numerical model

4 RESULTS WITHOUT FRACTURE SIMULATION

The implicit equation solver algorithm (Abaqus/Standard) was used to simulate the connection behaviour first. Up to a rotation of 2°, the calculated behaviour was very close to the test results. The simulation at higher rotations was not possible because of convergence problems due to large deformations.

The load-rotation behaviour of the tested connection, calculated by an explicit equation solver, is shown in Fig. 5 for ambient and elevated temperatures. It can be seen that test results and calculated load-rotation behaviour are correlating very well for rotations up to 5°. At higher rotations, the load capacity of the connection is overestimated by the numerical model. This can be seen at the test at 450°C.

To verify the calculation internal and external energies have been investigated. To avoid singular modes (c.f. hourglass control), artificial energies are added during the simulation. To ensure realistic results, the amount of this energy should be negligible compared to “real” energies. A value of 10% of internal energies was determined to be the maximum allowable fraction. This value has been reached for most calculations at a rotation of about 8°. As the calculation is quasi-static, the kinetic energy fraction should be marginal as well. The kinetic energy was found to be less than 1% of internal energies.

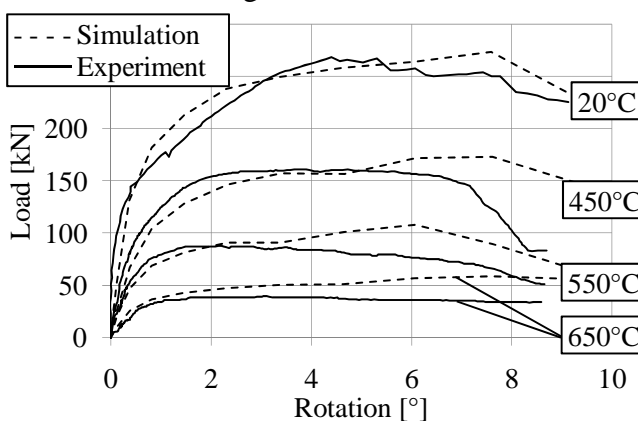


Fig. 5 Load-rotation behaviour at different temperatures (numerical and test results)

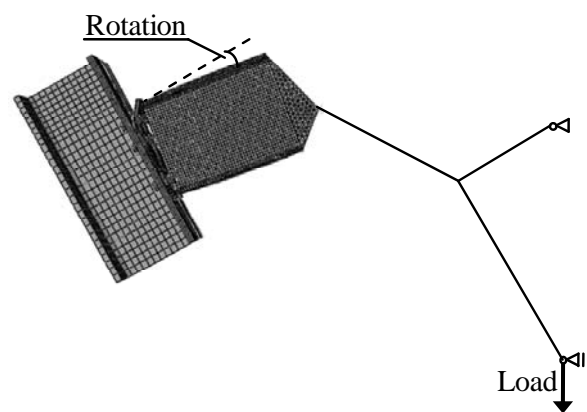


Fig. 6 Definition of load and rotation in Fig. 5, Fig. 8 and Fig. 11

5 COHESIVE ELEMENTS

As described in (Yu et al, 2008a), the test specimen showed two different failure modes. While at higher temperatures of 550°C and 650°C the bolts failed in tension, at 20°C and 450°C a shear fracture occurred very close to the beam web in the endplate.

A thin layer of cohesive elements has been implemented in the endplate next to beam web and flange to simulate this shear fracture. Failure of the cohesive layer has been simulated using material properties based on a fracture strain. As can be seen in Fig. 7, the stress strain relationship of the cohesive elements has been defined as linear elastic until a damage initiation criterion is reached. The damage initiation stress is defined as ultimate stress of the material. The Young's modulus has been defined as ultimate stress divided by the strain at the beginning of failure (c.f. Fig. 3). The failure strain, as defined in Fig. 7, has been determined to $\epsilon_{fail}=3$. For the reason of a very thin layer of cohesive elements, the influence of failure strain is negligible to the results, while the simulation is more stable using a higher strain.

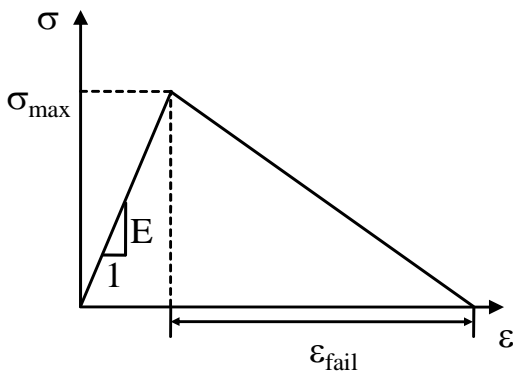


Fig. 7 Scheme of material behaviour of cohesive elements

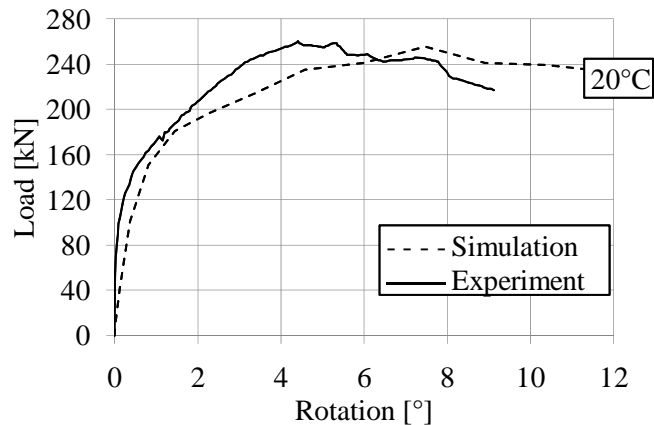


Fig. 8 Load-rotation relationship of connection at 20°C (numerical and test results)

In Fig. 8 the load rotation relationship for the test at ambient temperatures is compared to the calculation including cohesive elements. As can be seen, the curves are correlating very well and the decrease of load capacity can be simulated. The main benefit of the simulation including cohesive elements is the ability to visualise fractures. As can be seen in Fig. 9 and Fig. 10, it is possible to simulate the fracture which occurred in the test at ambient temperature.

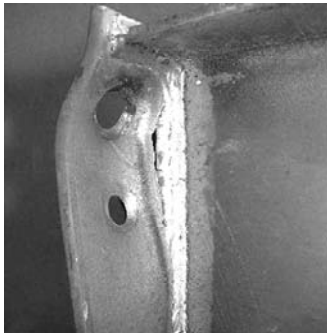


Fig. 9 Fracture of endplate in test specimen after test at 20°C

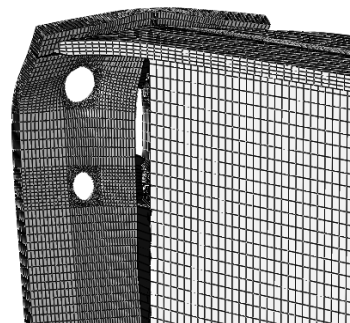


Fig. 10 Fracture of endplate in numerical simulation at rotation of 9°

6 GENERAL IMPLEMENTATION OF DAMAGE

Main problem of the use of cohesive elements in a fracture simulation is the need to know, where a fracture may occur. Otherwise, it is possible to implement a failure criterion to the general material properties.

The failure depends on a damage initiation strain, at which the stress reduction begins and failure strain at which the damage reaches 100%. The damage initiation strain can be described as strain-rate- and shear-stress-ratio-dependent. As there is no available data, the criterion has been set as constant for each temperature. The damage initiation strains have been determined to the strain at the beginning of stress reduction in the stress-strain-relationship (c.f. Fig. 3). Damage initiation strain and failure strain can be found in Tab 1.

Tab. 1 Temperature dependent strains for damage definition

Temperature [°C]	Damage initiation strain $\bar{\varepsilon}_s^{pl}$ [-]	Failure strain $\bar{\varepsilon}_f^{pl}$ [-]
20	0.200	0.5
400	0.200	0.5
500	0.275	0.5
600	0.400	0.5
700	0.575	0.5

The results of the simulation using a damage criterion for structural steel are shown in Fig. 11. It can be seen that the load-rotation-relationship is correlating very well for each temperature. While the results for tests at 550°C and 650°C are comparable to the calculation without a damage criterion, the results at 450°C are much closer to the test results especially at higher rotations and a decreasing load.

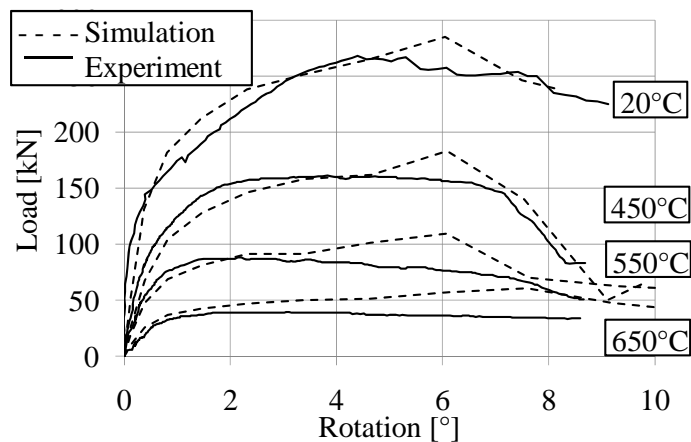


Fig. 11 Load-rotation behaviour of connection for different temperatures including a damage criterion for numerical results (for definition of load and rotation see Fig. 6)

As described in (Yu et al, 2008b), the failure at 20°C and 450°C was due to a shear fracture in the endplate at the beam web, while bolts failed due to tension at higher temperatures. This has been observed in the numerical simulation as well. In Fig. 12 the stress related to the ultimate stress at the specific temperature in the upper left bolt at a rotation of 7.5° is shown for the simulation at 20°C and 550°C. As can be seen by the low stress values in the bolt shaft at 550°C, the bolt has failed. For the reason of this failure, the load inside the endplate is reduced and the fracture at the beam web does not occur. As the bolt at 20°C is still functional, a fracture occurs in the endplate. In contrast to the experiments, the fracture in the simulation occurred as a tensional fracture. The reason for this slightly different behaviour may be found in the weld geometry or in the influence of the welding process in the heat affected zone.

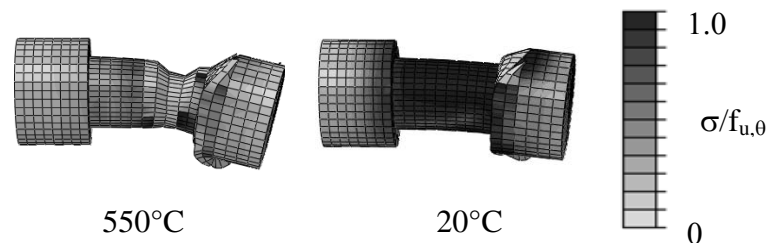


Fig. 12 Upper left bolt at rotation of 7.5° in numerical simulation at different temperatures

7 SUMMARY AND ACKNOWLEDGEMENT

In this paper, an experimental investigation in the load-rotation behaviour of flush endplate connections at ambient and elevated temperatures has been simulated. The simulation was conducted using a 3D finite element model including nonlinear material properties and large

deformations. As in some of the tests a shear fracture occurred in the endplate, different methods to simulate this failure mode were tested.

It was found that an implicit equation solver algorithm was not able to compensate large deformations. Thus an explicit algorithm was preferred and showed good correlations with the test results.

To simulate shear fracture, cohesive elements have been found to be a useful tool. Main disadvantage is the need to know, where the fracture may occur. If this is not known, the implementation of a general failure criterion is possible. This opportunity was investigated and comparisons to the test results showed very good correlation for the load-rotation-relationship. Additionally, the different failure modes at ambient and elevated temperatures were simulated correctly.

The authors would like to thank Ian Burgess and Shan-Shan Huang for providing information and help according to the experimental data. The IGF-Project No. 16586 N from FOSTA is funded by the German “Federal Ministry of Economics and Technology” via AiF.



Federal Ministry
of Economics
and Technology

REFERENCES

- Eurocode 3: Design of steel structures - Part 1-2: General Rules – Structural fire design; German version EN 1993-1-2:2005 + AC:2009, Beuth Verlag, Berlin, 2010
- Hu Y., Burgess I. W., Davison J. B., Plank R. J., Comparative study of the behaviour of BS 4190 and BS EN ISO 4014 bolts in fire, Proceedings of 3rd international conference on steel and composite structures, 2007.
- Hu Y., Burgess I. W., Davison J. B., Plank R. J., Modelling of flexible end plate connections in fire, Proceedings of 5th international conference Structures in Fire, Singapore, 2008.
- Krishnamurthy N., Two-dimensional finite element analysis of steel end-plate connections: parametric considerations, Auburn University, Report n. CE-AISC-MBMA-3, Auburn, 1974.
- Kruppa, J., Resistance on feu des assemblage par boulons, Centre Technique Industriel de la Construction Metallique, St. Remy Chevezese, France, 1976, CTICM Report, Document No. 1013-1, English translation available “Fire resistance of Joints with High Strength bolts”.
- Renner A., The effect of strain-rate on the elevated-temperature behavior of structural steel, Research dissertation, University of Sheffield, 2005.
- Sarraj M., Burgess I. W., Davison J. B., Plank R. J., Finite element modeling of steel fin plate connections in fire. Fire Saf J 42 (2007) 408-415, Elsevier, 2007.
- Schaumann P., Zhao B., Bahr O., Renaud, C., Fire performance of external semi-rigid composite joints , Proceedings of 6th International Conference Structures in Fire, Singapore, 2010.
- Wang W.-Y., Lia G.-Q., Dong Y.-L., Experimental study and spring-component modeling of extended end-plate joints in fire, Journal of Constructional Steel Research 63 (2007) 1127–1137.
- Wilson, W. M., Moore, H. F., Tests to Determine the rigidity of Riveted Joints in Steel structures, University of Illinois, Engineering Experimentation Station, Bulletin No. 104, Urbana, 1917.
- Yu, H., Burgess I. W., Davison J. B., Experimental investigation of the robustness of fin plate connections in fire, Proceedings of 5th ICASS (Advances in Steel Structures), 2007.
- Yu H., Burgess I. W., Davison J. B., Plank R. J., Experimental investigation of the behavior of flush endplate connections in fire, Proceedings of 5th international conference Structures in Fire, Singapore, 2008 (a).
- Yu H., Burgess I. W., Davison J. B., Plank R. J., Numerical simulation of bolted steel connections in fire using explicit dynamic analysis, JConstrStRes 64 (2008) 515–525, Elsevier, 2008 (b).
- Yu H., Burgess I. W., Davison J. B., Plank R. J., Experimental investigation of the behaviour of fin plate connections in fire, JConstrStRes 65 (2009) 723-736 2009.

THERMOMECHANICAL NONLINEAR ANALYSIS

Finite Element Analysis of Bolted Steel Connections Using Contact Mechanics

Andreas Kalogeropoulos^a, Georgios A. Drosopoulos^a, Georgios E. Stavroulakis^{a,b}

^a Institute of Computational Mechanics and Optimization, Department of Production Engineering and Management
Technical University of Crete, Chania, Greece

^b Department of Civil Engineering, Technical University of Braunschweig, Braunschweig, Germany

INTRODUCTION

Bolted steel connections have nonlinear mechanical behaviour due to unilateral contact and friction effects arising between the contacting parts as well as the elastoplastic material behaviour. Influence of elevated temperatures, indicating fire conditions, on the overall response of the joints is very important. In this framework, the thermomechanical behaviour of a 3 dimensional extended end-plate steel joint is investigated in the present study.

Simplified models as well as detailed finite element analyses have been used in the literature and compared with experimental measurements up to collapse. A number of experimental studies can be found in (Kruppa, 1976, Lawson, 1990, Al-Jabri et al, 1998, Spyrou et al, 2004, Spyrou et al, 2004, Daryan and Yahyai, 2009).

A lot of computational models for the study of steel connections under fire have also developed in the literature (Hu et al, 2009, Selamet and Garlock, 2010, Yu et al, 2008, Lien et al, 2009, Hozjan et al, 2007).

In the present study a 3 dimensional non linear finite element model has been developed, for the simulation of the thermomechanical behaviour of an extended end-plate steel joint. For the simulation between the end-plate and the column flange, a unilateral contact-friction law has been used. Degradation of the stress-strain non linear law at elevated temperatures together with large displacements, have been considered for the steel parts. Finally, three different load cases have been applied to the developed models. In the first loading scenario, the thermal and the concentrated mechanical load are applied both in the same analysis step, while in the second loading case the thermal loading precedes the point load. According to the third loading case, a small point load is followed by the thermal load; in a final step the total concentrated loading is applied to the connection. In all the aforementioned load cases an initial load step exists, namely the one with the application of the self-weight on the structure.

1 THE EXTENDED END-PLATE CONNECTION

The extended end-plate connection which has been used in this article, was tested to failure at ambient temperatures (Abdalla et al 2007). Eight high strength M20 bolts grade-8.8 with average yield and ultimate stresses $F_y=600\text{N/mm}^2$ and $F_u=800\text{N/mm}^2$ obtained from coupon tests, were used for the connection of the extended end-plate with the column flange. For each test, an IPE-360 beam section was attached to an HEA-220 column section (Fig. 1) through an extended end - plate. Beams, columns, and end-plates were made of steel having average yield and ultimate stresses $F_y=314\text{N/mm}^2$ and $F_u=450\text{N/mm}^2$, respectively, also obtained from three different uniaxial coupon tests. In Fig. 1 and Fig. 2 the geometry of the joint and the position of the point load, are shown.

2 FRAMEWORK OF THE NON-LINEAR MODEL

For the study of the thermomechanical behaviour of the extended end-plate, a three dimensional non linear finite element model has been developed. Unilateral contact law in the normal direction of the interface between the extended end-plate and the column flange, simulates the possible opening of the connected parts. Coulomb friction law is adopted to depict the contribution of the friction to the shear strength of the interface, together with the one obtained by the bolts.

At each point of the interface the basic unilateral contact mechanism can be described by the no-penetration inequality, the no-tension inequality, as well as a complementarity, either-or relation,

indicating that either separation with zero contact force or compressive contact force with zero gap appear.

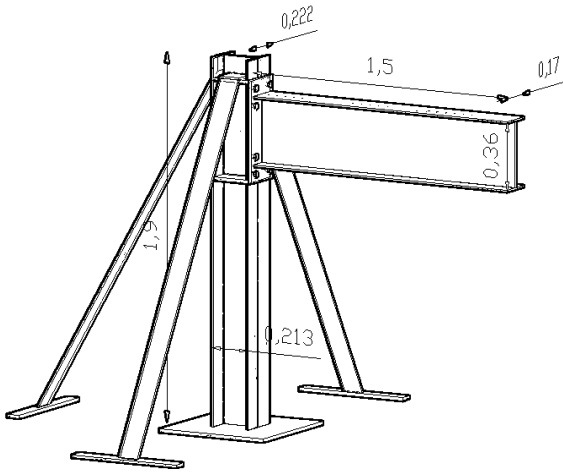


Fig. 1 Geometry of the steel connection

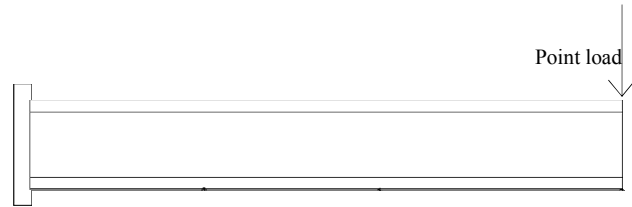


Fig. 2 Concentrated mechanical load

For a discretized structure the previous relations are written for every point of a unilateral boundary or interface by using appropriate vectors. The arising nonsmooth structural analysis problem has the form of a nonlinear complementarity problem. More details can be found, among others, in, (Panagiotopoulos, 1985), (Mistakidis and Stavroulakis, 1998), (Stavroulaki and Stavroulakis, 2002). The behaviour in the tangential direction of the interface is defined by a static version of the Coulomb friction model. Similarly with the contact problem, a complementarity problem arises for friction. The aforementioned scheme has been numerically implemented within commercial finite element packages.

3 THE FINITE ELEMENT MODEL

For the proposed finite element model three-dimensional 8-node brick elements have been used. For the satisfactory convergence of the analysis, a quite small average element size has been applied, resulting in a large number of finite elements (107.326 elements). The mesh which has been applied in the model is denser around the area of the connection while it becomes less dense away from it. In Fig. 3 and Fig. 4 the mesh as well as the structural parts of the joint are shown.

The friction coefficient for the beam–column interface is taken equal to 0.4. For the sake of simplicity, the interface between the bolt shank and the plate has not been considered, while interfaces between the bolts’ head and nut and the plate are simulated as tie connections which do not permit neither sliding nor opening. The Young’s moduli for the beam, the column and the bolts are approximately equal to 120GPa, as it is obtained from relevant coupon tests. The Poisson’s ratio for the whole structure is taken equal to 0.3. Finally, large displacement analysis as well as v. Mises plasticity have been considered for the structure.

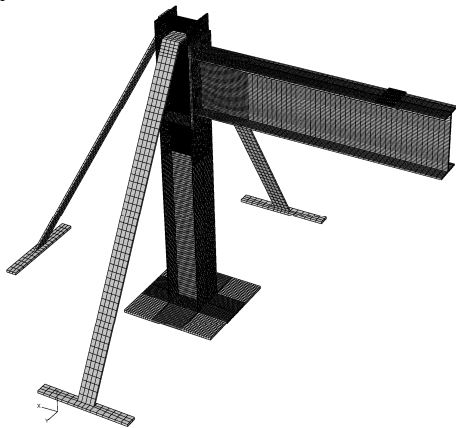


Fig. 3 Mesh of hexahedral 8-node finite elements

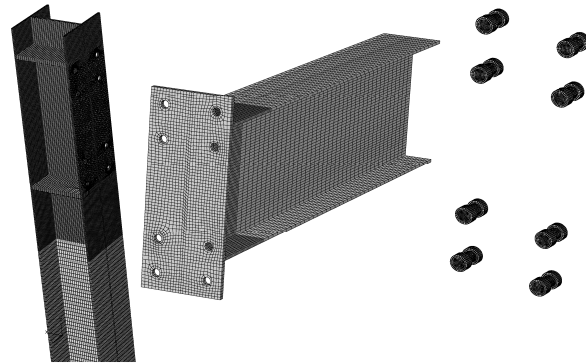


Fig. 4 Structural parts of the connection

4 FRAMEWORK OF THE THERMOMECHANICAL ANALYSIS

Within the aforementioned finite element analysis scheme, heat transfer analysis has been considered. Temperature boundary conditions have been applied as indicated in Fig. 5, Fig. 6 and Fig. 7.

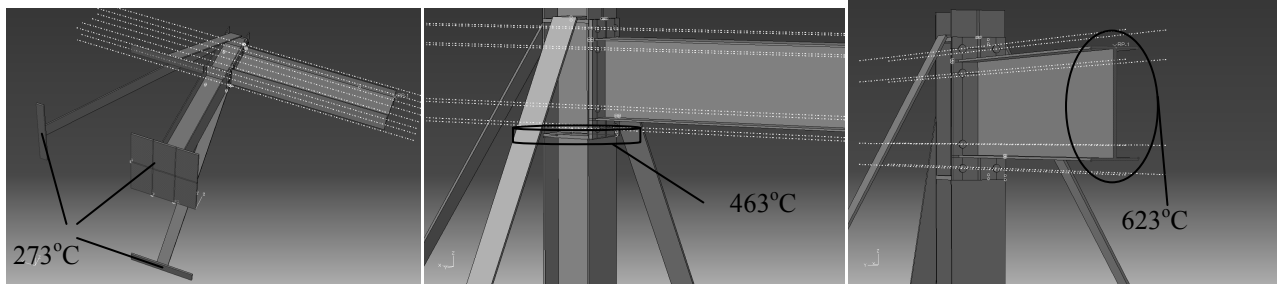


Fig. 5 Temperatures of 273°C Fig. 6 Temperatures of 463°C Fig. 7 Temperatures of 623°C

In addition, heat flux equal to 2KW/m² has been applied to the beam's web and to the column's web and front flange in the area below the connection, as it is shown in Fig. 8.

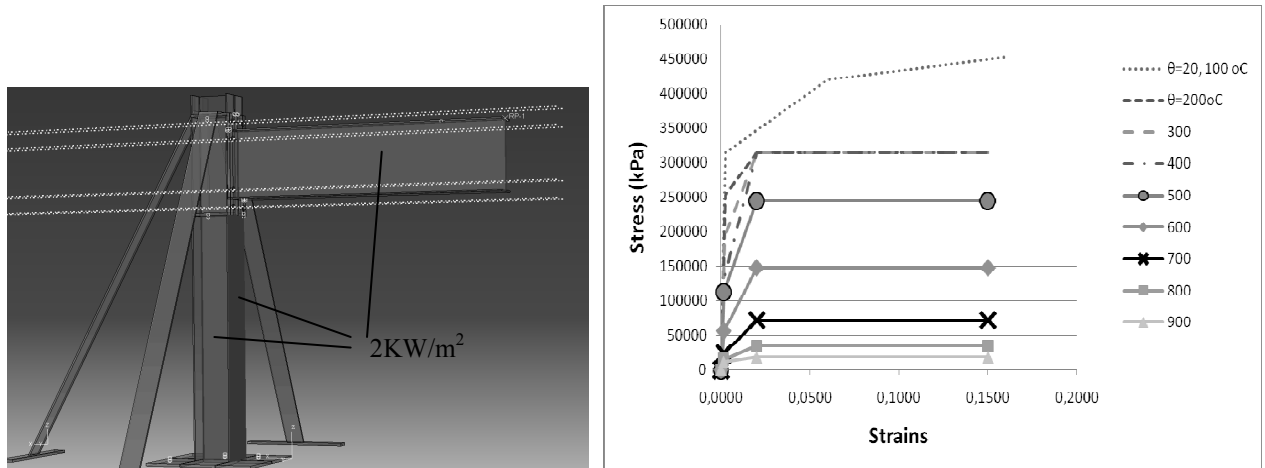


Fig. 8 Heat flux of 2KW/m²

Fig. 9 Degradation of the stress-stain laws

Thermal properties of the materials have been chosen to be as follows: thermal conductivity=45 W/m°C, thermal expansion for the steel parts=12x10⁻⁶ /°C, thermal expansion for the bolts=13x10⁻⁶ /°C.

Degradation of the Young's Modulus and the stress-strain materials laws at elevated temperatures have been considered, as it is represented in Fig. 9 (Eurocode 3, 2001).

Three load cases have been considered in the developed models. According to the first one, the thermal and the concentrated mechanical loads are concurrently applied in the same analysis step. Within the second load case the thermal loading precedes the point loading. At the third load case, a small point load (50KN) is followed by the thermal loading; in the final step the total mechanical load is applied to the connection. In all the aforementioned load cases an initial load step exists, in which self-weight of the structure is applied.

5 RESULTS

The sequence of application of the thermal and the mechanical load is proved to be quite significant for the overall behaviour of the connection. In case the thermal and the point load are concurrently applied to the structure, temperatures reach approximately 800°C at the collapse of the joint. Temperatures reach similar values for the third load case, where thermal loading follows a small concentrated load of 50KN. In both cases the connection emits a satisfactory strength to fire although the limit load is significantly reduced in comparison with the structure at ambient temperatures. However, supposing that thermal loading is initially applied to the connection when only the self-weight is present (before the point load, according to second load case), then

maximum temperatures become greater than 2000°C. Consequently, the structure can only support a quite small fragment of the point load which is applied afterwards. In Fig. 10 temperatures distribution at the failure of the connection for the first and the third load cases, are presented. In Fig. 11 and Fig. 12 temperatures distribution for the second load case as well as load-displacement diagrams, are shown. Moreover, if no reduction in the mechanical properties of the steel parts is considered, load-displacement diagram of the thermomechanical analysis is almost the same with the one obtained by the pure mechanical analysis (Fig. 12).

In Fig. 13 the plastic regions of the connection are depicted for the case the thermal and the concentrated load are concurrently applied (first load case). According to this, plastic yielding has been expanded to the whole beam, to the column web near the connection and to small regions of the column flange. In case the thermal load is initially applied with the self-weight and the point load follows in the next step, yielding of the joint is expanded to the whole beam at the end of the thermal loading step, before the application of the point load (Fig. 14). This is occurred due to the particular loading sequence which has been followed. Self-weight and the thermal load cause yielding to the beam, before the application of the concentrated load. As a result, when this is applied only a small part of it can be supported by the structure. For the third load case where the thermal load is applied after a small point load equal to 50KN, failure occurs before the end of the thermal loading step. Consequently, the ultimate load is equal to 50KN, which is smaller in comparison with the case where no fire is present, see diagrams of Fig. 12.

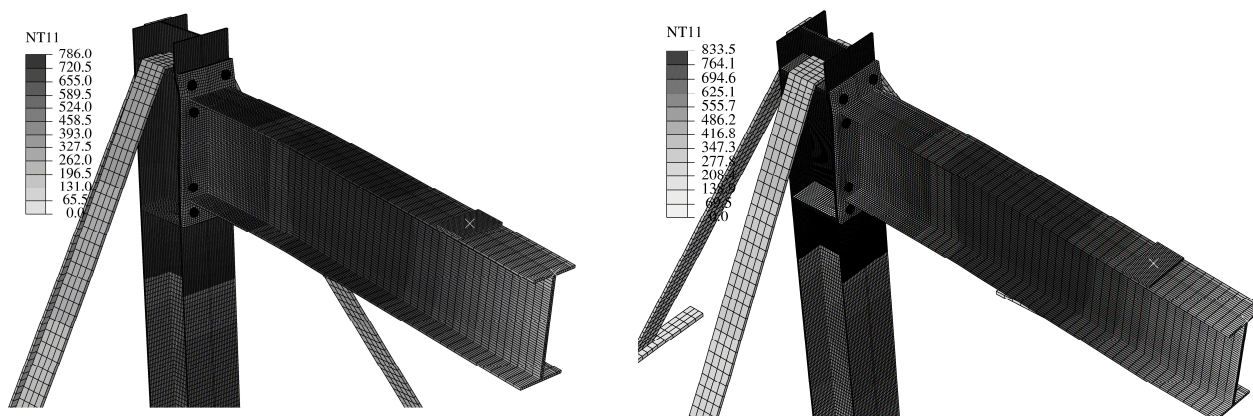


Fig. 10 Temperature distribution at failure for the first and the third load case

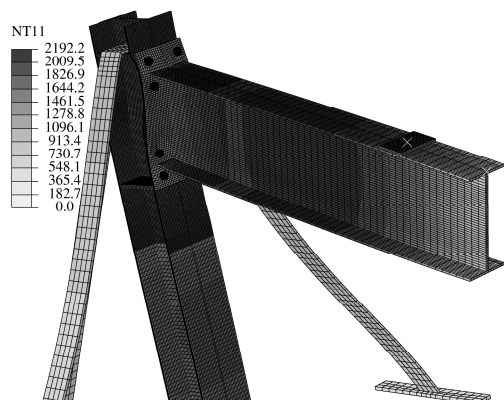


Fig. 11 Temperatures distribution for the second load case

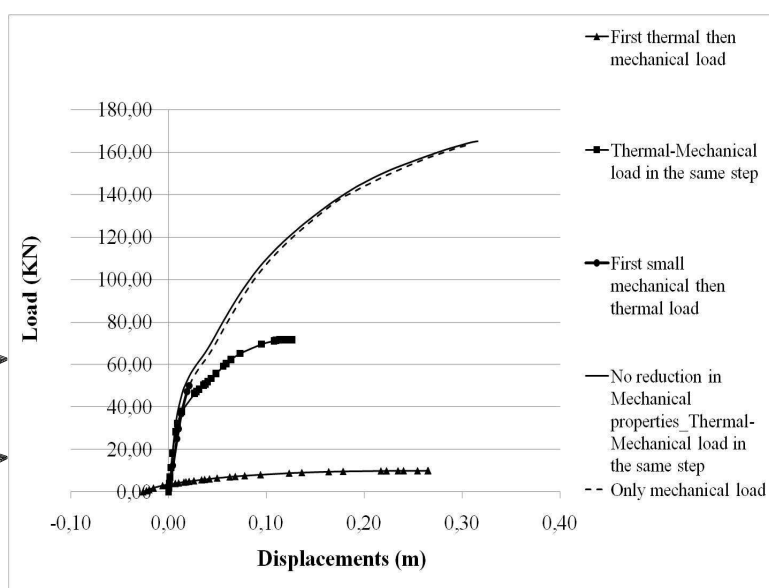


Fig. 12 Force-Displacement diagrams

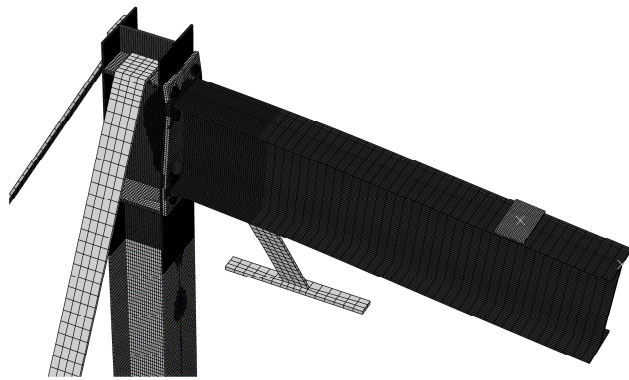


Fig. 13 Plasticity at the first load case

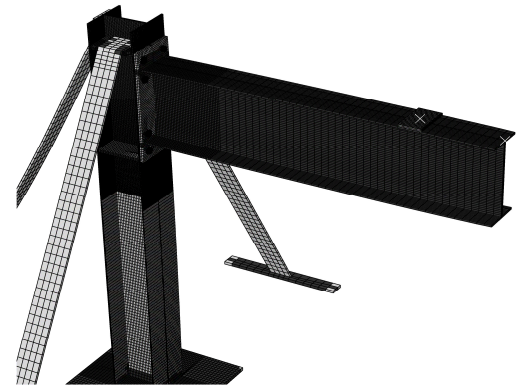


Fig. 14 Plasticity at the second load case

Another interesting aspect of the impact of the fire conditions on the steel connection is related with the opening of the connection. In Fig. 15a opening of the interface at the end of the analysis of the first load case, is shown. According to this, opening reaches a value of 18.7mm. In Fig. 15b opening of the interface at the end of the second load case, is shown. Opening in this case is bigger, thus equal to 38.7mm than the first load case. In addition, in the end of the thermal load step and before the application of the point load, there is a small opening in the interface (Fig. 15c). This is attributed to the total development of fire in the initial step of the analysis, where only the self-weight is present. Finally, in Fig. 16 are shown the opening of the interface for the third load case, where the point load precedes the thermal one. In Fig. 16a opening at the end of the point load of 50KN end before the application of the thermal load is shown. In Fig. 16b opening at the end of the analysis becomes approximately three times bigger than the one before the application of the thermal load (11.8mm instead of 3.5mm). This is due to fire conditions, as in the final step of the analysis the point load is constant and equal to 50KN.

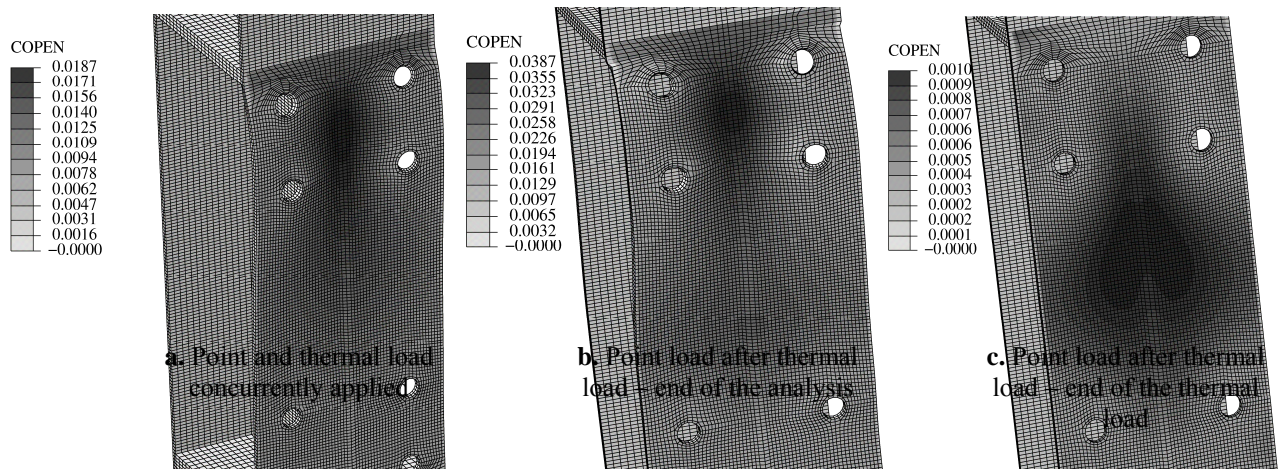


Fig. 15 Opening of the interface for the first (a) and the second (b), (c) load case

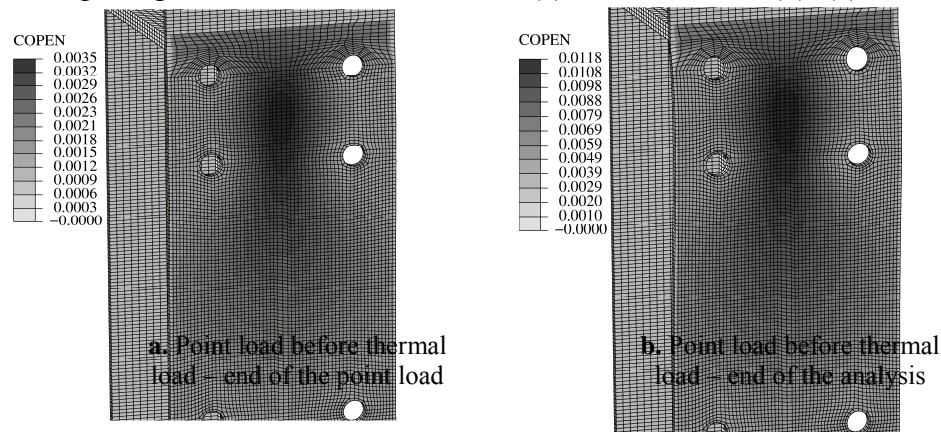


Fig. 16 Opening of the interface for the third load case

6 CONCLUSIONS

A thermomechanical analysis of a bolted steel joint has been performed in the present study, using a three-dimensional nonlinear finite element model. Three loading cases and the influence they have on the behaviour and the opening of the connection, are examined. The analysis has been performed up to collapse of the joint and the different collapse loads have been calculated. The results demonstrate that interaction of thermal and mechanical effects can be very complicated in structural elements. Comparable complexity is expected in the analysis of structures having such structural elements.

REFERENCES

- Kruppa J., Re'sistance en feu des assemblages par boulons, CTICM Report, Document No. 1013-1, Centre Technique Industriel de la Construction Metallique, St. Re'my les Chevreuse, France, 1976.
- Lawson R. M., Behaviour of steel beam-to-column connections in fire, *The Structural Engineer* 68, 1990.
- Al-Jabri K. S., Lennon T., Burgess I. W., Plank R. J., Behaviour of steel and composite beam-column connections in fire, *Journal of Constructional Steel Research* 46, 1998.
- Spyrou S., Davison J., Burgess I. W., Plank R. J., Experimental and analytical investigation of the "compression zone" component within a steel joint at elevated temperatures. *Journal of Constructional Steel Research* 60, 2004.
- Spyrou S., Davison J., Burgess I. W., Plank R. J., Experimental and analytical investigation of the "tension zone" component within a steel joint at elevated temperatures. *Journal of Constructional Steel Research* 60, 2004.
- Daryan A. S., Yahyai M., Behavior of bolted top-seat angle connections in fire, *Journal of Constructional Steel Research* 65, 2009.
- Hu Y., Davison B., Burgess I., Plank R., Component Modelling of Flexible End-plate Connections in Fire, *Steel Structures* 9, 2009.
- Selamet S., Garlock M. E., Robust fire design of single plate shear connections, *Engineering Structures* 32, 2010.
- Yu H., Burgess I. W., Davison J. B., Plank R. J., Numerical simulation of bolted steel connections in fire using explicit dynamic analysis, *Journal of Constructional Steel Research* 64, 2008.
- Lien K. H., Chiou Y. J., Wang R. Z., Hsiao P. A., Nonlinear behavior of steel structures considering the cooling phase of a fire, *Journal of Constructional Steel Research* 65, 2009.
- Hozjan T., Turk G., Srpacic S., Fire analysis of steel frames with the use of artificial neural networks, *Journal of Constructional Steel Research* 63, 2007.
- Abdalla K. M., Abu-Farsakh G. A. R., Barakat S. A., Experimental investigation of force-distribution in high-strength bolts in extended end - plate connections, *Steel and Composite Structures, An International Journal* 7, 2007.
- Panagiotopoulos P. D., Inequality problems in mechanics and applications. Convex and nonconvex energy functions, Birkhaeuser Verlag, Boston, Basel, Stuttgart, 1985.
- Mistakidis E. S., Stavroulakis G. E., Nonconvex optimization in mechanics. Algorithms, heuristics and engineering applications by the F.E.M., Springer/Kluwer, Dordrecht, Boston, 1998.
- Stavroulaki M. E., Stavroulakis G. E., Unilateral contact applications using FEM software, *International Journal of Applied Mathematics and Computer Science* 12, 2002.
- Eurocode 3: Design of steel structures part 1.2: general rules structural fire design ENV 1993-1-2:2001, Brussels (Belgium): European Committee for Standardization, 2001.

A COMPONENT-BASED MODEL FOR FIN-PLATE CONNECTIONS IN FIRE

Mariati Taib^a, Ian W. Burgess^a

^a University of Sheffield, Dept. of Civil and Structural Engineering, UK

INTRODUCTION

Connections can be classified according to their rotational stiffnesses, which are classed as rigid, simple or semi-rigid. Semi-rigid assumptions can be considered to assess the stiffness and capacity of steel framing systems most accurately. The benefits of this treatment are extensively documented, and there is a general acceptance that semi-rigid design results in efficiency, lightness and economical ambient-temperature design¹. In fire conditions, due to the combinations of thermal expansion and material weakening, beams can be subjected to high normal forces, both in compression (at fairly low temperatures) and tension (at high temperatures), in addition to extremely high rotations, if their ends are fixed horizontally. These beam forces have to be sustained by the connections unless some movement of the beam ends, which relieves the forces, is permitted. Such movements can occur because the connected members move, or because the connections themselves have enough ductility to reduce the forces transmitted. In any case, the vertical shear forces, which the connections are designed to sustain at ambient temperature, are generally largely unaffected by the effects of fire.

Incorporating semi-rigid connections into global thermo-structural analysis requires tools and methods to facilitate the analytical design process, as joint characteristics can clearly have a significant influence on the survival time of the structural assembly during a fire. Advanced finite element models of connections involve high preparation time and computational cost, hence limiting their use for practical design purposes, despite being capable of highly reliable nonlinear joint simulation. Due to the inadequacy of structural databases, full-scale or isolated fire testing is inevitably required to provide the most accurate representation of connection response, although this is unlikely to be an economically appealing solution.

An intermediate approach to incorporating connection behaviour, known as the component-based modelling approach, has now been widely developed for ambient-temperature design. Eurocode 3⁴ has implemented this approach to model the strengths and initial stiffnesses of steel joints for semi-rigid design. This approach constructs a connection from extensional zero-length “spring” elements and rigid links, representing the characteristics of its main structural zones realistically. Each active component makes its contribution independently, through its structural properties. This simplified method allows connections and structural system configurations to be varied rapidly, and thus the impact of various parameters on the system’s global performance can be analysed.

1 IDENTIFICATION OF ACTIVE COMPONENTS

A very widely used simple connection is the fin-plate connection, classed as a shear connection, which consists of a pre-drilled single plate, welded to the supporting column flange or web, and bolted to the beam web at a number of single- or double-bolted rows (Fig.1a). Simple connections are assumed to develop a moment at the beam end less than or equal to 20% of the fixed-end moment, while the end rotation is greater than or equal to 80% of the end rotation in a simply-supported beam². They are invariably cheaper to fabricate than moment-resisting connections as fabrication is simple, and fin-plates can be standardised. Cost advantages largely influence the choice of this connection, and erection on site is simple. As a simple shear connection, normal design concerns only the strength and ductility needed to transfer the vertical beam end reaction to its support. In fire conditions the connection also needs to provide sufficient rotational ductility to accommodate the rotation of the beam end, as well as a reasonable amount of horizontal movement.

Failure of fin-plate connections at high temperatures involves response to a combination of beam end shear and normal forces, and large rotations². In order to understand the load transfer via bolt shearing, it is convenient to represent a simple shear connection by a lap joint³ (Fig 1b).

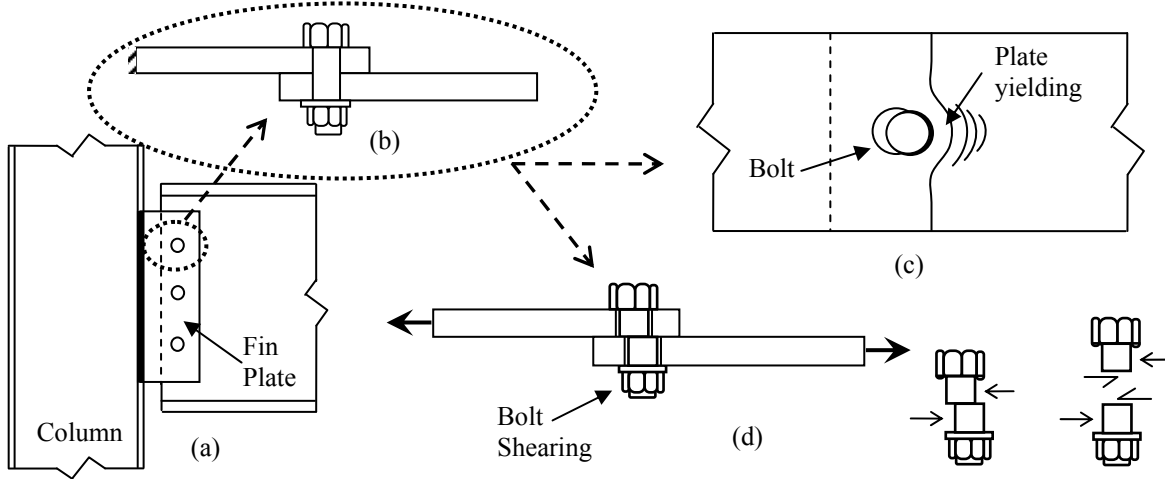


Fig. 1: (a) Fin-plate connection; (b) lap joint; (c) plate bearing; (d) bolt in shear.

1.1 Plate in bearing

Bearing failure of the plates is strongly affected by the lateral constraint to the contact zone by the surrounding material in its vicinity. Yielding of the plates does not cause a substantial loss of load capacity (Fig.1c), and is therefore generally treated as a ductile failure mode. The desired failure mode of a shear connection, as implied by the design guides^{4, 5} adopts the conservative design recommendation that plate bearing is the resistance which should govern design. When the bolt is close to the end of the plate, its edge distance controls the tear-out and bearing (which are treated as a single limit state). However, moving away from the end of the plate results in large bearing deformation of the bolt hole without occurrence of tear-out failure. A typical force-displacement relationship with respect to temperature is shown in Fig.2a.

Rex and Easterling³ concluded that the initial stiffness associated with a plate in bearing depends on three primary stiffness values (bending (K_b), shearing (K_v) and bearing (K_{br})) based on detailed investigation of a single-bolt lap plate connection. Sarraj⁶ distinguishes two cases of bearing from a finite element parametric study in order to determine the plate bearing resistance using the most effective curve-fit values; these involve bolts with a small end distance ($e_2 \leq 2d_b$) and with a large end distance ($e_2 \geq 3d_b$). The key difference between these studies was the degree of tightening of the nut on the outer surfaces of the plates. Rex and Easterling's equations are:

$$\text{Bearing stiffness, } K_{br} = \Omega t F_y (d_d / 25.4)^{0.8} \quad (1)$$

$$\text{Bending stiffness, } K_b = 32Et(e_2 / d_d - 0.5)^3 \quad (2)$$

$$\text{Shearing stiffness, } K_v = 6.67Gt(e_2 / d_b - 0.5) \quad (3)$$

$$\text{Initial stiffness, } K_i = \frac{1}{\frac{1}{K_{br}} + \frac{1}{K_b} + \frac{1}{K_v}} \quad (4)$$

Where e_2 is the end plate distance (mm),
 d_b is the diameter of the bolt (mm),
 Ω is a temperature-dependent parameter for curve fitting.

1.2 Bolt in shear

The bolt shear failure mode may significantly affect the integrity of the structural system because it has inadequate ductility to ensure simultaneous plastic distribution of the forces carried by the bolts, and may therefore allow progressive failure. The relationship between the bolt shear deformation

and the force is given in Eq. (5) by a modified Ramberg-Osgood⁶ expression for relative bolt deflection:

$$\Delta = \frac{F}{k_{v,b}} + \Omega \left(\frac{F}{F_{v,rd}} \right)^n \quad (5)$$

Where F is the level of shear force [N],

$K_{v,b}$ is the temperature-dependent bolt shearing stiffness [N/mm],

$F_{v,Rd}$ is the temperature-dependent bolt shearing strength [N].

In the study by Sarraj⁶, bolt shearing failure was assumed to occur immediately after the maximum shear resistance, $F_{v,rd}$ was reached. However, a gradual decrease of shear resistance was observed during tests carried out by Yu⁷ at elevated temperatures. It is therefore assumed here that the shear resistance decreases to zero at a displacement equal to the bolt diameter. Example characteristic curves with respect to temperature of a bolt in shear are shown in Fig.2b.

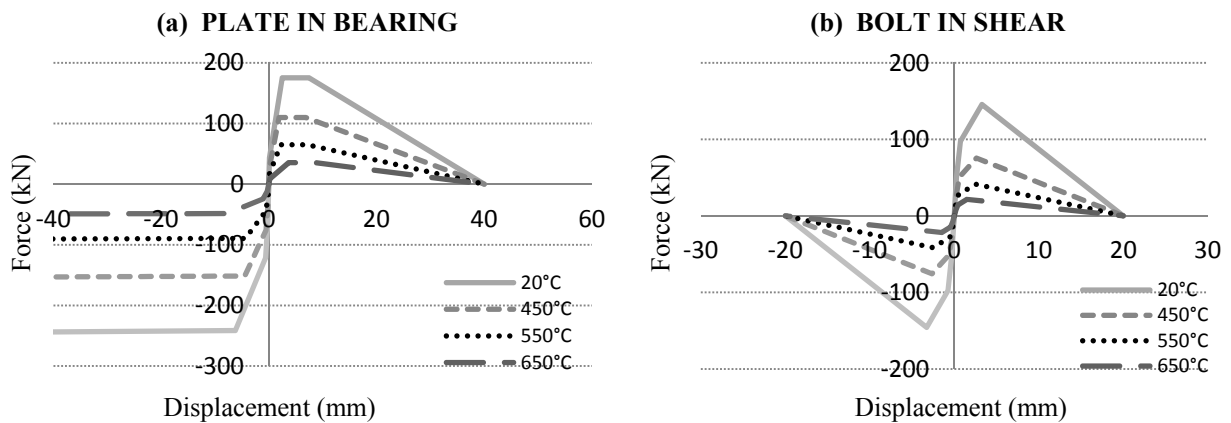


Fig. 2: Properties of components: (a) Plate in bearing; (b) Bolt in shear.

2 JOINT MODELLING

Previously, component-based models of fin-plate connections have been developed by Sarraj⁶ and Yu⁷ based on two-noded spring elements. The lap-joint zone consists of three fundamental components with no physical length, placed in series, for each bolt row: fin-plate in bearing; bolt in shearing; beam web in bearing. These component models include a friction spring in parallel with this basic spring series. The simplified friction load-deflection characteristic, however, generates low slip resistance, and has little influence on the connection's behaviour.

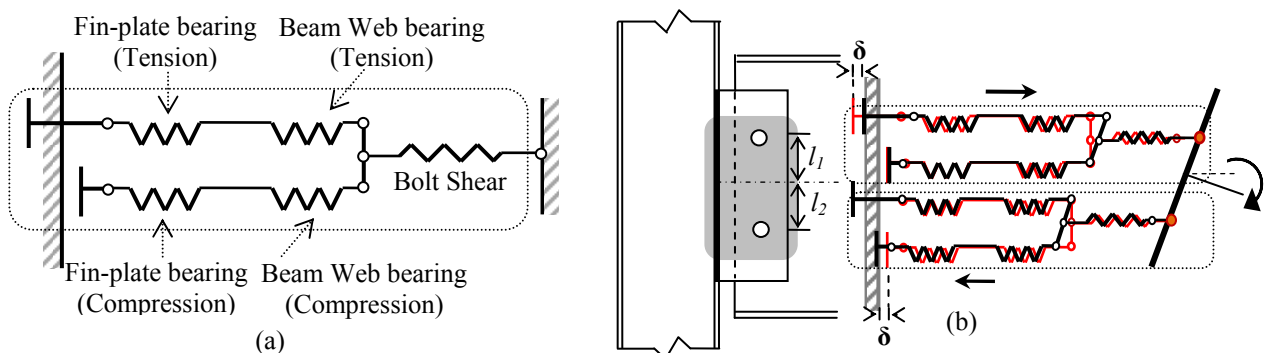


Fig. 3 : (a) Component-based model of a bolt row of a fin-plate connection (b) Component-based model subjected to tension and compression

A component-based model of a single-bolt-row of a fin-plate connection with no physical length is illustrated in Fig. 3a. The minimal effect of the frictional resistance between the two plates has been neglected here. The picture of the component-based model of a whole two-row fin-plate connection shown in Fig. 3b demonstrates that, during a complete analysis, tension and compression do not

follow the same lines of action. The load capacity is predominantly determined by the assembly of springs, from which the weakest individual component spring initiates failure.

2.1 Component-based model in VULCAN

The joint element is modelled as an assembly of component springs and rigid links, concentrating on the beam-to-column connection zone. An additional component spring at the lower beam flange level is adopted to account for contact between the lower flange of the beam and the column face at high rotation. A highly simplified version of the model consists of two horizontal rows; a single lap joint, the beam flange/column face contact, and a vertical shear spring, as shown in Fig. 4.

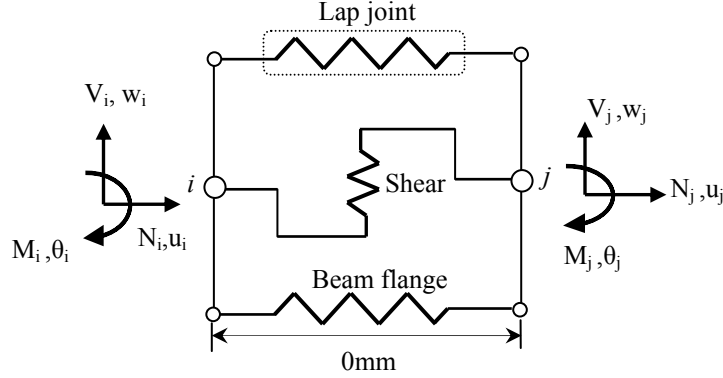


Fig. 4: Forces and displacements of a simplified connection element.

Each degree of freedom of the assembled springs is displaced individually to derive the stiffness matrix of the connection element, which eventually has three degrees of freedom (two translational u , w and one rotational θ) at each node. By solving for the global force and moment equilibrium of the whole element, the force-displacement relationships of the degrees of freedom can be calculated. The final tangent stiffnesses of the connection element are shown below.

$$K'_{11} = \sum_{i=1}^n k'_{lap,i} + k'_{beamflange,i} \quad (6)$$

$$K'_{15} = K'_{51} = \sum_{i=1}^n k'_{lap,i} l_{lap,i} + k'_{beamflange,i} l_{beamflange,i} \quad (7)$$

$$K'_{11} = k'_s \quad (8)$$

$$K'_{15} = K'_{51} = \sum_{i=1}^n k'_{lap,i} l_{lap,i} + k'_{beamflange,i} l_{beamflange,i} \quad (9)$$

In these equations, n is the number of component bolt rows, and the indices “lap” and “beamflange” indicate the lap joint assembly and beam flange spring respectively. The index s indicates the shear spring. Due to the simplicity of this mechanical model, the tangent stiffnesses can be incorporated in *VULCAN* using its existing spring element infrastructure. The component model subroutine subsequently provides the necessary incremental displacement vector for the connection element, and returns the tangent stiffness matrix and force vector to the main routines.

2.2 Loading and unloading of component model

The classic Massing rule⁸ is incorporated so that each individual component will respond realistically to load reversals. The hysteresis curve in unloading (Fig. 5a) from the point at which strain reversal occurs, is the loading curve, scaled by a factor of two and rotated 180°. A modification to the Massing rule is applied to account for the initial bolt-slip phase, and only allows force transition into the opposite quadrant when contact is re-established, as shown in Fig. 5b.

During the heating phase, the softening of the material is defined by force-deflection characteristics which are functions of temperature. The permanent plastic deformation, which is recalculated after each temperature change, is considered as unaffected if the temperature changes. Thus, each force-

displacement curve at different temperatures necessarily has to unload completely through the same point. The unloading curve for a new temperature intersects with the previous unloading path at the zero-force axis, and this point is used as the reference point, $\delta_{P,T1}$.

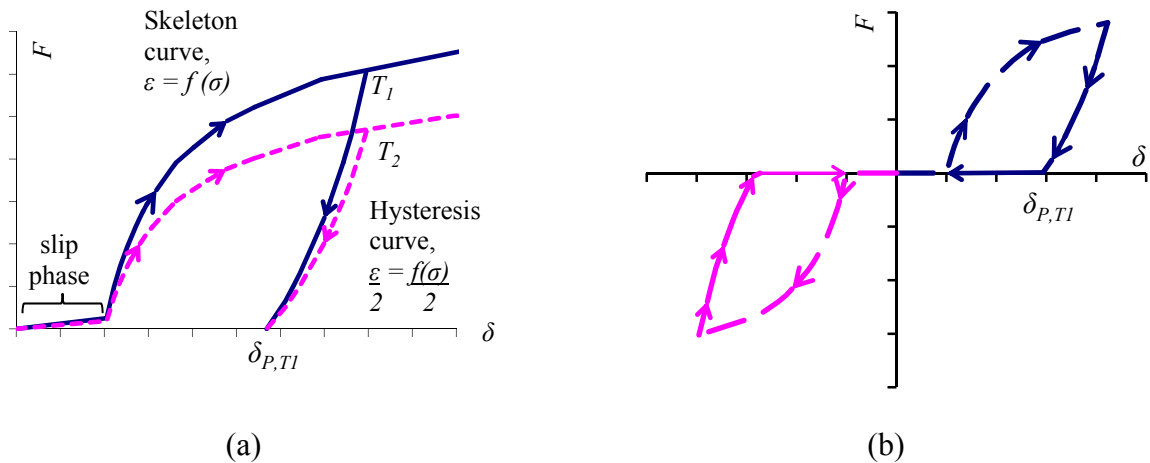


Fig. 5 Massing Rule for fin-plate connection at varying temperature.

3 EXPERIMENTAL VALIDATION AT ELEVATED TEMPERATURE

Yu *et al.*⁷ carried out an experimental investigation of the robustness of steel connections at elevated temperatures for flush endplates, flexible endplates, fin-plates and web cleats. The design setup for fin-plates used 200mm deep \times 8mm thick fin-plates with three rows of bolts, designed in accordance with UK design recommendations⁵. Inclined tying forces were applied to represent the catenary action phase of a beam in fire. The results shown in Fig. 6 are for applied force inclinations of $\alpha=35^\circ$ at ambient temperature and at 450°C , to represent a temperature range in which the properties of both structural and bolt steels have started to degrade rapidly.

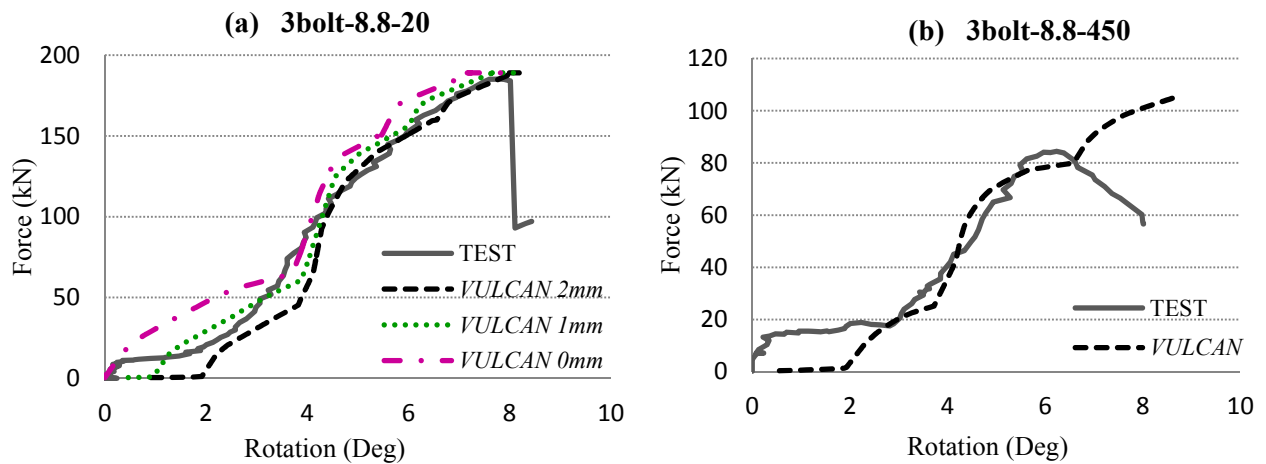


Fig. 6: Comparisons of test results to the component model (load angle 35°) at steady-state temperatures; (a) ambient temperature, (b) elevated temperature.

The responses of the component model and the test results are generally in close agreement for similar loading arrangements. Comparisons of the force-rotation relationship assume M20 bolts, initially installed centrally in clearance holes of 22mm diameter, producing 2mm initial slip between the plates. This initial slip ends with the first positive contact of the bolt against the bolt hole, which considerably influences the rotational response, as shown in Fig.6a. As the model is loaded, geometry changes cause the relationship between the force and rotational displacement to be non-linear. Subsequently, the second-order geometric effects, which create increased moments, are taken into account in the finite element analysis.

The resistance gradually increases after positive contact has been made by the bolt with the plate, until the maximum resistance of the top bolt is exceeded. The bottom flange subsequently comes into contact with the column face, resulting in a stiffer deformation response. The connection

strength is then controlled by consecutive bolt failures until the lowest bolt reaches its ultimate load. The component model was able to produce relatively close predictions of the maximum resistance and the rotational ductility of a connection, at both ambient and elevated temperatures.

4 CONCLUSION

A component-based connection model allows the behaviour of connections to be included in practical global thermo-structural analysis, provided that knowledge about the characteristics of key components is available from test data, numerical simulations or analytical models. At this stage, a basic component model for fin-plate connections has been developed and successfully incorporated in *VULCAN*. The stiffness matrix of the model has been derived to generate the connection's response to combinations of forces and displacements, and has subsequently been validated both at ambient and elevated temperatures. This component model, when embedded in *VULCAN*, allows direct analysis of whole structures or large substructures, including consideration of the interaction between realistic connection behaviour and that of the adjacent structural members.

A major modification to the model, which helps it to consider the real situation in fire, allows the lower beam flange to come into contact with the column face when the connection has undergone large rotation. It has been found that the complex nature of load reversal during a fire can be represented by adapting the Massing Rule, but with modification of the initial slip phase to account for the usual case where bolt holes are larger than the bolts. As part of the global structural assembly of beam-column, slab and connection elements, the component-based model will guarantee that the connection deformations are accounted for within the equilibrium of the whole assembly. This can be beneficial not only in design but also in assisting in the interpretation of experimental and analytical responses of connections within structures in fire.

5 ACKNOWLEDGMENT

The authors gratefully acknowledged sponsorship and support of the first author by the Malaysian Government for this research.

REFERENCES

- A. Astaneh (1989). "Demand and Supply of Ductility in Steel Shear Connections." *Journal of Constructional Steel Research* 14:1-19.
- E.Bayo, J.M. Cabrero, B.Gil (2006) "Component-Based Method to Model Semi-Rigid Connections for the Global Analysis of Steel and Composite Structures." *Journal of Engineering Structures* 28:97-108.
- Sarraj, M. "The behaviour of steel fin-plate connections in fire" .Ph.D. Thesis. University of Sheffield; 2006
- European Committee for Standardisation (CEN), BS EN 1993-1-8, Eurocode 3; Design of Steel Structures, Part 1.8: Design on Joints, UK :British Standard Institutions; 2005
- Yu, H., I. W. Burgess, et al. (2009). "Experimental investigation of the behaviour of fin-plate connections in fire." *Journal of Constructional Steel Research* 65(3): 723-736.
- Rex, C.O., Easterling, S.W. (2003). "Behaviour and modelling of a bolt bearing on a single plate." *Journal of Structural Engineering, ASCE* 129(6):792-800.
- BCSA, The British Constructional Steelwork Association, "Joints in Steel Construction : Simple Connection", The Steel Construction Institute (2002)
- Block, F.M. Development of a component-based finite element for steel beam-to-column connections at elevated temperature.Ph.D. Thesis. University of Sheffield; 2006
- European Committee for Standardisation (CEN), BS EN 1993-1-2, Eurocode 3; Design of Steel Structures, Part 1.2: General rules-Structural Fire Design, UK: British Standard Institutions; 2005

BEHAVIOUR OF HEATED COMPOSITE JOINTS

Preliminary numerical studies

Cécile Haremza ^a, Aldina Santiago ^a and Luís Simões da Silva ^a

^a Department of Civil Engineering, University of Coimbra, Portugal

INTRODUCTION

The work presented in this paper is part of the European RFCS ROBUSTFIRE project, in which the behaviour of steel and composite structures subject to an exceptional event is investigated. The study of the structural individual response of the affected structural elements is actually on progress and three approaches (experimental, numerical and theoretical) will be combined with the aim to derive behavioural models for elements. Some experimental tests on a composite steel-concrete beam-to-column frame are currently under development at the University of Coimbra. In order to define these tests and to justify some preliminary results, numerical models were performed with the non-linear finite element package ABAQUS, v6.10. This paper presents these numerical studies.

1 THE EXPERIMENTAL PROGRAMME

The main objective of the experimental tests is to observe the combined bending moment and axial loads in the heated joint when catenary action develops in the frame after the loss of the column. The composite joint zone is subjected to high temperatures in order to simulate the effect of the localised fire that leads to the column loss. Fig. 1 presents the seven beam-to-column frames being tested in Coimbra. According to previous experimental works performed in real composite steel-concrete open car park structures subjected to fire, a majority of the temperatures measured in the beam bottom flanges were lower than 500°C; however temperatures of 700°C were observed in recent tests performed in France (Simões et al., 2009). Based on these previous observations, five sub-structures are heated up to 500°C or 700°C; one sub-structure is tested at ambient temperature (test 1) and finally, a sub-structure is planned to be subjected to a demonstration test, for which the frame will be subjected to an increase of the temperature up to the failure of the column (test 7), see Fig. 1. The effect of the axial restraint to beam coming from the unaffected part of the building is also studied: tests 2 and 3 - no axial restraint to the beam; tests 4 and 5 - total axial restraint to the beam; and tests 1, 6 and 7 - realistic axial restraint to the beam. At this moment, three tests at elevated temperatures have been performed: tests 2, 3 and 4.

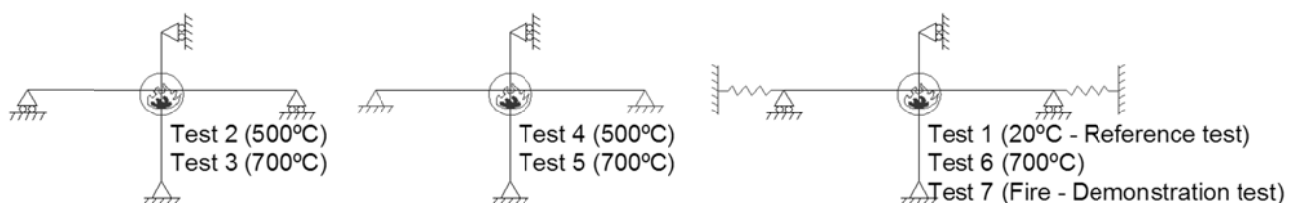


Fig. 1. Seven experimental tests

The two dimension sub-structure tested in Coimbra was selected from the actual composite building specially designed for the European ROBUSTFIRE project (Demonceau, 2010; Gens, 2011). This building was chosen to be the most general possible in order to obtain, at the end of the project, general rules on the design of such structures that ensure sufficient robustness under fire conditions. The selected structure is a braced open car park structure with eight floors of 3 m height, composite slabs, composite beams and steel columns. The sub-structure is defined by two unprotected composite beams with IPE550 steel cross-sections, grade S355, and one unprotected HEB300 cross-section steel column, grade S460 (Fig. 2). The steel beams are fully connected to the 130 mm thickness composite slab by 22 shear studs, and to the column by a flush end-plate with eight steel

bolts M30 cl. 10.9 (Fig. 3). In order to ensure the composite behaviour of the beam-to-column connections, ten steel rebars of diameter 12 mm are placed in the composite slab at each side of the column. Steel temperatures are increased using Flexible Ceramic Pad (FCP) heating elements. The heated zone consists of a length of 0.6 m of beam at each side of the joint, of the bolts and of 1 m of column. Servosis hydraulic jack ($F_{max.} = 1000 \text{ kN}$; $\Delta_{max.} = 280 \text{ mm}$) is used to apply the mechanical loading at the column top.

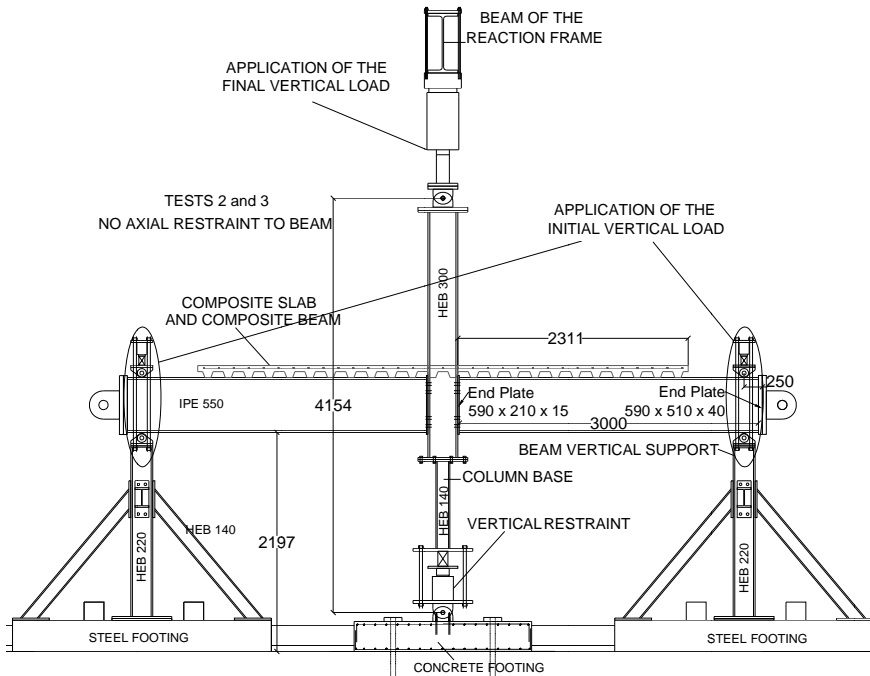


Fig. 2. General layout, longitudinal view of Tests 2 and 3



Fig. 3. Composite beam-to-column joint

2 NUMERICAL MODELS TO PREPARE THE EXPERIMENTAL TESTS

In order to define and to prepare the experimental tests, two simple preliminary models simulating the tests were performed in ABAQUS, v6.10. The first numerical model was used to define the initial loading: the initial load step reproduced the internal loads in the beam-to-column connections as in the actual car park. The applied hogging bending moment was predicted in this simple 2D model, using the loads at the service limit state (SLS) defined during the design of the car park structure (Fig. 4).

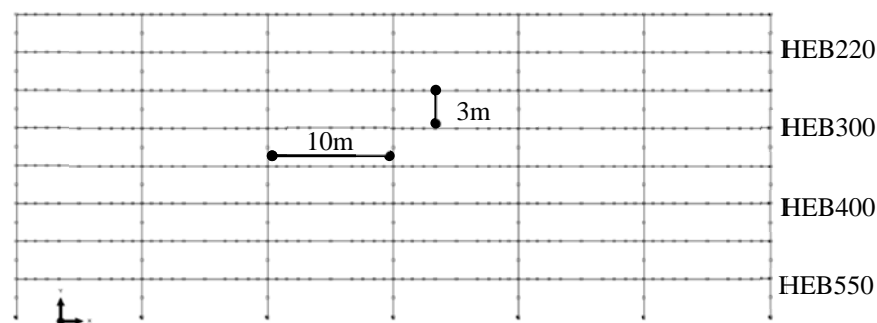


Fig. 4. Steel composite open car park modelled in ABAQUS

For the beam-to-column connections between the composite beams and the HEB 300 column, a hogging bending moment equal to -450 kNm was given in ABAQUS. According to EC1 part 1.2, effects of actions under fire may be deduced from those determined at ambient temperature, by

calculating a reduction factor η_{fi} (53% in this case), resulting in a target hogging bending moment of -236 kNm.

The second numerical model (sub-structure to be tested in the laboratory) was performed to define the required capacities of the load cells, displacement transducers, hydraulic jack and the axial restraints at the ends of the beams. Because the increase of the temperature with the FCP elements was not yet known before the tests, the temperatures into the cross-sections were obtained by a heat transfer analysis (ISO 834 fire curve was adopted). This heat-transfer problem involves conduction, and boundary radiation and convection (0.5 and 25 W/m²K respectively). The two heat transfer models (composite steel-concrete beam and steel column) were developed using 2D deformable elements DC2D4. The analyses were stopped once the beam bottom flange temperature reached 500°C or 700°C. After the heat-transfer analysis, a static analysis was performed. Materials temperature dependent properties were defined according to EC3 part 1.2 for steel and EC2 part 1.2 for concrete. The thermal expansion coefficient was defined constant equal to 1.4 x 10⁻⁵ /°C and 1.8 x 10⁻⁵ /°C for steel and concrete respectively. The true stress-logarithmic strain measures ($\sigma - \varepsilon$) calculated by the equation (1) were used in ABAQUS (Malvern, 1969):

$$\sigma = \sigma_{nom} (1 + \varepsilon_{nom}) \text{ and } \varepsilon = \ln(1 + \varepsilon_{nom}) \quad (1)$$

where σ_{nom} and ε_{nom} are respectively the nominal stress and nominal strain.

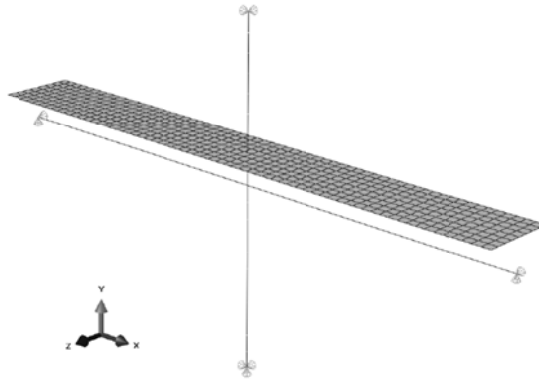


Fig. 5. Sub-frame modelled in ABAQUS (test 2)

Beams and columns were modelled by 3D beam elements B31, and the composite slab was simplified by a reinforced concrete slab using shell elements S4R (Fig. 5). Steel rebars were specified in the later by adding layers of reinforcement within the shell element virtual thickness at specified depth and angle of orientation. For the three tests with realistic axial restraint (tests 1, 6 and 7), connector elements were used to model the elastic linear behaviour of the “spring” restraint to beam (50 kN/mm). The full interaction between steel and concrete was modelled using a Tie constraint, and in this simple model, a Coupling constraint was used between beams and column simulating a rigid beam-to-column connection. No initial imperfections were applied. Each loading step was applied as to be performed in the laboratory (Haremza et al., 2011): step 1 – mechanical loading up to reach the target hogging bending moment in the joint (previously calculated); step 2 – heating of the joint zone with the temperatures obtained from the heat transfer analyses (applied as predefined fields); and step 3 – simulation of the loss of the column and increase of the sagging bending moment up to the failure of the joint, with the temperatures maintained constant. Thermal loading was defined at specific points through the beam/shell sections (ABAQUS Manual, 2010). From these analyses, the following conclusions were obtained: i) the maximum vertical load at the column top, leading to the failure of the joint under sagging bending moment (900 kN in the numerical model of test 1), was lower than the Servosis hydraulic jack capacity; ii) pins to link the axial restraint to the beam were designed according to the results of tests 4 and 5 (total axial restraint), for which the horizontal reaction load was the biggest (about 2200 kN in the numerical model); iii) load cells and displacement transducers were selected from the reaction loads and displacements numerical results.

3 NUMERICAL MODEL OF THE END-PLATE DEFORMATION

In the three experimental tests performed up to now, a localised deformation was observed at the steel end-plate centre (Fig. 10). A detailed three-dimensional model was developed in ABAQUS to reproduce and to study this end-plate local deformation. Steel temperature dependent properties are defined according to EC3 part 1.2, with steel S355 for the end-plate and S460 for the column. Bolts strain behaviour is estimated from previous experimental tests performed on M20 bolts grade 10.9 at ambient temperature, see Fig. 6 (Santiago, 2008). This curve is modified at elevated temperatures according to the reduction factors defined in EC 3 part 1.2 for the steel elastic modulus and for bolt tension and shear. The thermal steel expansion coefficient is defined constant ($1.4 \times 10^{-5} / ^\circ\text{C}$).

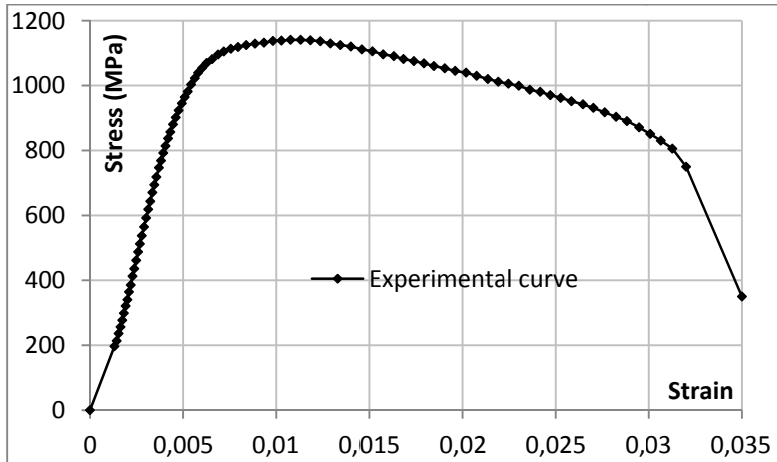


Fig. 6. Experimental and approximated bolt strain behaviour for grade 10.9 bolt (Santiago, 2008)

The symmetry of the joint is taken into account and half of the column, the end-plate and eight bolts are modelled combining C3D8R solid elements (Fig. 7). The axial displacement in the Y-direction is restrained, and at the bottom of the column, the displacements in the directions Y and Z are restrained. An initial deformation of the end-plate centre (0.6 mm) is measured before the experimental test 3 and is reproduced in ABAQUS.



Fig. 7. Numerical model in ABAQUS

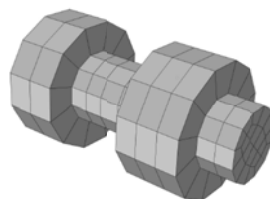


Fig. 8. Bolt mesh

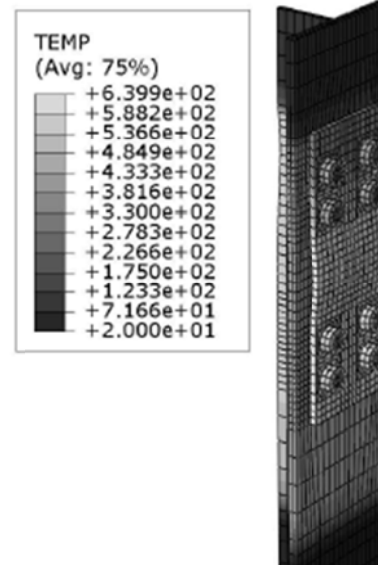


Fig. 9. Temperature results

Contact interactions are defined between the plate and the column flange, and between each bolt and the column flange and the end-plate: nut – column flange; bolt head – end-plate; bolt shank –

column flange hole; bolt shank – end-plate hole. Contacts are defined as surface-to-surface contact with a small sliding option. Normal contact is defined as “hard contact” with default constraint enforcement method, and separation is allowed after contact. The friction coefficient 0,25 is used in the tangential behaviour with penalty friction formulation. Bolts are meshed with the coarser mesh and their surfaces are defined as the master surfaces (Fig. 8). The static analysis algorithm is really difficult to solve once contact pairs are defined (33 in this model), and an easy way to pass through this is to pre-load the bolts at the beginning of the analysis, using the “Bolt load” option. A force is applied in each bolt equal to the pre-loading effectuated in the laboratory (120 kN). Bolt head and the nut are modelled circular as two washers are used.

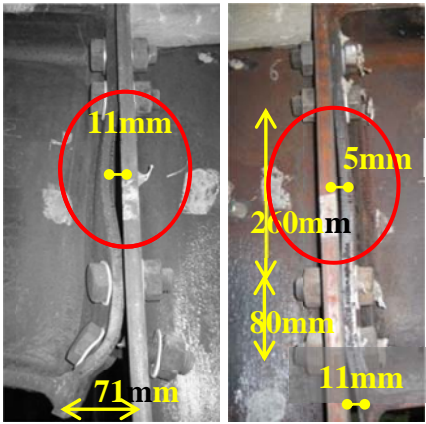


Fig. 10. Joint deformation in test 3

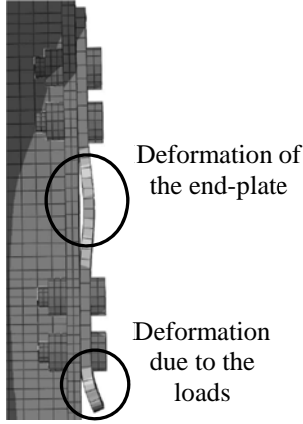


Fig. 11. End-plate deformation modelled in ABAQUS (Scale 2:1)

In this model, three load steps are defined: 1 – pre-loading of bolts, 2 – increase of temperatures, and 3 – increase of the horizontal displacement of the end-plate bottom part in order to approximate the real deformation under sagging bending moment (Fig. 11). Temperatures measured during test 3 are directly applied in the elements using the predefined temperatures. The temperature gradient measured in the end-plate and the column is applied, with four different temperatures in the plate and two different temperatures in the column web and in the column flange (Fig. 9). The comparison between the test and the numerical model is showed in Fig. 10 and Fig. 11. The end-plate deformation obtained by the numerical model is similar to the deformation obtained by the experimental test, and this local deformation happens during the increase of temperatures (step 2). Currently, the numerical model of the entire sub-frame tested in the laboratory is in development (Fig. 12). The composite slab is modelled with the steel rebars, concrete damaged plasticity material model, and ribs are modelled with a rectangular section in order to simplify the mesh of this part.

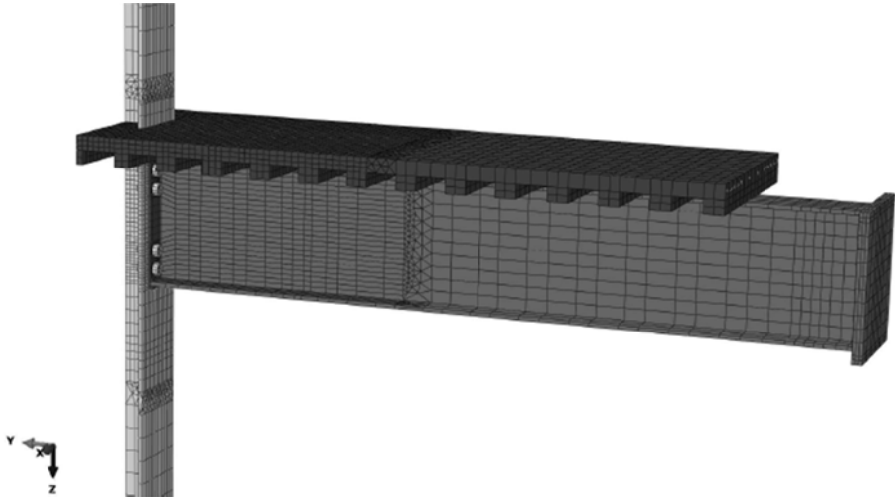


Fig. 12. Detailed 3D model in ABAQUS

A Tie constraint is used between concrete slab and the steel beam to model the total interaction. Because of the symmetry, only half of the frame is modelled. In this numerical model, the loading steps performed as in the experimental test are reproduced. Calibrations of the 3D finite element (FE) model against the test results are in development.

4 FINAL REMARKS

In this paper, preliminary numerical models, performed in order to prepare the experimental tests, and a more sophisticated 3D model of the localised joint deformation observed after some tests, were presented and described. As part of the ROBUSTFIRE project, the next step will be to experimentally study the influence of the axial restraint to beam and to observe the combined bending moment and axial loads in the heated joint when catenary action develops in the frame, and continue the calibration of the 3D FE models with the experimental tests results.

ACKNOWLEDGEMENTS

Financial support from the European Union (Research Fund for Coal and Steel) under contract grant RFSR-CT-2008-00036 and material support provided by PECOL, FELIZ and MARTIFER are gratefully acknowledged.

REFERENCES

- ABAQUS Theory Manual & Users Manuals, v. 6.10, Hibbitt, Karlsson and Sorensen, Inc. USA, 2010.
- Demonceau, JF, “ROBUSTFIRE Project - Design of the joints - notes”, Internal document, University of Liège, 2009.
- EN 1992-1-2:2004, “Eurocode 2: Design of concrete structures – Part 1-2: General rules – Structural fire design”, European committee for standardization, 2004.
- EN 1993-1-2:2005, “Eurocode 3: Design of steel structures – Part 1-2: General rules – Structural fire design”, European committee for standardization, 2005.
- Gens, F, “ROBUSTFIRE Project - Pre-dimensionning of the reference’s car park”, Internal document, Greisch, 2010.
- Haremza, C, Santiago, A, Simões da Silva, L, “ROBUSTFIRE Project, Document 6 – Experimental Tests – v2”, Internal document, University of Coimbra, 2011.
- Malvern L.E., “Introduction to the mechanics of a continuous medium”, Englewood Cliffs, NJ: Prentice-Hall, 1969.
- Santiago A., “Behaviour of beam-to-column steel joints under natural fire”, Ph.D. Thesis, Department of Civil Engineering, University of Coimbra, 2008.
- Simões da Silva, L, Santiago, A, Haremza, C, “ROBUSTFIRE Project, Document 1 – Car Parks – v1(11)”, Internal document, University of Coimbra, 2009.

A MACROSCOPIC FINITE ELEMENT BASED COMPUTER MODEL FOR EVALUATING THE FIRE RESPONSE OF FRP-STRENGTHENED REINFORCED CONCRETE BEAMS

Ahmed, A.^a, Kodur, V.K.R.^b

^a Principal Structural Engineer, Directorate of Design & Consultancy, Pakistan

^b Professor, Department of Civil and Environmental Engineering, Michigan State University, USA

INTRODUCTION

Fiber Reinforced Polymers (FRP) are widely used to strengthen and rehabilitate structural members mainly due to its high strength, light weight, durability, cost effectiveness and ease of application. In buildings, externally bonded FRP is effectively applied to increase the flexural capacity of existing reinforced concrete (RC) structures. When used in buildings, performance of FRP under fire exposure remains a major concern. However, there have been only limited experimental and numerical studies on fire resistance of FRP-strengthened RC beams. Thus, there is very little guidance available in codes and standards for the fire design of FRP-strengthened RC beams.

In recent years, limited fire tests have been conducted to study the fire performance of FRP-strengthened RC members and most of these were aimed at developing fire resistance ratings. However, the behavior of FRP-strengthened RC beams has not been studied under realistic fire, loading, restraint and bond conditions. In the case of numerical modeling, only thermal response has been studied under standard fire exposure, without giving any due consideration to overall structural response, effect of fire induced bond degradation and axial restraint force. Thus, the absences of reliable numerical models, and relatively high cost of fire tests are the two main reasons for lack of rational fire design provisions in codes and standards. To overcome this, a macroscopic finite element model has been developed for evaluating fire response of FRP-strengthened RC members. The proposed model accounts for high temperature properties for concrete, steel, FRP and insulation to capture the fire response of FRP-RC beams under realistic fire, loading and restraint scenarios. The, model also accounts for FRP-concrete substrate bond slippage in the analysis. A summary of the model features, together with its validation and case studies is presented in this paper.

1 COMPUTR PROGRAM

1.1 Calculation Procedure

A macroscopic finite element (FE) based computer model that utilizes moment-curvature relationships is developed to trace the response of FRP-strengthened RC beams under fire conditions (Ahmed 2010). In the analysis, the beam is idealized by dividing it into a number of segments along its length and the mid-section of each segment is assumed to represent the overall behavior of the segment. This mid-section is discretized into a number of elements as shown in Fig. 1.

In the analysis, the total fire exposure time is divided into number of time steps and at each time step, the response of the beam is traced through the following steps:

- Establishing temperatures due to fire exposure (standard and design fires).
- Conducting heat transfer analysis to determine temperature distribution in segmental cross-section.
- Calculating the slip (ϵ_{slip}) at the interface of FRP and concrete.
- Generating moment curvature ($M - \kappa$) relationships for each beam segment and performing beam analysis to compute internal forces and deflections.

The various steps involved in the fire resistance analysis are illustrated in the flow chart (see Fig. 2). At each time step, thermal analysis is carried out to determine the temperature distribution within

the cross-section of each segment utilizing high temperature thermal properties of constitutive materials. The computed cross sectional temperatures form the input to strength analysis, wherein, time dependent $M - \kappa$ relationships are generated for each beam segment. For evaluating these $M - \kappa$ relations, various strain components in each element of concrete, steel and FRP are added to obtain effective mechanical strains, and then stresses are evaluated using relevant high temperature stress-strain relationships. The initial strain (ϵ_{bi}) in FRP is evaluated based on dead loads at the time of retrofitting, while bond-slip (ϵ_{slip}) along the length of the beam segment is calculated as described in the Reference (Ahmed and Kodur 2011).

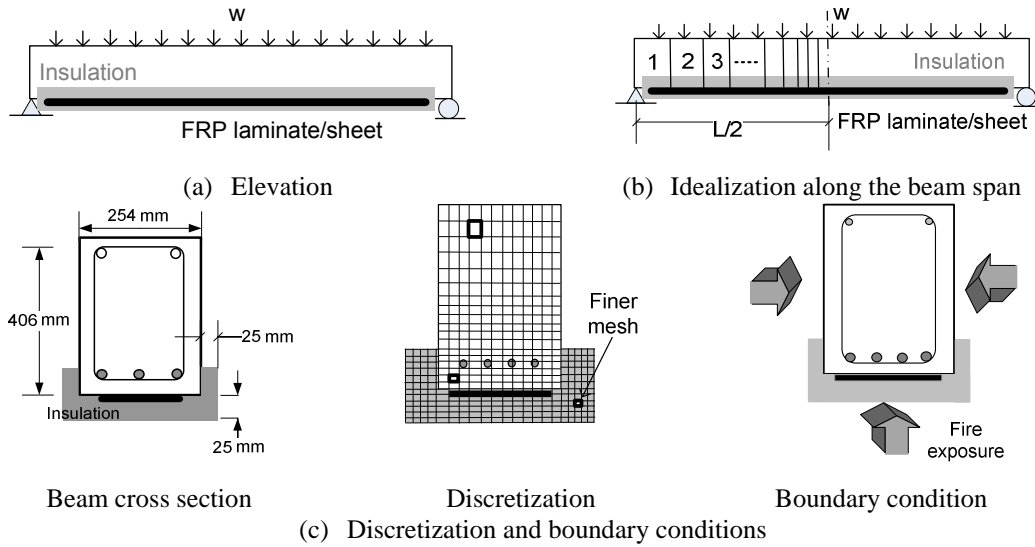


Fig. 1: Layout of typical FRP-strengthened RC beam, its idealization and discretization for analysis

At each time step, the computed forces are used to check force equilibrium. For an assumed total strain at the top layer of concrete ($\epsilon_{c,T}$), curvature (κ) is iterated until force equilibrium is satisfied. This iterative procedure is repeated till equilibrium, compatibility and convergence criterion are satisfied. Once these conditions are satisfied, moment and curvature corresponding to that strain is computed. Through this approach, various points on the moment-curvature curve are generated for each time step.

Following the generation of $M - \kappa$ relationships, an iterative procedure described by Cambell and Kodur (1990) is employed to evaluate deflections of the beam at each time step. In this approach, the stiffness matrix and the loading vector are computed for each longitudinal beam segment, assembled in the form of a nonlinear global stiffness equation, and solved to compute deflections at that time step:

$$[K_g] [\delta] = [P] \quad (1)$$

where: K_g = global stiffness matrix, δ = nodal displacements, $P = P_f + P_s$ where P_f = equivalent load vector due to applied loading and P_s = equivalent nodal vector due to $P - \delta$ effect.

The model generates various output parameters, such as cross sectional temperatures, stresses, strains, deflections and moment capacity for each time increment. These parameters are checked against pre-designated failure criterion, which include thermal and structural considerations. The time increment continues until one of the limiting criteria is reached. At this time step, the beam is said to have failed. The time duration to reach this failure point is the fire resistance of the beam. Full details on the development of the computer model, including the evaluation of various strains, stresses, bond-slip and forces are given by Kodur and Ahmed (2010).

In the model, any or all of the following limiting criteria can be applied to evaluate failure of the FRP-strengthened RC beam:-

- The moment due to applied load exceeds the strength capacity of the beam.
- The temperature in reinforcing steel (tension reinforcement) exceeds 593°C .

- The deflection of the beam exceeds $L/20$, where L is the length of the beam, at any fire exposure time.
- The rate of deflection exceeds the limit $L^2/9000d$ (mm/min) where L is the length of the beam (mm); and d , effective depth of the beam (mm).
- The temperature in FRP layer exceeds glass transition temperature (T_g) of FRP.

It should be noted that the user has the option to specify any (or all) of the five limit states to define failure.

1.2 High Temperature Material Properties

For modeling the response of FRP-strengthened beams, high temperature properties of concrete, steel reinforcement, FRP, adhesive and insulation are required. These properties include thermal, mechanical and deformation properties which vary as a function of temperature. In literature, there is reliable data on high temperature properties of concrete and steel. However, knowledge is limited on high temperature properties of FRP, adhesive and insulation. For concrete and steel, the properties suggested by ASCE Manual (Lie 1992) and for FRP and insulation, semi-empirical relationships suggested by Bisby (2003), have been incorporated into the model. To account for bond-slip at the interface of FRP-concrete, bond stress-slip curves presented by Leone et al. (2009) have been included in the model. These curves provide data for shear modulus (G) as function of temperature to compute bond-slip (ϵ_{slip}) at interface of FRP-concrete. For adhesive and insulation, properties available in the literature are utilized (Ahmed 2010).

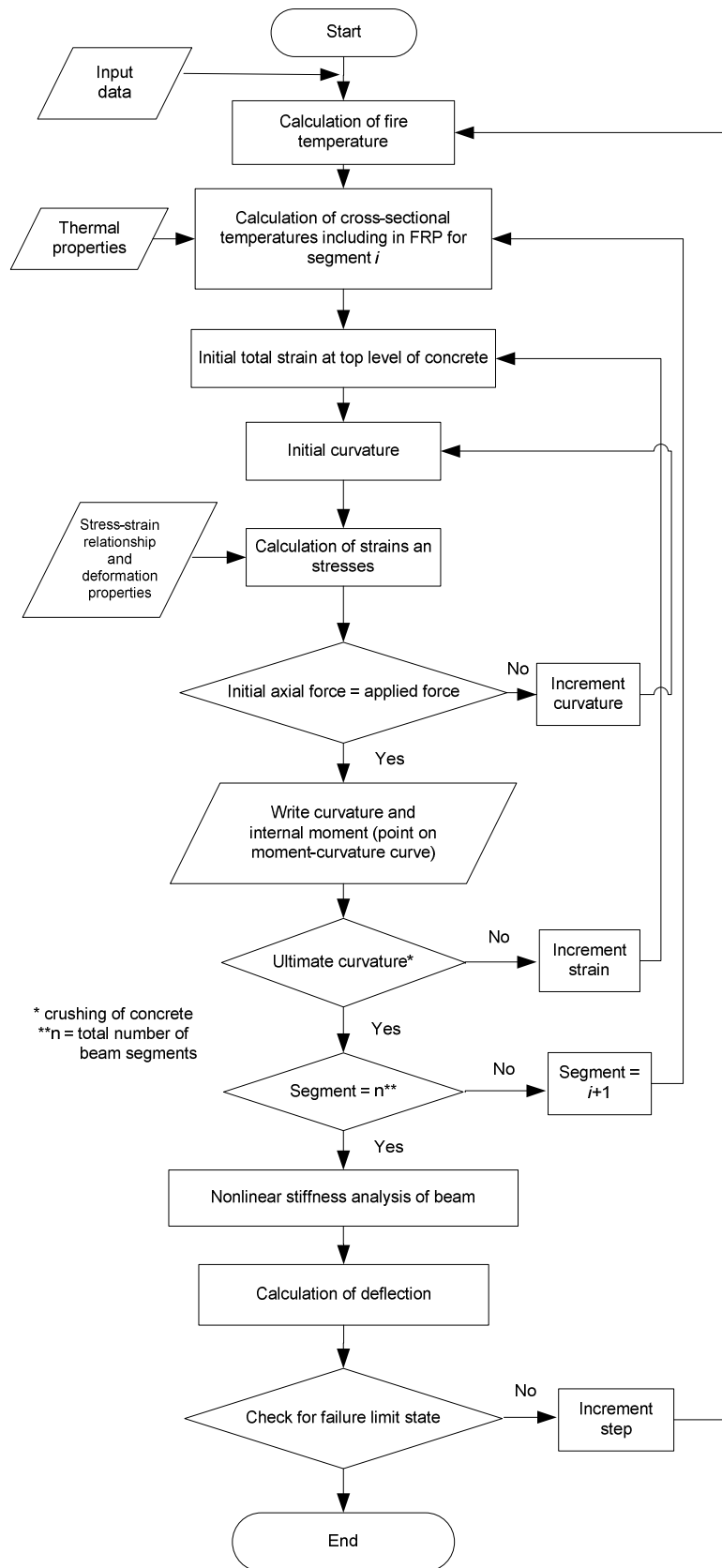


Fig. 2: Flow chart of analysis procedure used in computer program

2 VALIDATION OF MODEL

The above computer program is verified by comparing predictions from the model with measured data on a number of FRP-strengthened RC beams tested in Canada, USA and Europe. This paper presents validation on four FRP-RC beams (designated as Beams B1 to B4), tested as part of research at Michigan State University (Ahmed and Kodur 2010). Full details on the test beams are given by Ahmed (2010).

The thermal validation on one of the four tested FRP-RC beams (Beam B1) is presented here. Fig. 3 shows a comparison of temperatures at FRP/concrete and FRP/insulation interfaces, and at three different locations (TC5, TC6 and TC9) in the beam cross section. TC5 represent temperature in compression reinforcement, TC6 represent corner rebar temperature (flexural reinforcement) while TC9 is at mid-depth of beam cross section (203 mm). It can be seen (refer to Fig. 3 (a)) that the measured and predicted temperatures are in good agreement throughout the fire duration.

Fig. 3 (b) provides a comparison between predicted and measured temperatures at FRP/concrete and FRP/insulation (VG) interfaces. These temperatures are critical indicators of the performance of FRP under elevated temperatures. The model predicts temperature fairly well up to 40 minutes of fire exposure time. Beyond this, the model under predicts temperature at FRP/insulation interface and over predicts FRP/concrete interface temperatures. This could be attributed to the fact that measured temperature at FRP/insulation interface increase rapidly after 40 minutes due to localized burning of epoxy as a result of crack propagation in insulation. Due to this localized burning, measured temperatures are higher as compared to that predicted by the model. On the contrary, increase in temperatures recorded at FRP/concrete interface is slightly lower than predicted by the model. The possible reason for this temperature lag could be due to the formation of char layer as a result of thermal decomposition of epoxy (pyrolysis process) that acts as a thermal barrier and restricts heat flow to inner interface. The analysis of various other FRP-RC beams showed that the model predicts temperature progression reasonably well Ahmed (2010).

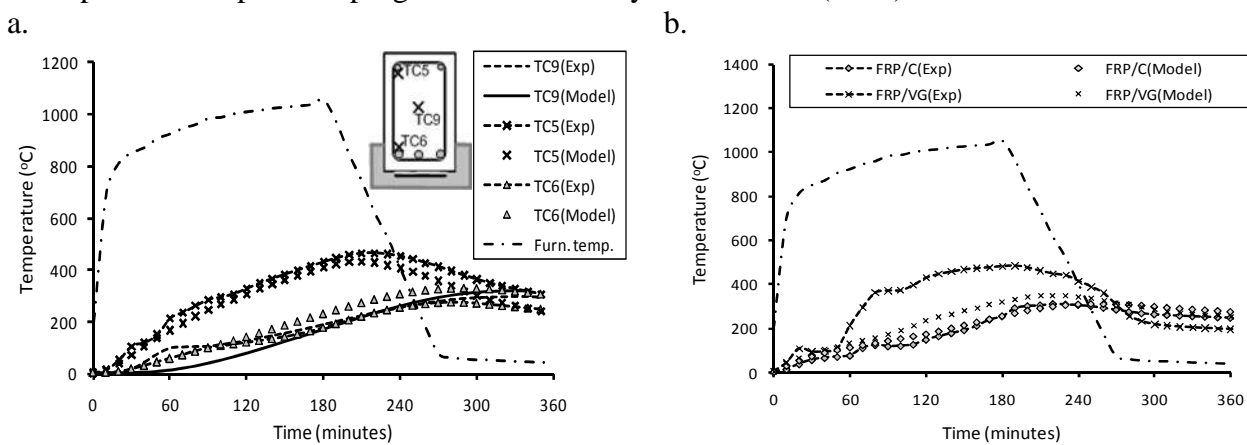


Fig. 3: Measured and predicted temperatures for FRP-RC Beam 1

The predicted and measured mid-span deflections for four tested FRP-RC beams are compared in Fig. 4(a). There is a good agreement between measured and predicted deflections for all four beams. Compared to observed time of FRP debonding at about 20-25 minutes, the model predicts it around 30 minutes. This variation can be attributed to the discrepancy between measured and predicted temperatures at interface of FRP as discussed above. For axially restraint beam B4, the result of predicted and measured axial restraint force is in good agreement for entire duration of the test (refer to Fig. 4(b)). Overall, the model provides reasonable estimates of cross-sectional temperatures, deflections and restraining force.

A comparison of fire resistance of FRP-RC beams as predicted in model and seen in tests is tabulated in Table 1. The time to reach failure is defined as the fire resistance of the structural member. All four FRP-strengthened RC beams sustained load during the entire fire tests (more than 3 hours). The results from the analysis show that the beams met the rebar temperature criterion and strength failure criteria specified in codes and standards. Analysis of the tests data showed that glass transition temperature of FRP exceeded in about 20-25 minutes which resulted in FRP debonding.

However, no strength failure occurred in FRP-strengthened beams. Thus, glass transition temperature failure criterion is overly conservative for insulated FRP-strengthened RC beams.

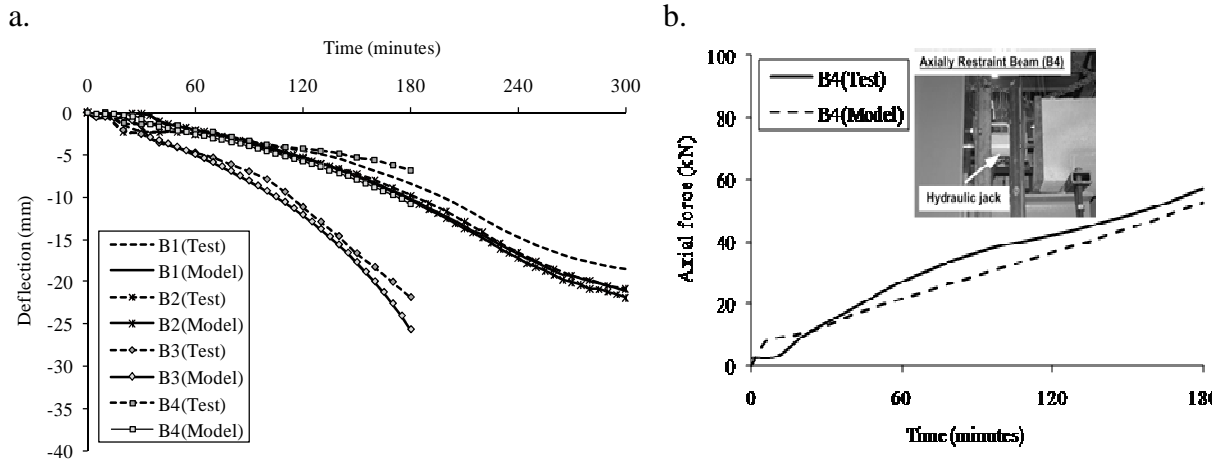


Fig. 4: Measured and predicted mid-span deflections and axial restraint force

Table 1 Summary of test parameters and of tested beams

Beam	CFRP strengthening	Insulation type	Insulation thickness (mm)		Fire scenario	Support condition	Load (kN)	Failure time (min)
			VG	EI-R				
B1	2 layers of 203 mm wide	Tyfo® WR AFP-Type A	25	0.1	Design fire	SS	70	NF*
B2		Tyfo® WR AFP-Type B	25	0.1	Design fire	SS	70	NF*
B3		Tyfo® WR AFP-Type A	25	0.1	ASTM E119	SS**	70	NF*
B4		Tyfo® WR AFP-Type A	25	0.1	ASTM E119	AR***	70	NF*

* NF – No failure ** Simply supported *** Axially restrained

3 CASE STUDY

The above developed computer program can be applied for evaluating fire response of FRP-strengthened RC beams and also for developing effective insulation schemes for achieving optimum fire resistance levels. This is illustrated through a numerical example. The selected beam (6.7 m in length and a cross section of 380×610 mm) is made with concrete of compressive strength $f'_c = 38\text{ MPa}$, yield strength of steel $f_y = 414\text{ MPa}$. The beam is strengthened in flexure by providing three layers of unidirectional CFRP at the tension face of the beam. These CFRP layers are applied at full width (380 mm) of the beam cross section. For fire protection, Tyfo® VG (vermiculite gypsum) insulation is applied at the bottom of the beam that extends 105 mm on two sides of the beam cross section. The thickness of insulation is kept 20 mm (constant) except when specified. The fire resistance of this beam was evaluated based on thermal, strength, and deflection failure criteria. Full details of analysis, including discretization and material properties, are given in Reference (Ahmed 2010).

3.1 Insulation Layout

In FRP-strengthened RC members, insulation layout is an important consideration for achieving fire resistance. The fire insulation helps to keep overall beam cross sectional temperatures low. Therefore, proper detailing of insulation can help to keep the temperatures low not only in FRP but also in tension steel reinforcement and help in achieving optimum insulation levels. An optimum geometric insulation configuration was developed to achieve good fire resistance in FRP-strengthened RC beams (Ahmed 2010).

The five insulation schemes that can be adopted for FRP-strengthened RC beam with rectangular beam cross section are shown in Fig. 4 (Ahmed 2010). It has been established that externally

bonded FRP without fire protection is not appropriate for FRP-strengthened RC beams (Gamage et al. 2006). Therefore, FRP without supplemental insulation is not recommended (refer to Fig. 4(a)). The two insulation configurations shown in Fig. 4(b) and (c) do not lead to optimum protection since rebar temperatures will not be kept for sufficient time to yield good fire resistance. From the parametric studies and fire tests, it was found that extending the insulation to two times the depth of concrete cover ($2C_c$) from bottom of the beam cross section (on either side) is required to achieve optimum fire resistance (Ahmed 2010). Based on these results, the two recommended insulation configurations are shown in Fig. 4(d) and (e). Both these insulation configurations can provide effective fire protection to overall beam cross section. However, the insulation scheme shown in Fig. 4(d) is the most preferred option, as compared to the one shown in Fig. 4(e), since applying insulation along complete exposed surfaces of the beam cross section is not practical and is an expensive proposition. A similar insulation schemes was also developed for FRP-strengthened T-beams (Ahmed 2010).

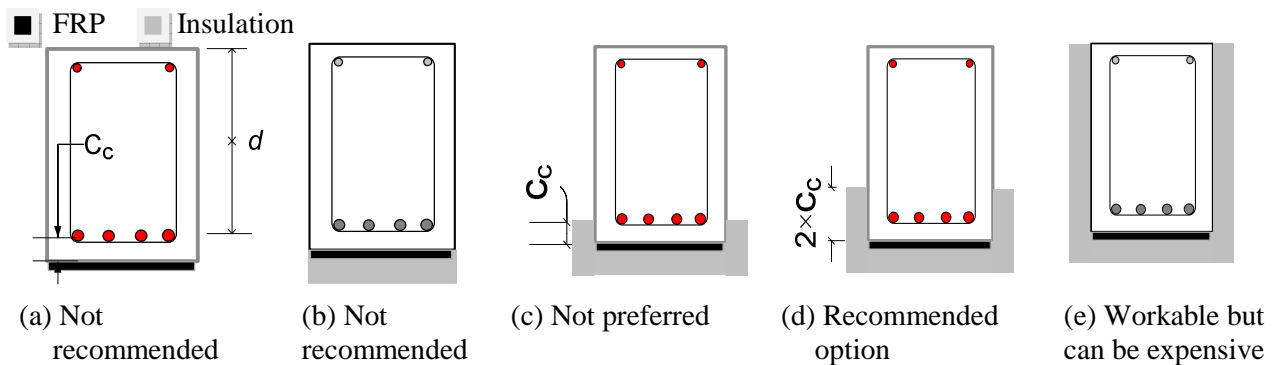


Fig. 4: Proposed geometric configuration schemes for fire insulation in FRP-strengthened RC beams

3.2 Insulation Thickness

Apart from the geometric configuration, insulation thickness is another key factor that governs fire resistance of FRP-strengthened RC beams. The effectiveness of insulation on fire resistance mainly depends on the thickness, specific heat and thermal conductivity properties of fire insulation. The fire resistance of FRP-strengthened RC beams increases with insulation thickness. However, there is a certain level of thickness beyond which any further increase in the thickness is not beneficial. This level of insulation thickness is referred to as "*optimum insulation thickness*".

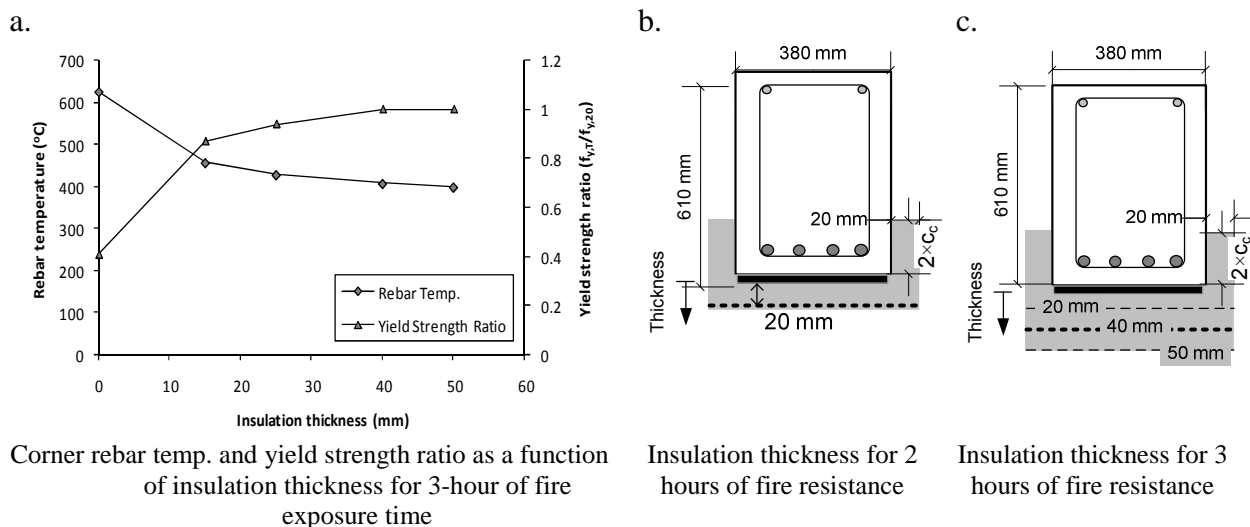


Fig. 5 Proposed optimum thickness for fire insulation in FRP-strengthened RC beams

For flexural members such as beams, it is not desirable to have insulation thickness beyond an optimum value since it adds to weight of the structures and accelerate insulation fall off under increased dead weight, especially when beam deflections increase under fire conditions. The insulation also limits the temperature rise in steel reinforcement and this in turn helps to achieve

higher moment capacity at a given fire exposure time. However, beyond optimum insulation thickness, at which steel rebar temperatures reaches about 400°C, any further reduction in steel reinforcement temperature does not result in higher tension force or capacity of the beam, as shown in Fig. 5(a) (Eurocode 2 2004). Figs. 5(b) and (c) shows the optimum insulation thicknesses recommended for FRP-strengthened RC beam and these thicknesses were derived through parametric studies for an insulation that has thermal conductivity of 0.12 W/m-°K (Ahmed 2010). An optimum insulation thickness of 40 mm is required to achieve 3 hours of fire resistance while a minimum of 20 mm thickness is needed to achieve a fire resistance up to 2 hours.

SUMMARY

The proposed macroscopic finite element based computer model, is capable of predicting the fire response of FRP-strengthened RC beams under wide range of design scenarios. The model accounts for high temperature material properties of constitutive materials, fire induced bond degradation, axial restraint force, and different strain components. The computer model can be applied to quantify the influence of various parameters (such as insulation schemes) on the fire response of FRP-strengthened RC beams and recommend broad guidelines for enhancing fire resistance. Such fire design guidelines, like the ones presented in this paper, will facilitate the wider use of FRP in strengthening of concrete members in buildings and other structures, where fire safety is one of the crucial issues.

ACKNOWLEDGEMENTS

The research presented in this paper is supported by the National Science Foundation (Grant No. CMMI 0855820) and Michigan State University through Strategic Partnership Grant (Award No. SPG 71-4434). Any opinions, findings, conclusions and recommendations expressed in this paper are those of the authors and do not necessarily reflect the views of the sponsors.

REFERENCES

- Ahmed, A. (2010). "Behavior of FRP-strengthened Reinforced Concrete Beams under Fire Conditions," Doctoral Thesis, Michigan State University, East Lansing, USA.
- Ahmed, A., and Kodur, V. K. R. (2010). "Performance of FRP-strengthened Reinforced Concrete Beams under Design Fire Exposure." Proceedings of Sixth International Conference on Structures in Fire, East Lansing, Michigan.
- Ahmed, A., and Kodur, V. K. R. (2011). "Effect of bond degradation on fire resistance of FRP-strengthened reinforced concrete beams." Composites Part B: Engineering, 42(2), 226-237.
- Bisby, L. A. (2003). "Fire behavior of fibre-reinforced polymer (FRP) reinforced or confined concrete," Doctoral Thesis, Queen's University, Kingston, Canada.
- Campbell, T. I., and Kodur, V. K. R. (1990). "Deformation controlled nonlinear analysis of prestressed concrete continuous beams." PCI Journal, 35(5), 42-90.
- Eurocode 2. (2004). "EN 1992-1-2: Design of concrete structures. Part 1-2: General rules - Structural fire design." European Committee for Standardization, Brussels, Belgium.
- Kodur, V. K. R., and Ahmed, A. (2010). "A Numerical Model for Tracing the Response of FRP Strengthened Reinforced Concrete Beams Exposed to Fire." Journal of Composites for Construction, 14(6), 85.
- Leone, M., Matthys, S., and Aiello, M. A. (2009). "Effect of elevated service temperature on bond between FRP EBR systems and concrete." Composites Part B, 40(1), 85-93.
- Lie, T. T. (1992). "Structural fire protection." ASCE Committee on Fire Protection, Structural Division, American Society of Civil Engineers, New York, NY, 225-229.

FIRE PROTECTION OF STEEL STRUCTURES USING AUTOMATIC WATER EXTINGUISHING SYSTEM

Jyri Outinen ^a

^a Rautaruukki Corporation, Vantaa, Finland

INTRODUCTION

A continuation to a previous research program [1] has been carried out in Finland in order to study further the cooling effect of water extinguishing system in fire situation to steel structures. The objective was to study how the temperatures of the load-bearing structures including steel trusses, columns, bracing and corrugated sheeting develop in fire situation, when there's a sprinkler system present and acting. Possibility to use unprotected steel structures within certain limits when a specified sprinkler network is installed was investigated in this research.

The research is based on experimental fire tests and numerical simulation [2,3] carried out by VTT, Technical Research Centre of Finland. On the basis of these researches a national product approval [4] was achieved. Also a European product approval is applied for the system.

1 BACKGROUND

It is very common to have a 60-120 minutes fire resistance requirement to load-bearing structures in typical buildings in Finland and also in other European countries. Normally quite expensive passive fire protection, e.g. fire protection paint, gypsum boards, rock wool or other material to cover and protect the structure is needed to fulfil this requirement for steel structures. These are naturally simple ways of achieving the fire resistance, but there are also some problems with these solutions and high costs.

The objective of this research was to study whether the cooling effect of quite effective sprinkler systems ensure the fire protection of steel structures with no need for passive fire protection. It is known that automatic water suppression also keeps the fire local in most cases when functioning properly [5].

The fire protection is always expensive whether it is done by passive or active measures. That is why there's also a financial benefit when either of these can be totally or partly left out. The sprinkler system is more important when talking about protecting the people, which of course is more essential than the building itself. Naturally in some cases the passive protection is still more reasonable than using active measures.

When automatic water suppression is required to a building for common fire safety reasons, the use of it also as structural fire protection can be very cost-effective. With this system the structural fire resistance can be achieved simultaneously ensuring the life safety of the occupants or users of the building. When the fire sprinkler system is designed, installed and maintained properly, the risk that it won't work is very little [5]. As it is known the sprinkler systems are required in certain types of buildings with certain criteria. This differs from country to another, even within EU countries [6].

In some countries the structural fire resistance can be lowered when the fire sprinklers are present. Almost in every country some other benefits in fire safety design can be gained, e.g. bigger fire-compartments, compromises in smoke extraction etc. This is also the case in Finland and especially the fire-compartment size is a normal compensation.

The Authorities can then decide whether the water suppression system can also be used to lower e.g. the structural fire resistance requirements.

2 TESTING FACILITIES

2.1 Test arrangements

The previous fire tests were conducted in Finland in 2009. A small steel framed hall was constructed, the sprinkler system was installed to the ceiling and the studied steel trusses, beams and columns and other parts of the building were equipped with temperature detectors. The outer walls were left enough open from the bottom so that there would be enough oxygen for the fire. In Figure 1 the basic geometry and the sprinkler locations of the tested system are presented. The outer walls were constructed from sandwich panels and the roof was built from load-bearing corrugated steel sheets with insulations above it. Temperatures were measured also from the corrugated steel sheeting.

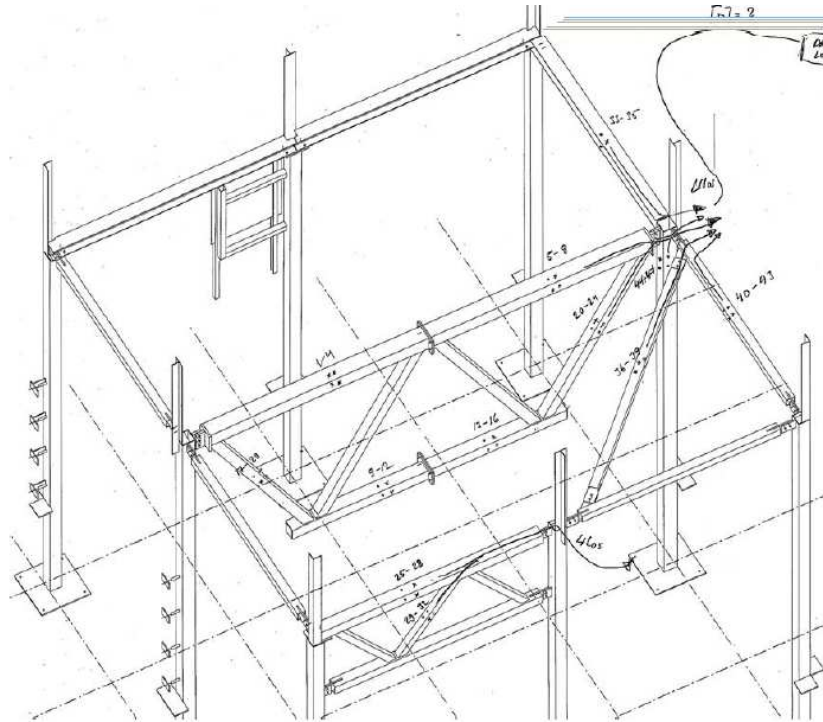


Fig. 1. Skeleton of the structures

2.2 Fire scenario

The system was tested against standard ISO-fire. The fire load was produced by heptan-spray burner, which was situated centrally under the studied structures spreading the fire with three nozzles. The test was run so far as to get enough information about the temperature development in the test room and in the structures to get the needed data for the product approval of the system.

2.3 Tested structures

The temperatures were measured from tubular steel trusses, beams and columns. Also the temperatures from the connections, bracing and steel sheeting were measured. The height of the steel truss was about 1,5m and it was built from different sized cross-sections. The temperatures were measured from different parts of the truss. The other structures were also selected so that they represented the smaller sized structures normally used, in order to widen the use of the results to bigger sections.

2.4 Water extinguishers

In the tests, three kind of sprinkler nozzle types were tested, ESFR (early suppression fast response), normal spray-nozzles and also conventional sprinklers. The water flow was set to a normal value used in building design. The pressure was set to quite low level. In ESFR tests only half of the nozzles could be used because of the huge amount of water produced by the system.

The sprinklers produce an umbrella shaped water flow. The watering is determined mainly to put down or at least restrict the fire from spreading around. At the same time water cools down the structures directly and very effectively as was found out in the research. Different sprinkler heads, or nozzles are presented in the following figure.

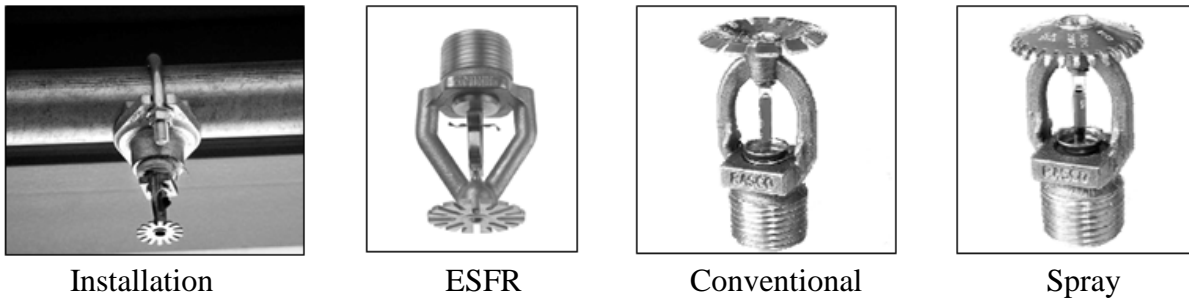


Fig. 2 Sprinkler nozzle types

2.5 Simulations

The fire test was also simulated using FDS (Fire Dynamics Simulator). The heating of the structures was studied. In the picture below the system is in use in a real commercial building in Finland. E.G this kind of system was simulated in fire situation.

Simulating sprinkler's effect is quite complicated, but the tools in FDS are being developed all the time. A separate 3-year project was carried out in Finland in 2008-2010. Ruukki was financing and participating to this research. The project "Fire Suppression" was carried out by VTT and the final report will be published soon.

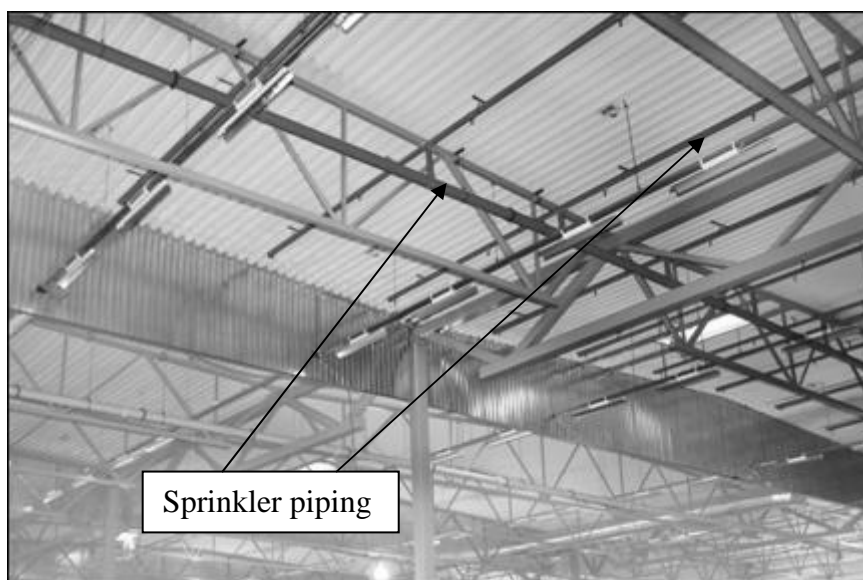


Fig. 3 Steel structures, sprinkler piping and nozzles

3 RESULTS

In the fire tests a standard fire exposure was set by using heptan-spray burners underneath the structure system. Temperatures from the installed structures were measured during the test. For the defined set of cross-sections, the temperatures of the steel structures did not raise above critical level in standard fire exposure. This can be noted from the figures 3 and 4.

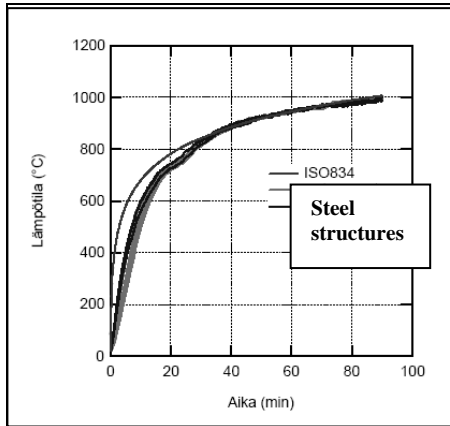


Fig. 4 Temperatures of the steel structures in free burn test. No sprinklers

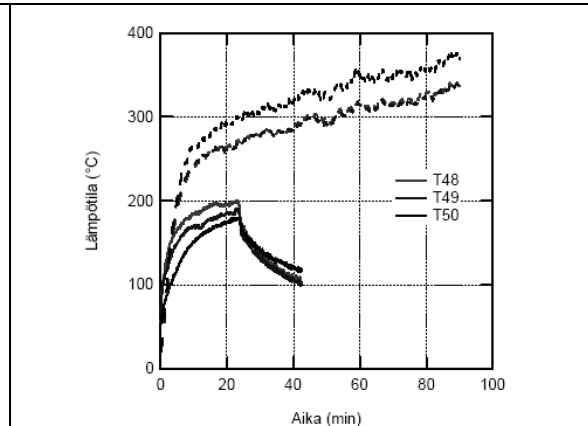


Fig. 5 Temperatures of the steel sheeting in sprinkler test. Dotted lines from simulation, solid lines from tests.

All in all the temperatures of the structures stayed at adequate level. On the basis of these tests product approval for 90 minutes fire rating was got to the systems. The tests went well and the measurements and simulations were carried out successfully.

On the basis of the tests a short design guide for structural design and also for the design of the water sprinkler system was introduced. In these instructions the limitations to the structures, cross-sections, structures' dimensions are set. For the water sprinklers the design principles concerning the water flow, number and location of the sprinkler nozzles are instructed.

4 SUMMARY

A research concerning the fire protection of steel structures in standard fire exposure was carried out in Finland. Structural fire protection of steel structures was studied using automatic water extinguishing systems. Several different sprinkler types were used to study the temperatures in selected steel structures. The research was carried out with fire tests and also simulations.

The aim was to study the possible fire resistance rating to the system and according to the research results; fire rating of R90 was accomplished. The temperatures of the steel structures stayed at very low level so that there is no need for additional fire protection in this kind of case.

This kind of systems will be used typically in 1-2 storey building at the moment, but the field of application will be widened in the future.

More research is planned to investigate different scenarios and structural systems.

REFERENCES

Outinen, Kansa, Fire protection of steel structures using water sprinklers, ASFE conference, Prague, 2009.

Fire protection of steel structures using sprinkler systems”, VTT Research report VTT-R-1871-10.

Fire protection of steel structures using sprinkler systems”, VTT Research report, VTT-R 7226-10

Steel structure with a water sprinkler system fire-protection, VTT Certificate VTT-C-4921-10, 2011.

Hietaniemi, J., Cajot, L.-G., Pierre, M., Fraser-Mitchell, J. Joyeux, D. & Papaioannou, K. Risk-Based Fire Resistance Requirements. Final Report. Luxembourg: Office for Official Publications of the European Communities 2005.

European sprinkler organisation homepage, www.eurosprinkler.org

ROLE OF CFD IN THE QUANTITATIVE ASSESSMENT OF STRUCTURAL PERFORMANCE IN FIRE SCENARIOS

Filippo Gentili, Luca Grossi, Franco Bontempi

Sapienza University of Rome, School of Engineering, Rome, Italy

INTRODUCTION

The quantitative assessment of the structural performance is based on a multiphysics analysis. In the process of calculating the structural behaviour, three essential models can be identified: a fire model, a heat transfer model and a structural model (Buchanan, 2002).

Computational fluid dynamics (CFD) simulation plays an important role in fire research. It allows evaluating the fire development and provides a new, efficient, reliable and economic path for fire investigations. As a consequence, it is considered nowadays an important fire research tool (Yeoh and Yuen, 2008). With the wide adoption of performance-based fire safety design, CFD simulation is becoming a routine practice for obtaining the necessary fire design information. With new developments in modelling techniques, fast increase of computing power, and quick drop of hardware price, it is expected that CFD simulation will keep gaining popularity in the fire research community. A CFD model permits a quite realistic representation of fire scenarios, because it takes into account the distribution of fuel, the geometry and the occupancy of individual compartments in a structure.

In this paper, an industrial hall has been considered as a case study. The development of fire of wooden pallets has been studied by means of a CFD code, FDS (McGrattan et al, 2009), considering different positions of the combustible material and different ventilation conditions. The adiabatic surface temperature (AST), (Duthinh et al, 2008), solves the heat transfer model and creates a link with FE codes in order to assess the structural performances.

1 CASE STUDY

The industrial hall considered as a case study is shown in Fig. 1. This structure has been previously investigated by Vassart et al. (2004). The system is composed by 5 frames, jointed by means of purlins. The length of the main slightly inclined beams is 20 m, and the height of the 15 columns is 5 m.

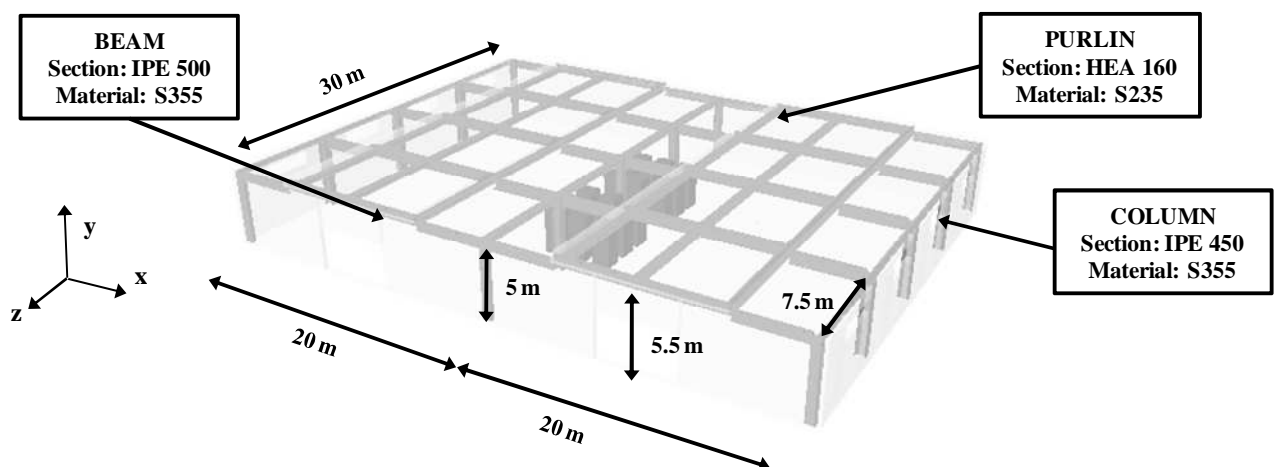


Fig. 1. Structure taken as case-study.

Due to the doors located on the longest building facade with an area of 30 m^2 , and due to the windows located on the shortest sides with an area of 28 m^2 , the opening factor of the structure is

equal to $0.265 \text{ m}^{1/2}$ and the fire results to be ventilation controlled, being the fire load significant as can be seen below. In the FDS model, the presence of structural elements is not important for the evaluation of the fire development, but it allows to compute the heat transfer model.

2 FIRE AND HEAT TRANSFER MODEL

2.1 Identification of the fire scenarios

The identification of the appropriate fire scenarios is essential to the design of a building that fulfils the fire safety performance objectives (ISO 13387, 1999). Fire scenarios define the ignition and fire growth process, the fully developed stage and the decay stage. In this case the fire triggered by the ignition of wood pallets has been considered. Conceptually, a wood pallet is a similar arrangement to a wood crib (Drysdale, 1999). The geometry, however, is different. Instead of being composed of identical rows of square-section sticks, pallets are made up of rectangular elements, whose typical setup is shown in Fig. 2.

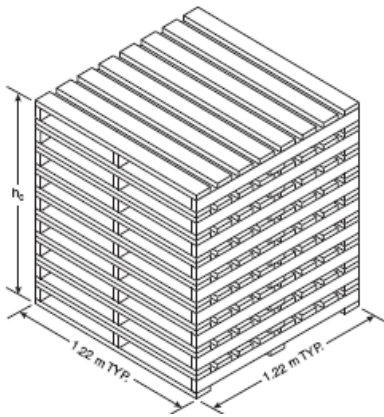


Fig. 2 Wood pallets

Height	3.05m
Size	1.2m x 1.2m
Weight of one pallet	15 kg
Weight of one stack of pallets	300 kg
Weight of all stacks	5400 kg
$HRR_{S,max}$	6810 MW/m^2
t_g	80 s
Where $HRR_{S,max}$ the maximum of heat-release-rate per unit area, t_g the characteristic time of fire	

Tab. 1 Properties of pallets

A typical experimental Heat-Release-Rate (HRR) curve shows that a constant plateau can be seen if the stack is reasonably high (Krasner, 1968). The burning of 18 stacks of pallets has been considered as a fire scenario. Tab. 1 shows the most important characteristics of considered pallets.

2.2 Optimization and validation of the model

The reliability of the fluid dynamic prediction of events is influenced by the size of the grid. In the Fire Dynamic Simulator there is a parameter that should always be considered, which is called characteristic fire diameter D^* and whose value is given in Eq. (1), (McGrattan et al, 2009):

$$D^* = \left(\frac{\dot{Q}}{\rho_\infty \cdot c_p \cdot T_\infty \cdot \sqrt{g}} \right)^{2/5} \quad (1)$$

where: \dot{Q} is the heat release rate, ρ_∞ is the ambient density, T_∞ is the ambient temperature, c_p is the specific heat, and g is the acceleration of gravity.

The description of the fire depends on the quality of this parameter, since it affects the combustion model by acting in the calculation of the fraction mixture, which describes the stoichiometric reaction that takes place. FDS employs a numerical technique known as Large Eddy Simulation (LES) to model the irresolvable or “sub-grid” motion of the hot gases. The effectiveness of the technique is largely a function of the ratio between the fire characteristic diameter D^* , the size of a grid cell δx . In a few words, the greater the ratio $D^*/\delta x$, more the simulation is accurate, due to the fact that the fire dynamics is resolved more directly. A ratio of 4 to 16 usually produces favorable

results at a moderate computational cost (McGrattan et al, 2009). According to other studies on the LES (Baum and McCaffrey, 1989), a good representation is obtained by using values of δx within $0.1 \cdot D^*$ and $0.3 \cdot D^*$. Tab. 2 synthesizes the studied models. In order to get a simpler feedback on the model validation and to choose the correct mesh, a strong and unrealistic hypothesis of simultaneous involvement of all pallets has been initially considered in this study. Following the directions given in ISO-13387, it is possible to calculate point B and point C of heat release rate curve shown in Fig.3, according to what is reported in Tab 3.

dx	$\% D^*$	$\frac{dx}{D^*}$	Number of cells
0.3	0.15	6.89	298080
0.4	0.19	5.17	126360
0.5	0.24	4.14	64512
0.6	0.29	3.45	38880

Tab. 2 Models with different mesh sizes

A size of 50 and 60 cm does not provide an adequate simulation of the phenomenon in terms of the heat release rate (Fig. 4), maximum temperature (Fig. 5) and height of the smoke (Fig. 6). With a discretization of 40 cm fire is better modeled as a whole, but if a strong temperature gradient occurs, the result accuracy is still not satisfactory. For these reasons, for the investigations presented in the following paragraphs, a model with the mesh size of 30 cm has been used.

	time [min]	HRR [MW]
t_0	0	0
t_F	10	54
t_A	11	176
t_B	14	176
t_C	18	0

Tab 3 Values of the HRR

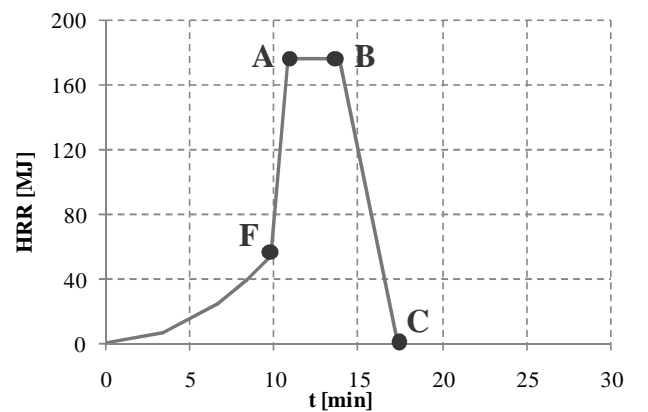


Fig. 3 Considered HRR curve

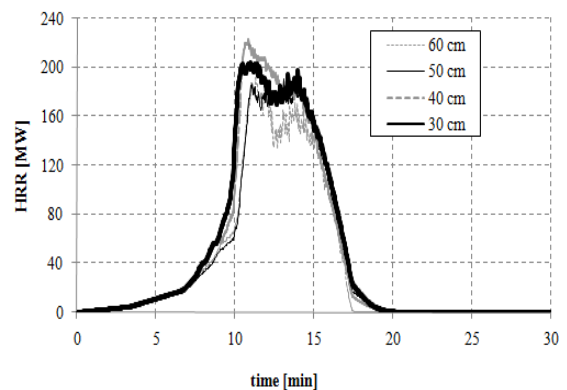


Fig. 4 Heat release rate curve

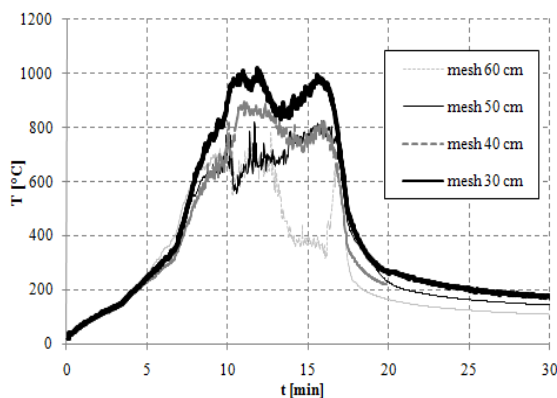


Fig. 5 Maximum temperature

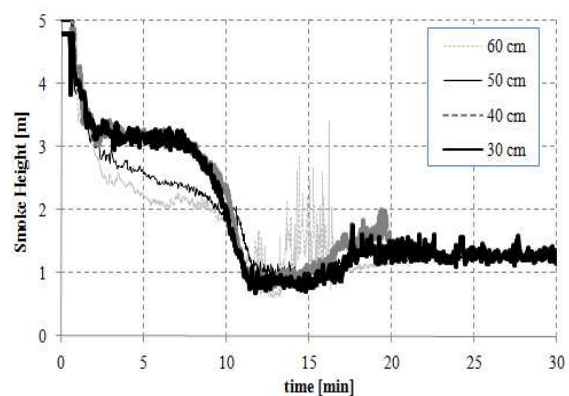


Fig. 6 Height of smoke

2.3 Fire scenarios: variation of the fuel position

The fire development is greatly influenced by the position of the fuel in relation to the geometry of the compartment. In particular, a decisive factor is the proximity of the combustible material to the openings. The first scenario consists of 18 pallets on fire, which are located in the proximity of a corner near one of the windows; in the third scenario instead the pallets are in the middle of compartment; finally in the second and fourth scenario the pallets are positioned along one long wall: the difference between the last two cases is that in the second scenario the fuel is near to a door, while in the fourth, the pallets are very far from the vents (Fig. 7).

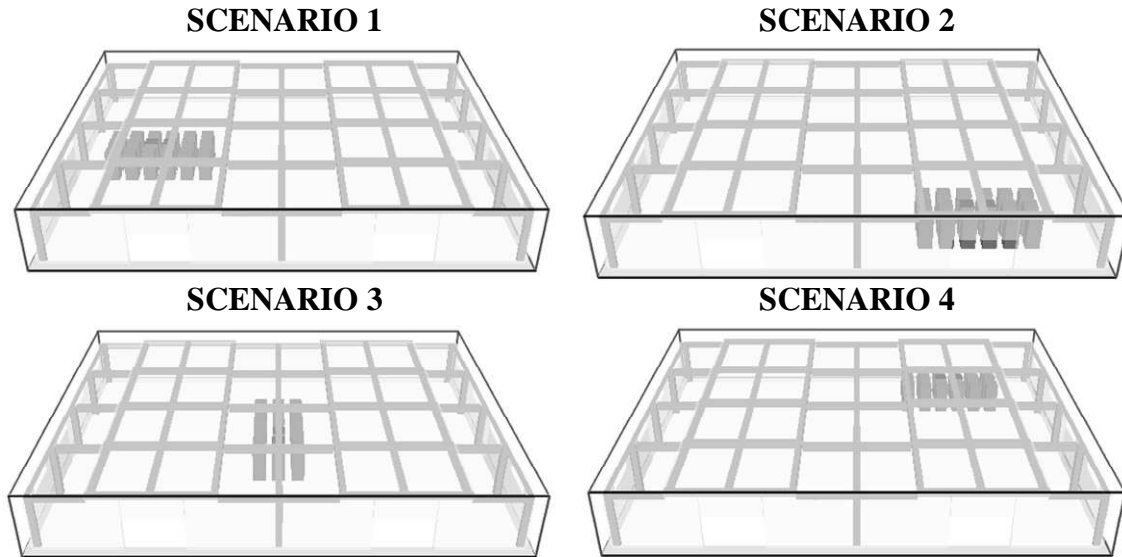


Fig. 7 Fire Scenarios: variation of the fuel position

NFPA 555 (2009), indicates an expression for estimating the minimum values of thermal power that can lead only to radiant heat ignition of combustible materials. This calculation determines whether the ignition of a material is able to determine the spread to others. The equation used is Eq. (2).

$$HRR_{\min} = 30 \cdot \frac{(d + 0.02)}{0.0092} \quad (2)$$

where: HRR_{\min} is the minimum heat release rate necessary for the ignition;

d distance between materials

In Fig. 8 a possible subsequent involvement of group of pallets is shown with respect to the first fire scenario. For the second and the fourth scenario, a similar sequence has been assumed; while some differences are present in the third scenario due to the presence of a column between the pallets. The different hypotheses concerning the diffusion of fire ignition are visible in Fig. 9. The heat release rate measured in FDS for all scenarios is shown in Fig. 10, while in Fig. 11 the highest temperatures of the structural elements are reported for each scenario. The fire development in scenarios 1, 2 and 3 determinates a quite similar heating in elements. In the fourth scenario instead the heating is slower, as shown in Fig. 11.

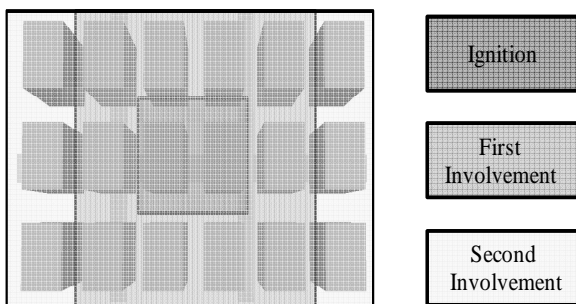


Fig. 8 Involvement of pallets in the first scenario

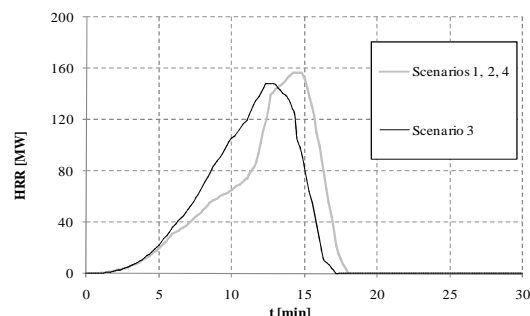


Fig. 9 Calculated heat release rate

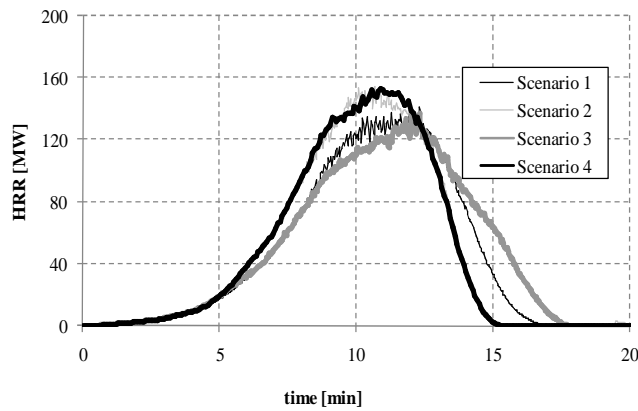


Fig. 10 Registered HRR in FDS

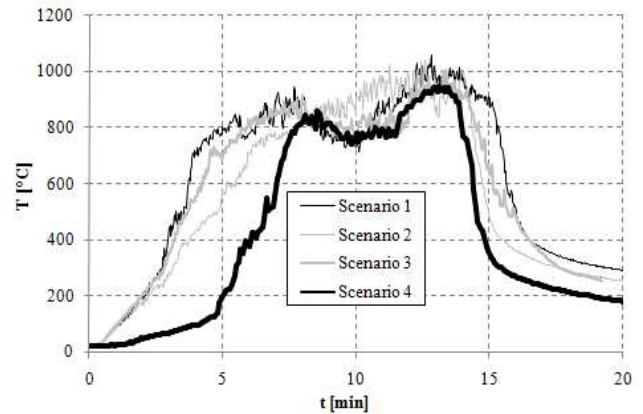


Fig. 11 Maximum temperature

2.4 Fire scenarios: variation of the ventilation

The development of the fire is determined by the opening factor. In particular, with reference to position 3 of the fuel (Fig. 7), the evolution of the fire has been studied in the following cases:

1. openings all closed;
2. breaking of the windows;
3. doors opening after 600 s;
4. smoke extractors activated at 68°C.

The sudden variation of the ventilation conditions determinates a strong change in development of fire, as Fig. 12 shows. The highest temperatures (Fig. 13) are reached when doors are open from the beginning. When all openings are closed instead, the fire extinguishes at an early stage by lack of oxygen. The sudden opening of the doors leads to a resumption of the fire and in an increment of the temperatures, which at a later stage reach the values of the first case, where the doors were open since the beginning. The smoke extractors lead to a change in the height of the gas, in the visibility and in the toxicity, but do not cause a big change for the purposes of structural analysis.

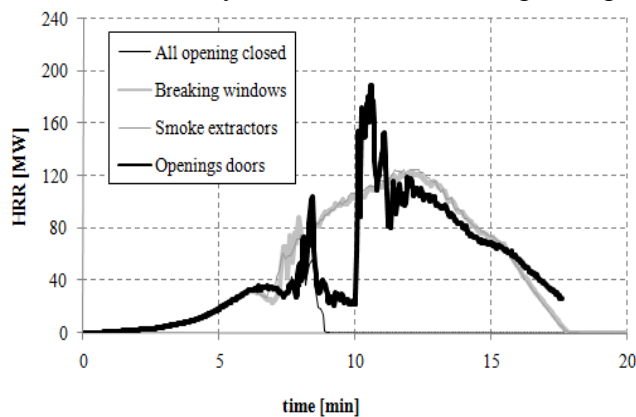


Fig. 12 Heat release rate

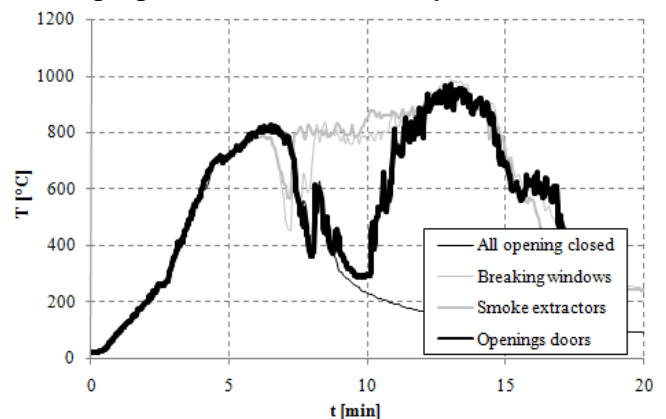


Fig. 13 Maximum temperature

2.5 Comparison between experimental and analytical heat release rate curve

The setting of the HRR value is a crucial point in CFD analyses finalized to assessing the fire development. For this reason, with reference to a fire of 30 stacks of pallets (dimensions 1.30m x 1.00m x 0.90), an experimental heat release rate curve (Averill et al, 2010) is compared with an analytical curve (Babrauskas, 2002), as shown in Fig. 14. The formula (3) proposed by Babrauskas is taken from Krasner (1968).

$$HRR_{s,max} = 919 \cdot (1 + 2.14h_p) \cdot (1 - 0.03M) \quad (3)$$

where: h_p is stack height (m) and M is moisture (%).

The experimental test was conducted by NIST in 2010. In Fig. 15 the highest temperatures of structural elements are shown. The possibility of referring to the experimental data rather than analytical assessments leads to a stronger validation.

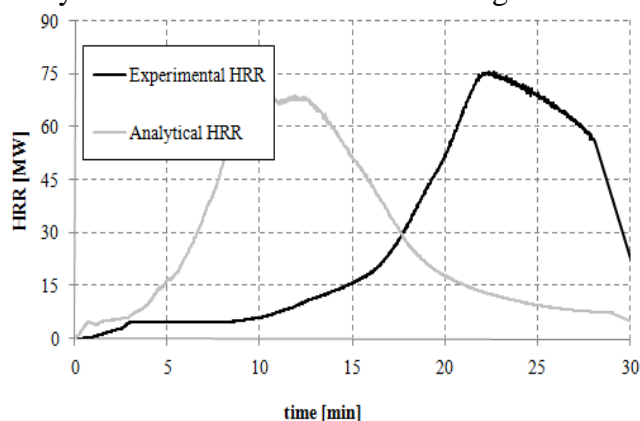


Fig. 14 Heat release rate curves

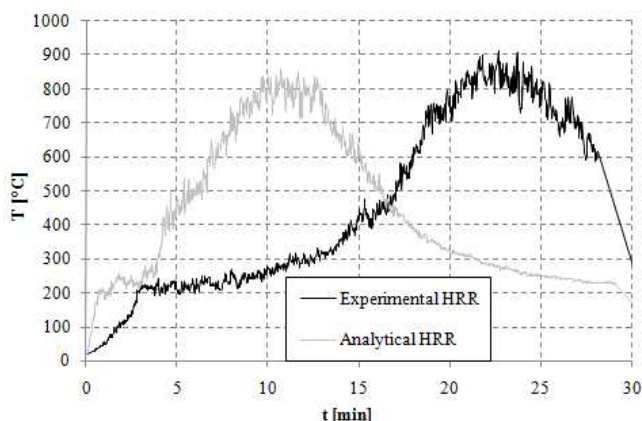


Fig. 15 Maximum temperature curves

3 CONCLUSION

In this study, aspects concerning the role of CFD analyses in the quantitative assessment of the structural performance in fire scenarios have been inquired. An application on a steel structure shows that CFD allows a more refined representation of the fire compared to an analytical evaluation. It can consider issues relevant to the development of the fire (e.g. ventilation, fuel location) and take into account significant variations of the boundary conditions in time.

REFERENCES

- Buchanan A. H., *Structural Design for Fire Safety*, Wiley, 2002.
- Yeoh G. H., Yuen K. K., *Computational Fluid Dynamics in Fire Engineering*, Butterworth Heinemann, 2009.
- Vassart O. et al., 3D simulation of Industrial Hall in case of fire. Benchmark between ABAQUS, ANSYS and SAFIR, 10th International Fire Science & Engineering Conference, Interflam, Edinburgh, 2004.
- ISO/TR 13387-1:1999 (E) Fire Safety Engineering - Part 1: Application of fire performance concepts to design objectives. Technical Report. Geneva: International Organization for Standardization.
- Krasner L.M., *Burning Characteristics of Wooden Pallets as a Test Fuel, Serial 16437*, Factory Mutual Research Corp., Norwood, MA, 1968.
- Babrauskas V., Heat release rate. In: *SFPE handbook of fire protection engineering*, 3rd edn. National Fire Protection Association, Quincy, MA, 2002.
- Baum H. R., McCaffrey B.J., *Fire-Induced Flow – Theory and Experiment*, Fire Safety Science, 2nd International Symposium, ed. T. Wakamatsa et al., 129-148, Hemisphere, Washington, 1989.
- NFPA 555: *Guide on Methods for Evaluating Potential for Room Flashover*, 2009.
- McGrattan K., Klein B., Hostikka S., Floyd J., *Fire Dynamics Simulator (Version 5) – User guide*, NIST, Special Publication 1019 – 5, Washington, USA, 2009.
- Averill et al, *Report on Residential Fireground Field Experiments*, NIST, Washington, 2010.
- Drysdale D., *An Introduction to Fire Dynamics*, Second Edition, Wiley, 1999
- Duthinh D., McGrattan K. B., Khashkia A., 2008, Recent advances in fire-structure analysis, *Fire Safety Journal*, Vol. 43, No. 2, 161-167.

EVALUATION OF THE FIRE RESISTANCE OF THE STEEL STRUCTURE OF A WASTE TREATMENT PLANT USING STRUCTURAL FIRE SAFETY ENGINEERING

Paulo Vila Real ^a, Nuno Lopes ^b

^a Professor, University of Aveiro, LABEST - Department of Civil Engineering, Portugal

^b Assistant professor, University of Aveiro, LABEST - Department of Civil Engineering, Portugal

INTRODUCTION

It is the purpose of this paper to present a study performed on the fire resistance of the steel structure of a waste treatment plant.

In the Portuguese Technical Regulations for Buildings Fire Safety, on the Decree No. 1532/2008 (MAI, 2008), which is now implemented, two approaches are recommended for assessing the safety of structures exposed to fire: a prescriptive approach using the standard fire curve ISO 834; and a performance based design using the natural fire development concept.

The natural fire curve definition takes into account the size of the fire compartment, the ventilation conditions and the surrounding walls coatings, in opposition to the standard fire curve that does not depend on any of these parameters.

In addition, in the last decade several European projects (EC, 1999a,b, RFCS, 2008) have shown that in large compartments, the prescriptive regulation based on the standard fire curve is too conservative and unrealistic.

According to Part 1-2 of Eurocode 3 (EC3) (CEN, 2005a), the stability verification can be made verifying that:

- a) with the standard fire, the structure collapse does not occur before the fire resistance time defined by the regulation; or
- b) with the natural fire and advanced calculation methods the structure collapse does not occur during the complete duration of the fire, including the decay phase or during a required period of time, which may coincide with the fire resistance time defined by the regulation.

In this work, the studies, performed to assess the needs of passive protection in the steel structure of a waste treatment plant in Gaia (Portugal), are presented.

Advanced calculation methods were used (Franssen, & Vila Real, 2010), both for the natural fire characterization (programme Ozone (Cadorin 2003, Cadorin et al., 2006), developed at the University of Liege and Arcelor Profil Luxembourg Research Centre) and to simulate the thermo-mechanical behaviour (finite element program SAFIR (Franssen, 2005, 2008) also developed at the University of Liege).

It was also considered the occurrence of possible localized fires, in accordance with Part 1-2 of Eurocode 1 (EC1) (CEN, 2005b). This methodology from Eurocode was implemented in the program Elefir-EN (Vila Real et al., 2010) (developed at the Universities of Aveiro and Liege).

The fire compartment temperature definition was determined, as defined in Part 1-2 of EC1, with each of the following fire models: the localise fire and 1 or 2 zone models, according to whichever is more appropriate. These models correspond to different types of fire and different phases of the same fire.

The waste treatment plant is composed of 3 main units, one building dedicated to the reception (being this the central building), another to the post-composting and finally one dedicated to the storage. The structures have steel trusses as their primary structural elements, and self-supporting roofs composed of thin-walled cold formed steel sheeting, which had to be analysed through shell finite elements. This last structural system incorporates as well a tie rod connecting both supports.

This study, on the steel structure fire behaviour, aimed at determines the fire resistance for each of the building structures.

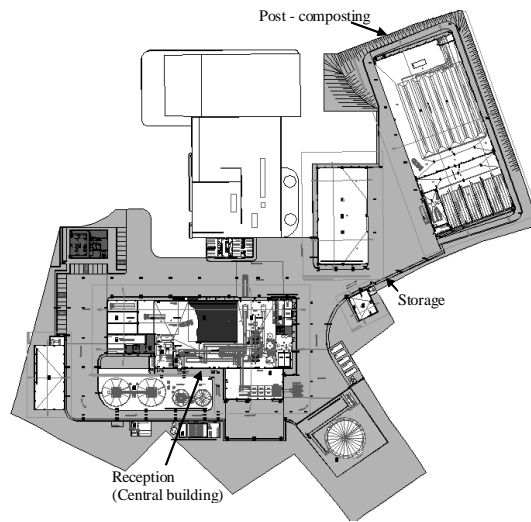


Fig. 1 Waste treatment plant.

1 FIRE SCENARIOS

The temperature evolutions were determined using the calculation software Ozone V2.2 (Cadorin 2003, Cadorin et al., 2006).

Although, as it will be shown, in all studied fire scenarios occurred flashover, on the localized fires, the maximum flame height L_f was evaluated according to EC1 and based on the Heskestad model (Heskestad, 1983, CEN, 2005b, Vila Real et al., 2010). In these analyses the rate of heat release was $RHR_f = 500 \text{ kW/m}^2$, it was also considered a high fire growth rate (CEN, 2005b), and a combustion factor with the value of 1 was considered. The openings were completely open during the all fire.

1.1 Compartment fires

The considered compartment fire scenarios were:

Scenario 1 - Fire in the reception unit (central building). This compartment as an height of 12.1 m. The considered maximum area was $A_{f,max} = 4992 \text{ m}^2$, and the fire area $A_{fi} = 4992 \text{ m}^2$. It was considered an openings area of 68 m^2 , and the fire load density was $q_{f,k} = 4960 \text{ MJ/m}^2$.

Scenario 2 - Fire in the Post - composting unit. This compartment as an height of 7.8 m. The considered maximum area was $A_{f,max} = 2688 \text{ m}^2$, and the fire area $A_{fi} = 2688 \text{ m}^2$. It was considered an openings area of 283.5 m^2 , and the fire load density was $q_{f,k} = 45753 \text{ MJ/m}^2$.

Scenario 3 - Fire in the storage unit. This compartment as an height of 7.8 m. The considered maximum area was $A_{f,max} = 1250 \text{ m}^2$, and the fire area $A_{fi} = 1250 \text{ m}^2$. It was considered an openings area of 220.5 m^2 , and the fire load density was $q_{f,k} = 13888 \text{ MJ/m}^2$.

The temperature evolutions of all the compartment fire scenarios are plotted in Figure 2.

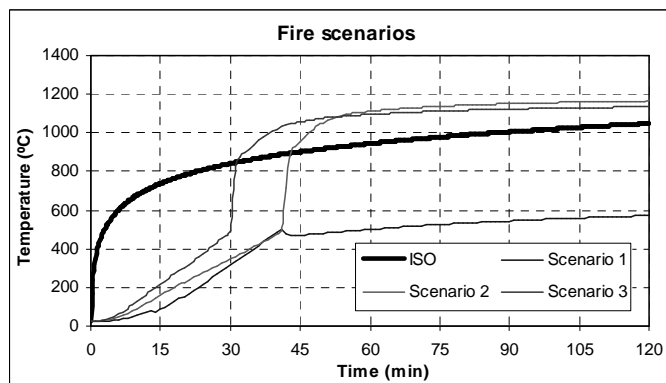


Fig. 2 Temperatures evolution in the compartments.

1.2 Localised fires

A localised fire with a $A_{fi} = 78.5 \text{ m}^2$ (EC, 1999b, Heskestad, 1983) was considered. The fire load density was $q_{f,k} = 45753 \text{ MJ/m}^2$. As the maximum temperature reached in this fire at the level of the roof was only $400 \text{ }^\circ\text{C}$ at 15.67 min, being the maximum flame length 5.94 m (see figure 3), this fire scenario was not considered on the mechanical analysis.

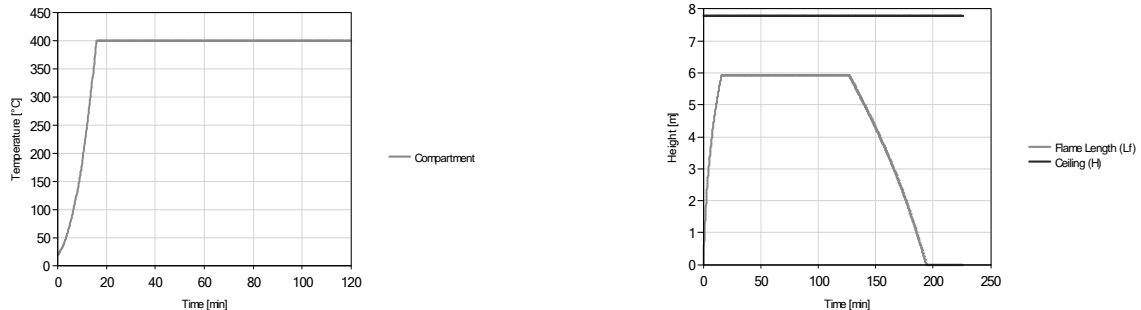


Fig. 3 Localised fire: fire compartment temperature evolution; flame length.

2 MECHANICAL ANALYSIS

A 3D mechanical analysis using the software SAFIR (Franssen, 2005, 2008), with beam and shell finite elements was used.

2.1 Mechanical actions

The fire is considered an accidental action, which means that the design value of the action effects in fire situation, should be obtained using an accidental combination as defined in EN 1990 (CEN, 2005c) and in accordance with the Portuguese National Annex of the EN 1991-1-2 (CEN, 2005a):

$$\sum G_k + \psi_{1,1} \cdot Q_{k,1} + \sum \psi_{2,i} \cdot Q_{k,i} + \sum A_d \quad (1)$$

The roof loads were determined, in accordance with Annex A1 of the EN 1990 (CEN, 2005c), adopting the category H for roofs, which corresponds to the accidental combination:

$$1.0G_k + \psi_{1,1}Q_{k,1} = 1.0G_k + 0.0Q_{k,1} = G_k \quad (2)$$

where G_k refers to the permanent loading and Q_k to the variable action.

2.2 Cross-sections analysis

The thermal analyses of the cross sections were performed with the program SAFIR. From these analyses it was obtained the temperature field of the cross sections for each of the considered fire scenarios, which was later applied to the mechanical analysis. No fire protection was considered in the thermal analysis.

In the main structural elements was considered that the cross sections were subjected to fire in all their four sides. Commercial sections such as SHS100x100x40 and HEA200 were used on these structural systems. In the roof it was considered fire on one side only (the underside). Figure 3 shows one of the sections analyzed (BNTA700) (Blocoltha, 2010).

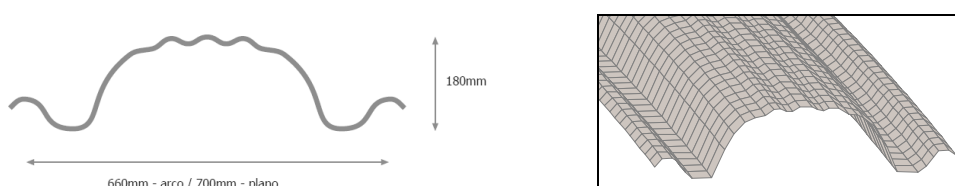


Fig. 3 Cross-section of the roof plate.

Three different roof plate sections (corresponding to the three units) were analysed. Their thickness varies between 0.8 and 1.5 mm, their geometry are also slightly different in each of the cross-sections.

2.3 Analyzed structural system

The main structural systems studied correspond to three-dimensional lattice girders. These truss structures were modelled with beam finite elements. Some of the truss structures were simply supported and others were continuous beams. Each unit of the waste treatment plant had a different truss structure as main structural system and different cold formed cross section for the roof sheeting, additionally the unit Post – composting had a continuous beam supporting the roof sheeting.

Several analyses were performed, being the structural elements subjected to the natural fire curves obtained from:

- a) Widespread fire in the reception unit (scenario 1 as defined in Section 1).
- b) Widespread fire in the post-composting unit (scenario 2 as defined in Section 1).
- c) Widespread fire in the storage unit (scenario 3 as defined in Section 1).

The following figure 4 shows the deformed beam lattice of the storage unit, subjected to the natural fire scenario 3, just before collapse (on 31 minutes).

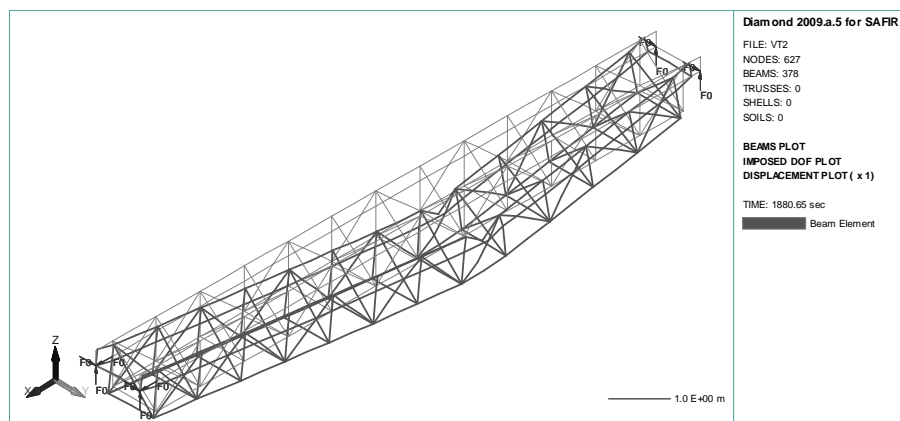


Fig. 4 Deformed shape of the truss structure of the storage unit, just before collapse (x1).

The self-supporting roof cold formed steel sheeting was analyzed using shell finite elements. This structural system was also composed of a tie rod connecting both extremities. Simplification of symmetry was used, thus considering only half of the coverage and a double support at one end and a "slide" at middle span. It were analysed the self-supporting roof sheeting with and without a tie rod with a diameter of 12 mm, also subjected to natural fire curve, and modelled using beam finite elements. Higher steel strengths on the steel sheeting due to the cold formed fabrication process (folding) were neglected.

The figures 5 and 6 show the deformed shape of the self-supporting roof of the composting unit, subjected to the natural fire scenario 2, just before collapse (43 minutes). Figure 5 illustrates the behaviour of the roof sheeting without the tie rod, while figure 6 presents the deformed shape when considering the tie rod. The time for collapse with and without the tie rod was the same

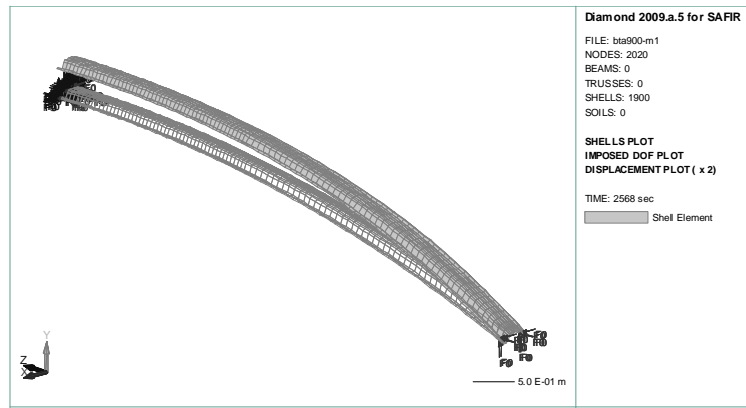


Fig. 5 Deformed shape of the roof sheeting of the composting unit, just before collapse (x2).

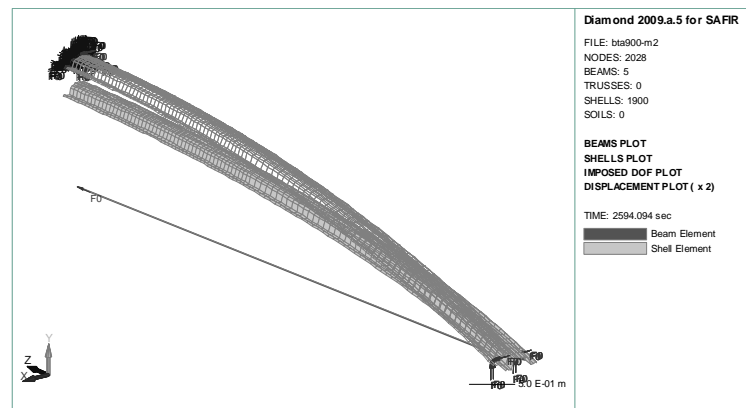


Fig. 6 Deformed shape of the roof sheeting with a tie rod, just before collapse (x2).

From the studies it was concluded that the steel structures of the various units comprising the waste treatment plant have, in the absence of passive fire protection, the resistance shown in tables 1 and 2.

Table 1 provides the fire resistance obtained for the main structures when subjected to the standard curve ISO 834 and to the fire scenarios obtained with the natural fire modeling.

Tab. 1 Fire resistance of the main structures

	ISO 834 (min)	Natural fire (min)
Reception truss structure	10	70
Post - composting truss structure	14	43
Post - composting continuous beam	37	47
Storage truss structure	9	31

Table 2 presents the fire resistance obtained for the cold formed self-supporting roof sheeting when subjected to natural fire scenarios.

Tab. 2 Fire resistance of the steel roof sheeting

	Natural fire (min)
Reception self-supporting roof sheeting (700x1.12)	> 120
Reception self-supporting roof sheeting (700x1.12) with a tie rod	> 120
Post - composting self-supporting roof sheeting (900x1.5)	43
Post - composting self-supporting roof sheeting (900x1.5) with a tie rod	43
Storage self-supporting roof sheeting (700x0.8)	30
Storage self-supporting roof sheeting (700x0.8) with a tie rod	30

As it can be observed, the instant of collapse with and without the tie rod is the same, meaning that the collapse is due to the sheeting and not due to the tie rod.

It can be also concluded that, according to the deformed shape of all the analyzed structural systems, the collapse, when it occurs, is towards the inside of the building, thus resulting in no danger to fire-fighters intervention.

3 CONCLUSION

In this work it was presented a case study to the fire resistance of the steel structure of a waste treatment plant using simplified and advanced calculation methods.

Based on studies conducted within European projects (EC, 1999a,b, RFCS, 2008), the steel structure temperatures development, resulted from a fire in a waste treatment plant, in Gaia Portugal, was analysed, in which the several compartments fit the classification of a large compartments.

The temperatures obtained with this analysis are relatively high, when compared to a prescriptive assessment following the standard ISO 834 fire curve.

The use of finite element models, on the mechanical analysis, has also revealed to be decisive, on better predict the actual behaviour of these structures in case of fire.

REFERENCES

- Blocotelha, Catálogos de chapas metálicas autoportantes de coberturas, (in portuguese), 2010.
- Cadorin, J.-F., Compartment Fire Models for Structural Engineering, Thèse de doctorat, University of Liege, Belgium, 2003.
- Cadorin, J.-F., Franssen, J.-M., Pinteá, D., Cajot, L. G., Haller, M., Schleich J. B., Software Ozone V2.2. University of Liege, Belgium and Arcelor Profil Luxembourg Research Centre, Luxembourg, 2006.
- CEN (European Committee for Standardization), EN 1991-1-2, Eurocode 1 – Basis of design and actions on structures – Part 1-2: General rules – Structural fire design, 2005a.
- CEN (European Committee for Standardization), EN 1993-1-2, Eurocode 3 – Design of steel structures – Part 1-2: Actions on structures exposed to fire, 2005b.
- CEN (European Committee for Standardization), EN 1990, Eurocode – Basis of structural design, 2005c.
- EC (European Commission), Development of Design Rules for Steel Structures Subjected to Natural Fires in Closed Car Parks, EUR 18867 EN, 1999a.
- EC (European Commission), Development of Design Rules for Steel Structures Subjected to Natural Fires in Large Compartments, EUR 18868 EN, 1999b.
- Franssen J.-M., SAFIR. A Thermal/Structural Program Modelling Structures under Fire, Engineering Journal, A.I.S.C., Vol 42, No. 3, 143-158, 2005.
- Franssen, J.-M., User's manual for SAFIR 2007a, a computer program for analysis of structures subjected to fire, Structural Engineering, ArGENCO, University of Liege, Belgium, 2008.
- Franssen, J.-M. & Vila Real, P., Fire Design of Steel Structures. Eurocode 1: Actions on Structures. Part 1-2 – Actions on Structures Exposed to Fire. Eurocode 3: Design of Steel Structures. Part 1-2 – Structural Fire Design, ECCS, Ernst & Sohn, 2010.
- Heskestad, G., “Luminous heights of turbulent diffusion flames”, Fire Safety Journal, Elsevier, 1983.
- MAI (Ministério da Administração Interna), Portaria n.º 1532/2008 (in portuguese), 2008.
- RFCS (Research Fund for Coal and Steel), DIFISEK+ - Dissemination of Structural Fire Safety Engineering Knowledge, 2008.
- Vila Real, P., Franssen, J.-M., Software Elefir-EN – Fire design of steel structural members according to Eurocode 3. <http://elefired.web.ua.pt>, 2010.

FIRE RESISTANCE OF STEEL TRUSSES WITH OPENSEES

Panagiotis Kotsovinos^a, Asif Usmani^a

^a University of Edinburgh, School of Engineering and Electronics, Edinburgh, United Kingdom

INTRODUCTION

Steel trusses are an efficient structural system, widely used in practice in order to support loads over long spans. Hence, a structural failure of a truss can have enormous consequences. Steel truss sections can be especially vulnerable to fire because of typically high surface area to volume ratios and lots room for exposure from all sides. Fire resistance of trusses is therefore a very important research topic.

Many finite element codes, both commercial or research based, have been developed and are commonly used for modelling structures in fire. However most of these do not offer sufficient flexibility for adding new capabilities and are also not normally accessible to users or researchers for modification. The object oriented nonlinear finite element framework (OpenSees), primarily designed for earthquake engineering simulations, offers the necessary flexibility and access needed to further expand its capabilities.

Element formulations have been implemented within the OpenSees framework to model the behaviour of truss structures subjected to fire. The geometric nonlinearity caused by large displacements and material nonlinearity due to the stiffness and strength reduction experienced in a real fire have been accounted for.

It should be also noted that this extension allows for fire following earthquake analyses in a combined framework. The implementation includes modules for temperature dependent material properties according to the Eurocode and the effects of thermal expansion of structural members. Hence, the inelastic effects are accounted for by utilizing appropriate constitutive relationships. Although the implementation procedure is similar for different types of structures, this paper focuses on trusses. Several numerical examples are presented to demonstrate the accuracy of the proposed numerical procedure.

Different finite element formulations for truss elements are used based on the Total Lagrangian and Co-rotational formulation.

Excluding the strain due to creep effect the total strain is equal to the mechanical strain and the thermal strain:

$$\varepsilon_t = \varepsilon_m + \varepsilon_{th}$$

Where the thermal strain for a truss element, which considers only thermal expansion of the member, will be

$$\varepsilon_{th} = \alpha \Delta T = \alpha (T_{heated} - T_{ambient})$$

The total strain varies for different formulations. For the TL formulation the total strain will be equal the Green-Lagrange strain, while for the co-rotational formulation it will be equal to the engineering strain.

Furthermore, for elastoplastic problems the mechanical strain includes both the elastic and plastic strain

$$\varepsilon_m = \varepsilon_e + \varepsilon_p$$

The thermal strain does not produce any stress, therefore

$$\sigma = \sigma(\varepsilon_m)$$

Stress has to be work conjugate with strain, so for the total Lagrangian formulation the stress measure will be the second Piola-Kirchoff stress (S) while for the co-rotational formulation it will be the simple engineering stress.

For elastoplastic problems the stress in an element will be equal to

$$\sigma = E(T) \varepsilon_e = E(T) (\varepsilon_t - \varepsilon_{th} - \varepsilon_p)$$

The axial force in the element is given by

$$N = \sigma A$$

While the internal resisting force of the element is given by

$$P = \sigma A L_0 B^T$$

Where B is the classical strain-displacement matrix

1 LOAD CONTROLLED STEP BY STEP NUMERICAL ANALYSIS

Analysis of structures in fire is usually performed into two load steps. The mechanical load is first applied as the first load step and remains constant for the second thermal load step. Such an analysis often involves the use of a step by step numerical method. The most used step by step method is the load controlled Newton-Raphson method. The temperature of the element is provided as an input. The temperature is multiplied by the load factor, as in mechanical analysis, to give the first temperature increment. During that increment, the material tangent and the thermal strain are queried from the material class in order to obtain a guess for the thermal force in the element for the first iteration which will be equal to $EA\varepsilon_{th}$. Then, further iterations follow until the equilibrium conditions are satisfied inside a convergence limit and the next increment is then applied. During each iteration the tangent stiffness matrix of the element gets updated as well as the material stress gets calculated. At the end of the iterations and before the next increment, the resisting force gets updated by removing the thermal force found in that increment from the load resulting from the material stress in order to find the actual force in the element.

For each load step during the analysis an incremental displacement is found out according to equation below.

$$\{\Delta F\} = [K] \{\Delta u\}$$

where ΔF is the Vector of Incremental forces

K is the Stiffness Matrix

Δu is the Vector of Incremental Displacements

Furthermore to remove the residual or unbalanced forces (R), iterations are included inside an increment to determine the converged displacement. The unbalanced forces are computed as the difference between total applied loads (P) and the internal resisting forces of the structure (F) as shown in the equation below for the j^{th} iteration of the i^{th} incremental step

$$\{R_{j-1}^i\} = \{P_{j-1}^i\} - \{F_{j-1}^i\}$$

The drawback of this load controlled procedure is that it cannot follow the equilibrium path beyond the limit points. This is the point where failure of the element takes place or a temporary loss of stability is experienced and then a post buckling path is followed. This drawback is not important for some simple or determinate structures, but for redundant structures local failure does not imply global failure of the whole structure which may be able to continue to carry the loads, without the contribution from the failed member. This is because redundant structures can find different load paths by which to support additional load when its local strength is reached at a single location (Rotter et al, 1999). Hence, alternative step by step procedures have also to be employed to check if the structure will continue to be stable or collapse. For this reason a dynamic procedure (Franssen & Gens, 2004) has been developed to make to analyse structures in fire in the OpenSees framework. An example of such an analysis is given in example 3.3.

In case of a dynamic analysis, the residual equation provided before becomes

$$R = P - Ma - Cv - F$$

Where P is the external force, Ma is the inertia force, Cv is the damping force and F is the internal force due to deformation.

2 MATERIAL MODELS OF STEEL

Several fire resistance tests of structural steel members have shown that high temperature causes material degradation so the reduction of material properties like Young's modulus and Yield Stress have to be accounted for by utilizing appropriate constitutive relationships. Hence, new uniaxial elastic plastic material models have been developed by modifying appropriately the existing ones under the OpenSees framework that take into account the material degradation under elevated temperatures, the bilinear material model (Steel01Thermal) and the elliptic material model (Steel02Thermal) (Usmani et al, 2010).

2.1 Bilinear Material

Steel01Thermal is a uniaxial bilinear steel material with kinematic hardening. The information required for this material are yield strength (F_y), Young's modulus (E_0) and strain hardening parameter (b). This material is approximate but computationally efficient at the same time. It should be noted that this material is allowed to have both constant strain hardening and temperature dependent strain hardening as suggested by Shen and Zhao (1995).

2.2 Elliptic Material

Steel02Thermal is a uniaxial Giuffre-Menegotto-Pinto steel material with isotropic strain hardening. Here the material depends on the young modulus and the strain hardening parameter as before but also from the yield stress at the start of the elliptic curve as well the yield stress at the end of the elliptic curve. Compared to the Steel01Thermal material it is considered to provide more realistic results.

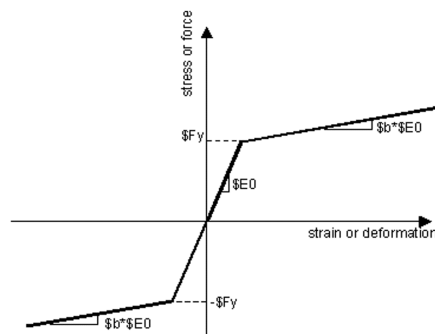


Fig. 1 Bilinear Material

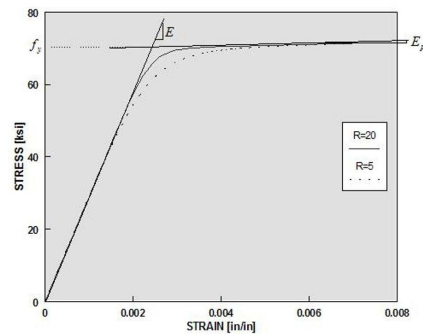


Fig. 2 Elliptic Material

3 NUMERICAL MODELLING

Some numerical examples are presented to validate the procedures developed.

3.1 Restrained truss

The first example is a restrained truss which is restrained against thermal expansion and half of it is heated. This truss is modelled using two elements but only the left one is heated (Figure 3). The aim of this example is to demonstrate that the developed procedure captures both geometrical (thermal expansion) and material (yielding) effects. The length of each element is 1000mm. The area of the elements was selected as 100mm^2 . The boundary conditions of the truss were restrained both horizontally and vertically. The example was solved by both Total Lagrangian and Co-rotational formulations and for constant strain hardening equal to 0.1 as well as temperature dependent properties using the values suggested by Shen and Zhao (1995). The results of the analyses are shown in Figure 4.



Fig. 3 Restrained truss

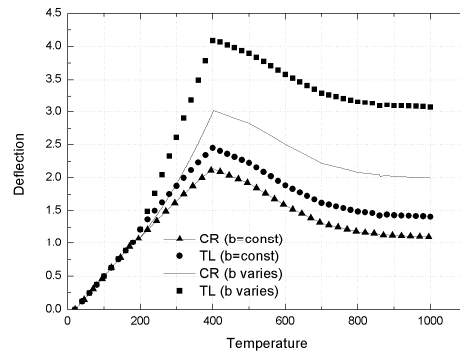


Fig. 4 Load-deflection curve

The results show that the model can capture both geometric and material phenomena. In the case of the formulations with constant strain hardening it can be seen that although the members yield early (at a temperature of about 200°C), they continue to expand almost linearly until the temperature reaches about 400°C when the yield stress of the material drops. Then the members deform towards the opposite direction.

For the case of temperature dependent strain hardening it can be seen that the curve shows a similar behaviour. The difference with the previous case is that because the strain hardening changes here the members have different behaviour after the yield point.

3.2 One member truss

The example selected is the benchmark provided by Lin et al (2010) which was solved analytically by the authors using a Total Lagrangian approach. For comparison purposes both Total Lagrangian and Co-rotational procedures developed are examined here. The temperature increments for the OpenSees modelling were applied in 10°C steps.

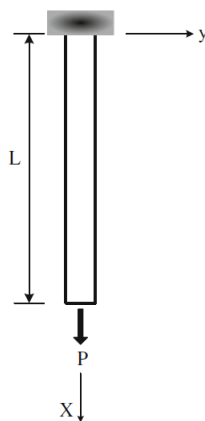


Fig. 5 One member truss

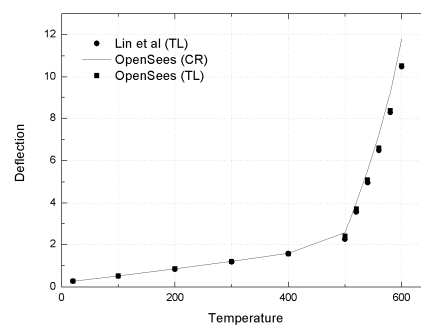


Fig. 6 Load-deflection curve

The comparison between the authors and OpenSees results shows very good agreement. Furthermore, as expected the OpenSees TL solution is almost identical to the analytical one as it is also based in a TL formulation. The CR solution finds a slightly higher result by 1mm.

3.3 Two Member Truss

This example was also solved by Lin et al (2010) using a Generalised Displacement Control (GDC) method and loses stability through snap-through buckling. In order to analyse this example a

dynamic procedure was followed. Further details of the dynamic approach for modelling the post-buckling behaviour will not be discussed here as it is outside the scope of the present paper.

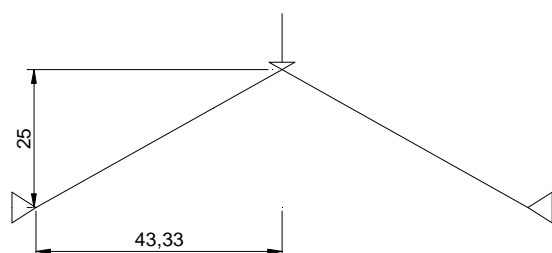


Fig. 7 Two member truss

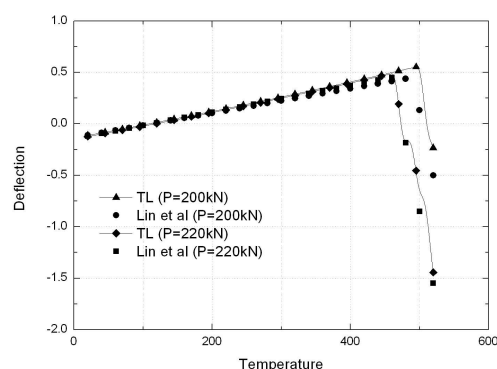


Fig. 8 Load-deflection curve

The results of the dynamic analysis agree well with those obtained from Lin et al (2010) using Generalised Displacement Control (GDC). The slight difference between the results is attributed to the different analysis technique. A static analysis using the GDC method will show convergence for most problems (except when snap-back problems are involved) but does not take into account the inertia forces that are developed.

For the particular example it is also of interest to note that as the temperature increases the truss deflects upwards but when the members have yielded, the deflection of the truss changes direction towards the other side. Moreover, the differences of the final deflection for the 200kN and 220kN cases show that the effect of preloading plays a role in the behaviour of the truss.

4 SUMMARY

This paper presented the procedures developed for modelling the fire resistance of trusses in the object oriented and open source framework OpenSees. More specifically Total Lagrangian and Co-rotational formulation based elements to account for the nonlinear effects. Several numerical examples have been presented to demonstrate the procedures developed. A dynamic approach was also followed to examine the postbuckling response of a truss that loses stability through snap-through buckling.

5 ACKNOWLEDGMENTS

Thanks to Jian Zhang for providing the modified temperature dependent material classes and for all the help. Assistance from Dr McKenna of PEER and UC Berkeley is also appreciated.

REFERENCES

- Franssen J.M., Gens F., Dynamic analysis used to cope with partial and temporary failures, Proceedings of International Workshop on Structures in Fire, Ottawa, 2004, 1089-94
- Lin T.J., Yang Y.B., Huang C.W., Inelastic nonlinear behaviour of steel trusses cooled down from a heating stage, International Journal of Mechanical Sciences 52 (2010) 982-992.
- J.M.Rotter, A.M.Sanad, A.S.Usmani, and M.A.O'Connor. Structural performance of redundant structures under local fires. In *Proceedings of Interflam'99*, Edinburgh, Scotland, June-July 1999.
- Usmani A. S. , Rotter J. M., Lamont S., Sanad A. M., Gillie M., Fundamental principles of structural behaviour under thermal effects, *Fire Safety Journal*, 36(8), 721-744 (2001).
- Usmani A., Zhang J., Jiang J., Jiang Y., Kotsovinos P., May I., Zhang J., Using OpenSees for Structures in Fire, Proceedings of International Conference on Structures in Fire, Michigan, 2010, 1089-94

- Shen J.Y., Zhao J.C., Modelling fire resistance behaviour of multi-storey steel frames, Proceedings of International Conference on Computing in Civil and Building Engineering, Berlin, 1995, 1089-94
- Wang P., Li G., Guo S., Effects of the cooling phase of a fire on steel structures, Fire Safety Journal 43 (2008) 451-458.

TEMPERATURE OF STEEL COLUMNS EXPOSED TO LOCALISED FIRE

Zdeněk Sokol ^a

^a Czech Technical University Prague, Faculty of Civil Engineering, Prague, Czech Republic

INTRODUCTION

Temperature of steel structures exposed to fire is the critical factor influencing the resistance. The temperature depends on the fire behaviour, position of the element with respect to the fire and fire protection. There are simple models for prediction of temperature of both unprotected and protected steel elements. These models can be easily used for compartment fires and for beams exposed to localised fires.



Fig. 1. Column exposed to localised fire, fire test Mittal Steel, Ostrava, June 2006

1. STEEL STRUCTURES EXPOSED TO LOCALISED FIRE

Gas temperature at localised fire depends on distance from the fire. The highest temperature can be observed in the plume and in the hot zone directly above the fire. The temperature in far from the fire is quite low.

As a result, the temperature of elements exposed to localised fire is variable along their length. The highest temperature of beams is observed above the fire, but it is decreasing at larger distances. There are two models for beams: the Heskestad model applicable at situation when the beam is not engulfed in flames and Hasemi model for beams engulfed in flames. These models are included in standard EN 1993-1-2.

The standard does not give any rules for evaluation the column temperature. Application of step-by-step method in combination with Heskestad model for localised fire is given in this paper.

2. MODEL OF LOCALISED FIRE

The model for localised fires in situation when the flames do not impact the ceiling gives the length of the flames and temperature along the vertical axis of the fire. The model is given in Annex C of EN 1991-1-2.

The input parameters include:

- Fire growth rate given as time t_{α} to reach the rate of heat release 1 MW,
- Fire load in MJ,
- Maximum rate of heat release for fuel-controlled fire RHR_f produced by 1 m² of the fire, depending on type of combustible materials,
- Maximum fire diameter D .

These input data are used to derive the rate of heat release Q . The concept of t-square fires is included in EN 1991-1-2, Annex E, see Fig. 2. The picture indicates the rate of heat release at any time of the fire and consists of three phases: the growing phase of the fire, steady state represented by horizontal plateau and the decay phase. It is assumed the fire is fuel-controlled. In case when the fire is ventilation-controlled, the maximum rate of heat release needs to be reduced according to amount of oxygen available in the fire compartment, see Fig. 3, where H_u is net calorific value of combustible materials, m is combustion factor, ($m = 0,8$), A_v is opening factor and h_{eq} is height of the opening. The details are given in EN 1991-1-2.

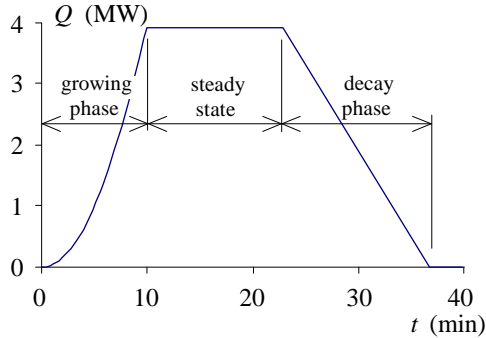


Fig. 2. Model of rate of heat release according to EN 1991-1-2

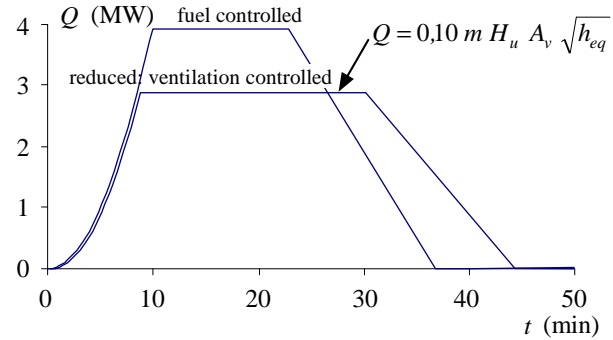


Fig. 3. Model of rate of heat release for fuel-controlled fire

The gas temperature along the vertical axis of the fire is given by:

$$\theta_g = 20 + 0,25 Q_c^{2/5} (z - z_0)^{-5/3} \quad (1)$$

where Q_c is the convective part of the rate of heat release

$$Q_c = 0,8 Q \quad (2)$$

and the virtual origin z_0 is

$$z_0 = -1,02 D + 0,00524 Q^{2/5}. \quad (3)$$

The length of the flame L_f as function of time t (depending on rate of heat release Q) is given by

$$L_f = -1,02 D + 0,0148 Q^{2/5} \quad (4)$$

where the fire diameter D at time t can be obtained from

$$D = \sqrt{\frac{4 Q}{\pi RHR_f}}. \quad (5)$$

3. TEMPERATURE OF COLUMN NOT ENGULFED IN FLAMES

The prediction of column temperature is not described in the standard EN 1993-1-2. In cases when the flames impact the ceiling the Hasemi model can be used also for columns giving their temperature of the upper part. As an alternative, zone model can be used and the column temperature can be derived from the hot zone temperature. This approach can be used for relatively small compartments and compartments with low height where the hot zone temperature is high and the column temperature is significant.

However, for columns in large and high compartments, the above method does not give satisfactory results as the hot zone spreads to large area, therefore its depth and temperature is low. The column temperature in the upper part is not significant, but the lower part might be heated by radiation from the localised fire and the column temperature can be much higher than temperature at the top.

The column temperature can be calculated when the effect heat gained from radiation and heat „loses“ by convection and surrounding space is taken into account, see Fig. 4. Standard step-by-step method as in EN 1993-1-2 can be used and is described in the paper with these assumptions:

- The fire temperature is calculated according to model described above (EN 1991-1-2, Annex C), flames do not impact the ceiling,
- the localised fire is replaced by cylindrical surface with diameter equal to diameter of the fire. The position of the column with respect to the fire, see Fig. 4,
- the column is not engulfed in the flames, the heat is transferred to the column by radiation only,
- the emissivity of the fire is 1,0,
- the column is surrounded by cold air, the ambient temperature is 20°C,
- the temperature is variable along the column height,
- non-uniform temperature of the cross-section is neglected,
- the effect of heat conduction along the column length is neglected, this is conservative assumption leading to higher column temperature.

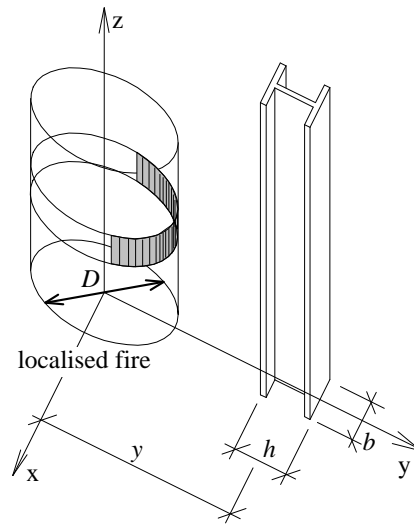


Fig. 4. Model of column exposed to localised fire

The heat gained by the column can be calculated from the heat flux received from any point of the flames (cylindrical surface) as

$$h_{net,gain} = \Phi \varepsilon_{res} \sigma \left((\theta_g(z) + 273)^4 - (\theta_m + 273)^4 \right), \quad (6)$$

where the flame temperature (temperature of the radiating surface) $\theta_g(z)$ is variable with respect to distance from the floor of the compartment z .

The heat which is lost from the column because of convection and radiation to surrounding space is obtained from the corresponding heat flux given by

$$h_{net,loss} = (1 - \Phi) \varepsilon_m \varepsilon_f \sigma \left((\theta_m + 273)^4 - (20 + 273)^4 \right) + \alpha_c (\theta_m - 20), \quad (7)$$

where the heat transfer coefficient $\alpha_c = 25 \text{ W/m}^2\text{K}$.

As the flame temperature depends on height, the radiating surface needs to be divided to rings according to Fig. 4. Temperature of the ring is assumed to be uniform, and the total heat flux to any location on the column is obtained as sum of the fluxes from all the rings (including the heat loss) as

$$h_{net} = \sum h_{net,gain} - h_{net,loss} \quad (8)$$

The column is exposed to radiation on three sides only, Fig. 5, and the shadow effect is taken into account by considering the envelope of the column cross-section.

4. CONFIGURATION FACTOR

The effect of radiation include the configuration factor Φ . General formula for its evaluation is

$$\Phi = \int_{A_1} \frac{\cos \varphi_1 \cos \varphi_2}{\pi r^2} dA_1, \quad (9)$$

where the angles of source area A_1 and target area A_2 are shown on Fig. 6.

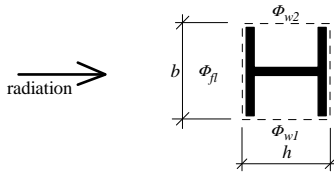


Fig. 5. Envelope of the column cross-section and surfaces exposed to radiation

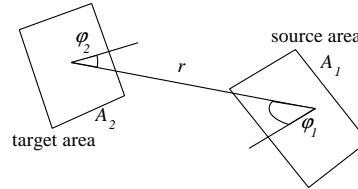


Fig. 6 Configuration factor Φ

The configuration factor is evaluated for each rectangle comprising the ring of the radiating surface. Only the visible part of the ring is taken into account, see Fig. 4. The total heat flux from that ring is therefore given as sum of the heat fluxes from these small rectangles at equal temperature.

The configuration factor was calculated numerically using the equation above. It is calculated separately for the front surface of the column (column flange, Φ_{fl}) and for both side surfaces (column webs, Φ_{w1} and Φ_{w2}).

The resulting configuration factor from the single ring to any location on the column is given by

$$\Phi = \frac{b \Phi_{pas} + h (\Phi_{st1} + \Phi_{st2})}{b + 2h}. \quad (10)$$

5. RESULTS

The method described above was used to evaluate the column temperature of single storey industrial building sized 60×150 m with height 7 m. The building is used for metal forming and assembling of final products. Only non-combustible materials are presented in the building and the assumption of localised fire fits to the nature of the building. The next pictures show results from two fire scenarios: localised fire of metal-forming machine and localised fire of a fork lift. Fire resistance 15 minutes is required.

5.1 Localised fire of metal-forming machine

Exact evaluation of the fire load is difficult as there are no data available. The fire load is based on estimation of amount of combustible material and its calorific value (electric components, cables, switches, covers, oil fill). The characteristic value of fire load is

$$Q_{f,k} = \sum m H_u = 10 \cdot 40 + 5 \cdot 43,2 = 616 \text{ MJ}.$$

and the design value of fire load (based on compartment size and danger of fire activation)

$$Q_{f,d} = \delta_{q1} \delta_{q2} \prod \delta_{n,i} m Q_{f,k} = 2,2 \cdot 1,22 \cdot 1,0 \cdot 0,8 \cdot 616 = 1326 \text{ MJ}.$$

Medium fire growth rate with $t_\alpha = 300$ s, maximum fire diameter $D = 2$ m and maximum rate of heat release $RHR_f = 500 \text{ kW/m}^2$ were chosen as the parameters for the localised fire. The maximum rate of heat release RHR_f and fire growth rate t_α were chosen in such way the end of the steady state is the same as the required fire resistance, i.e. 15 minutes.

The rate of heat release derived from the parameters above is shown on Fig. 7.

The length of the flame is shown on Fig. 8.

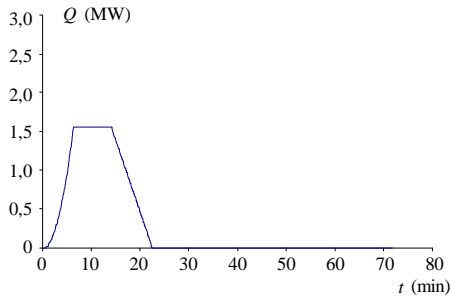


Fig. 7 Rate of heat release

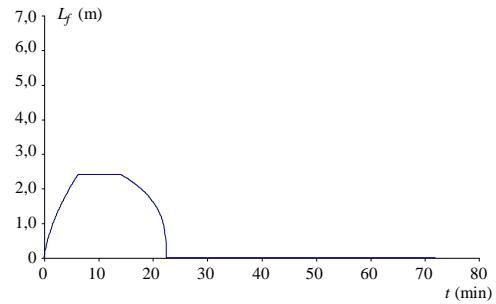


Fig. 8 Flame length

The maximum flame length is 2,41 m, the flame does not impact the ceiling. Temperature of the hot zone below the ceiling was calculated using zone model (Ozone software). Because the maximum gas temperature is only 60°C, the temperature of the upper part of the column does not to be considered as significant for the column resistance.

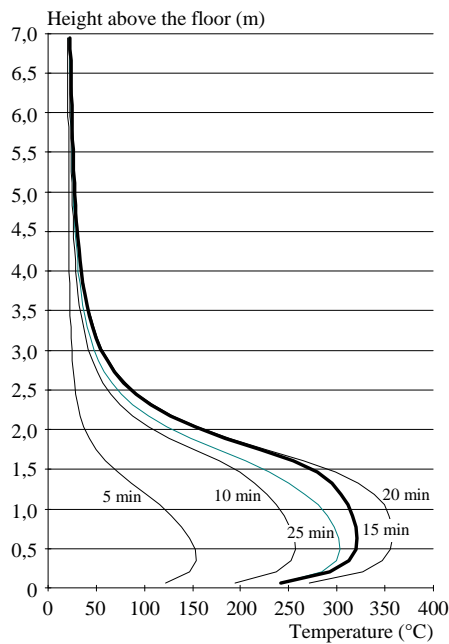


Fig. 9 Temperature of column section HEA 260 along the height

The maximum column temperature 320°C at time 15 minutes is reached 0,65 m above the floor.

5.2 Localised fire of forklift

The parameters of localised fire were of the forklift were adopted from research focused on fires in car parks, as rate of heat release of the forklift is not available. Diameter of the fire was chosen to be the same as length of the forklift, i.e. $D = 2,70$ m. Rate of heat release is shown on Fig. 10.

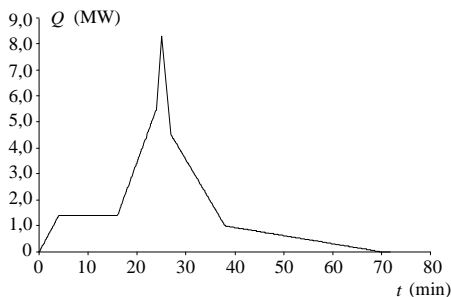


Fig. 10 Rate of heat release

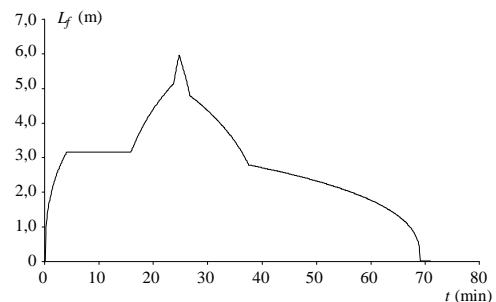


Fig. 11 Flame length

The maximum flame length is 5,91 m, the flames do not impact the ceiling.

The gas temperature of the hot zone is only 90°C, therefore the temperature of the upper part of the column is not significant for the column resistance.

The maximum column temperature 345°C at time 15 minutes is reached 1,10 m above the floor.

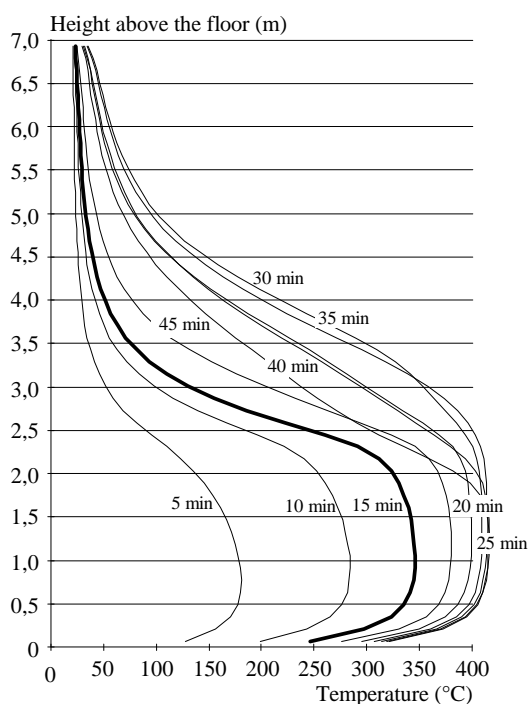


Fig. 12. Temperature of column section HEA 260 along the height

6. SUMMARY

The method described in this paper can be used to evaluate temperature of steel columns exposed to localised fire which is not dealt in European standards. It is compatible with EN 1991-1-2 and EN 1993-1-2. It is necessary to use numerical calculation of configuration factor and step-by-step method. Results from practical application are included.

ACKNOWLEDGEMENT

This paper was prepared with help of grant MSM 6840770001.

REFERENCES

- EN 1991-1-2, Eurocode 1:Actions on structures – Part 1-2: General actions – Actions on structures exposed to fire, Brussels: CEN, November 2002.
- EN 1993-1-2, Eurocode 3: Design of steel structures – Part 1-2: General rules – Structural fire design, Brussels: CEN, December 2003.
- Buchanan A.H., Structural design for fire safety, Wiley, New Zealand, 2002.
- Franssen J.M., Zaharia R., Design of Steel Structures Subjected to Fire, Background and Design Guide to Eurocode 3, University Liège, 2005.
- Development of design rules for steel structures subjected to natural fires in closed car parks, CEC Agreements 7210-SA/211/318/518/620/933: Validation of the method & Measured rate of heat release of burning cars.
- Sokol, Z. - Wald, F.: Prediction of Column Temperature Exposed to Localised Fire. In Technical Sheets 2008 - Part 3. Praha: CIDEAS-Centrum integrovaného navrhování progresivních stavebních konstrukcí, 2009, vol. 3, p. 59-60.
- Sokol, Z. - Wald, F. - Kallerová, P. - Bonnet, N.: Column Behaviour during Localised Fire Test. In Proceedings of the Fifth International Conference Structures in Fire. Singapore: Nanyang Technological University, 2008, p. 256-263.

BEHAVIOUR OF FRAME COLUMNS IN LOCALISED FIRES

Ruirui Sun^a, Ian Burgess^a, Zhaohui Huang^a

^a University of Sheffield, Department of Civil and Structural Engineering, Sheffield, UK

INTRODUCTION

Column behaviour plays a key role in the robustness of framed structures in fire, and a key research topic in recent years [1-4] has been the effect of axial restraint from superstructure on column buckling. As a result of these studies, the limiting (initial buckling) temperature of a column can now be predicted with reasonable accuracy. However, most studies have concentrated on isolated columns with clearly defined boundary and loading conditions. It is well recognised that the behaviour of a column in a complete building differs from that of an isolated column, because of the effects of structural continuity. In a frame, both the critical temperature of a column and its capacity to re-stabilize after initial buckling are important aspects of preventing a progressive collapse mechanism from developing. A conventional static analysis is terminated when a local instability takes place. To evaluate frame behaviour after initial instability the analysis should be continued beyond this instability until total collapse or re-stabilisation happens. In this paper, a simplified method to predict the behaviour of an individual column as a result of its interactions with other frame members is described and tested against a newly-developed static/dynamic analysis.

1 STATIC/DYNAMIC PROCEDURE AND FRAME ANALYSIS

In order to overcome the propensity of conventional static analysis to fail at the first singularity and to enable the analysis to continue through its unstable stage, a combined static and dynamic procedure has been developed for *Vulcan*. With this extended capability, it has been possible to trace the structural behaviour of single members or whole frames from initial static response, through local failure or instability, to stable post-buckling behaviour. The dynamic analysis is carried out by an explicit scheme. It has the benefit of avoiding convergence checking, and is therefore less time-consuming within each time step. The explicit scheme has been widely used for structural progressive collapse analysis. This particular implementation has been validated [5] using several practical cases. In this study, it is used to carry out structural analysis of steel frame under localised fire conditions. A planar frame shown in Fig.1 has been tested under localised fire conditions. The central column at ground floor level is assumed to be heated by an IS0834 fire curve.

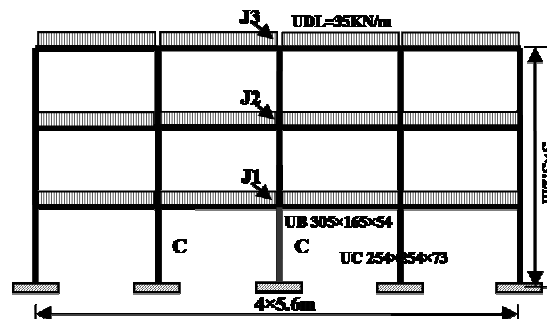


Fig. 1: The test frame.

Failure of the frame develops through three stages, as shown in Fig.2. In Stage I the column is heated progressively, and its thermal expansion against restraint provided by its superstructure increases its compressive force. When this force rises to the level of the capacity of the column, degraded by its increased temperature, the column will buckle. In Stage II, the ends of the beams attached to the column and its upper storeys move downwards with the vertical buckling deflection of the heated column. Moments then develop at the ends of these beams as this deformation

increases. If these moments exceed the beams' plastic moment capacity, plastic hinges will be generated at their ends. During this stage, catenary action is gradually activated. The catenary force is highest in the beams directly connected to the failed column. The axial forces in these beams will pull the adjacent columns inwards; the forces in the upper-storey beams are much lower since the upper storeys of these columns stay vertical. If the lateral restraint from the outer bays is not stiff and strong enough to stabilise this deformation, Failure Stage III is initiated. Plastic hinges are generated in the neighbouring columns, and the total collapse of the frame happens.

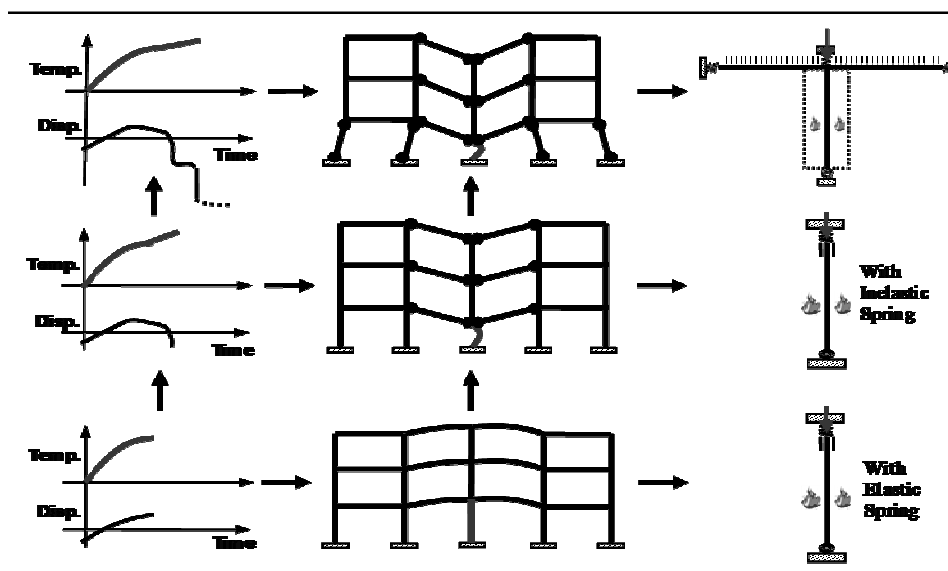


Fig. 2: Failure process and proposed simplified model.

On the basis of these three stages, the simplified model has been proposed. The key to Stage I is the buckling, or critical, temperature of the heated column, which depends on the stiffness of the axial restraint provided by the upper-storey beams above the column. This can be simulated by a simple model containing a single column with an axial elastic spring at the top end. For Stage II, the simultaneous yielding of the beam directly attached the column's upper storeys can be considered implicitly in the force-displacement characteristic of the spring. In order to take into account catenary action, the beams connected to the heated column are included in an extended simplified model, and the lateral restraint provided by surrounding bays are also simulated by horizontal springs. Several terms are clarified as follow:

Initial critical temperature of column: the temperature at which the column initially buckles.

Collapse temperature of column: the temperature beyond which the column restrained by inelastic restraints cannot achieve any re-stabilisation.

Collapse temperature of frame: the temperature beyond which no re-stabilisation position can be achieved by model with column and beams.

2 SIMPLIFIED MODEL

2.1 Restrained column model

The column model with elastic axial restraint has been studied by other researchers such as Poh and Bennetts [6], Shepherd [1] and Ali *et al.* [3]. As discussed above, these researches mainly focus on studying the buckling temperatures of restrained columns. The post-buckling behaviour of columns and their interaction with other members of the frame are outside their scope. Recently, a simplified spreadsheet calculation to predict the column behaviour from pre-buckling, through the buckling stage, and then in the post-buckling stage, has been proposed by one of the authors on the basis of the simplified model described previously. In this study, the simplified restrained column model, analysed by the static/dynamic version of *Vulcan* will be used to validate this calculation method, and this model will also be extended later to study the column behaviour considering the interaction

with other members of the frame. The comparison of results from the *Vulcan* analysis and the spreadsheet calculation method is shown in Fig.3.

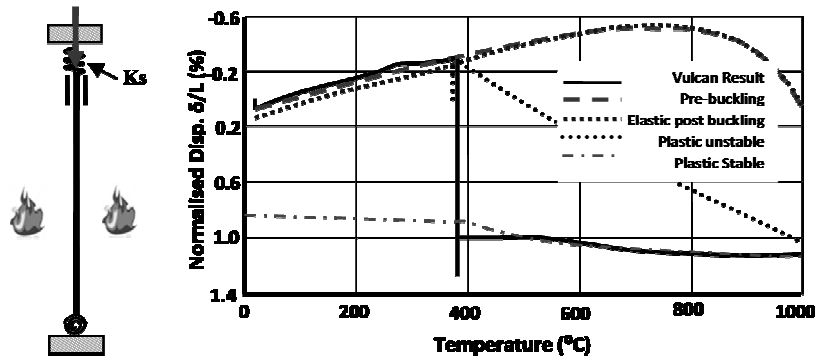


Fig. 3: Comparison of results from different simplified models.

2.2 Restrained column model considering beam yielding effects

In Stage I the restraint stiffness from beams above the heated column (Fig. 4) is:

$$K_s = \frac{12E \sum I_s}{L_s^3} \quad (1)$$

This calculation of lateral beam stiffness assumes that both ends of the beams are completely fixed against rotation, but this is not the case in a real structure. If the rotational stiffness of connections is considered, the lateral stiffness of a beam can be modified to:

$$Ks = \frac{1}{\frac{L^2}{2K_\theta} + \frac{L^3}{12EI}} \quad (2)$$

where K_θ is the initial rotational stiffness of the semi-rigid connections.

A purely elastic spring cannot represent the restraint conditions realistically if beam yielding takes place. When the beams above the affected column yield the restraint stiffness provided by these beams to the column will be lost, and the restraint condition of the column changes. When the plastic hinges are formed at the ends of a beam, the vertical shear force carried by the beam can be calculated as strength (see Fig. 5):

$$F_{pb} = 2 \times \frac{M_p}{L} \quad (3)$$

The restraint strength provided by the other beams above the column is determined as:

$$F_p = \sum F_{pb} \quad (4)$$

If taking connections into consideration and assuming that the plastic hinge forms in connections, this restraint strength can be estimated as:

$$F = \sum F_p = \sum \frac{2M_\theta}{L} \quad (5)$$

where M_θ is the aggregated moment capacity of the connections.

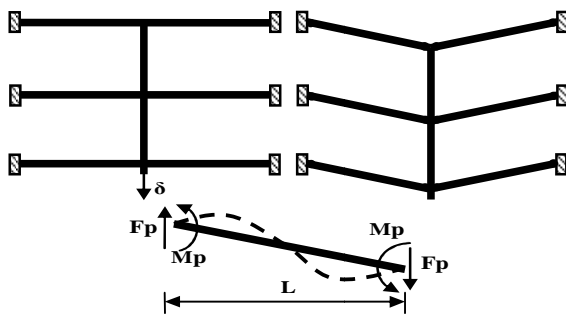


Fig. 4: Beam yielding effects.

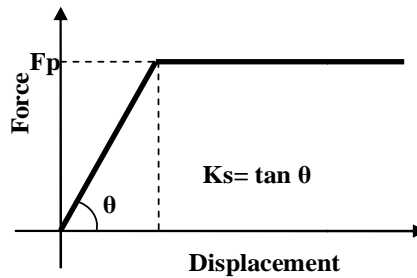


Fig. 5: Force-Displacement Curve.

2.3 Extended model

After the column has initially failed, large deformations develop in the attached beams. The force shed by the failed column transfers to the adjoining members through catenary action. To investigate the effect of this catenary action, a sub-frame with column and beam members is shown in Fig.6. The top of column and the outer ends of the beams are restrained by springs. As discussed above, the spring at the top of the column is inelastic, while the lateral stiffness provided by the adjoining columns is represented by elastic springs. The stiffness of the lateral restraint springs at the ends of the beams provided by neighbouring column bays, and is calculated as:

$$K_C = \frac{12E \sum I_s}{L_s^3} \quad (6)$$

In order to test the ability of the extended model to predict the column behaviour in a frame, the results from this model have been compared with those from full-frame analysis. As can be seen from Fig.7, the extended model can predict very well not only the initial failure temperature of the column but also the re-stabilisation of the frame.

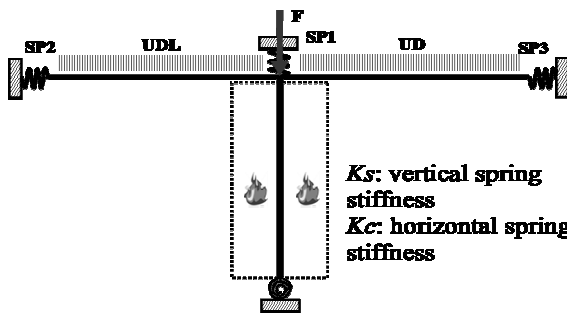


Fig. 6: Simplified model.

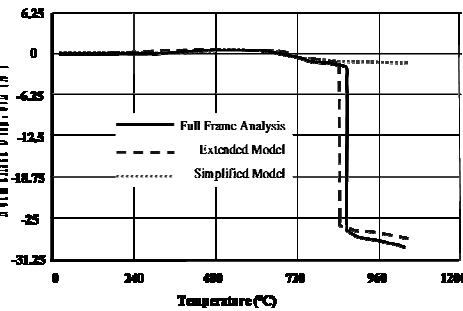


Fig. 7: Comparison of results.

3 PRELIMINARY PARAMETRIC STUDIES

With the simplified model, the key behaviour of frame can be predicted rather than carrying out complex full frame analysis. Three stages of failure have been described above. The restraints from above beams and lateral supports significantly affect the structural behaviour during these three stages. In first stage, the axial restraint of column influences the critical temperature of column buckling; in second stage, the strength of restraints determines whether the beam above yields or not; in last stage, the centenary force develops in beam and connections and lateral restraints would be important for re-stabilisation of frame. Several parameters have been studied to identify their influence on the behaviour of column considering the interaction with surrounding members.

3.1 Strength and stiffness of restraints from superstructure

When the heated column has buckled, the beams will support an increased proportion of the superimposed load. If the beams are strong enough, the column will not necessarily collapse completely. The ultimate collapse temperature will relate not only to the stiffness of restraints but also to their strength. Columns with restraints of different stiffnesses and strengths have been tested. The change of strength and stiffness are indicated by the strength ratio F_p/F_b , and the stiffness ratio K_s/K_c , respectively. K_s is the restraint stiffness and K_c is the axial stiffness of the column; F_p is the aggregate strength of restraints, and F_c is the axial resistance of the column (based on Eurocode 3 values). As shown in Fig.8, for cases with restraints of low strength, the model is effectively a simply supported column under axial force, so the collapse temperatures for different restraint stiffness are identified. As the strength of restraints increases, the collapse temperatures of columns increase and vary with different stiffness ratio of restraints. With the same strength of restraints, the higher stiffness achieves higher collapse temperatures. This is shown in by Fig.9. There are two points during a fire at which the beams may yield. The first occurs during the initial column heating, when the beams resist the thermal expansion of the column and reverse moments increase at the ends of beams. It is possible for the beams to yield under this scenario. The second occurs

when the heated column has buckled, and the beams cannot support enough of the superimposed load. Two lines, “Pre-buckling yield” and “Post-buckling yield” locate these two conditions. Each has two intersection points with the axial force curve for the column with elastic restraint. The first intersection point with the “Pre-buckling yield” indicates beam yielding before column buckling, while the second intersection with “Post-buckling yield” indicates beam yielding after initial column buckling. The axial force curve for columns with inelastic restraint should be obtained as shown in this figure. The results shown in Fig. 8 are only for stocky columns (slenderness ratios 30 and 60); for slender columns the results could differ, but the rationale implied by Fig. 9 can also be used for slender columns.

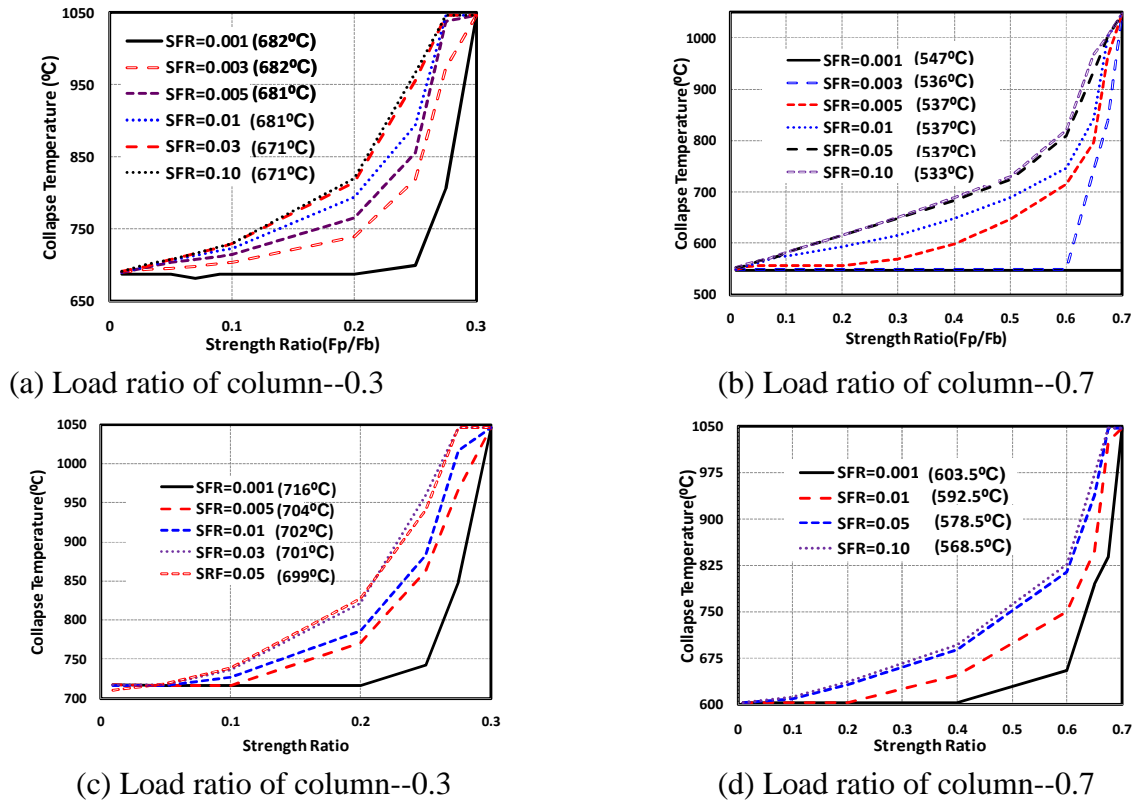


Fig.8: Collapse temperatures of column: (a), (b) for slenderness 30; (c), (d) for slenderness 60.

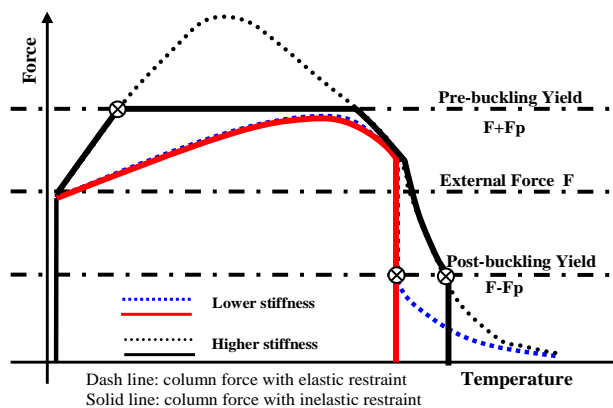


Fig. 9: Axial force development in column with rising temperature.

3.2 Stiffness of lateral restraints and connection rigidity

After the collapse of column, lateral restraint becomes the most important factor to determine whether (or when) re-stabilisation occurs. The three failure stages are indicated in Fig.10. Stiffer lateral stiffness provides a lower displacement at re-stabilisation, but a smaller axial force in the beams. Connections are vulnerable, and may fracture, at this stage. As mentioned previously, the model can take rotational stiffness of connections into consideration. As indicated in Fig.11,

different connection rotational stiffnesses do not change the failure temperature or re-stabilisation displacements significantly.

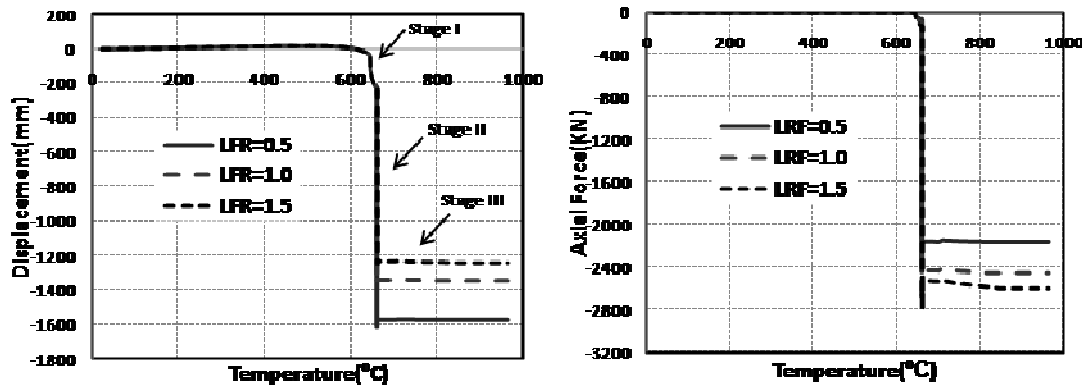


Fig. 10: Displacement of column top and axial force in beam with different lateral restraint stiffnesses ($LFR=K_v/K_c$).

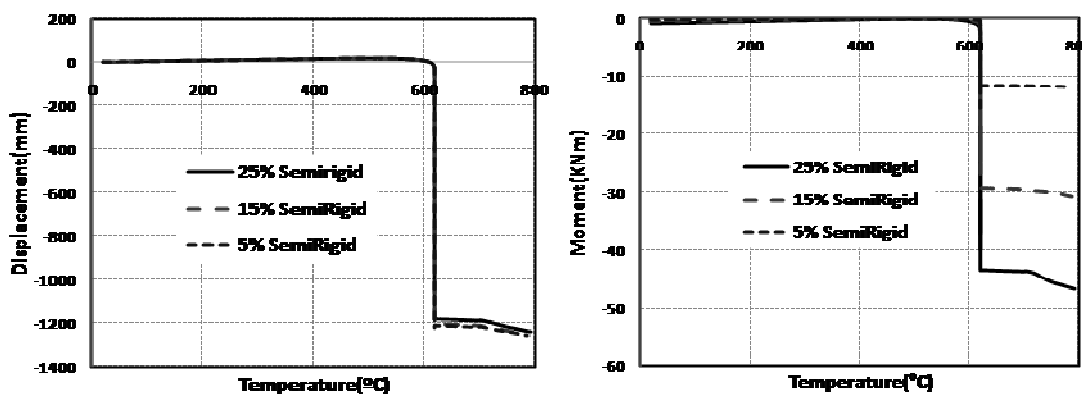


Fig. 11: Displacement of column top and moment with semi-rigid connections.

4 CONCLUSION

A simplified model has been proposed to study the column behaviour in framed structures based on the collapse mechanism of frame under localised fire. The boundary restraints from surrounding members are modelled by springs. The influence of stiffness and strength of restraints on the collapse temperature of column, and the effect of lateral restraints and connection rigidity on the behaviour of frame after column fails have been studied. It is an effective way to predict the structural behaviour under fire without carrying out complex detailed analysis. This method can be adopted to propose different simplified models for different frame under various fire scenarios. This model is based on 2D frame containing beam, column and connections. It is also feasible to include slabs into simplified models to investigate behaviour of composite frame under fire scenarios.

REFERENCES

- Shepherd P., The Performance in Fire of Restrained Columns in Steel-framed Construction, Phd Thesis, University of Sheffield, 1999.
- Y.C. Wang, Post-buckling behaviour of Axially Restrained and Axially Loaded Steel Columns under Fire Conditions, Journal of structural Engineering, March 2004.
- Franssen, J. M., Failure temperature of a system comprising a restrained column submitted to fire. Fire Safety Journal, 34, 191-207, 2000.
- Ali F., Nadjai A., Effect of Rotational Restraint on Performance of Steel Column in Fire, Journal of Applied Fire Science, 21-34, Volume 13, Number 1/2004-2005.
- RR Sun, ZH Huang, IW Burgess, A Static/dynamic Procedure for Collapse Analysis of Structure in Fire, Fireseat, Edinburgh, 2010.
- Poh K W, Bennetts I D. Analysis of structural members under elevated temperature conditions. J Struct Eng, 1995, 121(4): 664–675.

THE ROLE OF ACTIVE FIRE PROTECTION MEASURES IN A NATIONAL FIRE SAFETY CONCEPT IN GERMANY

Christoph Klinzmann^a

^ahpbberlin - Ingenieure für Brandschutz GmbH, Hamburg, Germany

INTRODUCTION

At the moment the building codes in Germany that regulate the fire protection of structural elements are prescriptive. This means that these codes contain requirements regarding the necessary fire resistance class of structural members which depend on the usage of the building.

With the implementation of the fire parts of the Eurocodes in 2011, realistic natural fire models are allowed for to be applied in structural fire design. The Eurocodes will make it possible that the structural members can be designed economically according to the boundary conditions like fire load, ventilation conditions and the geometry of the building. The application of the Eurocodes must be embedded within a holistic safety concept that ensures that the overall safety level is not reduced to an unacceptable level due to reduced design requirements. For the application in Germany a new safety concept was developed, which replaces the informative Annex E of Eurocode 1 part 1-2 (DIN EN 1991-1-2, 2010).

In this paper the main focus lies on the effect of the interaction of different safety measures, the resulting overall safety level and their consideration in the safety concept.

1 ACTIVE FIRE PROTECTION MEASURES

In Germany, the main focus of fire protection lies on structural fire protection measures. They have the advantage to be very effective in means of performance. Other countries like Great Britain follow different philosophies with a reduced amount of structural protection measures and more active fire protection measures like fire alarm systems or sprinklers in some cases. Active protection measures are usually composed of more or less complex technical systems. This means that they are at least subjected to potential failures or malfunctions under certain conditions. More complex and possibly less redundant systems lead to a higher probability of failure of a measure.

The aim of all active fire protection measures is to control the fire in one way or another. In the ideal case the fire can be extinguished, in some cases the fire size can only be reduced or the fire can be controlled to prevent it to spread beyond the compartment of origin. The measures can be considered as barriers preventing the starting fire from becoming a fully developed fire that affects the rest of the building concerned.

Active protection measures can be classified by their type and their influence on the fire. Direct measures, like the fire brigade or a sprinkler system affect the fire directly, e. g. by its extinction. Indirect measures like fire alarm systems only have impacts on the direct fire protection measures or on the consequences of a fire.

One of the main targets of the investigation described in this article was to quantify the safety benefit of active fire protection measures in structural design. This was achieved using the methods of probabilistic system analysis.

2 EFFECT OF ACTIVE PROTECTION MEASURES IN DESIGN FIRES

The definition of the design fire is the starting point of a performance-based fire safety design. In most applications, a design fire usually consists of the so called heat release rate (HRR) that describes the release of energy due to the fire over a period of time. Figure 1 exemplarily shows the different stages of a design fire for different types of fires. The fire starts with the ignition and is followed by the fire spread. It is widely assumed that the energy release during the fire spread follows a quadratic law ($\alpha \cdot t^2$ approach, ISO/CD 13388). After reaching the maximum heat release

rate (ventilation or fuel controlled), the energy release is assumed to remain constant until a decaying phase starts which leads to a subsequent extinction of the fire when all available fire load has been burnt.

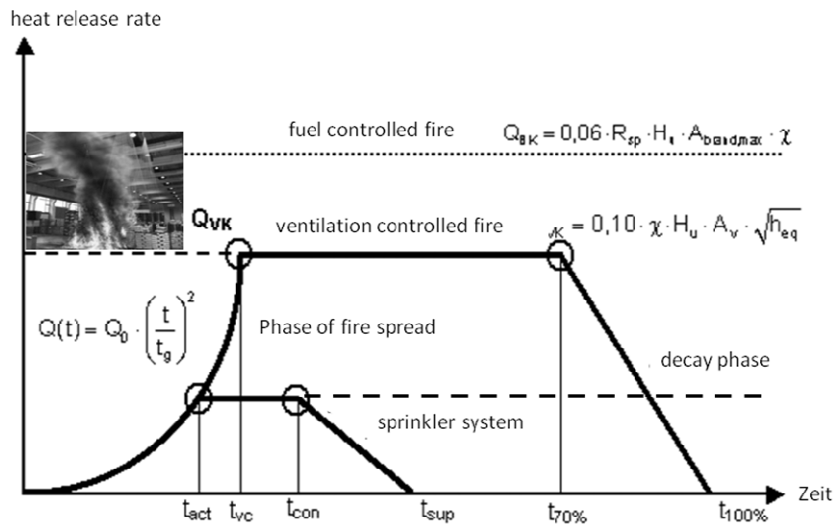


Figure 1: Heat release rates for different types of fires

Active fire protection measures can affect the release of energy during a fire, but some measures are only able to affect the consequences of the fire (e. g. temperature or toxic combustion products).

A sprinkler system is usually able to control or even to extinguish the fire at an early stage. In this case, the energy release into the room is reduced significantly. This is shown in figure 1, the sprinkler system is activated at the time t_{act} and controls the fire at t_{con} and is able to extinguish the fire at t_{sup} .

The work of the fire brigade can be considered in a similar way, with the difference that due to a longer response time of the plant or the public fire brigade, the fire spread takes longer, leading to a higher amount of energy release compared to a fire controlled by sprinklers. Plant fire brigades with better knowledge of the premises and significant shorter driving times usually have significant shorter response times.

A fire alarm system is an example for an indirect measure. In most cases a fire alarm system shortens the time of detection of the fire, leading to an earlier response of the fire brigade and lower energy releases.

Smoke and heat exhausts usually do not affect the heat release rate fuel controlled fires that are most relevant for structural fire design. For that reason, the consideration of smoke and heat exhausts was omitted in the safety concept for the moment.

It was already mentioned that every technical system can malfunction, active fire protection measures are no exception. Apart from their effect on the fire, the quantification of a safety benefit of a measure requires knowledge about its reliability. The available information will be discussed in the following chapter. A deeper discussion can be found in Klinzmann and Hösler, 2009.

3 RELIABILITY OF ACTIVE FIRE PROTECTION MEASURES

In Germany statistics about fire events are not collected systematically, at the moment no centralised fire database or statistics are available for the public. For that reason the data used for the analysis described here was based on literature studies (e.g. of VDS, 1990).

It was found that the probability of failure of a fire alarm system is likely to lie between $p_{f,fa} = 0,05$ and $p_{f,fa} = 0,10$. Analogous to fire alarm systems, sprinkler systems must be serviced well to achieve to relatively low probability of failure of $p_{f,sprinkler} = 0,02$ that was found in the studies.

The determination of a probability of failure of fire fighting is more complicated. It is common knowledge that fire fighting measures can fail as well. For the analyses it was assumed that this is

the case when the fire is able to spread beyond a size that cannot be controlled anymore. It was assumed that this is the case if the fire has reached an area of 200 m². The benefit of fire alarm systems in terms of the increased reliability of fire fighting measures was modelled by a gain of time in the overall response time of the fire brigade of 5 minutes. The reliability data acquired is required to quantify the overall safety benefit of the different measures and their combinations or interactions. This is the basis for the determination of safety factors that can be applied on the parameters of design fires in order to consider positive effects of installed active fire protection measures. In the following, the probabilistic system analyses carried out to quantify the safety levels and safety benefits in the different scenarios as well as some exemplary results are explained.

4 PROBABILISTIC SYSTEM ANALYSES

The effect of the different active fire protection measures on the reliability of a structural member in a fire was investigated in a research project during which the safety mentioned concept was developed (Hosser et al., 2009).

The probabilistic system analyses that were carried out had to consider all possible outcomes of fire scenarios evolving from of functional and not working active fire protection measures. This can be seen in figure 2, where a system consisting of an automatic and a manual fire alarm system, a sprinkler system, an on-site plant fire brigade as well as a public fire brigade is illustrated via an event-tree.

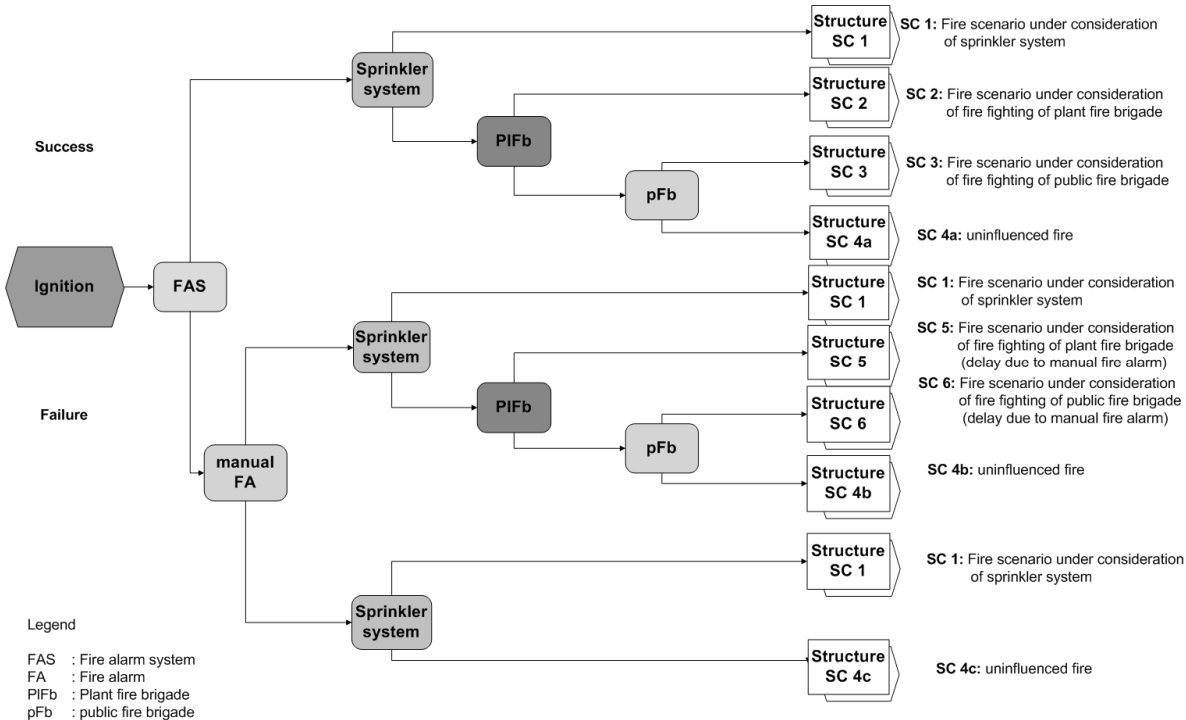


Figure 2: Event-tree for the system of active fire protection measures

Event tree analyses help to investigate how the different measures (barriers) affect the development of the fire in the compartment, the size of the fire and its consequences starting from the event “ignition of a fire in the compartment”. Each failure of a barrier increases the probability that the fire becomes a fully developed fire that can spread beyond the compartment of origin and stresses the structural members with higher temperatures.

The probabilistic system analysis computes the probability of failure of a structural member due to the different scenarios at discrete time intervals. The overall probability of failure p_{fi} or the reliability index β_{fi} respectively of the whole system of active fire protection measures and the structural element is computed in a subsequent step via the logical relations determined with the help of the event-tree. The boundary conditions of the different scenarios and the stochastic models that were analysed and the models used can be found in [Klinzmann, 2009 and Hosser et al., 2009].

In many cases more than a single type of active fire protection measures has to be considered. Especially buildings like high-rise towers, shopping malls, stadiums and large atria are equipped with different types of measures that interact with each other. The problem is that the effects of the protection measures are not necessarily independent.

The interaction of plant and public fire brigades that are called to the same fire scene can be taken as an example. Usually the plant fire brigade responds to the fire earlier than the public fire brigade due to longer distances and less knowledge of the premises. This means that the additionally called public fire brigade is not able to increase the reliability of the structural members in the burning room significantly in case a well working plant fire brigade is present. The safety concept must ensure that the actual safety level is not overestimated because of the interaction of non-independent active fire protection measures. For that reason the additional consideration of a public fire brigade in case a plant fire brigade is present is not allowed according to the safety concept.

5 RESULTS

In the system reliability analyses carried out the following protection measures and combinations of active fire protection measures were investigated in addition to the uninfluenced fire:

- a fire brigade with an overall response time of 20 minutes
- a fire brigade with an overall response time of 20 minutes and a well serviced sprinkler system
- a fire brigade and a fire alarm system (FAS)

The analyses were carried out on the basis of the event tree in figure 3 that was simplified according to the measures considered, leading to four different design fires for the structural member. The results of the analyses are shown in figure 3.

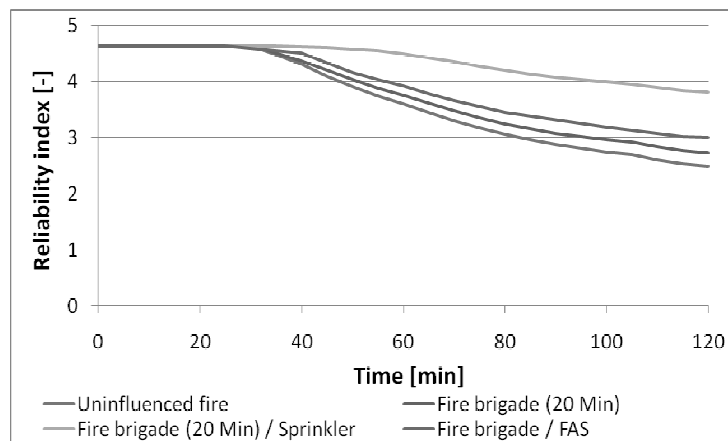


Figure 3: System reliability index under consideration of different active fire protection measures

The graphs show the development of the reliability index at discrete points in time for the 4 different scenarios. It can be seen that in all solutions the reliability starts to decrease after a time span of approximately 30 minutes. This means that up to this time the structural member under no circumstance reaches a critical temperature. The structural member used in this case is an insulated steel beam, which shows a performance similar to members made of concrete. Unprotected steel beams would reach lower reliability indexes earlier due to the quicker heating.

It can be seen that the active fire protection measures have different impacts on the overall reliability level. The blue line represents the uninfluenced fire and is taken as reference solution. Its minimum is obtained after 120 minutes and lies around a value of $\beta=2.50$ for the reliability index. The scenario with the next higher reliability is the one with the consideration of fire fighting by a fire brigade with an overall response time of 20 minutes. The probability of failure of the fire fighting lies around $p_{f,FW} = 0,50$. The minimum reliability index of this scenario after 120 minutes is approximately $\beta=2.75$. In the next scenario a fire alarm system that provides a gain in response time of the fire brigade of 5 minutes is considered, leading to a minimum reliability index of approximately $\beta=3.00$. In an earlier study [10] it was found out, that a fire alarm system is able to

reduce the probability of failure of the fire fighting by a factor of around 0.5, depending on the overall response time. The scenario with the highest reliability considers a sprinkler system with a probability of failure $p_{f,sprinkler}=0.02$ in addition to the fire fighters. The minimum reliability index in this scenario lies at around $\beta=3.85$.

The investigations described were able to quantify the reliability benefit of the different measures. Additionally, it was found out that the scenario of the uninfluenced fire, occurring if all active fire protection measures fail, is the representative scenario. This phenomenon is independent of the active fire protection measure and the complexity of the event-tree. This is shown in table 3. The table compares the reliability index computed within the system analysis with a reliability index computed based on the reliability index calculated from the reliability index of the uninfluenced fire. The probability of failure can be computed from the reliability index via the relation $p_f=\Phi(-\beta)$ and vice versa via the relation $\beta=-\Phi^{-1}(p_f)$, being Φ the Gaussian distribution and Φ^{-1} its inverse.

Table 3: Comparison of reliability indexes

Scenario	Reliability index (System analysis)	Reliability index (calculated with probability of failure)
Uninfluenced fire	~ 2.50 ($p_f=6.2E-3$)	$-\Phi^{-1}(6.2E-3)=2.5$
Fire fighters	~ 2.75	$-\Phi^{-1}(6.2E-3*0.5)=2.74$
Fire fighters and fire alarm system	~ 3.00	$-\Phi^{-1}(6.2E-3*0.5*0.5)=2.96$
Fire fighters and sprinkler system	~ 3.85	$-\Phi^{-1}(6.2E-3*0.5*0.02)=3.84$

The safety concept developed for Eurocode 1 that is published in DIN EN 1991-1-2, 2010 makes use of the described results. It provides representative data for the probability of failure of different active fire protection measures and formulas to consider this information in the calculation of the required reliability level. A higher amount of active fire protection measures leads to a lower required reliability. This influences the values of the partial safety factors for the maximum heat release rate and the fire load density. A lower required reliability leads to lower partial safety factors. This shows that active fire protection measures can be used to reduce the requirements demanded of structural members. More details can be found in Klinzmann, 2009.

6 IMPLEMENTATION INTO SOFTWARE

With the introduction in 2011, the described safety concept will be applicable in Germany. The partial safety factors that are required for the leading input parameters are either tabulated or can be programmed easily. They will be available in the relevant software packages within short time.

7 CONCLUSION

The first part of this article briefly analysed different active fire protection measures and their effect on natural fires. In a subsequent step, the available data regarding the probability of failure of these measures was discussed. In Germany, no centralised statistics regarding the availability of such data exists. This leads to the problem that all analyses must rely on eventually biased information from manufactures or not in all cases representative data from different countries.

In the second part of this article, the probabilistic analyses carried out for the development of a safety concept for German National Annex of Eurocode 1 were explained. The main focus lays on the consideration of the active fire protection measures in the design fires for structural fire design. It was shown that a fire uninfluenced by active fire protection measures is the representative scenario that should be used as a basis of the design fire. The safety concept developed provides a methodology to consider the rareness of such an event positively via the probability of failure of the active fire protection measures available.

The probability of occurrence of the mentioned scenario of an uninfluenced fire in the building of concern must be analysed. Especially in large buildings with separations with a determined fire

resistance an uninfluenced fire in a whole storey of the building is unlikely and usually not representative. In these cases, a different fire, e. g. under consideration of active fire protection measures can be representative.

It must be mentioned, that these facts apply only for the fire design of structural members. The simulation of the egress of people from the building and of the smoke distribution in the building usually requires different design fires. The uninfluenced fire usually is representative due to the fact, that the egress of people from the building takes place during the phase of fire spread and should be finished long before the fire becomes a fully developed fire. In Germany, the safe egress of all people in the building is guaranteed by short escape routes. In most cases, the verification of a minimum smoke height, e. g. in convention centres, shall ensure safe and effective fire fighting measures. The representative scenario in this case must include the consideration of the effects for fire fighting.

REFERENCES:

- DIN EN 1991-1-2/NA: Nationaler Anhang - National festgelegte Parameter — Eurocode 1 - Einwirkungen auf Tragwerke — Teil 1-2/NA: Allgemeine Einwirkungen – Brandeinwirkungen auf Tragwerke; December 2010
- DIN EN 1991-1-2: 2003-09. Eurocode 1 - Einwirkungen auf Tragwerke - Teil 1-2: Allgemeine Einwirkungen; Brandeinwirkungen auf Tragwerke, Beuth Verlag, Berlin, Germany
- Hosser, D.; Weilert, A.; Klinzmann, C.; Schnetgöke, R.; Albrecht, C.: Erarbeitung eines Sicherheitskonzeptes für die brandschutztechnische Bemessung unter Anwendung von Ingenieurmethoden gemäß Eurocode 1 Teil 1-2“ (Sicherheitskonzept zur Brandschutzbemessung). Abschlussbericht zum DIBT-Forschungsvorhaben ZP 52-5-4.168-1239/07. Institut für Baustoffe, Massivbau und Brandschutz (iBMB), Technische Universität Braunschweig, November 2008
- ISO/CD 13388 Committee Document, *Fire Safety Engineering. Design Fire Scenarios and Design Fires*, ISO/TC92/SC4, 1997.
- Klinzmann, C.; Hosser, D.: Berücksichtigung abwehrender und anlagentechnischer Maßnahmen beim brandschutztechnischen Nachweis von Bauteilen, vfdb-Zeitschrift (2), April 2009, Kortlepel Verlag Zweigniederlassung der Ebner Verlag, GmbH & Co. KG, Bremen, Germany
- VdS Schadenverhütung, Jahresbericht 1990 / 91, Köln, Germany

COMPUTATIONAL MODELLING FOR PERFORMANCE BASED FIRE ENGINEERING (PBFE)

Francesco Petrini, Konstantinos Gkoumas

Sapienza University of Rome, School of Engineering, Rome, Italy

INTRODUCTION

Modern codes endorse two different methods for the design of structures subjected to fire: either by means of a prescriptive approach or with a performance-based approach. A prescriptive-based code provides for fire safety by prescribing some combination of specific requirements, without referring to the desired safety level or how it is achieved. In comparison, a performance-based code allows any solution that can lead to an *a priori* imposed safety level. In some cases, for example when dealing with complex structures where it is impossible to comply with all the architectural prescriptions specified by a prescriptive approach, a prescriptive-based code proves to be inadequate, and a performance-based approach is more appropriate in obtaining the optimal structural behaviour under fire.

On the basis of the above premises, this paper focuses on the application of the performance-based approach (in the context commonly referred as PBFE – Performance Based Fire Engineering) to an exhibition pavilion with a relatively complex geometry subject to fire. The structure is of interest since, due to its occupancy, it is prone to elevated fire risk.

Conceptually the paper is organized as follows: chapter one describes the case study and the fire scenarios considered under a performance based approach. Chapter two deals with the determination of the fire load using a computational fluid dynamic code (FDS - Fire Dynamics Simulator). Finally, chapter three reports the performed structural analysis, accounting for the non linearity of materials and the decay of their mechanical characteristics with the temperature

1 THE PERFORMANCE BASED FIRE DESIGN APPROACH

The performance based fire design (Pbfd) in the last years gained a lot of ground mostly for facilities prone to elevated fire risk. The focus is on the structural performance in the presence of fire and includes requirements of fire resistance both for the structural elements (e.g. beams, slabs, columns) or for the structural system as a whole (avoidance of excessive vibrations, of progressive collapse, etc.). A very important step to guarantee an assigned level of safety is to verify that the resistance of the structure under fire is higher than the fire severity (fire resistance > fire severity). In general, there are three techniques for checking the fire resistance: in the time, temperature or strength domain. An outline of the performance based approach implemented in this study is synthesized in the following paragraphs.

1.1 Design goals

It is necessary to predict not only the structural resistance, but also the level of damage in case of fire in order to assure an appropriate performance. In this study, the design goal set is that the structure has to resist to fire, withstanding the total combustion of any combustible material, within the whole building or in a specific zone, without intervention from the fire-fighters.

1.2 Structural collapse and performance metrics

The definition of structural collapse is delicate, especially when considering a strongly redundant structure. In fact, the failure of a single steel member does not lead to the collapse of the entire structure. In that case, it is possible to consider a limited deformability for a group of elements, so that the vertical displacement of some key points can be assumed as performance metrics.

1.3 Fire scenarios

In accordance with ISO/TS 16733 (2006), for a comprehensive description of the fire scenarios, the following aspects need to be specified:

- the fire source;
- the nature and physical characteristics of the combustible;
- the growth rate of the fire and the peak of rate of the released heat.

In the specific case, the structure is a strongly redundant rectangular building with sides of 144m and 72m (Fig. 1). It consists in 24 concrete columns. The horizontal elements consist in 3 steel reticular beams in the principal direction and 11 in the minor direction. The structure has two openings of 36x6 m in the centre of the smaller sides.

Given the structure's occupancy (exposition pavilion), it is realistic to consider inside the presence of stands. Each of these is assumed formed by a wooden table on top of which some paper is deposited, surrounded by three plastic shelves and two sofas.

In order to estimate the fire evolution in the structure, six scenarios have been considered. The source of ignition is considered to be the paper on the table. The position of the fire ignition according to the six scenarios is shown in Fig. 2.

In accordance with what is prescribed by EN 1991-1-2 (2002), the value for the Rate of Heat Release (RHR) has been defined on the basis of the occupancy of the structure. From table E.5 (EN 1991-1-2, 2002), the RHR considered is the one for a shopping centre. In this context the development of fire is fast. The following values have been considered to describe the fire development: $\alpha=0.04444 \text{ kW/s}^2$ (fire growth factor), $\text{RHR}_f=250 \text{ kW/m}^2$, $t_a=150 \text{ s}$ (time needed to reach a rate of heat release of 1 MW).

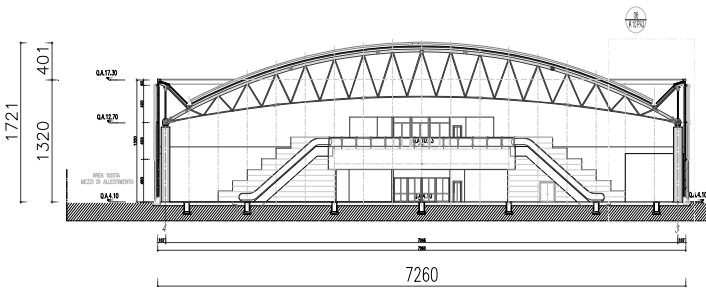


Fig. 1 Cross Section of the structure

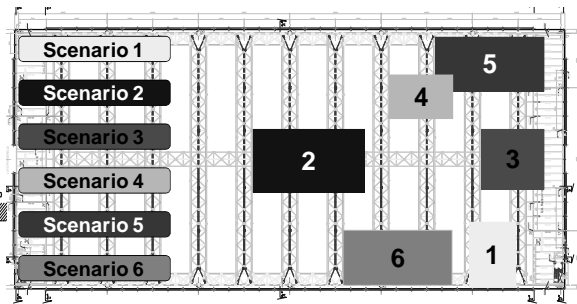


Fig. 2 Location of the six scenarios

In order to obtain the corresponding natural fire curves, standard procedures have been implemented (see for example, Karlsson and Quintiere, 2000). After the flashover, the RHR remains constant until the beginning of the decay that at this stage occurs according to a linear law. Following prescriptions from the ISO/TR 13387-1, 1999 and considering a fire load density of $q_{f,k}=600 \text{ MJ/m}^2$, taken from table E.4 of EN 1991-1-2, 2002, the characteristics of the RHR curve for the six scenarios are those indicated in Table 1.

Tab. 1 Values of the RHR curve in specific time points

Scenario	Area [m^2]	RHR_{max}	t_A [s]	t_B [s]	t_C [s]
1-3-4	216	54000	1102	1552	2512
2-5-6	432	108000	1559	2959	3919

Fig. 3 shows the two RHR-time curves used in all six scenarios. The analysis is divided in two steps:

- the determination of fire load (Joyeux et al, 2002);
- the characterization of the fire effects on the structure (Buchanan, 2008).

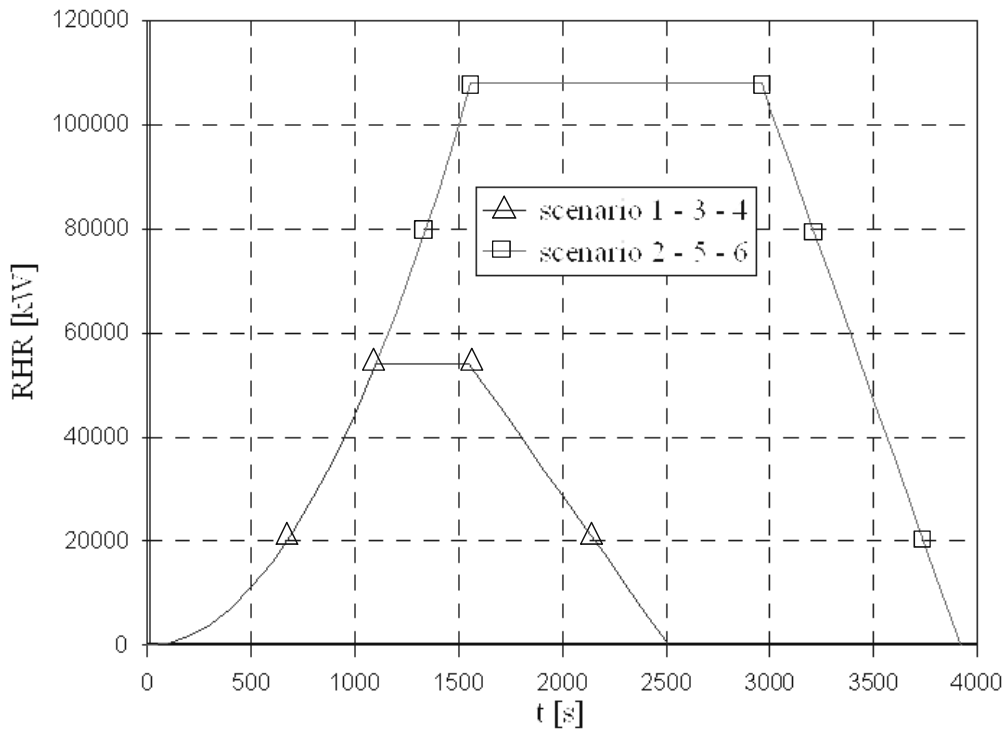


Fig. 3 RHR-time curves for the six scenarios

2 DETERMINATION OF THE FIRE LOAD

Three different analyses have been performed by means of a computational fluid dynamic (CFD) code (McGrattan et al, 2009) in order to determine the fire action in the structure:

- analysis of the sensitivity to the mesh;
- study of the boundary conditions;
- determination of the thermal map for each of the considered scenarios.

In the first analysis, the external environment has been considered as a solid at 20°C. Consequently, a sensitivity analysis has been carried out in order to establish the accuracy of the mesh.

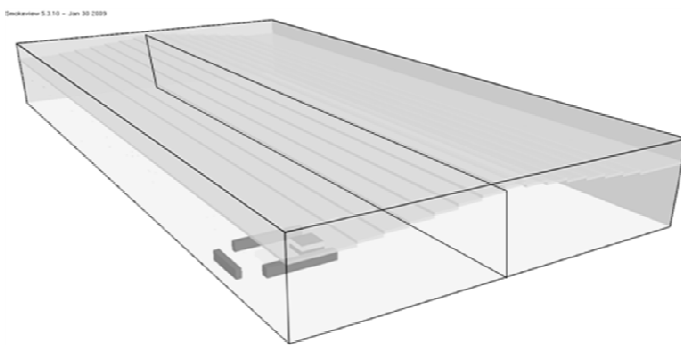


Fig. 4 Tridimensional model without external environment

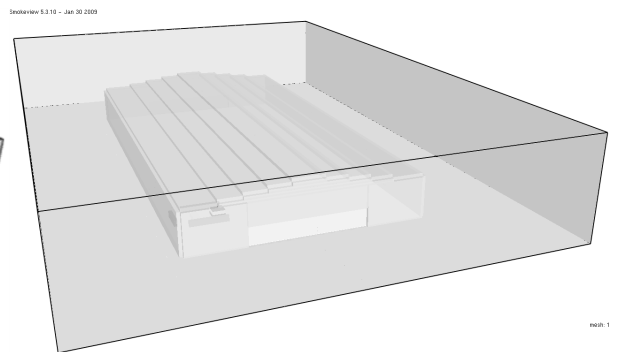


Fig. 5 Tridimensional model with external environment

In the analysis (Fig. 4), rectangular parallelepiped elements are used with base dimensions between 1.5 m and 0.5 m and height 1 m, or elements with a square base of 1 m and a variable height between 1.5 m and 0.5 m. Due to the lack of convergence of the phenomenon, a finer model has been realized. This model is composed by concentric cubic elements. As a consequence, a large amount of elements (about 440060) has been used, with a very high computational load (corresponding to analyses lasting about 70 hours).

In this model, scenario 1 has been analyzed, and the flashover occurs after 930 seconds.

The computation of temperature is strongly influenced by the boundary conditions. Thus, the model has been included in a larger environment in order to verify the role of the boundary conditions (Fig. 5). In a first place, the initial volume has been extended 4 m beyond the structure in the minor direction, 8 m in the major one, and 4 m in vertical direction. In the final configuration of the model, it extends respectively of 28 m, 36 m and 8 m.

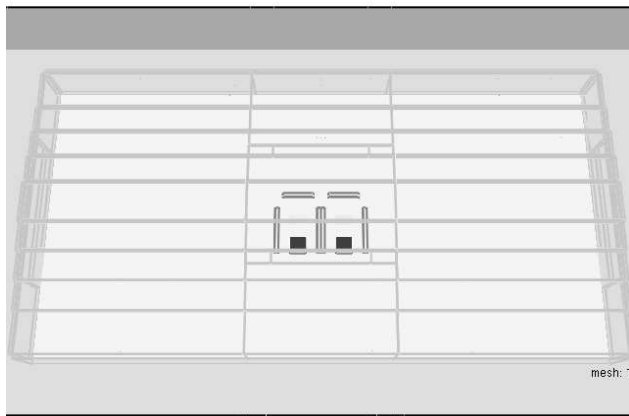
This model is characterized by a great amount of elements (more than 1 million) and by a huge computational load (with analyses running up to 10 days on a multi core PC).

In both cases, the validation of the model is based on the:

- qualitative analysis of the propagation of flames;
- global analysis by means of the RHR curve;
- local analysis applying temperature-time curves on the structural elements and the significant sections.

Once the model has been validated, a thermal map of the structure is realized by applying it to the six scenarios. Fig. 6 shows the modelling of scenario 2 in FDS. Fig. 7 illustrates the heat release distribution at the flashover development. The significant difference between the application of the ISO 834 nominal curve and the application of the natural curves obtained with the FDS software is highlighted in Fig. 8.

Smokeview 5.3.10 - Jan 30 2009



Smokeview 5.3.10 - Jan 30 2009

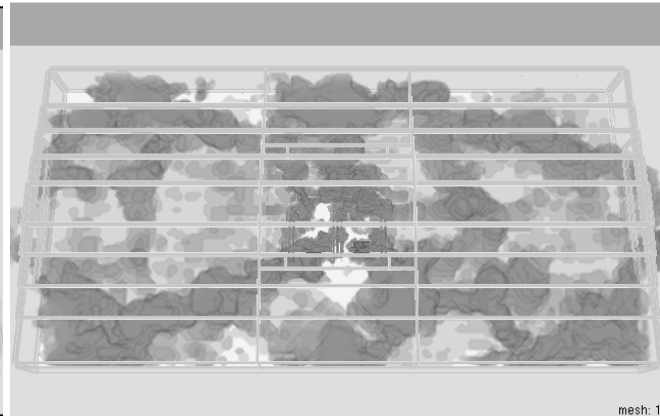


Fig. 6 Scenario 2 modelled in FDS

Fig. 7 Fire peak (flashover development)

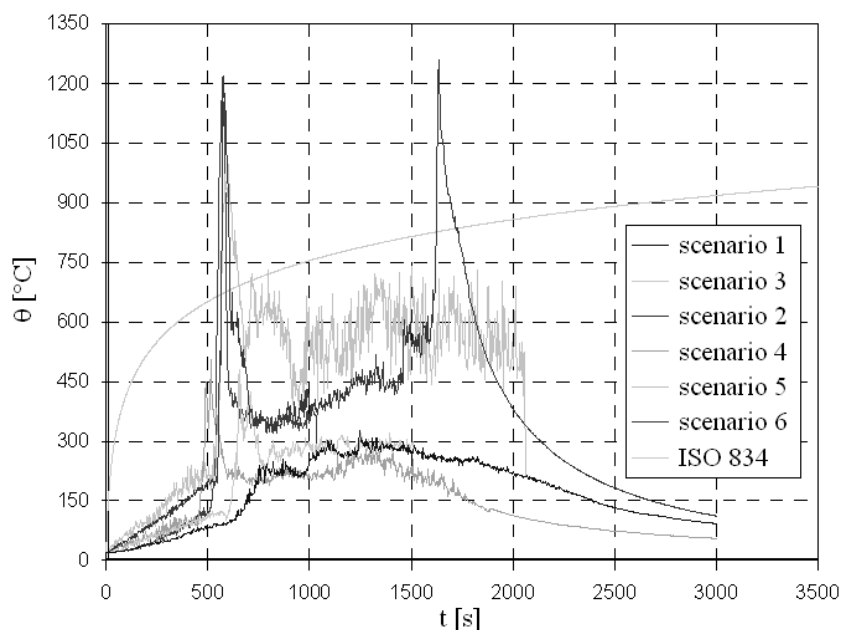


Fig. 8 Temperatures registered during the fire peak

3 STRUCTURAL ANALYSIS

The obtained fire load has been applied using the finite element code Straus7/Strand7 in order to inquire on the structural response (Usmani et al, 2001, Crosti et al, 2009). Figs. 9 and 10 show the vertical displacements corresponding to scenario 2 after the application of the nominal and the natural curves.

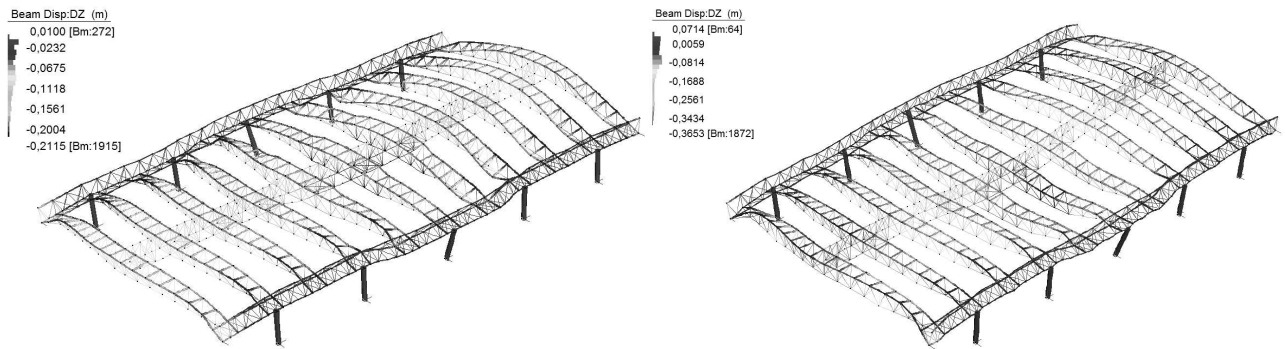


Fig. 9 Global displacements for scenario 2 with the nominal curve Fig. 10 Global displacements for scenario 2 with a natural curve

For the same load scenario, considering the critical node 322 (Figs. 11 and 12), Figs. 13 and 14 illustrate the vertical displacement. This analysis accounts for the non linearity of the materials and the decay of their mechanical characteristics due to the temperature variation (Crosti et al, 2009, Petrini and Bontempi, 2009).

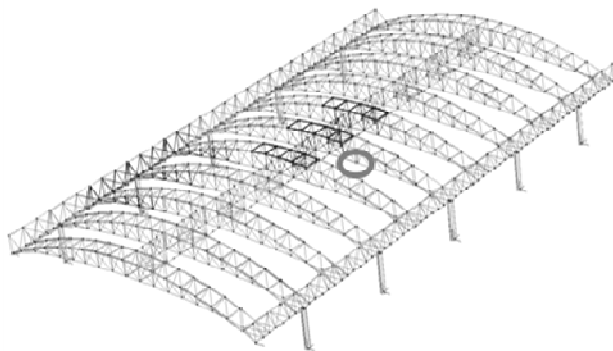


Fig. 11 Position of node 322

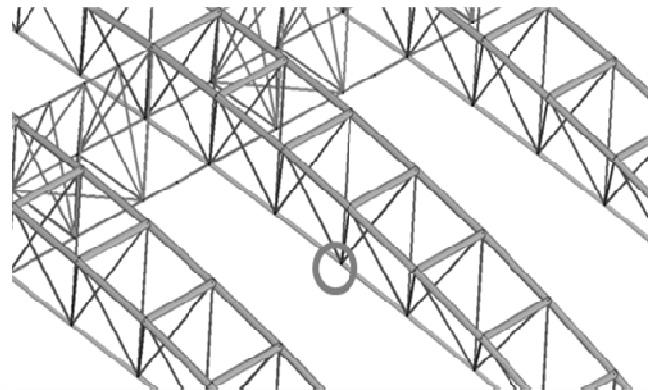


Fig. 12 Position of node 322 (detail)

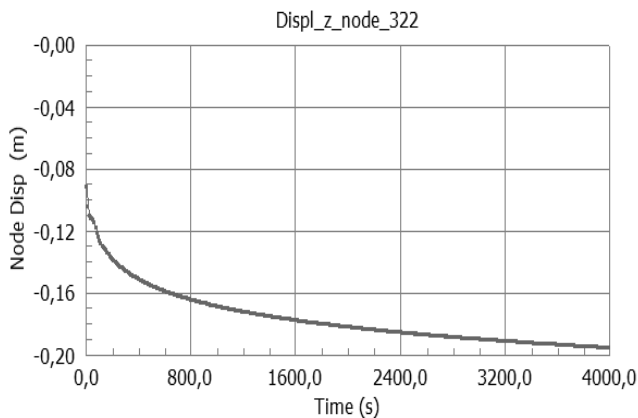


Fig. 13 Vertical displacements for scenario 2 with the nominal curve

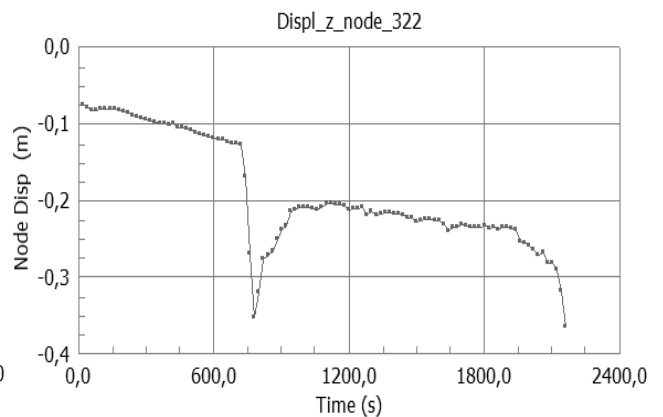


Fig. 14 Vertical displacements for scenario 2 with a natural curve

The difference between the two curves can be explained considering the differences between the temperature distributions obtained in two cases. In fact, whereas a thermic load can be applied outside the nominal area of the scenario using natural curves, it is not realistic to consider the nominal curve outside the scenario area.

The adequate behavior of the structure under fire, leads to the accomplishment of the prescribed performance. Moreover, the alternative load paths among the elements emerge. Conclusively, it is important to highlight the local collapse in some fire scenarios.

4 CONCLUSION

In the present paper, aspects concerning the numerical analyses for the performance based fire design of complex structures has been inquired. An application on a complex steel structure has been presented, where both computational fluid dynamic analyses for the assessment of the fire development and structural analyses for the structural response investigation are developed. The analyses show that use of advanced methods for the numerical simulation of fire is fundamental in order to obtain reliable results in assessing the structural behaviour.

Even though simplified methods for the fire modelling, using nominal fire curves, apparently conduct to similar results (in terms of the deformed shape under fire), using more advanced methods with CFD, a detailed description of the structural response (e.g. the detail on the vertical displacement time history for critical nodes) highlights the great difference of the two methods in obtaining the structural response. Considering the above, the use of advanced numerical simulations is recommended, especially for complex structures.

ACKNOWLEDGMENTS

The authors wish to thank Prof. Franco Bontempi, Prof. Luca Grossi and Mr. Filippo Gentili of the Sapienza University of Rome, Piergiorgio Perin of HSH srl and Dr. Luisa Giuliani of the Technical University of Denmark - DTU for their fundamental support to this study.

REFERENCES

- Buchanan A. H., Structural Design for Fire Safety, Wiley, 2008.
- Crosti C., Giuliani L., Gkoumas K., Bontempi F., Structural analysis of steel structures under fire loading, Applications of Structural Fire Engineering, Prague 19-20 February 2009.
- EN 1991-1-2, Eurocode 1: Actions on structures – Part 1-2: General actions – Actions on structures exposed to fire, European standard, 2002, CEN, Brussels.
- ISO/TR 13387-1:1999 (E) Fire Safety Engineering - Part 1: Application of fire performance concepts to design objectives. Technical Report. Geneva: International Organization for Standardization.
- ISO/TS 16733: Fire safety engineering – Selection of design fire scenarios and design fires, Technical Committee ISO/TC 92, 2006.
- Joyeux D., Kruppa, J., Cajot L., Schleich J., Van de Leur P., Twilt L., Demonstration of Real Fire Tests in Car Parks and High Buildings, Final Report, Contract No. 7215 PP 025, CTICM, Metz, France, 2002.
- Karlsson B., Quintiere J.G., Enclosure Fire Dynamics, CRC Press, 2000.
- McGrattan K., Klein B., Hostikka S., Floyd J., Fire Dynamics Simulator (Version 5) – User guide, NIST, Special Publication 1019 – 5, Washington, USA, 2009.
- Petrini F., Bontempi F., Performance-Based Fire Engineering, Atti del XXII Convegno Collegio dei Tecnici dell'Acciaio (CTA), Padua, Italy, 28-30 September 2009, (in Italian).
- Straus7/Strand7, www.strand7.com.
- Usmani A.S., Rotter J.M., Lamont S., A.M.Sanad, Gillie M., 2001, Fundamental principles of structural behavior under thermal effects, Fire Safety Journal, 36, 721-744.

LOADING-BEARING CAPACITY METHOD FOR STRUCTURAL FIRE SAFETY DESIGN – A CASE STUDY

Du Yong^a, Li Gou-qiang^b

^a Nanjing University of Technology, School of Civil Engineering, China

^b Tongji University, School of Civil Engineering, China

INTRODUCTION

Since the Cardington frame fire tests in UK in the 1990s, structural design for fire safety based on single element behavior in the standard fire resistance test has been negated. A great deal of work on the behavior of steel structures in large space buildings fire has been developed since 2000s in China [1]~[3]. It is revealed that the temperature during a large space fire is different from that in compartment fire described schematically by the Fig.1 and Fig.2 which show the non-uniform temperature field for the horizontal plane at a given height of large space and the typical temperature history of growth and full development phase. The non-uniform temperature field remains some parts of the structure at relatively low temperature. These cooler parts adjacent can provide adequate restrain and stiffness to the heated area, and restrained thermal expansion will lead to thermal stress in the heated area during fire period. Structural collapse will occur if load sharing exceeds the structural loading capacity, although the maximum temperature shown in Fig.2 is lower than the standard test. On the other hand temperature histories in large space fire should be gotten instead of ISO-834 and other standard temperature curves for large space structural fire safety design. The behavior of single structural element heated in a furnace with a standard fire exposure dose not consider the real boundary and load situation, the result from standard test can't represent of the real structural element response in whole structure in large space fire. These are proved by centenary action in beams and tensile member action in slabs found in the behavior of real structure [4]. However calculation methods are developed in advanced fire-resistance design.

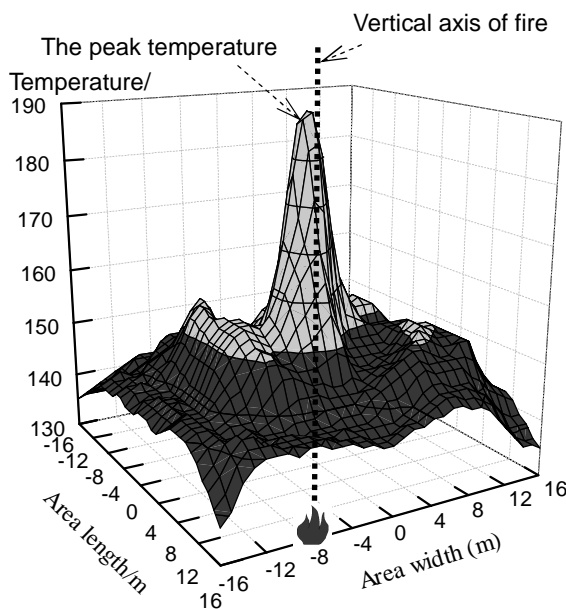


Fig. 1 FDS simulated temperature distribution in the horizontal plane at 6m height from fire

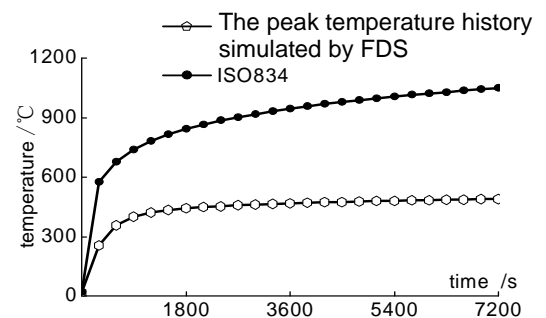


Fig. 2 Comparison of FDS simulated the maximum temperature history and ISO834 curve

1 LOADING-BEARING CAPACITY METHOD

Experimental and analytical methods are suitable for evaluating the performance of structural fire resistant if the boundaries fit to the real structure. Whereas it is difficult to simulate the boundary

conditions of elements in real structures and natural fires, the standard fire test bears very little resemblance to the behaviour of any but the simplest of real structure. The whole structure fire test isn't widely employed in routine structural design for its expensive and complex.

Some fire design codes have now been introduced for designing structures to resist fire by calculation. In principle fire loading can be treated as any other form of load. However, the structural behaviour in fire in all but the simplest case is much more complex than normal temperature for the material characteristics varied with temperature. Computer-based finite element methods are employed which include the non-linear material properties temperature dependent and the effects of thermal expansion. The loading-bearing capacity method carries out a structural analysis for the fire situation with the method discussed above, and check structures loading-bearing capacity in fire ultimate limit stat. The basic steps in loading-bearing capacity method for structural fire safety design are:

- (1) design fire scenarios based on fire performance and determine the fire temperature distribution,
- (2) determine critical temperature based on FE calculated,
- (3) guess the thickness of fire protection for members (without fire protection is permitted),
- (4) calculate the maximum temperature in members,
- (5) if the maximum temperature in member is lower than critical temperature, come back step (3).

2 THE BUILDING

As a part of the complex cultural center, the auditorium covers 896m² with 1100 seats shown in Fig. 3~Fig.5. Because of the long span a steel grid structure roof was chosen, which is supported on the concrete columns above 13.965m high from the auditorium ground. The two rows of columns have 30m span and are space at 9m. The active fire protections are set in the auditorium to prevent the spread of fire and structural collapse during natural fire.



Fig. 3 Air photo of the auditorium

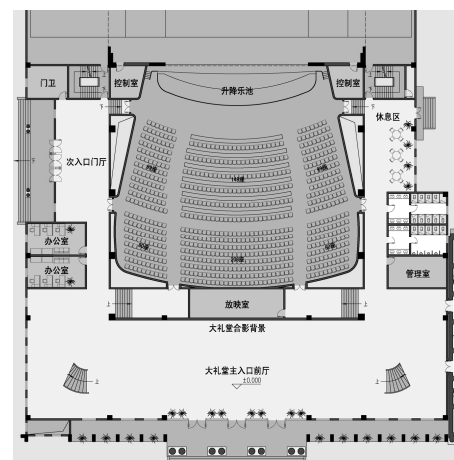


Fig. 4 Plan of the auditorium

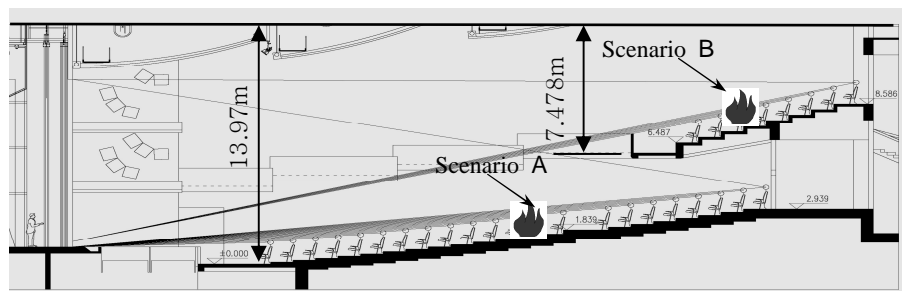


Fig. 5 Fire scenario in the auditorium

3 DESIGN FIRE

3.1. Fire scenarios

Scenario A– the auditorium covers $32\text{m}\times 28\text{m}=896\text{m}^2$ and with the height of 13.965m. The localized fire is in the middle of the compartment shown in Figure 5.

Scenario B – the balcony covers $32\text{m}\times 10\text{m}=320\text{m}^2$ and with the height of 7.478m. The localized fire is in the middle of the balcony shown in Figure 5.

3.2. Estimating rate of heat release

Stackable sofas are most commonly used in auditorium and are regarded as the main fire resource. The heat release rate of the fire must be known for calculation of fire behavior in auditorium. The test on HRR for real products have been run by Babrauskas and colleagues since 1980s at NIST. The highest HRR is 3MW recorded in Fig. 6 and the whole fire last 20min.

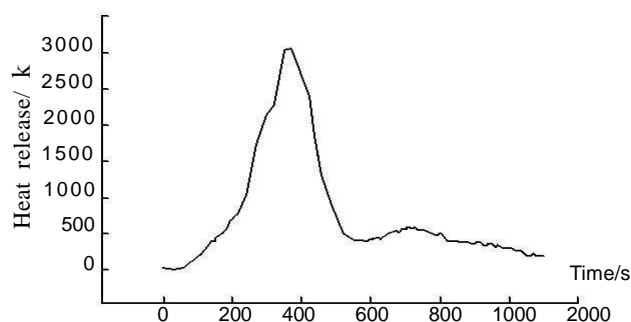


Fig. 6 Heat release history

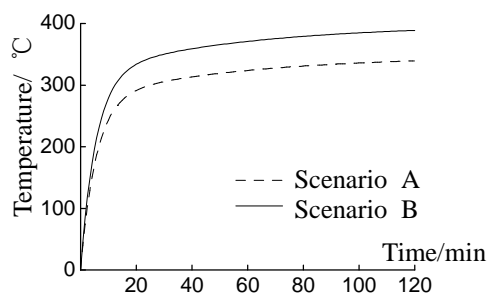


Fig. 7 The maximum temperature history for scenario A and B

The fire grows as the t-squared fire and fire growth coefficient for the fast fire is 0.04689kW/s^2 .

Taking account of the fire duration of members and fire traveling it has been considered as the most critical fire load that four sets of stackable sofa covered $3\text{m}\times 3\text{m}$ combust in the meantime, and the highest HRR is 12MW during fire course 1.5h.

3.3. Smoke temperature distribution

Due to the large dimension of the auditorium, a prescriptive rule using the standard fire curve ISO 834 isn't available and quite unrealistic. Temperature distribution in large space fires obtained from the parameter equation (1), which bases on the computational fluid dynamics [5].

$$T(x, z, t) = T_g(0) + T_g^{\max} \cdot f(t) \cdot k_{\text{sm}} \quad (1)$$

where $T(x, z, t)$ the smoke temperature at the point above floor and from the vertical axis of fire through the whole fire

$T_g(0)$ ambient temperature

x, z the horizontal distance from the vertical axis of fire, and the height above the floor

t the time in the temperature history

T_g^{\max} the maximum temperature of smoke, given by Eq.(2)

$$T_g^{\max} = (20Q + 80) - (0.4Q + 3)H + (52Q + 598) \times 10^2 / A_{\text{sp}} \quad (2)$$

where A_{sp}, H the floor area, and the height of the internal space respectively

Q the fire power

$$f(t) = 1 - 0.8e^{(-\beta t)} - 0.2e^{(-0.1\beta t)} \quad (3)$$

where β the regression parameter dependent on the fire growth types listed in table 1

$$k_{sm} = \eta + (1 - \eta)e^{(D/2-x)/7}, \quad \text{if } x \leq D/2, \text{ then } x = D/2 \quad (4)$$

$$D = 2\sqrt{A_q/\pi} \quad (5)$$

Where η the shape factor dependent on the floor area, A_{sp} , and the height of the internal space, H , listed in table 2

D the effective diameter of fire source

A_q the area of the fire.

Input each coefficient into Eq.2 and the maximum temperatures can be got as 347°C and 398°C in the scenario A and B respectively, and decrease from the vertical axis as the Eq.4. As large shape coefficient of chords, the temperatures in steel chords is the same as these hot smoke temperature.

Tab. 1 Factor β with fire growth types

	Fire growth type			
	Slow	Medium	Fast	Ulter
β	0.001	0.002	0.003	0.004

Tab.2 Factor η with volumes of large space building

A_{sp} (m ²)	H (m)				
	6	9	12	15	20
500	0.60	0.65	0.70	0.80	0.85
1000	0.50	0.55	0.60	0.70	0.75
3000	0.40	0.45	0.50	0.55	0.60
6000	0.25	0.30	0.40	0.45	0.50

4 STRUCTURAL FIRE ANALYSIS

4.1 Loading combination rule

For each load case, design value for the effects of actions shall be determined from accidental combination rule given as[5]

$$S_m = \gamma_{0T}(S_{GK} + S_{TK} + \phi_f S_{QK}) \quad (6)$$

$$S_m = \gamma_{0T}(S_{GK} + S_{TK} + \phi_q S_{QK} + 0.4S_{WK}) \quad (7)$$

where S_m the design value of the accidental actions

S_{GK} , S_{TK} , S_{QK} , S_{WK} the characteristic value of permanent actions, thermal actions in fire situation, occupational variable actions and wind action respectively

ϕ_f , ϕ_q the frequent and the quasi-permanent coefficient of the occupational variable actions respectively

γ_{0T} the safety coefficient of buildings in fire.

The more serious action between Eq.6 and Eq.7 will be employed.

4.2 Global FE model

The finite element model was developed using commercial software ANSYS to analysis the behavior of the space truss above auditorium during the design fire. Fig. 8 graphically shows a half of globe structure. The material properties assumed in FE model are given in Tab. 3, and the stress-strain curves at elevated temperature was shown in Fig. 9. The supports provide restraint in the horizontal directions and fixed in the vertical direction, but rotationally free. 3D axial elements were used to represent the steel tubes in space truss shown in Fig.10. Each element is associated with its appropriate section properties and material characteristics at elevated temperature. In the meantime the model elements were fully geometrically nonlinear. The temperature distribution as the result of Eq. 4 is loaded on each element node according to the maximum temperature, T_g^{\max} , in Eq.2. The heat transfer model of ANSYS software was used to establish the gradient through the longitudinal of the 3D Link8 element in response to Eq.1.

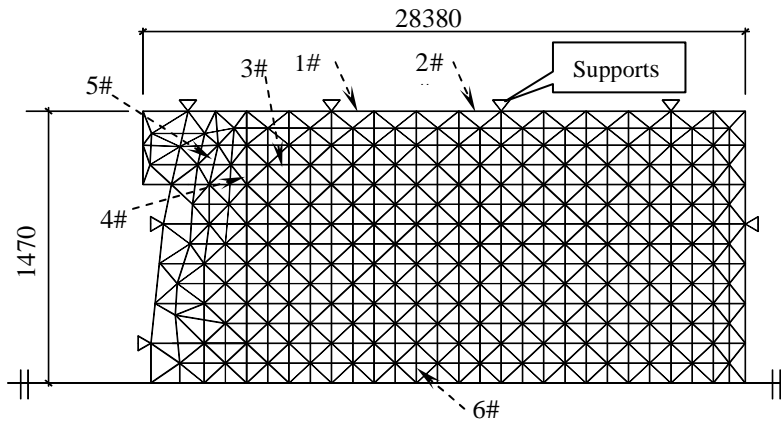


Fig.8 The space truss global model

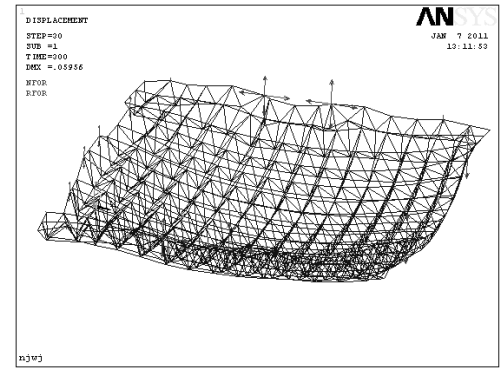


Fig.9 Deformation of FE model

Tab. 3 Material properties at elevated temperature

Parameter Name	symbol	value	unit
Thermal expansion coefficient	α_s	1.4×10^{-5}	$m/(m \cdot ^\circ C)$
Thermal conductivity	λ_s	45	$W/(m \cdot ^\circ C)$
Specific heat	c_s	600	$J/(kg \cdot ^\circ C)$
Density	ρ_s	7850	kg/m^3
Poisson 's ratio	ν_s	0.3	—

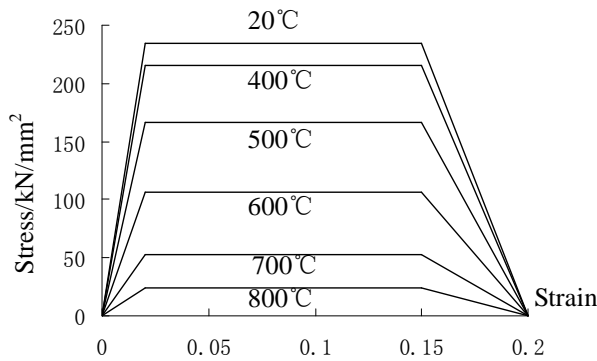


Fig.9 Stress-strain relation for steel at elevated temperatures

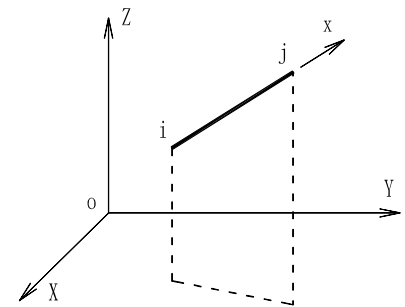


Fig.10 3D element for FE analysis

4.3 Failure criteria

To assess the result obtained from the FEA, ‘failure’ rule must be established. At ultimate limit state, stability of the structure would be maintained throughout the design fire. This is primarily assessed by checking in the rate of deflections during the fire. Runway deflections (a rapid increase in the rate of deflection) are assumed to indicate incipient failure of the structure. On the basis of the accidental combination rule, the following verification condition must be satisfied.

$$T_d \leq T_m \quad (8)$$

where T_d the maximum temperature of structures (or elements) subjected to design fire

T_m the critical temperature of structures (or elements) given by structural fire analysis as follow.

4.4. Thermo-mechanical analysis

In Fig. 11, the top chord 1# failed at 90°C for the strong restraint along the longitudinal axis, which connects the support directly, then bottom chord 3# and the web chord 4# failed at 410°C and 520°C respectively, finally the top chord 6# in the midspan of the space truss failed at 770°C. The sharp variations shown as Fig.11 reflect the internal forces redistributed performance as other member

failure, and the compress forces increased due to axial restrain. These thermo-mechanical coupling effects caused the chords failure. When one element lost its loading capacity, high redundant structures can redistribute to other stiffer and stronger elements. In Fig. 12 the greatest downward displacement in the midspan of the space truss increases with the maximum temperature elevated during fire history. At 770°C, the displacement increased rapidly and the global structure lost its loading capacity. The analysis indicated that the critical temperature, 770°C, at accidental load combination is higher than the maximum temperature, 398°C, in structure caused by the design fire scenario B. The space truss covered the auditorium design is fitted to the fire limit state without fire protection measures.

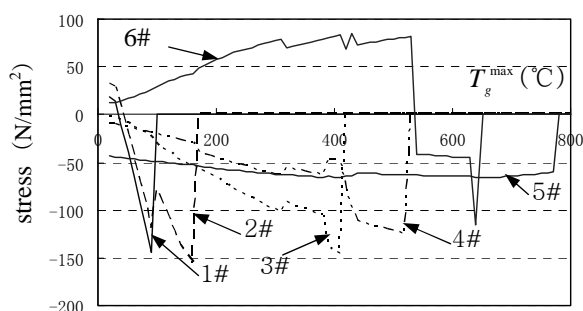


Fig. 11 Stress history curves

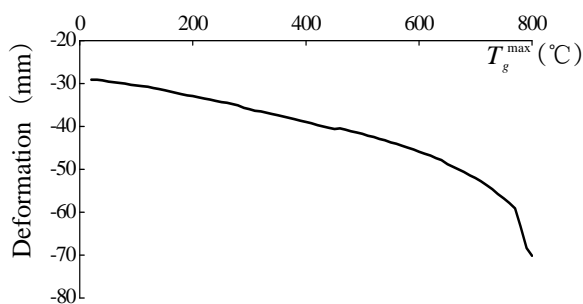


Fig.12 The great displacement history curve

5 CONCLUSIONS

This paper provides a snapshot of information and analysis to demonstrate the loading-bearing capacity method is sufficient for fire safety design.

A detailed FEA of the space truss with a credible design fire was carried out to determine the deflections and forces in the space truss.

The performance-based structural fire safety design showed that the space truss above the auditorium can maintain its structural loading capacity without fire protection while the active fire protection is out of work in design fire scenario.

REFERENCES

- Li G. Q., Du Y., Analyses the parameters of fire temperature elevation at the top of large space buildings, *Fire Science and Technology*, 2005, 1, pp.19-21(in chinese)
- Du Y., Li G. Q., Fire radiation effect on steel member at elevated temperature in large space fire, *Fire Safety Science*, 2006, 4, pp.189-199(in chinese)
- Du Y., Li G. Q., Utility temperature elevation empirical formula in large space fire, *Fire Science and Technology*, 2005, 3, pp.283-287(in chinese)
- Izzuddin B. A., Song L., Elnashai A. S. and Dowing P. J., An integrated adaptive environment for the fire and explosion analysis of steel frames—Part II: verification and application, *Journal of Constructional Steel Research*, 2000, 3, pp.87-111.
- National Institute of Standards for Engineering, Technical code for fire safety of steel structures in buildings, CECS 200: 2006 China
- Kevin B., Grattan M. C., Glenn P. Forney, Kuldeep P., *Fire Dynamics Simulator(Version3)—User's Guide*, NISTIR 6784,2002 Ed.: 2002 U.S.

RC FRAME EXPOSED TO FIRE AFTER EARTHQUAKE

Ljupco Lazarov^a, Koce Todorov^a, Meri Cvetkovska^a

^a University “Ss. Cyril and Methodius”, Faculty of Civil Engineering, Skopje, Macedonia

INTRODUCTION

Earthquakes represent an extreme event causing enormous damage to buildings, infrastructure, not to mention a loss of human lives. The occurrence of a fire following an earthquake can understandably produce a disastrous effect. Although ground shaking is the major concern in most earthquakes, subsequent fire could be even more dangerous to urban infrastructure. The post earthquake fire if ignited could grow, intensify, and spread out of control in the neighborhood. Therefore, besides satisfying structural design requirements for normal loads, such as dead and live loads including the seismic hazard, buildings should also be designed to withstand the fire following earthquakes for a certain minimum duration as required for a desired level of performance. Fire resistance requirements for specific building members and structures are provided in building codes. However, much of these criteria are developed for fire exposure under normal conditions without a cumulative damage from preceding earthquake (Iding, 2003, Mousavi et al., 2008).

The behavior of a particular reinforced concrete structure exposed to fire after surviving strong earthquake is presented. The seismic response of the structure was evaluated using a nonlinear static pushover analysis.

1 BASIC THEORY

A computational procedure for nonlinear analysis of reinforced concrete frame subjected to fire loading exposed to different fire models is analyzed. For that purpose the program FIRE (Cvetkovska, 2002) is used. A coupled thermal - structural analysis approach is implemented in the program. In each time step, the fire behavior of a structural member is estimated using a complex, coupled heat transfer - strain equilibrium analysis, based on theoretical heat transfer and structural mechanics principles. The analysis is performed in three sub steps within each time step: namely, calculation of fire temperatures to which the structural members are exposed, calculation of temperatures in the structural members, and calculation of resulting deflections and internal forces including an analysis of the stress and strain distribution. The program FIRE carries out the nonlinear transient heat flow analysis (modulus FIRE-T) and nonlinear stress-strain response associated with fire (modulus FIRE-S) (Iding et al., 1977).

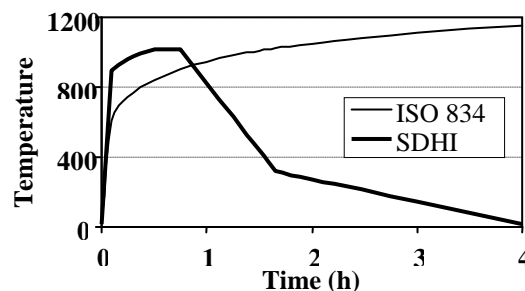


Fig. 1 ISO 834 and SDHI fire models

The solution technique used in FIRE is a finite element method coupled with time step integration. The computer modulus FIRE-T solves the governing differential equation of heat transfer in conduction and in that purpose the following assumptions are made: a fire can be modeled by a single valued gas temperature history: ASTM E119, ISO 834 or SDHI (short duration, high

intensity) fire model, Fig. 1; no contact resistance to heat transmission at the interface between the reinforcing steel and concrete occurs; the fire boundary conditions can be modeled in terms of both convective and radiating heat transfer mechanisms; the temperature dependant material properties are known (recommended in Eurocode 2, part 1.2); while cracks appear, or some parts of the element crush, the heat penetrates in the cross section easier, but in this study it is neglected. It has been assumed that the heat flow is separable from the structural analysis. The response of a reinforced concrete elements and plane frame structures exposed to fire is predicted by modulus FIRE-S. This modulus accounts for: dimensional changes caused by temperature differences, changes in mechanical properties of materials with changes in temperature, degradation of sections by cracking and/or crushing and acceleration of shrinkage and creep with an increase of temperature. To define the fire response of reinforced concrete structure is thus a complex nonlinear analysis problem in which the strength and stiffness of a structure as well as internal forces continually change due to restraints imposed by the structural system on free thermal expansion, shrinkage, or creep. Pushover analysis, representing dynamic effects of an earthquake via static nonlinear procedure, is incorporated in the program as an option that precedes the post earthquake fire analysis.

2 NUMERICAL EXAMPLE – CASE STUDY

2.1 Structural Geometry and Material Characteristics

The object of the numerical analysis is a two-story three bay planar reinforced concrete frame structure. Frame geometry, element cross-sections and reinforcement of all cross sections are schematically presented in Fig. 2. Concrete compressive strength is $f_c=30\text{MPa}$, reinforcement yield strength is $f_y=400\text{MPa}$. Structure self weight is included in the permanent and live loads, applied on beams as cumulate uniformly distributed, $q=45\text{kN/m}'$. Total weight of the structure is $W=2 \times (45.0 \times 15.0) = 1350\text{kN}$. The reinforcement of beam cross sections is taken in such a way that the stresses in steel bars due to nominal load q are approximately 60% of the yield strength. The percentage of column reinforcement is taken to be 1%.

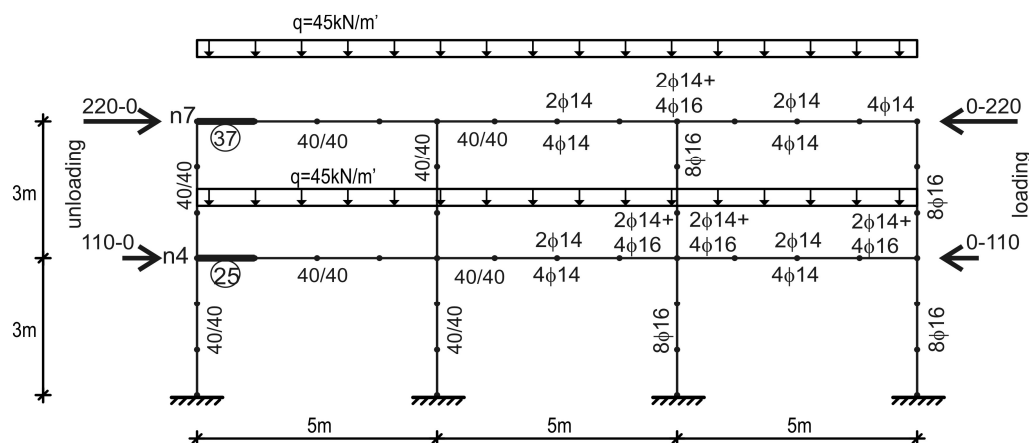


Fig. 2 Geometry and loading

2.2 Description of Analysis Cases

Thirteen different loading cases have been analyzed:

1. Gravity load ($q=45\text{kN/m}'$), (abbreviated as “g” in figures and tables)
2. Gravity load + ISO fire scenario 1
3. Gravity load + SDHI fire scenario 1
4. Gravity load + ISO fire scenario 2
5. Gravity load + SDHI fire scenario 2

6. Gravity load + Pushover (loading + unloading) + ISO fire scenario 1
7. Gravity load + Pushover (loading + unloading) + SDHI fire scenario 1
8. Gravity load + Pushover (loading + unloading) + ISO fire scenario 2
9. Gravity load + Pushover (loading + unloading) + SDHI fire scenario 2
10. Gravity+Pushover (loading+ unloading +opposite loading+ unloading) + ISO fire scenario 1
11. Gravity+Pushover (loading+unloading+opposite loading+ unloading)+ SDHI fire scenario 1
12. Gravity+Pushover (loading+unloading +opposite loading+ unloading)+ ISO fire scenario 2
13. Gravity+Pushover (loading+unloading +opposite loading+ unloading)+SDHI fire scenario 2

Fire scenario 1 assumes fire in the first story left compartment and fire scenario 2 assumes fire in the second story left compartment of the frame. In the pushover analysis a triangular load distribution in horizontal direction is applied, Fig. 2. In loading case 6 up to loading case 9, the horizontal forces are incrementally increased from 0 to 220kN on the second floor and from 0 to 110kN on the first floor pushing the rightmost floor nodes of the structure (applied in direction from right to left).

2.3 Results of Analysis Cases

The value for the base shear of 330kN (220kN + 110kN) corresponds to 0.244W and is chosen in such a way that the structure is pushed into nonlinear range and rather large number of plastic hinges are formed. Total base shear has been reached corresponding to top story horizontal displacement of 4.23cm, Fig. 3a. Once the loading phase up to corresponding base shear of 330kN is completed, unloading phase takes place. After unloading the corresponding residual plastic displacement at node 7 was 1.09cm, Fig. 3b.

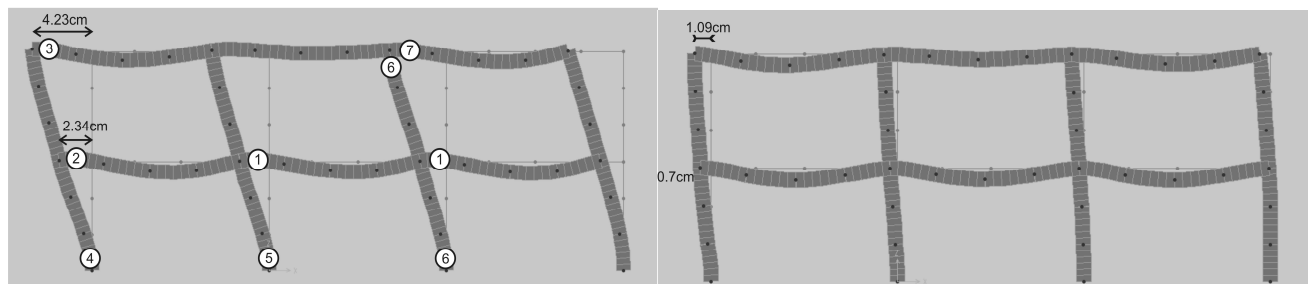


Fig. 3 a) Sequence of plastic hinges formation and horizontal displacements due to pushover
b) Residual displacements after pushover

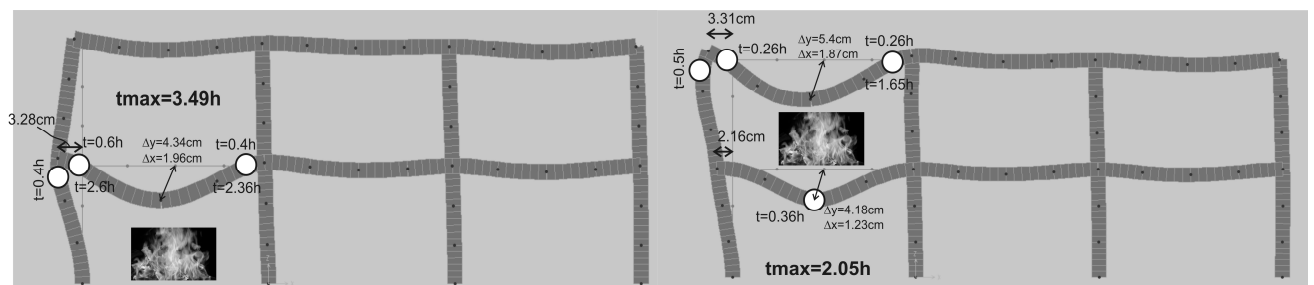


Fig. 4 a) L. case 6, sequence of hinges due to fire, b) L. case 8, sequence of hinges due to fire

To accomplish loading cases 6 to 9, after unloading the structure is exposed to two different fire scenarios for two different fire load models. In loading case 10 up to loading case 13, the horizontal forces are applied to the structure that is already plastically deformed in the previous cycle of pushover analysis and are incrementally increased from 0 to 220kN on the second floor and from 0 to 110kN on the first floor, pushing the leftmost floor nodes (node 7 and node 4) of the structure (applied in direction from left to right). Again, to accomplish loading cases 10 to 13, after unloading the structure from total base shear of 330kN in the opposite direction, the frame is exposed to two different fire scenarios for two different fire load models. Some of the obtained results are graphically presented.

Base shear-displacement relations from loading case 10 for nodes 7 and 4, due to ISO fire scenario 1, are presented in Fig. 5. Loading, unloading, loading in opposite direction and unloading from opposite direction are assigned as: L1PO, UL1PO, L2PO and UL2PO consequently. The sequence of formation of plastic hinges on Fig. 3a are shown on the L1PO branches of Fig. 5. Additional results for displacements of nodes: 4, 7, 9 and 12 for characteristic moments of the analysis in fire scenario 1 or 2 and for fire models ISO and SDHI, are presented in Tab. 1, Tab. 2 and Tab. 3.

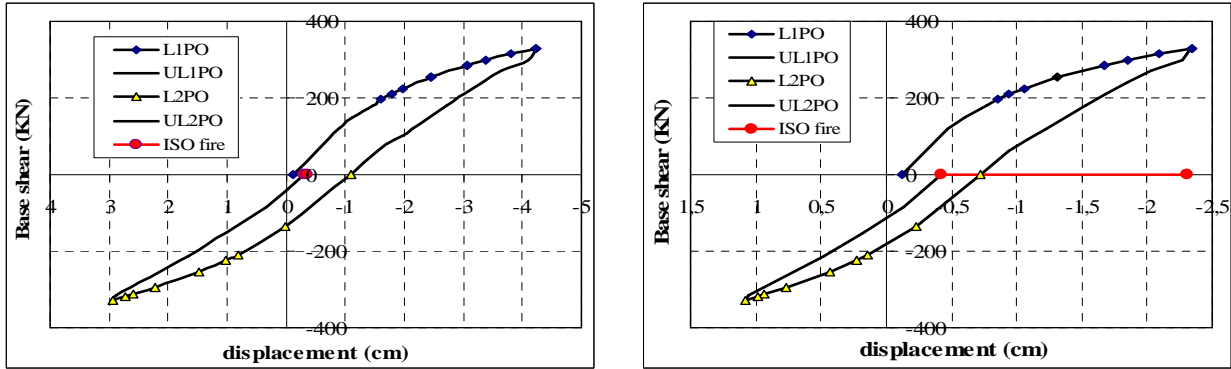


Fig. 5 Base shear-displacement relations for nodes 7 and 4, due to ISO fire scenario 1

Tab. 1 Fire scenario 1

node	Displac. (cm)	only “g” and fire action				“g”+ seismic action + fire action					
		g	g+ISO t=3.3h	g+SDHI		g	g+LPO	residual displac.	residual + ISO t=3.49h	resid.+SDHI	
				t=1.1h	t=5h					t=1.1h	t=5h
4	Δ_x	-0.12	-2.85	-1.83	-1.08	-0.12	-2.34	-0.72	-3.28	-2.23	-1.49
7	Δ_x	-0.13	-0.27	-0.20	-0.19	-0.13	-4.23	-1.09	-1.12	-1.03	-1.01
9	Δ_y	-0.43	-4.14	-1.27	-1.61	-0.43	-0.64	-0.78	-4.34	-1.45	-1.78

Tab. 2 Fire scenario 2

node	Displac. (cm)	only “g” and fire action				“g”+ seismic action + fire action					
		g	g+ISO t=2.0h	g+SDHI		g	g+LPO	residual displac.	residual + ISO t=2.0h	resid.+SDHI	
				t=1.1h	t=5h					t=1.1h	t=5h
4	Δ_x	-0.12	-1.62	-1.22	-0.70	-0.12	-2.34	-0.72	-2.16	-1.79	-1.27
7	Δ_x	-0.13	-2.62	-1.98	-1.89	-0.13	-4.23	-1.09	-3.31	-2.67	-2.25
9	Δ_y	-0.43	-3.67	-2.68	-1.53	-0.43	-0.64	-0.78	-4.18	-3.23	-2.46
12	Δ_y	-0.56	-5.34	-3.29	-4.26	-0.56	-0.59	-0.73	-5.41	-3.27	-4.29

Tab. 3 Fire scenario 1 and 2

node	Displac. (cm)	“g”+ seismic action in two directions+ fire action						
		g	g+L1PO	residual displac.1	g+L2PO	residual displac.2	residual + fire 1 t=3.54h	residual + fire 2 t=2.43h
4	Δ_x	-0.12	-2.34	-0.72	+1.12	-0.42	-2.31	-1.60
7	Δ_x	-0.13	-4.23	-1.09	+3.05	-0.30	-0.36	-1.55
9	Δ_y	-0.43	-0.64	-0.78	-0.87	-0.96	-3.70	-4.20

As expected, residual horizontal displacements of nodes 4 and 7 as well as the residual vertical displacements of nodes 9 and 12, are slightly higher when fire action is applied after pushover, then in the case when no seismic action was applied. This trend is observed in both fire scenarios and both fire models. Interesting results are obtained for the capacity of this reinforced concrete structure to sustain fire load. Namely, the duration of time that the structure survived the ISO fire after a pushover episode was higher than the duration of time that the structure survived the ISO fire without a seismic action in fire scenario 1, 3.49 hours against 3.3 hours (loading case 6). In fire scenario 2 the duration of time, for both cases, was almost equal, t=2.0 hours (loading case 8). That

was even more emphasized in loading cases 10 and 12, when a full cycle (loading, unloading, loading in opposite direction and unloading from opposite direction) was completed, Tab. 3.

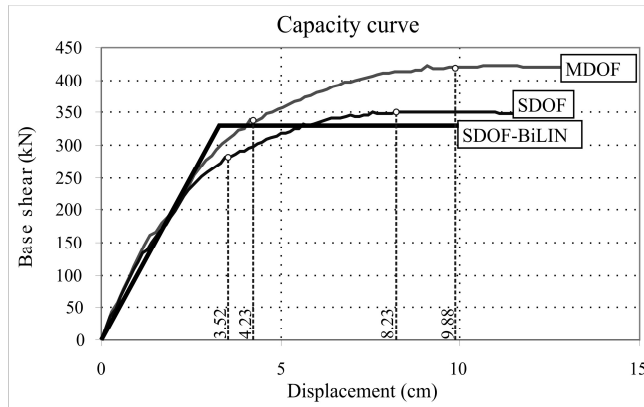


Fig. 6 Pushover curve – capacity curve

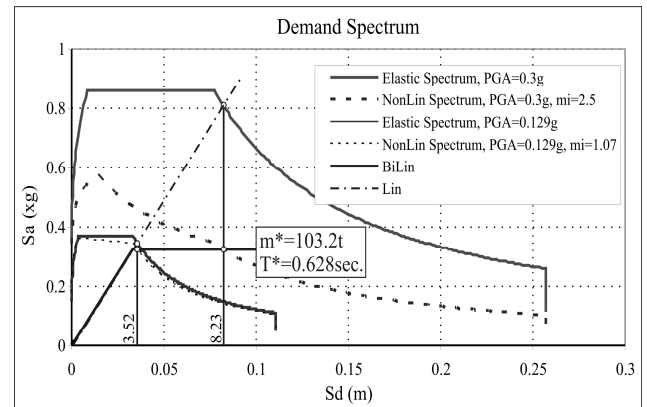


Fig. 7 Elastic and demand spectra

The reinforcement of the RC frame cross sections is defined from criteria that do not take into account seismic provisions. In order to see what is the seismic capacity of the structure and to what level of seismic demand corresponds the assumed base shear of 330kN, the N2 method was implemented (Fajfar, 2000). Final results of capacity-demand calculations are graphically presented in Fig. 6 and Fig. 7. Base shear of 330kN and the obtained displacement of 4.23cm at node 7 corresponds to elastic demand spectrum for PGA=0.129g. By inverse procedure, it was found that this RC frame has capacity (base shear of 420kN and target displacement of 9.88cm) to sustain elastic demand spectrum for PGA=0.3g. All loading cases were reapplied such that the horizontal forces were increased up to a base shear of 393kN (corresponding approximately to 94% of frame's capacity). Due to limited space only few results for displacements for nodes 4 and 7 are listed. For base shear=393kN, $\Delta_{x4}=4.19\text{cm}$, $\Delta_{x7}=7.31\text{cm}$. For base shear=0kN (unloading), $\Delta_{x4}=1.98\text{cm}$, $\Delta_{x7}=3.04\text{cm}$ (residual displacements). It is worth mentioning also, that increased resistance in case of fire scenario 1 was observed. The structure has sustained fire load after earthquake in duration $t=3.76$ hours.

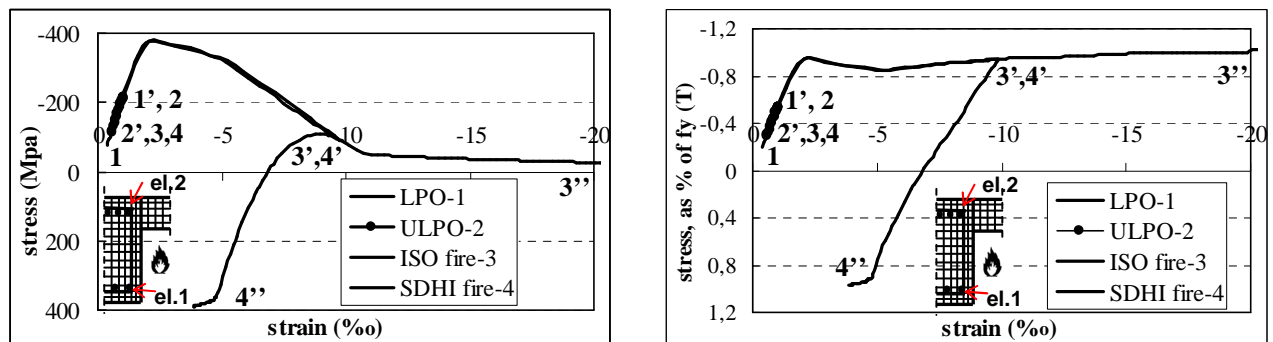


Fig. 8 Bottom bar, Node 4, fire scenario 1

Stress-strain hystories for reinforcing bars in beam cross sections of nodes 4 and 7 for applied loading cases are presented in Fig. 8 thru Fig. 11. The interpretation of the numbers next to particular stress-strain curve is such that, for example on Fig. 8 the stress-strain history for ISO fire-3 starts at point 3, continues thru point 3' and finishes at point 3''. Also, the stress-strain relation for some reinforcement bars is doubly presented, as for example bottom bar, Node 4, fire scenario 1 on Fig. 8. The left graph presents real stress-strain relations during time history of loading and on the right graph stresses are normalized as percentage values of the reduced yield stress due to elevated temperature, $f_y(T)$.

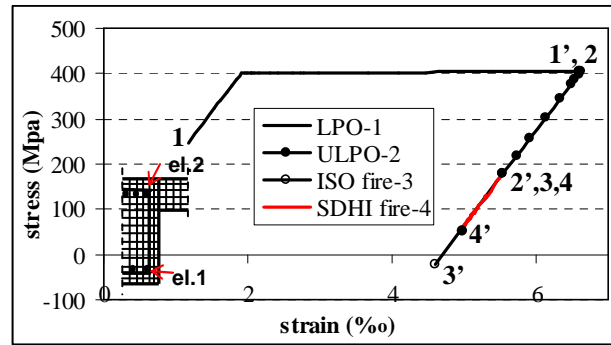
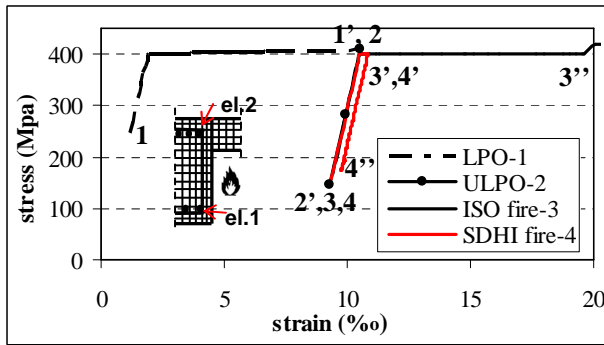


Fig. 9 a)Top bar, Node 4, fire scenario 1, b)Top bar, Node 7, fire scenario 1

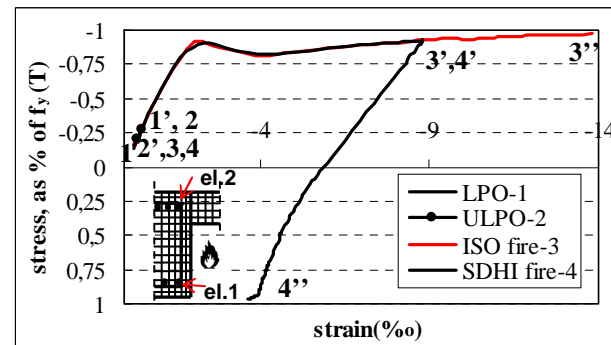
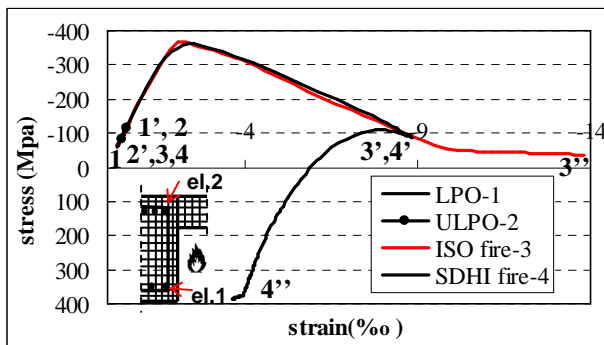


Fig. 10 Bottom bar, Node 7, fire scenario 2

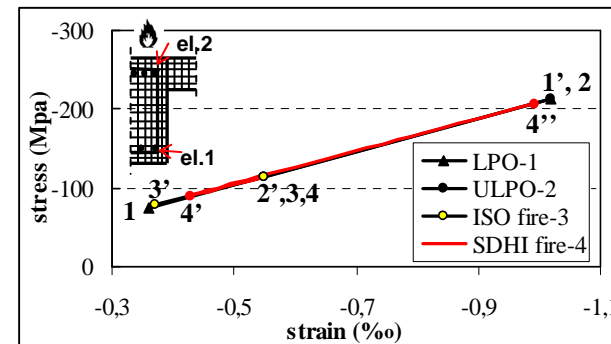
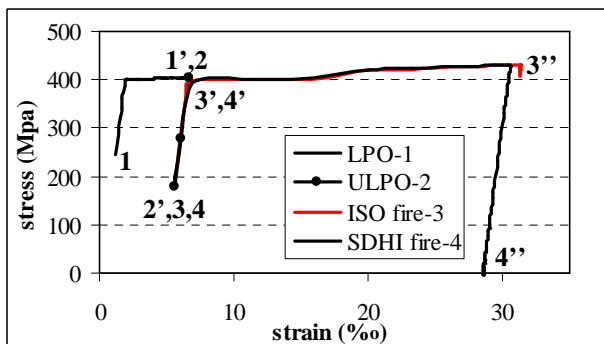


Fig. 11 a)Top bar, Node 7, fire scenario 2 , b)Bottom bar, Node 4, fire scenario 2

REFERENCES

- EUROCODE 2, "Design of Concrete Structures, Part 1-2: General rules - Structural Fire Design", CEN - European Committee for Standardization, 2004.
- Cvetkovska M. "Nonlinear stress strain behaviour of RC elements and RC frames exposed to fire", Phd. thesis, University St.Cyril and Methodius, Skopje, 2002 (in Macedonian).
- Fajfar P., "A nonlinear analysis method for performance-based seismic design", Earthquake Spectra, 2000, 16(3): 573-92.
- Iding R., Bresler B. and Nizamuddin Z., "FIRES-RC II-A Computer Program for The Fire Response of Structures-Reinforced Concrete Frames", Report no.UCB FRG 77/8, Structural Engineering and Structural Mechanics, department of Civil Engineering, University of California, Berkeley, California 1977.
- Iding R., "Calculating Structural Response to Fire", Fire Protection Engineering, 2003.
- Mousavi S., Bagchi A., Kodur V., "Review of post-earthquake fire hazard to building structures", Canadian Journal of Civil Engineering, Jul. 2008.

ADAPTATION OF FEA CODES TO SIMULATE THE HEATING AND COOLING PROCESS OF TIMBER STRUCTURES EXPOSED TO FIRE

Mechanical Behaviour

Danny Hopkin ^{a/c}, Jamal El-Rimawi ^a, Vadim Silberschmidt ^b, Tom Lennon ^c

^a Loughborough University, Department of Civil and Building Engineering, Loughborough, UK

^b Loughborough University, Wolfson School of Mechanical Engineering, Loughborough, UK

^c BRE Global, Garston, Watford, Herts, WD25 9XX, UK (HopkinD@bre.co.uk)

INTRODUCTION

Computer analysis of timber structures exposed to fire is not a widely undertaken task. Typically, such modelling is limited to simplified sectional analysis tools based on spreadsheets and underpinned with basic code. In the case of timber, additional complexities related to its orthotropy and differences in tensile and compressive stiffnesses at elevated temperature mean that the analysis of timber structures in fire does not lend itself easily to more powerful generic finite element software packages, such as TNO DIANA and ABAQUS.

When using the properties of timber at increasing temperatures, an assumption of identical reduction of the modulus of elasticity (MOE) under both tensile and compressive stresses is not suitable; simple correlations between temperature and tensile and compressive strengths are also inadequate. In the case of the former, the compressive MOE of timber at increasing temperatures degrades at a much higher rate than the tensile MOE. As a result, in a uniformly heated symmetrical section, the neutral axis is not central as would be expected. The effect of temperature on the strength of timber is also unusual. Unlike other materials, timber undergoes a very noticeable physical change upon heating. At a temperature of approximately 300°C timber chars, leaving a friable weak residual mass. Therefore, characterising strength on the basis of temperature alone would result, in some instances, in an artificial strength recovery in char zones upon cooling. Clearly, the full temperature history of an element, together with its current temperatures, is important in the determination of any strength recovery upon cooling.

In this paper, the development of a number of sub-routines for characterising the behaviour of timber elements exposed to both heating and cooling is described using simple examples. Developed codes for the determination of MOE, compressive and tensile strength under both cooling and heating are discussed. The subroutines are coupled with DIANA total strain-based constitutive models, which describe yielding and fracture. The potential for these developments to be adopted in the fire design of large-section timber structures is also evaluated.

1 MODELLING FIRE-EXPOSED TIMBER STRUCTURES

The modelling of timber exposed to fires has largely focussed upon temperature development either in unprotected large-section or light-weight gypsum-lined structures. The mechanical modelling of timber exposed to fire is a recent endeavour instigated by Thomas (1997) followed subsequently by Konig & Walleij (2000). More recently, further investigations were undertaken by Schmid *et al.* (2010) who conducted simulations of cross-laminated timber (CLT) members exposed to fire. However, in almost all instances the modelling has been performed using in-house *ad-hoc* sectional analysis codes, which are only appropriate for single-member analyses. If buildings are to be designed in a performance-based manner, whereby full building interactions are considered, then modelling approaches need to be advanced and more powerful codes adopted.

The adoption of more general finite element packages, such as DIANA and ABAQUS, for modelling timber has yet to become common due to a number of complexities relating to the behaviour of timber. For example, it is brittle and fractures in tension, while being more ductile and plastic when subject to compression.

A more interesting behaviour of timber is that, with increasing temperature, the degradation in its constitutive behaviour in tension is different from that when it is in compression. As a result, its MOE depends on its state of stress. Therefore, a single MOE-temperature relationship cannot be defined. Finally, upon heating timber undergoes a phase change whereby wood becomes friable char. Upon cooling, char still has little or no strength or stiffness. Therefore, it is not appropriate to specify timber strength on the basis of temperature alone when cooling is to be considered; knowledge of the full temperature history is required. Most commercial finite element programs do not incorporate many of the above characteristics in a direct way. Therefore, it is necessary to adapt such codes to accommodate these behaviours. An approach for doing this is described in the remainder of this paper. Implementation of the approach in the FEA software TNO DIANA (Manie 2010) via FORTRAN user-supplied subroutines (USS) is also described.

2 USRYOU- A SUBROUTINE FOR DETERMINING MOE OF TIMBER

DIANA offers a number of subroutine options for customising the analyses performed. One such subroutine is the USRYOU option, which allows users to return MOE based upon a number of inputs, including integration point strain and temperature. The authors have developed a USRYOU USS for determining the MOE of timber exposed to both heating and cooling.

Firstly, integration point and element numbers are called from the program along with temperature at the given integration point. Temperature history of elements is recorded via a common block, which determines whether the temperature of the timber (a) exceeded the charring temperature of 300°C, (b) exceeded the moisture evaporation temperature of 100°C, or (c) below 100°C, that is, timber neither charred nor suffered moisture evaporation. Based on this, the temperature-history common block is updated incrementally, which allows state history to be recorded. The latter allows for a number of hypotheses to be investigated, which will be discussed below.

Using the recorded temperature history the stress state may be investigated. The strains in the local element co-ordinates are called from DIANA. The dominant integration point strain is determined, which is then used to evaluate MOE appropriate to temperature and the strain state. For example, if ϵ_{xx} is found to be the largest element strain and the strain is negative (that is compressive), the MOE is returned, based upon EN 1995-1-2 (BSI 2004) compression (-ve) reduction factors (K_{EC}) and element temperature. The converse case would be adopted if ϵ_{xx} was found to be positive (+ve). In this instance reduction factors are defined as K_{ET} . This process is shown diagrammatically in Figure 1.

3 USRCST/TST- A SUBROUTINE FOR DETERMINING COMPRESSIVE/ TENSILE STRENGTH OF TIMBER

Two more USSs, namely USRCST and USRTST, are available in DIANA for determining the tensile and compressive strength, respectively. These routines in particular are for implementation with Total Strain Based constitutive models, which are discussed in a supporting paper (Hopkin *et al.* 2011b). The routines utilise the temperature-history common block initialised in the above USRYOU routine to calculate tensile and compressive strength using EN 1995-1-2 reduction factors. The element number and integration point number are used to reference allocated memory slots, where temperature state variables are stored. Compressive and tensile strengths (limiting stresses) are passed to DIANA for implementation in the adopted Total Strain Based Constitutive model. This process is shown in a flow diagram in Figure 2.

4 THE USE OF TEMPERATURE STATE VARIABLES IN THE COOLING DOWN PHASE

When the temperature reaches a certain limit within a timber section its moisture content will be completely lost through evaporation. As the section's temperature increases, charring of certain parts may also occur. The charred timber will not contribute to the strength and stiffness of the section. Clearly, this damage is irreversible. However, little is known about the strength and stiffness of the remaining un-charred part of the section and how the section behaves during cooling

down. To study this, the concept of temperature history state variables (SVs) has been introduced. This allows for a number of hypotheses to be investigated.

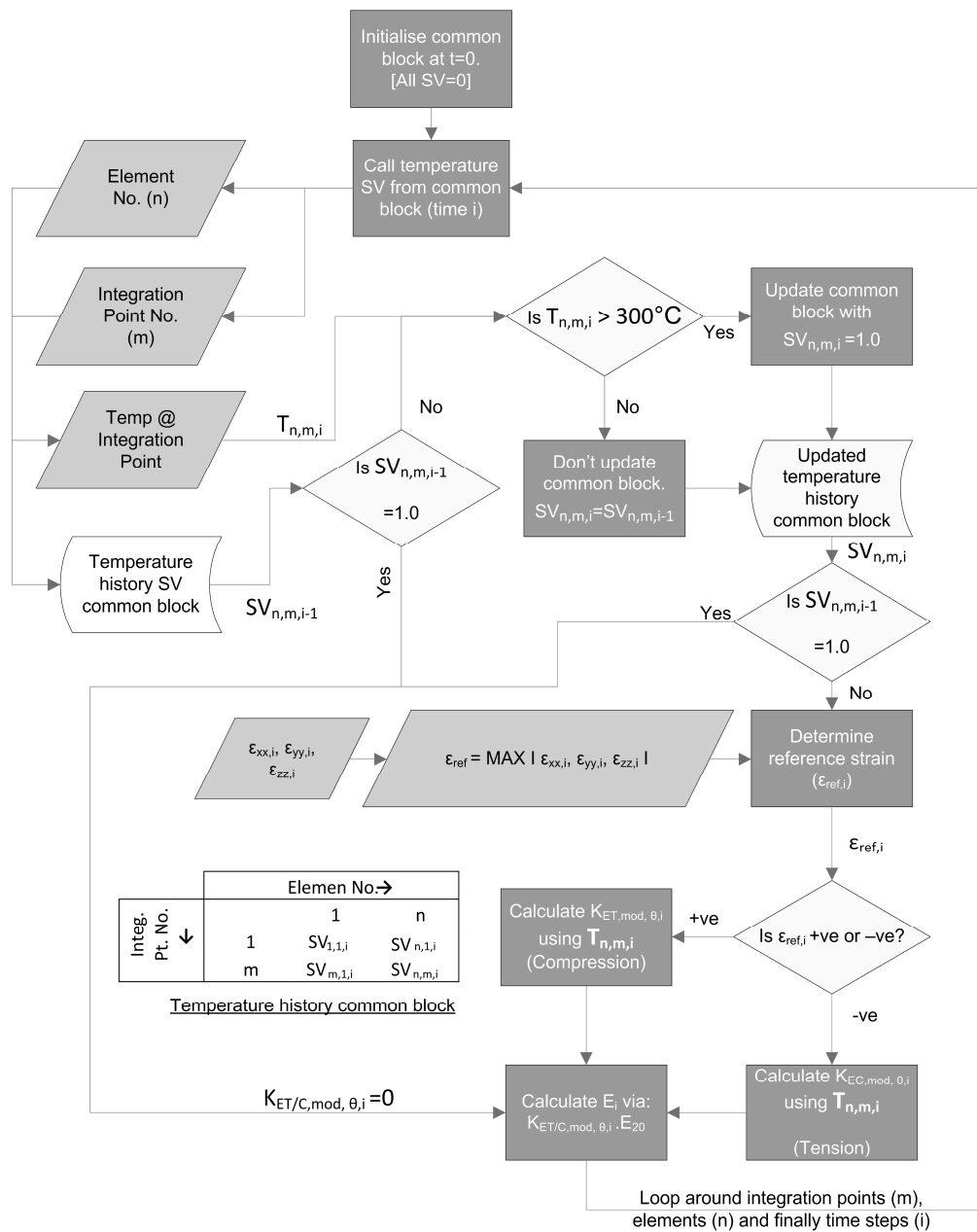


Fig. 1 Flow chart for USRYOU routine

The first hypothesis is based on the assumption that, during cooling down, undamaged timber recovers none of its strength or stiffness. This would be the case if temperature changes during the cooling phase are ignored. In this case, the maximum temperature reached during heating up governs the behaviour during cooling.

In the second hypothesis it could be argued that moisture lost during the heating phase cannot be regained during cooling down. This means that strength and stiffness of timber whose temperature, upon heating, did not exceed 100°C will be fully recovered to that appropriate to its temperature during cooling down. However, timber heated beyond 100°C, but not charred, may recover its strength and stiffness but only up to the maximum value applicable to dry moisture-free timber. The latter condition implies that reduction factors corresponding to 100°C should remain applicable even when timber temperature drops below this limit.

A third and final hypothesis is that, while cooling down, all non-charred timber will recover the entire strength and stiffness appropriate to its temperature. This implies that loss of moisture during heating had no effect on the recovered properties. Clearly, this approach may be implausible as it

suggests the return of moisture into the timber during cooling. Although timber is a hygroscopic material the return of free moisture would take time much in excess of the decay phase of most fires. The implications for these three hypotheses can be observed through a number of simple numerical tests on single quad elements or simply supported beams. This testing process is discussed in the following section.

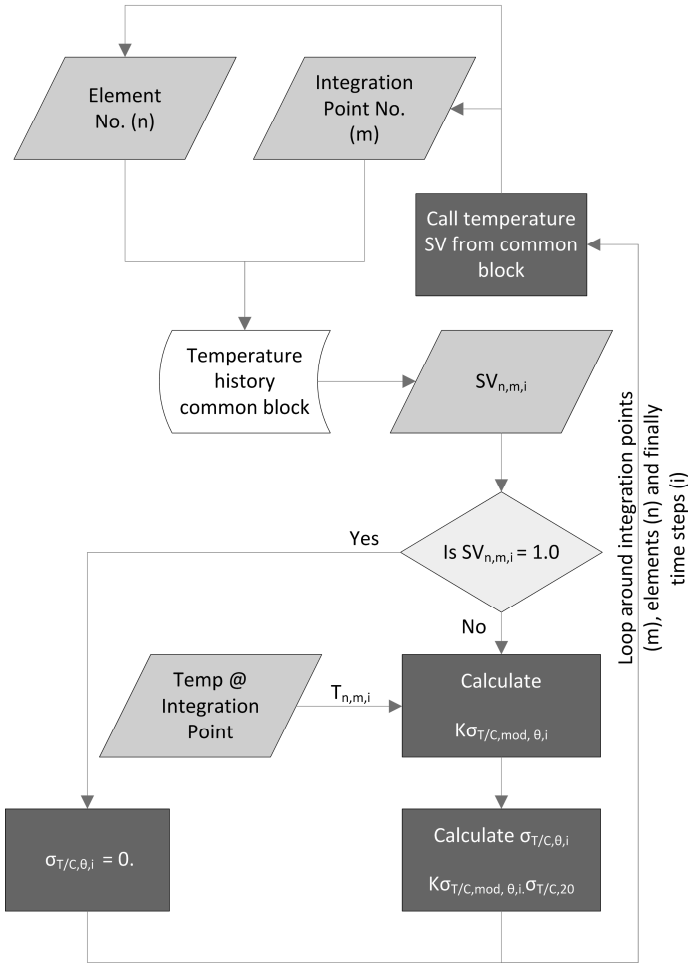


Fig. 2 Flow chart for USRCST/TST routine

5 SUBROUTINE TESTING AND IMPLEMENTATION

The testing of the USSs was conducted at a number of different scales. Firstly, trials of hypotheses 1–3 were conducted using single first-order quad elements uniformly heated and cooled down, and subject either to a compressive or tensile strain. In these trials, only the USRYOU subroutine is implemented so that non-linear elastic solutions can be sought without either cracking or plasticity. Resulting strain-temperature plots are shown in figure 3 for all three hypotheses. A constant load was applied throughout. In such trials it is not possible to indicate permanent charring damage as it would result in numerical instability. Thus, the maximum applied temperature was 210°C. Tensile and compressive loads of identical magnitude were applied to allow for the difference in MOE degradation with temperature for different strain states to be checked. However, only one set of results (compressive) is shown as the other indicated the same pattern.

The second element of USS testing is concerned with the behaviour of simply supported beams subject to a temperature gradient. A beam was modelled simply in DIANA using a number of first-order 2D beam elements. Temperatures were specified at 11 integration points through the cross section of beam elements. Integration point distribution was according to a Simpson integration scheme. The adopted temperature profiles are shown in Figure 4a. The legend indicates fire from below with 11 integration points numbered from the top down. The temperatures applied are fictitious temperatures and serve only to demonstrate implementation of the USS. The modelled

beam is 4 m in length and has a 100 mm x 250 mm cross-section. The beam is subject to a nominal load of 5 kN/m. The development of deflection upon heating, followed by cooling can be seen in Figure 4b. In this case, the beam temperature developed beyond 300°C. Therefore, permanent deformation due to charring was apparent, including the case with full un-charred timber strength recovery (hypothesis 3).

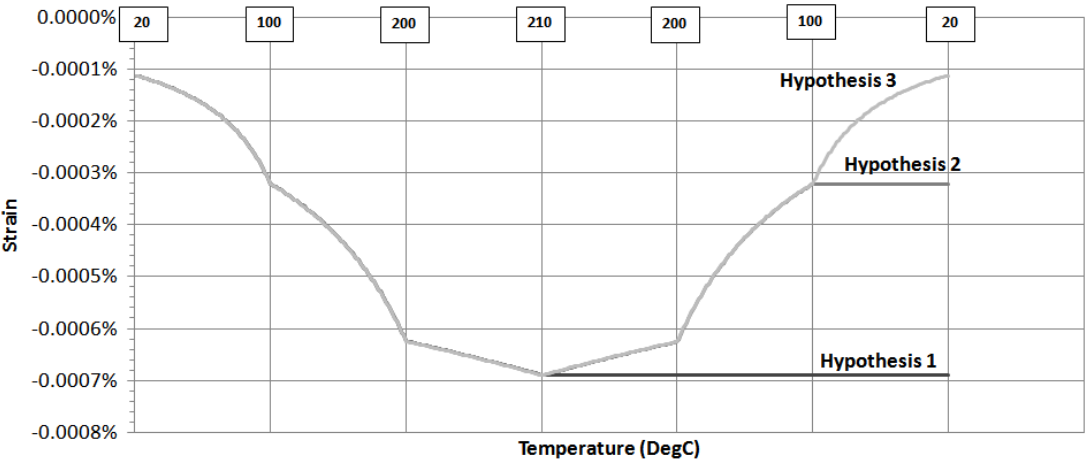


Fig. 3 Single-element implementation of USRYOU subroutine: temperature-strain plots for a constant nominal load

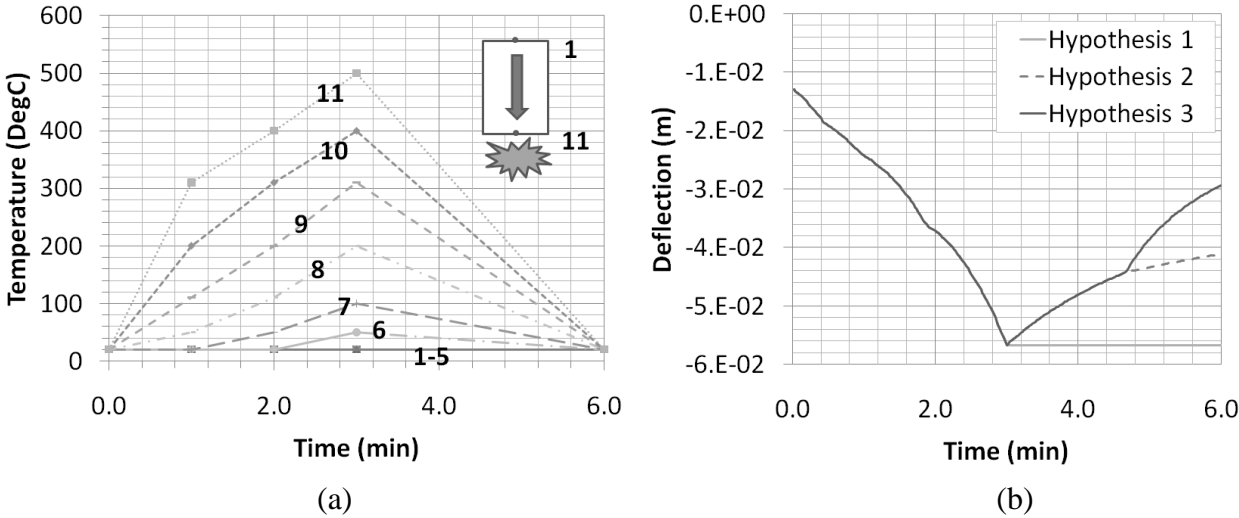


Fig. 4 Beam implementation of USRYOU and USRCST/TST subroutines: (a) Temperature profiles at integration points (b) Deflection–time plots.

6 SUMMARY

A number of relatively simple modifications to a commercial finite element code have been presented. The modifications allowed for timber in fire to be modelled in potentially much more complex scenarios than previously considered. Until recently, the thermo-mechanical modelling of timber using commercial codes has not been widely undertaken. Where attempts have been made it has been done with simple *ad-hoc* codes having limited fields of application. If more advanced simulations of timber are to be conducted then either specialist codes need to be developed or commercial codes adapted.

The adaptation of a commercial code, such as DIANA, by means of FORTRAN user-supplied subroutines is desirable for a number of reasons. Firstly, with simple modifications to the stress relations, outlined above in the USSs presented, any number of element variations, from beam, through shell, to block elements, can be considered depending upon the problem encountered. Secondly, the powerful robust solvers, which are heavily tested in commercial codes, can be adopted with only the aspects of material behaviour which need to be appropriately represented by

the USS, such as MOE, tensile and compressive strength with increasing (and decreasing) temperature.

In relation to the strength and stiffness recovery of timber upon cooling, experimental evidence suggests that the first two hypotheses may be more realistic (Lennon *et al.* 2010 & Hopkin *et al.* 2010). In the many experiments conducted by BRE on timber structures over the last decade, there appears to be little evidence to suggest any strength or stiffness recovery in timber structures exposed to fire, upon cooling.

Our papers presented at this event (Hopkin *et al.* 2011a/b), coupled with the developments proposed in this paper, give an integrated procedure for modelling large-scale timber assemblies exposed to fire. The modified conductivity model (MCM) proposed in a supporting paper (Hopkin *et al.* 2011a) provides a means of determining transient reduced cross section during parametric design fires, which can be adopted with the USS presented herein in thermo-mechanical analyses. A further study (Hopkin *et al.* 2011b) discusses implementation of the constitutive behaviour of timber in FEA models using relatively simple Total Strain Based models, with appropriate fracture energies. All the approaches presented will be developed further. However, initial findings appear to give consistent results with many empirical methods present in EN 1995-1-2 for isolated structural members. Thanks to the growth of timber constructions market share, both in the UK and continental Europe, it is becoming increasingly important to develop tools appropriate for structural fire design. As timber buildings become increasingly larger and more complex, numerical simulations would become a valuable resource.

7 ACKNOWLEDGEMENTS

The authors would like to thank EPSRC and BRE Global for their support.

REFERENCES

- BRITISH STANDARDS INSTITUTION, 2004. Eurocode 5: Design of timber structures – Part 1-2: General – Structural fire design. BS EN 1995-1-2. London: BSI.
- HOPKIN, D., EL-RIMAWI, J., SILBERSCHMIDT, V., LENNON, T., A numerically derived modified conductivity model for softwood exposed to parametric design fires. In: Proceedings of applications in structural fire engineering, 29th April 2011, CTU, Prague.
- HOPKIN, D., EL-RIMAWI, J., SILBERSCHMIDT, V., LENNON, T., The impact of assumed fracture energy on the fire performance of timber beams. In: Proceedings of applications in structural fire engineering, 29th April 2011, CTU, Prague.
- HOPKIN, D.J., LENNON, T., EL-RIMAWI, J. and SILBERSCHMIDT, V., 2010. Failure mechanisms of structural insulated panel (SIP) systems under natural fire conditions, V.R. KODUR and J.M. FRANSSSEN, eds. In: Proceedings of the sixth international conference on structures in fire (SiF), 2-4th June 2010, DEStech pp520-527.
- KONIG, J. and WALLEIJ, L., 2000. Timber frame assemblies exposed to standard and parametric fires part 2: A design model for standard fire exposure. I0001001. Stockholm: SP Tratek.
- LENNON, T., HOPKIN, D.J., EL-RIMAWI, J. and SILBERSCHMIDT, V., 2010. Large scale natural fire tests on protected engineered timber floor systems. Fire safety journal, **45**(3), 168–182.
- MANIE, J., 2010. DIANA User's Manual. 9.4 edn. Delft: TNO.
- THOMAS, G., 1997. Fire resistance of light timber framed walls and floors. PhD Thesis. New Zealand: University of Canterbury Press.
- SCHMID, J., KONIG, J. and KOHLER, J., 2010. Design model for fire exposed cross-laminated timber, V.R. KODUR and J.M. FRANSSSEN, eds. In: Proceedings of the sixth international conference on structures in fire, 2-4th June 2010, DEStech pp511-519.

SIMULATION OF THE STRUCTURAL BEHAVIOR OF STEEL-FRAMED BUILDINGS IN FIRE

Filippo Gentili^a, Luisa Giuliani^b

^aSapienza University of Roma, Structural and Geotechnical Engineering Department, Rome, Italy

^bTechnical University of Denmark, Department of Civil Engineering (DTU-BYG), Lyngby, Denmark

INTRODUCTION

Structural integrity of buildings and safety of people in urban areas have been often endangered in the past by malevolent or accidental fires. Among all buildings in particular, high-rise structures pose particular design challenges with respect of fire safety for a number of reasons (Craighead, 2003), which refer not only to enhanced difficulties in evacuating the building, but also to the developing of the fire (i.e. the characteristic of the action) and to the response of the buildings (i.e. the characteristic of the structural system).

From the point of view of the fire action, either it is difficult for the fire-fighters to extinguish the fire, due to reduced accessibility and the limited length of ladders and fire hoses, and the fire might easily propagate upwards and spread to higher floors through the internal façade ducts or externally through windows as a consequence of the buoyancy effect on the thermal plume: Andraus Building fire of Sao Paulo in 1972, the First Interstate Bank fire in 1988 and the One Meridian Plaza fire of Philadelphia in 1991, are some of the worst cases where external fire spread was identified as a significant factor (Crooke, 2002). In order to reduce the increased risk due to the high elevation (BS 5588-5, 2004; NFPA 101, 2009), building codes of several countries nowadays require special fire safety systems for high-rise building, including, smoke venting, sprinkler systems and special fire alarms for an early detection of the fire and a prompt intervention of the fire-fighters. External shelters and window protrusions can also be effective for avoiding external fire propagation (Galea et al., 1996). Nevertheless, the design of active fire safety measures proved to be insufficient in several cases: some examples are the Parque Central Tower fire of Caracas in 2004, where the sprinkler system was not in working condition due to lack of maintenance, and the Mandarin Oriental Hotel fire of Beijing in 2009, where the sprinkler system was not installed yet, since the building was under construction.

Under those circumstances, the passive fire resistance of structural elements (MSB-6, 2008) and the intrinsic robustness of the system are the only measures to rely on, in order to maintain the structural integrity of the building during and after the fire and avoid major economic losses and additional casualties due to collapsing members. High-rise buildings of different typologies have been susceptible to progressive collapses induced by fire, such as the Windsor Tower fire of Madrid in 2005 (steel and concrete), the Architecture Faculty Building fire of Delft in 2008 (concrete) and the Odd Fellow Palace fire of Copenhagen in 2010 (wood and masonry). The first and the last ones in particular seem to have experienced pancake-type collapses (Starossek, 2009) that originate when the an initial the loss of vertical load bearing members cause the failure and separation of the horizontal slabs, which, impacting the slabs below, would propagate the collapse downwards. A different possible collapse mechanism have been instead recently highlighted (Usmani et al., 2003) for the case of the WTC collapse of New York in 2001 (steel), where the initial buckling of the heated floor slabs induced by hindered thermal expansion would have subsequently caused the buckling of the columns, as a consequence of the loss of horizontal restrains of the floors. It seems plausible to extend this type of mechanism to other type of steel framed buildings too, in particular those with a strong column - slender beam system, such as the one considered here as case study.

1 CASE STUDY

In this paper, a 3-dimensional substructure representing one floor of a high rise building has been investigated under different fire scenarios, with the avail of a finite element commercial code.

Particular attention is devoted to the description of the i) methodology followed for building the model, ii) setting the analyses and iii) interpreting the results.

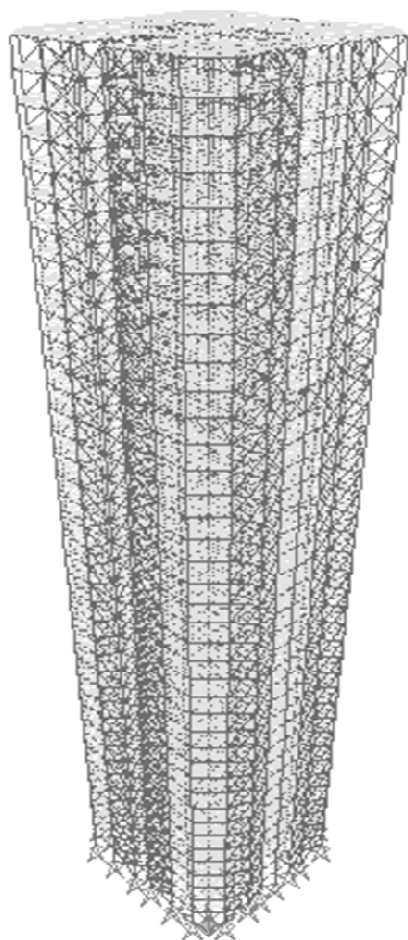


Fig.1 Model of the high-rise building

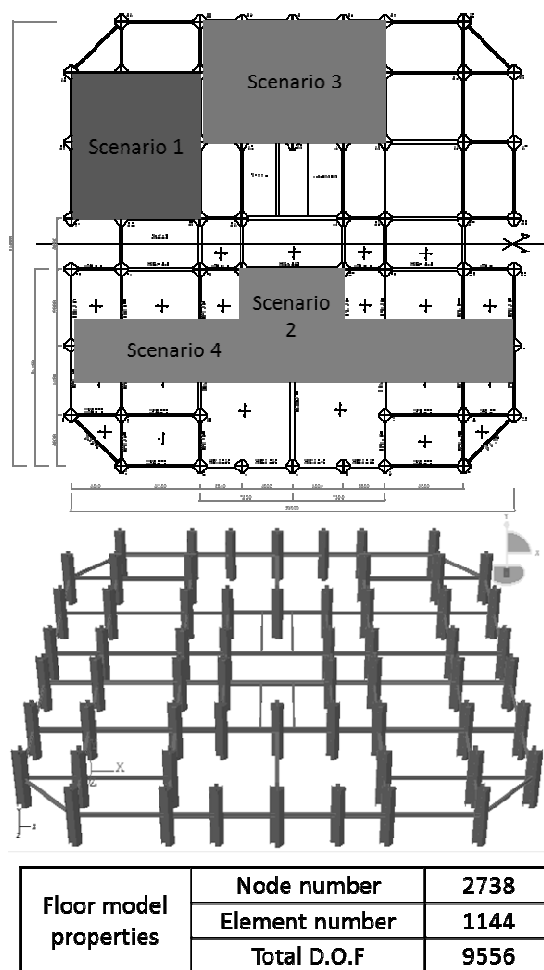


Fig. 2 floor plan FEM model and fire scenarios

1.1 Description of the structure

The building considered as case study is a multi-storey building, whose premises are devoted to offices and residential use and has been designed on the basis of the geometry and characteristic of a building recently built up in Latina, Italy.

The building has a steel framed structural system. A vertical bracing system provides stiffness against horizontal actions, while no horizontal bracings are present in the floor planes: the stiffness within the floor planes is achieved by means of bidirectional concrete floor slabs, which maintain the biaxial symmetry of the floors and are lightened by spherical hollows. The slab characteristics allow for long spans and slender beams, which can be contained within the height of the slabs.

1.2 Fire scenarios and thermal model

Some relevant fire scenarios can be pragmatically identified on the structure (Bontempi, 2010): for this study it is assumed that the vertical compartmentalization of the building remains intact and the fire originates and spreads in one floor only. In principle, different fire scenarios along the building height should be considered, since floors have different elements and loads and vertical propagation of the failure can be different. However, in the following, only four fire scenarios will be investigated, which refer to fire on the 5th floor of the building and are reported in Fig.1.

The temperature-time curve considered for the fire is the ISO 834, while the heating curves of the beams involved in each fire scenario have been calculated under the assumption of uniform temperature in the element, according to the Eurocodes formula for unprotected steel, using

a convective coefficient $\alpha = 25 \text{ W/(m}^2\text{K)}$ and a total emissivity $\varepsilon = 0.5$ (no shadow effect considered).

1.3 Structural model

The modelling of a complex construction requires formulating some assumptions and starting with the investigations of simpler substructures, where the collapse mechanisms can be identified more easily and the validity assumptions can be checked. Judging by the results of this preliminary investigation, the model can be refined in a later stage and bigger substructures can be considered.

In the following investigations therefore, only beams have been preliminarily assumed to be directly involved in the fire. It is expected that under these conditions, the primary initial effects of the fire will be localised to the elements of the floor, so basic preliminary investigations are carried on a substructure, which represents the 5th floor of the building (Fig.2 bottom). This condition can be representative of a construction stage, where the beams, which are not insulated, are left unprotected by the absence of the floors. It can also be significant for understanding the effect of beam failures on the adjacent elements and highlight a possible propagation of the failures to zones of the structure not directly involved in the fire.

As a matter of fact, a particular dangerous situation for high-rise buildings under fire is represented by an indirect involvement of the columns, which are either pushed outside by the horizontal thermal expansion of the beam, or pulled inwards by the vertical runaway of the beams (Song et al., 2009). This mechanism is particularly relevant for frames where the stiffness of the beam is significant and comparable with the flexural stiffness of the columns (EUR 24222 EN, 2010), while for strong column – slender beam system, the involvement of the column can be due to the stress redistribution and loss of lateral restraint consequent to the buckling of the horizontal members, as mentioned above. In both cases, the collapse would not remain localized and would propagate downwards through failures of columns and other floors.

In order to see a possible influence of the fire effects on the columns and to model with a sufficient accuracy the translational and rotational capability of the beam end nodes, columns are included in the model to the extent of half-length of the columns pertinent to the 5th floor (below the floor level) and half length of the columns pertinent to the 6th (above the floor level). The columns are continuous and restrained by hinges at bottom, and by vertical sliding support at the top and are considered to be unloaded in this preliminary investigation. In case a possible significant overloading of the column is evidenced in the analysis, a refined model should be considered, where more floor planes have to be modelled and a more realistic loading condition should be considered for the columns.

1.4 Analysis and collapse criterion

The analyses take into account thermo-plastic material and geometric nonlinearities. Dead and live loads pertinent to beams are applied as line forces and considered in a first static analysis step, together with self-weight, while in a second load step the temperatures of the calculated steel heating curves of the beams are applied to the beam nodes and an implicit dynamic solver has been used in order to overcome convergence problems due to local mechanisms and be able to follow the propagation of failures.

Depending on the safety level considered and on the design objectives of the investigation, a nominal collapse condition can be assumed when displacements overcome a given limit, which in this work has been taken equal to $L/20$, where L is the beam length. Another possibility is to consider the runaway of the beam, with this term meaning the accelerating and irreversible downward displacement (Usmani et al. 2003) of the beam mid-span node. In the following the time resistance of the structure is evaluated and compared for the four fire scenarios considered, with reference to both the above mentioned collapse criteria.

2 RESULTS

In the following, the main outcomes are presented and discussed, with reference to each fire scenario. The first fire scenario is analysed in detail, with the aim of outlining a methodology for the interpretation of the results in this kind of investigations. The resistance times corresponding to each fire scenario is evaluated and compared on the basis of the collapse criteria discussed above.

2.1 First fire scenario

The results of the analysis on the first scenarios highlight the following sequence of failures in the area involved in the fire:

1. After 2 min of fire, an out of plane buckling mechanism triggers, involving the three beams that converge in the middle external column (i.e. the two external transversal beams and the longitudinal beam between them). Almost contemporarily also the most internal beam on the left (indicated as InB on the left bottom image of Fig.3) buckles out of plane. The early failure of those beams is only due to the eigenstresses induced by the hindered thermal expansion of the beams (dotted and continuous lines in the top graphs at the right of Fig.3), consequent to the strong column- slender beam frame type and also due to the absence of the restraint provided by the slab: specifically, the three beams have IPE270 profiles, while the columns adjacent to them have HEM1000* profiles. As a consequence, the beam failures trigger when the temperatures are very low (around 100 °C) and no degradation of the steel mechanical properties, which typically plays a determinant role in fire-induced collapses, has occurred yet.
2. Shortly after the first four beams, the two transversal beams in the middle, which have a slightly bigger profile (IPE300), buckle out of plane too.
3. At about 10 and 15 minutes of fire respectively, also the last two beams directly involved in the fire buckle out of plane. The higher resistance of those beams is due to the different profile of the sections, which is a HEA240.
4. At this point the temperature are quite high (ca. 600 °C) and the internal beams, which carry higher load than the external ones, experience a runaway and exceed the maximum acceptable displacement considered as nominal collapse criterion (right top graph of Fig.3). It is the material degradation which is responsible for the runaway, which determines the overcoming of the collapse condition and the lack of convergence of the analysis at about 20 min of fire.

It seems relevant to highlight the fact that the same design characteristic that is responsible of the early failure of the beams, i.e. the strong column – slender beam system, ensures on the other side a compartmentalization of the collapsing sections of the structure and avoid the propagation of the collapse to the vertical elements, which are only slightly overloaded (last two row of graphs on the right of Fig 3) by the stress redistribution consequent to the beam failures and would therefore be hardly involved in the collapse mechanism.

The results in term of deformed configurations and element displacements and forces are summarized in Fig. 3. In the left part of the figure the deformed configurations at 14 (top) and 20 min of fire (bottom) are represented. In the top figure, the progression of beam failure is indicated by numbers from 1 to 4, which correspond to the steps illustrated above. In the right part of the figure the result history is shown with reference to one external and one internal beam (indicated as ExB and InB in the left figure). The first row shows the horizontal and vertical displacement of the beam mid-spans, while the second row shows the axial stresses of the two beams: in order to highlight the effect of material degradation, the displacement and axial forces obtained without consideration of material degradation are reported in the graphs as dotted lines. The last two rows show instead the overloading of the columns adjacent to the monitored beams (indicated as ExLFC, ExRgC, InLFC and InRgC in the bottom left image of Fig.3), in term of axial and shear forces at the bottom node.

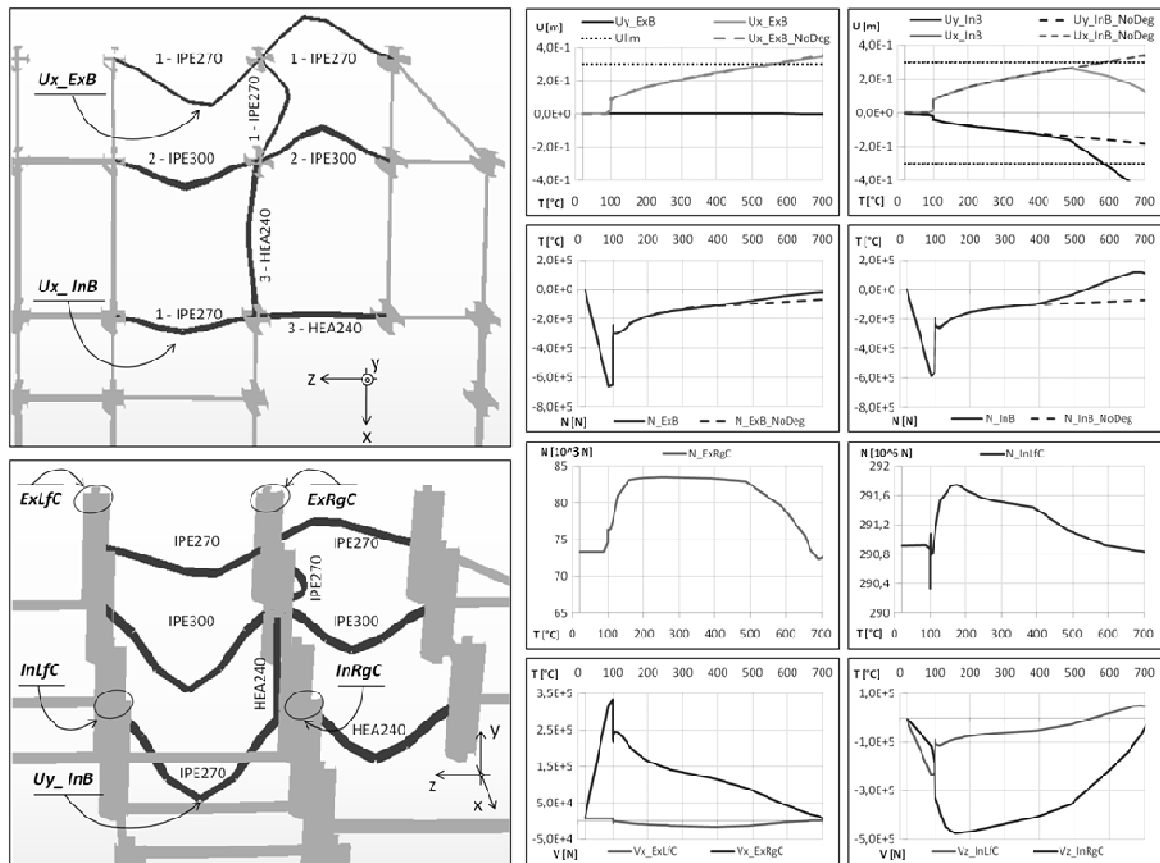


Fig. 3 Results for fire scenario 1, in term of deformed configurations, forces and displacements.

Other fire scenarios

The deformed configurations for the other 3 scenarios are reported in Fig. 4, together with the horizontal and vertical displacements of the nodes, identified by the points A, B, C in the figures.

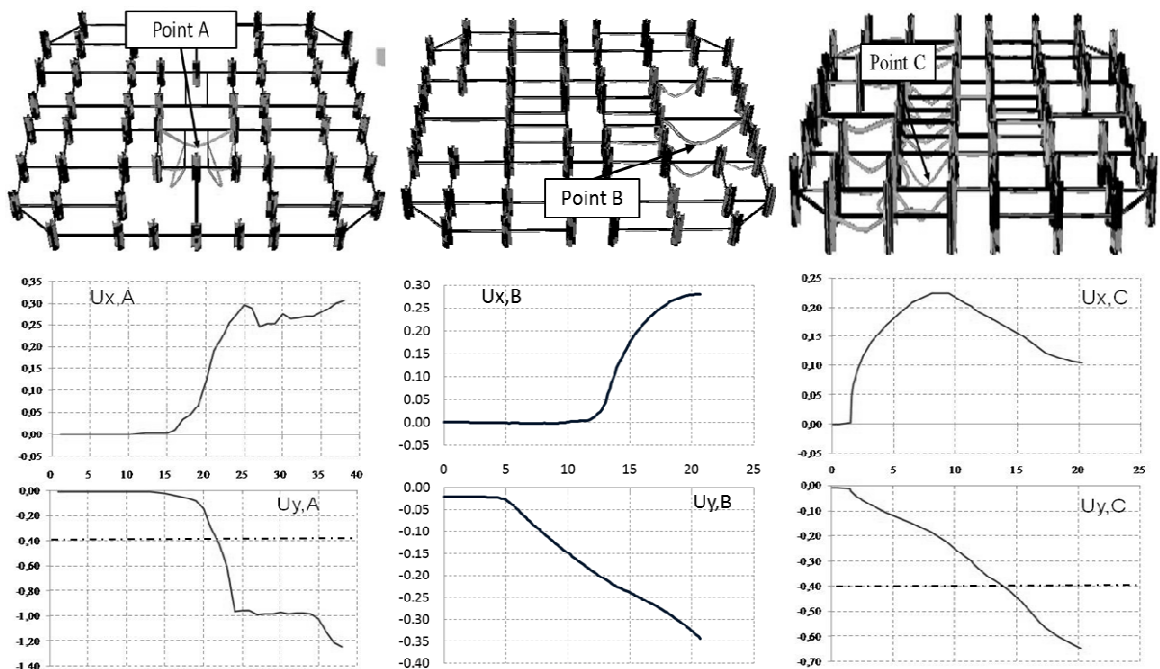


Fig. 4 Results for fire scenario 2, 3, 4 (from left to right) in term of deformed configurations (top) and trend of the horizontal and vertical displacements (in m) versus time (in min) of monitored points (bottom).

These nodes identify the mid-span point of the beams that experience the highest displacement in each fire scenario.

It can be seen that all the monitored beams experience high displacements both in the horizontal and vertical direction. In the second scenario however, a discontinuity in the trend of the vertical displacement can be observed, which is followed by an almost horizontal branch that indicates a regain in stiffness of the element. This can be imputed to the triggering of a catenary action, occurring as a consequence of the significant vertical displacement of the beam, which support also two perpendicular beams, and of the high horizontal restraint offered by the columns. The same considerations apply to the monitored beam in the third scenario. In the fourth scenario instead, the monitored beam experience an out of plane buckling, which is followed by a significant but gradual increment in the vertical displacement, so that an actual runaway point cannot be identified.

3 CONCLUSIONS

By comparing the resistance times of the four scenarios summarized in Tab.1, the most critical scenarios seem to be the first and the fourth ones. However, whereas the in the fourth scenario a large portion of the floor is involved in the fire as a result of an assumed loss of the horizontal compartmentalization of the building, in the first scenario only few elements are directly involved in the fire. The second and third scenarios have a longer resistance in term of maximum nominal displacement: however the value of $L/20$ refers to beam of standard dimension and seem to allow very big displacement for long beams such as the one monitored in the third scenario, which even if experiencing very big displacements doesn't reach the collapse condition within the analysis time.

Tab. 1 Resistance times in term of nominal maximum displacement and runaway of critical beams.

Scenario Time (in min) at	1 - InB	2 - PointA	3 - PointB	4 - PointC
$L/20$	9	22	>20	14
Runaway	12	20	---	---

REFERENCES

- Bontempi F., Petrini F., Fire-Induced Collapses in Structures: Basis of the Analysis and Design, Proceedings of The Fourth International Conference on Structural Engineering, Mechanics and Computation (SEMC2010), Cape Town (South Africa), 6 - 8 September 2010.
- BS 5588-5:2004. Fire precautions in the design, construction and use of buildings - Part 5: Access and facilities for fire-fighting, British Standard, 2004.
- Craighead G., High-rise security and fire life safety, Elsevier Science, U.S., 2003
- Crooke C., External fire spread via windows - closing report, Building Research Establishment, Fire and Risk Sciences Division, report nr. 203141, United Kingdom, 2002.
- EUR 24222 EN, Fire safety of industrial hall - A valorization project, Final report, Research Fund for Coal and Steel, European Commission, DOI: 10.2777/90662, 2010
- Galea ER, Berhane D, Hofmann NA. CFD analysis of fire plumes emerging from windows with external protrusions in high rise buildings, Interflam '96, Cambridge, UK, March 1996.
- MSB-6, Multi-storey steel buildings - Part 6: Fire Engineering, Steel Building in Europe design manual, Research Fund for Coal and Steel of the European Community, 2008.
- NFPA 101:2009 Life Safety Code®, National Fire Protection Association, MA, U.S., 1988
- Song Y.Y., Huang Z., Burgess I.W., Plank R.J., The Behaviour of Single-Storey Industrial Steel Frames in Fire. International Journal of Advanced Steel Construction, 5 (3), pp. 289-302, 2009
- Starossek U., Progressive collapse of structures, Thomas Telford Publishing, London, 2009
- Usmani A.S., Chung Y.C., Torero J.L., How Did the WTC Collapse: A New Theory, Fire Safety Journal, 38, 6, 501-591, 2003.

NUMERICAL ANALYSIS OF STRUCTURES IN FIRE USING OPENSEES

Jian Jiang^a, Asif Usmani^a, Jian Zhang^b, Panagiotis Kotsovinos^a

^a School of Engineering, The University of Edinburgh, Edinburgh EH9 3JF, United Kingdom

^b School of Built Environment, Heriot-Watt University, Edinburgh EH14 4AS, United Kingdom

INTRODUCTION

Many finite element program codes have been written to simulate the structural behaviour at elevated temperature and the results compare well with the test data from Cardington test. These include specialist programs such as ADAPTIC (Song 1995; Izzuddin 1996), FEAST (Liu 1988; Liu 1996), SAFIR (Franseen 2000), VULCAN (Bailey 1995; Huang 2000) and commercial packages such as ABAQUS and DIANA. The specialist programs can be cost-effective compared to commercial packages but lack generality and versatility because they are always developed to focus on some special feature of structural behaviour in fire. OpenSees is an open-source object-oriented software framework developed at UC Berkeley. OpenSees has so far been focussed on providing an advanced computational tool for analysing the non-linear response of structural frames subjected to seismic excitations. Given that OpenSees is open source and has been available for best part of this decade it has spawned a rapidly growing community of users as well as developers who have added considerably to its capabilities over this period, to the extent that for the analysis of structural frames it has greater capabilities than that of many commercial codes.

The OpenSees framework is being extended to deal with the frame structures in fire conditions by a team at the University of Edinburgh. New load classes are created to define the temperature distribution across the section of the element, which is built up with “fibres”. Existing material classes are modified to account for the temperature-dependent material properties according to the Eurocode3. The existing beam-column element classes are modified to include interfaces to the updated material at elevated temperature and section with temperature field and to take account of the thermally induced forces and deformations. Some benchmark cases are studied to validate the thermo-mechanical analysis in OpenSees followed by the modelling of the restrained beam test at Cardington test. The analysis procedures being developed for structures under fire in OpenSees will make it easier to perform coupled heat-transfer and thermo-mechanical analyses allowing for non-uniform temperature distribution along an element resulting from local fires.

1 THERMO-MECHANICAL ANALYSIS IN OPENSEES

The OpenSees framework was chosen to develop thermo-mechanical analysis of frame structures by adding new thermal load class and modified temperature dependent material classes (shown in Fig. 1). Based on existing beam element *dispBeamColumn2d* (Taucer and Filippou 1991), the flowchart of the thermo-mechanical analysis in OpenSees is shown in Fig. 2. New thermal load class *<Beam2dTemperatureLoad>* is created to store the temperature distribution along the section consisting of temperature and coordinate, the temperature of each fibre will be determined by the interpolation of the temperature at the nearest coordinate point according to its location. Also the temperature dependent material properties are modified from the existing bilinear steel material class according to Eurocode 3 (ENV 1993-1-2).

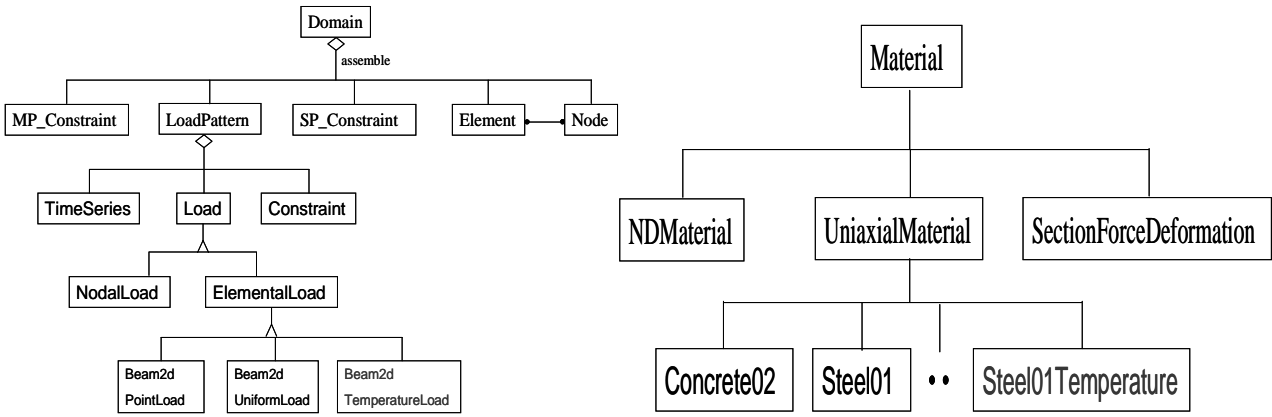


Fig. 1 Class diagram for thermal load and material in OpenSees

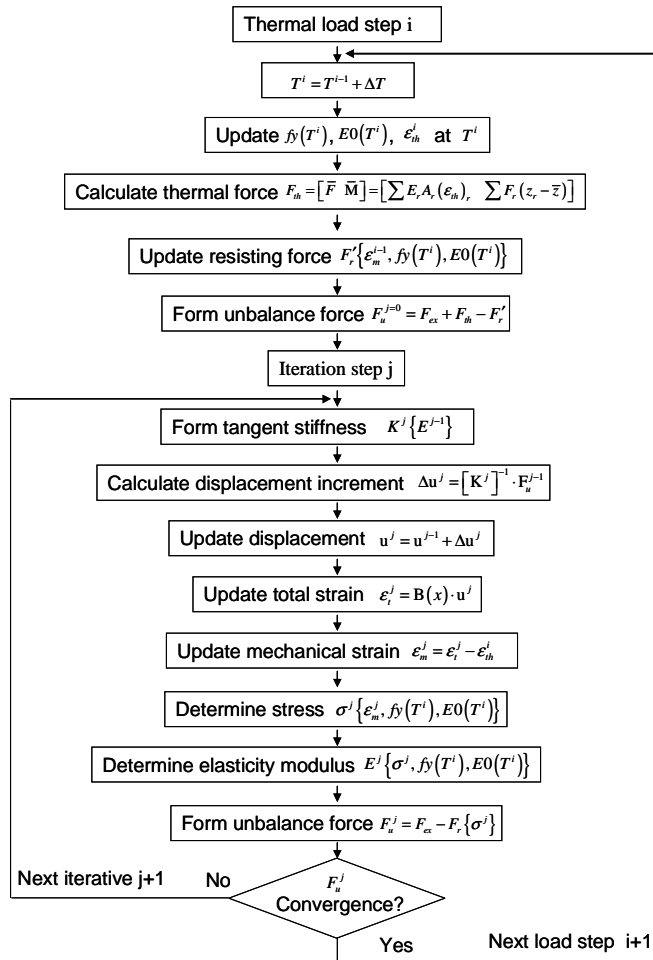


Fig. 2 Flowchart for thermo-mechanical analysis in OpenSees

2 VALIDATION

In order to establish the validity of the thermo-mechanical analysis in OpenSees, a number of benchmark problems are solved involving a beam subjected to temperature gradient and comparing the results against ABAQUS solutions. Further validation is obtained from modelling a uniformly heated steel frame test (Rubert and Schaumann, 1986).

2.1 Simply supported beam with varying restraint to lateral translation

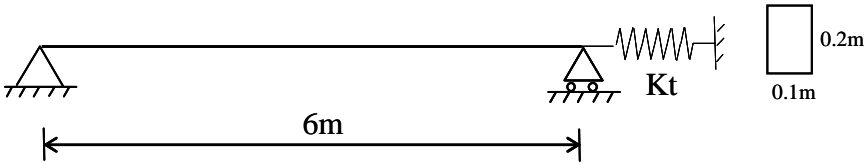


Fig. 3 Simply supported beam with a translational spring at end

The deformation of structures under fire conditions is sensitive to its boundary condition. Fig. 3 shows a 2D single beam with finite end restraint. The beam subjected to a uniformly distributed load (UDL) and a linear thermal gradient along the section height. The finite end restraints are represented by a translational spring of constant stiffness K_t . Different boundary conditions can be obtained by varying K_t . Thermo-mechanical analysis of beam members with these boundary conditions was conducted and the results were compared with ABAQUS.

The temperature at top of the beam is assumed 0°C and the temperature at bottom varies linearly from 100°C to 1000°C . Temperature dependent elastic material is used for the model and constant expansion coefficient $\alpha = 12 \times 10^{-6} / ^{\circ}\text{C}$ is assumed. The modulus of elasticity at elevated temperature is varied according to Eurocode 3 (ENV 1993-1-2) with an initial value of 20000MPa at ambient temperature. The details of the model are listed in Table 1.

Table 1. Input parameters of the beam model

Length (m)	Area (m^2)	E (0oC) (N/m^2)	UDL (N/m)	Thermal gradient ($^{\circ}\text{C}/\text{m}$)	α ($^{\circ}\text{C}$)	K_t (N/m)
6	0.02	2e11	1000	500-5000	12×10^{-6}	6.7e8

Three kinds of translational restraint were applied to the beams such as free end, finite translational end restraint and pinned end shown in Fig. 4. The predicted results shown in Fig. 5 and Fig. 6 agree well with that of ABAQUS.

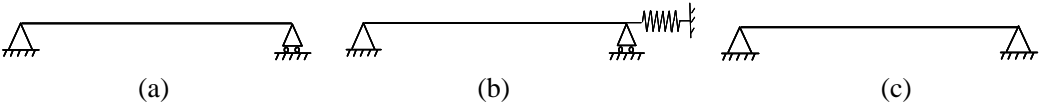


Fig. 4 Schematic of beams with different translational end restraint: (a) free end; (b) spring end; (c) pin end

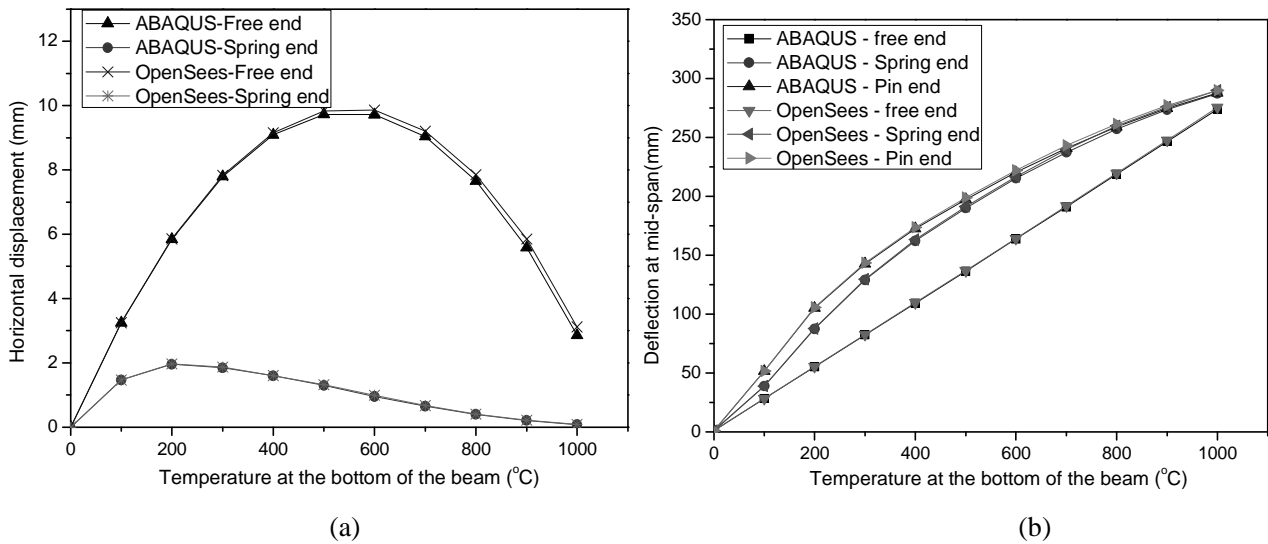


Fig. 5 Displacement of beam with different translational end restraint: (a) Horizontal displacement; (b) mid-span displacement

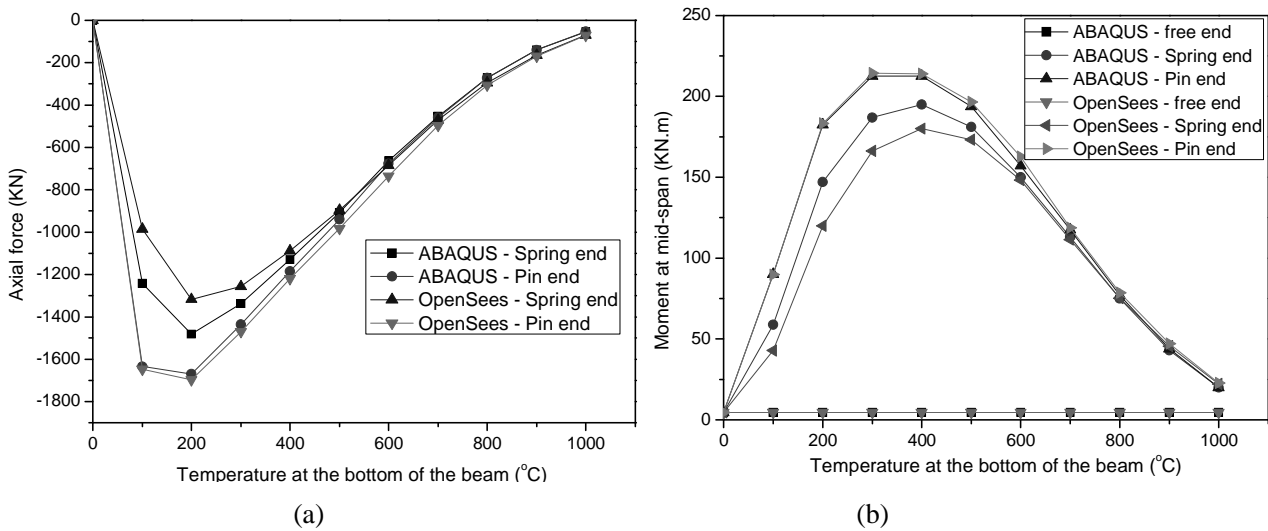


Fig. 6 Forces in the beam with different translational end restraint: (a) axial force; (b) mid-span moment

2.2 Steel frame test

Two steel frames as shown in Fig. 7 were tested by heating them directly to a high temperature. The results from an OpenSees analysis shown in Fig. 8 agree relatively well with the experimental data (Rubert and Schaumann, 1986), showing a qualitatively similar behaviour.

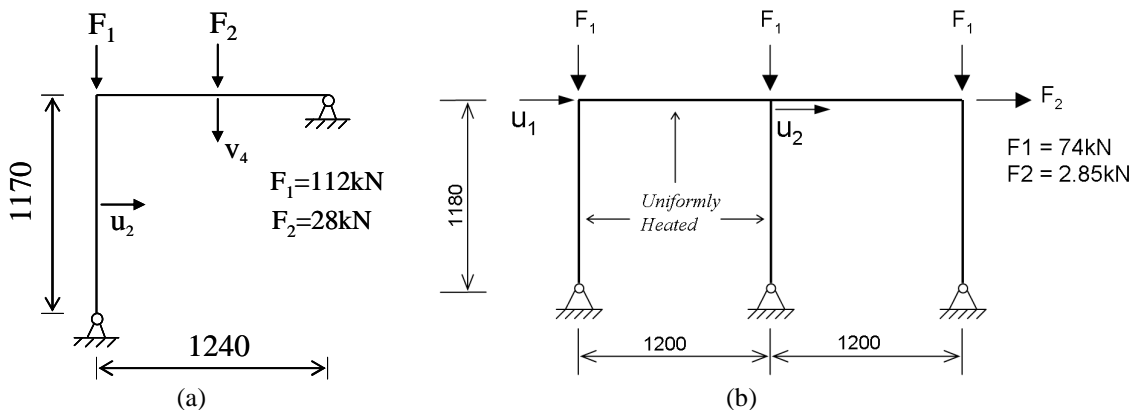


Fig. 7 Schematic of the tested steel frames (mm): (a) frame EHR3; (b) frame ZSR1

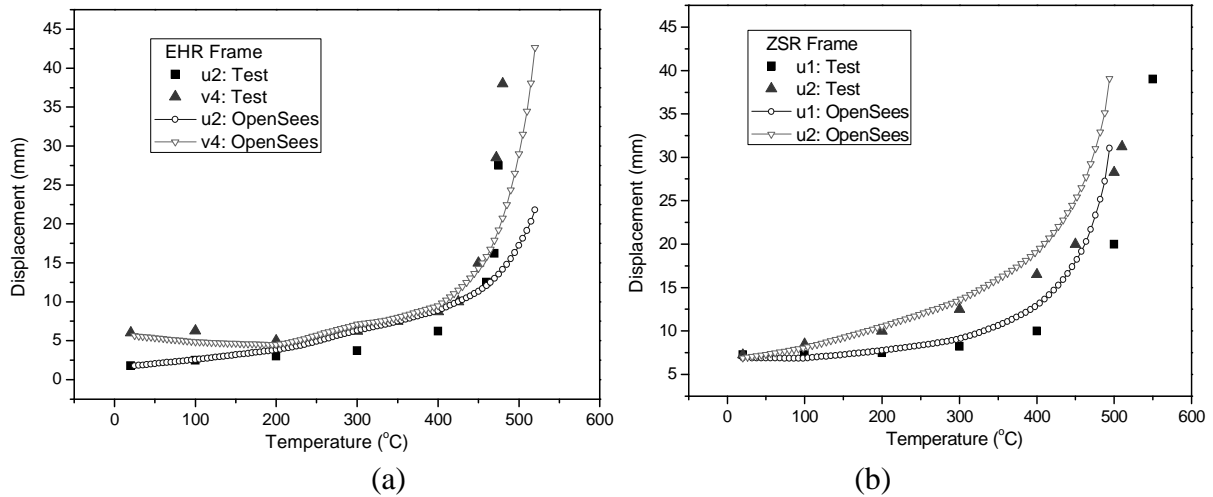


Fig. 8 Comparison between predicted and test deflection results: (a) frame EHR3; (b) frame ZSR1

3 CONCLUSION

The extended OpenSees framework (still under development) seems to be able to adequately deal with the thermo-mechanical analysis of structures under fire conditions. Further work is being done to develop 3D beam element and shell element classes for thermo-mechanical analysis.

REFERENCES

- Bailey, C. G. "Simulation of the structural behavior of steel-framed buildings in fire", PhD thesis, Department of Civil and Structural Engineering, University of Sheffield, UK, 1995
- ENV 1993-1-2. Design of steel structures, Part 1.2: general rules — structural fire design. Eurocode 3 Part 1.2, 2005
- Franssen, J. M., Kodur, V. K. R. and Mason, J. User's manual for SAFIR2001, A computer program for analysis of structures submitted to the fire, University of Liege, Belgium, 2000
- Huang, Z. H., Burgess, I. W. and Plank, R.J. "Effective stiffness modeling of composite concrete slabs in fire", *Engineering structures* 22: 1133-1144, 2000
- Izzudin, B. A. "Quartic formulation for elastic beam-columns subject to thermal effects", *ASCE Journal of Engineering Mechanics* 122(9): 861-871, 1996
- Liu, T. C. H. "Thermal modeling of steel portal frame behavior", PhD thesis, Department of Civil Engineering, University of Manchester, UK, 1988
- Liu, T. C. H. "Finite element modeling of behavior of steel beams and connection in fire", *Journal of Constructional Steel Research* 36(2):181-199, 1996
- Rubert, A. and Schaumann, P. "Structural steel and plane frame assemblies under fire action", *Fire Safety Journal*, 10, 173-184, 1986
- Song, L., Izzudin, B.A., Elashai, A. S. "Nonlinear analysis of steel frames subjected to explosion and fire loading", *Proceedings of the International Conference on Structural Dynamics, Vibration, Noise and Control*, Hong Kong, December, 1995
- Taucer, F. F. Filippou, F. C. "A Fiber Beam-column element for seismic response analysis of reinforced concrete structures". Report of University of California, Berkeley, 1991

DEVELOPMENT OF HEAT TRANSFER MODELLING CAPABILITY IN OPENSEES FOR STRUCTURES IN FIRE

Yaqiang Jiang ^a, Asif Usmani ^a, Stephen Welch ^a

^a University of Edinburgh, School of Engineering, UK

INTRODUCTION

An advanced analysis for structures subjected to fire typically involves a fire model, a heat transfer model and a structural model. Generally speaking, two categories of software may be used to achieve this purpose (Wang, 2002). The first group represents commercial packages which are generally powerful with well designed GUI based pre-processing and post-processing functionalities as well as rich element libraries. However, due to their intrinsic attributes, these packages may cause inflexibilities in dealing with new and unusual couplings such as an integrated fire-thermal-structural analysis (Welch et al, 2009) and therefore may impose restrictions on the users. The second group consists of in-house programs developed on the basis of research outcomes at certain research and academic institutions. Even if soundly validated, most of them have been developed using procedural programming languages which leads to weak modularity resulting in difficulties in software maintenance and further development. Object-oriented design and programming outweighs conventional procedural paradigm in building and maintaining large and complicated software systems (Rumbaugh et al, 1991). One of the first applications of the object-oriented design to finite element analysis was presented by Forde (Forde et al, 1990). Since then, increasing attention has been given to this topic due to the intrinsic complexity of finite element data structures (Zimmermann et al, 1992; Cross et al, 1999).

OpenSees, the Open System of Earthquake Engineering Simulation, is an object-oriented and open source software framework developed at the University of California, Berkeley (McKenna, 1997). It was initially designed to simulate structural frames subjected to seismic excitations using the finite element method. The framework has been known for its computational efficiency, flexibility, extensibility and portability (McKenna, 2010). One can conveniently introduce into OpenSees a new element, a new material model or even a new analysis procedure without the knowledge of every single piece of codes in the framework.

The authors have been motivated to add a structures-in-fire modelling capability into the OpenSees framework by utilizing its well-designed software architecture (Usmani et al, 2010). To achieve this purpose, a dedicated heat transfer module, addressing transient nonlinear heat conduction in structural members whose surfaces are exposed to spatially and temporally variable heat fluxes, has been developed using the finite element method. By adopting object-oriented programming paradigm, the software structure is consistent with that of OpenSees, which made it possible to reuse some of the existing components such as graph numbering classes and numerical classes. Important class diagrams and the detailed interactions between associated classes are described in this paper. Verification is conducted through running a series of benchmark tests using four-noded and eight-noded quadrilateral elements.

1 SOLUTION ALGORITHM

The discretised nonlinear heat transfer equation using the finite element method and generalised trapezoidal time-integration rule is expressed as

$$\mathbf{C}_{n+1} \dot{\mathbf{T}}_{n+1} + \mathbf{K}_{n+1} \mathbf{T}_{n+1} = \mathbf{Q}_{n+1} \quad (1)$$

where $T_{n+1} = T_n + \Delta t \{ (1 - \alpha) \dot{T}_n + \alpha \dot{T}_{n+1} \}$

In equation (1), \mathbf{C} is called heat capacity matrix, \mathbf{K} is conductivity matrix and \mathbf{Q} represents the load vector which includes the effects of boundary heat fluxes $\bar{q}(T)$ over all the external surfaces. The users are referred to other publications for more details (Huang & Usmani, 1994). A general expression for $\bar{q}(T)$ describing heat flux boundary conditions is given as

$$\bar{q}(T) = q_{pr} + h(T - T_g) + \varepsilon\sigma T^4 - q_{ir}(t) \quad (2)$$

The first term, second term and the last two terms represent, respectively, prescribed heat flux, convective heat flux and radiation heat flux. It should be noted in the above equation the incident radiation flux does not come from a blackbody with constant temperature, but from all other radiating sources (smoke gas, flame, other solid surfaces, etc.) within a fire compartment. This assumption facilitates the fire-thermal coupling where the incident radiant fluxes can be computed by a separate CFD program.

Besides heat flux boundary conditions(except for prescribed ones), material properties such as specific heat and conductivity can be temperature-dependent as well, which together bring nonlinearities into equation (1). Therefore, an iterative algorithm should be used to obtain the converged solution. A typical predictor-corrector algorithm with Newton iteration method is reproduced here (Winget & Hughes, 1985)

<p>Solution predictor(when $ir = 0$)</p> $\mathbf{T}_{n+1}^{ir} = \tilde{\mathbf{T}}_{n+1} = \mathbf{T}_n + \Delta t(1 - \alpha)\dot{\mathbf{T}}_n \quad (3)$ $\dot{\mathbf{T}}_{n+1}^{ir} = \tilde{\dot{\mathbf{T}}}_{n+1} = 0$ <p>Solution Corrector(iterating until converged)</p> $\mathbf{M}_{n+1}^{*ir} \Delta \dot{\mathbf{T}}_{n+1}^{ir} = \Delta \mathbf{Q}_{n+1}^{ir} \quad (4)$ $\dot{\mathbf{T}}_{n+1}^{ir+1} = \dot{\mathbf{T}}_{n+1}^{ir} + \Delta \dot{\mathbf{T}}_{n+1}^{ir}$ $\mathbf{T}_{n+1}^{ir+1} = \tilde{\mathbf{T}}_{n+1} + \alpha \Delta t \dot{\mathbf{T}}_{n+1}^{ir+1}$
--

The linearized tangent matrix here is defined as

$$\mathbf{M}_{n+1}^{*ir} = \mathbf{C}(\mathbf{T}_{n+1}^{ir}, t_{n+1}) + \alpha \Delta t (\mathbf{K}(\mathbf{T}_{n+1}^{ir}, t_{n+1}) + \mathbf{K}_q(\mathbf{T}_{n+1}^{ir}, t_{n+1})) \quad (5)$$

which approximates the exact tangent matrix by keeping symmetric terms only.

The residual vector here is defined as

$$\Delta \mathbf{Q}_{n+1}^{ir} = \mathbf{Q}(\mathbf{T}_{n+1}^{ir}, t_{n+1}) - \mathbf{C}(\mathbf{T}_{n+1}^{ir}, t_{n+1}) \dot{\mathbf{T}}_{n+1}^{ir} - \mathbf{K}(\mathbf{T}_{n+1}^{ir}, t_{n+1}) \mathbf{T}_{n+1}^{ir} \quad (6)$$

2 PROGRAM DESIGN AND IMPLEMENTATION

A comprehensive review on object-oriented finite element programming (specific to structural analysis) was reported and the software architecture for OpenSees was proposed by McKenna (McKenna, 1997). As with its initial purpose, most classes in OpenSees have attributes and behaviours specific to structural analysis only and are not applicable to heat transfer analysis. However, in object-oriented software design, a class should describe objects with similar attributes, common behaviours, common association relationships, and common semantics (Rumbaugh et al, 1991). For this reason, a separate set of classes specific to heat transfer analysis has been created, which will be presented in the rest of this section in detail.

Standard UML (Unified Modelling Language) class diagrams represented by graphical notations are used here for demonstrating the structure of the system (Rumbaugh et al, 1999). Fig. 1 shows the high-level classes for the heat transfer module. A **HeatTransferDomain** creates the analysis environment for a **HeatTransferAnalysis** object by aggregating components of a finite element model. Methods to add, remove and access those components are provided. A **HeatTransferAnalysis** object has to be associated with a specific **HeatTransferDomain** object to perform the analysis. A **HeatTransferNode** corresponds to a specific node in FE discretization, which knows its coordinates and holds its temperatures and temperature derivatives (with respect to time).

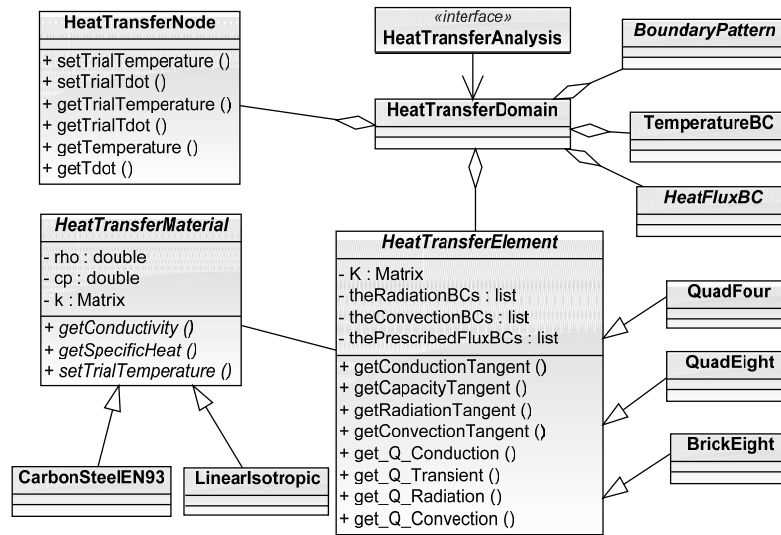


Fig. 1 Diagram for high-level classes for heat transfer module

Methods to modify and query those quantities are provided. Similarly, a *HeatTransferElement* object represents a specific element in the FE discretization and it is the basic computational unit returning the tangent matrix and residual vector at elemental level. As shown in equation (5) and (6), both the tangent and residual vector can be decomposed into four parts by considering contributions from the transient storage, conduction, convection and radiation. Methods are designed to support this decomposition for a more flexible architecture which facilitates using different solution algorithms and time integration rules. *HeatTransferElement* is an abstract class and its instantiation relies on the subclasses. Currently four-noded and eight-noded quadrilateral elements are implemented to solve two dimensional heat conduction problems. Each element is associated with several *HeatTransferMaterial* objects depending on the number of quadrature points used. A *HeatTransferMaterial* object holds values of conductivity and specific heat at a given temperature and allows access to those quantities. Subclass *LinearIsotropic* is designed to define any arbitrary temperature-independent material information. Subclass *CarbonSteelEN93* is implemented for steel by using material information given in Eurocode 3. Other material models can also be introduced easily by subclassing *HeatTransferMaterial*. With this design, elements can be assigned different materials and heat transfer in structures with multiple material layers can be modelled.

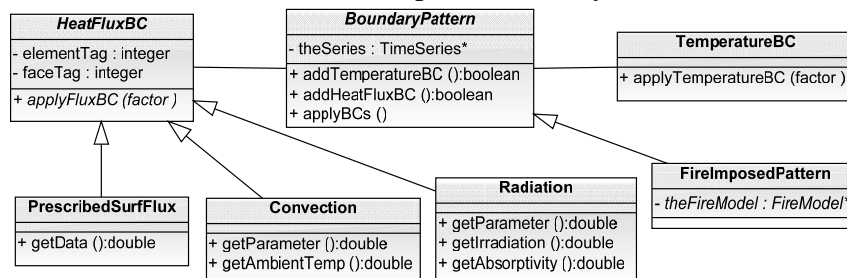


Fig. 2 Diagram representing classes for specifying boundary conditions

A *TemperatureBC* object specifies the existence of Dirichlet boundary condition at solid boundaries and a *HeatFluxBC* object specifies Neumann boundary conditions. Some of the attributes and public operations for these two classes are shown in Fig. 2. A *HeatTransferElement* object keeps a record of *HeatFluxBC* objects acting on its faces and enables imposition of multiple flux boundary conditions on any of its faces. Objects of *TemperatureBC* and *HeatFluxBC* can only deal with constant boundary conditions. A *BoundaryPattern* class, which has a *TimeSeries* object as its attribute, is introduced to define arbitrary time-varying boundary conditions. Object of this class can be associated with a number of *HeatFluxBC* and *TemperatureBC* objects by invoking *addTemperatureBC()* and *addHeatFluxBC()* methods. Subclass *FireImposedPattern*, which has a *FireModel* object as its attribute, will be implemented to specify temporal heat flux boundary conditions imposed by a specific type of fire. As indicated by equation (2), there are generally three types of boundary heat fluxes:

prescribed heat flux, convective heat flux and radiative heat flux; thus three subclasses of HeatFluxBC are provided, whose public operations returning relevant quantities are also given in Fig. 2.

Fig. 3 illustrates a general picture of relationships between classes relevant to heat transfer analysis procedures, where HT_TransientAnalysis is a subclass inheriting from HeatTransferAnalysis class and an instance of this class is associated with several instances of other classes to perform a transient analysis. The architecture of this analysis system is fundamentally the same as that of OpenSees. A HT_DOF_Number object employing algorithms based on graph theory numbers all the degrees-of-freedom in the domain with the aim of reducing the bandwidth of the tangent matrix. A HT_DOF_Group object keeps a reference to a HeatTransferNode object in the domain and deals with the mapping between degrees-of-freedom and global equation numbers. Similarly, a HT_FE_Element is linked to a HeatTransferElement in the domain and it provides methods to set and retrieve equation numbers for degrees-of-freedom relevant to that element. It also provides methods to return elemental residual vector and tangent stiffness matrix. A HT_AnalysisModel holds all the HT_DOF_Groups and HT_FE_Elements in an analysis and also provides methods to update the state of the domain. HeatTransferIntegrator class provides methods to assemble the system of equations by adding elemental contributions. Subclasses of HT_TransientIntegrator provide methods to set the solution predictor and updater for a transient problem. BackwardDifference implements the time-integration algorithm shown in equation (1) with α being set one, which removes the need of computing initial temperature derivatives. TemperatureBCHandler is an abstract class, which provides interfaces for imposing the Dirichlet boundary condition on the global system of equations. Subclasses provide the implementation details, such as using penalty method. HT_SolutionAlgorithm implements the algorithms such as Newton's method to solve a system of equations.

By instantiating some of the heat transfer classes and OpenSees' solver classes, one can produce stand-alone executable applications to solve any heat conduction problem. In addition, it is also possible to integrate these heat transfer classes into the main application of OpenSees, which allows users to run heat transfer analyses with scripting languages such as Tcl.

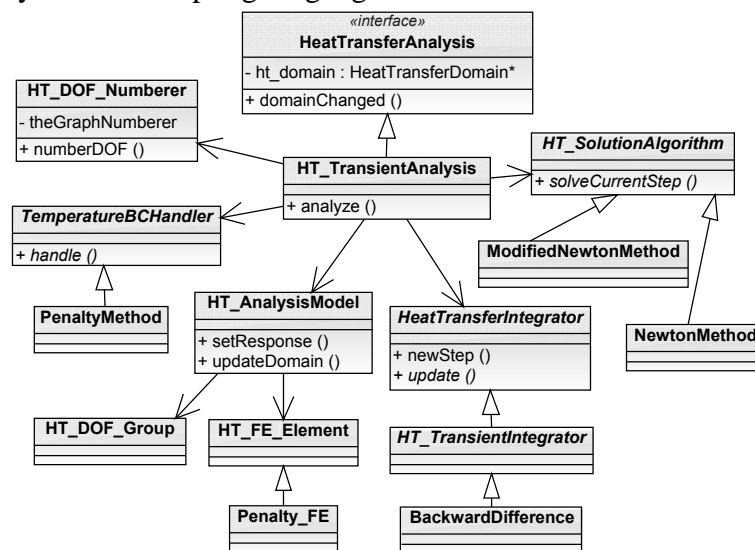


Fig. 3 Class diagram representing heat transfer analysis algorithms

3 VERIFICATION

The heat transfer module discussed in the foregoing section is verified through three benchmark tests. The comparison between FE solutions and analytical solutions are given below.

The first example shown in Fig. 4 can be used to examine the general performance of solution procedures of a finite element program and its transient modelling capability in particular (Huang & Usmani, 1994). The physical problem is a two dimensional bar with fixed temperature on its left end and with sinusoidal temperature changes at its right-end. Steel material is assumed here, where mass density $\rho = 7200 \text{ kg/m}^3$, specific heat $c_p = 440.5 \text{ J/kgK}$, heat conductivity $k = 35.0 \text{ W/mK}$.

Both four-noded and eight-noded quadrilateral elements together with backward difference time-integration scheme are used in this test. A uniform mesh with ten elements is shown in Fig. 4(b).

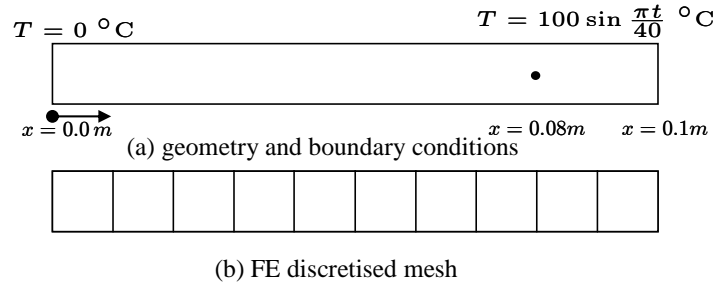


Fig. 4 Benchmark test with transient temperature boundary condition

Fig. 5 presents the temporal solution at a target point ($x = 0.08\text{m}$). It can be seen that both the linear and quadratic quadrilateral elements produce results rather close to analytical solutions while the quadratic ones show larger deviation. However, as shown in Fig. 6, eight-noded quadratic elements give better prediction of the spatial temperature distribution especially in the vicinity of the right-end, where the gradient-reversal behaviour is totally missed by using linear elements. One may also notice that 8-noded elements still give a slight error at $x = 0.095\text{m}$, which was demonstrated to be produced by backward-difference time integration scheme and may be improved by using Crank-Nicolson method due to its higher accuracy.

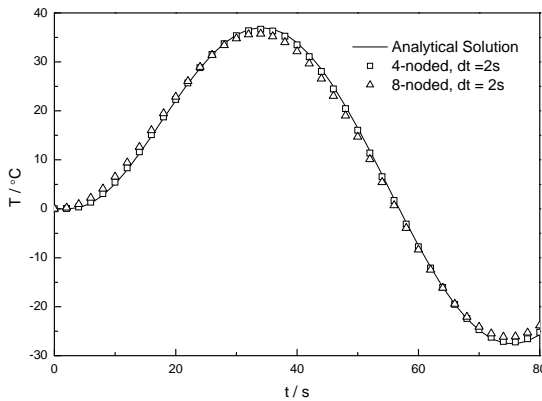


Fig. 5 Temporal solution at target point

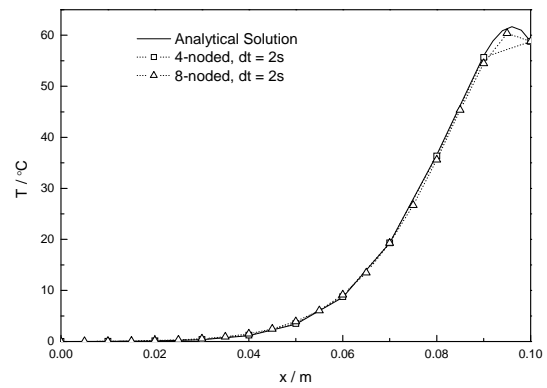


Fig. 6 Spatial distribution along length

The second test problem is shown in Fig. 7, where a two dimensional plate has a fixed temperature boundary condition at its bottom and is insulated along its left-side boundary. The top and right are subjected to the convective boundary condition with ambient temperature $T_a = 0\text{ °C}$ and convective heat transfer coefficient $h = 750\text{ W/m}^2\text{K}$. Other material properties are listed in the figure.

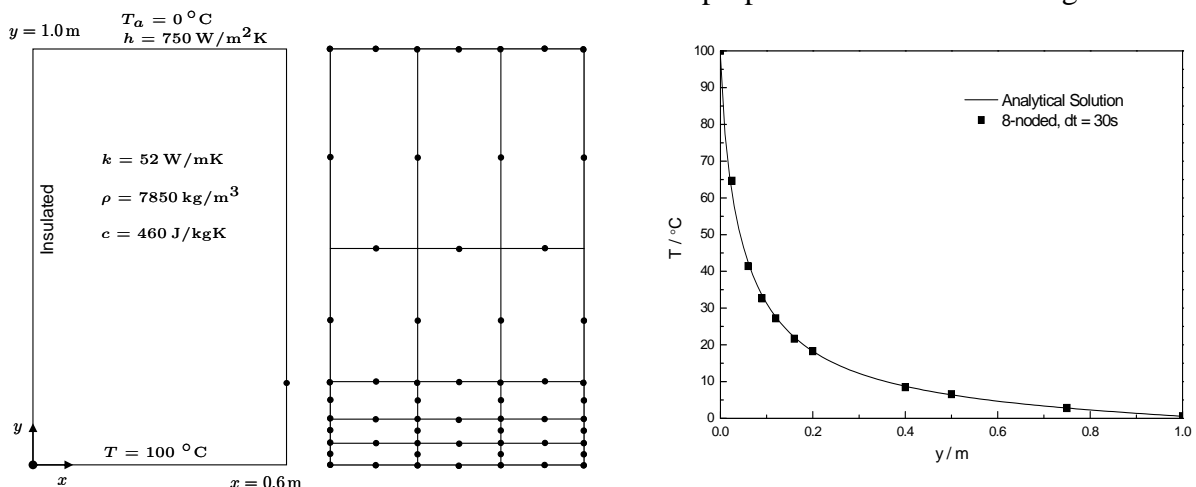


Fig. 7 Benchmark test with convection boundary condition Fig. 8 Temperature distribution along right-side boundary

The steady state analytical solution suggests a strongly nonlinear temperature distribution along the right-bottom boundary. Therefore, a graded mesh shown in Fig. 7 with eight-noded elements is

used. The steady state solution given Fig. 8 is obtained by using backward-difference time-integration scheme with a step of 30s. It can be seen that the FE solution agrees with analytical solution very well and the large temperature gradient along the right-side boundary is accurately captured. A local examination at the target point (0.6, 0.2) also gives a good result with 18.28 °C which closely approaches the analytical solution of 18.3 °C.

The purpose of the last test is to examine the program's capability of handling radiation boundary conditions which introduces a nonlinear source into the system of equations. The problem itself shown in Fig. 9 is rather simple, which is again a bar with fixed temperature at its left-end and with its right-end radiating to ambient, where surface emissivity $\varepsilon = 0.98$, Stefan-Boltzmann constant $\sigma = 5.67 \times 10^{-8} \text{ Wm}^{-2}\text{K}^{-4}$. In the current test, Newton-Raphson algorithm is used and a converged solution of 927.008 K at the right-end is obtained with nil error.

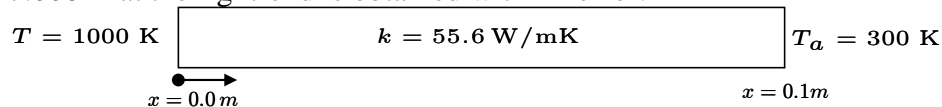


Fig. 9 Benchmark test with radiation boundary condition

3 SUMMARY AND ACKNOWLEDGMENT

A flexible and extensible heat transfer module dedicated to structures-in-fire modelling is developed for OpenSees. A series of benchmark tests are carried out by comparing the modelling results with analytical solutions. It is shown that results from the two agree very well and the module behaves desirably as expected. Future work would be directed to the development of the fire module and the implementation of fire-thermal-structural coupling techniques.

The first author gratefully appreciates the China Scholarship Council and The University of Edinburgh for providing a joint scholarship on his PhD project. The authors also would like to thank Dr Frank McKenna at UC Berkeley for his assistance during the development process.

REFERENCES

- Cross J., Masters I., Lewis R., Why You Should Consider Object-oriented Programming Techniques for Finite Element Methods, *International Journal of Numerical Methods for Heat and Fluid Flow*, 9(3), 333-347, West Yorkshire, England: MCB University Press, 1999.
- Forde B., Foschi R., Stiemer S., Object-Oriented Finite Element Analysis, *Computers & Structures*, 34(3), 355-374, 1990.
- Huang H. C., Usmani A. S., *Finite Element Analysis for Heat Transfer: Theory and Software*, London: Springer-Verlag, 1994.
- McKenna F. T., *Object-Oriented Finite Element Programming: Frameworks for Analysis, Algorithms and Parallel Computing*, PhD Dissertation of University of California, Berkeley, 1997.
- McKenna F., Nonlinear Finite-Element Analysis Software Architecture Using Object Composition, *Journal of Computing in Civil Engineering*, 24(1), 95-107, 2010.
- Rumbaugh J., Jacobson I., Booch G., *Unified Modeling Language Reference Manual*, Reading, MA: Addison-Wesley, 1999.
- Rumbaugh J., Blaha M., Premerlani W., Eddy F., Lorensen W., *Object Oriented Modeling and Design*, West Nyack, NY: Prentice Hall, Book Distribution Center, 1991.
- Usmani A., Zhang J., Jiang J., Jiang Y., Kotsovinos P., Zhang J., and May I., Using OpenSees for structures in Fire, 6th International Conference on Structures in Fire, 919-926, Michigan, USA, 2010.
- Winget J., Hughes T., Solution Algorithms for Nonlinear Transient Heat Conduction Analysis Employing Element-by-element Iterative Strategies, *Computer Methods in Applied Mechanics and Engineering*, 52(1-3), 711-815, 1985.
- Welch S., Miles S., Kumar S., Lemaire T., Chan A., FIRESTRUC – Integrating Advanced Three-dimensional Modelling Methodologies for Predicting Thermo-mechanical Behaviour of Steel and Composite Structures Subjected to Natural Fires, 9th International IAFSS Symposium, Vol. 22, 1315-1326, Karlsruhe, Germany, 2009.
- Wang Y., *Steel and Composite Structures: Behaviour and Design for Fire Safety*, London and New York: Spon Press, Taylor & Francis, 2002.
- Zimmermann T., Dubois-Pèlerin Y., Bomme P., Object-oriented Finite Element Programming: I. Governing principles, *Computer Methods in Applied Mechanics and Engineering*, 98, 291-303, 1992.

A NUMERICALLY DERIVED MODIFIED CONDUCTIVITY MODEL FOR SOFTWOOD EXPOSED TO PARAMETRIC DESIGN FIRES Background, Benchmarking and Adaptation for Cooling

Danny Hopkin ^{a/c}, Jamal El-Rimawi ^a, Vadim Silberschmidt ^b, Tom Lennon ^c

^a Loughborough University, Department of Civil and Building Engineering, Loughborough, UK

^b Loughborough University, Wolfson School of Mechanical Engineering, Loughborough, UK

^c BRE Global, Garston, Watford, Herts, WD25 9XX, UK.

INTRODUCTION

Recommendations for designing timber structures, as well as other structures made of concrete or steel, under fire conditions are given in the relevant parts of the fire Eurocodes. However, unlike other parts, the scope for using the part relevant to the fire design of timber structures (Eurocode 5 part 1.2) is quite limited. This is because, with the exception of a single annex, it is only applicable to structures subjected to standard fire exposure. The only exception to this is Annex A which gives guidance on the charring rates of initially un-protected timber members in parametric fires. However, in the UK the use of this Annex is prohibited as specified in its national annex to the Eurocode.

1 BACKGROUND TO THE MODIFIED CONDUCTIVITY MODEL (MCM)

The complex phenomena present in heated timber elements are difficult to model explicitly and, hence, to date, ‘effective properties’ are often defined. Such properties implicitly account for the effects of complex behaviour, such as the flow of pyrolysis gases and water vapour, through calibration against known temperatures in limited experimental configurations. König and Walleij (2000) have been instrumental in initiating such a process for timber. They calibrated ‘effective’ thermal properties for standard fire exposure conditions. These properties form the basis of the advanced calculation models contained in Annex B of EN 1995-1-2. However, additional studies by König (2006) proved (both experimentally and numerically) that those properties exhibited very conservative predictions of char depth when applied to non-standard (parametric) fire conditions with heating rates in excess of those given by the standard-fire curve. Similarly, the properties from the code were shown to result in non-conservative predictions of timber temperature and depth of char for heating rates lower than that of the standard-fire curve. As a result, EN 1995-1-2 explicitly states that the thermal properties present in Annex B should only be adopted for standard-fire exposure and not for parametric fire exposure.

König (2006) previously proposed that consistency between parametric charring measurements in experiments and computational predictions, under standard-fire exposure, could be achieved via subtle modifications to the conductivity-temperature relationships proposed in Annex B of EN 1995-1-2. In addition, he noted that only those properties in excess of 350°C should be modified as they represent the ‘effective’ properties of the char layer. Phenomena in the char area, such as ‘reverse cooling pyrolysis flows’, cracking and ablation, appear to be influenced by heating rate. Although König (2006) made the observation that the thermal properties present in Annex B of EC5-1-2 were not appropriate for parametric fire applications and that better agreement could be seen through adaptation of the char-layer conductivity, no follow-on research has been conducted to quantify the necessary modification of the char-layer conductivity.

In an earlier publication the authors proposed a modified conductivity model (MCM) for softwood timber (Hopkin *et al.* 2010) based upon the principles outlined in König’s research and upon EN 1995-1-2 specific heat modifications proposed by Cachim and Franssen (2009). The MCM was derived using numerical calibrations of a fire load- (q_{td}) and heating rate- (Γ) dependent modification factor and the depths of char present in parametric design fires. In the latter case the depth of char in such fires was determined using the Annex A approach of EN 1995-1-2.

The full derivation of the proposed model can be found elsewhere (Hopkin et al. 2010). However, the resulting relations are shown in Tab 1. and Eqn 1.

Tab. 1(a) Summary of MCM

Temperature (°C)	Conductivity (W/m K)
20	0.12
200	0.15
350	0.07
500	$0.09k_{\lambda,mod}$
800	$0.35k_{\lambda,mod}$
1200	$1.50k_{\lambda,mod}$

Tab. 1(b) Specific heat after Cachim & Franssen (2009)

Temperature (°C)	Density ratio G	Cachim and Franssen moisture modified specific heat (J/kg K)
20	$1+\omega$	$(1210+4190\omega)/G$
99	$1+\omega$	$(1480+4190\omega)/G$
99	$1+\omega$	$(1480+114600\omega)/G$
120	1.00	$(2120+95500\omega)/G$
120	1.00	2120/G
200	1.00	2000/G

$$k_{\lambda,mod} = k_{\Gamma,mod} k_{qtd,mod} \quad (1)$$

$$\text{with } k_{\Gamma,mod} = 1.5\Gamma^{-0.48}, \quad k_{qtd,mod} = \sqrt{\frac{q_{td}}{210}} \quad \text{and } \Gamma = \frac{(O/b)^2}{(0.04/1160)^2},$$

where ω is the moisture content of timber (%), O is an opening factor ($m^{0.5}$) and b is compartment thermal inertia ($J/m^2s^{0.5}K$).

The above, when coupled with specific heat properties and appropriate densities, were found to give rather consistent transient depth-of-char predictions for the heating phase of a parametric fire, when compared to EN 1995-1-2 Annex A. However, from a structural-engineering view point, the definition of the depth of char in Finite Element analysis (FEA) simulations is sufficient to fully characterise the mechanical response of a member exposed to high temperatures. In timber only those temperatures below 300°C are of concern. Above this threshold the timber is charred and friable. As a result, the MCM must not only be able to place the char line correctly within a cross section, but it must also accurately simulate temperature in the intact member. This allows the sectional response to be determined using strength, stiffness and temperature relations. Given the limited number, and limitations, of experiments conducted on timber exposed to parametric fires, the authors were only able to investigate temperature development using the test data developed by Konig and Walleij (1999). The modelling conducted and the comparisons made are discussed in the section that follows.

2 BENCHMARKING AGAINST KONIG TEST DATA

At the turn of the century Konig and Walleij (1999) reported 6 experiments on timber blocks exposed to parametric fires. The experiments, as best as possible, exposed timber panels to one-dimensional heat transfer via a gas-powered furnace following parametric curves. From this it was first observed by Konig (2006) that the thermal properties present in Annex B of EN 1995-1-2 were inappropriate for use with non-standard fire exposure. The timber used in the experiments was a generic softwood with an estimated moisture content of 12% and a mean density of 420-430 kg/m³. Although Konig and Walleij (1999) attempted to follow parametric curves, this was not entirely possible due to the furnace configuration. As a result, the authors fitted EN 1991-1-2 parametric curves to the measured gas temperature-time relationships via trial and error. The resulting key parameters are noted in Tab. 2. From observation of the test data it is apparent that experiments C1 to C3 follow the standard fire curve and then cool, whilst C4 to C6 follow a different accelerated heating regime. Given this the authors decided to attempt to simulate experiments C4 to C6 as they represent an obvious deviation from the standard fire curve. In addition, as the authors' MCM was developed for the heating phase of parametric fires, only the heating phase of Konig and Walleij's (1999) experiments is considered at present.

Tab. 2 Fitted parametric curve parameters

	C4	C5	C6
q_{td} (MJ/m ²)	93.8	109.4	114.6
Γ (-)	2.7	3.0	4.5

Using these parameters it is possible to determine the appropriate values of $k_{\lambda,mod}$ for each test thus yielding modified conductivity properties.

As the moisture content was estimated as 12% by Konig & Walleij (1999) then the specific heat relationship from EN 1995-1-2 can be adopted without modification. Using the gas temperature measured in each experiment as a boundary condition, coupled with boundary coefficients of $\epsilon = 0.7$ and $\alpha = 35$ W/m² K, the one-dimensional heat flow was simulated using TNO DIANA. In all instances first-order quad elements with dimensions of 0.5 mm were adopted. Temperatures at depths of 0, 6, 18, 30, 42 and 54 mm, denoted 1, 2, 3, 4, 5 and 6, respectively, were measured by Konig & Walleij (1999). Therefore, temperatures for corresponding nodes are used as output in DIANA (Manie 2010). In addition, simulations were conducted with unmodified conductivity properties as per EN 1995-1-2 for comparison. Plots of the resulting temperature development are shown in Figure 1(a-c).

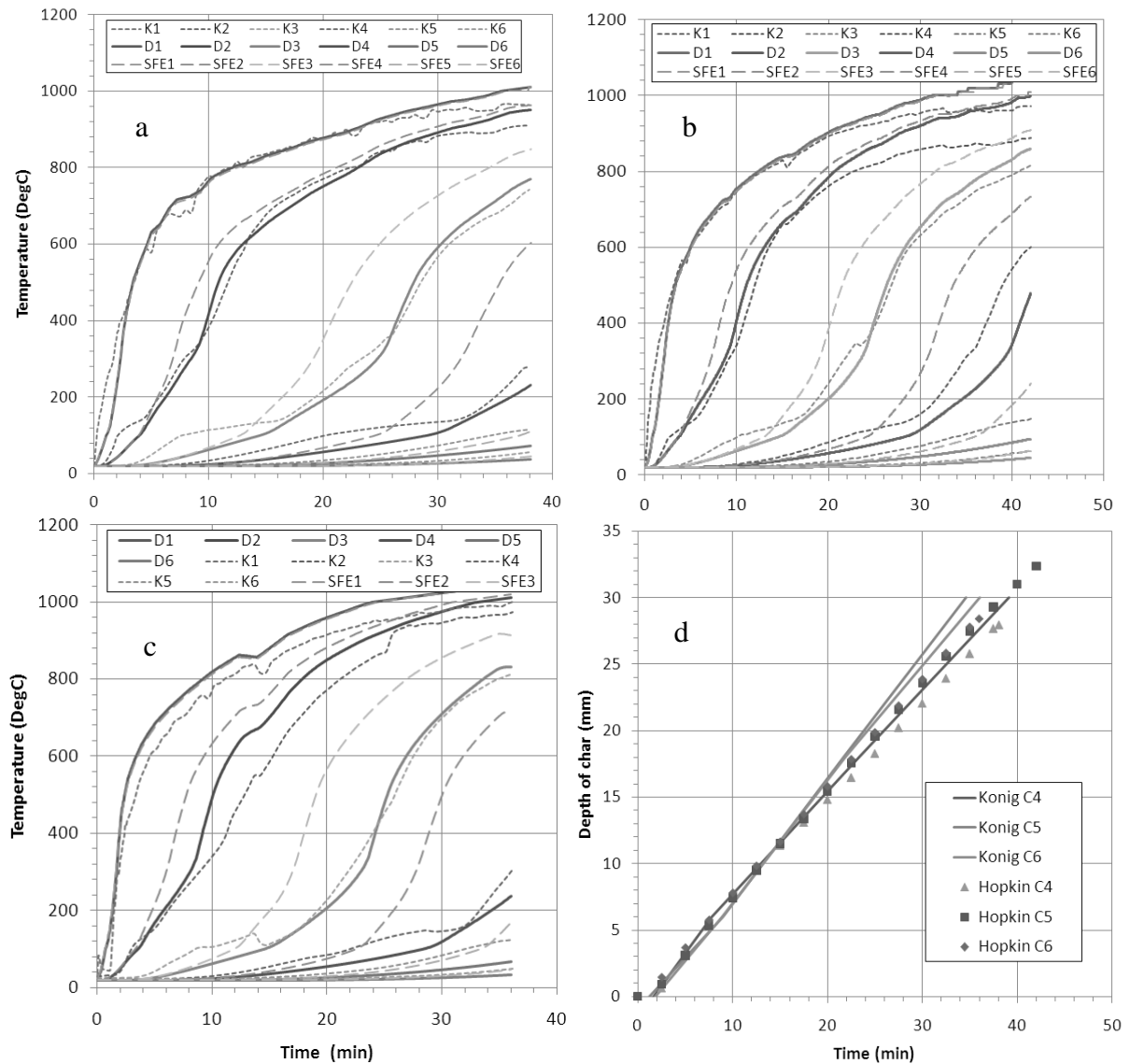


Fig. 1 (a-c) Temperature development, comparison of MCM (D), Konig (K) and EN 1995-1-2 (SFE) simulations/experiments; (d) Transient depth of char- simulation (Hopkin) versus experiment (Konig)

It is apparent from the limited temperature validation conducted that the MCM proposed by the authors for softwood results in a vastly improved prediction of temperature development in timber members exposed to the heating phase of parametric fires (compared to EN 1995-1-2 Annex B properties). However, the experiments of Konig and Walleij (1999) are not well defined, and, as a result, stronger conclusions cannot be drawn without further benchmarking against more robust experiments.

3 EXTENSIONS TO COOLING TIMBER

The modified conductivity model (Hopkin *et al.* 2010) was derived by numerically calibrating timber char conductivity to heating rate by positioning the 300°C isotherm (or char line) so that the method yielded the same charring depth as set out in Annex A of EN 1995-1-2. This calibration was conducted so that the depth of char after a period of t_0 minutes was consistent when calculated using both FEA simulations and Annex A. The period t_0 is defined as the ‘constant charring phase’. It describes a linear relationship between depth of char and time. During this period char of a thickness βt_0 develops. However, after this period and during cooling, according to EN 1995-1-2, a further char layer with thickness βt_0 develops, giving a total depth of char of $2\beta t_0$. The term β is the parametric charring rate in mm/min. Given that the MCM was developed for the heating phase of parametric fires (i.e. up to t_0), its applicability in the cooling phase of fire development is uncertain. To verify its applicability further benchmarking was conducted against Annex A of EN 1995-1-2 by conducting simulations with the proposed conductivity changes and a fully defined parametric fire (inclusive of cooling). An example finding is shown in Figure 2.

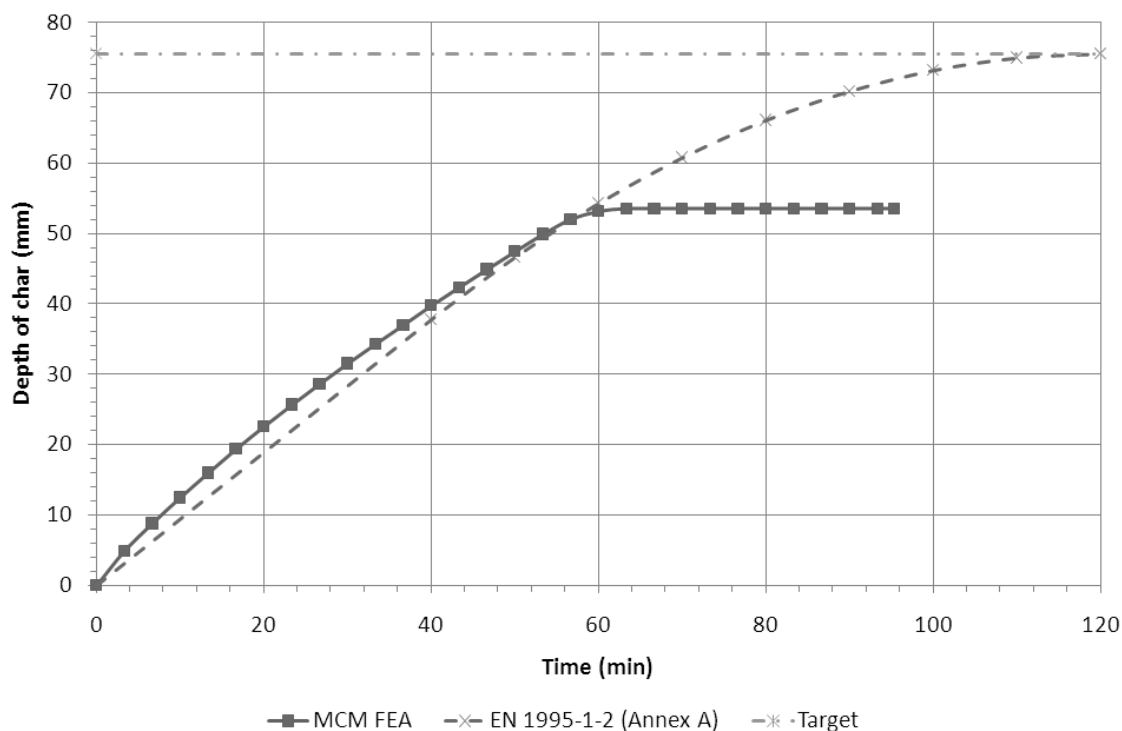


Fig. 2 Comparison of FEA, MCM and EN 1995-1-2 calculation of depth of char

Clearly, even with the proposed modifications to conductivity, char formation in the cooling phase of parametric fires is still not satisfactorily addressed. This could be attributed to a number of reasons, a most critical one is that the pyrolysis and associated energy release of the timber surface is not considered in the design fire characterisation. Konig (2006) proposed that either an artificial fire load, to account for timber member ignition, is incorporated in the cooling phase of a parametric fire, or different timber thermal properties are adopted for the cooling and heating phases of fire development. However, the authors are proposing a more pragmatic solution, which would allow for the performance-based design of timber structures using FEA. This proposal is discussed in the following section.

3.1 An engineered approach to design for cooling

Since charring is a dominant phenomenon, and that transient effects and thermal expansion of timber appear to have little bearing on behaviour in fires, it becomes less important to accurately simulate temperature and char development as a function of time.

By definition, performance-based design is a process whereby a structure is designed to survive the entire duration of a fire, and, in crude terms, the resulting building has infinite fire resistance. It follows that to design a timber member for such an event, it is only necessary to determine the maximum depth of char (at the end of cooling) and the maximum temperature apparent in any undamaged residual timber. This process is semi-independent of time.

Further numerical calibrations performed by the authors showed that, via a slight modification to the fire load-dependent term ($k_{qtd,mod}$) in the MCM, the total depth of char can be determined accurately using FEA simulation. The calculated char depth is inclusive of the additional char that develops during cooling. The modified term is given by:

$$k_{qtd,mod} = \sqrt{\frac{4 \cdot q_{td}}{210}} \tag{2}$$

This simple modification yields the following relationships between depth of char and time for different parametric fire exposures, see Figure 3. In all instances $q_{td}=210 \text{ MJ/m}^2$:

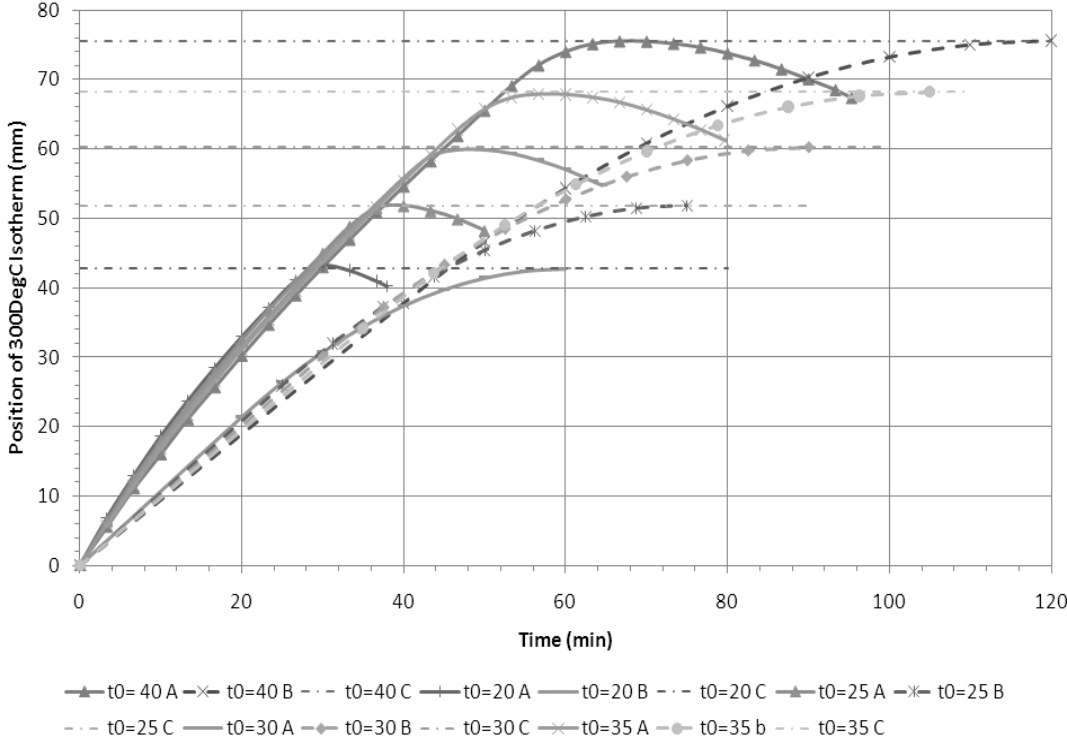


Fig. 3 Position of 300°C isotherm using modified $k_{qtd,mod}$ (A) and EN 1995-1-2 Annex A (B). Target depth of char shown as (C).

Figure 3 shows that in all instances the maximum depth of char determined via simulation is consistent with the Eurocode approach. As a result, although in transient terms the depth of char is inconsistent, the residual cross-section determined in both cases at the end of the fire is identical. From a scientific view point the method proposed does not accurately simulate the physical complexities that occur in timber on cooling. However, this is also the case for the many empirical methods contained in EN 1995-1-2. To gauge the applicability of such an approach, determining the charring depths alone is not sufficient. It must also be shown that ultimate temperature development in uncharred timber is compatible with that apparent in reality. To verify this, further benchmarking will be conducted against the test data of Konig and Walleij (1999).

4 SUMMARY

A modified conductivity model for timber, derived on the basis of numerical calibrations between parametric depth of char and char layer conductivity, has been introduced. The full derivation of the model is outlined elsewhere (Hopkin *et al.* 2010). It was found that with such a modification the depth of char (or position of the 300°C isotherm) can be located with relative accuracy during the heating phase of a parametric fire. In addition, through benchmarking against experimental data provided by SP Tratek, it has been found that the proposed conductivity modifications also result in vastly improved predictions of temperature development in timber members exposed to non-standard fires.

Further benchmarking of depth of char predictions, using the modified properties, and the empirical Annex A charring method indicate that the proposed adaptations still do not fully adequately simulate char formation and temperature development in the cooling phase of a parametric fire. This is likely to be due to char oxidation, which results in additional ‘fire load’, thus increasing the temperature of a timber member beyond that of the cooling surrounding gas temperature. Such a conclusion was supported by the findings of König and Walleij (1999).

The simulation of temperature development in cooling timber members is a complex and difficult task. König (2006) suggested that different thermal properties should be adopted in the heating and cooling phases of fire development. From a design perspective this is an awkward approach. As a result, the authors proposed a pragmatic engineered solution, which should, theoretically, but subject to further verification, allow for the design of timber buildings exposed to parametric fires, using computational techniques. This approach will be further investigated, and additional benchmarking will be conducted against any available test data. In general, the developments presented herein are believed to be a meaningful step towards the whole-building analysis of timber structures exposed to non-standard fires. If such an approach can be realised then many of the beneficial aspects of holistic behaviour associated with steel, concrete and composite construction may be capitalised upon to design more efficient large-section timber structures.

5 ACKNOWLEDGMENTS

The authors would like to acknowledge EPSRC, BRE Global and Jürgen König of SP Tratek for their support.

REFERENCES

- BRITISH STANDARDS INSTITUTION, 2004. Eurocode 5: Design of timber structures – Part 1-2: General – Structural fire design. BS EN 1995-1-2. London: BSI.
- CACHIM, P.B. and FRANSSEN, J.M., 2009. Comparison between the charring rate model and the conductive model of Eurocode 5. *Fire and Materials*, **33**(3), 129-143.
- HOPKIN, D.J., EL-RIMAWI, J, SILBERSCHMIDT, V., and LENNON, T., 2010. An effective thermal property framework for softwood in parametric design fires: Comparison of the Eurocode 5 parametric charring approach and advanced calculation models. *Journal of Construction and Building Materials*, doi: 10.1016/j.conbuildmat.2010.12.002.
- KONIG, J., 2006. Effective thermal actions and thermal properties of timber members in natural fires. *Fire and materials*, **30**(2), 51-63.
- KONIG, J. and WALLEIJ, L., 2000. Timber frame assemblies exposed to standard and parametric fires part 2: A design model for standard fire exposure. I0001001. Stockholm: SP Tratek.
- KONIG, J. and WALLEIJ, L., 1999. One-dimensional charring of timber exposed to standard and parametric fires in initially unprotected and postprotection situations. I9908029. Stockholm: SP Tratek.
- MANIE, J., 2010. DIANA User's Manual. 9.4 edn. Delft: TNO.

TRAVELLING FIRES IN LARGE COMPARTMENTS

Realistic fire dynamics for structural design

Guillemro Rein ^a, Jamie Stern-Gottfried ^{a,b}

^a University of Edinburgh, School of Engineering, UK

^b Arup, London, UK

INTRODUCTION

Close inspection of real fires in large, open compartments reveals that they do not burn simultaneously throughout the whole compartment. Instead, these fires tend to move as flames spread, partitions or false ceilings break, and ventilation changes through glazing failure. These fires have been labelled ‘travelling fires.’

Despite these observations, fire scenarios currently used for the structural fire design of modern buildings are based on one of two traditional methods for specifying the fire environment; the standard temperature-time curve, which has its origins in the late 19th century, or parametric temperature-time curves, such as that specified in Eurocode 1 (EN 1991-1-2, 2002). These methods are based on the extrapolation of existing fire test data, which stems from tests performed in small compartments that are almost cubic in nature. This test geometry allows for good mixing of the fire gases and thus for a uniform temperature distribution throughout the compartment.

While both of these methods have great merits and represented breakthroughs in the discipline at their times of adoption, they have inherent limitations with regards to their range of applicability (Rein et al., 2007; Stern-Gottfried et al., 2009). For example, Eurocode 1 states that the design equations are only valid for compartments with floor areas up to 500 m² and heights up to 4 m, the enclosure must have no openings through the ceiling, and the compartment linings are also restricted to a thermal inertia between 1000 and 2200 J/m²s^{1/2}K, which means that highly conductive linings such as glass facades and highly insulating materials cannot be taken into account. As a result, common features in modern construction like large enclosures, high ceilings, atria, large open spaces, multiple floors connected by voids, and glass façades are excluded from the range of applicability of the current methodologies. These limitations, which are largely associated with the physical size and geometric features of the experimental compartments on which the methods are based, ought to be carefully considered when the methods are applied to an engineering design. This is particularly relevant given the large floor plates and complicated architecture of modern buildings.

A recent simple survey of buildings at the University of Edinburgh campus (Jonsdottir and Rein, 2009) underlines the narrow design fire specifications in the Eurocodes. For buildings built over a long period of time starting in the early 20th century, 66% of their total volume falls within the limitations. However, in a newly constructed, modern building that has open spaces and glass facades, only 8% of the total volume is within the limitations. This suggests that modern building trends are moving out of the limits of current design practices.

The limitations of the existing methods arise from the assumption of uniform temperature conditions throughout the whole floor of a compartment. A fire that would cause these uniform conditions burns uniformly within the enclosure and generates high temperatures for a relatively short duration. This is opposed to a travelling fire that burns locally but spreads through the enclosure with time, generating lower temperatures for longer times. Post-flashover fires in open plan offices are unlikely to burn throughout the whole space at once. Real, large fires that have led to structural failure, such as those in the World Trade Center towers 1, 2 and 7 in September 2001, the Windsor Tower in Madrid, Spain in February 2005 and the Faculty of Architecture building at TU Delft in the Netherlands in May 2008 were all observed to travel across floor plates, and vertically between floors, rather than burn uniformly for their duration.

1 NEW METHODOLOGY FOR TRAVELLING FIRES

While the traditional methods have inherent assumptions of fire behaviour different from that observed in real fires, they have generally been deemed to be conservative, and therefore appropriate, tools for structural fire design in the absence of better and more relevant data. Although these methods might be considered acceptable for most design cases, the need for better optimisation of structural behaviour in fire will eventually require a more performance-based definition of the fire. This is particularly relevant given that computational methods for determining structural behaviour have matured over the last decade and have enabled analysis of more complex structural systems. This has led to an understanding that many modern structures do not behave in the same manner as simpler, more traditional frame based systems. Thus, in order to address these differences, and continue to enable innovation in structural design, a more sophisticated characterisation of fire scenarios is required.

Therefore a methodology is being developed that allows for a wide range of possible fires, including both uniform burning and travelling fires, by considering the fire dynamics within a given building (Rein et al., 2007; Stern-Gottfried et al., 2009, Angus et al. 2011). This methodology also facilitates the collaboration between fire safety engineers and structural fire engineers, which is an identified need within the structural fire community, to jointly determine the most challenging fire scenarios for a structure.

The key aspect of the new methodology is to characterise the thermal environment for structural analysis accounting for the fire dynamics specific to the building, including a wide range of possible fires. In order to achieve this, a simple fire model is selected that enables capturing the spatial and temporal changes of the fire-induced thermal field. This model is then applied to a particular floor of the building accounting for a family of fires that range between one that burns in a small area and travels across the floor plate for a long duration and one that is well distributed across the whole floor plate but burns for a short duration.

2 TEMPERATURE FIELD

The methodology divides the effect of a fire on structural elements into the near field and the far field. The near field is when a structural element is exposed directly to the flames of the fire and the far field is when it is exposed to the hot gases, i.e. the smoke layer away from the flames, as shown in Figure 1. This division of the thermal field allows the methodology to avoid the well-known inaccuracies of flame temperature prediction of most fire models.

In previous work, a CFD fire model (Rein et al., 2007) was selected to study the temperature field as a function of distance from the fire. In this paper, a ceiling jet correlation was used. The ceiling jet correlation developed by Alpert (1972) and given below in Eq. (1) was selected in this case as the simple fire model to study the temperature field as a function of distance from the fire. The use of such a correlation is deemed appropriate if the floor area is large and the smoke layer is thin relative to the floor to ceiling height.

$$T_{\max} - T_{\infty} = \frac{5.38(\dot{Q}/r)^{2/3}}{H} \quad (1)$$

where T_{\max} is the maximum ceiling jet temperature (K)

T_{∞} is the ambient temperature (K)

\dot{Q} is the total heat release rate (kW)

r is the distance from the centre of the fire (m)

H is the floor to ceiling height (m)

Note that while Alpert gives a piecewise equation for maximum ceiling jet temperatures to describe the near field ($r/H \leq 0.18$) and far field ($r/H > 0.18$) temperatures, only the far field equation is utilised in the present case study as the near field temperature is assumed to be the flame temperature.

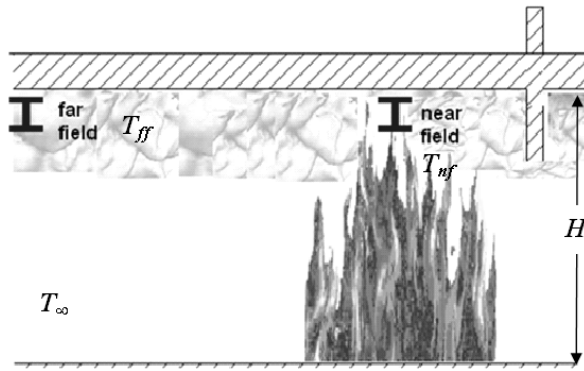


Fig. 1 Illustration of near and far fields

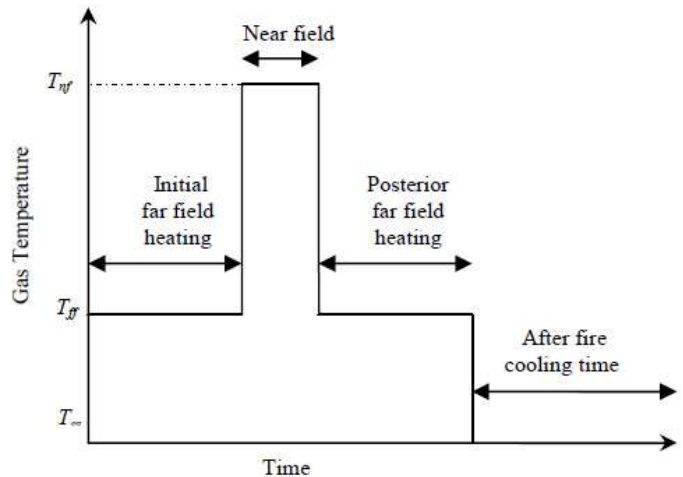


Fig 2 Temperature-time curve at one ceiling location for a travelling fire

The ceiling jet correlation characterises the spatial variation of the temperature field only as a function of the distance from the fire. This simple correlation was chosen to provide a straightforward description of the temperature field that is qualitatively sufficient to progress the development of the methodology. Alternative fire models, including computational fluid dynamics, can be utilised instead.

3 FAMILY OF FIRE SIZES

A family, or set, of fires that covers the range of possible fires, both travelling and uniformly burning, needs to be selected as an input for the temperature field. To do this it was assumed that each fire in the family would burn over a surface, A_b , which is a percentage of the total floor area, A_t , of the building, ranging from 1% to 100%. The burning area of the fire that is equal to 100% of the floor area is a well distributed fire. All other burning areas represent travelling fires of different sizes.

It is assumed that there is a uniform fuel load across the fire path and the fire will burn at a constant heat release per unit area typical of the building load under study. Thus the burning time can be calculated by Eq. (2).

$$t_b = \frac{q_f}{\dot{Q}''} \quad (2)$$

where t_b is the burning time (s)

q_f is the fuel load density (MJ/m^2)

\dot{Q}'' is the heat release rate per unit area (MW/m^2)

For the case study presented below, the fuel load density, q_f , is assumed to be $570 \text{ MJ}/\text{m}^2$, as per the 80th percentile design value for office buildings. The heat release rate per unit area, \dot{Q}'' , is taken as $500 \text{ kW}/\text{m}^2$ which is deemed to be a typical value for densely furnished spaces, as typical design guidance gives this value for retail spaces. Based on these two values, the characteristic burning time, t_b , is calculated by Eq. (2) to be 19 min.

Note that the burning time is independent of the burning area. Thus the 100% burning area and the 1% burning area will both consume all of the fuel over the specified area in the same time, t_b . However, a travelling fire moves from one burning area to the next so that the total burning duration, t_{total} , across the floor plate is extended. This time is given in Eq. (3).

$$t_{total} = \frac{t_b}{A_b/A_t} \quad (3)$$

This means that there is a longer total burning duration for smaller burning areas. For example, the 100% burning area has a total burning duration of 19 min and the 1% burning area a total burning duration of 1900 min.

In the case of the 100% burning area, all of the structure will experience near field (flame) conditions for the total burning duration (which is equal to the burning time, t_b). However, for the travelling fire cases, any one structural element will feel far field (smoke) conditions for the majority of the total burning duration and near field conditions for the burning time as the fire burns locally to the element. The time one element experiences far field conditions prior to the arrival of the flame is defined as t_{pre} and the time the element experiences far field conditions after the departure of the flame is defined as t_{post} . Figure 1 illustrates the difference between the near field and far field.

The near field temperature, T_{nf} , is taken here as the flame temperature, which for the accuracy levels required in structural fire analysis, is more or less constant and approximately 1200°C to 1300°C for a typical office fire. The far field conditions vary as a function of distance away from the fire. However, it is desirable to express the results in simple terms but without loss of generality in order to be of valuable engineering use. Thus, the far field is reduced to a single characteristic temperature, T_{ff} , which keeps the amount of information passed to the structural analysis manageable. To do this, the far field temperature is taken as the fourth-power average of T_{max} (to favour high temperatures in a bias towards radiation heat transfer and worst case conditions) over the distance between the end of the near field, r_{nf} , and the end of the far field, r_{ff} . This average is calculated by Eq. (4).

$$T_{ff}^4 = \frac{\int_{r_{nf}}^{r_{ff}} T_{max}^4 dr}{r_{ff} - r_{nf}} \quad (4)$$

Once the far field temperature is determined for a given fire size, the temperature time history of a point can be described, as shown in Figure 2. Determining both t_{pre} and t_{post} is dependent on the path of the fire and the exact position being examined. However, it is not possible to establish a fire's path of travel a priori, as there are many potential paths in principle; therefore assumptions must be made for worst case conditions.

The growth and decay phases of the gas temperatures for the travelling fires detailed in this paper are assumed to be very fast. This is because the larger an enclosure is, the lower the importance of the thermal inertial of its linings are, thus the faster the growth and decay phases will be. In other words, the transport of the hot gases in the smoke layer is faster than the heat transfer to the surfaces. Note that the cooling is not neglected in the structural analysis, only the decay phase is eliminated from the fire environment.

4 A CONCRETE STRUCTURE

The methodology has been applied to a large compartment with a floor area of 1000 m² made of concrete slabs (see details in Law et al., 2011). The resulting family of fires is shown in Figure 3 as the far field temperature vs. total burning duration. When these fire temperatures are fed into a heat transfer model (Abaqus) of the concrete structure, the resulting rebar temperature are those in Figure 4.

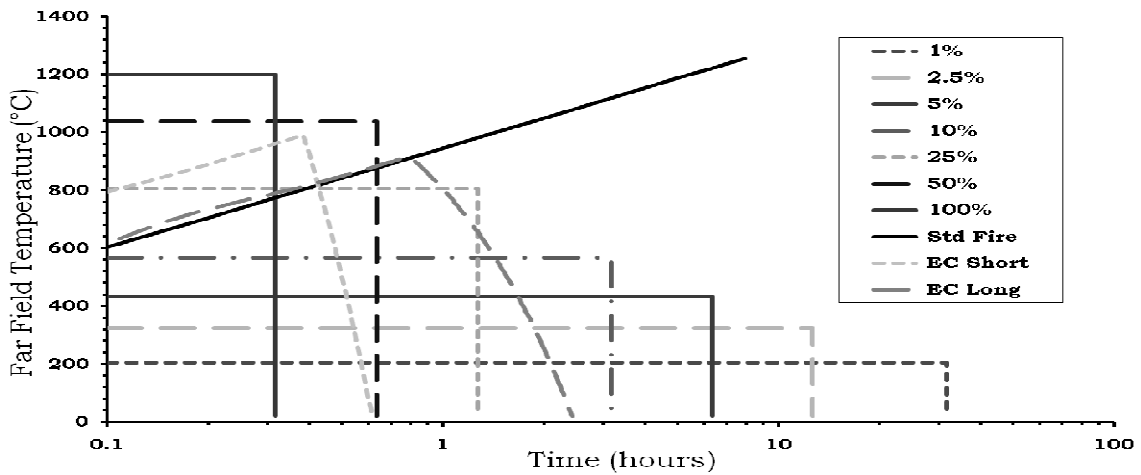


Fig. 3 Fire temperature in the family of fire sizes (Law et al., 2011)

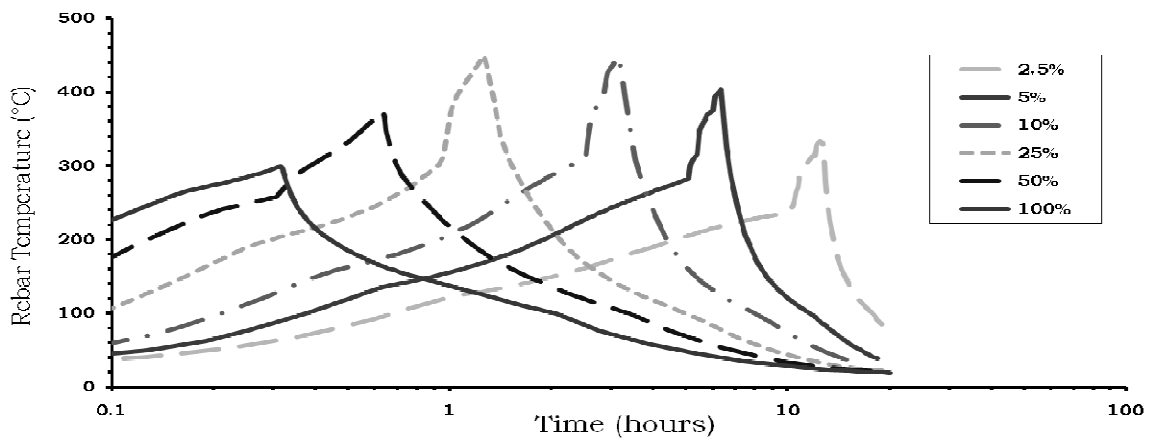


Fig. 4 Resulting temperature of the rebar in the concrete slabs for the family of fire sizes (Law et al., 2011)

5 A STEEL STRUCTURE

The methodology is applied to The Informatics Forum, a modern building in Edinburgh, using simple analytical calculations to obtain the steel temperatures (see details in Jonsdottir et al. 2010). Analysis of three protected steel beams, and comparison to those from traditional design methods (standard and parametric fire curves) are shown in Figure 5.

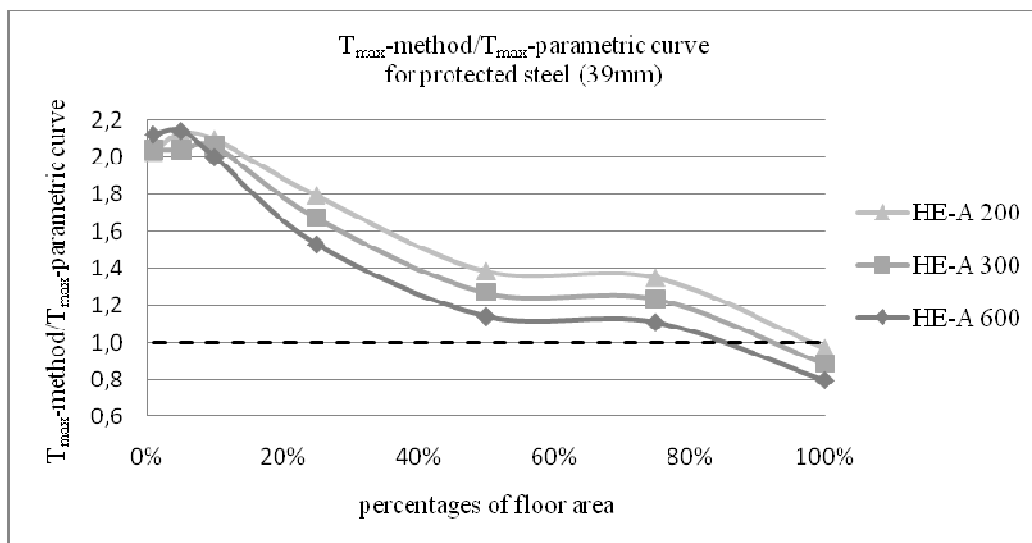


Fig. 5 Maximum steel temperature using the travelling fire method normalised by the maximum steel temperature using the parametric curve - protected steel (Jonsdottir et al. 2010).

The results indicate that more severe conditions are predicted for small travelling fires of size 5 to 10% of the floor plate than for uniform fires assumed in traditional methods. Compared to the parametric fire curve, travelling fires lead up to 95% higher steel temperatures for unprotected steel, and up to 110% for protected with 39mm-gypsum. Traditional methods are more conservative only when compared to travelling fires larger than 85% of the floor plate.

6 CONCLUSIONS

This paper has presented a performance based methodology for specifying design fires for structural analysis using travelling fires. The method allows for inclusion of a family of fires, to cover a wide range of possible fire dynamics in a building, ultimately leading to quantification of a range of possible structural responses. This range includes more challenging cases than are included in the traditional design methods.

7 ACKNOWLEDGMENT

The authors acknowledge collaborators Law, Gillie, Jonsdottir and Torero, and funding from Arup.

REFERENCES

- Eurocode 1: Actions on structures – Part 1-2: General actions – Actions on structures exposed to fire, European standard EN 1991-1-2, 2002. CEN, Brussels.
- Rein, G. et al, “Multi-story Fire Analysis for High-Rise Buildings,” 11th International Interflam Conference, London, 2007. <http://www.era.lib.ed.ac.uk/handle/1842/1980>
- Stern-Gottfried, J., Rein, G., and Torero, J. L, “Travel Guide”, Fire Risk Management, Nov 2009, pp. 12-16. <http://www.era.lib.ed.ac.uk/handle/1842/3184>
- Jonsdottir, A. and Rein, G. “Out of Range”, Fire Risk Management, Dec 2009, pp. 14-17. <http://www.era.lib.ed.ac.uk/handle/1842/3204>
- Alpert, R.L., “Calculation of Response Time of Ceiling-Mounted Fire Detectors,” Fire Technology, Vol. 8, 1972, pp. 181–195.
- Law, A., Gillie, M., Stern-Gottfried, J., Rein, G., The Influence of Travelling Fires on a Concrete Frame, Engineering Structures, (in press) 2011. doi:10.1016/j.engstruct.2011.01.034
- Jonsdottir, A., Rein, G., Stern-Gottfried, J, Comparison of Steel Temperatures using Travelling Fires and Traditional Methods, 12th Interflam, Nottingham, July 2010.

APPLICATION OF A VIRTUAL RESISTANCE FURNACE: Fire resistance test simulation on a plasterboard membrane

François Cayla^a, H. Leborgne^b, D. Joyeux^c

^a Efectis France, Bordeaux, France

^b Efectis France, Maizières-Lès-Metz, France

^c Efectis France, Saint-Aubin, France

INTRODUCTION

Furnaces are necessary to perform fire resistance tests on building elements. The European standard **EN 1363 -1** imposes mainly two constrains which must be achieved simultaneously:

- The static overpressure must be maintained to 20 Pa at the top of a vertical tested element placed as the closing wall of the furnace.
- The thermal program delivered by the furnace burners is defined by a time dependant logarithmic curve ranging from 20°C at the start of the test to approximately 1050 °C after 2 hours of test as given by *Eq. (1)*:

$$T = 345 \log_{10}(8t + 1) + 20 \quad (1)$$

With T in °C and t in minutes

In order to have a better understanding of such fire resistance furnace behaviour, experiments have been carried out and concerned measurement methods (Sultan et al 1986, Sultan 2006). However, few studies are addressed to the numerical simulations of those furnaces (Bressloff et al 1995, Welch et al 1997).

In this work, a fire resistance test furnace simulator is presented. It has been designed in such a way to be representative of the vertical furnace of Efectis France Laboratory. This furnace is warmed up by 12 natural gas burners. Its geometry is showed on Fig. 1.

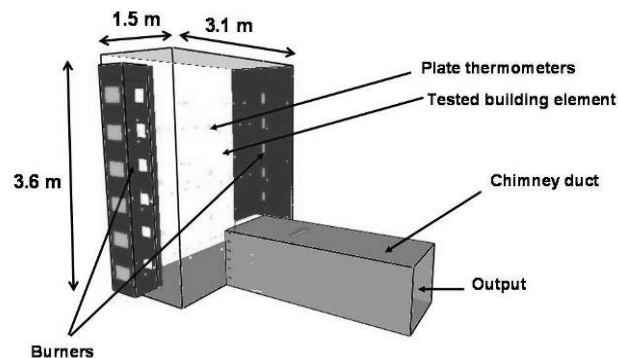


Fig. 1 Outline of the virtual furnace structure

This paper addresses a simulation using the virtual furnace coupled with a plasterboard membrane as tested element. The main characteristics of the simulator and of its coupling with the building element will be summarised in part 2. Results obtained with this simulator on a plasterboard membrane will be exposed in part 3.

1 MAIN CHARACTERISTICS OF THE FURNACE MODEL

The modelling of realistic simulator requires simulating both the furnace behaviour and its interaction with the tested building element.

1.1 The furnace model

The computational fluid dynamics code FDS (Fire Dynamic Simulator) version 5, developed by NIST institute, is used for the furnace design.

This program has been modified to satisfy to the constraints imposed by the European standard EN 1363-1. Thus, automatic controls have been introduced to regulate the 12 gas burners combustion and to assure an imposed output volume flow at the chimney exit. Both combustion mixture and hot gases extraction conditions are iteratively corrected at each time step of the simulation driven on this modified FDS 5 version.

Each gas burner is modelled as a block in which natural gas and combustion air are injected to perform the combustion. Proportions of injected gas and air are based on experimental measurements carried out during calibration tests on the EFECTIS France vertical furnace.

The evolution of temperatures in the virtual furnace is controlled by 6 modelled plate thermometers designed in full compliance with **EN 1363-1** requirements. They are constituted by an Inconel steel sheet insulated on their backside by a refractory board. An Inconel thermocouple is welded on the Inconel steel sheet. This type of thermometer has been developed by the European fire laboratories to harmonize the thermal impact delivered by European furnaces and must be used to perform fire resistance tests (see Fig. 2). This design makes plate thermometers quite sensitive to the radiative heat flux coming from flames of burners and lining of furnaces.

Those plate thermometers are placed as indicated in Fig. 3 in x and z directions and at 10 cm from the tested element in y direction. The steel sheet of each plate thermometer is oriented towards the furnace cavity.

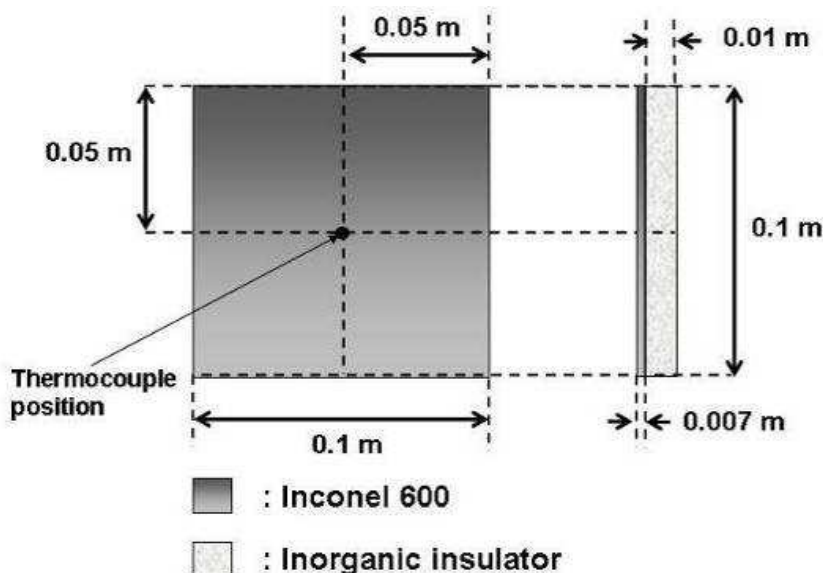


Fig. 2 Outline of the plate thermometer structure

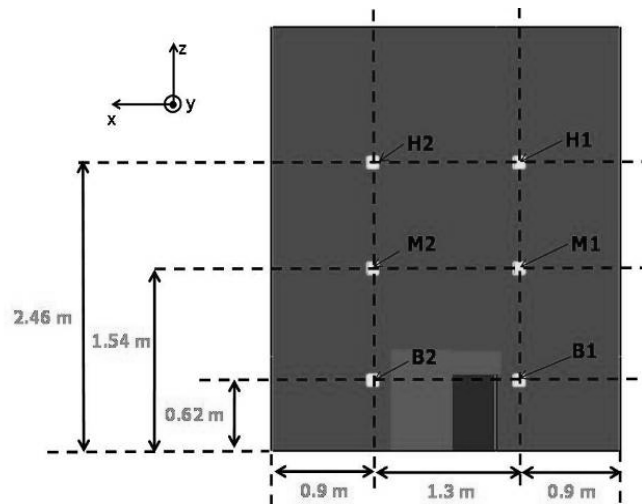


Fig. 3 Position of the plate thermometers

1.2 The building element coupling

The tested building element is modelled by using the code CAST3M. This finite element code is developed by the C.E.A. (French Alternative Energies and Atomic Energy Commission). It is mainly dedicated to thermomechanical behaviour of solids.

An interface has been created between this code and the modified version of FDS 5 to ensure the thermal coupling between the virtual furnace and the element. Thermal constraints delivered by FDS 5 are refreshed regularly on the fire exposed element surface. They are constituted by a radiative flux coming from the furnace lining, a convective flux due to hot gasses in the vicinity of the element and a radiative flux emitted by the exposed side of the tested element (see Fig. 4).

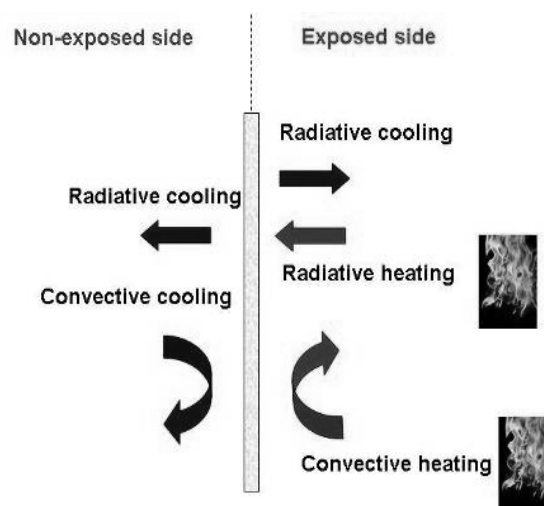


Fig. 4 Heat flux at the exposed and non-exposed sides of the tested element.

Those constraints allowed the determination of the temperature field on the exposed side of the element. This field constitutes the new boundary conditions for the calculation of the thermodynamic equilibrium of the furnace inner volume at the next time increment step.

2 RESULTS

The furnace simulator has been assessed in a combination with a full size plasterboard membrane. The dimensions of this membrane are 3.1 x 3.6 x 0.0125 m (w x h th).

The rear side of the membrane is submitted to an ambient temperature equal to 20 °C coupled with

a free convection factor of $4 \text{ W.m}^{-2}.\text{K}^{-1}$. The emissivity of the plasterboard is taken as 0.7 in this simulation.

On fig. 5 and 6, the temporal evolutions of the temperatures calculated by the virtual plate thermometers are presented. The EN 1363-1 temperature curve and its accepted tolerance ($\pm 100^\circ\text{C}$) are shown too. We observe that the furnace simulator permits to follow strictly the EN 1363-1 thermal program after 10 minutes simulated. Before 10 minutes, temperatures of points M1 and M2 are not lining up with the EN 1363-1 curve because furnace wall are still colder than ambient gas inside furnace.

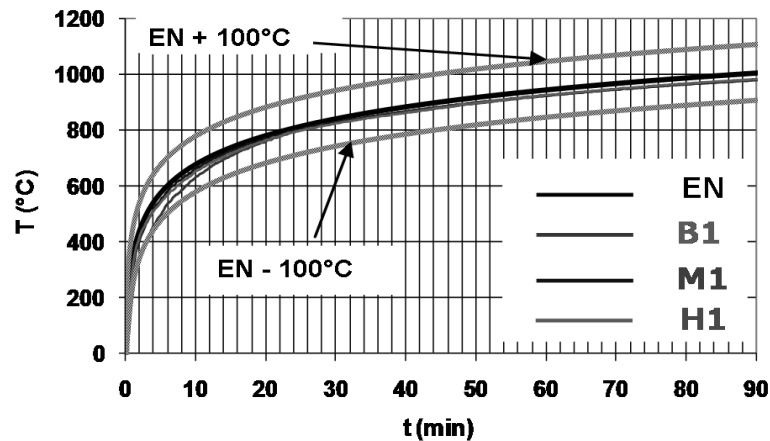


Fig. 5 Temperatures calculated by Plate Thermometers B1, M1 and H1 as function of time.

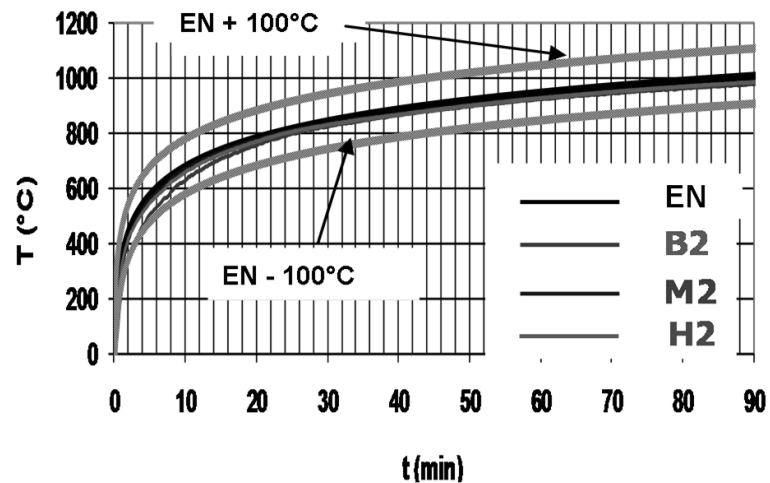


Fig. 6 Temperatures calculated by Plate Thermometers B2, M2 and H2 as function of time.

The Fig. 7 shows the static over pressure time evolution at the top of the tested membrane. We observe that this pressure is pretty well maintained around the 20 Pa level as recommended by the European standard after 10 minutes of simulation. Before this time, the pressure is enhanced because of the fast turning on of the burners, and reaches a maximum of 78 Pa.

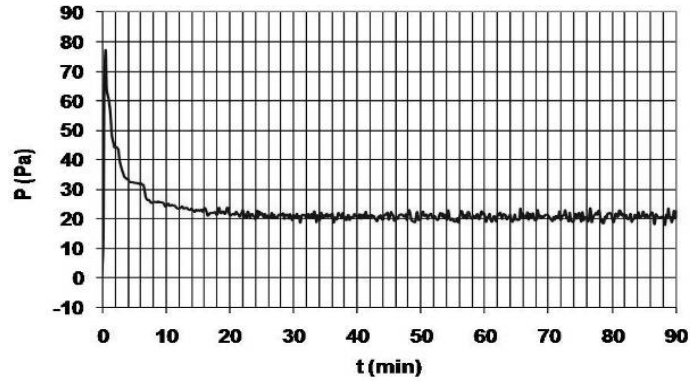


Fig. 7 Over pressure at the top of the furnace as function of time

Fig. 8 presents the temperature gradient evolution in the centre of the membrane. Temperature of the exposed side (a) is below the European standard evolution curve. This is explained by the water evaporation in the core and on non-exposed side of the plasterboard membrane.

On the non-exposed side (c) the hygroscopic effect leads to the slowing down of the temperature around 100°C. This phenomenon is representative of experimental measurements during actual fire tests.

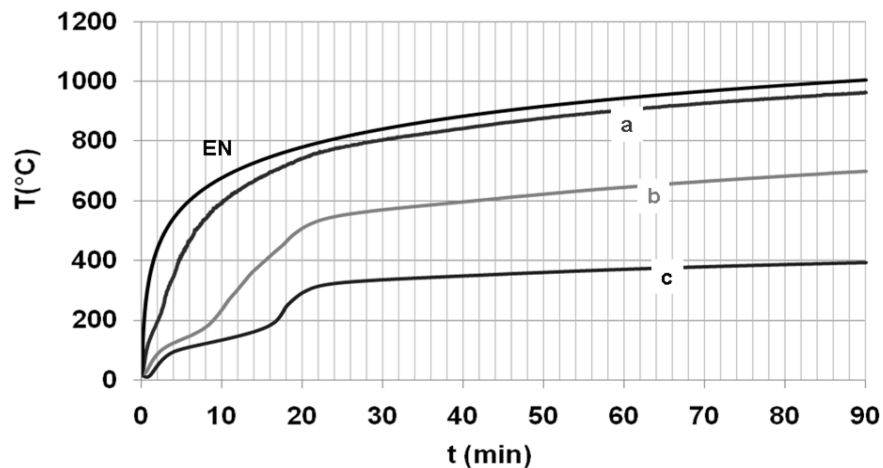


Fig. 8 Temperatures evolutions at the centre of the tested element as a function of time (EN: standard curve, a: exposed side, b: mid-thickness position, c: non-exposed side)

3 SUMMARY AND ACKNOWLEDGMENT

This paper presents a summary of the fire resistance furnace simulator modelled by coupling the code CAST3M and a modified version of the CFD code FDS 5.

The modified version of FDS 5 permits to control temperature and pressure conditions in the virtual furnace to achieve the EN 1363-1 requirements.

The strong coupling of the virtual furnace with the code CAST3M gives results in good agreement with experiments concerning the temperature of the tested element.

To confirm the relevance of the furnace simulator, more sophisticated elements as fire resistant doors will be soon tested. A more complete and elaborate physical model needs also to be developed to take into account more properly the vaporisation plateau supplied by hygroscopic material as plasterboard or calcium silicate boards when submitted to EN 1363-1 thermal program.

We acknowledge P. Verpeaux, A. Millard and Th. Charras of the CEA/DM2S/LM2S (Saclay, France) for their help concerning the use of CAST3M software.

REFERENCES

- Sultan M.A., Harmathy T.Z., Mehaffey J.R., Heat transmission in fire test furnaces, 10(2): 47-55, 1986
- Sultan M.A. Incident heat flux measurements in floor and wall furnaces of different sizes. *Fire and Materials*, 30: 383-396, 2006
- Sultan M.A. Fire Resistance Furnace Temperature Measurements: Plate Thermometers vs Shielded Thermocouples. *Fire Technology*, 42(3): 253-267, 2006
- Bressloff N., Rubini P. Cox G. Computational Fluid Dynamics Modelling of a Fire Resistance Furnace. 1st European symposium on Fire Safety Science, Zurich, Switzerland, 1995.
- Welch S., Rubini P.A. Three-dimensional Simulation of a Fire-Resistance Furnace. Proceedings of 5th International Symposium on Fire Safety Science, Melbourne, Australia, 1997.

THE IMPACT OF ASSUMED FRACTURE ENERGY ON THE FIRE PERFORMANCE OF TIMBER BEAMS

A Numerical Study

Danny Hopkin ^{a/c}, Jamal El-Rimawi ^a, Vadim Silberschmidt ^b, Tom Lennon ^c

^a Loughborough University, Department of Civil and Building Engineering, Loughborough, UK

^b Loughborough University, Wolfson School of Mechanical Engineering, Loughborough, UK

^c BRE Global, Garston, Watford, Herts, WD25 9XX, UK.

INTRODUCTION

The behaviour of timber at elevated temperature is complex. Timber is not only combustible but also has complex mechanical properties; it is orthotropic and its tensile and compressive strengths and stiffnesses vary at differing rates with increasing temperature. In addition, timber is brittle when exposed to tensile stresses and ductile when subject to compression. All of the above, and the fact that its thermal properties are dependent upon heating rate, make the simulation of timber structures in fire a difficult task.

EN 1995-1-2 gives guidance on the properties, both thermal and mechanical, that should be adopted in the simulation of timber structures exposed to fire. It is apparent from the literature that at ambient temperature strain energy is not instantaneously dissipated at the moment a crack forms in timber under tensile loading (i.e. its behaviour is not perfectly brittle). After cracking, tension softening is apparent whereby the fracture energy is gradually dissipated with increasing crack strain. Modelling this behaviour is not only desirable from a physical point of view but is often necessary to ensure numerical stability in simulations. However, no guidance is given in EN 1995-1-2 regarding a magnitude of fracture energy at ambient or elevated temperature.

In this study the finite element software DIANA has been used to investigate the impact of fracture energy and tension softening regime on the structural behaviour of a simply supported timber beam, subject to a standard fire from below. Timber beams, subject to one-dimensional heating from below in a 2D plane stress formulation, are studied at different load ratios. In enabling this study to be conducted, FORTRAN subroutines were incorporated to determine the elastic modulus of timber depending upon the governing strain state, i.e. tensile or compressive. This user routine is implemented with a Total Strain-based cracking and plasticity model to evaluate the consequences of adopting fracture energies ranging from 600 to 5000 Nm/m². In addition, the impact of the shape of the tension softening branch is also evaluated.

1 FRACTURE ENERGY AND TENSION SOFTENING

The fracture energy of timber, more specifically softwoods, is an area well researched at ambient temperature. Many textbooks give fracture energies for different cracking modes, which are shown to be highly dependent upon density (Thelandersson & Larsen 2003). Larson & Gustafsson (1990/91) give one such correlation for notched timber members subject to bending, where:

$$G_f = 1.07\rho - 162 \quad (1)$$

where G_f is fracture energy (Nm/m²) and ρ is density in kg/m³.

For typical softwood this gives fracture energies ranging from 160-480 Nm/m² for mixed mode cracking. However, little, if anything, is known about the fracture energy of timber or other brittle materials at elevated temperature.

The numerical mechanical modelling of timber at elevated temperature is rare. To date, simplified models are often adopted using spreadsheets and sectional analysis tools (Konig & Walleij 2000, Schmid, et al. 2010). As a result of such an approach, it is not necessary to define fracture energy as timber in tension can be treated as a perfectly brittle material.

However, such an approach cannot be adopted in more general FEA computations as this may lead to numerical instability. To this end, tension softening regimes are often defined to describe the descending branch of a materials constitutive relation (See figure 1). The definition of such behaviour requires either knowledge of fracture energy (i.e. the integral of the deformation stress curve) or ultimate crack strain, i.e. the strain at which all crack stress has vanished. Neither codes and standards nor academic research give an insight into the effect of increasing temperature on fracture energy or ultimate crack strain. As a result, it is often necessary to assume values, which can have a very large influence upon deformation behaviour and upon the ultimate load carrying capacity.

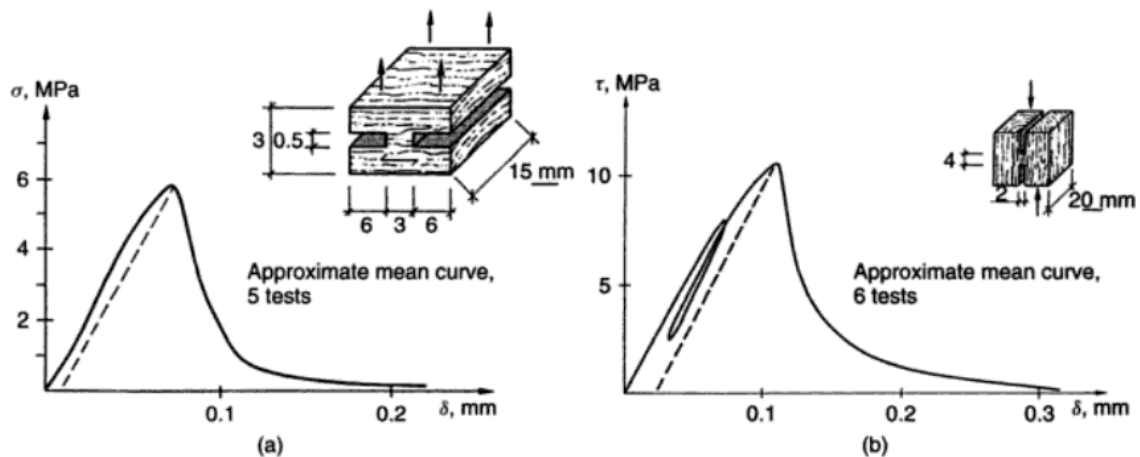


Fig. 1 Indicative fracture behaviour of timber in (a) tension and (b) shear (displacement vs. stress) after Thelanderson and Larsen (2003)

In the DIANA FEA package it is possible to define a number of tension-softening relationships based upon fracture energy, crack bandwidth and/or ultimate crack strain. To investigate the impact of these parameters, a parametric study was designed to study the behaviour of simply supported beams, loaded to different utilisation levels, under standard fire exposure. To undertake the study, it has been necessary to make a number of modifications to DIANA in order to extend characterisation of the behaviour of timber. These developments are discussed in a supporting paper (Hopkin *et al.* 2011). The concept of total strain-based cracking as implemented in DIANA is introduced briefly in the following section. The design of the parametric study is discussed in further detail later on in the paper.

2 TOTAL STRAIN-BASED CRACKING

The DIANA constitutive model based on total strain is developed along the lines of the Modified Compression Field Theory, originally proposed by Vecchio & Collins (1986). The three-dimensional extension to this theory is proposed by Selby & Vecchio (1993). A constitutive model based on total strain describes the stress as a function of the strain. This concept is known as hypo-elasticity, when the loading and unloading behaviour is along the same stress-strain path. In the current implementation in DIANA, the behaviour in loading and unloading is modelled differently with secant unloading.

One commonly used approach is the coaxial stress-strain concept, in which the stress-strain relationships are evaluated in the principal directions of the strain vector. This approach, also known as the *Rotating crack model*, has been applied to the constitutive modelling of reinforced concrete for a long period and has shown that the modelling approach is well suited for such structures.

More appealing to the physical nature of cracking is the fixed stress-strain concept, in which the stress-strain relationships are evaluated in a fixed coordinate system that is fixed upon cracking. Both approaches are easily described in the same framework, where the crack directions *nst* are either fixed or continuously rotating with the principal directions of the strain vector.

The basic concept of total strain crack models is that the stress is evaluated in the directions given by those of the crack. The strain vector ϵ_{xyz} in the element coordinate system xyz is updated with the strain increment $\Delta\epsilon_{xyz}$ according to:

$$(t + \Delta t_{i+1})\epsilon_{XYZ} = t\epsilon_{XYZ} + (t + \Delta t_{i+1})\Delta\epsilon_{XYZ}. \quad (2)$$

This is transformed to the strain vector in the crack directions with the strain transformation matrix \mathbf{T} giving:

$$t + \Delta t_{i+1}\epsilon_{nst} = T(t + \Delta t_{i+1}\Delta\epsilon_{XYZ}). \quad (3)$$

The strain transformation matrix \mathbf{T} is either fixed upon first cracking or depends on the current strain vector (Rotating crack model). The Total Strain crack models, be it the fixed or rotating crack model, are appealing as they are numerically very stable when compared to smeared strain decomposed alternatives. In such cases the total strain is decomposed into elastic and crack components, i.e.:

$$\epsilon = \epsilon_E + \epsilon_{cr}. \quad (4)$$

This decomposition of the strain allows also for combining the decomposed crack model with, for instance, a plastic behaviour of the concrete in a transparent manner. The sub-decomposition of the crack strain ϵ_{cr} gives the possibility of modelling a number of cracks that simultaneously occur. However simplistically, in a total strain based formulation, the compressive (ductile) and tensile (brittle) characteristics can be idealised within a single material model describing both aspects of physical behaviour.

3 PARAMETRIC STUDY DESIGN AND MODELLING APPROACH

In DIANA the tension softening relations of a material can be described either via fracture energy or ultimate crack strain. Both of these parameters can be specified as a function of temperature. DIANA offers linear, exponential or Hordyk tension-softening regimes, which describe the stress-strain relations of an open crack (see figure 2). More information on the tension softening regimes can be found in Manie (2010).

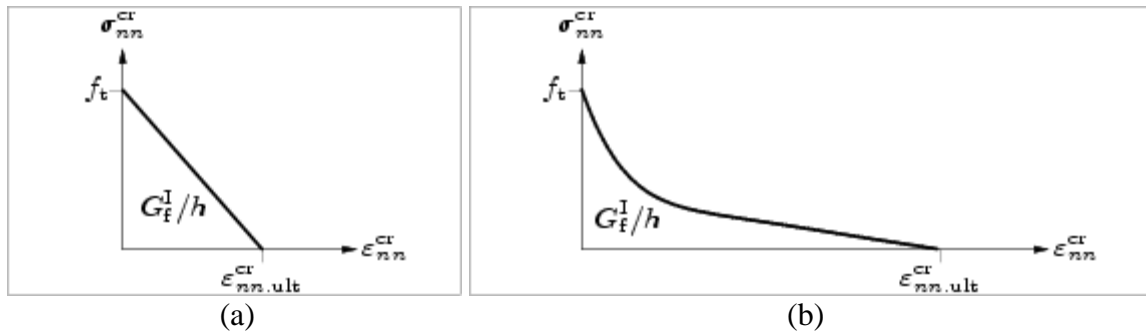


Fig. 2 Tension-softening relationships available in DIANA (Manie 2010):- linear (a) and Hordyk (b)

In the parametric study conducted, both of the above were adopted to investigate the apparent failure time of a simple timber beam exposed to fire (ISO834) from below and subject to varying degrees of load level (via a mid-span point load). A simple bi-linear model describes the plasticity behaviour of timber in compression as part of a total strain-based crack model incorporating the above. The beam is modelled as continuum using second-order quad plane-stress elements.

The analysis is conducted as a staggered thermo-mechanical model whereby second-order structural elements are converted to first-order flow elements. Thermal and boundary properties are as per EN 1995-1-2 and EN 1991-1-2, respectively (BSI 2002/2004). Grade C30 timber is assumed throughout with a characteristic density of 300 kg/m^3 . Tensile strength is derived according to Thunnel (1941) assuming 80% fractile strength. The Modulus of Elasticity (MOE) as a function of temperature is determined using a subroutine proposed by Hopkin *et al.* (2011).

Timber beams 150 mm deep and 2 m long are subject to different utilisation ratios of 25, 50, 75 and 90%. The required loads to achieve such utilisation levels are derived using the reduced cross section method set out in EN 1995-1-2 for standard fire exposure. Target ‘failure times’ are also derived using this method. Where a “mixed” fracture energy is referenced, this implies an increasing fracture energy with temperatures as per figure 3.

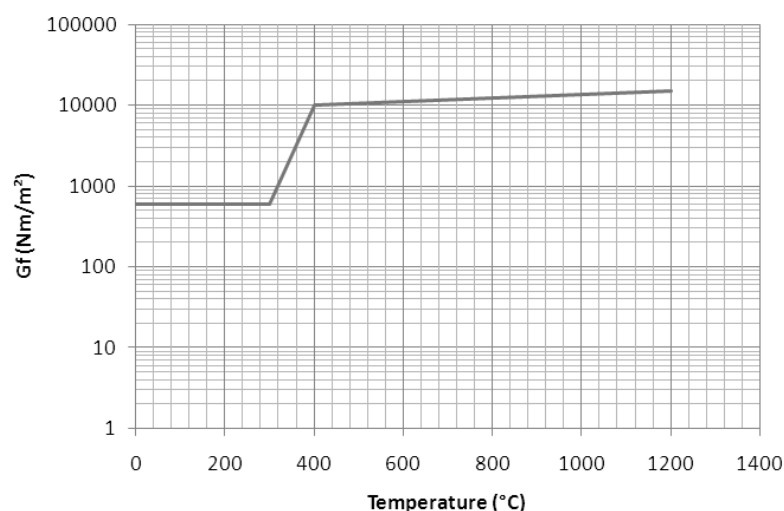


Fig. 3 Mixed fracture energy adopted in simulations

The mixed fracture energy concept is introduced as a potential solution to numerical instability. Large strains can develop in the char zone of a beam, which contributes little to the mechanical resistance yet may govern the termination time of a simulation, should the total strain at the extreme char fibres exceed that of the ultimate crack strain. The application of a single large fracture energy for all temperatures (i.e. 5000Nm/m² for all temperatures) may overpredict the load-carrying capacity of a timber beam and, as such, it is important to maintain realistic fracture energy values for uncharred timber.

Tab. 1 Parametric study summary

Group No.	Utilisation (%)	Fracture energy (Nm/m ²)	Tension softening	Target failure time (min)
1 (A-E)	25	600 (A), 1000 (B), 2000 (C), 5000 (D), Mixed (E)	Linear	66 (3960 s)
2 (A-E)			Hordyk	
3 (A-E)	50		Linear	34 (2040 s)
4 (A-E)			Hordyk	
5 (A-E)	75		Linear	13.5 (810 s)
6 (A-E)			Hordyk	
7 (A-E)	90		Linear	5 (300 s)
8 (A-E)			Hordyk	

Simulation failure is crudely taken as the last converged step. It is recognised that such a termination can be brought about due to numerical instability and not a physical failure. However, where fractures develop without alternative means of load redistribution, it is highly likely that failure is due to a violation of the stress-strain relationship for the material and thus can be considered as a ‘true failure’. This is particularly the case for instances where large fracture energy values, and thus large ultimate crack strains, are specified for the char layer, i.e. the mixed case.

4 FINDINGS

Without supporting experimental data the authors have chosen to measure the relative impact of fracture energy on ‘failure’ time by comparing simulation termination times with predicted failure times using the reduced cross-section method of EN 1995-1-2. Results are divided by tension-softening regime and as such plots of apparent simulation failure time and EN 1995-1-2-derived failure time are shown for linear and Hordyk tension-softening regimes in figures 4 and 5, respectively.

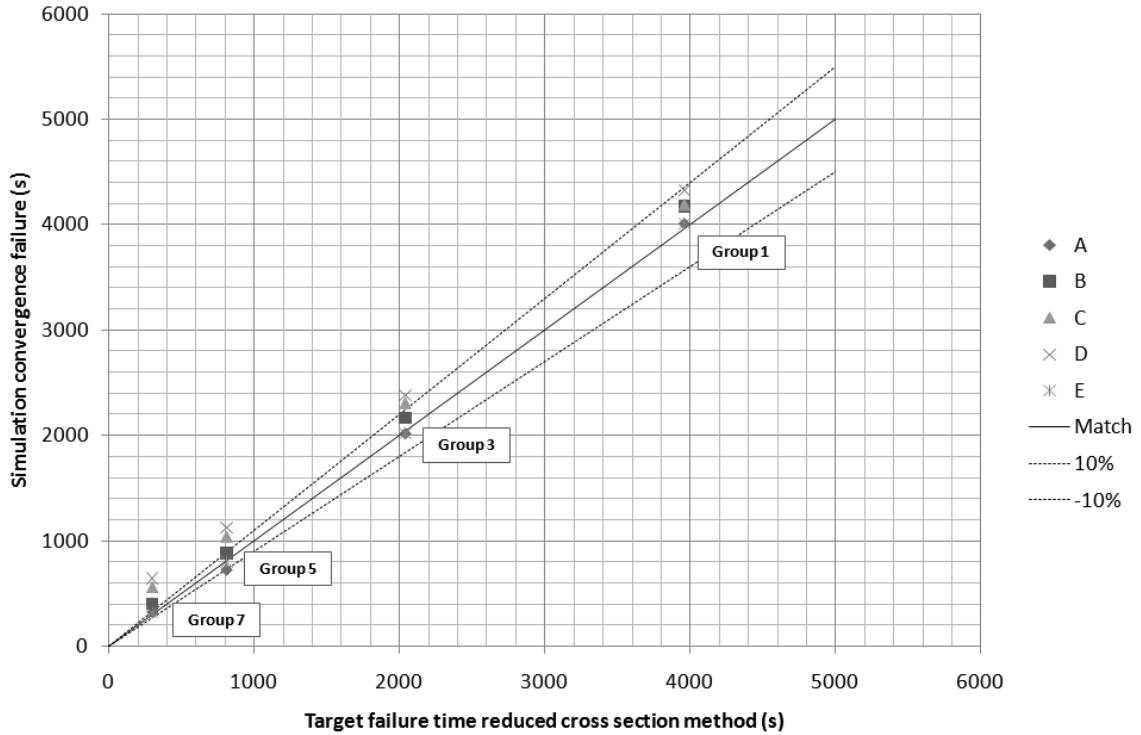


Fig. 4 Simulation termination time vs. predicted failure time from EN 1995-1-2 (linear tension softening)

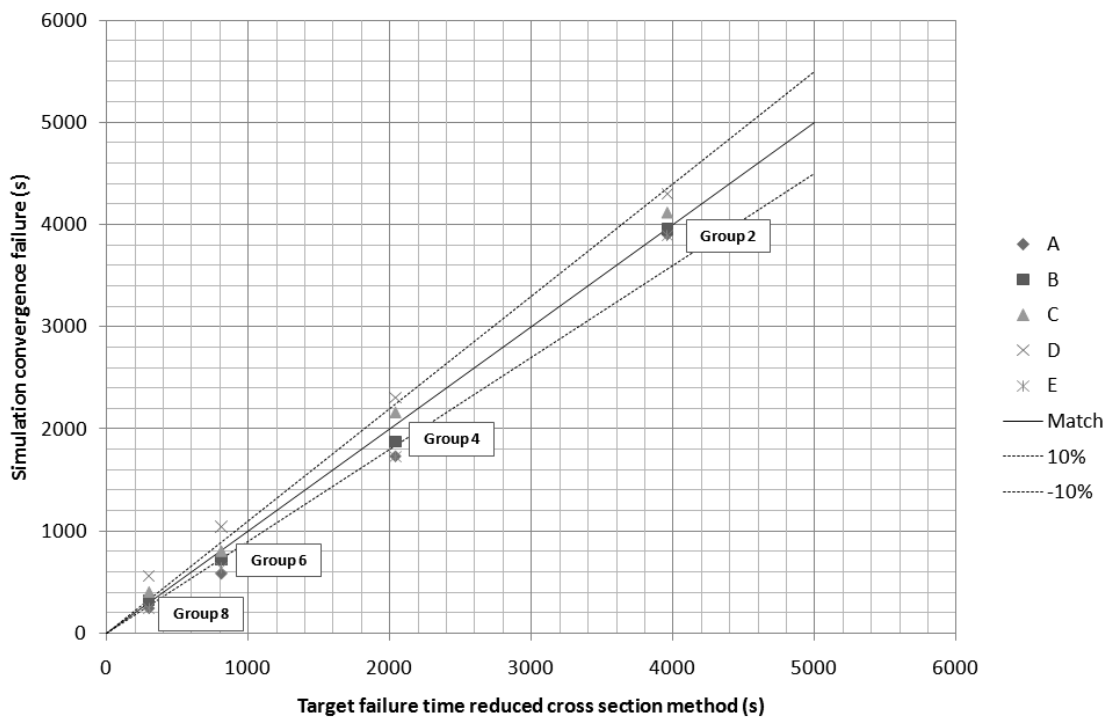


Fig. 5 Simulation termination time vs. predicted failure time from EN 1995-1-2 (Hordyk tension softening)

5 SUMMARY

Figures 4 and 5 demonstrate that the assumed fracture energy has an important influence on the simulation termination time when a timber beam is exposed to fire from below and is subject to different levels of load. The larger the fracture energy, the more ductile a structural member behaves as crack stress is dissipated over a much larger crack strain.

In numerical simulations the incorrect input of fracture energy can result in overall reductions in tensile strength as the values specified should be sufficient for the full tension-softening regime to be defined. In DIANA the limiting tensile strength is dependent upon the tension softening regime, fracture energy, MOE and crack bandwidth. Where small crack bandwidths and fracture energies are introduced, reductions in tensile strength can occur, which impact heavily upon apparent 'failure time'. This behaviour was found to be more critical when Hordyk tension softening is adopted over Linear.

For the purposes of modelling timber beams exposed to fire it has been found that linear tension softening is adequate. A mixed fracture-energy approach (i.e. increasing G_f with temperature) can ensure that numerical instability does not develop in the char zone, where strains are high, whilst also giving realistic strength characteristics and brittleness behaviour in the undamaged residual cross section.

6 ACKNOWLEDGEMENTS

The authors would like to thank EPSRC and BRE Global for their support.

REFERENCES

- BRITISH STANDARDS INSTITUTION, 2004. Eurocode 5: Design of timber structures – Part 1-2: General – Structural fire design. BS EN 1995-1-2. London: BSI.
- BRITISH STANDARDS INSTITUTION, 2002. Eurocode 1: Actions on structures – Part 1-2: General actions – Actions on structures exposed to fire. BS EN 1991-1-2. London: BSI.
- HOPKIN, D.J., EL-RIMAWI, J., SILBERSCHMIDT, V., 2011, The adaptation of TNO DIANA for the modelling of timber exposed to fire. Proc. of ASFE, Prague, Czech Republic.
- KONIG, J. and WALLEIJ, L., 2000. Timber frame assemblies exposed to standard and parametric fires part 2: A design model for standard fire exposure. I0001001. Stockholm: SP Tratek.
- LARSEN, H.J., and GUSTAFSSON, P.J.H, 1991. The fracture energy of wood in tension perpendicular to the grain. Paper CIB-W18A/24-19-2, Proc. of CIB-W18A Meeting 23, Oxford, UK.
- LARSEN, H.J., and GUSTAFSSON, P.J.H, 1990. The fracture energy of wood in tension perpendicular to the grain- results from a joint testing project. Paper CIB-W18A/23-19-2, Proc. of CIB-W18A Meeting 23, Lisbon, Portugal.
- MANIE, J., 2010. DIANA User's Manual. 9.4 edn. Delft: TNO.
- SCHMID, J., KONIG, J. and KOHLER, J., 2010. Design model for fire exposed cross-laminated timber, V.R. KODUR and J.M. FRANSSSEN, eds. In: Proceedings of the sixth international conference on structures in fire, 2-4th June 2010, DEStech pp511-519.
- SELBY, R. G., AND VECCHIO, F. J., 1993. Three-dimensional Constitutive Relations for Reinforced Concrete. Tech. Rep. 93-02, Univ. Toronto, dept. Civil Eng., Toronto, Canada.
- THELANDERSON, S. and LARSEN, H.J., 2003. Timber engineering. 1st edn. Sussex: Wiley.
- THUNNEL, B., 1941. Hallfastetsegenskaper hos svenskt furuvirke utan kvistar och defekter. Handlingar Nr. 161. Stockholm: Ingenjorsvetenskapsakademien.
- VECCHIO, F. J., AND COLLINS, M. P., 1986. The modified compression field theory for reinforced concrete elements subjected to shear. *ACI Journal* 83(22), 219-231.

STOCHASTIC ANALYSIS OF STRUCTURES IN FIRE BY MONTE CARLO SIMULATION

Kaihang Shi ^a, Qianru Guo ^a, Ann E. Jeffers ^a

^a Department of Civil and Environmental Engineering, University of Michigan, Ann Arbor, MI, USA

INTRODUCTION

Current methods for investigating structural response in fire are based on the assumption that the parameters affecting the fire behavior and the corresponding structural response are deterministically known. However, research in the area of structure-fire interaction demonstrates that a large number of uncertainties exist in the nature of the problem and in our ability to accurately represent the fundamental behaviors with numerical models. Furthermore, as the profession develops performance-based approaches to structural fire design, there is a significant need for design methods that allow structural performance to be assessed in a rational way. Deterministic methods are not well-suited for performance-based design because they do not account for uncertainty and fail to quantify the reliability of a given design, thus preventing a logical assessment of the response given uncertainties in the fire load and subsequent structural response.

To overcome current limitations, a reliability-based framework was utilized to assess the performance of structural systems given uncertain fire effects. The framework involves (i) characterizing the sources of uncertainty, (ii) quantifying the probabilistic characteristics of each uncertain parameter, (iii) defining performance criteria for the structure based on strength, stability, and serviceability requirements, (iv) evaluating the structural response stochastically (e.g., by Monte Carlo simulation), and (v) calculating the probability of failure. Once the probability of failure is determined, the adequacy of the design can be evaluated in terms of an acceptable level of risk. The methodology is illustrated here by an example in which the fire resistance of a steel beam was evaluated based on uncertainties in fire load and structural resistance. Stochastic analyses were carried out by performing finite element analyses within a Monte Carlo simulation. The paper focuses specifically on the implementation of a sequentially coupled stochastic analysis in the finite element analysis software Abaqus (2010) using Python scripting commands. Although the example considered here is relatively simplistic and does not include all possible uncertain parameters, it effectively demonstrates the application of the proposed reliability method and provides insight into the practicalities of extending the approach to more complex structural systems.

1 ANALYTICAL METHODOLOGY

The work described herein seeks to explore the effects of uncertainty in the fire behaviour and structural response using Monte Carlo simulation. Monte Carlo simulation is an iterative method in which random values for each uncertain parameter are generated based on their probabilistic characteristics, and the response is evaluated deterministically for each combination of random values. Once all simulations have been carried out, probabilistic information about the system can be synthesized from the results. For the purposes of evaluating structural reliability, the probability of failure p_f can be determined by observing the number of simulations for which the response exceeds a given failure criterion, i.e.,

$$p_f = \frac{N_f}{N}, \quad (1)$$

where N_f is the number of simulations for which the system failed, and N is the total number of simulations. While the Monte Carlo method has been used extensively to evaluate uncertainty in a wide range of applications, it tends to be very computationally expensive because a large number of

iterations are required to achieve a desired level of accuracy. Efficiency can be improved with special sampling techniques such as Latin hypercube sampling (Bergmeister et al., 2009). As shown in Fig. 1, structure–fire interaction involves a propagation of uncertainty that affects each stage of the sequentially coupled analysis. For example, uncertainties in the compartment geometry, type and distribution of fuel, and ventilation conditions result in a fire load that cannot be predicted with great precision. Additional uncertainties associated with the material properties of the structure, the thermal and structural boundary conditions, and magnitude of applied loads lead to further challenges in determining how the structural system will respond in an actual fire scenario. The Monte Carlo method was adopted here to simulate the stochastic response of a of a structure given uncertainties in the fire and structural parameters. In the following analysis, random values were generated for each uncertain parameter based on assumed probabilistic characteristics. Three stochastic analyses were then carried out to evaluate the fire behaviour, the thermal response of the structure, and the mechanical response of the structure. Data from the stochastic simulations were then used to determine the reliability of the system using Eq. 1. Details about the analysis are provided in the following section.

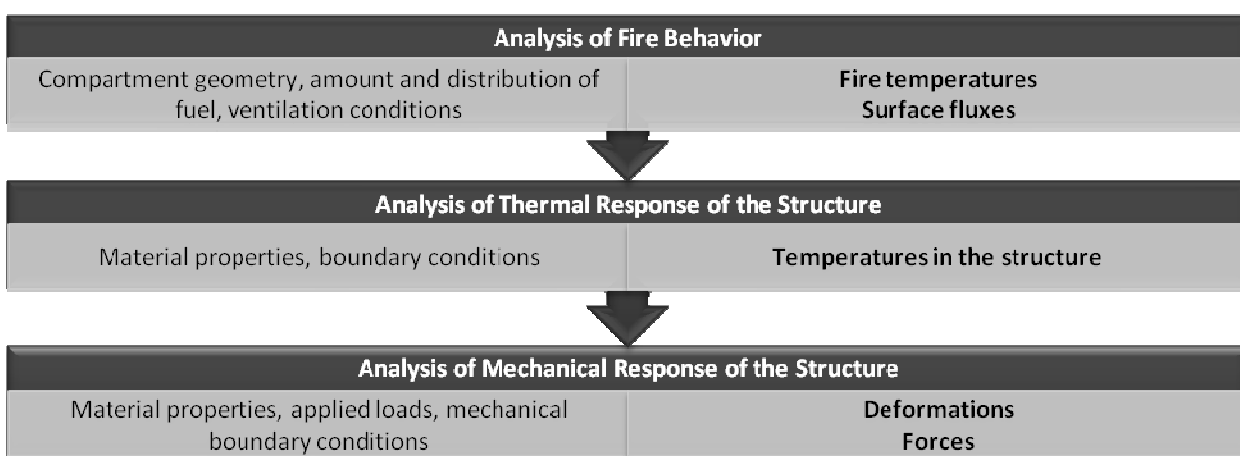


Fig. 1 Propagation of uncertainty in the structural fire simulation

2 PROBLEM STATEMENT

To illustrate the stochastic simulation of structural performance in fire, Monte Carlo simulations were conducted for a protected steel beam exposed to natural fire. As illustrated in Fig. 2a, the beam was simply supported and carried a uniformly distributed load w . In addition to the applied loads, the beam also supported a concrete slab, which was assumed to act non-compositely with the beam. The steel had a nominal yield strength of 345 MPa. A cross-section of W28x8 was required to resist the assumed design load based on the U.S. steel design specification (AISC, 2005) and to meet the ANSI/UL 263 requirements for prescriptive fire resistant design in the U.S. The beam’s cross-section is shown in Fig. 2b. The beam was protected by a spray-applied fire resistant material such that the beam provided a 1h fire resistance.

The purpose of the analysis was to evaluate the response of the protected steel beam exposed to natural fire given uncertainties in the fire, material, and loading parameters. Natural fire exposure was modelled using the Eurocode parametric fire curve as modified by Buchanan (2002). To evaluate the thermo-mechanical response, two sequentially coupled analyses were conducted in Abaqus (2010). Heat transfer over the cross-section was modelled using two-dimensional continuum elements. The mechanical response was subsequently modelled using two-dimensional beam elements. Temperatures in the flanges and web were obtained from the heat transfer analysis and transferred directly into the structural model by specifying the flange and web temperatures as *predefined fields* in Abaqus.

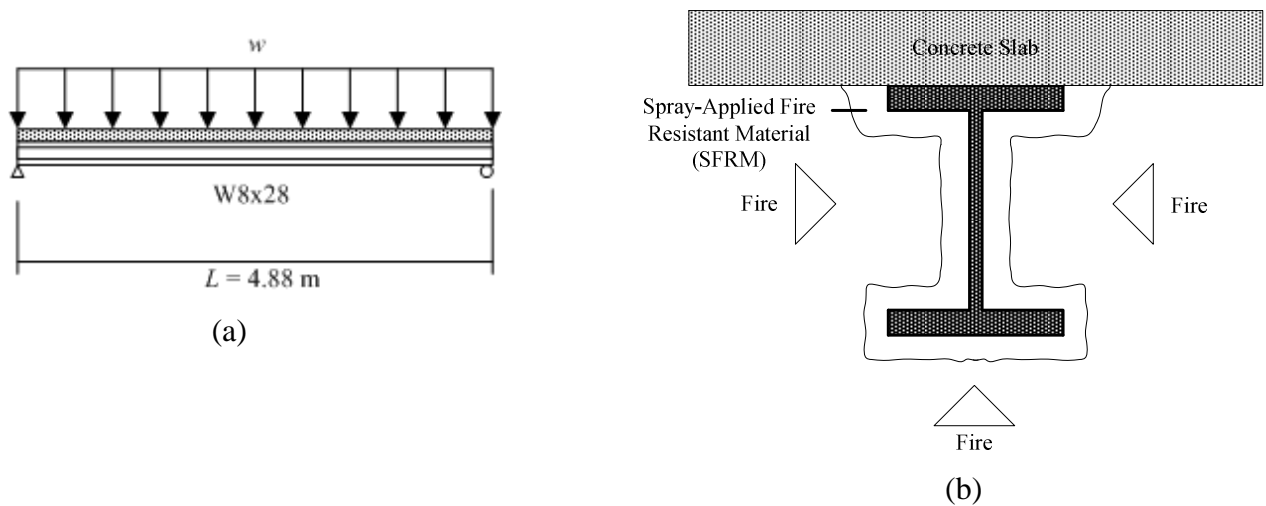


Fig. 2 Problem statement: (a) Loading and support conditions; (b) Cross-section

One thousand Monte Carlo simulations were carried out using Latin Hypercube sampling to reduce the total number of simulations required for the analyses. As illustrated in Fig. 3, two parametric studies (i.e., one for the heat transfer analysis, one for the structural analysis) were run in Abaqus, each of which utilized a Python script file that generated an Abaqus model for each combination of random parameters. To perform the parametric study, the input file (.inp) for the finite element analysis was written in terms of the uncertain parameters associated with the particular heat transfer or structural analysis. Random values for each parameter were generated in Matlab (2010) using the appropriate, mean, covariance, and probability distribution. Values for the random parameters were then entered in the Python script file along with commands to define the combination of parameters for each case and options for executing the analysis. The analysis was executed by running the Python script from the Abaqus command prompt. Once the analysis was completed, a separate Python script was executed to compile the results from each of the simulations.

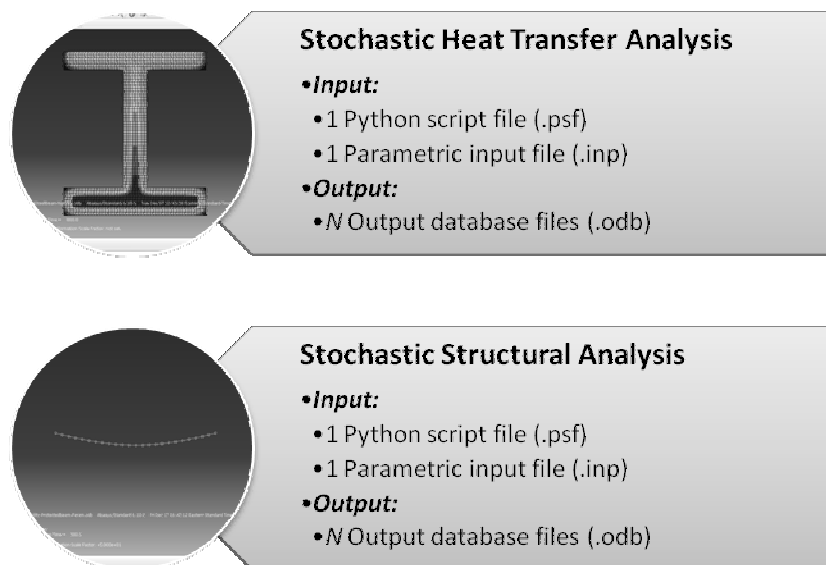


Fig. 3 Sequentially coupled stochastic simulation in Abaqus

2.1 Fire Analysis

Natural fire exposure is modelled using the temperature-time curve recommended by Buchanan (2002). For stochastic simulation of the fire, the fire parameters were assumed to have realistic mean values and probability distributions based on the works of Culver (1976) and Iqbal and Harichandran (2010). Specifically, the ventilation factor F_v was assumed to have a mean value of 0.04, a coefficient of variation (COV) of 0.05, and normal distribution. It was also assumed that the walls and ceiling were made of gypsum board, which has a mean value of $b = 423.5 \text{ W s}^{1/2}/\text{m}^2\text{K}$, a

COV of 0.09, and normal distribution. Based on an assumed compartment geometry, the fire load per total area e_t was determined to have a mean value of 132.54 MJ/m^2 with a COV of 0.62 and Gumbel (Extreme Type 1) distribution.

Random values for each of the fire parameters were generated in Matlab and subsequently inserted in the fire model to obtain a series of natural fire curves that represent the range of potential compartment fires expected in the current case study. As illustrated in Fig. 4, fires varied in duration and intensity, with the expected (mean) fire reaching a maximum temperature of approximately 1100 C and burning steadily for 15 min before decay.

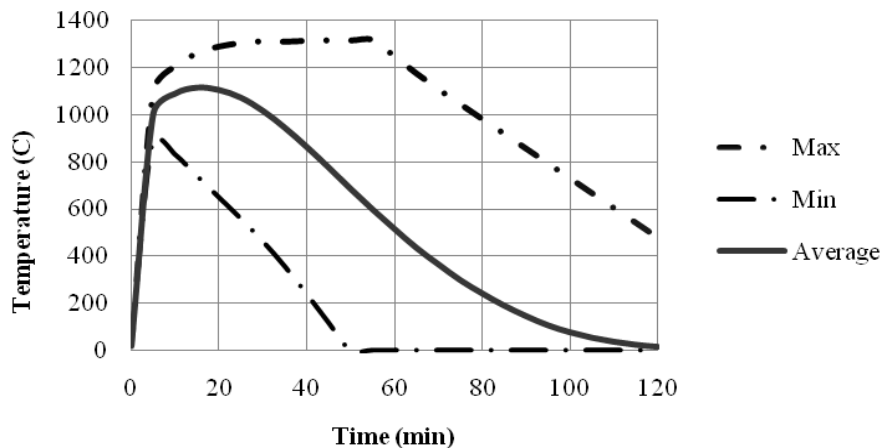


Fig. 4 Compartment temperature

2.2 Heat Transfer Analysis

The fire temperatures computed from the previous step were subsequently used in a two-dimensional heat transfer analysis of the beam’s cross-section, which is shown in Fig. 2b. Heat is transferred from the fire to the steel by convection and radiation. Mean values for the convection heat transfer coefficient and effective emissivity ε were taken from the Eurocode, while both constants were assumed to be normally distributed with coefficients of variation of 0.10 due to lack of existing data.

To achieve the 1h fire resistance rating, the SFRM was required to have a thickness of 11.1 mm. The mean value for the SFRM thickness was taken as the nominal thickness plus 1.6 mm, resulting in a mean thickness of 12.7mm. The COV was assumed to be 0.20 and variability that follows a lognormal distribution. The density, thermal conductivity, and specific heat for the SFRM were assumed to be independent of temperatures using mean values reported in the Eurocode and probability distributions given by Iqbal and Harichandran (2010).

Conduction at the steel-concrete interface was modelled by treating the concrete as a semi-infinite medium with constant temperature of 20 C (Incropera and DeWitt, 2002). Thermal properties for the concrete were assumed to be constant and independent of temperature, while thermal properties for the steel were assumed to follow the temperature-dependent Eurocode models. Variability in the steel and concrete properties was ignored in the present analysis for simplicity.

There were a range of steel temperatures obtained due to the variability in the fire temperatures and thermal properties of the beam. Average temperatures from the heat transfer analysis are shown in Fig. 5. Note that the average steel temperatures around 500 C for the expected fire load. However, more severe fire loads combined with low fire protection thicknesses resulted in the possibility of steel temperatures in excess of 1000 C .

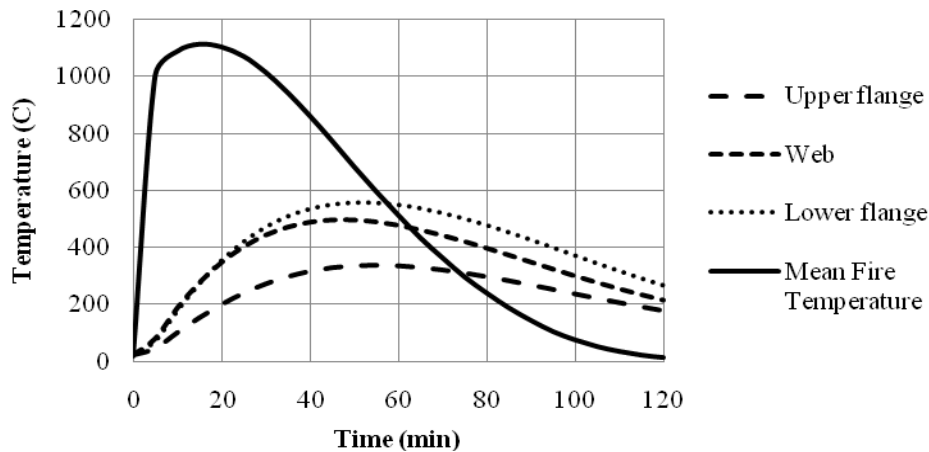


Fig. 5 Average temperatures in the steel

2.3 Structural Analysis

The steel temperatures from the heat transfer analysis were subsequently specified in the mechanical model of the beam that is shown in Fig. 2a. The stochastic simulation considered uncertainties in the yield strength and magnitude of the applied loads. While the beam was designed for a nominal yield strength of 345 MPa, a statistical analysis of data presented by Wainman and Kirby (1988) showed that this grade of steel has a mean strength of 380 MPa and a COV of 0.08 (normal distribution). The uniformly distributed dead and live loads had design values 5.15 kN/m and 3.65 kN/m, respectively, based on typical office loading in U.S. construction. For stochastic simulation, arbitrary-point-in-time dead and live loads were used based on the calculations of Ellingwood (2005). Thus, the dead load had a mean value of 5.41 kN/m, COV of 0.10, and normal distribution, and the live load had a mean value of 0.88 kN/m, COV of 0.60, and followed a gamma distribution.

The mid-span displacement for each simulation was measured at each time step in the analysis. Results are illustrated in Fig. 6. Note that the expected (mean) mid-span displacement reaches a value of 58 mm before cooling. Due to the range of potential fire loads, material parameters, and magnitudes of applied loads, there were many cases in which the deflections became excessively large.

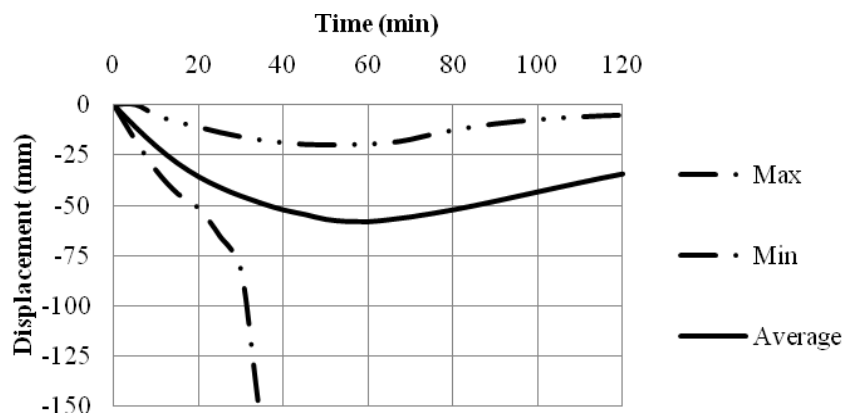


Fig. 6 Mid-span displacement

For the purposes of assessing the reliability of the structure, failure was defined as the time at which the mid-span displacement exceeded a limiting value of $L/30$. The probability of failure was computed according to Eq. 1, yielding a failure probability of 1.3%. Thus, despite the potential for catastrophic failure based on a potential “worst-case” scenario, the beam (as designed according to the current prescriptive codes) appears to be sufficiently designed to resist the natural fire, as expected. Note that the analysis only considered 1000 Monte Carlo simulations, and so the margin of error in calculating the probability of failure is high. Therefore, the findings of this study are

inconclusive at this point in time. Further work is being done to explore the problem in greater depth.

3 SUMMARY AND CONCLUSIONS

This paper presents a preliminary study into the stochastic simulation of structures in fire. Specifically, the Monte Carlo method was used with finite element simulation in Abaqus to evaluate the response of a protected steel beam given uncertainties in fire load and structural resistance. While the application shows much promise for future investigations into the probabilistic mechanics of structures at extreme temperatures, the computational demands required to perform three sequentially coupled Monte Carlo simulations with embedded finite element simulations calls for a more computationally efficient approach. On-going work is being conducted to explore the parallelization of the simulation to improve the efficiency of the Monte Carlo method for structure-fire applications.

ACKNOWLEDGMENT

This research was supported by the U.S. National Science Foundation under Grant No. CMMI-1032493

REFERENCES

- Abaqus, v.6-10 (2010). Dassault Systemes, Providence, RI.
- AISC (2005). Steel Construction Manual, 13th Ed., American Institute of Steel Construction, USA.
- Buchanan, A.H. (2002). Structural Design for Fire Safety, John Wiley and Sons Ltd, England.
- Bergmeister, K., Novak, D., Pukl, R., and Cervenka, V. (2009). "Structural Assessment and Reliability Analyses for Existing Engineering Structures, Theoretical Background," *Structure and Infrastructure Engineering*, 5, 267-275.
- Culver, C.G. (1976). Survey Results for Fire Loads and Live Loads in Office Buildings, National Bureau of Standards, Washington, D.C.
- Ellingwood, B.R. (2005). "Load Combination Requirements for Fire-Resistant Structural Design," *Journal of Fire Protection Engineering*, 15, 43-61.
- Incropera, F. P., and DeWitt, D. P. (2002). Fundamentals of Heat and Mass Transfer, 5th Ed., John Wiley and Sons, Inc., New York.
- Iqbal, S., and Harichandran, R.S. (2010). "Capacity Reduction and Fire Load Factors for Design of Steel Members Exposed to Fire," *Journal of Structural Engineering*, 136, 1554-1562.
- MATLAB, v.7.11 (2010). MathWorks, Inc., Natick, MA.
- Wainman, D. E., and Kirby, B. R. (1988). Compendium of UK Standard Fire Test Data: Unprotected Structural Steel - 1, Report No. RS/RSC/S10328/1/87/B, British Steel Corporation, England.

INTEGRATED NUMERICAL MODELING IN FIRE SAFETY ASSESSMENT

Current needs, challenges, potentiality and perspectives.

Paweł A. Król

Warsaw University of Technology, Faculty of Civil Engineering, Warsaw, Poland

INTRODUCTION

Building fire safety is one of the six requirements imposed by the local building law act of European Union's member states, which must be strictly complied in the design and execution of buildings and structures. Ongoing adoption of Eurocodes - European standards for structural design imposes new challenges for the engineering community in Poland and elsewhere. It should be expected that, in the near future, as fire safety engineering develops, the global and advanced analyses of civil engineering structures will be absolutely necessary to consider the special design case of a fire. Such analyses will play a vital role in the attempts to assess and ensure high level of structural safety, in particular in the case of buildings and structures, for which the consequences of their destruction are serious, i.e. for those where the risk of human life and health loss is high, and for buildings with a special economic status. EN 1991-1-2: Eurocode 1, Directive 89/106/EEC as well as the state technical and building regulations stipulate that buildings and structures must be designed and built in order that, in the event of a fire: – load-bearing capacity of the construction can be assumed for a specific period of time, – the generation and spread of fire onto adjacent buildings and structures is limited, – residents can leave the building or be rescued in another way, – the safety of rescue teams is taken into consideration. The above requirements are in most cases met by analyzing the load-bearing capacity of the structure in the case of fire impact, using the conventional fire scenarios (nominal fires) or "natural" (performance-based) fire scenarios, whereas in the execution phase, passive and active fire safety measures, respectively, are used. Parts of the constructional Eurocodes identified by numbers 199x-1-2, which relate to the impact on the construction of temperatures generated by fire, discuss specific aspects of passive fire safety, considering the methodology for the design of structures and parts thereof, in order to ensure their appropriate load-bearing capacity, and to minimize the spread of fire. Two approaches exist in the structural design: conventional and performance-based. The conventional approach is based on certain simplified assumptions and uses the concept of nominal fire which generates thermal action described by a function of temperature distribution in time, where the function is not dependent on other physical and chemical parameters, which are often of vital importance. The approach based on performance models uses the principles of fire safety engineering and describes thermal action as a concept that depends on multiple physical and chemical parameters, which values are determined individually, considering the specific features of a given structure, which renders the approach much closer to the actual behavior of the construction in the case of a real fire, but is also much more difficult to describe from the computational standpoint. The state-of-the-art knowledge contained in the provisions of the new construction design standards stipulates that structural fire safety assessment can be made at three levels of detail: at the level of an individual component, part of the structure, or the entire load-bearing system. The approach based on simplified computational models does not reflect the actual action of the construction, or the actual behavior of load-bearing components in the case of a fire. These simplified models are mostly based on the assumptions which stipulate an even temperature distribution over the length and/or cross-section of the analyzed component, and usually lead to overestimated fire load-bearing capacity. Many researchers consider the adoption of such design solutions as not justified from the economic perspective. Fast urban development and technology advance poses new challenges for the actors in the building processes involving highly-complex structures (in particular in the case of high-rise buildings or buildings with complex geometric shapes) and increasingly often necessitates a design approach based on performance, known in the literature as "performance-based design". This

approach to structural analysis, especially in the case of large and complex buildings and structures, is much more valid, but requires advanced computational techniques, both to determine temperature fields, which vary over time and space, as well as to determine the response of the structure to the simultaneous mechanical and thermal loads. To respond to the first challenge, computational software is used that draws on the Finite Volume Method and methodologies more broadly used in fluid dynamics. In the case of structural stress analysis, both at the ambient temperature and at fire-generated temperatures, Finite Element Method-based software is in most cases used. Increasingly more often, a need arises to conduct fully combined numerical studies which, in a single computational cycle, consider a two-way interaction between heat transport and the generated temperature fields on the one hand, and the deforming structure on the other. Such combined structural analysis, convenient from the user perspective, generates additional computational problems which, should be identified and at least partially solved.

1 DETAILED PROBLEM DESCRIPTION

Rapid development of fire safety engineering in recent years has stimulated the ever-more widespread interpretation of a fire as a special design case, where limit states of the structure's load bearing capacity are tested. Primary information on the subject is provided in a collection of standards recently published in Europe and being continuously adopted in the UE's member states as national standards. These are the following Eurocodes: EN 1991-1-2: Eurocode 1, EN 1992-1-2: Eurocode 2, EN 1993-1-2: Eurocode 3, and EN 1994-1-2: Eurocode 4. All these standards consider computational analyses conducted at one of the three levels of detail: single structural component, a detached, representative section of the structure, or global, advanced analysis of the entire structure. The more advanced the level of analysis, the greater its reliability and accuracy of the results.

The primary purpose of analyzing civil engineering structures in the event of a fire is the need to anticipate the fire's impact on the building, and in particular to assess the resistance of the structure in the event of a fire, and its behavior at the stage of temperature rise or cooling. Results of such analysis may find a direct application in the design of passive and active fire safety systems, for safety assessment of new or existing structures, as well as a supplementation of, or addition to, usually very expensive experimental studies.

Although the procedures for the assessment of bearing capacity of a single component are relatively detailed in the provisions of the said standards, details on the analysis of detached sections of structural systems, and on global analysis of entire structures, exist only as general guidelines, providing conceptual assumptions on the methodology only, and do not lead to any clear-cut conclusions which could be used as final and unambiguous guidelines by the individual designer, and which could translate into their direct application in the design practice.

The methodology for the fire safety of civil structures adopted by the said standards is not perfect and results in economically unjustified, overestimated computations. Formulas used to verify the capacity of any individual member in fire situation are designed so that they are close to their corresponding formulas used to determine limit states of load bearing capacity in the event of the persistent design situations. Such verification procedures are valid in the case of single and simple structural elements, but are not fully adequate to reliably assess entire structural systems, as they do not allow a reliable estimation of the thermal and mechanical response of the structure exposed to a fire, leave out the impact of non-linear effects, which can be considered only if the advanced computational models are used. Further, what provokes certain doubts in the research community is the way thermal loads are treated in fire-related static and structural resistance analysis. The conventional design theory assumes that fire-generated loads are quantified using deterministic methods in the same way like in case of typical mechanical loads which come from the structural components' self-weight (dead load), or such as finishing materials, snow and wind, are quantified. The resistance analysis is essentially limited to pure mechanical factors, and the effect of temperature is considered only indirectly, with the use of adjustment coefficients, which are to account for e.g. structural material resistance parameter degradation.

Next to analytical methods reflected by the design standards, fire-related analysis of civil structures or their components may also be conducted experimentally, or with the use of advanced computer

software, which is authorized based on delegations under the provisions of the relevant technical regulations.

The experimental method appears the most reliable of all, but it has a number of limitations, both of technical and economic nature. Micro-tests, using research furnaces can be applied only for individual structural components, whose dimensions are typically reduced. On the other way the natural-scale tests (the best-known of which are the Cardington and the Mokrsko tests) are very expensive are rarely conducted, although they represent a very valuable source of information on the actual behavior of structures during a fire, fully reflect the nature of physical and chemical phenomena and, when correctly conducted, provide important information on the core of the problem, (Wald at al, 2010). The complexity of the tests in which furnaces are used is also revealed by the some specific uncertainties, which can be partially reduced by e.g. increasing the accuracy of measurement techniques, or cannot be reduced owing to the structure of the research equipment. Disappointingly, in the case of experiments conducted during fires, numerous technical problems arise, related to correct determination of mechanical and thermal factors having a bearing on the tested element or the entire structure during the test, such as ensuring the actual support conditions that fully reflect the conditions which prevail for the actual structure, etc. Also the quantity of information obtained in the course of the experiment is markedly limited. An ideal case of repeating the identical thermal and mechanical conditions is not feasible, and, from the economic perspective, involves huge expenses. Similarly, the determination of certain values on completion of the test is not possible.

The application of numerical methods currently encounters serious difficulties, too. There are no popular and simple-to-use numerical tools available on the market, which would enable structural designers or experts at fire safety to conduct computational studies themselves, and, even worse, the most popular computer programs used for computer-assisted design are not compliant with the provisions of key European standards on construction design in the persistent design situation. Approximate analytical methods which could be used in the design practice provide results which often markedly depart from the actual conditions, in particular in the case of innovative and complex structural systems, or where new technologies and materials are used.

The concept of fire safety based on the natural fire approach provides a more realistic view of the phenomenon over time and space, as compared against other simplified methods based on the conventional fire concept. The design of new civil engineering structures, or the assessment of the existing load-bearing systems based on the performance parameters is one of the methods for approving structural safety stipulated by the European design standards. The need for the fire safety procedures to consider the individual nature of each building, the presence and type of ventilation systems used, passive and active protection systems, as well as other furnishings which have a direct impact on the fire-spread scenario, was formulated in the final conclusions from the European research project developed a few years ago, (Kumar at al, 2008).

The actual understanding of the behavior and actions of the structure in the event of a fire, as well as the assessment of its bearing capacity, may be fully reliable only when using the methods that apply the performance parameters, in particular: type of building, premises or designated fire zone, occupancy method (magnitude of fire load), shape and geometrical dimensions, possible hypothetical changes to the building arrangement, occupancy or furnishings over the life of the building, possible fire scenarios, considering the likelihood of a fire that follows a given scenario, etc. A thorough analysis and understanding of the nature of the phenomenon and a more precise analysis of the structure may demonstrate a higher level of structural safety than previously assessed based on the design standard procedures. From the economic perspective, this approach can lead to "greater value for money".

It is widely expected that the natural fire safety concept-based research tasks can be executed only with the use of advanced numerical tools which enable a simultaneous thermal and mechanical analysis of the structure, when both types of analysis are combined and coupled. The only tools that allow the conduct of such analyses at an advanced level (still beyond the reach of engineering practitioners) are specialty numerical programs (software) based on the Finite Volume Method or the Finite Element Method, which, however, require relatively deep theoretical knowledge. The first

of the two methods allows the adoption of time- and space-variable temperature field factor, and is used in computational fluid dynamics (CFD) (e.g. FDS, ANSYS-CFX, ANSYS-FLUENT, JASMINE, SOFIE). Phenomenon modeling with the use of Computational Fluid Dynamics has been, until recently, relatively often used in engineering and technical sciences to model heat transport processes. The last 20 years have seen a faster CFD development and application of its methods to model fire scenarios, which considerably spurred the development of a research discipline called “fire safety engineering”. Until now, however, coordinated attempts at harnessing the potential of the method to assess the occurrence and magnitude of thermal impact on fire-struck buildings have been few and far between.

The FEM is widely used in the structural stress analysis, both for ambient and increased temperatures, and utilizes such software as ABAQUS, ANSYS, LS-DYNA, SAFIR, to name but a few. Fully relevant structural analysis requires a combination and coupling of thermal analysis with stress analysis, where, in a single computational cycle, a two-way interaction is considered between heat transport and the generated temperature fields on the one hand, and the deforming structure on the other, and where secondary static schemes and changes to the degrees of freedom, etc. are incorporated.

2 JUSTIFICATION OF THE PROPOSED RESEARCH METHODOLOGY

Numerical computational models used both for analysis of individual components and global analysis of complete load-bearing systems can be evaluated as fully reliable if they appropriately render the nature of the phenomena they study through, an appropriate selection of the type of analysis, integration methods, system geometry, variability of material resistance parameters, along with the change in temperature field, mechanical support and load conditions, as well as temperature distribution over time and space. Numerical methods (sometimes called as computer simulations) offer a vast potential and are successfully used in many other technical disciplines, such as fluid and solid mechanics, or structural mechanics.

What raises most serious doubts when it comes to the application of using numerical analyses is the question of how reliable the results are, and to what extent those complex numerical analyses are able to anticipate the actual behaviour of structures. It should be noted that formal evidence of reliability of numerical solutions using the FEM exist for linear problems only, where the response of the structure is in proportion to the cause (of the mechanical load). Owing to the nature of the phenomena, linear analyses are insufficient for structures struck by a fire. High temperatures are accompanied by essentially non-linear effects, the sources of which lie in the variable material properties, which change as the temperature rises, geometrical relations between deformations and movements, or which result from the very methods of load application and support, and from interactions between structural components.

3 CURRENT KNOWLEDGE AND EXISTING TECHNOLOGICAL SOLUTIONS

The descriptions of assumptions accompanying building fire safety assessment based on the natural fire safety concept can be found in final reports of the research projects conducted under "Natural Fire Safety Concept" programme, (Kumar at al, 2005 and 2008), whereas results of the attempts to incorporate the method's assumptions into structural design can be found in numerous conference papers, articles in specialty press and some guidebooks (e.g. Parkinson at al, 2010).

The body of literature on advanced computational models for fire-exposed structures is even smaller. There are no comprehensive research studies on integrated fire-exposed structure modeling, with the exception of isolated cases of articles published in recognized international magazines, and papers delivered at international fire safety conferences. Literature on the subject provides some information on the attempts to use numerical tools to model physical phenomena that structural components are impacted by when exposed to high temperatures. Divergent opinions are presented on the potential establishment of standardized procedures for review and validation which could be valid regardless of the case in question. There are also extremely skeptical arguments, which entirely reject the possibility of reliable validation of numerical models. In the case of varied

and complex non-linear issues, the going practice in the engineering and technical circles, is to verify the correctness of given solutions based on "a posteriori" tests only, which essentially involve drawing conclusions based on results of the experiments. Over the last decade, thanks to the participation of researchers working in the US National Laboratories, numerous standards and guidelines emerged on the verification and validation of numerical models. The said standards do not provide detailed ways of working, but rather give an overview and terminology on the subject. The standards differ amongst themselves owing to different research foci and specificity of individual applications, and their non-universal nature precludes their application in any given research case.

4 INNOVATION OF THE DESCRIBED RESEARCH METHODOLOGY

The review of the literature on the subject reveals that the proposed research methodology for building fire safety assessment using advanced numerical tools based on the natural fire safety concept is a unique case as compared to the current knowledge on the subject and is in line with the overall research trends with respect to the area covered. Laying the foundations for improved structural safety using the natural fire safety concept represents a need identified by the construction industry, real estate maintenance market, building control bodies and the state fire services, and has recently been a research priority of numerous research centers, both in the European Union's member states and leading American centers, as well. A vast potential and repository of knowledge which still awaits and requires exploration resides in the proposed methodology and the research scope.

Advanced numerical models are primarily used in such areas of science and technology, where, owing to geometrical complexity of the tested structures, or complexity of the tested phenomena, it is not feasible to create ready-made, finite analytical solutions to apply in a given case, as well as in any field where, for various, and often economic reasons, experimenting is not feasible or insufficient. Complex numerical methods come in particularly useful in such computational cases, where geometrical non-linearity of the structures, or non-linearity of material parameters, need to be considered, or where certain values bear a non-linear relation to other values, which are also variable in a non-linear manner. This is the case with both thermal and mechanical response of steel structures exposed to fire temperatures. A natural reaction is that everything new and not thoroughly explored arouses certain controversies and doubts, and sometimes even denial. For instance, in the case of numerical analysis, a controversy is whether it is suitable for correct anticipation of outcomes of the physical problems in question. Adaptation of numerical models to meet the challenge of reflecting physical phenomena usually takes place upon their verification and validation, which is considered as the most objective method for reliability assessment of non-linear computer simulations. Validation should be preceded by verification, which seeks to check the correctness of the broadly understood discretizing process that is transformation of the mathematical model into a numerical (discrete) model. Verification usually proceeds by comparing numerical computations with high-accuracy reference-standard analytical or numerical solutions. The core element, although not the only one, of verification conducted by the user is to check the consistency of the solution based on tests with the refined grid of finite elements. In turn, validation consists in comparing numerical solutions with experimental results in order to check whether the numerical and mathematical model correctly reflect the physical model, expressed by the way the structure behaves, by the type of phenomenon in question, etc.

An important role in the process of adapting a numerical model to the physical nature of the analyzed phenomena is played by correct mapping of properties of the materials used in the model, which are typically variable as the temperature rises.

5 PRACTICAL SIGNIFICANCE OF THE PROPOSED RESEARCH METHODOLOGY

The proposed numerical research method is of material importance from the perspective of fire safety engineering economy, design practice with emerging new challenges and owing to the social aspect of the problem. Regardless of leaders' political agendas, safety of the population and

property is or should be a prioritized objective. From the economic standpoint, notably in a period of global crisis, it is essential that the proposed design solutions in this respect meet not only the essential requirements relating to structural safety, and safety of people and property as well as rescue teams, but are also cost-effective.

Fire safety has been a subject of research across the world already a dozen or so years ago, but it had not been until the attacks on the World Trade Centre in New York that the research work accelerated considerably. Many countries across the world, including the European Union's member states, introduce new standards for building design, which necessitate incorporation of a specific case of fire into the structural safety assessment. The procedures adopted by the European standards are not equally proper for the assessment of various structural components, as they rely on certain simplified assumptions, resulting from the adopted validation methods, and from the attempt to align the adopted procedures with those that apply for the analysis of bearing capacity limit states in the persistent design situations. The conventional approach to fire-related structural safety assessment may be accepted only for uncomplicated cases, where load-bearing systems can be quantified with static computations. In the case of complex structural systems, however, the application of the latter may lead to considerable inaccuracies, resulting from the aggregation of non-linearity owing to changes in a number of vital construction material resistance parameters, generation of secondary effects, generation of large additional internal forces in the components following the limitation of deformation freedom caused by the temperature rise. Conventional, analytical methods for fire-related structural safety assessment are marked by significant inaccuracies resulting from the simplified methodology and, as a rule, lead to significant overestimations, whereas actual-scale experimental studies are extremely expensive and have a number of technical limitations.

The utilization of numerical tools to conduct analyses may lead to development of new, advanced and less expensive fire-related method of structural safety assessment based on "virtual testing" of the structure through numbers of numerical analyses, which represent a convenient alternative to the conventional experiment, and allow multiple computations for parameter-based studies or probabilistic simulations. Next to the assessment of new building safety, there is also a need for safety assessment of the existing structures marked by complex load-bearing systems. Since there are no consistent regulations and methodology for the assessment of the actual safety level, large discrepancies tend to occur between safety assessments of various buildings serving the same purpose, and marked by similar technical and geometrical parameters.

It is expected that the development and implementation of the proposed research methodology, notably among local corporations of engineers and architects, will change the present, conventional approach to design, marked by a task-based execution methods.

REFERENCES

- Wald F., Kallerová P., Chlouba P., Sokol Z., Strejček M., Pospíšil J., Štroner M, Křemen T, Smítka V., Fire Test on an Administrative Building in Mokrsko. Summary of the Results from the Fire Experiment, 2010
- Kumar S., Welch S., Miles S. D., Cajot L.-G., Haller M., Ojanguren M., Barco J., Hostikka S., Max U., Röhrle A., Natural Fire Safety Concept - The development and validation of a CFD-based engineering methodology for evaluating thermal action on steel and composite structures, European Commission Report EUR 21444 EN, 2005
- Kumar S., Miles S., Welch S., Vassart O., Zhao B., Lemaire A D., Noordijk L. M., Fellingner J. H. H., Franssen J. M., Integrating advanced three-dimensional modeling methodologies for predicting thermo-mechanical behaviour of steel and composite structures subjected to natural fires, Research Fund for Coal and Steel, Contract No RFSR-CT-2003-00030, Final Report, 2008
- Parkinson D. L., Kodur V., Sullivan P. D., Performance-Based Design of Structural Steel for Fire Condition. A Calculation Methodology, ASCE Manuals and Reports on Engineering Practice No. 114, 2009

NUMERICAL INVESTIGATION OF PLASTERBOARD SEPARTING ELEMENTS SUBJECTED TO FIRE

Hung Tran ^{a,b,c}, Hervé Leborgne ^b, Bin Zhao ^c, Alain Millard ^{a,d}

^a Ecole Normale Supérieur de Cachan, Avenue du président Wilson, 94235 Cachan Cedex, France

^b Efectis France, Espace technologique – L'orme des merisiers – Immeuble Apollo, 91193 Saint-Aubin, France

^c Centre Technique Industriel de la Construction Métallique (CTICM), Espace technologique – L'orme des merisiers – Immeuble Apollo, 91193 Saint-Aubin, France

^d Commissariat à l'Energie Atomique (CEA), 91190 Gif-sur-Yvette, France

INTRODUCTION

Plasterboard separating partitions are widely used in the complexes, commercial and industrial buildings. They consist of regularly spaced steel studs fixed on both sides with the facings by screws. Each facing is composed of a single or a double layer of plasterboard. The plasterboard is reinforced with help of glass fibres to ensure its mechanical resistance. The steel studs which have in general a lipped C-section or I-section play the role of a supporting frame. The advantage of such type of partition is lightweight, easy for installation and its high fire resistance performance. The building fire regulations always require the partition elements to have sufficient fire resistance in terms of load-bearing stability, thermal insulation and integrity criteria. For the time being, the common way to validate the fire resistance of such type of partition is to conduct full-scale fire tests. However, these tests are often very expensive and many tests need to be carried out to finalize a new product. Moreover, the limited maximum height of the furnace (5 m at present) constitutes a problem for the manufacturers when they need to validate higher partition elements.

Therefore, the development of a numerical tool becomes very useful in order to carry out on one hand the preliminary design of new products as well as their optimization and on the other hand, to extend the application of experimental results to configurations different from those of the tests (change of dimensions, of components, of boundary conditions ...). Up to now, many researchers have studied and proposed heat transfer models to predict the temperature distribution in the plasterboard partitions but there was little research on their structural behaviour under fire conditions.

In consequence, this paper presents a study which led to the development of a numerical model capable of predicting the thermo-mechanical behaviour of plasterboard partitions when they are subjected to standard thermal action of EN 1363-1 on one side. The developed model allows treating not only non-linear heat transfer but also the non-linear structural behaviour of the plasterboard partition under thermal stresses taking into account the rigidities versus temperatures for the punctual screwing of plasterboards on the steel studs. The prediction of the numerical model was compared with experimental results in terms of temperature and out-of-plane displacements of the partition. The comparisons permit to show the capability of the numerical model to predict appropriately the fire behaviour of plasterboard partitions.

1 PROCEDURE FOR MODELLING OF PLASTERBOARD PARTITIONS

In order to model the fire behaviour of plasterboard partitions, the first step was the development of a thermal model in order to determine accurately the temperature distributions through the partition. These temperatures were used as input data for the thermo-mechanical model. One assumed a weak coupling of the two models.

1.1 Heat transfer model

The heat transfer numerical analysis was performed using the software Cast3M from which was determined the temperature distribution in the cross-section of the partition when it was exposed to the standard fire. The assumptions used for the thermal analysis were as follows:

- The temperature field was uniform throughout the height of the partition. This assumption leads to a 2D thermal model instead of a 3D one, which reduces largely the computation time;
- Double plasterboards layers constituting the two facings were considered as an equivalent homogeneous material. The contacts between the different elements of the partition were assumed to be perfect and the fixing system (screws) was not modelled.

Thermal analysis was conducted on a 2D model using 4-node linear elements (Q4). The facings were subdivided into several layers depending on the thickness of the facing. The thermo-physical properties of steel are those given in Eurocode 3 (Part 1-2), while those of the plasterboards were identified versus temperature by a characterization program and shown in fig. 1 and 2. It must be noted that the evolution of the water content, the phase change due to evaporation of water and mass transfer due to migration of water vapour in the material were implicitly taken into account via the variations of its properties.

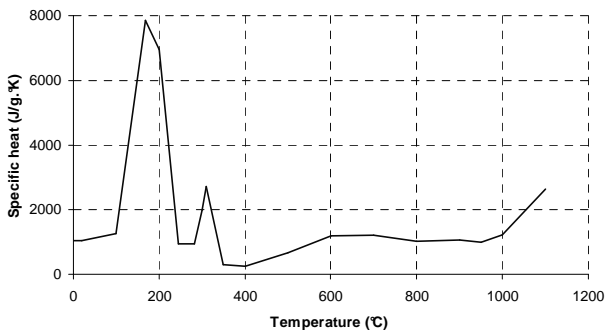


Fig. 1 Specific heat of plasterboard

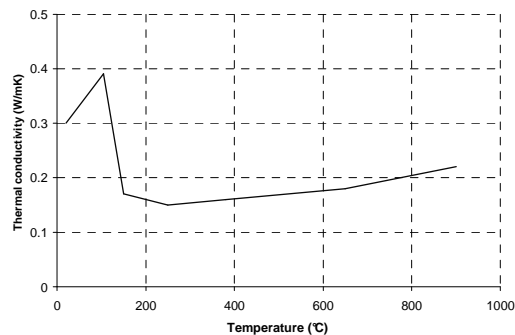


Fig. 2 Conductivity of plasterboard

In the model, one introduced a parameter t_{fall} in order to represent the time at which the exposed facing fell. One supposed that after this time, only the unexposed facing was still in place. This time, which was determined from the test, was used to define the two periods of calculation: period 1 (from 0 to t_{fall}) and period 2 (from t_{fall}). The boundary conditions and thermal loading for the two periods (example $t_{fall} = 100$ minutes) are presented in fig. 3 and 4.

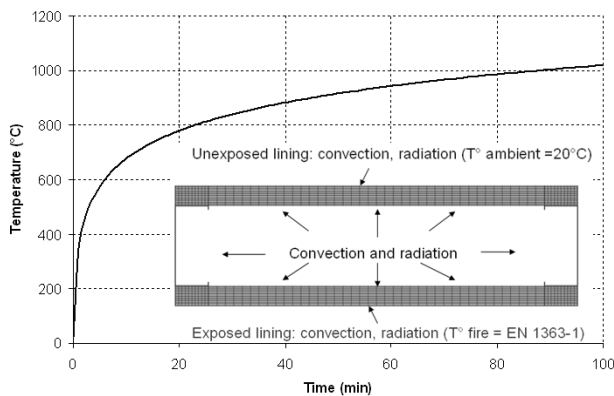


Fig. 3 Boundary conditions and thermal load for period 1

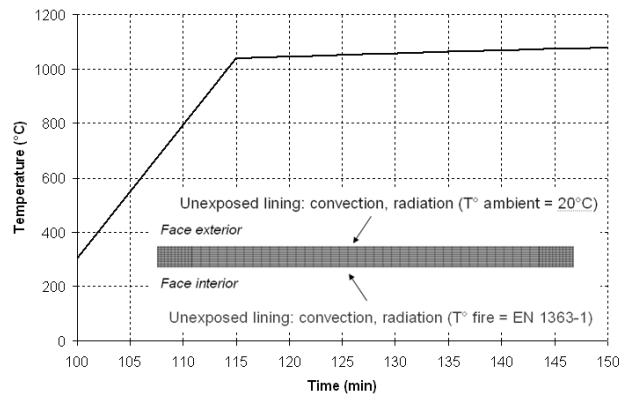


Fig. 4 Boundary conditions and thermal load for period 2

1.2 Thermo-mechanical model

The numerical modelling of structural response to fire action was carried out using the software Cast3M. The assumptions made for the thermo-mechanical analysis were as follows:

- The facings were considered as a continuous membrane without interruption along the full height (no horizontal joints between boards of a same layer). The double layers of plasterboard were considered as a equivalent homogeneous material;
- The exposed facing was supposed to remain in place during the simulation. Its loss was taken into account through the drastic reduction of its thermo-mechanical properties.

The plasterboard partition was modelled in 3D as an assembly of finite multi-layer shell and interface elements. The finite multi-layer shell elements with non-linear evolution of the temperature between the two faces were adequate. To do this, Cast3M uses the Kirchhoff theory (thin plate) for the formulation of its four-node shell element. The thermal expansion, geometric and material non-linearities were taken into account for all elements. Screws for connections were modelled by the interface element (JOINT3D) of Cast3M (Pegon et al, 2001) with an elastic behaviour. The Eurocode 3 (Part 1-2) steel properties were used. For plasterboard, Young's modulus and yield strength were determined by a 4-point bending test at different temperatures up to 400°C. When the temperature of the gypsum exceeds 400°C, i.e. when the cardboard of plasterboard is totally charred, its elastic modulus and yield strength can be assumed to decrease down to zero at 1200°C. It is noted that with a new product, the same characterization program must be performed to identify its thermo-physical and thermo-mechanical properties. Fig. 5 and 6 show the variation of the thermo-mechanical properties of plasterboard versus temperature:

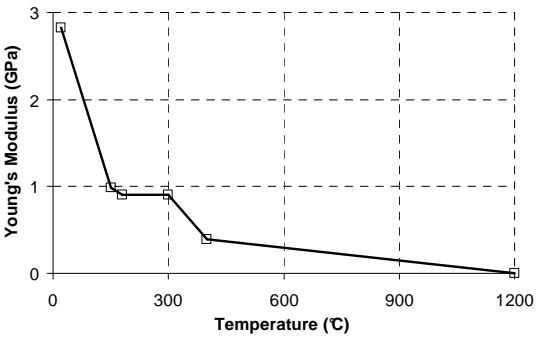


Fig. 5 Elastic modulus of plasterboard

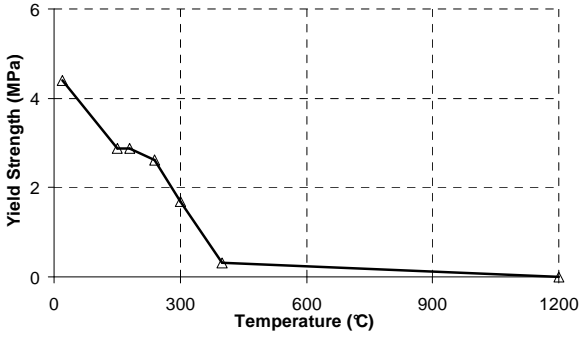


Fig. 6 Yield strength of plasterboard

2 VALIDATION OF DEVELOPED NUMERICAL MODEL

2.1 Experimental reference test

The reference fire test was conducted with a 5x4 m (h x w) partition. The frame of the partition was made of 8 lipped C-section steel studs 100 x 50 x 0.6 mm (h_{web} x w_{flange} x t_h) spaced at 600 mm. A 50 mm gap was provided at the top of the steel studs to allow free expansion. The facings were made of two 15 mm layers of fire quality plasterboards. The joints between boards of both layers were staggered. Boards of both layers were screwed together along horizontal joints. The facings were fixed on studs by screws at 300 mm centres and at 100 mm centres on upper and lower tracks. Fig. 7 shows the plasterboard partition.

This partition was heated on one side according to the standard fire curve EN 1363-1 and expressed by the following formula: $T_f = 345 \log(8t + 1) + T_{amb}$, where t is the time in minutes and T_{amb} is the ambient temperature in the furnace at 100 mm from the exposed side, in Celsius degrees. Temperatures measuring sections and out-of-plane displacements at different levels were distributed over the partition. On the studs, the thermocouples were placed on the exposed and unexposed flanges as well as at 1/4 and 3/4 height of the web. On both facings, thermocouples were installed at interface between double layers and on unexposed sides. The out-of-plane displacements were measured in 3 locations by displacement sensors placed on the unexposed side. Locations of the instrumentation are shown in Fig. 8.

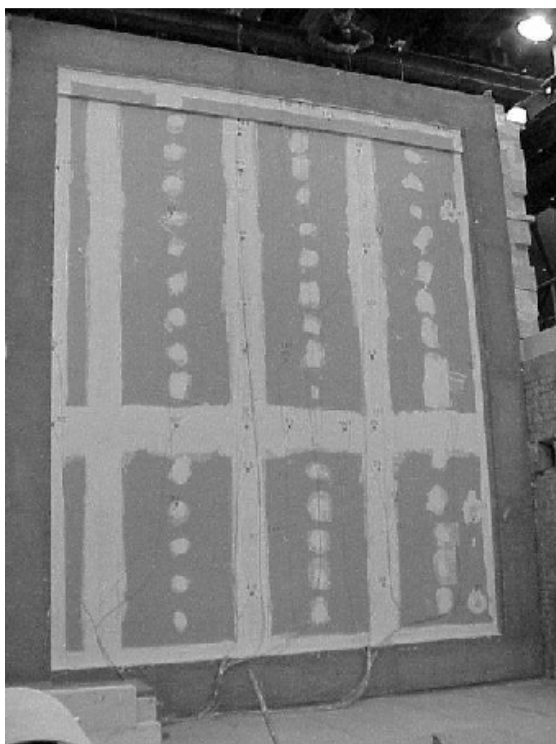


Fig. 7 Plasterboard partition

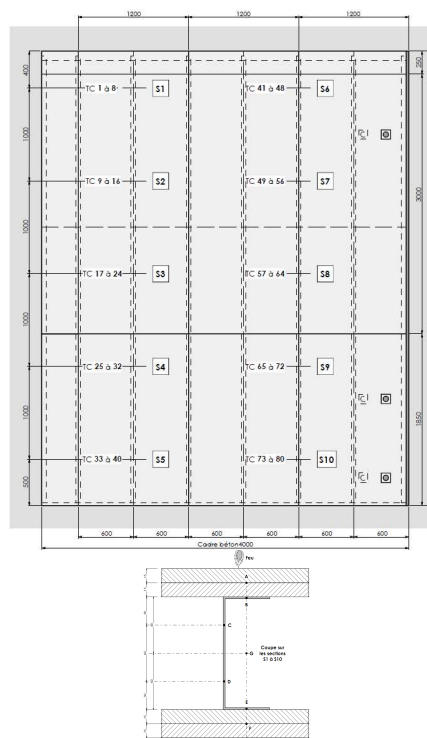


Fig. 8 Locations of the instrumentation

During the fire test, the partition bent towards the furnace, due to the expansion of the studs. One observed that the horizontal joints were a weak point of the partition. They tended to open earlier than the vertical joints. This opening allowed the passage of hot gases inside the cavity, which raised quickly the temperature of the steel studs and also increased considerably the deformation of the studs. At 100 min around, the first fall-down of parts of exposed facing occurred. This phenomenon was progressive and did not affect the whole exposed area of the partition at the same time. When the exposed facing fell, the steel studs were directly exposed to fire and their temperatures increased rapidly and quickly exceeded 900°C , a sufficient temperature to ensure that there was no more load-bearing capacity still present in any part of the studs. The studs eventually buckled and failed locally. After this moment, one observed the displacement of the partition towards the side opposite to the fire because of the contraction of the unexposed facing as it was still attached to the studs and both tracks. At the end of test, unexposed facing was still in place and one did not observe any rupture on it.

2.2 Calibration results

The developed numerical model is validated against a full-scale fire test of plasterboard partition which was described above. Before modelling the structural behaviour, a thermal analysis was conducted by using the thermal model to predict the temperature distribution within the cross-section of the partition. To simplify the model, it was reduced to a common part between two consecutive studs of 600 mm along width (see fig. 9). This choice led to consider as a closed internal volume between the two studs and adiabatic conditions on both lateral edges of the model. Fig. 10 shows a mesh of the model. Based on the experimental test, one assumed that the exposed facing fell at 100 minutes ($t_{\text{fall}} = 100$ minutes). The predictions from the thermal model were compared with experimental results at several points in the cross-section. The comparisons are presented in fig. 11 and 12. One can note a small difference between average experimental temperatures and those calculated.

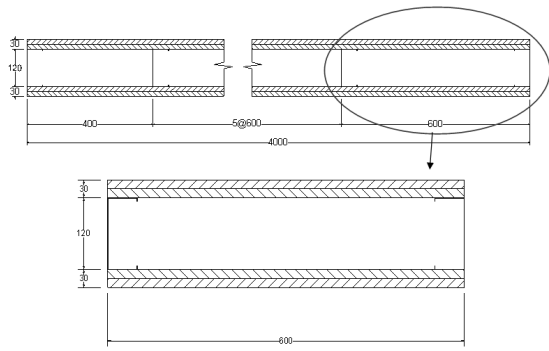


Fig. 9 Geometry for the thermal analysis

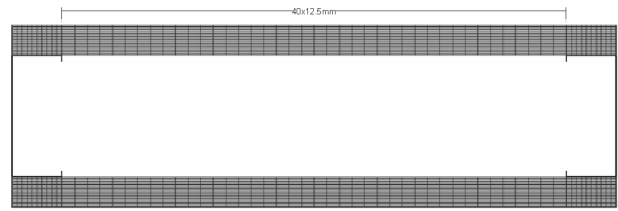


Fig. 10 Mesh of finite element model

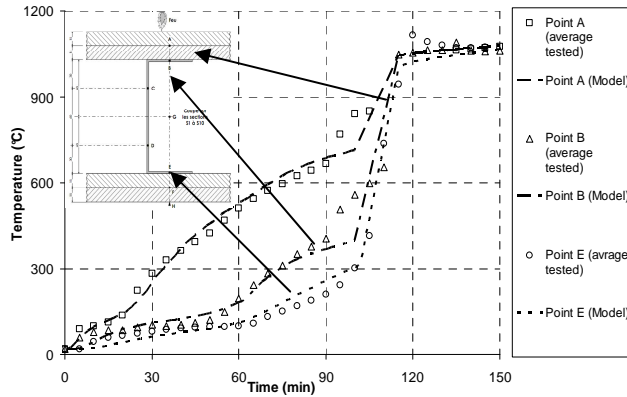


Fig. 11 Comparison between model and measure

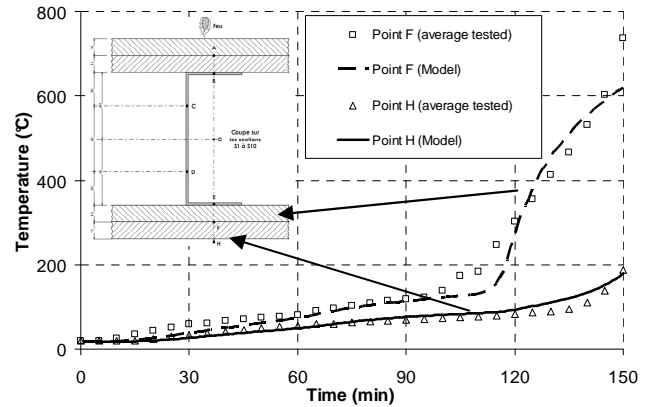


Fig. 12 Comparison between model and measure

Non-linear temperatures distributions calculated from the thermal analysis were incorporated into the temperature input file in order to simulate the structural behaviour of the partition. Fig.13 shows the finite-element mesh and boundary conditions considered for the thermo-mechanical model.

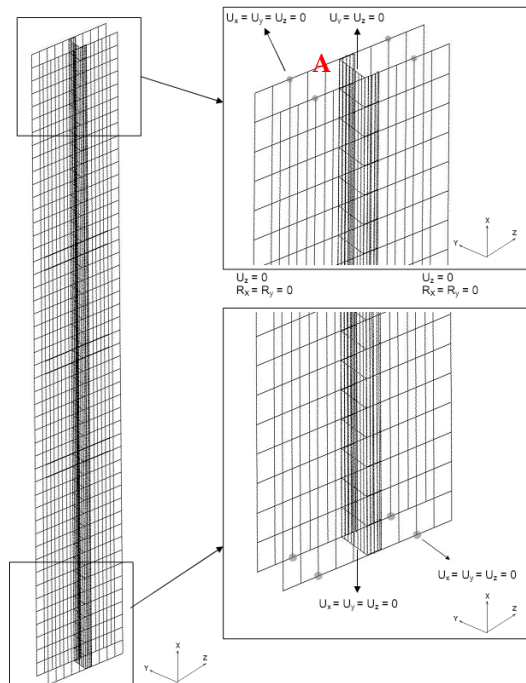


Fig. 13 Mesh and boundary condition

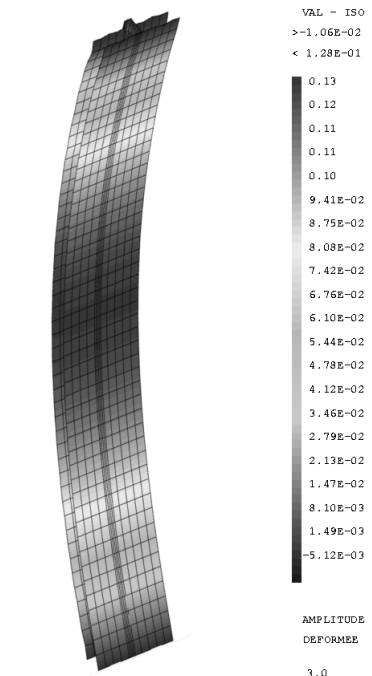


Fig. 14 Deformed shape at 107 minutes

Both longitudinal sides of facing, rotations about the X and Y axes and displacements in the Z axis were restrained. All displacements of eight points of the two facing were blocked in order to simulate the screwing on top and bottom tracks of the partition. For point A (see fig. 13) on the stud, displacements were restrained in the Y and Z directions, and allowed in the X direction.

The coefficient of thermal expansion assigned to the exposed facing was assumed without pre-drying. On the unexposed face, during the first 60 minutes, its temperatures were less than 100°C. It can therefore be assumed that the facing was subjected to a pre-drying for the first 60 minutes at least. The latter led to use different thermal expansion coefficients for the exposed and unexposed facings. Fig. 14 shows the deflection shape of the partition at 107 minutes (maximum deflection). Fig. 15 shows the comparison of the maximum deflection at mid-height of the partition between the prediction of the model and the test result. One can observe that the predictable displacement from the model was under-estimated of about 20 mm when compared to measured displacement. This difference might be caused by the deformation of the concrete frame used as supporting construction for the tested partition and not taken into account in the model.

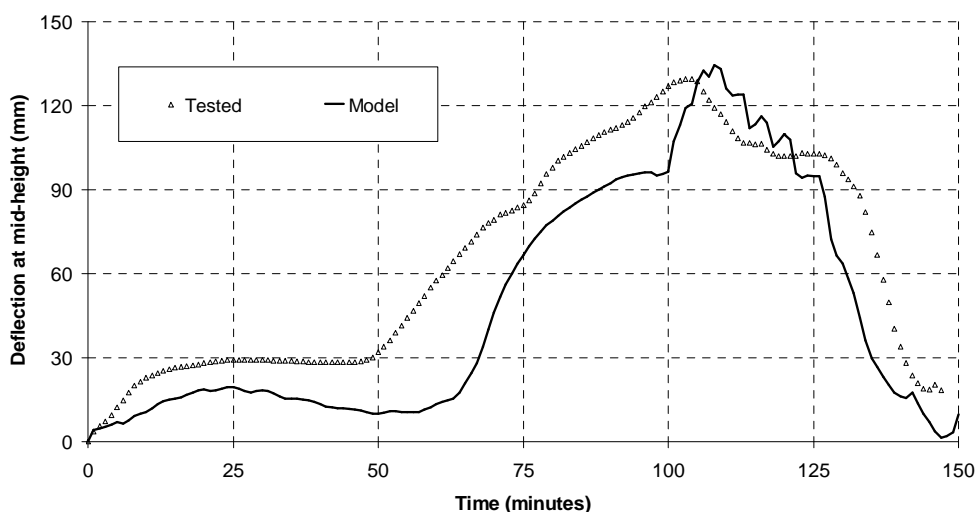


Fig. 15 Comparison of predicted deflection at mid-height of the partition with test result

3 CONCLUSIONS

In this paper, the development of thermal and thermo-mechanical models to simulate the plasterboard partition in fire has been described. The proposed model allows dealing with non-linear heat transfer as well as non-linear structural behaviour of the plasterboard partition from thermal stresses, taking into account specific rigidities versus temperatures for the punctual screwing of plasterboards on the steel studs. The predictions of model show a good correlation with the test results.

REFERENCES

- Cast3M, Finite element software (version 2010), <http://www-cast3m.cea.fr/>
- Cramer S. M., Friday O. M., White R. H., Sriprutkiat G., Mechanical Properties of Gypsum Board at elevated temperatures, Fire and materials 2003: 8th International Conference, 2003
- Feng M., Wang Y. C., Davies J. M. Thermal performance of cold-formed thin-partitioned steel panel systems in fire. Fire Safety Journal 38, 365–394, 2003.
- Chen C. J., Lee T. L., Jeng D. S. Finite element modeling for the mechanical behavior of dowel-type timber joints. Computers and Structures 81, 2731-2738, 2003.
- Eurocode 3 – Part 1.2: Calculation of steel structures – Fire behaviour, 1993.
- Pegon P, Pinto A.V., Gérardin M., Numerical modelling of stone-block monumental structures, Computers and Structures 79, 2165-2181, 2001.

FIRE SIMULATION APPLICATION IN FIRE SAFETY DESIGN FOR TUNNEL STRUCTURES

Aleš Dudáček^a, Isabela Bradáčová^a, Petr Kučera^a

^a VŠB – Technical University of Ostrava, Faculty of Safety Engineering, Ostrava, Czech Republic

INTRODUCTION

The developing Trans-European Rail network made up of the high-speed and conventional rail networks must ensure safe, uninterrupted, efficient, high-quality and user-friendly transport for users as well as operators.

The rail transport network also includes tunnel structures. A possible occurrence of a tunnel incident may have considerable negative impacts on people and property.

The consequence of a tunnel incident is then traffic suspension of quite long duration together with direct endangering people in the tunnel and possible great material loss of and damage to cargo, rail vehicles and tunnel structure and its equipment.

When comparing the probability of an incident in a road tunnel with that of an incident in a railway tunnel it is possible to state that the probability of an incident in a railway tunnel is, owing to the nature and method of rail traffic control, substantially lower than in the case of road tunnels. With regard to a large number of people carried by passenger trains, a potential incident can however affect a markedly greater number of people under worse conditions of their evacuation (difficult quick leaving the coach, limited width of the escape walkway along the train, etc.).

On the basis of risk analysis, scenarios for specific incidents in tunnels, such as collision, derailing, fire, explosion, toxic gas release, and spontaneous evacuation have been developed.

To ensure interoperability and required level of safety, European regulations lay down essential requirements that must be fulfilled in the trans-European rail system:

- safety
- reliability and availability
- health
- environmental protection
- technical compatibility.

In the area of fire safety, the satisfaction of the essential requirements is shown by means of fire safety design on all levels of land-planning and design for tunnel construction. Minimum safety limits are set, e.g. in Commission Decision 2008/163/EC (TSI, 2007), and other requirements are stated in thematically relevant national standards (ČSN 73 7508, 2002).

However, the complexity of showing the fulfilment of generally formulated requirements calls, more and more frequently, for choosing approaches different from standard (conservative) approaches which do not provide any integrated view of the situation being solved, and which often are not able to consider it at all.

More and more experts all over the world are thus concerned with more general, mathematically describable models based on selected fire scenarios. Subsequently, efforts appear to describe, as trustworthy as possible, a fire, to model its development, smoke and combustion product spread, to express opacity, to deal with the transfer of heat through a structure, and to describe other important manifestations of the fire.

1 EVACUATION ANALYSIS

To verify the safe evacuation of people in case of fire on a train set in a railway tunnel, the following tasks were solved:

- development of temperatures during a fire in a tunnel
- smoke stratification during a fire in a tunnel
- evacuation time assessment.

2 MODELLING OF TEMPERATURE DEVELOPMENT AND SMOKE STRATIFICATION

In the design of escape walkways, the worst variant is usually considered, namely a fire on a coach in the vicinity of entry into the escape walkway (cross-passage or escape shaft). People thus can escape merely along unprotected escape walkways leading to the entry to a neighbouring cross-passage or escape shaft or to the exit through tunnel portals. In addition, in the identification of the most unfavourable site of the fire it is necessary, in the case of a longitudinally inclined tunnel tube, to consider the stack effect owing to which people escaping in the direction chosen incorrectly may be directly exposed to the products of combustion.

In the determination of temperature and smoke distributions in the tunnel, the program FDS (Fire Dynamics Simulator), current version 5 was used.

2.1 Geometry of a Tunnel Model

In Fig. 1 the part of the tunnel tube that will be used not only for modelling the spread of fire and combustion products but also for the assessment of evacuation of people is given. People can escape along an unprotected escape walkway towards the entry to an escape shaft situated 605 m from a portal. The model tunnel length is selected at 610 m, width at 12 m and the maximum height of the tunnel arch at about 8 m. Fire simulation time is 20 minutes.

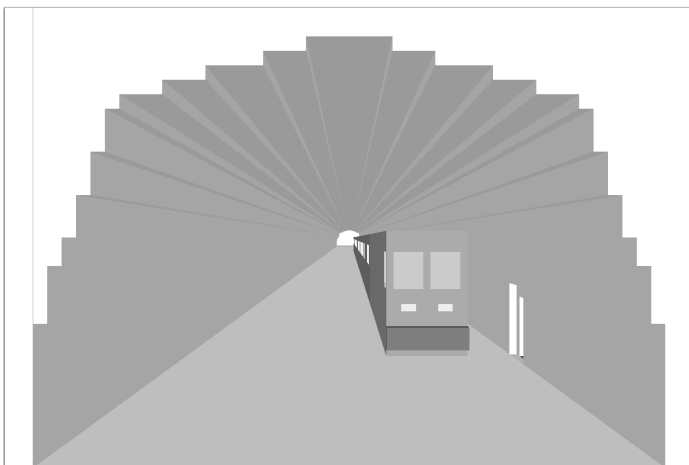


Fig. 1 Simplified cross-section of bi-directional tunnel tube

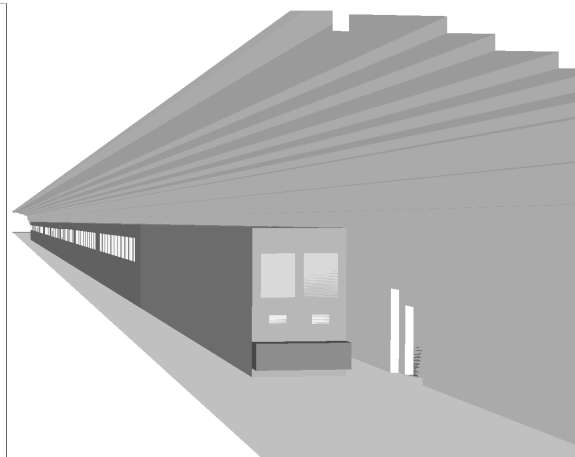


Fig. 2 Geometry of train set

2.2 Geometry of a Train Set

For simulation, a passenger train set consisting of eight coaches and a locomotive of the total length of 225 m is selected. The shape of train of this train set is simplified to one elongated rectangle divided into the locomotive and 8 passenger coaches, divided from each other by partitions. Along the sides of the coaches, window openings are distributed evenly. The front of the train is placed near the exit portal. A fire in the first coach is assumed.

2.3 Definition of a Fire

A fire is defined by means of heat release rate determined on the basis of data from the German railways (Deutsche Bahn AG, 2000). Values of passenger train fire development during the first 20 minutes grow gradually to 21 MW.

2.4 Graphic representation of results concerning the distributions of temperatures and smoke in the tunnel

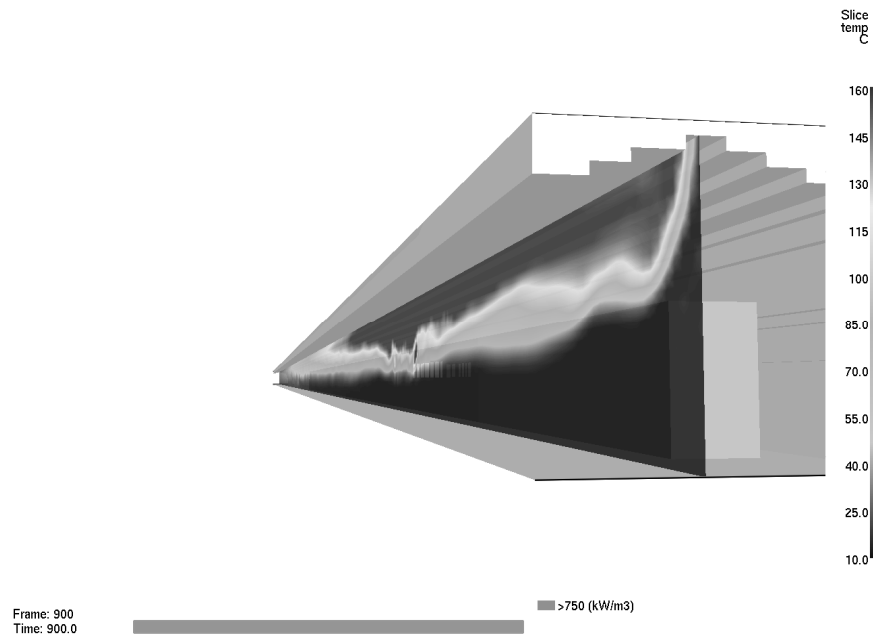


Fig. 3 Isotherm in the longitudinal cross-section of tunnel in the vicinity of fire seat in the 15th minute



Fig. 4 Isotherms just behind the train set at 40 °C - 60 °C in the 15th minute

Note: These limit temperatures will not occur at heights less than 2.5 m on the walkway; they will not endanger in any way people escaping towards the entry to the escape shaft. Total evacuation time according to program SIMULEX is about 12 minutes.

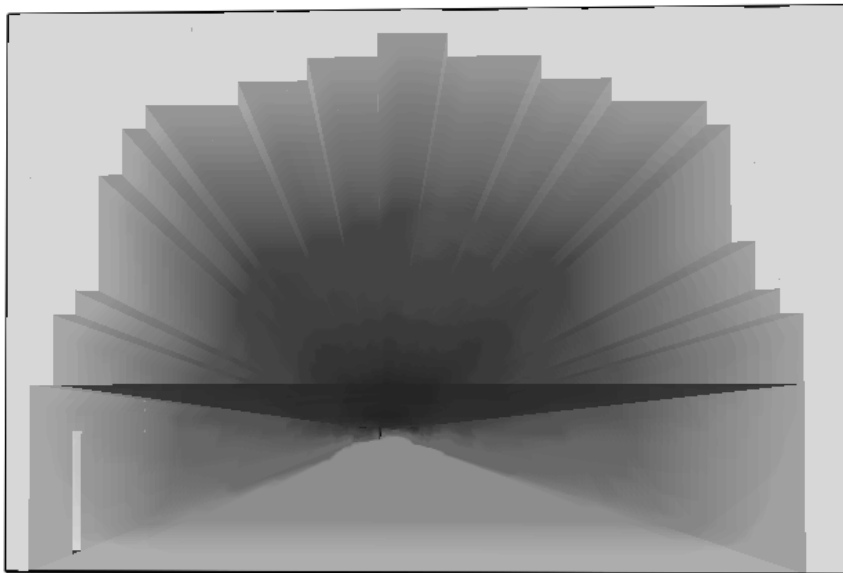


Fig. 5 Smoke layer at the entry to the escape shaft in the 12th minute
(line across the tunnel tube represents the 2.5 m height)

Note: Cooled smoke layer will diminish visibility on the escape walkway already at the end of evacuation; however, escaping people will not be endangered.

3 EVACUATION TIME ASSESSMENT

The aim of evacuation assessment using a SIMULEX model is to identify critical points for evacuation in the railway tunnel concerned, and to verify whether the designed escape walkways will enable people to leave through the tunnel escape shaft the space of affected tunnel tube in a sufficiently short time.

3.1 Geometry of the Tunnel Model and Preconditions for Evacuation

For the purpose of evacuation assessment, the evacuation of people from the train set, which considered a stop of the train set near the exit portal, in the point of smallest height, was selected. Evacuating people thus can escape in two directions along the unprotected escape walkway along the tunnel tube – towards the tunnel portal and towards the entry to the escape shaft. A distance between the portal and the entry to the escape shaft is 605 m, escape walkway width is 1.1 m and width of door to the tunnel shaft is 1.4 m. The estimated number of passengers in the set is 840.

The escape of people from the train set takes place in both the directions; that is why at setting calculations in the program SIMULEX, one half of the passengers of the train set (320 passengers) is designed to escape towards the portal and the other half of the passengers towards the entry to the escape shaft. People making for the portal will walk along the far escape walkway to avoid the effects of heat from the burning coach.

The walking speed of people is 1.0 m/s on a flat surface (corresponds to the dimensions of an average man). However this speed is not constant; it changes depending on the density of people at a certain place and time.

Before starting the evacuation of people, a 30 s time delay, which expresses the time required for informing the passengers by the train crew about the start of evacuation, is considered.

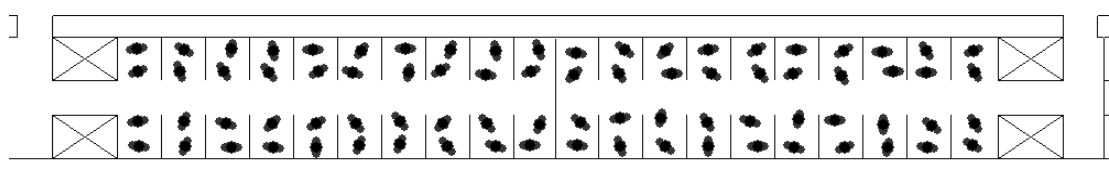
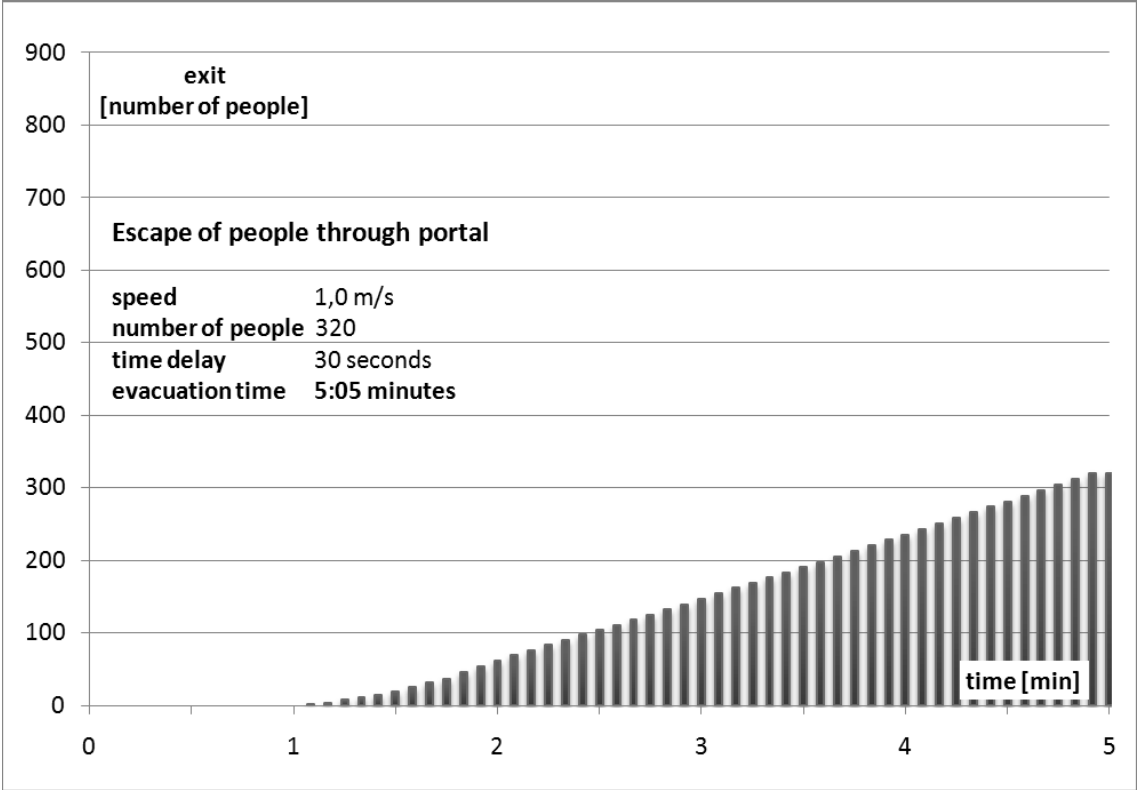


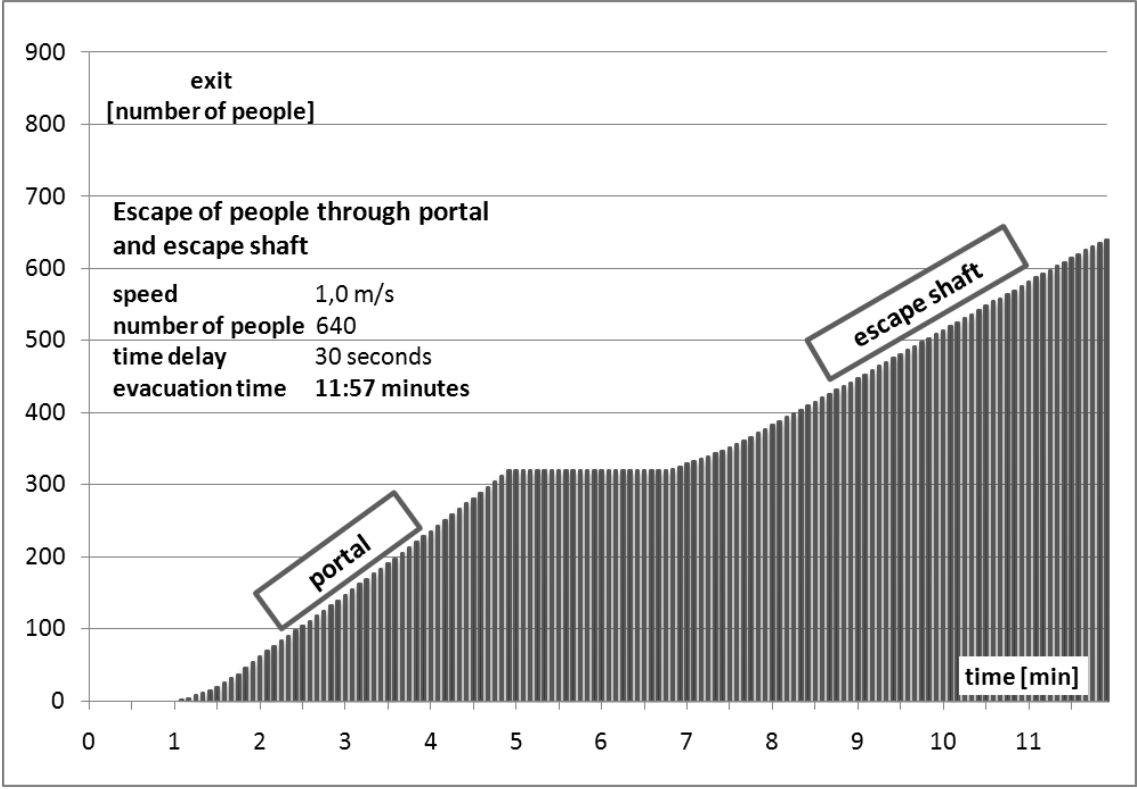
Fig. 6 Visualisation of placement of people in a coach

The placement of people in individual coaches is even. The space is divided longitudinally into two parts by an escape aisle. To direct the evacuation better an auxiliary dividing line is there in the median part of the coach, which guides evacuating people towards the nearer escape door.

3.2 Output Data



Graph 1 – Dependence of number of people escaping through the portal on time



Graph 2 Dependence of number of people escaping through the portal and the escape shaft on time

4 SUMMARY

By the program SIMULEX the time necessary for the evacuation of people was determined. The evacuation was carried out in two directions – towards the tunnel portal and towards the entry to the escape shaft. In spite of the fact that the division of evacuating people was made into two equal parts, the times of evacuation in individual directions were markedly different. The evacuation of people towards the tunnel portal took only 5 minutes, whereas the evacuation towards the entry to the escape shaft lasted 11:57 minutes and was thus the factor decisive of the determination of total evacuation time. The cause of the longer evacuation time was especially the distance-to-exit, i.e. the length of unprotected escape walkway.

Using the program FDS, the distribution of temperatures, the level of smoke layer and visibility during the fire on the train set in the tunnel were determined.

On the basis of simulation performed using the program FDS for the selected fire scenario (14 MW in the 15th minute at flow of 2 m/s) it is possible to state that the isotherm of 40 °C below the upper hot layer will not shift in the course of evacuation (12 minutes) below the height of 2.5 m above the escape walkway. Toxic combustion products will be accumulated mainly in the upper hot layer, it means above this isotherm. The isotherm of 40 °C was selected as acceptable temperature for the short-term stay of people during evacuation in the affected tunnel tube.

By means of program FDS visibility was also verified; the limit value of visibility is 10 m. In the course of evacuation, the visibility changed minimally, the value of 30 m decreased merely in the vicinity of the burning coach; otherwise, the visibility above the escape walkway during evacuation of people will not be less than 30 m.

5 CONCLUSION

By modelling using the computer programs it has been verified that people will leave the tunnel within 12 minutes and that in the course of evacuation they will not be endangered by high temperatures and smoke. Moreover, it has been verified that the visibility (opacity) along the walkways is satisfactory.

REFERENCES

TSI – Commission Decision 2008/163/EC concerning the technical specification of interoperability relating to safety in railway tunnels in the trans-European conventional and high-speed rail system 2007.

ČSN 73 7508: Železniční tunely, ČNI, září 2002.

Deutsche Bahn AG – Ergebnisbericht zur Beurteilung von Branden an Schienenfahrzeugen als Bemessungsbrände zur brandschutztechnischen Auslegung von oberirdischen Personenverkehrsanlagen der Deutschen Bahn AG; Deutsche Bahn AG, DB Station & Service, Fachstelle Brandschutz, Frankfurt am Main, September 2000.

ČSN 73 0802. Požární bezpečnost staveb. Nevýrobní objekty. ÚNMZ 2009.

SIMULEX 11. 1. 3 – User's Guide, Copyright Integrated Environmental Solutions Ltd. 1998.

FIRE ANALYSIS OF RC PRECAST SEGMENTAL TUNNELS

Giovanna Lilliu ^a, Alberto Meda ^b

^a TNO DIANA BV, The Netherlands

^b Universita' di Roma "Tor Vergata", Italy

INTRODUCTION

Tunnel construction with Tunnel Boring Machine (TBM) is today the most extensively adopted method both in soft soil and rock. The tunnel lining is usually made of precast reinforced concrete segment elements. Study of the tunnel behaviour under fire conditions is a relevant topic (Pichler et al. 2006, Savov et al. 2005, Ulm et al. 1999, Varley and Both 1999), also due to several accidents that have occurred in recent years.

The effect of fire exposure is not related to the material degradation solely, but the actions that can arise due to the thermal expansion can jeopardise structural safety. Regarding the material degradation, the main effect on this kind of structure is related to concrete spalling: in fact, precast segments are usually produced with high strength concrete, in order to speed the production process. However, spalling can be avoided with the use of a proper mix design or by adding polypropylene fibres. The other aspect is related to material degradation under elevated temperature: this effect should be considered coupled with the stresses that can occur due to the thermal expansion of the tunnel lining.

The analysis of a lining with the typical characteristics of a tunnel built in soft soil is considered in this paper. Analyses are performed with the FE program DIANA. In the analysis, excavation of the tunnel is modelled first in order to predict stresses in the lining due to the soil pressure and after this the fire exposure is considered. The nonlinear behaviour of the reinforced concrete lining is taken into account in order to simulate the actual behaviour.

The results show the importance of a complete analysis of the structure, the ability to consider the interaction with the soil and the degradation of the concrete lining.

1 TUNNEL MODELLING

The tunnel is modelled in 2D, under the assumption of plane strain. A construction phase analysis is performed in order to simulate the different construction phases and the exceptional event due to the fire.

In the first phase, only the soil is considered and stresses are initialized adopting the K0 procedure. Three layers of soil are present: the most superficial layer, 1 m deep, is modelled as linear elastic. The second layer, with a depth of 10 m, is made of non-cohesive material with Young's modulus $E = 340$ MPa and friction angle $\phi = 35^\circ$. Finally, the third layer is a cohesive soil with a depth of 50 m, $E = 400$ MPa, cohesion $c = 3000$ Pa and $\phi = 27^\circ$. The second and third layers of soil are modelled with a Mohr-Coulomb model (Fig. 1). In order to prevent volume expansion in case of unloading of the soil, the Young's moduli adopted in the analysis are those obtained in a triaxial test, during unloading.

In the second phase, excavation and installation of the tunnel are considered, with the tunnel segment being connected to the surrounding soil with interface elements following a friction Coulomb material model with tension cut-off. The thickness of the tunnel segment is 400 mm. Reinforcement is placed at the extrados and the intrados of the tunnel, with a cover of 50 mm.

Finally, effect of fire is considered on the inner part of the tunnel segment. The adopted fire curve (temperature versus time) is the RWS law (Efectis Nederland 2008), typical for hydrocarbon fire (Fig. 2). Fire is considered only on the tunnel lining above road level.

For modelling the effect of the fire, a partially-coupled thermo-mechanical analysis is performed. In the thermal analysis the effect of increasing temperature in the structure is modelled by solving the Fourier equation for heat transfer considering conduction, convection and radiation effects.

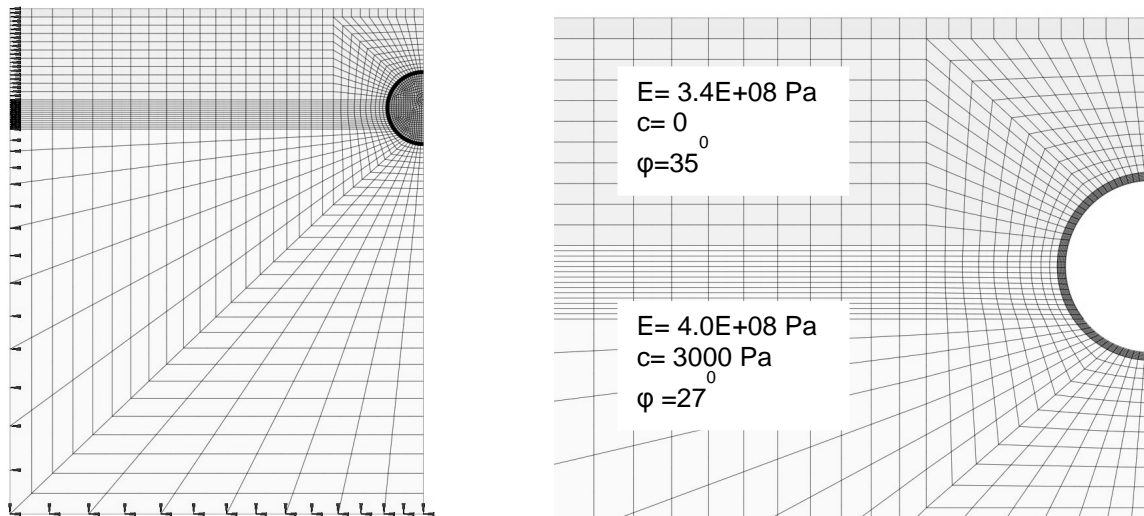


Fig. 1 Soil model.

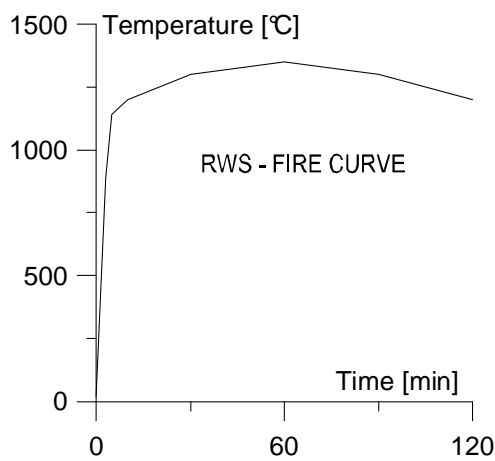


Fig. 2 RWS fire curve.

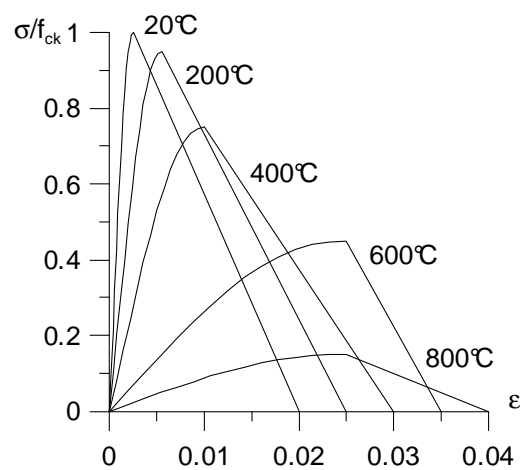


Fig. 3 Concrete in compression.

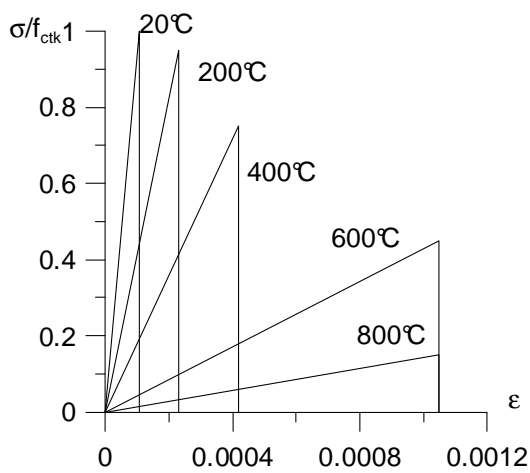


Fig. 4 Concrete in tension.

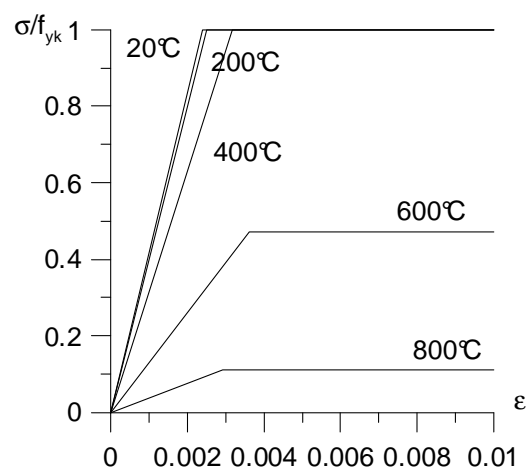


Fig. 5 Steel reinforcement.

In the stress analysis, the adopted constitutive material laws are those suggested in the Eurocode 2 (EN1992-1-2). The stress-strain curve for concrete in compression is shown in Figure 3. Eurocode 2 does not give any indication for concrete in tension. In this analysis it has been chosen to use an

elastic-brittle relationship for concrete in tension, with tensile strength and Young's Modulus decaying with temperature as they do in compression (Fig. 4).

The steel reinforcement, considered embedded in the concrete elements, follows an elasto-plastic behaviour with yielding strength decaying with temperature as described in the Eurocode 2 (Fig. 5).

2 RESULTS

Figure 6 shows results at the analysis step corresponding to installation of the tunnel. On the left, the vertical stresses in the soil surrounding the tunnel is depicted, while the principal stresses in the lining are shown on the right. It can be observed that the lining is subjected to prevalent bending moment with part of the structure under tension. This is a typical situation of a tunnel excavated in soft soil near the surface.

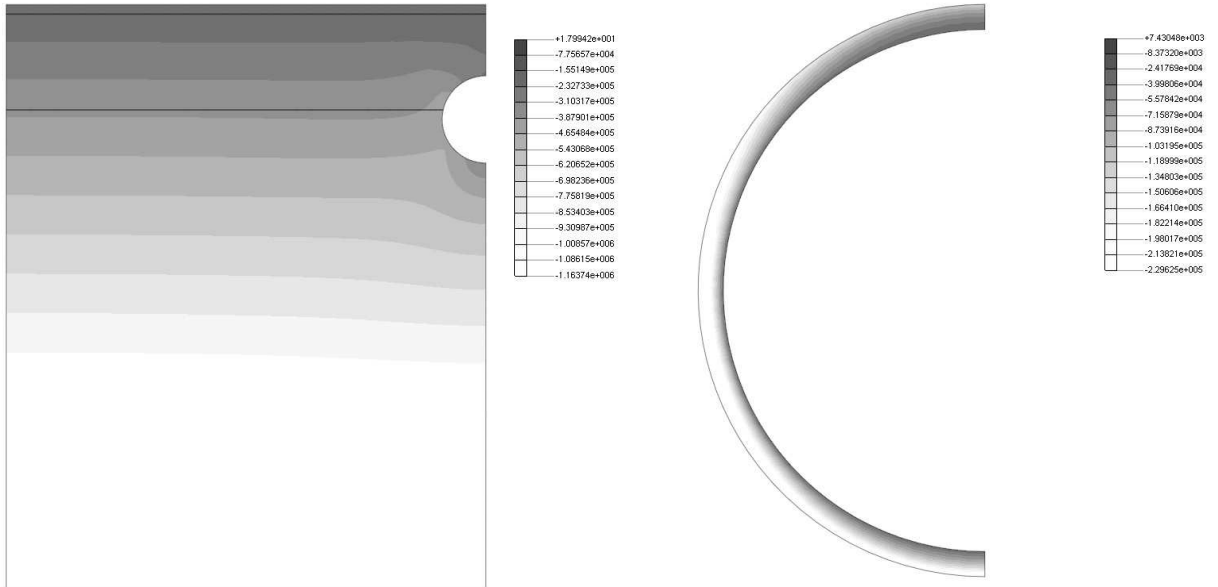


Fig. 6 Stresses in the soil and in the lining after installation of the tunnel (values in N/m²).

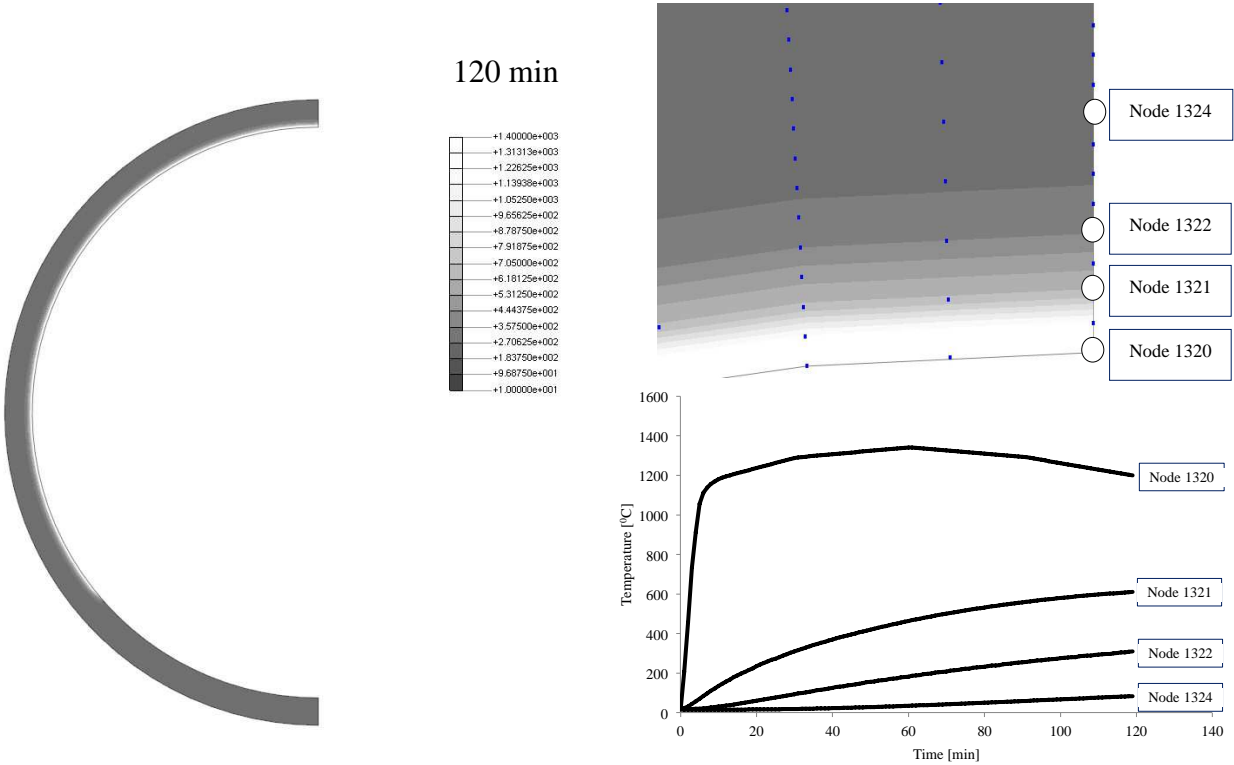


Fig. 7 Temperature development.

After this step the fire is considered. The thermal analysis is performed in steps of 1 minute up to 120 minutes of fire exposure. Figure 7 shows the temperature distribution in the lining after 60 minutes of fire exposure. It can be observed that after 120 minutes of fire exposure, only the first 60 mm of the lining reaches temperatures higher than 400 °C while temperatures of about 100 °C develop at a depth of 150 mm.

Figure 8 shows the crack propagation in the lining. The first cracks appear after 25 minutes of fire exposure. Several cracks are present after 30 minutes, with a concentration in the lower part of the lining at the road level. After 60 minutes all the lining is cracked.

Figure 9 shows the number of newly formed cracks versus time: it is evident that most of the cracks develop in the first 45 minutes of fire exposure.

It can be noticed that cracks are present at the outer part of the lining (Fig. 8) and they are caused by stresses induced by the differential thermal expansion. This aspect is important on the structural point of view: crack propagation causes a stiffness reduction in the lining, thus limiting the effect of the differential thermal expansion.

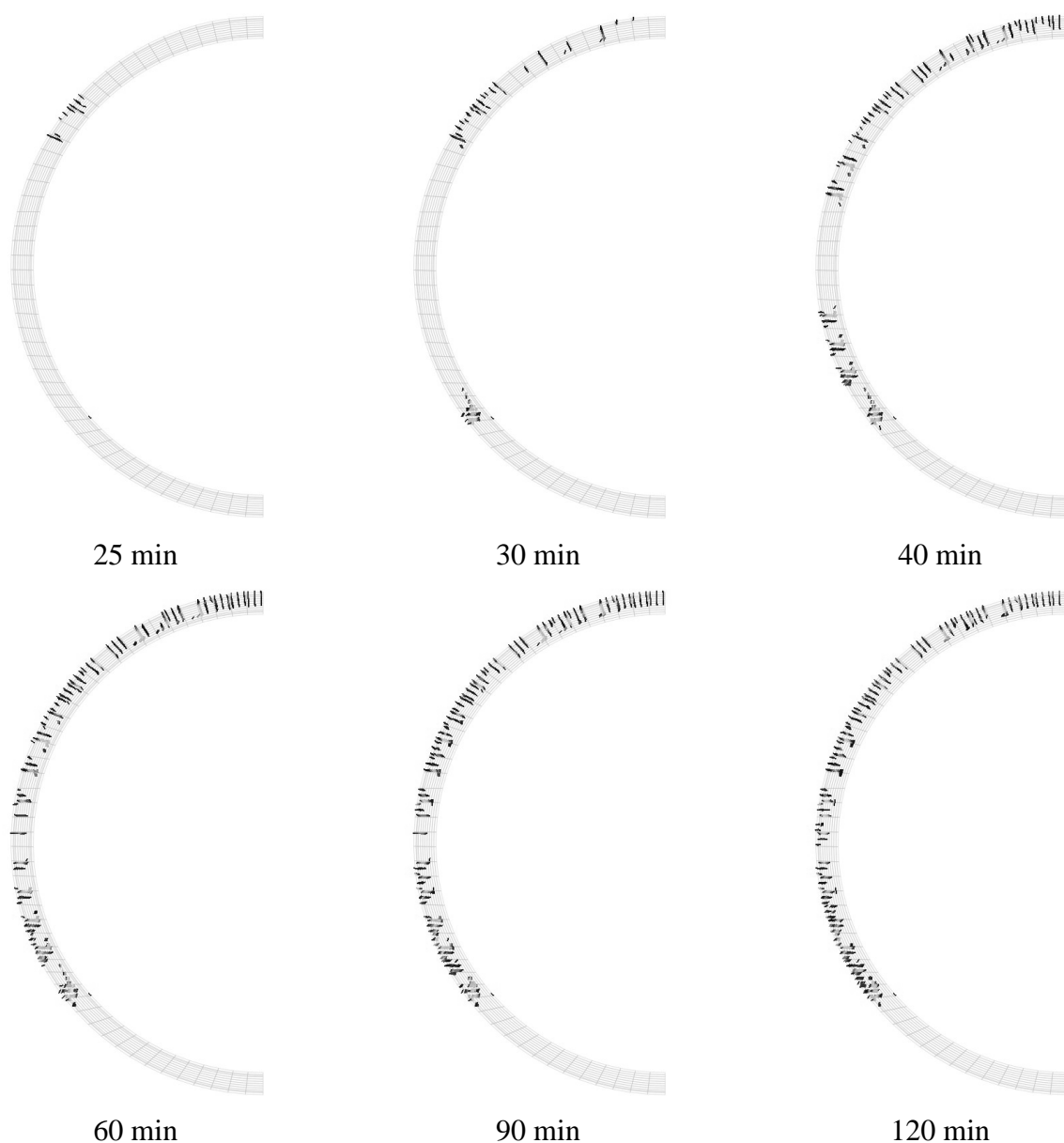


Fig. 8 Crack patterns during fire.

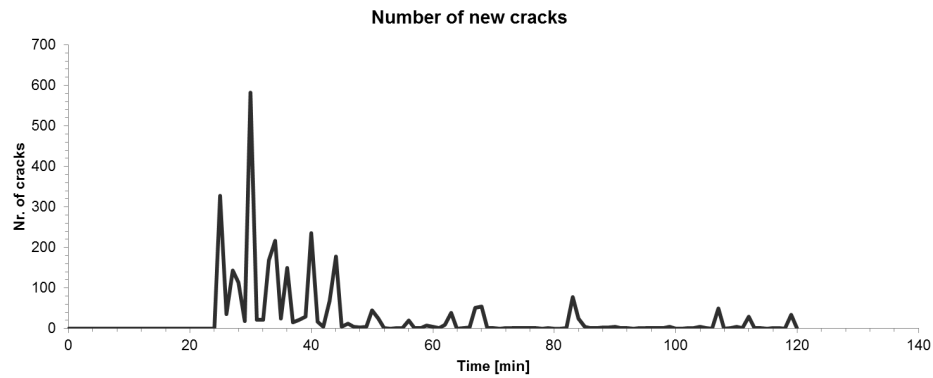


Fig 9 Crack development versus time.

At the inner part of the tunnel, only a small portion of the tunnel thickness appears to be damaged: this effect is not related to a high stress level but to the dramatic material degradation, due to the high temperatures that are reached. Figure 10 shows the equivalent plastic strain in the lining after 120 minutes fire duration.

The reinforcement remains elastic at the extrados whereas it yields at the intrados, due to the thermal degradation. Figure 11 shows the plastic strains in the reinforcements at the intrados, after 120 minutes fire exposure.

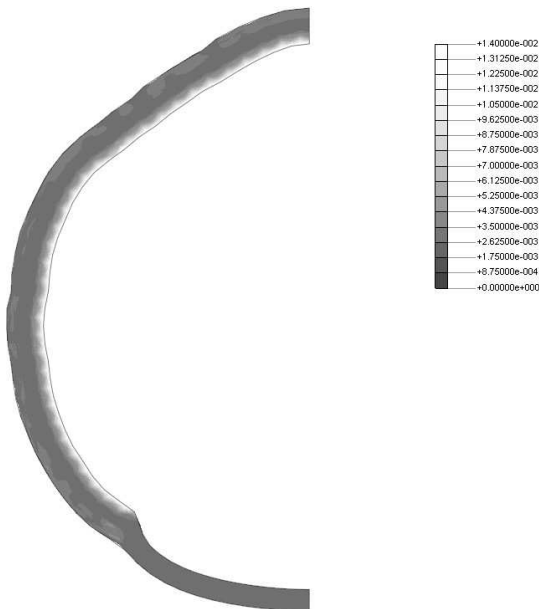


Fig. 10 Equivalent plastic strains.

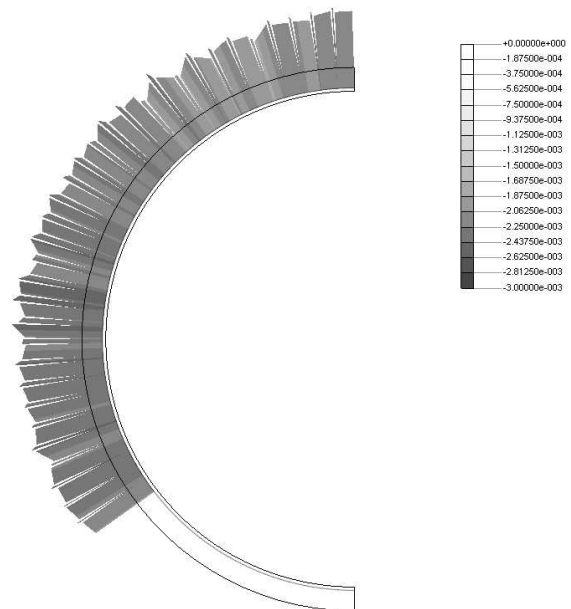


Fig. 11. Plastic strains in the reinforcement.

RESULTS

This paper presents a procedure for analysing the behaviour of segmental lining tunnels in soft soil under fire. The analysis considers construction of the tunnel and application of the fire afterwards. A partially coupled thermo-stress analysis is performed for modelling effects of fire, that cause both degradation of the material and stresses due to differential thermal expansion.

The results show that the lining is subjected to extensive cracking that allows a reduction of the stiffness and, as a consequence, a reduction of the stresses induced by the thermal expansion. Furthermore, damage in the concrete at the inner part of the tunnel is very limited and caused by the material degradation induced by the fire. Despite cracking and yielding of reinforcements, structural stability of the tunnel is ensured up to 120 minutes of fire duration.

This type of analysis requires the use of an adequate non-linear finite element code, able to consider soil-structure interaction, non-linear material behaviour and cracking in concrete, and the coupling between the thermal and the mechanical problem.

REFERENCES

- DIANA Users' Reference Manual, release 9.4, 2010.
- Efectis Nederland, Fire testing procedure for concrete tunnel lining, 2008.
- EN1992-1-2. Eurocode 2: Design of Concrete Structures - Part 1-2: General rules – Structural Fire Design. December 2004.
- Pichler C., Lackner R., Mang H.A., Safety assessment of concrete tunnel linings under fire load, ASCE Journal of Structural Engineering. Vol. 132, No. 6, 2006.
- Savov K., Lackner R., Mang H.A., Stability assessment of shallow tunnels subjected to fire load, Fire Safety Journal, Vol. 40, 2005.
- Ulm F.J., Acker P., Levy M., The ‘‘Chunnel’’ Fire. II: analysis of concrete damage, ASCE Journal of Engineering Mechanics. Vol. 125, No. 3, 1999.
- Varley, N., Both, C., Fire Protection of Concrete Linings in Tunnels, Concrete, May 1999.

PREDICTION OF TEMPERATURE VARIATION IN AN EXPERIMENTAL BUILDING

Xudong Cheng^{a,b}, Milan Veljkovic^a, Alexandra Byström^a, Naveed Iqbal^a,
Joakim Sandström^{a,c}, Ulf Wickstöm^{a,d}

^a Division of Structural Engineering –Steel Structures, Luleå University of Technology, Luleå, Sweden

^b State Key Laboratory of Fire Science, University of Science and Technology of China, Hefei, China

^c Brandskyddslaget AB, Karlstad Sweden

^d Swedish National Testing and Research Institute (SP), Borås, Sweden

INTRODUCTION

In view of recent large fires in tall buildings, structures have been observed to have easily lost stability or even collapse during fire. To understand such events, structural behavior under fire loading is more and more of a concern for researchers. Some numerical models have been developed to simulate the behavior of isolated structural components, but lack of validation with full-scale experimental data limit the use of models in fire safety design of structures (Buchanan, 2001 and Usmani et al, 2001). A series of fire resistance tests have been carried out during the last decade. Liu (Liu et al, 2002) and Buchanan (Buchanan, 2003) have completed some fire tests on isolated structural element, e.g. beams, columns and connections, in furnaces to help the development of design models. Some fire tests on reduced scale frame assemblies have also been conducted by Hosam (Hosam et al, 2004) and Yang (Yang et al, 2006). However, many aspects of structural behavior which occur due to the interaction between adjacent members could not be observed and the structural response of reduced scale models may be different from those of a real structure in fire. It is necessary to carry out some large scale fire tests under real nature fire. Dong (Dong et al, 2009) carried out some full-scale fire experiments of steel composite frames under furnace loading. Wade (Wade et al, 2006, Chlouba et al, 2009 and Wade et al, 2009) investigated the global structural behavior of steel-concrete composite frame building during large-scale natural fire tests at the Cardington laboratory and Mittal Steel Ostrava. Due to the high cost of full-scale fire tests and size limitations of existing furnaces, these valuable fire tests are not easy to be conducted frequently.

Two full-scale fire tests to investigate structural behavior under natural fire will be carried out in a two-storey composite frame building in Jilemnice, Czech Republic in September 2011 within the RFCS research project COMPFIRE Design of joints to composite columns for improved fire robustness, RFS-PR-08009. It is necessary to conduct some numerical calculation work to simulate the fire development and obtain prediction of fire development before the real fire tests. Fire dynamics simulator (FDS) is a program, which is frequently used by researchers to simulate different fire scenarios (Ryder et al, 2004 and Pope et al, 2006). In this paper, four fire scenarios with different locations of ignition sources for the full-scale fire test are simulated by FDS without mechanical load. The temperature variation of upper hot smoke layer is also obtained, which is important for the behavior of beam and connection. The effect of ignition on fire development was analyzed.

1 FDS MODEL OF FIRE SCENARIOS

FDS is a large eddy simulation (LES) model, which was developed by the National Institute of Standards and Technology (NIST). The primary assumption behind the LES technique is that the larger scale turbulence that carries the majority of the energy of the system, which needs to be directly resolved in order to accurately represent flow (McGrattan et al, 2010). FDS solves numerically a form of the Navier-Stokes equation appropriate for low-speed, thermally-driven flow with an emphasis on smoke and heat transport from fires.

The dimension of the two-storey composite frame building in Jilemnice is 12 m by 9 m by 8 m. There are five composite columns as shown in figure 1. A steel beam is mounted under the ceiling

and included in the FDS model of the fire. None of the structural components are fire protected. A door and a window are located on the wall for natural ventilation during the fire; the total opening area is 14m². The fuel consists of 24 timber cribs with the size of 1.0 m by 1.0 m by 0.6 m are uniformly distributed on the floor as shown in figure 2.

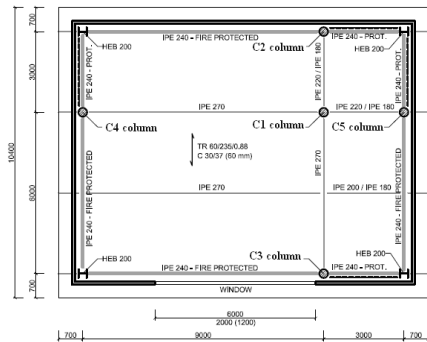


Fig. 1 Ground plan of the building

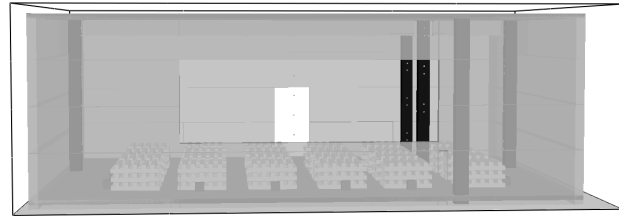


Fig. 2 FDS model of the building (one-storey)

In the FDS model, three different kinds of material are used: concrete, steel and wood. The thermal properties of these materials are shown in table 1, which are assumed to be constant during the fire. The timber crib is ignited by small ignition sources. There are four fire scenarios depending with different locations of the ignition source, such as four sides, center, four corners and one side of the wood fuel stacks. These are named as case1, case2, case3 and case4, respectively, in this paper. The heat release rate of the ignition sources is assumed to be developing in three steps, which linearly increases to the peak at 50 s at first, and keeps that state until 300 s, and at last decreases linearly to zero at 400 s. The approach for describing the pyrolysis here is assuming the solid fuels burn at a specific rate, which is dependent on the properties of the fuel, such as ignition temperature, thickness, heat of vaporization and heat release rate per unit area. The cell size within this model is 0.1 m by 0.1 m by 0.1 m except the area around the steel beam, where it is 0.05 m by 0.05 m by 0.05 m. The computational domain is divided into eight parts, so the parallel FDS calculation is used in these models to save running time.

Tab. 1 Properties of materials used in FDS model

Material	Density [kg/m ³]	Heat conductivity [W/K.m]	Specific heat capacity [J/kg.K]	Heat of combustion [kJ/kg]	Component member
Wood	400	0.2	1300	18000	fuel
Steel	7850	46.0	460	/	Column, beam
Concrete	2100	2.0	950	/	wall, ceiling, column

2 RESULTS AND DISCUSS

2.1 Heat Release Rate

Figure 3 shows the heat release rate (HRR) curves of the four different fire cases. The natural fire development process included four basic stages: ignition stage, fire growth stage, fully developed stage and decay stage. The fire develops as t-square fire model with different fire growth rates in the four fire cases. There are a series of small ignitions around the wood fuels in case 1, which can be seen from figure 2. The outer timber cribs are ignited at the same time, which probably will be used in real fire test. The fire develops so quickly that flashover appears at about 500 s, and the fire growth rate is about 32 W/s². In case 2 and case 3, the fire spreads from center and four corners, respectively, through various directions. There are no obvious differences between these two cases. The fire growth rate is about 5.4 W/s². In case 4, the fuels are ignited along one side and the fire travels from left to right. The fire develops very slowly with low fire spread rate. All the fuels are ignited after 3500s, and the fire growth rate of this case is only about 0.2 W/s², which is much lower than that of the other three cases because of the initial ignition condition.

The peak values of heat release rate in four cases are almost the same, which are about 26 MW. The period of fully developed stage is about 800 s. During this period, the compartment is nearly full of hot smoke, and the fire is controlled by the ventilation conditions. The peak value of heat release rate could also be calculated by *eq. (1)* (Karlsson et al, 2000), which assumes complete combustion of all the oxygen entering the compartment. The peak value from FDS simulation is a little lower than that from hand calculation, which should be caused by complete combustion assumption of oxygen. The performances of structural components are degraded and most buildings may collapse during this period. As the fuel consuming, the fire turns into the decay stage.

$$Q_{peak} \approx 1500A_0\sqrt{H_0} = 1500 \times 14 \times \sqrt{2} kW \approx 29674 kW = 29.67 MW \tag{1}$$

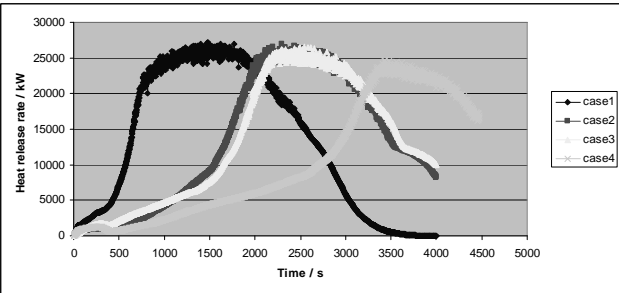


Fig. 3 Heat release rate of four fire cases

2.2 Hot Smoke Temperature

During the fire development, there are two main layers in the compartment: hot smoke layer and cold air layer. The temperature of hot smoke layer is the boundary condition of beam, ceiling, connections and others. Figure 4 gives the results of hot smoke temperatures of the four fire cases. The thermocouple sensor in FDS model is positioned in the center of compartment and 200 mm below the ceiling. The temperature values for the four fire cases reaches to about 600 °C before flashover with different increasing rates. During the fully developed stage, hot smoke temperature continues to increase with lower rate. The final peak value reaches to about 900 °C, which is similar with the temperature in a standard fire test.

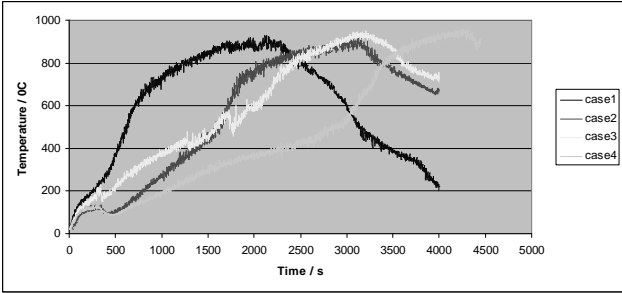


Fig. 4 Hot smoke temperatures in four fire cases (center position)

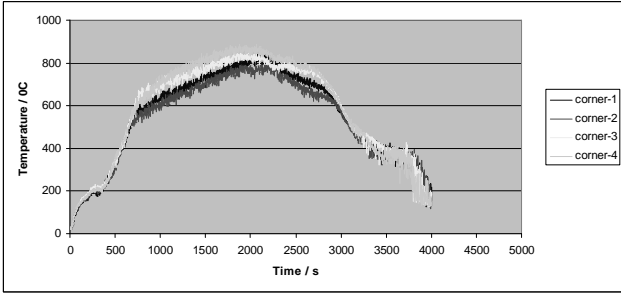


Fig. 5 Smoke temperatures of four corners around the connections (Case 1)

Connections between beams and columns are important structural components with great importance to the robustness of a steel framed structure. The fire gas temperatures around the four corners are also predicted in the FDS model. Figure 5 presents the temperature results around the corners in case 1. In case 1, the uniformly distributed fuel is ignited around four sides, and the temperature distribution is also nearly uniformly. It can be seen that the smoke temperature variation trends around four corners are nearly the same. During the fully developed stage, the peak values reach to about 800 °C, which is close to the temperature in the center position.

The average value of smoke temperature in ventilated enclosure fire could also be approximately estimated by energy balance theory (Karlsson et al, 2000), as shown in *eq. (2)*. The compartment is made up of 200 mm thick concrete blocks, the thermal penetration time of which could be calculated as *eq. (3)*. The calculation time is assumed to 1200 s. The final smoke temperature could

be calculated as *eq. (4) and eq. (5)* shown. The result is about 1000 °C, which is a little higher than the FDS simulation result for using higher heat release rate in hand calculation.

$$Q = m_g c_p (T_g - T_a) + q_{loss} = m_g c_p (T_g - T_a) + h_k A_T (T_g - T_a) \quad (2)$$

$$t_p = \frac{\delta^2}{4\alpha} = \frac{0.2^2}{4 \times 5.7 \times 10^{-7}} \approx 17544s = 292 \text{ min} \quad (3)$$

$$h_k = \sqrt{\frac{k\rho c}{t}} = \sqrt{\frac{2 \times 10^6}{1200}} \approx 40.7W / mK = 0.041kW / mK \quad (4)$$

$$\Delta T = 6.85 \left(\frac{Q^2}{A\sqrt{H}h_k A_T} \right)^{1/3} = 6.85 \times \left(\frac{29674^2}{14 \times \sqrt{2} \times 0.041 \times 370} \right)^{1/3} \approx 980K \quad (5)$$

2.3 Ceiling Temperature

The roof of the compartment is made up of concrete. Its top side is exposed to ambient temperature, and the low side to hot smoke. The temperature of ceiling increases during the fire by absorbing radiative heat from the flames and by convection from hot fire gases. The temperature results in the C1 column position from FDS simulation are shown in figure 6. The variation trend is a little different from heat release rate and hot smoke temperature, especially during the fully developed period. During fire growth stage, the temperatures reach to about 500 °C for case2, 3 and 4. But in case 1, the temperature only reaches to 350 °C before flashover due to the limited combustion time. During fully developed stage, the temperature continues to increase until 800 °C because of energy accumulation, except case4 due to the long combustion time. As the fuel consuming, the temperature also decreases gradually.

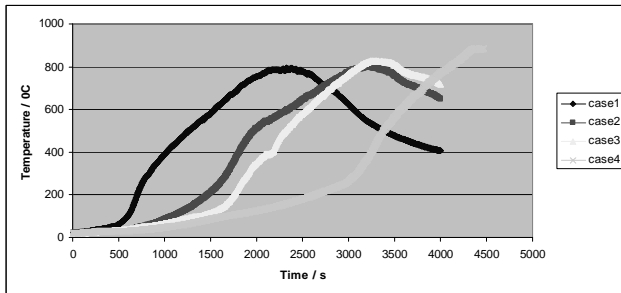


Fig. 6 Ceiling temperature at C1 Column position in four fire cases

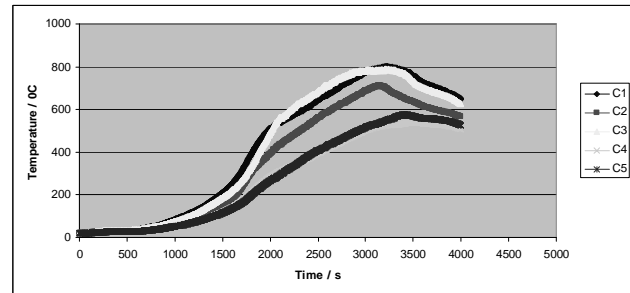


Fig. 7 Ceiling temperature at five column positions (case 2)

In large compartment fire, although the hot smoke nearly fills up the compartment, there are still some differences between ceiling temperature at different positions. Figure 7 gives the ceiling temperatures of five column positions in case 2, in which the ignition sources are in the center. Since the C1 column is positioned near the center and the C3 column is positioned near the big opening, the ceiling temperatures at C1 and C3 column positions are higher than the others, which reaches to about 800 °C. The peak values of ceiling temperature near C4 and C5 columns are less than 600 °C. The assumption of uniform ceiling temperature distribution within the compartment is not very valid. It is good to divide the ceiling into several parts when analyzing the mechanical behavior of ceiling in FEA model.

2.4 Column Temperature

The column in this compartment is made up of steel hollow section filled with concrete. The cross section is assumed as a square shape with dimensions 250 mm by 250 mm, and steel hollow thickness equals to 15 mm. Figure 8 shows the surface temperature of C1 column at the height of 3.5m in these four cases. The temperature of the column increases slowly by absorbing heat from hot smoke and flame. During fully developed period, the temperature still increases with the same rate, which is different from that for the ceiling. The peak value of temperature is about 700 °C in

case 1, 2 and 3, but higher in case 4 due to the long combustion time. The mechanical behavior of column would be affected greatly.

Heat transfer inside column is also investigated by FDS, which is a one dimensional heat conduction issue. Figure 9 gives the temperatures at different inside depths of C1 column in case 3. It can be seen that there was a higher temperature gradient near the surface, but lower temperature gradient near the kernel. Most of the heat is absorbed by the steel hollow section. Part of the concrete in contact with the steel hollow section is affected by steel, and the highest temperature reaches to about 500 °C. The temperature inside the concrete is increasing very slowly during the whole period, even when the fire is decreasing.

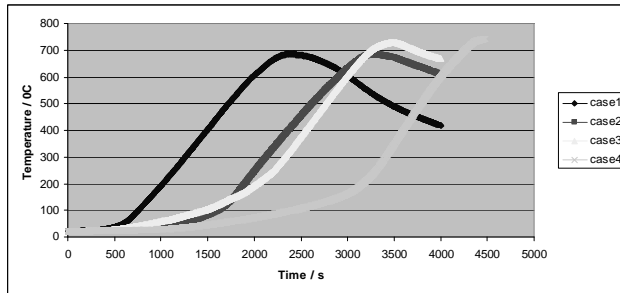


Fig. 8 Surface temperature of C1 column in four fire cases (3.5m high position)

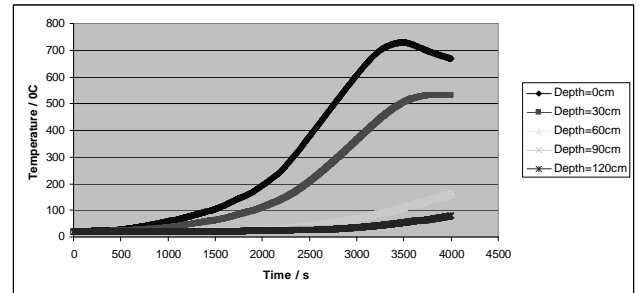


Fig. 9 Temperatures at different inside depths of A1 column (Case 3)

2.5 Beam Temperature

The solid steel beam is positioned between two columns under the ceiling. During the whole fire development, the beam is exposed to the hot smoke completely. The beam temperature increases rapidly as shown in figure 10, which is similar to column temperature due to the same material. The peak values of four cases reaches to about 800 °C, which is very close to the hot smoke temperature. In the fire growth stage, beam temperature is determined by both radiation and convection. As the temperature is increasing, the difference between beam and hot smoke is decreasing gradually. During fully developed period, beam temperature continues to increase with an obvious lower increase rate mainly due to the radiative heat.

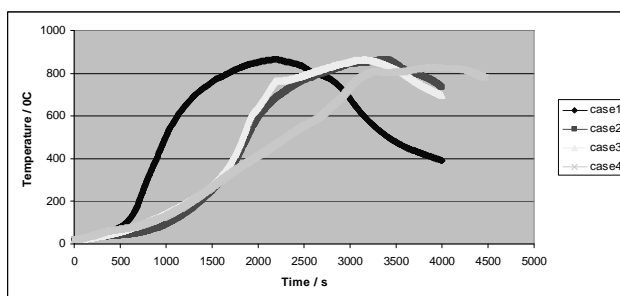


Fig. 10 Beam (left part) temperatures in four cases

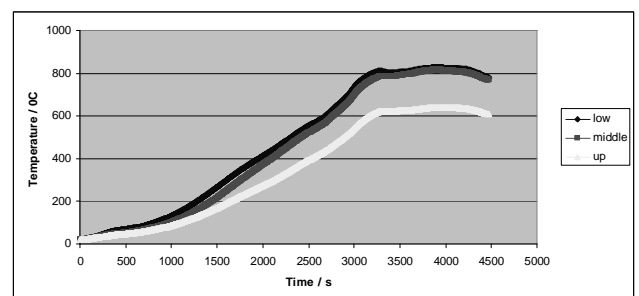


Fig. 11 Beam temperatures of different parts (Case 4)

The steel beam is made up of three thin steel plates. The boundary conditions of bottom flange and middle part are hot smoke, but the top part is just tightly under the ceiling. In FDS model, the environment temperature is assumed to be 20 °C immutably. There is only a one dimensional heat conduction calculation in FDS. Actually the heat conduction effect along the plane is feeble because of the low heat conductivity of concrete. Then the temperature of the top part of the beam is lower than that of the other two parts. Figure 11 gives the temperature variation of different parts in case 4. There are no differences between the bottom flange and the middle part, because the hot smoke temperatures around them are almost the same. The temperature of the top part increases with a low rate. The peak value of the top part is only 600 °C, which is 200 °C lower than the other parts. The difference should be considered carefully when analyzing the mechanical performance of beam in a fire scenario.

3 CONCLUSION

In this paper, compartment fire scenario with uniformly distributed wood cribs is simulated by FDS. Four different ignition sources were considered. The temperature variations during fire of structural components are obtained from the FDS calculations. Simulation results indicate that the fire growth rate is greatly affected by the position of ignition sources and the peak value of heat release rate during flashover period is controlled by the ventilation condition. The fire development process could be divided into four stages clearly as: ignition, growth, fully developed and decay. The temperature variation trend is mainly determined by heat release rate. The highest temperature of hot smoke reaches to about 900 °C, which is not uniform at that level. The surface temperature of the concrete ceiling is similar to the smoke temperature, but there are big differences of their values at different positions. The highest temperature of the column surface is about 700 °C. There is a large temperature gradient along the depth near the surface, but low temperature gradient near the kernel inside the column. The temperature of the beam under the ceiling is also increasing rapidly during the fire, with the same peak value as that of the smoke and the ceiling. The temperature of the top flange of the beam is obviously lower than the other two parts, which should be taken into account in an FE-analysis. Based on these simulation results and the experimental results, further analysis of structural performance in fire using FEA tools will be carried out.

4 ACKNOWLEDGMENT

Authors gratefully acknowledge financial support provided by Tillväxtverket project NSS, Nordic Safety and Security and from the European Union (Research Fund for Coal and Steel) under contract grant RFSR-CT-2008-00036”, research project COMPFIRE, Design of joints to composite columns for improved fire robustness, RFS-PR-08009.

REFERENCES

- A.H. Buchanan, *Structural Design for Fire Safety*, Wiley, Chichester, 2001.
- A.S. Usmani, J.M. Rotter, S. Lamont, A.M. Sanad, M. Gillie, *Fundamental principles of structural behaviour under thermal effects*, *Fire Safety Journal*. 36 (8) 721–744, 2001.
- Liu, T. C. H. “Experimental investigation of behavior of axially restrained steel beams in fire.” *J. Constr. Steel Res.*, 58, 1211–1230, 2002.
- Buchanan A. H. *Structural design for fire safety* John Wiley & Sons, ISBN 0-471-89060-X, 2003.
- Hosam, M. A., Senseny, P. E., and Alpert, R. L. “Lateral displacement and collapse of single-story steel frames in uncontrolled fires.” *Eng. Struct*, 26, 593–607, 2004.
- Yang, K. C., Lee, H. H., and Chan, O. “Experimental study of fire-resistant steel H-columns at elevated temperature.” *J. Constr. Steel Res.*, 62, 544–553, 2006.
- Dong Y, Zhu C and Prasad K. Thermal and structural response of two-storey two-bay composite steel frames under furnace loading. *Fire Safety Journal*, Volume 44, 439–450, 2009.
- Wald, F., Simoes da Silva, L., Moore, D.B., Lennon, T., Chladná, M., Santiago, A., Beneš, M. and Borges, L. Experimental behaviour of a steel structure under natural fire. *Fire Safety Journal*, Volume 41, Issue7, pp. 509-522, 2006.
- Chlouba J, Wald F, and Sokol Z. “Temperature of Connections during Fire on Steel Framed Building.” *Steel Structures* 9, 47-55, 2009.
- F.Wald, J.Chlouba, A.Uhlir, P.Kallerova, M.Stujberova. Temperatures during fire tests on structure and its prediction according to Eurocodes. *Fire Safety Journal* 44 135– 146, 2009.
- Ryder N L, Sutula J A, Schemel C F, Hamer A J and Brunt V V. Consequence modeling using the fire dynamics simulator. *Journal of Hazardous Materials* 115 149–154, 2004.
- Pope N.D. and Bailey C.G. Quantitative comparison of FDS and parametric fire curves with post-flashover compartment fire test data. *Fire Safety Journal* 41 99–110, 2006.
- McGrattan K, McDermott R, Hostikka S, Floyd J, *Fire Dynamics Simulator (Version 5)-User’s Guide*, NIST Special Publication 1019-5, 2010.
- Karlsson B and Quintiere J G. *Enclosure fire dynamics*. Boca Raton, Florida: CRC Press, 2000, pp. 117-127, 129-132.

EFFECTIVE THERMAL CONDUCTIVITY OF FIRE PROOF MATERIALS And The Measuring Method

Jun HAN ^a, Guo-Qiang LI ^b, Guo-Biao LOU ^b

^a College of Civil Engineering, Tongji University, Shanghai, China

^b Safe Key Laboratory for Disaster Reduction in Civil Engineering, Tongji University, Shanghai, China

INTRODUCTION

Steel structures have poor fire resistance, due to the great decrease of steel strength as temperature elevate and the high thermal conductivity of steel thereby leading to quick temperature rise. The fire endurance of non-protected steel members is only 15 ~ 20min, so easily destroyed in fire (Li et al., 2006).

Fire proof materials are widely used to provide passive fire protection of steel structures. The basis is preventing direct heat transfer to the steel members from external heat source, thus delaying the steel temperature rise and improving the fire-resistance of steel members (CECS 200: 2006). Therefore, insulation property, commonly characterized with thermal conductivity is the most important parameter to predict steel temperature in fire. However, thermal conductivity of fire proof materials generally has a great change as temperature elevate while steel temperature usually range from room temperature to over 1000 °C in fire. Thus, calculation based on thermal conductivity at room temperature will lead to large errors despite its great convenience in calculation.

Part 11 of *Assessment method of fire protection system applied to structural steel members* (ISO/CD 834) provides a method to calculate thermal conductivity of fire protection materials based on steel components standard fire test and can comprehensively reflect the performance of fire coating in fire. In this method, the thermal conductivity of fire proof materials was calculated directly by iterative formula and non-explicit relationship lies between temperature and thermal conductivity, so manual computation is difficult. In addition, the method proposed the thermal conductivity of fire proof material by every temperature range of 50 °C, which apparently lead to more accurate result but more complicated calculation in determining the steel temperature in fire. Moreover, the existing furnaces used for standard fire test of steel components are of large sizes, such as the beam and plate furnace sized 3m×4m×1.5m and the column furnace sized 3m×4m×4m, which are extremely time consuming and expensive for small-scaled tests.

In view of this, this paper proposed the concept of effective thermal conductivity and developed measuring method and test setup based on steel components standard fire test, in order to reflect the actual performance of fire insulation in fire. In total, 15 steel specimens with 5 different schemes of layer thickness were fire tested in the new-developed furnace of Tongji University. Comparison of experimental results and theoretical calculations will be presented to show that the effective thermal conductivity can accurately model the performance of steel members protected with fire proof material in fire.

1 THE EFFECTIVE THERMAL CONDUCTIVITY

1.1 Calculation of thermal conductivity

In fire condition, the equilibrium between the heat absorbed by the steel member and the heat transmitted through the insulation can be expressed as (Li et al., 2006; CECS200:2006; EN 1993-1-2,2005):

$$T_s(t + \Delta t) - T_s(t) = \frac{\alpha}{\rho_s c_s} \cdot \frac{F_i}{V} \cdot [T_g(t + \Delta t) - T_s(t)] \Delta t \quad (1)$$

$$\alpha = \frac{1}{\frac{1}{\alpha_c + \alpha_r} + R_i} \quad (2)$$

$$R_i = \frac{d_i}{\lambda_i} \quad (3)$$

- where
- t time (s);
 - Δt time intervals (s);
 - T_s, T_g temperature inside the steel members and ambient temperature ($^{\circ}\text{C}$);
 - ρ_s density of steel (kg/m^3);
 - c_s specific heat of steel ($\text{J}/\text{kg}\cdot\text{K}$);
 - F_i cross-sectional area of steel member in unit length (m^2/m);
 - V volume of steel member in unit length (m^3/m);
 - R_i thermal resistance of fire insulation ($\text{m}^2/\text{W}\cdot\text{K}$);
 - d_i thickness of fire insulation (m);
 - λ_i thermal conductivity of fire insulation ($\text{W}/\text{m}\cdot\text{K}$);
 - α complex heat transfer coefficient ($\text{W}/\text{m}^2\cdot\text{K}$);
 - α_c convective heat transfer coefficient, fire to insulation, $\alpha_c=25$ ($\text{W}/\text{m}^2\cdot\text{K}$);
 - α_r radiative heat transfer coefficient, fire to insulation ($\text{W}/\text{m}^2\cdot\text{K}$).

Usually, the thermal resistance R_i is much larger than $1/(\alpha_r + \alpha_c)$, so the complex heat transfer coefficient can be expressed approximately as Equation 4.

$$\alpha = \frac{1}{R_i} \quad (4)$$

As a iterative formula, Equation 1 is inconvenient in practice, so Equation 5 was developed as a simple formula of Equation 1 by mathematical fitting approach to determine the temperature of the steel members protected with fire proof material in ISO834 fire.

$$T_s = \left(\sqrt{5 \times 10^{-5} \times \frac{1}{R_i} \cdot \frac{F_i}{V} + 0.044} - 0.2 \right) t + 20 \quad (5)$$

The comparison between Equation 1 and Equation 5 indicated that the simple formula is close to Equation 1 especially in the temperature zone of $400\sim 700^{\circ}\text{C}$, which covers the critical temperature of most steel members, as is shown in Fig.1. The explicit formulation greatly simplifies the calculation of the temperature of steel members.

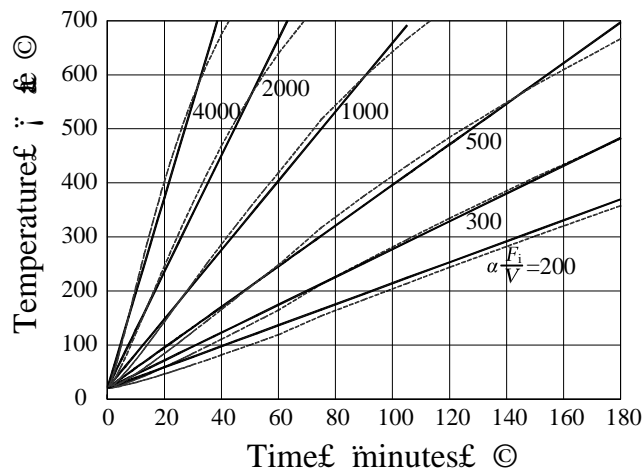


Fig. 1 Comparison between the calculating results of Eq.1 and Eq. 5

Thermal resistance of the fire insulation can be easily obtained, if temperature-time curve is known, as Equation 6 shows. Afterwards, the thermal conductivity of fire insulation can be calculated from Equation 7.

$$R_i = \frac{5 \times 10^{-5}}{\left(\frac{T_s - 20}{t_0} + 0.2 \right)^2 - 0.044} \cdot \frac{F_i}{V} \quad (6)$$

$$\lambda_i = \frac{d_i}{R_i} \quad (7)$$

1.2 Definition of effective thermal conductivity

The relationship between thermal conductivity and temperature can be derived from Equation 7 according to the specimen temperature-time curve in steel structures standard fire test. The time-dependent thermal conductivity brings much difficulty to determine the temperature of steel members. Consequently, the concept of effective thermal conductivity is proposed to represent the insulation property of fire proof materials with a constant, and the two definitions of effective thermal conductivity are drawn as follows:

(1) Def.1: the average of the thermal conductivities when the specimen temperature was 400~600°C
The critical temperature of most steel members is in the temperature zone of 400~600°C, in which the calculated temperature should be as close as the measured temperature. The average of thermal conductivities in this temperature zone can accomplish this object.

(2) Def.2: the thermal conductivity when the specimen temperature was 540°C (1000°F)

In *Standards Test Methods for Fire Tests of Building Construction and Materials* (ASTM E119), the standard fire test will be stopped if the temperature of steel members is higher than 1000°F (538°C), which is defined as the critical temperature. Defining the thermal conductivity of fire proof material when the specimen temperature was 540°C (1000°F) as the effective thermal conductivity can greatly simplify calculation.

Comparison of the two definitions has been made and detailed below.

2 TEST SETUP AND SPECIMENS

2.1 Test setup

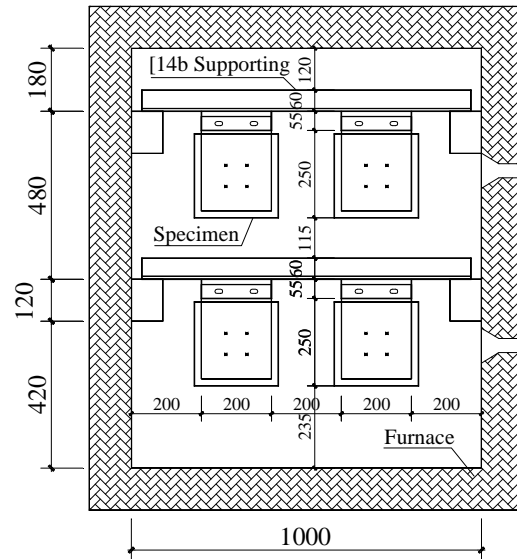
A mini-sized furnace was developed for small-scaled test of fire coating, whose technical specifications are as follows:

- 1) Furnace size: 1.0m×1.0m×1.2m;
- 2) Furnace Temperatures: ISO834 fire, Hydrocarbon fire and customized heating curves are available and ISO 834 fire was employed in the experiment;
- 3) Data Acquisition and Control: the pressure and the temperature of the furnace, loading and unloading, the data acquisition, the secure alarm are all integrally controlled with a computer, so as to reach the convenient operation.

As is shown in Fig.2, four standard specimens can be placed on channel steel [14b with fire protection in the furnace.



a) Furnace



b) The cross-section and the arrangement of specimens

Fig. 2 Testing furnace and the arrangement of specimens

2.2 Test specimens

As shown in Fig. 3, steel plate specimens with dimensions of 16mm×200mm270mm were chosen in the test based on the following considerations:

- 1) The shape and configuration of specimens should be as simple as possible, so steel plate was selected;
- 2) The size of the steel plate should be as small as possible to reduce cost but not too small to ensure the uniformity of temperature field of steel plate, which is necessary to simulate one-dimensional heat transfer.
- 3) The typical thickness of steel plates was chosen as 16mm, because steel plates with thickness of 6mm~25mm are usually used in practice. Moreover, shape parameter of the selected specimen is 145m^{-1} , which is similar with the shape parameter of specimens used in *Fire resistive coating for steel structure* (GB 14907-2002), as is shown in Tab. 1.
- 4) Specimens with five different thickness (10mm, 17mm, 20mm, 30mm, 40mm) were carried out to determine the effects of layer thickness on the thermal conductivity, and then the appropriate thickness will be select as a typical thickness.
- 5) Fig. 2 shows three measuring points on every steel plate and the temperature will be measured with thermal couples. Theoretically, the temperatures at point 1 and point 3 are the same, while the small deviation in practice can confirm the uniformity of the temperature field inside the steel plates.

Tab. 1 Shape parameter F_i/V of the specimen used in GB 14907-2002

Specimen Type	Shape Parameter F_i/V (m^{-1})	
	Four sides in fire	Three sides in fire
I36b	142.1	125.6
I40b	137.0	121.7

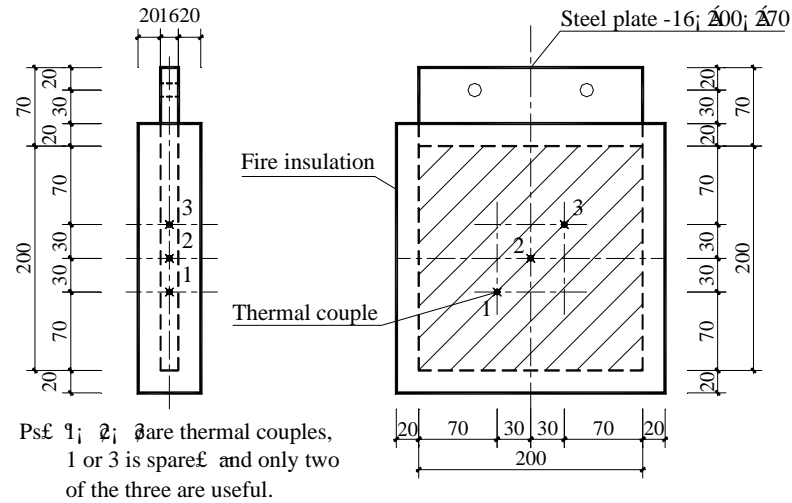


Fig. 3 Dimensions of specimens and arrangement of thermal couples

3 TESTING RESULTS

The fire insulation showed peace performance with no obvious change and the temperature of the steel member rose steadily in fire (Han, 2009). Cracks appeared on the surface of the insulation after fire, as is shown in Fig. 4.



Fig. 4 Reaction of spray coating in fire

Fig. 5 ~ Fig. 8 shows the temperature-time curve of steel members, furnace temperature-time curve and the thermal conductivity of fire insulation (calculated by Equation 7). Tab. 2 shows the comparison between the thermal conductivity calculated by the two definitions indicating that the definitions of effective thermal conductivity are reasonable and available. The following conclusions are derived from the experiments:

- 1) The thermal conductivity calculated in Equation 7 was at first increased and then decreased and reached peak value when steel temperature was around 540°C (the largest difference was not over 4% for all the specimens).
- 2) Calculated temperature matched well with the measured temperature, especially when the steel temperature was higher than 400°C, verifying that the method proposed above are available.
- 3) The effective thermal conductivities derived by the two definitions are similar. However, the second definition is suggested for its more convenience than the first one.
- 4) The thickness of fire insulation has little effect on the effective thermal conductivity. 20mm was chosen as typical thickness for its wide use.

Tab. 2 Testing results of effective thermal conductivity

Specimen ID	Design Fire-resistance (h)	Design Thickness (mm)	Actual Thickness (mm)	Shape Parameter F_t/V (m ⁻¹)	Time of Ts=540°C (min)	Effective Thermal Conductivity (W/m·K)			
						By Def.1	Average of Def.1	By Def.2	Average of Def.2
1-1	0.5	10	11.2	145	41	0.2271		0.2277	
1-2	0.5	10	11.6	145	39	0.2472	0.2359	0.2448	0.2349
1-3	0.5	10	12.5	145	43	0.2334		0.2323	
2-2	1.0	17	14.2	145	41	0.2827	0.2597	0.2834	0.2604
2-3	1.0	17	14.5	145	47	0.2366		0.2373	
3-1	1.5	20	18.5	145	55	0.2476		0.2498	
3-2	1.5	20	18.0	145	62	0.2031	0.2339	0.2055	0.2366
3-3	1.5	20	18.0	145	53	0.2511		0.2545	
4-1	2.0	30	33.0	145	86	0.2373		0.2456	
4-2	2.0	30	31.0	145	91	0.2050	0.2299	0.2125	0.2374
4-3	2.0	30	31.5	145	81	0.2475		0.2542	
5-1	2.5	40	36.0	145	94	0.2300		0.2378	
5-2	2.5	40	36.0	145	98	0.2182	0.2272	0.2251	0.2342
5-3	2.5	40	36.0	145	94	0.2335		0.2396	

Ps: the steel plates are all sized 16 mm×200 mm×270mm;

Def.1—the average of the thermal conductivity when the specimen temperature was 400~600°C,

Def.2—the thermal conductivity when the specimen temperature was 540°C (1000°F).

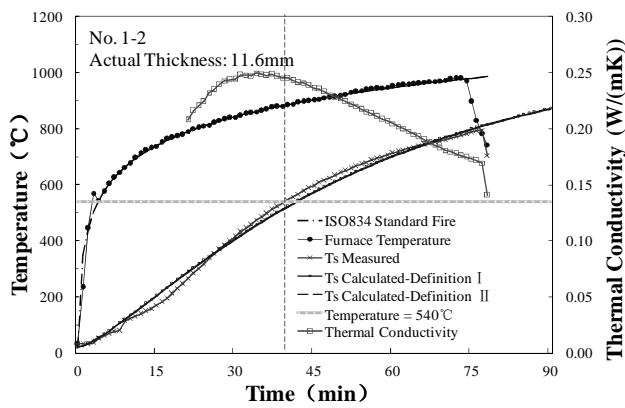


Fig. 5 Comparison between Ts calculated and Ts measured (No.1-2)

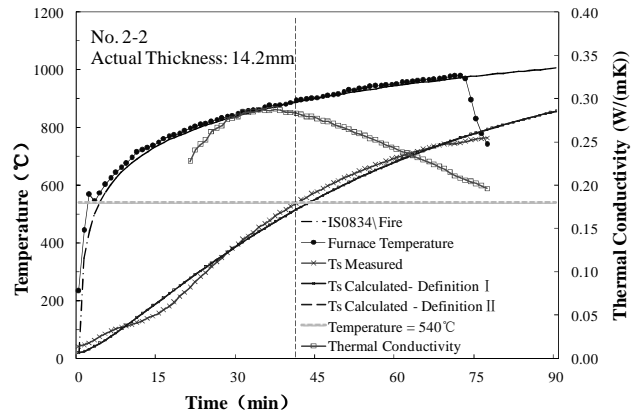


Fig. 6 Comparison between Ts calculated and Ts measured (No.2-2)

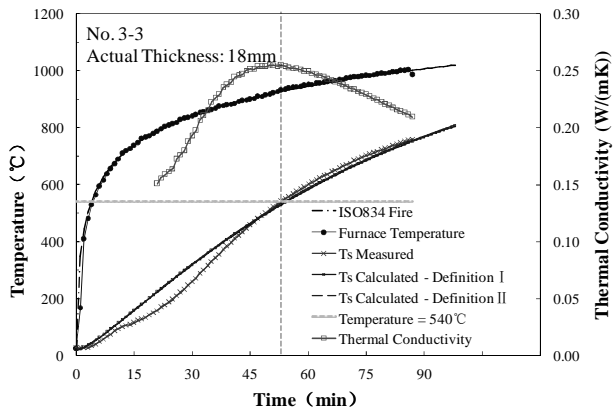


Fig. 7 Comparison between Ts calculated and Ts measured (No.3-3)

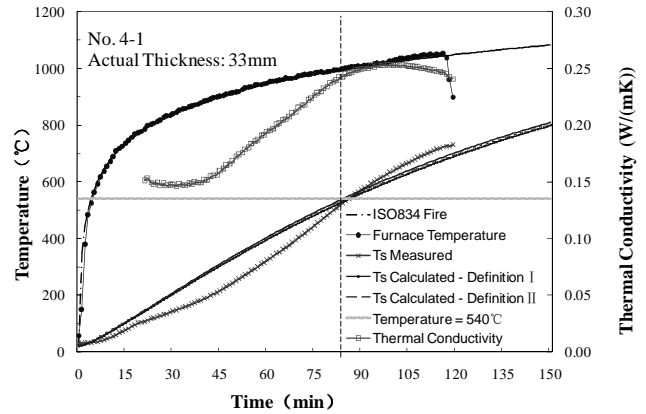


Fig. 8 Comparison between Ts calculated and Ts measured (No.4-1)

3 SUMMARY

The thermal conductivity generally changes a lot with temperature elevate. Therefore, predicting steel temperatures in fire with the thermal conductivity at room temperature brings large errors, while variable thermal conductivity makes calculation complicated. In view of this, this paper proposed the concept of effective thermal conductivity and developed measuring method and test setup based on steel components standard fire test, which represented actual performance of fire proof materials in fire. The deviation between calculated temperature and measured temperature met the engineering requirements, indicating that the test-based method is available. The main work and conclusions may be drawn as follows.

- 1) Proposed a measuring method suitable for thermal conductivity of fire proof materials and developed the corresponding test setup.
- 2) Proposed two definitions of thermal conductivity. Def.1: the average of thermal conductivities when the specimen temperature was 400~600 °C ; Def.2: the thermal conductivity when the specimen temperature was 540°C (1000°F).
- 3) Verification and comparison of the two definitions were proposed. Comparison between the calculated temperature and the measured temperature indicated that the two definitions met the engineering requirements. In practice, the second definition is suggested for its more convenience than the first one.
- 4) The thickness of fire insulation has little effect on the effective thermal conductivity. 20mm was chosen as typical thickness taking actual use into consideration.

REFERENCES

- Li G. Q., Han L. H., Lou G. B., Jiang S. C., Fire-resistant Design of Steel and steel - concrete composite structure ,China Architecture & Building Press, Beijing, China, 2006
- CECS200:2006, Technical code for fire safety of steel structure in buildings, China Association for Engineering Construction Standardization, China Planning Press, Beijing, 2006
- ISO/CD 834-11: 2003, MOD. Fire Resistance Tests— Elements of Building Construction, Assessment method of fire protection system applied to structural steel members, International Organization for Standardization, 2003
- EN 1993-1-2. Eurocode 3, Design of Steel Structures, Part 1.2: Structural Fire Design, 2005.
- ASTM E 119-00a, Standards Test Methods for Fire Tests of Building Construction and Materials, American Society of Testing and Materials (ASTM), July 10, 2000
- GB 14907-2002, Fire resistive coating for steel structure, General Administration of Quality Supervision, Inspection and Quarantine of PRC, 2002
- HAN, J., Measuring method of fire insulation parameters of steel structures, Bachelor Thesis, Tongji University, Shanghai, China, 2009

FIRE LOAD SURVEY OF COMMERCIAL PREMISES IN FINLAND

Jouni Björkman ^a, Veli Autio ^a, Heikki Ylihärtilä ^a, Peter Grönberg ^b, Markku Heinisuo ^c

^a Seinäjoki University of Applied Sciences, Seinäjoki, Finland

^b Technical Research Centre of Finland (VTT), Espoo, Finland

^c Tampere University of Technology, Seinäjoki, Finland

INTRODUCTION

Fire load is the most important parameter to know for different types of enclosures in building fire safety design. Fire load is the integral against time of fire heat release curve, which can be used, when fire development in an enclosure is evaluated by calculations, e.g. numerical simulations. They give temperatures, smoke layer depth and amount of poisonous gases in an enclosure in a building. By using temperatures, the temperatures in structures can be calculated and thereby determine the integrity of structures in case of fire. In Finland and many other European countries the new Eurocodes are being taken into account in building design. The new European standards (Eurocodes) in building engineering will be applied in Finland as of 2011. In the Eurocodes relating to fire safety, the fire load densities are given according to (EN 1991-1-2, 2003). However, the national annex in Finland (NA, EN 1991-1-2, 2007) does not allow applying the above mentioned Eurocode-tables of fire load densities to different room types. The fire loads may vary a lot in shopping malls and shops. Accordingly, this fire load study concentrates on those types of premises. In fire safety related Eurocodes, building fire load densities, growing factor and heat release rates are given according to the use of the building. Design fire load density is then calculated according to the standard (EN 1991-1-2, 2003) by applying a formula, where an average fire load density, efficiency factor, ignition risk according to the enclosure size, ignition risk according to the use and coefficient describing active fire protection arrangements are multiplied together. In this study the fire load density is given in unit MJ/m^2 , where the square meters refer to the floor area. Fire loads have been determined since 1920. Traditionally the fire load is determined by surveying the burnable objects in existing buildings and multiplying the masses of those by calorific values of materials. Burning is expected not to be oxygen or fire load restricted. Fire load is divided into movable and fixed fire load. Linings (floor, walls, ceiling) are included into the fixed fire load. Movable fire load is separated according to material type. The total fire load is the sum of all those different fire loads for a space according to the use. The datapoints are then fitted to some statistical functions. Applied distributions related to the fire load density measurements are normal, logarithmic normal (lognormal), 3-parametric gamma- and Gumbel distributions. In the Eurocodes the Gumbel-distribution has been applied. Design parameters applied are average and the fractiles of 80, 90 and 95 %. In this study fire loads were measured in 30 commercial premises in the Seinäjoki area in Finland and design parameters for Eurocode based fire safety design were derived. We hope that the results of this study, besides the results of former and ongoing other research projects, will give the basis for the Eurocode based fire load density determining in building design.

1 FIRE LOAD

1.1 Fire load calculation

Fire load is divided into movable and fixed fire load. Linings (floor, walls, ceiling) are included into the fixed fire load. Movable fire load is separated according to material type. The total fire load is the sum of all those different fire loads for a space according to the use of space. Fire load is defined as total released heat in full burning in an enclosure where the fire is situated (Sleich & Cajot 2001). Fire load Q can be expressed mathematically as follows

$$Q = \chi m \Delta H \quad (1)$$

where χ is burning efficiency factor, m mass, H calorific value. According to Eurocodes all movable items and linings are included into fire load. The parts of the burnable material which do not char during the fire do not have to be taken into account in fire load (EN 1991-1-2 Appendix E 2003). According to the Finnish building rules, E1: Building fire safety, the fire load is the total released heat, when the materials in the enclosure burn completely. Bearing, stiffening, separating and other pieces of building as well as movable objects are included in the fire load (E1: Building fire safety 2002). First of all, fire loads are defined according to the use of the building. Many studies dealing with fire loads have been carried out in Finland and worldwide (Autio et al 2011).

2 MEASUREMENTS

The premises investigated were shops with different sizes and types in Seinäjoki and its surroundings in Finland. It was assumed that the geographical situation of a shop does not have any significant meaning. The shops were chosen so that the premises with small as well as big fire load densities could be taken into account in the study. Measurements were carried out in 30 commercial premises and their relating spaces. Those relating spaces were storages and social rooms. The floor area investigated was almost 28000 m². The smallest shop was 54 m² and the largest one was 4550 m² with a 800 m² storage. There were shoe shops, textile shops and bookshops as well as furniture shops and nine groceries.

The measuring method given by (Theyvoven et al 2008) was applied, where burning materials were divided into wood, textiles, plastic, paper and miscellaneous materials. Measurements of the fixed fire load were carried out at the linings without damaging them. Measuring devices such as typical weighers, rulers and laser-systems were used. In small places all materials were weighed and parts of different materials were evaluated. The weight of the bigger items was measured from the volume or just evaluated. In the biggest places parts of the materials were weighed e.g. kg/m² and then multiplied by the evaluated dimensions. Into the fixed material all floor, wall and ceiling lining materials were incorporated. The amount of the material was evaluated by measuring the area of material multiplied by the thickness. The gained volume was multiplied by the material density that yielded the mass.

In addition to the fire load data, many other fire safety related things were collected, too. In the premises information about openings, fire safety class, and distance from the fire station, evacuation plans and active fire safety equipment was also collected. A floor plan was also drawn if not already available.

The fire load was calculated by using the Equation 1, by using calorific values of materials from literature (DiNunno et al 2002, EN 1991-1-2, 2003, Kumar & Rao 1995). See Table 1.

Tab. 1 Average calorific values used in calculations

Material	Average calorific value (MJ/kg)
Wood	17,5
Paper	20
Plastic	30
Textiles	20
Food	15

3 RESULTS

3.1 Fire load densities: Shops and associated spaces

Thirty commercial premises with floor area of 54 ... 4550 m² were analysed. The smallest shops were typically special shops situated in shopping malls. The largest premises were groceries, building material shops and household appliance and furniture shops. The studied types of shops

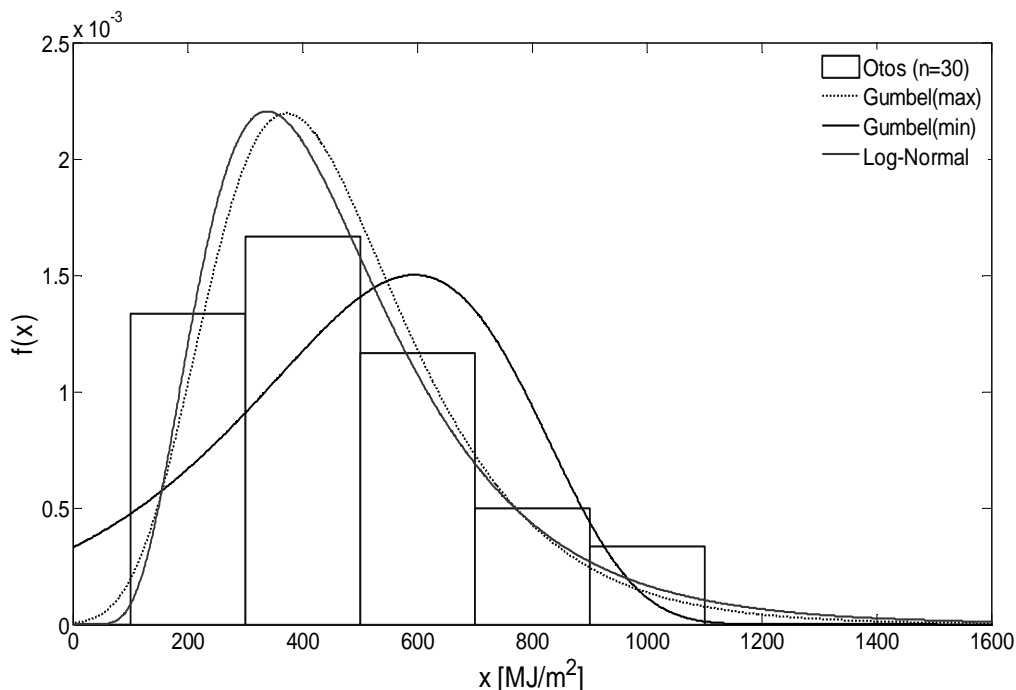
were: grocery (9), furniture shop (2), decoration shop (1), household appliance shops (2), ironmongers shop (1), video hiring (2), toyshops (1), sports shop (1), draper shop (1), optician (1), book-shop (2), shoe-shops (2), clothing store (3), bag-shop (1) and chemist's shop (1).

Associated spaces relating to the shops were mostly storages (17), social premises (4) and offices (3). Fixed (burnable parts of the building and linings) and movable fire loads in premises were measured. In percentages, the biggest part of the fire load of the shops was movable. In associated premises there were spaces where the amount of fixed fire load was bigger than that of movable. On the other hand, there were associated spaces where the amount of fixed fire load was smaller than in shops at its minimum. The variation of the fire load of associated spaces was bigger than in shops. Movable fire load was divided into five material classes: wood, paper, textile, plastics and miscellaneous. The fire load diversity of certain shop types was very similar. For example in textile shops there were mostly textiles. The share of plastics is the biggest in household appliance and toyshops. In furniture and decoration shops there is a lot of wood in the fire load. Miscellaneous fire load can be found in groceries and at chemist's shops. Paper is a common material, of course, in book shops, but also in shoe shops. (Autio et al 2011)

3.2 Fitting

It has been claimed that the fire load density in buildings is often assumed to follow logarithmic normal (lognormal) (DiNunno et al. 2002) or Gumbel-distribution (Eurocode EN 1991-1-2). In this study the suitability of these two stochastic models to calculated fire load densities was considered. The curves were fitted into the fire load density data collected. The parameter estimates of the biggest probability (MLE) of fitted curves, average value, standard deviation and fractiles of cumulative functions were determined. The fitted density and cumulative functions and their parameters for shops and associated spaces are given in (Autio et al 2011).

In Figure 1 there are the density $f(x)$ and cumulative $F(x)$ functions of fitted distributions with the fire load densities x calculated based on the measured data of shops. It is clearly to be seen that logarithmic normal and Gumbel (maximum) –distributions match the data well.



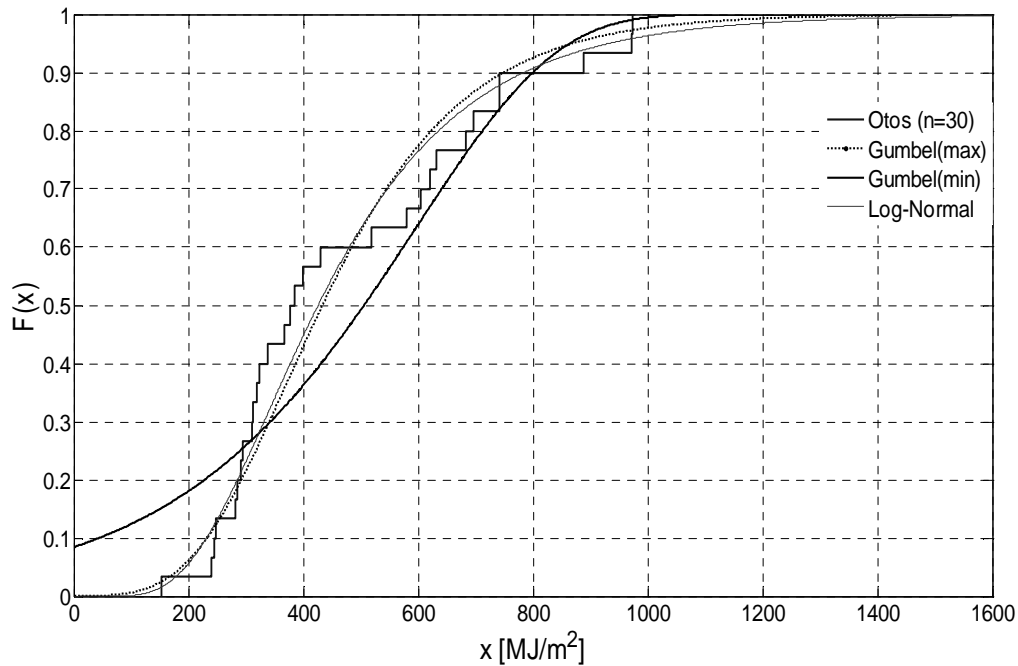


Fig. 1 Fitted density functions and cumulative functions for shops. Measured based fire load densities are expressed by using histograms and the cumulative fire load density by using step curve.

Fitted density functions $f(x)$ and cumulative functions $F(x)$ for associated spaces are in (Autio et al 2011).

It can be seen in figures that the logarithmic normal distribution and the Gumbel (maximum) – distribution fit well with the fire load density histogram and the cumulative step curve.

When looking at the curves of cumulative functions it can be seen that the logarithmic distribution matches best the fire load data. However, evaluation by eye is difficult and uncertain. Accordingly, the quality of fitting was investigated by using χ^2 –test. It was found that measured and calculated fire load density function follows logarithmic normal distribution significantly more reliably than the Gumbel (minimum) –distribution, and a bit more reliably than Gumbel (maximum) –distribution. In the case of associated spaces the results are corresponding. The final result can be concluded so that the logarithmic normal distribution describes the measurement based fire load densities in the most reliable way. However, in the case of Gumbel (maximum) –distribution, the deviation is not significant.

The results of the additional measurements: Active fire safety arrangements were also investigated in the shops. There was at least one portable extinguisher in every shop. In 10 places there was a rescue plan available. In one place there was none. In 19 places it was not known if a rescue plan was available. Safety and escape illumination was sufficient in 28 shops. Automatic fire detection system was installed in 22 buildings and 12 shops were equipped with an automatic extinguishing system. A smoke exhausting system was installed in 15 shops and a water supply was found in 14 places. In some buildings the water supply may exist somewhere but not in the vicinity of the shops investigated. (Autio et al. 2011)

4 DISCUSSIONS

The inventory in the shops was rather a demanding task. The biggest problem was the large material diversity and material identification. For example, there was a lot of different plastics. They were partly equipped with material data, but some of them were impossible to classify. Almost all items were packed in some way. Thus the mass of an item itself and its packaging material had to be separated. The mass of big items, which could not be weighed, was evaluated based on their volumes. This was especially difficult to accomplish. Accordingly, at the later phase of the work

previously calculated values in the case of items of the same type were used. The most difficult items to evaluate were the items which consisted of many materials.

Fire load densities are typically reported to follow logarithmic normal or Gumbel- distribution. Which one of them suits best requires investigation in every case. Essential factors affecting the suitability and the form of the distributions are the variation coefficient of the measured data set, the structure of the premises i.e. it can be asked if the space is a one- or multi-room space and if the fire load type is fixed or movable as well as what the distribution model itself is.

When the variation coefficient of measured data approaches zero, many distributions converge towards normal distribution. On the other hand, fire load can be assumed to be some kind of sum of masses of burnable materials and specific heats. The fire load of a certain room or building is the sum of fire loads of rooms. It can be assumed that the cumulative process of a fixed fire load is based on different mechanisms from that of a movable fire load. A phenomenon, which is the sum of independent variables which are distributed by different ways, follows normal distribution. A phenomenon which is the product of independent in a different way distributed variables follows lognormal distribution if the ensemble is large. It was found that there is a significantly linear correlation between the fire load and the room volume, which partly may cause lognormal behaviour.

5 SUMMARY AND ACKNOWLEDGEMENTS

In the 30 commercial premises, which were studied, the measured and fitted fire load density follows logarithmic normal distribution significantly more reliably than the Gumbel (minimum) – distribution and slightly more reliably than the Gumbel (maximum) –distribution. On the basis of this study and corresponding foreign studies, it can be claimed that 80 % fractile of the Eurocode of 730 MJ/m² is a suitable characteristic value for the fire safety design of commercial premises of shopping malls except for storages and associated rooms. In this study, the fire loads of storages and associated spaces were 1,5 times bigger than in shops. Especially the fire loads in storages may vary a lot and they must be determined according to the type, amount and location of goods. We suggest fire load measurements in theatres, cinemas and libraries and corresponding premises according to the same measuring and analysing methods as in this study.

We are indebted to the students of building engineering of Seinäjoki University of Applied Sciences who assisted in the fire load inventory and the shops who allowed the measurements in their premises. Members of the steering committee and funding by Ministry of Interior (Palosuojelurahasto), Ministry of Environment, Teräsrakenneyhdistys ry, City of Seinäjoki and Tampere University of Technology are highly acknowledged.

REFERENCES

- Autio, V., Björkman, J., Grönberg, P., Heinisuo, M. & Ylihärsilä, H. 2011. Fire load survey of buildings. Publications of Seinäjoki University of Applied Sciences. Reports B 47. 65 p. (In Finnish)
- DiNenno, P. et al. 2002. Handbook of Fire Protection Engineering. 3. ed. The National Fire Protection Association (NFPA).
- E1: Finnish Building Code. Building fire safety. 2002. Ministry of Environment.
- EN 1991-1-2. 2003. Eurocode 1: Rakenteiden kuormat: Palolle altistettujen rakenteiden rasitukset. Helsinki: Suomen Standardisoimisliitto. (In Finnish)
- Annex NA, EN 1991-1-2, 2007. EN 1991-1-2. 2003. Eurocode 1: Rakenteiden kuormat: Palolle altistettujen rakenteiden rasitukset. Helsinki: Suomen Standardisoimisliitto. (In Finnish)
- Kumar, S. & Rao, C.V.S. K. 1995. Fire Loads in Residential Buildings, Building and Environment 30 (2), 29–305.
- Schleich, J.B. & Cajot, L-J. 2001. Valorisation project. Natural fire safety concept. Profil Arbed.
- Thayvoye, C, Zhao, B, Klein, J & Fontana, M. 2008. Fire load survey and statistical analysis. Fire safety science – Proceedings of the 9th international symposium 991–1002, IAFSS.

SYSTEMATISATION OF DESIGN FIRE LOADS IN AN INTEGRATED FIRE DESIGN SYSTEM

Markku Heinisuo ^a, Mauri Laasonen ^a, Jyri Outinen ^b, Jukka Hietaniemi ^c

^a Tampere University of Technology, Faculty of Built Environment, Tampere, Finland

^b Rautaruukki Oyj, Vantaa, Finland

^c Markku Kauriala Ltd, Fire Engineering and Fire Safety Design Consultants, Espoo, Finland

INTRODUCTION

Definition of design fires is the starting point of fire safety engineering. Fire scenarios should be defined with care in close co-operation between the client, the designers and the authorities. Different fires must be taken into account depending on the intended use of the building, as is done when defining the mechanical actions on buildings. In Europe design fires and the corresponding minimum fire loads have been defined in Standard EN 1991-1-2, 2003 based on the occupancies of buildings. However, no standard values exist for many types of fires, such as rack-stored commodity fires and vehicle fires, which requires defining design fires based on literature or tests and analyses. It is also true that the EN standards have not yet been approved by all European countries (Heinisuo et al, 2010) which requires defining design fires in them based on literature or by other means.

It is believed by the authors that fires based on occupancies of buildings, rack-stored commodity fires and vehicle fires are similar across Europe. Rack and vehicle fires depend on the types of stored items and vehicles, but if they are known the fire loads of similar types can be assumed to be the same. In many countries these fires are defined differently even by different local authorities. The standardisation of fire loads is extremely important for the operations of contractors globally. It is also important in creation of design tools for designers.

This paper looks into the systematisation of design fire loads. Systematisation is hoped to lead in the future to the standardisation of fire loads. The implementing environment of the design fire loads of this study is an integrated fire design system developed during the last three years (Heinisuo et al, 2009). Integration starts in BIM (Building Information Model, Tekla Structures) and continues with fire simulations ending with resistance checks of steel members. BIM provides the geometrical entities and required physical properties for defining the fire loads needed to run fire simulations. The fire simulations are done using NIST FDS (Fire Dynamics Simulator). Member resistance checks are done using SCIA Engineering software (Nemetschek) after obtaining the gas temperatures from FDS.

By these means the fire design process can be facilitated and the quality of the simulations improved. Fire simulations can be run taking into account only the conditions of the building to be built in the design phase.

This paper presents the modelling of Eurocode fires based on occupancies of buildings as well as special fires such as rack-stored commodity fires and vehicle fires (Hietaniemi, Mikkola, 2010; Haack, 2001; Shleich, 2010). The effects of sprinklers are also examined. When presenting the Eurocode fires based on occupancy, a so-called chessboard system is utilised which proved to give more reasonable results than applying the fire load of FDS to the entire floor area. Simple rules are included in the definitions of the fire loads to enable sensitivity studies.

1 EUROCODE FIRES BASED ON OCCUPANCIES OF BUILDINGS

During systematisation of the fire loads, idealisations of real fires should be done to put the fire actions into a form readable by computers. The idealisations should be safe and describe all relevant features of the fires. The relevant features depend on the effects we are examining. For example, the most simplified representation of the heat release rate of the fire in Fig. 1 cannot predict the growth

and decay phases of fires which are important in some cases, but may be enough when considering the ultimate resistance of the structures.

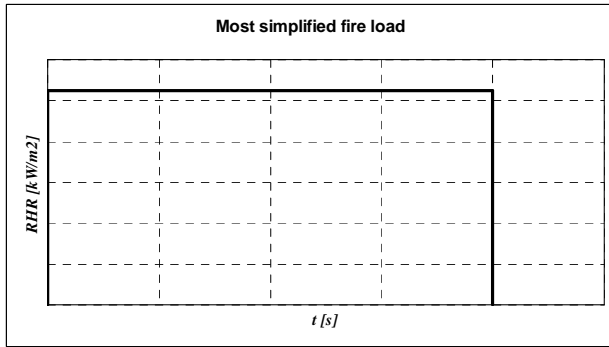


Fig. 1 Simplified fire load

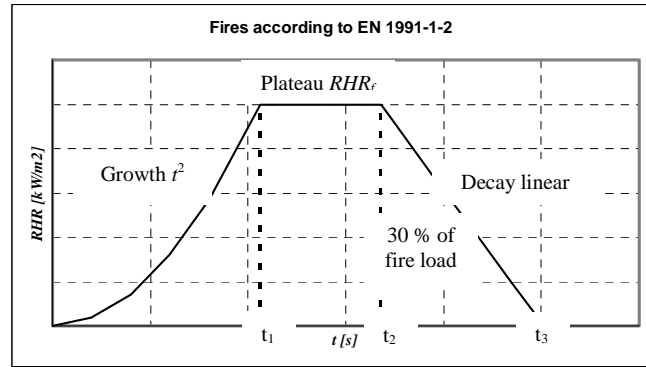


Fig. 2 Eurocode fire loads

Fig. 2 presents the idealisation of the rate of heat release (RHR) used in Eurocodes for fires based on occupancies of buildings. The parameters needed to specify the fire of Fig. 2 are:

- RHR_f [kW/m^2], (maximum heat release rate per area, plateau value),
- t_α time to reach 1MW [s] (controls the growth phase of the fire, t^2 rule used),
- $q_{f,k}$ [MJ/m^2], (maximum fire load density per area),
- A_{fi} [m^2], (the maximum area of the fire, which is the fire compartment in case of a uniformly distributed fire load, but which may be smaller in case of a localised fire).

The 30% rule shown in Fig. 2 defines the time t_3 when the fire ends, and this 30% can be considered the parameter given in the Eurocodes. The first three parameters in the Eurocodes are given based on the occupancy of the building. The fourth parameter A_{fi} should be defined by the designer. When these parameters are known, the times t_1 , t_2 and t_3 can be calculated using the equations:

$$q_{f,k} = \int_0^{\infty} RHR_f dt \quad (1)$$

$$t_1 = t_\alpha \cdot \sqrt{\frac{RHR_f \cdot A_{fi}}{1MW}} \quad (2)$$

$$q_1 = \int_0^{t_1} \frac{1MW}{A_{fi}} \cdot \left(\frac{t}{t_\alpha}\right)^2 dt = \frac{1}{3} \cdot \left(\frac{1MW}{A_{fi}}\right) \cdot \frac{t_1^3}{t_\alpha^2} \quad (3)$$

$$q_2 = RHR_f \cdot (t_2 - t_1) = q_{f,k} - q_1 - q_3 \Rightarrow t_2 = t_1 + \frac{q_{f,k} - q_1 - 0.3 \cdot q_{f,k}}{RHR_f} \quad (4)$$

$$t_3 = t_2 + \frac{2 \cdot 0.3 \cdot q_{f,k}}{RHR_f} \quad (5)$$

Fig. 3 illustrates all Eurocode fires based on different occupancies for $A_{fi} = 200 \text{ m}^2$ using Eqs. (1)-(5).

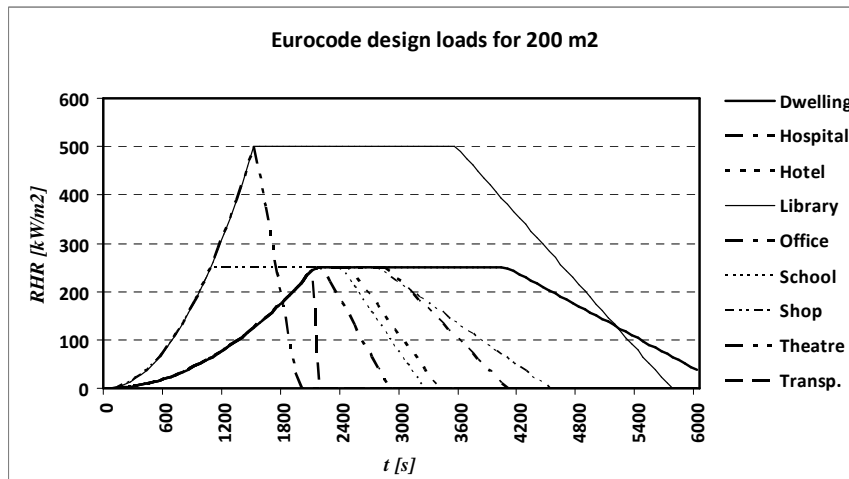


Fig. 3 Eurocode fires based on occupancies

The Eurocodes assume that the fire load is located across the entire floor area. However, when considering e.g. the resistances of roof structures, the fire may be located above floor level. In this study the fire loads are located about 1 m above floor level across about 1x1 m² horizontal areas, which are conservatively supposed to ignite simultaneously. Moreover, these fire sources are located randomly at 1 m +/- one grid length in the vertical direction. The exact locations of the fire sources are defined so that they will fit the computational grid. Horizontal distances twice (N=2) the grid size in corresponding directions between the fire sources (chessboard) were found most critical in numerical tests for distances 1, 2, 3 and 4 times grid size. The criteria were the maximum temperatures near the ceiling of the 7x7 m² classroom at a height of 3 m. The heat release rates of the chessboard areas should be increased so that the total heat release matches the original.

Fig. 4 shows the FDS result for one classroom simulation and Fig. 5 shows the temperatures near the ceiling, Point 8. The resolution in Fig. 5 is defined in (Heinisuo et al, 2008) and is used to define the proper grid size for the fire simulations. Note, that resolution 7 is much smaller than recommended, but it gave about the same results as using the recommended value in this case.

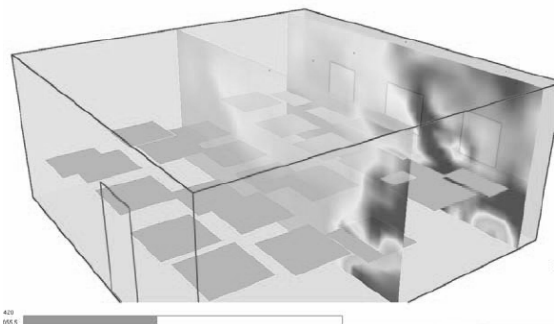


Fig. 4 Classroom FDS model

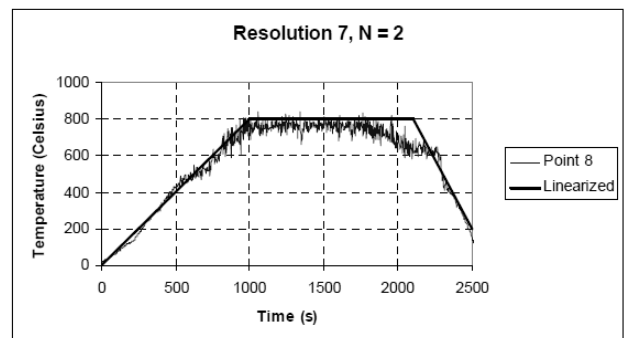


Fig. 5 Gas temperatures near ceiling

Fig. 5 also shows the linearisation of gas temperatures in fire. When defining the resistances of structures, this kind of linearisation is essential to reduce the computing time in post-processing. The exact definition of the linearisation will be considered in further studies.

It is recommended that at least two simulations are done in the case of sensitivity studies. The second run is done by varying the grid size whereby the levels of the fire sources change automatically, because they are defined using random processing. Variation of the grid size is not necessary if the original grid size is defined using the definition of (Heinisuo et al, 2008).

The effects of sprinklers are taken into account based on two scenarios: a local sprinkler fire and a global sprinkler fire. The local sprinkler fire is defined so that the fire ignites just above the broken sprinkler, which is a conservative assumption (Heinisuo et al, 2010). Other sprinklers stop the fire

in other areas and we end up with a local fire without sprinklers. The fire area A_{fi} is defined as the area covered by the broken sprinkler, typically about $3 \times 3 \text{ m}^2$.

The global sprinkler fire is defined by modelling the sprinklers as they are in the FDS analysis while otherwise using the input data given above. This means that the fire is not stopped by sprinklers. They only cool down gas temperatures. In this case we should also assume that some of the sprinklers will not work by reducing the flow rate of the sprinklers by, say, 10% in the input file of the FDS. Typically, a local sprinkler fire is more severe than a global sprinkler fire. The sprinkler data should correspond to the planned properties of the sprinklers of the project.

Fig. 6 shows the critical model (this study used three models corresponding to the three different locations of broken sprinklers) for the local sprinkler fire 3 and the corresponding temperatures at the control points of the $7 \times 7 \text{ m}^2$ classroom in the Eurocode classroom fire. Control points are located near the ceiling and windows. Fig. 7 shows the temperatures at the same control points in the global sprinkler fire. The default K11 sprinklers were located 2.5 m from each other near the ceiling.

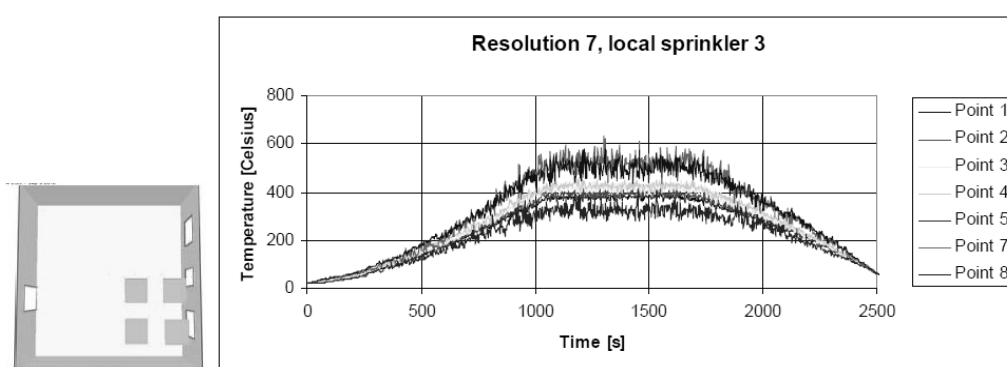


Fig. 6 Critical local sprinkler fire

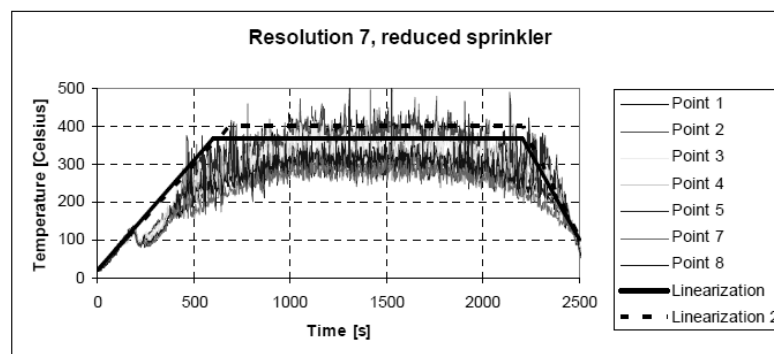


Fig. 7 Global sprinkler fire

The Eurocodes give reduction factors for design fire loads with sprinklers. If an automatic water extinguishing system exists and the number of independent water supplies varies from 0 to 2, then the reduction factors are: at 0 $0.61 \times 1.00 = 0.61$ (load 1), at 1 $0.61 \times 0.87 = 0.53$ (load 2), at 2 $0.61 \times 0.70 = 0.43$ (load 3). The temperatures based on Eurocode reductions for the fire loads with sprinklers were very high (maximum near 800°C) compared to the global sprinkler fire defined above (see Fig. 7).

2 RACK FIRES

Five categories of rack-stored commodity fires are proposed (Hietaniemi, Mikkola, 2010):

1. 150 kW/m^2 which corresponds to a typical fire load of cellulose materials such as wood and paper products.

2. 300 kW/m² which corresponds to a typical fire load that may consist of cellulose materials and some fire retardant or otherwise not very highly combustible plastics such as PET, POM, etc. A furniture fire load may fall in this or the next category.
3. 500 kW/m² which corresponds to fire loads consisting of mixtures of cellulose materials (major ingredient) and highly combustible plastics such as ABS, PE, PP and PS, or where plastics such as PET, POM, PMMA are the principal ingredient. A furniture fire load may also fall in this category.
4. 1 000 kW/m² which corresponds to a typical fire load consisting of significant amounts of non-fire retardant, highly combustible plastics such as ABS, PE, PP and PS. The other ingredients may be e.g. cardboard boxes, etc.
5. 2 000 kW/m² which corresponds to fire load consisting of a very high percentage of non-fire retardant, highly combustible plastics such as ABS, PE, PP and PS. E.g. a boat store fire.

All rack fires are modelled using combinations of basic fuel boxes. The nominal dimensions of the basic box are 100x800x400 mm³. The actual dimensions of the boxes are fitted to the computational grid of the FDS. The distance between boxes in every direction is one grid length in the direction in question. As many full boxes as possible are fitted in the rack area. The box direction is perpendicular to the rack area direction. In this study the shelves are modelled as non-combustible plates with a nominal thickness of 100 mm. The properties of each box are:

- Ignition temperature 320 °C,
- Density 500 kg/m³,
- Specific heat 1.5 kJK⁻¹kg⁻¹,
- Thermal conductivity 0.2 WK⁻¹m⁻¹.

One box is used for ignition. The others ignite after reaching the ignition temperature. Burn away option of the FDS is used for boxes. An ignition box is located at the bottom and at the top of the rack - both cases should be simulated. Sprinklers are modelled as above, locally or globally. Fig. 9 shows a case of a category 1000 kW/m² rack fire without sprinklers with an ignition box at the bottom or at the top.



Fig. 9 Ignition bottom

Ignition top

It is recommended that both bottom and top ignition be studied. Moreover, it is recommended that the required resolution factor be used to define the proper grid size for rack fires. A lot of CPU time will unfortunately be required for small heat release rate categories (150 - 300 kW/m²).

3 VEHICLE FIRES

Based on (Hietaniemi, Mikkola, 2010) and (Haack, 2001) a so-called Type 2 car fire (e.g. Renault Megane) in the case of a 2x5 m² floor area was implemented in this study to study fire loads of car parks in Finland. The critical locations of the cars were defined using the rules of (Shleich, 2010).

The heat releases from one and three cars are shown in Fig. 10. The equations for the design curves are given in (Heitaniemi, Mikkola, 2010). An adjacent car ignited 12-15 minutes after a car had started to burn based on tests. The heat release from three Type 2 cars is the sum of the heat releases from three individual cars as shown in Fig. 11 using 12 minute ignition delay.

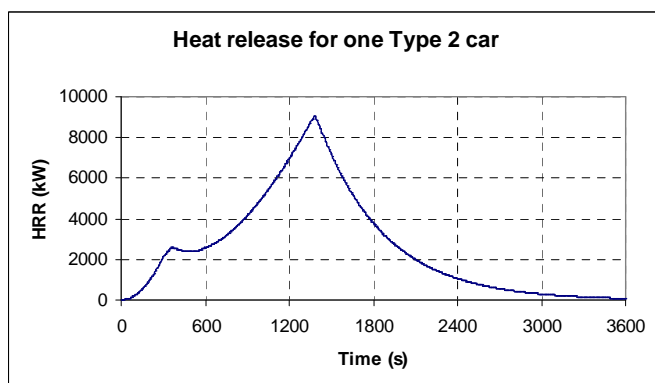


Fig. 10 Heat release for one Type 2 car

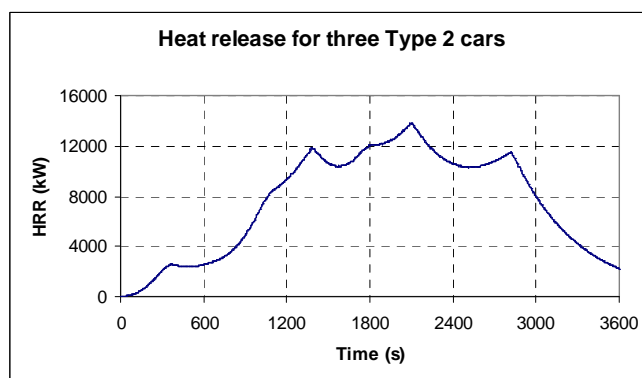


Fig. 11 Heat release for three cars

Heavy goods vehicle (HGV, 40 MW), petrol tank (the most severe 200 MW) and bus fires (20 and 34 MW) were also implemented in this study. HGV and petrol tank design fires (heat release rates, kW/m²) are presented for the top surface of the geometrical entity shown in (Hietaniemi, Mikkola, 2010). Two bus fires for a 3x10 m² area 1 m above the floor level are presented after the definitions of (Hietaniemi, Mikkola, 2010).

4 SUMMARY

Eurocode, rack and vehicle fires were implemented in this study for the integrated fire design system. Comprehensive experimental and theoretical background studies on rack and vehicle fire loads can be found in literature which form a solid basis for the standardisation of these fire loads. Eurocode fires based on occupancies are presently being checked and in the near future they may be revised for use in practical projects.

REFERENCES

- EN 1991-1-2, Eurocode 1: Actions on structures, Part 1-2: General actions, Actions on structures exposed to fire, CEN, Bryssels, 2003.
- Haack A., Rapporteur, STUVA, Design Fire Scenarios, technical Report – Part 1, Thematic Network, FIT- Fire in Tunnels, Contract no G1RT-CT-2001-05017, WTC, Brussels, 2001.
- Heinisuo M., Laasonen M., Hyvärinen T., Berg T. Product modeling in fire safety concept, effects of grid sizes and obstacles to steel temperatures, In: Proc of IABSE Helsinki Conference, 2008.
- Heinisuo M., Hietaniemi J., Kaitila O., Laasonen M., Outinen J., Integrated fire engineering of steel skeleton using well established fire sources. In: International Conference, Application of Structural Fire Engineering, Prague, 19-20 February, 2009. pp. 380-385.
- Heinisuo M., Laasonen M., Outinen J., Fire design in Europe. in: Cost Action C26, Urban Habitat Constructions under Catastrophic Events, CRC Press/Balkema, London, 2010, pp. 375-402.
- Hietaniemi J., Mikkola E., Design Fires for Fire Safety Engineering, VTT Working Papers 139, VTT, 2010.
- Shleich J-B, Modern Fire Engineering, Fire Design of Car Parks, Arcelor Profil, Luxembourg Research Centre. (Internet publication), 2010.

A STRUCTURAL FIRE ENGINEERING PREDICTION FOR THE VESELÍ FIRE TESTS, 2011

Shan-Shan Huang^a, Ian Burgess^a and Buick Davison^a

^aThe University of Sheffield, Dept. of Civil and Structural Engineering, UK

INTRODUCTION

When a fire occurs in a building the internal forces in the joints change substantially during the course of the fire, even though the external forces applied to the structure remain unchanged. This results mainly from restraint to thermal deformations and degradation of the mechanical properties of the building materials at high temperature. These phenomena were observed in both full-scale tests (Newman *et al*, 2004) and actual fires (NIST 2005, 2008). Because current design methods for connections are solely based on ambient-temperature behaviour, the additional forces and rotations generated in fire are not taken into account. If, at any stage of fire exposure, a connection does not have sufficient resistance to accommodate the large rotations and co-existent forces, fracture will occur. This may lead to extensive damage or progressive failure of the structure. Therefore, how the joints perform in a building fire will be critical to whether it would be able to survive the fire attack.

The Structural Fire Engineering Research Group of the University of Sheffield is participating in the European-funded project COMPFIRE (RFCS 2008), a collaboration between research teams at universities in Manchester, Coimbra, Luleå and Prague, Desmo Ltd in the Czech Republic, and TATA Steel Tubes Europe. The objective of this project is to investigate the behaviour and robustness in fire of practical connections between steel beams (both composite and non-composite) and two types of composite columns - concrete-filled tubular (CFT) and partially-encased H-section columns. Two natural fire tests on a full-scale composite structure are planned to take place in Veselí, in the Czech Republic (Wald 2011). One task of the Sheffield research team has been to predict the structural behaviour of the tests before they are conducted. The assessment was conducted using the specialist structural fire engineering FEA program *Vulcan*, and this paper reports the results of this predictive analysis.

1 TEST DESCRIPTION

The objectives of the Veselí tests are to provide experimental data on the response of composite frames to a natural fire, and to demonstrate the impact of improved detailing of joints on structural robustness in fire. The tests are scheduled to be conducted on the 6th and 15th of September 2011. They have been designed and are to be carried out by the Prague team of COMPFIRE (Department of Steel and Timber Structures of the Czech Technical University) and the Sheffield team has checked the design of the connections. Two fire tests will be performed on the test structure in sequence, one on each storey. During the first test (hereafter referred to as Test 1), the upper storey will be heated without mechanical loading applied on the slab above. This test does not aim to cause failure; the objectives are to observe the heat transfer in the compartment and to measure the temperature distributions in the structure, particularly in the beam-to-column connections. The second test (Test 2) is to be performed in the lower storey, which is subject to both mechanical and fire loading, with the upper floor cool. It aims to collect temperature data and to demonstrate the robustness in fire of the particular types of joints investigated in this project. Failure of the connections is expected.

The test has been set up as a 9m high, 10.4m x 13.4m two-storey office building structure as shown in Figures 1 and 2. The floor system consists of 120mm thick composite slabs with trapezoidal decking and Grade C30 concrete. The slabs act compositely with the steel beams with TRW Nelson 19mm diameter and 100mm height shear connectors in each rib. The slabs are reinforced

with a plain bar mesh, providing a steel area of $196\text{mm}^2/\text{m}$ in each direction, situated 20mm below the top of the slab. There is also a $\phi 8\text{mm}$ reinforcement bar in each rib, with 20mm cover from the bottom of the slab.

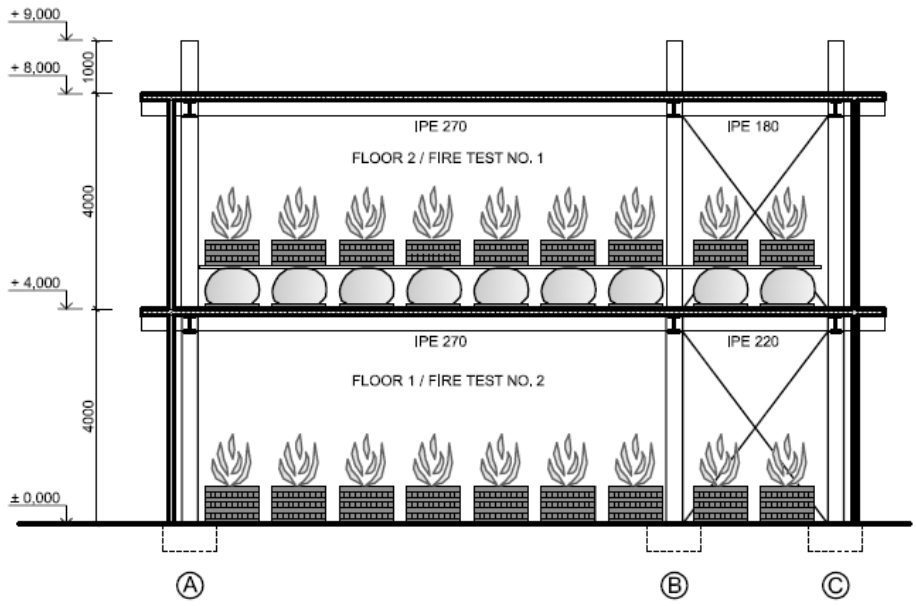


Fig. 1 Test setup (Wald 2011)

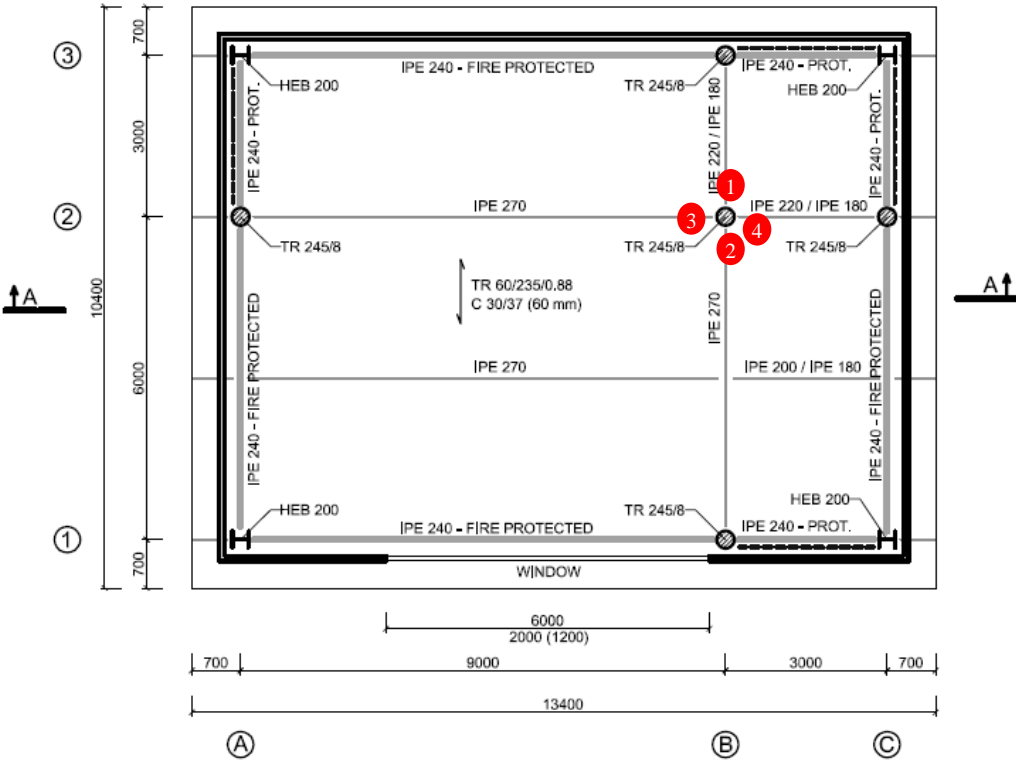


Fig. 2 Floor plan of the test structure (Wald 2011)

The edge beams are all IPE 240, while IPE 270 beams are used for the 9m span interior beams and IPE 220, IPE 200 and IPE 180 are used for the shorter-span ones. The floor arrangement is supported by five circular CFT columns (TR 245/8 filled with Grade C30 concrete) and four HEB 200 steel columns at the corners. All columns and beams are of Grade S355 steel. Two types of connections, reverse-channel and fin-plate, are adopted. The horizontal stiffness of the building is provided by two sets of cross bracing of tubular section in each direction of each floor. The columns, edge beams, bracings and connections in the lower floor are fire-protected to a standard

resistance R60. All the other elements are unprotected. The cladding walls, which are composed of liner trays, mineral wool and external corrugated sheets, form a fire compartment on each floor. The applied mechanical load has been designed to represent that of a typical office building. The imposed load of 3.0kN/m^2 on the slab is generated by bags filled with gravel and recycled concrete. The self-weight of the floor system (including the slabs and floorings) is 2.85kN/m^2 and that of the partitions is 0.5kN/m^2 . The fire load is generated by timber cribs of size $50\text{mm} \times 50\text{mm} \times 1000\text{mm}$ to simulate a natural fire in a regular office building. A $2\text{m} \times 6\text{m}$ unglazed opening in the front wall of each floor provides ventilation to the fire. More details of the test setup can be found in Wald (2011).

2 PRE-TEST MODELLING USING *Vulcan*

This section reports the pre-test predictions of the structural response of the loaded test (Test 2). The modelling was conducted using the structural fire engineering FEA program *Vulcan* (VSL).

2.1 Model setup

Based on the design brief, the model was set up as shown in Figure 3. For simplification the flooring system and the beams of the upper floor were not modelled, but their self-weight (2.85kN/m^2) was applied on the column tops as concentrated loads. The applied load on the slab was 6.35kN/m^2 , which is the overall actual (unfactored) load. The column base was assumed to be fixed. Since the frame is braced, the top ends of the upper-floor columns were restrained against lateral movement but free to deform axially, so thermal elongation is unrestrained. All the other elements had neither translational nor rotational restraints. While waiting for the actual temperature data, the first predictions were made by relating the beam, column and slab temperatures to a Eurocode 1: Part 1.2 (CEN 2002) type of fire curve (Figure 4) which reaches 1000°C at 60 minutes and then starts to descend linearly. The upper-floor elements were exempted from this assumption, as they were assumed to remain cool throughout the analysis.

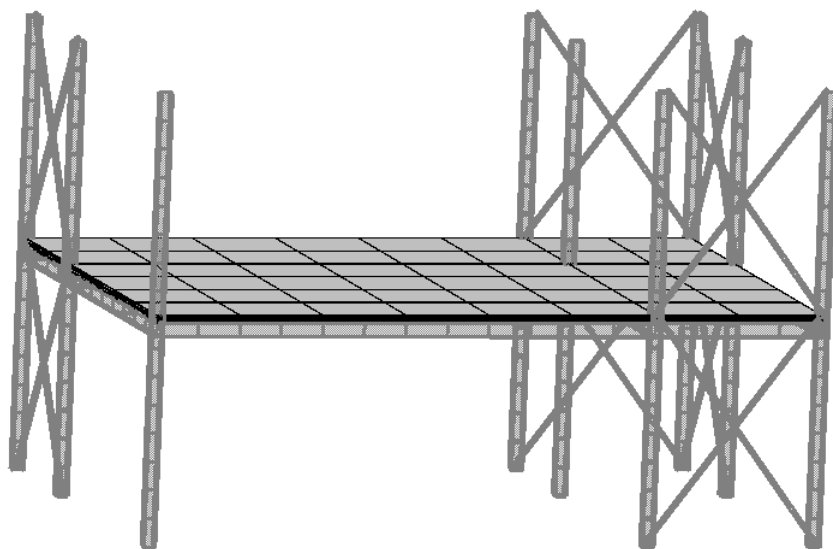


Fig. 3 Vulcan model setup

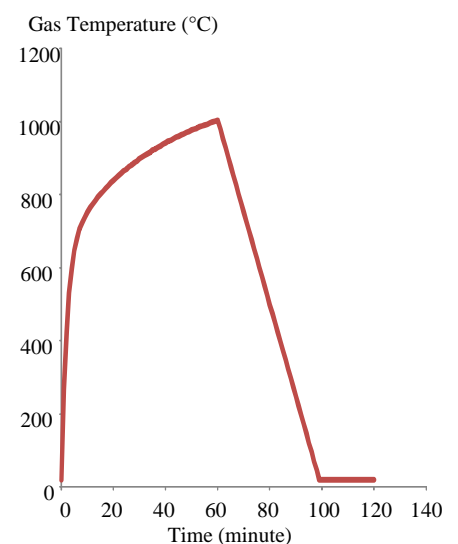


Fig. 4 Fire curve

For the unprotected beams, the temperatures of their bottom flanges and webs were assumed to be 95% of the fire temperature, and the top flanges to be at 80% of the fire temperature. The temperatures of the bottom flanges and webs of the protected beams were assumed to be 50% of the gas temperature, and the top flanges to be at 45% of the fire temperature. The lower-floor columns and bracings, which will be protected, were set as uniformly heated to 50% of the gas temperature. The temperature gradients through the slab depth were represented as a bilinear distribution, in which the slab lower surface was as hot as the fire; the temperature was 50% of the gas temperature 30% into the depth from the bottom, and the top surface reached only 15% of the fire temperature.

After the tests have been conducted, the recorded temperature data will be used as more accurate input data to the *Vulcan* model.

For the diagonal bracing members, RHS 60mm x 60mm x 6mm of Grade S275 steel were assumed in the model. Due to the limitation on mesh shape in *Vulcan*, and the resulting complexity of modelling circular sections, the circular CFT columns were modelled as equivalent (in terms of cross-section area and second moment of area) square columns of 215mm width. The connections were represented using rotational spring elements at this pre-test stage. As a part of the COMPFIRE project, a comprehensive component-based connection element is being established in *Vulcan*; the model will be upgraded using this connection element after the tests. The connections were assumed as rigid, pinned or semi-rigid by varying the rotational stiffnesses of the springs. The orthotropic nature of the slab was accounted for by using the *Vulcan* effective stiffness approach (Huang *et al.* 2000). The full depth of the composite slab was modelled as a flat slab with different bending stiffnesses in the two orthogonal directions to account for the contribution of the ribs. The shear studs connecting the composite slabs and beams, each of which was assumed to have an ultimate shear strength of 350N/mm², were modelled using the shear-connector elements embodied in *Vulcan*, providing partial interaction between the slabs and beams.

2.1 Results

The results of the *Vulcan* analyses are summarised in Table 1. Five models with different connection rigidities were analysed by varying the rotational stiffnesses of the spring elements, which were used to model the connections.

Tab. 1 *Vulcan* analysis results

Model No.	Connection Rigidity	Rotational Spring Stiffness (Nmm/rad)	Fire Resistance Period (minutes)	Max. Slab Displacement (mm)	Max. Connection Tying Force (kN)
1	Pinned	100	29	891	118
2	Semi-rigid	5x10 ⁵	49	939	119
3	Semi-rigid	1x10 ⁹	120	728	268
4	Semi-rigid	1x10 ¹⁰	120	666	309
5	Rigid	1x10 ¹²	120	642	354

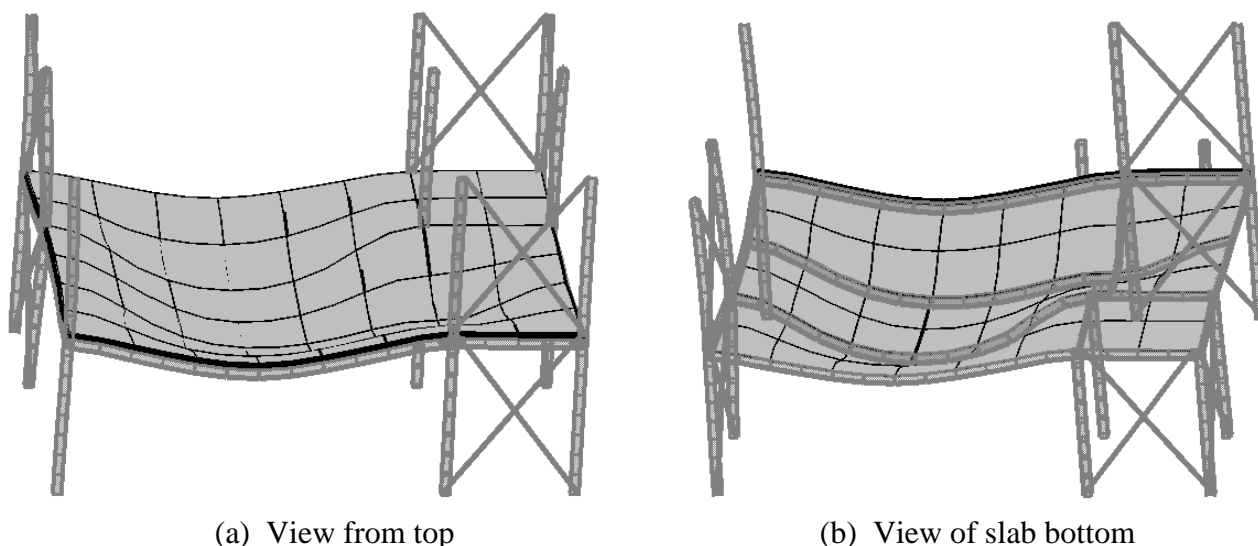


Fig. 5 Deformed *Vulcan* model

The model with pinned connections failed at 29 minutes. Unsurprisingly, the fire resistance period was extended with increasing connection rigidity, and Models 3, 4 and 5 survived through the whole course of loading and heating without experiencing failure. The deformed shapes of the models are similar. One example is shown in Figure 5, in which the deflections are magnified three

times. The centre of the slab panel A1-B3 experienced the highest vertical displacement. Figure 6 shows the development of the slab displacement at this point over time for each model, and the maximum displacement which occurred throughout the course of analysis is given in Table 1. The model with rigid connections deflected substantially less than the one with pinned connections, even though it was subject to much higher temperatures. On the other hand, Model 2 (with semi-rigid connections) experienced a larger deflection than Model 1 (with pinned joints), due to its extended fire resistance period compared to that of the latter.

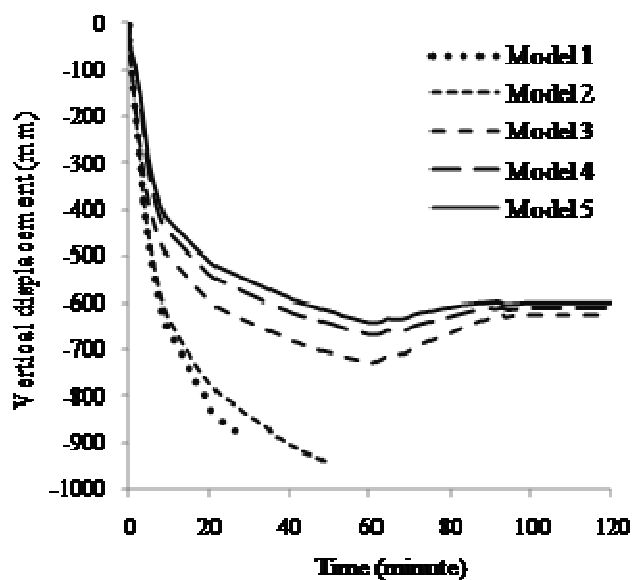


Fig. 6 Maximum displacement of slab

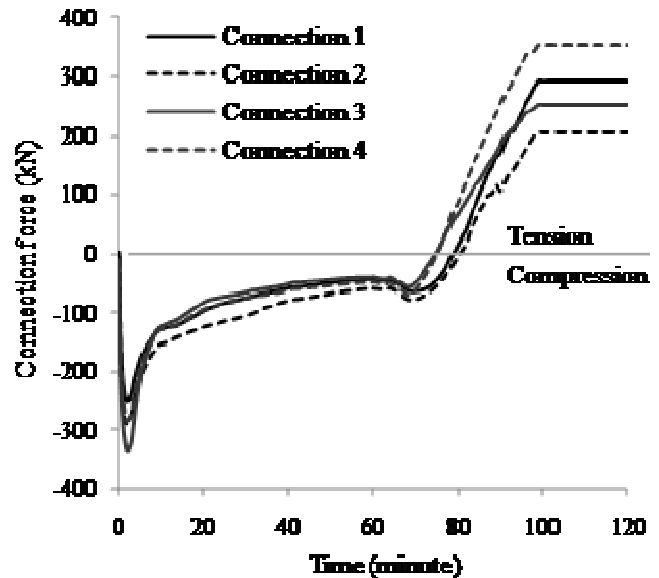


Fig. 7 Connection forces of Model 5

Due to its higher structural continuity and exposure to higher temperatures, the maximum tying force generated in the connections of Model 5 (with rigid connections) was significantly larger than those of the other models, as given in Table 1. The forces in the connections to Column B2 of this model are plotted in Figure 7. The numbering of these connections is marked on the floor plan (Figure 2). The connections were initially in compression due to the restraint to thermal expansion, but as heating continues and the beams deform further, the compressive forces decrease and finally turn into tension during cooling. This phenomenon corresponds closely with the horizontal displacement of Column A2. It can be seen that, after an initial outward movement due to thermal expansion of the structure, this column moved inwards due to pull-in by the vertically-deflecting beams. This observation may prompt speculation about a possible cause of the failure of Models 1 and 2. Further in-depth analyses will be carried out after the tests, in the light of measured temperature and structural data.

3 CONCLUSION

In this paper, an initial prediction has been made of the response to natural fire of the composite structure to be tested later in 2011 at Veselý using the finite element program *Vulcan*. While awaiting precise data (such as the temperature distributions) which will only be confirmed when the tests are performed, conservative assumptions have been made at this pre-test prediction stage. Since the robustness in fire of the connections is of particular interest in these tests, five models of identical setup but different connection rigidities were analysed, and the following behaviour has been observed:

- The deformation shapes of the models are similar;
- Initially, the floor system expanded, which pushed the edge columns outwards and induced high compression in the connections due to restrained thermal expansion;
- This action reversed as the beam deflected further: the columns moved inwards due to pull-in by the deflecting beam, and the connection forces eventually reversed, becoming tensile;

- The effect of connection rigidity on the fire resistance and deformability of the structure is considerable; the fire resistance of the structure is enhanced by increasing the rotational stiffnesses of the connections;
- For the models with more rigid connections, the maximum tying forces in the connections are greatly increased, although the maximum slab displacements are not necessary smaller, since these models experience higher temperatures.

ACKNOWLEDGMENT

The research leading to these results has received funding from the European Community's Research Fund for Coal and Steel (RFCS) under grant agreement n° RFSR-CT-2009-00021.

REFERENCES

- European Committee for Standardization (CEN), BS EN 1991-1-2, Eurocode 1. Actions on structures. General actions. Actions on structures exposed to fire, British Standards Institution, UK, 2002.
- Huang, Z., Burgess, I. W. and Plank, R. J., Effective Stiffness Modelling of Composite Concrete Slabs in Fire, *Engineering Structures*, Volume 22(9), pp 1133-1144, 2000.
- Newman, G. M., Robinson, J. T. and Bailey, C. G. *Fire Safety Design: A New Approach to Multi-Storey Steel-Framed Buildings*, The Steel Construction Institute, Ascot, 2004.
- NIST, *Final Report on the Collapse of the World Trade Center Towers*, National Institute of Standards and Technology, USA, 2005.
- NIST, *Final Report on the Collapse of World Trade Center Building 7*, U.S. Department of Commerce and National Institute of Standards and Technology, USA, 2008.
- RFCS, *Design of Joints to Composite Columns for Improved Fire Robustness*, Research Fund for Coal and Steel, Grant agreement n° RFSR-CT-2009-00021, European Commission, Belgium, 2008.
- Vulcan Solutions Limited: <http://www.vulcan-solutions.com>
- Wald, F., *Demonstration Fire Test on Real Object - Veselí 2011*, The Czech Technical University, Czech Republic, 2011.

STRUCTURAL FIRE ENGINEERING IN BUILDING RENOVATION

Application of Natural Fire and Heat transfer Models to guarantee Fire Safety

Tom Molkens ^a

^a StuBeCo, Engineering Office, Overpelt, Belgium

INTRODUCTION

Till the years seventy or nearly eighties of previous century most of the concrete structures are developed just to resist loads in so far “cold” situations. Due to this reason there rise often problems at the moment of structural renovations. This at two levels; the deformations seems to be unexpected big and the fire resistance of the structural elements are insufficient to guarantee the required level. The deformation problem in the scope of this study no issue.

By the aid of a case study with a problematic concrete floor and cover we want to show the possibilities of software tools to calculate different options which finally must lead to an integrated fire risk management and guaranteed fire stability.

The limitations of this approach don't stop with concrete because this is the main problem in this case study. It seems that also existing wood, masonry and steel structures have the same problems and can be solved on a similar way.

1 DESIGN CONSIDERATIONS

1.1 Juridical

Strictly juridical spoken there is in a lot of cases no need for a proven fire stability. In most of the cases the need for application of a law will be linked to buildings with a building permit request after the publishing date of the law (for example Annexes R.D., 1997). So existing building (or parts) escape, even in rather heavy transformation, to the regulation for new buildings.

For our case study the special Belgian regulation for school buildings (IBN/BIN, 1982) is valid and requests only one half hour of fire stability, with only day-use of the building. Only for buildings/parts with permit requests after 1997, the normal regulations for low buildings are valid which would ask a fire resistance of at least one hour. Because his higher order this regulation is mostly used, but like already said not on application for existing buildings.

Unless this juridical possibilities or call it leaks, the school authority wants to assure in our case-study a higher level of security instead of the half hour (maximum which can be achieved by application of tabulated data). This to be in order with their own conscience. Just for the case if something must happen with the knowledge that there building didn't fit actual regulations.

1.2 Scientific

To solve this conscience problem we presented the school a natural fire with the criterion that the existing structure must withstand the whole duration of the fire. There is no longer an estimated time because we're speaking about a natural fire and not about a comparison criterion like the ISO834 is. Belgian regulation (Annexes R.D., 1997) allows such an approach but the calculations must be approved by the interrogation commission of the ministry of internal affairs.

The advantage for an old building of this approach is that because there is no regulation valid, we can skip this verification by the interrogation commission. This becomes therefore more cost effective because of lesser administration and lesser retarding effects on the building process. This latest is important because mostly the inconvenience comes clear in the demolishing phase just before rebuilding. However in our opinion the missing of verification can be a disadvantage, because such natural fire models can be sensitive for boundary conditions.

With the presence of rather heavy masonry, concrete floors and not a real high amount of windows, it can be estimated that the fire will be smouldered and not very explosive.

1.3 Software use for structural fire engineering

After juridical and scientific considerations we've got to solve the problem and therefore rather easy to use software solutions are available, sometimes even free. For our approach we made use of a 2-zone model (Ozone V2) to determine the fire load. This fire load is introduced in a basic commercial available thermo elastic frame work software called Powerframe. To reduce the problem to a 2D-frame we made a slice of 1 m width. This allows us to regard not only the thermal behaviour of the sections but also to the thermal expansion effects of the structure as whole. With those rather simple "in use" software tools we can obtain much more guarantees about the behaviour of the structure in case of fire as before.

2 DESCRIPTION OF THE CASE STUDY

2.1 Geometry

The involved building part was build in 1939 and in the 50's of previous century extended, the oldest part dates from 1881. The connection between those 3 building phases was partially demolished to create a new entrance with some new facilities. Partial, because a part of the building (with an audience) was protected by the ministry of monuments and sites, this must be kept in his original shape.

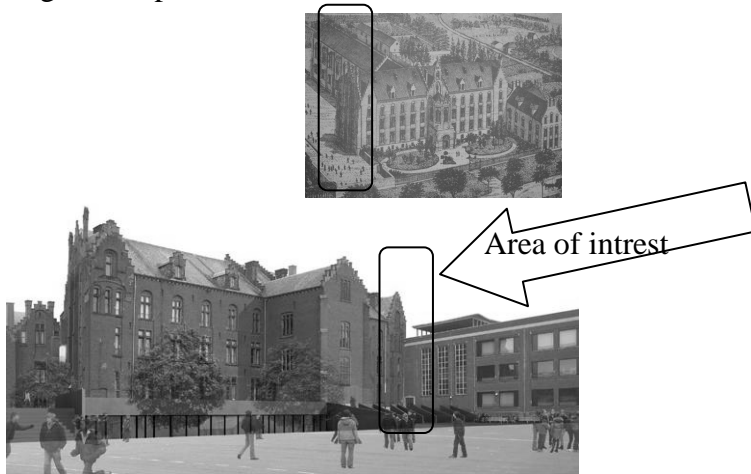


Fig. 1 Elevation views



Fig. 2 View from demolished area

Besides previous images the ground floors and section made by the architect gives a much better idea of the dimensions of the structure.

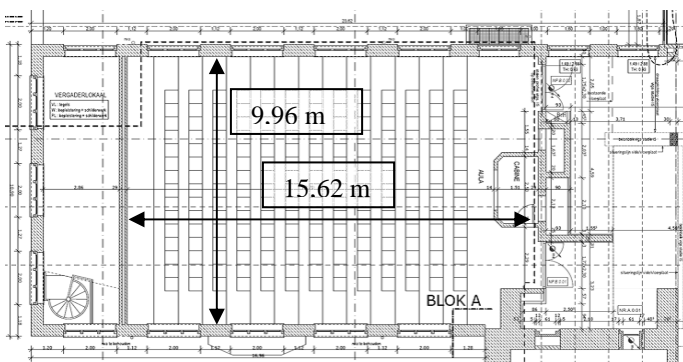


Fig. 3 Ground view; 9,96x15,62 m²

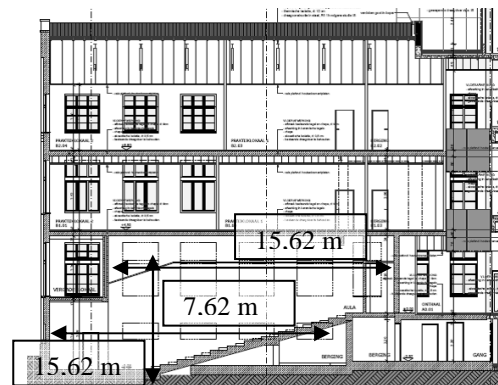


Fig. 4 Section; 7,62 m

The structure exists of bearing masonry and ribbed concrete slabs. The slabs support from elevation to elevation without any intermediate support. Besides the auditorium at 0-level we've also classes at the first and second floor level. Above the second level there are steel truss beams which were in tender foreseen to be protected with anti-combustion painting.

2.2 Materials

All material properties corresponds with the relevant EN-standards for concrete, steel and masonry. We've summarized those in Tab. 1.

Tab. 1 Material properties

Material	ρ [kg/m ³]	$\Delta L/L$ [mm/mK]	λ [W/mK] at 20°C	c [J/kgK]
Masonry	1600	5	0,70	840
Concrete	2300	10*	1,60*	1000*
Steel	7850	12*	14,6*	450*

* Those values are at 20°C and are only automatically adapted in function of temperature in the frame work model to calculate the mechanical response

3 FIRE LOAD

To limit fire risks it was obtained that each schoolroom or auditorium will be executed as a separated compartment. Only fire doors were not yet foreseen, so the extra cost was not an obstacle. Due to the EN 1991-1-2 the fire load exists of uniformly distributed 347 MJ/m² for a typical schoolroom (tab E.4, 80% fractile). Because of the presence of a wooden false ceiling we raised it for the audience till 511 MJ/m² (+ 21 mm of wood).

For the fire a NFSC fire curve was chosen; fire growth was taken as medium, with a rate of heat release equal to 250 kW/m², danger of activation = 1, reduction for heat detection (0,87), off site brigade (0,78) and raise because of the surface (1,43). The combustion efficiency factor was putted on 0,80 (wood based fire). Because the building can't be air-closed a constant ratio of 2% of the vertical surface is introduced as a kind of natural ventilation factor + windows and doors without REI value of course.

3.1 Audience

Thanks to the software several scenario's where investigated, in particular the influence of the window openings was investigated. Hereby was not only the temperature of importance but also the delay till flash-over. It was mentioned by the school authority that this time must me be as big as possible, at least 10 minutes to be similar with the other existing class rooms. In addition an extra exit bellow the audience seems to be absolutely needed to prevent evacuation problems. We start simulations with the actual situation:

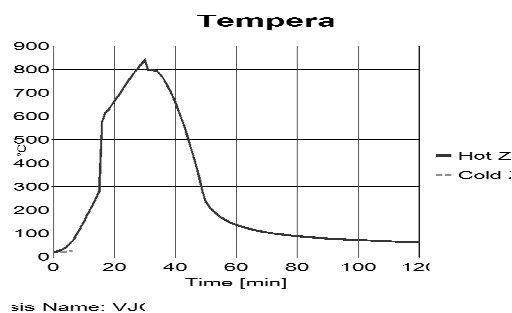


Fig. 5 Gas temperature actual situation

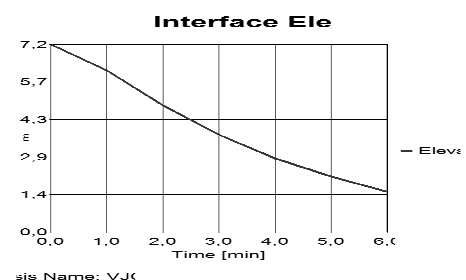


Fig. 6 Cold layer

It is rather clear that after 30 minutes we achieve a temperature which is almost the same as predicted by an ISO 834 conventional fire. But the peak value is only there in a shorter and limited time interval. The switch to one zone happens already after 6 minutes with a cold layer of only 1,54 m = first approximation of smoke free layer.

In the past they closed all window opening, because there is no need for day light in the audience. This avoid entrance of oxygen but also the evacuation of heated smoke. Therefore we did a new calculation with the upper part opened. There is certainly an influence on the temperature decreases from 900 till bellow 600 °C but the time till flash over stays still to big. This figures are not shown.

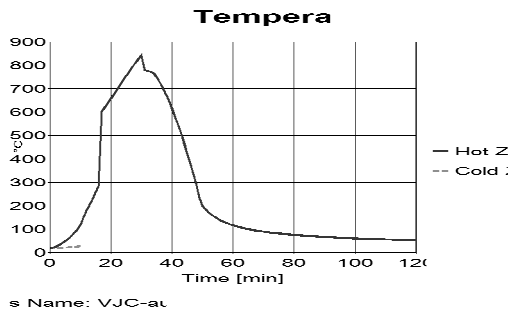


Fig. 9 Gas temperature + S&H system

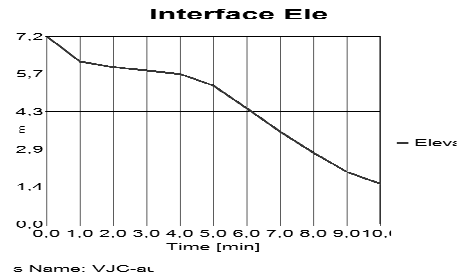


Fig. 10 Cold layer

By changing the ventilation group by a more advanced model which can act as a smoke and heat evacuation system (S&H system with 12 m³/s) we've reached the needed improvement of the time till flash over but the temperature stays still high. By removing the false ceiling (it is a fire load of 347 instead of 511 MJ/m²) only the time interval with higher gas temperatures can be reduced with about 6 minutes. There is no effect on other parameters.

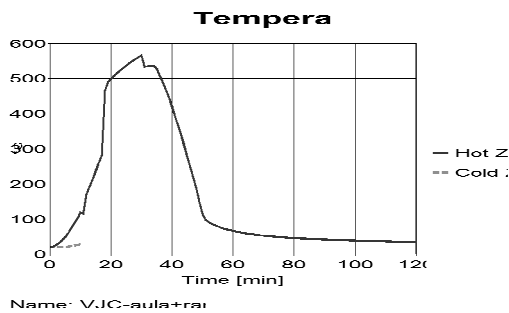


Fig. 11 Gas temperature + S&H system

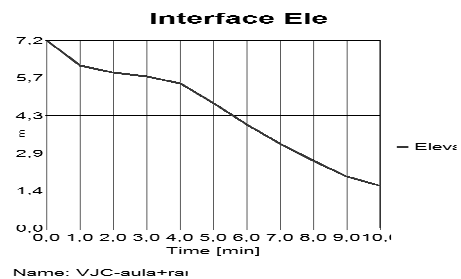


Fig. 12 Cold layer

It seems that a combination of passive (making high openings in masonry) and active equipment (S&H system with 10 m³/s) can lead to low temperature profiles, limited in time and with an acceptable delay till flash over. This option was therefore proposed and chosen.

3.2 Class room at first level

We've looked for the classroom that has the highest ratio window/wall surface to obtain the most worst fire scenario = room 1.01.

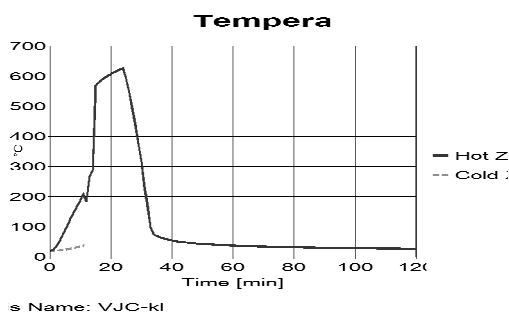


Fig. 13 Gas temperature + S&H system

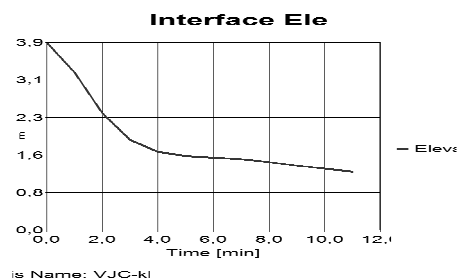


Fig. 14 Smoke layer

Because there are in relation to the elevation surface more opening the temperature rises, due to the limited fire load (347 MJ/m², no wooden false ceiling) the width of curve with higher temperatures is however more limited.

3.3 Class room at second level

As before we made the same exercise but for room 2.04, unfortunately we don't have any more a heavy ceiling but only a plasterboard covering of the steel structure.

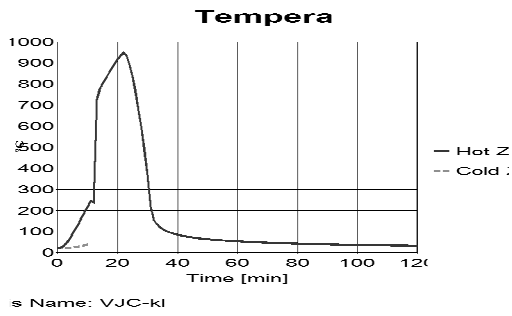


Fig. 15 Gas temperature + S&H system

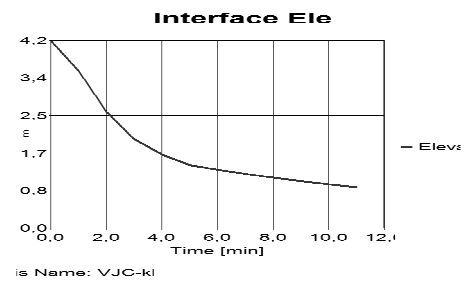


Fig. 16 Smoke layer

The temperature rise higher and quicker as before without “damping” mass

4 REACTION OF THE STRUCTURE

At this moment we’ve calculated several fire loads which are different for each level. Those fire loads are incorporated in a slice-model of the structure. The width is taken equal to 400 mm (= distance between ribs) except at the location of windows where it is limited to the ratio sum of all windows/overall width of the elevation. Spring constants equal to $3EI/L$ are integrated at the hinges to avoid a mechanism and making a realistic approach of stiffness boundaries.

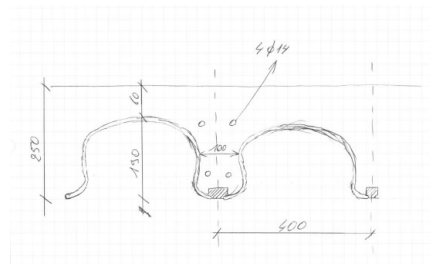


Fig. 17 Section of one rib



Fig. 18 Slice model

For the concrete elements we made a model with only concrete because it was said that the influence of the reinforcement would be of lesser importance, it gives an extra reserve.

4.1 Concrete elements

With the mentioned fire loads above we can calculate following temperature profiles with maximum reinforcement temperature:

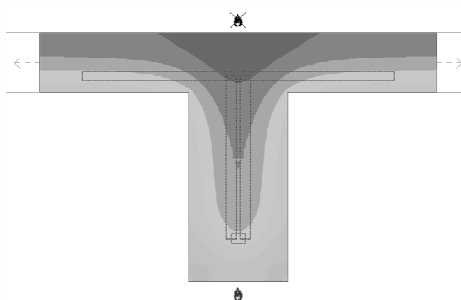


Fig. 19 Audience max after 43 min.

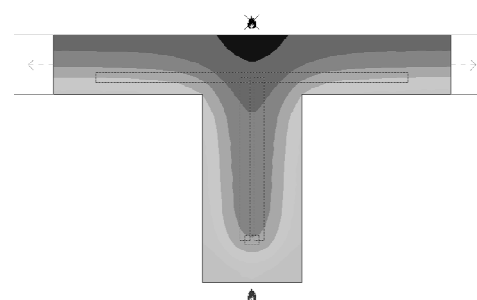


Fig. 20 Class 1.01 max after 31'

At the moment the highest temperatures are reached at the level of the reinforcement the surface subjected to smoke is already in cooling phase. Therefore the natural fires makes that the reinforcement never reaches 500°C , at maximum only about 200°C .

4.2 Steel structure

It seems that also for the steel, thanks to the double layer of gypsum board, the temperature never reaches 500°C , 150°C becomes the maximum. This caused by the very thin peak in the curve.

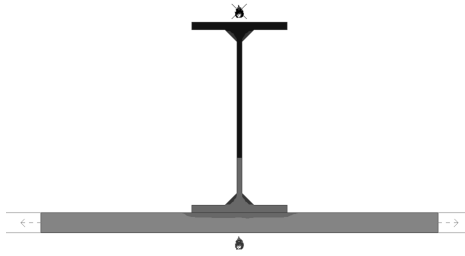


Fig. 21 Steel, max after 55 min.

For the steel is besides the double gypsum board no further protection needed.

4.3 Masonry structure

With the acting bending moments and temperature profiles coming out of the model we could check and confirm on a manual way the bearing capacity of the masonry walls on several levels.

5 CONCLUSIONS

With the aid of easy to use 2-zone models and a thermo elastic stability check we were in the possibility to build up a tailor made solution for this particular problem. This with build in security there were needed, without overkill and perhaps more important without underestimation of some effects.

Some extra costs were needed but otherwise we could realise also some efforts for the steel construction. The proposed solution is approved by the school authority and executed.

REFERENCES

- NBN S21-204 Fire protection in buildings – School buildings – general requirements an fire reaction, Belgian standard institute IBN/BIN, 1982.
- Annexes to add at the Royal Decree of 19/12/1997, modification of the Royal Decree of 07/07/1994: published the 30/12/1997: Terms and rules for low, medium and high buildings + reaction on fire of materials, Moniteur Belge 1997.
- EN 1990:2002+National Annexe NBN EN 1990-ANB:2007, Eurocode 0: Basis of structural design, European Committee for Standardization CEN, 2002.
- EN 1991-1-2:2002+National Annex NBN EN 1991-1-2-ANB:2008, Eurocode 1: Actions on structures - Part 1-2: General actions - Actions on structures exposed to fire, European Committee for Standardization CEN.
- EN 1992-1-2:2005+Nationale Bijlage NBN EN 1992-1-2-ANB:2010, Eurocode 2: Design of concrete structures - Part 1-2: General rules - Structural fire design, European Committee for Standardization CEN, 2005.
- A tool to design steel elements submitted to compartment fires OZone V2. Part 1: pre- and post-flashover compartment fire model, Cadorin J.-F. & Franssen J.-M., Fire Safety Journal, Elsevier, 38 (2003), 395-427, <<http://hdl.handle.net/2268/29650>>
- A tool to design steel elements submitted to compartment fires OZone V2. Part 2: Methodology and application, Cadorin J.-F., Pintea D., Dotreppe J.-C. & Franssen J.-M., Fire Safety Journal, Elsevier, 38 (2003), 429-451, <<http://hdl.handle.net/2268/29651>>
- PowerFrame version 2010 and Diamonds by BuildSoft, version 2011.
- SAFIR. A Thermal/Structural Program Modelling Structures under Fire, Franssen J.-M., Engineering Journal, A.I.S.C., Vol 42, No. 3 (2005), 143-158.

FAILURE PROBABILITY ASSESSMENT FOR FIRE SITUATION WITH A CERTAIN TYPE OF THE NETWORK DIAGRAM Example of application

Mariusz Maślak ^a

^a Cracow University of Technology, Faculty of Civil Engineering, Cracow, Poland

INTRODUCTION

Failure probability is usually adopted as an objective measure of the safety level if accidental fire conditions are considered in the analysis. However, estimation of its value, being reliable and precise enough, is not easy. In general such probability depends on a great amount of factors, connected between each other in a complex and intercorrelated network. For this reason, solutions obtained by traditional design methodology not always can be unequivocally interpreted. Moreover, the assessed value will be significantly different from the previous one if further factors influencing the fire safety are additionally considered or even if the order of the occurrence of the examined factors changes. In the presented paper specific and user friendly calculation technique is discussed by the author in detail, helpful for the accurate evaluation of the probability that fire which has already occurred will not be extinguished in any way and, consequently, the failure of the analysed structural member will take place. This approach is based on the study of a certain type of the network diagram, suggested by *R. W. Fitzgerald* (Fitzgerald, 2004). Such diagram contains both AND and OR-type logical gates, which are identified respectively with the conjunction and the alternative of independent and complementary random events. The examined scheme can be extended by the addition of the next level of the analysis if considered fire may expand from one fire compartment to the adjoining one. The proposed design procedure of the assessment of searched failure probability is in the article widely illustrated by a representative numerical example.

1 VARIOUS INTERPRETATIONS OF THE FAILURE PROBABILITY

Application of failure probability p_f as a basic safety measure in classical structural analysis made for accidental fire situation explicitly determines the understanding of the limit state phenomenon, danger to some people or to the building structure. This limit state is not reached exactly at the point-in-time when such considered unexpected event really takes place, but earlier, when the probability of its occurrence is no longer possible to accept. Conclusively, the ultimate condition is in general formulated as follows:

$$p_f \leq p_{f,ult} \quad (1)$$

where $p_{f,ult}$ is the maximum value of p_f which can be acceptable to the designer or, more frequently, to the suitable authorities. Values of $p_{f,ult}$, linked with the right side of Eq. (1), are assigned arbitrarily, to be adequate for the assumed reliability class. In the presented paper some aspects of the assesment of the probability p_f , associated with the left side of this inequality, are discussed. However, before the detailed analysis how to correctly evaluate its value will be presented we have to precisely define what kind of the probability is considered. It is crucially important because at least two different interpretations can be distinguished in this field. They are as follows (Maślak, 2005), (Maślak and Domański, 2008):

- probability of failure, caused by fire, if it is known that fire ignition has occurred and; moreover, that this fire has reached the flashover point (it may be described as a fully developed fire) – in further analysis such probability will be marked by the symbol p_f ,
- probability of failure, caused by potential fire which can take place; however, it has not yet occurred (so the designer has no information about its ignition and flashover) – let us appoint the symbol p_{ff} for its designation.

Relation between p_f and p_{ff} is given by *T. T. Lie* (Lie, 1972):

$$P_{ff} = P_t P_f \quad (2)$$

where p_t means the probability of fire occurrence (the most frequently not only of fire ignition but also of reaching the flashover point). As we can see, probability p_f should be interpreted as a conditional one with the condition that fire has already occurred and the temperature of exhaust gas in the whole compartment is uniform (the fire is fully developed). Not only qualitative but also quantitative distinction between those both probabilities, p_f and p_{ff} , seems to be very significant. Even if conditional probability p_f is large, probability p_{ff} is usually quite small and does not seem to be apprehensive, because in reality the value of probability p_t is also slight (Maślak, 2005).

2 LOGICAL GATES IN FAILURE PROBABILITY ASSESSMENT

Let us assume, developing the example given by *R. W. Fitzgerald* (Fitzgerald, 2004), that failure (F) in this analysis is connected with the case when fully-developed fire in considered compartment will not be extinguished. Only three ways of its extinction are then specified as possible in real conditions:

- $E1$ - fire will burn out spontaneously,
- $E2$ - fire will be extinguished owing to the working of active fire protection measures (sprinklers, water curtains etc.), without any activity of a fire brigade,
- $E3$ - fire will be extinguished due to the activity of a fire brigade.

Let the symbol \bar{E} denote for each identified way of the extinction the event contrary to event E . It is also the event complementary to E in mathematical sense, so that $P(E) \cup P(\bar{E}) = 1$. It is important that all considered ways of fire extinction have to be understood as independent in statistical sense. For this reason the event, formally possible, that fire is only partially suppressed by active fire protection measures, but definitively extinguished only when the fire brigade firefighting action is successfully finished, should be classified explicitly as the $E3$ manner. Finally, the following evaluations can be performed:

- fire which has started will not be extinguished at all if event $\bar{E1}$ AND event $\bar{E2}$ AND also event $\bar{E3}$ occur, so failure probability $P(F)$ can be assessed by the formula:

$$p_f = P(F) = P(\bar{E1}) \cdot P(\bar{E2}) \cdot P(\bar{E3}) = [1 - P(E1)] \cdot [1 - P(E2)] \cdot [1 - P(E3)] \quad (3)$$

- fire which has started will be extinguished as a result EITHER of the occurrence of event $E1$, OR event $E2$, OR event $E3$. Occurrence of only one from those three events is sufficient to cause the extinction of fire. However, in this case the scheme of calculation of searched probability is not so simple. Let us notice that the event $E2$ can occur only if the event $E1$ does not occur (i.e. if the event $\bar{E1}$ occurs). Similarly, the event $E3$ can occur only if the events $E1$ AND $E2$ do not occur previously (i.e. if the events $\bar{E1}$ AND $\bar{E2}$ occur). In conclusion the final formula applied for its calculation has the form:

$$\begin{aligned}
1 - p_f &= P(\overline{F}) = P(E1) + P(\overline{E1})P(E2) + P(\overline{E1})P(\overline{E2})P(E3) = \\
&= P(E1) + [1 - P(E1)]P(E2) + [1 - P(E1)] \cdot [1 - P(E2)]P(E3)
\end{aligned}
\tag{4}$$

which means that the fire will be extinguished only when the event $E1$ occurs, OR when the event $E2$ takes place provided that the event $\overline{E1}$ will have happened previously, OR if the event $E3$ appears in the case when not only the event $\overline{E1}$ but also the event $\overline{E2}$ will have come into being.

As we can see two types of the logical gates are taken into account in such analysis. The first kind is the classical AND-type gate. It is the synonymous with the conjunction of independent random events. Probability $p_f = P(F)$ is in this case calculated as a simple product of component probabilities (see Eq. (3)). The second one is the OR-type gate which can be identified with the alternative of considered random events. This is the reason why the probability $P(\overline{F})$ is estimated as an ordinary sum of component probabilities (see Eq. (4)). Let us notice that also some internal AND-type gates can be identified in the evaluation of the probability $(1 - p_f)$. Correctness of the obtained solution may be verified by checking the following equation:

$$P(F) = 1 - P(\overline{F}) \tag{5}$$

If the considered fire is not extinguished in the analysed compartment $\Omega1$ (i.e. when the event F with respect to Eq. 3 takes place) then it will be the imminence that flames can expand to the adjoining room $\Omega2$. This case will be possible if the fire-break division (fire-partition or fire-resisting door), being a barrier (B) for fire increasing, damages and - as a consequence - it does not fulfil imposed insulating requirements. Such event will be denoted in further analysis by the symbol \overline{B} . Let us assume that only two causes may be specified for such disaster (Fitzgerald, 2004):

- $\overline{B1}$ for the situation when the fire isolation limit state is reached,
- $\overline{B2}$ for the alternative situation when the fire tightness limit state is reached.

Consequently, the event marked by the symbol B will concern the case when the barrier is sufficiently strong and it does not admit to expand the fire.

3 THE FITZGERALD'S-TYPE NETWORK DIAGRAM

Application of the network diagram can be very helpful for practical evaluation of failure probability $p_f = P(F)$ with the calculation procedure presented above. Many types of such diagram can be found in the professional literature. In the presented article the author proposes to use in this field the scheme given by *R. W. Fitzgerald* (Fitzgerald, 2004). It is shown in Fig. 1 for the case when fire can expand from one fire compartment to adjoining one. Let us notice that all connections marked with the solid line are always linked with the AND-type logical gates. On the other hand, connections drawn by means of the broken line can be identified with the OR-type logical gates. To describe in detail how to correctly use such assessment methodology the numerical example has been prepared by the author (Maślak, 2008). Its fundamental solutions are presented below.

4 NUMERICAL EXAMPLE

Let us assume that in the fire compartment $\Omega1$ we have:

$$P(E1) = 0,4; P(E2) = 0,8; P(E3) = 0,7.$$

Probability that the considered fire will not be extinguished at all in the fire compartment $\Omega1$:

$$P(F\Omega1) = [1 - P(E1)] \cdot [1 - P(E2)] \cdot [1 - P(E3)] = 0,6 \cdot 0,2 \cdot 0,3 = 0,036$$

Probability that this fire will be extinguished successfully in the fire compartment $\Omega1$ in any way:

$$P(\overline{F\Omega 1}) = P(E1) + P(\overline{E1})P(E2) + P(\overline{E1})P(\overline{E2})P(E3) = 0,4 + 0,6 \cdot 0,8 + 0,6 \cdot 0,2 \cdot 0,7 = 0,964$$

Formal checking:

$$0,036 + 0,964 = 1,0.$$

Let us assume that:

$$P(B) = 0,75; P(\overline{B1}) = 0,15; P(\overline{B2}) = 0,10.$$

Formal checking:

$$P(B) + P(\overline{B1}) + P(\overline{B2}) = 0,75 + 0,15 + 0,10 = 1.$$

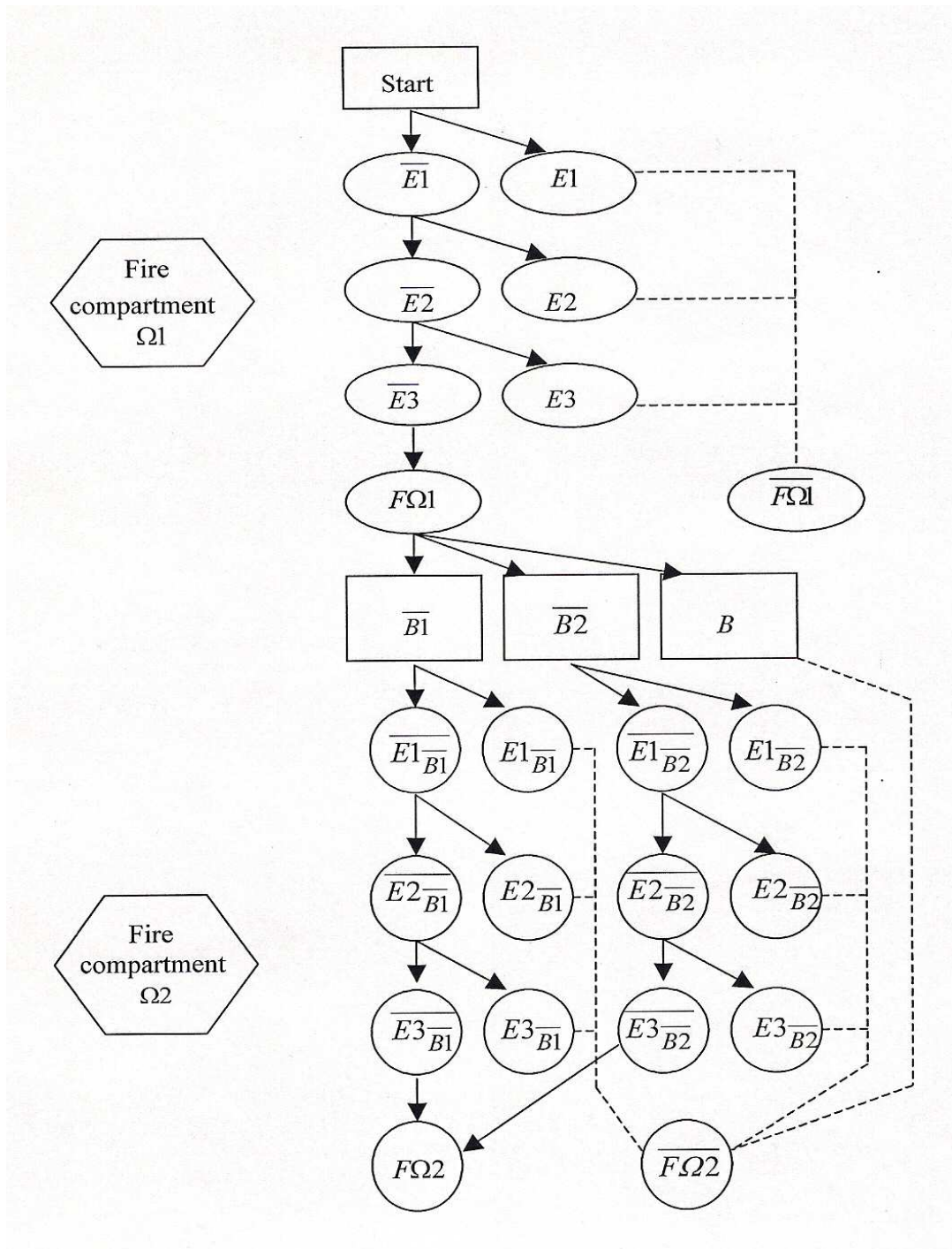


Fig. 1 Network diagram proposed by R. W. Fitzgerald (Fitzgerald, 2004) for the case when the considered fire can expand from one fire compartment to adjoining one.

Let, in the fire compartment Ω_2 , us have:

$$P(E1_{\overline{B1}}) = 0,3; P(E2_{\overline{B1}}) = 0,7; P(E3_{\overline{B1}}) = 0,9, P(E1_{\overline{B2}}) = 0,1; P(E2_{\overline{B2}}) = 0,2; P(E3_{\overline{B2}}) = 0,3,$$

Probability that the fire which has not been extinguished in the fire compartment Ω_1 will not be extinguished also in the adjoining fire compartment Ω_2 :

$$P(F\Omega_2\overline{B1}) = P(F\Omega_1)P(\overline{B1})P(\overline{E1_{\overline{B1}}})P(\overline{E2_{\overline{B1}}})P(\overline{E3_{\overline{B1}}}) = 0,036 \cdot 0,15 \cdot (1-0,3)(1-0,7)(1-0,9) = 1,134 \cdot 10^{-4}$$

$$P(F\Omega_2\overline{B2}) = P(F\Omega_1)P(\overline{B2})P(\overline{E1_{\overline{B2}}})P(\overline{E2_{\overline{B2}}})P(\overline{E3_{\overline{B2}}}) = 0,036 \cdot 0,10 \cdot (1-0,1)(1-0,2)(1-0,3) = 1,814 \cdot 10^{-3}$$

$$P(F\Omega_2) = P(F\Omega_2\overline{B1}) + P(F\Omega_2\overline{B2}) = 1,134 \cdot 10^{-4} + 1,814 \cdot 10^{-3} = 1,927 \cdot 10^{-3}$$

Probability that the fire which has not been extinguished in the fire compartment Ω_1 will be extinguished succesfully in the adjoining fire compartment Ω_2 :

$$P(\overline{F\Omega_2\overline{B1}}) = P(F\Omega_1)P(\overline{B1}) \cdot [P(E1_{\overline{B1}}) + P(\overline{E1_{\overline{B1}}})P(E2_{\overline{B1}}) + P(\overline{E1_{\overline{B1}}})P(\overline{E2_{\overline{B1}}})P(E3_{\overline{B1}})] = 0,036 \cdot 0,15 \cdot [0,3 + (1-0,3) \cdot 0,7 + (1-0,3)(1-0,7) \cdot 0,9] = 5,287 \cdot 10^{-3}$$

$$P(\overline{F\Omega_2\overline{B2}}) = P(F\Omega_1)P(\overline{B2}) \cdot [P(E1_{\overline{B2}}) + P(\overline{E1_{\overline{B2}}})P(E2_{\overline{B2}}) + P(\overline{E1_{\overline{B2}}})P(\overline{E2_{\overline{B2}}})P(E3_{\overline{B2}})] = 0,036 \cdot 0,10 \cdot [0,1 + (1-0,1) \cdot 0,2 + (1-0,1)(1-0,2) \cdot 0,3] = 1,786 \cdot 10^{-3}$$

$$P(\overline{F\Omega_2\overline{B}}) = P(F\Omega_1)P(\overline{B}) = 0,036 \cdot 0,75 = 0,027$$

$$P(\overline{F\Omega_2}) = P(\overline{F\Omega_2\overline{B1}}) + P(\overline{F\Omega_2\overline{B2}}) + P(\overline{F\Omega_2\overline{B}}) = 5,287 \cdot 10^{-3} + 1,786 \cdot 10^{-3} + 0,027 = 0,03407$$

Hence, the probability that the considered fire will be exinguished at all (in the fire compartment Ω_1 or in the adjoining compartment Ω_2):

$$P(\overline{F}) = P(\overline{F\Omega_1}) + P(\overline{F\Omega_2}) = 0,964 + 0,03407 = 0,99807$$

Formal checking:

$$P(F\Omega_2) + P(\overline{F}) = 1,927 \cdot 10^{-3} + 0,99807 = 1,0$$

5 CONCLUDING REMARKS

Classical calculation technique, used for the evaluation of failure probability in the case when the fully developed fire broke out in considered compartment and when the flames can spread from one room to adjoining one, is usually based on the analysis of typical logical tree, reflecting the hierarchy of all factors influencing the fire safety as well as the internal connection structure between them. Therefore, the methodology of the analysis of complex hierarchical process is suggested to be used to assess its value precisely and reliably enough (Ginda and Maślak, 2006). Mathematical formalism taken from the examination of the so called Markov chains is also very promising in this field. However, the construction and the study of the network diagrams still remains the assessment approach being the most illustrative and imaginative. Such schemes should be less or more adequate for the reality, depending on their complexity and accuracy. The Bayesian networks are implemented the most frequently in the professional literature for this purpose (Holicky and Schleich, 2001). The simple network proposed by *R. W. Fitzgerald* (Fitzgerald, 2004) and discussed in this article seems to be very useful and friendly for practical application when the fire scenario and accompanying circumstances are not very complicated and when they can be explicitly identified.

Consideration of the complementary random events gives the designer the opportunity to apply for the estimation of searched safety level the well known formalism of complete probability analysis (Holicky and Schleich, 2001), (Maślak 2008). The logical tree based on such concept can be further developed and complicated, the most frequently through the addition of the next subsequent levels to its internal structure. Let us notice that in such case previously evaluated value of failure probability will change. Therefore, if we want to increase the precision of the probability assessment, and for that reason we take into account in the next step some additional factors influencing the fire safety, then we can easily obtain a value even significantly different from the previous one. The approach presented above is on that score safer for the implementation because the final result of the evaluation does not depend on the order of occurrence of particular component events.

The interpretation of searched probability should be clearly and unequivocally defined. In classical structural safety analysis probability p_f , which is conditional with the condition that fire has already occurred, is usually estimated. However, in many cases we want to evaluate the failure probability related to some people, for example to building occupants who will be able to inhabit in considered compartment if fire ignition and flashover takes place or even to firemen taking part in potential firefighting action. In such context probability p_{ff} , understood in a different way than the previous one (see Eq. 2), is commonly assessed.

6 ACKNOWLEDGMENT

This paper was elaborated with the financial support of the project granted by Polish Ministry of Science and Higher Education (N N506 243938).

REFERENCES

- Fitzgerald R. W., Building Fire Performance Analysis, John Wiley & Sons Ltd., Chichester, England, 2004, p. 534.
- Ginda G., Maślak M., Assessment of Factors Influencing the Fire Safety for Building Users, Proceedings of IABSE Symposium "Responding to Tomorrow's Challenges to Structural Engineering", Budapest, September 13-15, 2006, IABSE Report, vol. 92.
- Holicky M., Schleich J. –B., Modelling of a Structure under Permanent and Fire Design Situation, Proceedings of the IABSE International Conference "Safety, Risk, Reliability – Trends in Engineering", Malta, 2001, pp. 1001-1006.
- Lie T. T., Optimum Fire Resistance of Structures, Journal of the Structural Division, 98, No. ST1, 1972, pp. 215-232.
- Maślak M., Failure Probability of Building Load-bearing Structure under Fire Conditions (in Polish), Czasopismo Techniczne, 12-B/2005, pp. 67-80.
- Maślak M., Fire Resistance of Steel Bar Structures (in Polish), Monography No 370, Series "Civil Engineering", Publishers of Cracow University of Technology, Cracow, 2008, p. 203.
- Maślak M., Domański T., Safety Factors in Design of Steel Member for Accidental Fire Situation, Proceedings of the International Conference "Design, Fabrication and Economy of Welded Structures", Miskolc, Hungary, Horwood Publishing, Chichester, UK, 2008, pp. 563-570.

APPLICATION OF FIRE SAFETY ENGINEERING FOR OPEN CAR PARKS IN ITALY

Emidio Nigro^a, Anna Ferraro^a, Giuseppe Cefarelli^a, Gaetano Manfredi^a, Edoardo Cosenza^a

^a University of Naples FedericoII, Department of Structural Engineering (D.I.ST.), Naples, Italy

INTRODUCTION

In fire structural design, current Italian and European codes (D.M.14-01-2008, 2008; EN 1991-1-2, 2002; EN 1993-1-2, 2005) allow the use of a performance approach through the concept of Fire Safety Engineering based, among other things, on the mechanical and geometric nonlinear structural response in fire situation. According to ISO/TR 13387-1, the “Fire Safety Engineering” (FSE) is the application of engineering principles, rules and expert judgement based on a scientific assessment of the fire phenomena, the effects of fire and both the reaction and behaviour of peoples, in order to a) save life, protect property and preserve the environment and heritage, b) quantify the hazards and risks of fire and its effects, c) evaluate analytically the optimum protective and prevention measures necessary to limit, within prescribed levels, the consequences of fire.

The Directive 89/106/CEE on Construction Products of the European Community introduced the definition of the requirement of “safety in case of fire” in Europe, which is the base for the application of the Fire Safety Engineering. This requirement, implemented in the National Codes of European member countries, is explained by achieving the following five objectives:

- 1) the load-bearing capacity of the construction can be assumed for a specific period of time;
- 2) the generation and spread of both fire and smoke within the works is limited;
- 3) the spread of fire to neighbouring construction works must be limited;
- 4) occupants have to be able to leave the works or be rescued by other means;
- 5) the safety of rescue teams must be taken into consideration.

Focusing on the structural safety, the European codes are established by the “Fire Parts” of Structural Eurocodes. In Italy, the new Technical Code for Constructions has been published in 2008. For the first time in Italy, the fire action is introduced within the definition of the actions on constructions, as an “exceptional load”. This document defines the performance safety levels of buildings according to the safety objectives required by the Directive 89/106/CEE. The Italian Technical Code for Constructions defines five safety performance levels depending on the importance of the building, which establish the damage level that can be accepted. These rules define the fire structural performance requirements and they refer to specific technical codes issued by the Italian Ministry of Interior for all activities under the control of the National Fire Brigades.

In this scenario the FSE allows a more precise adjustment of the safety level of the building through qualitative and quantitative criteria (namely acceptance criteria). However, it is important to note that in the current code the performance approach does not replace the prescriptive one, but both the approaches coexist. The technical solutions imposed by the prescriptive approach remain one of the possible ways that the designer may choose for the structural fire design.

The following describes the application of FSE (namely the structural behaviour in fire situation) to the car parks in the new buildings of the “C.A.S.E. Project for L’Aquila”. This Project was developed in L’Aquila (province of Abruzzo, Italy), after the seismic event of 06/04/2009, in response to the housing emergency. The car parks, placed at the ground floor of the buildings, are mainly built with steel columns that support the seismically isolated superstructure. The Italian prescriptive code provides, for car parks, a fire resistance class for the load-bearing criterion of 90 minutes in standard fire exposure (R90). However, for obtaining the fire resistance class R90 the adoption of protective coatings of steel columns is needed, for which a continuous and accurate maintenance is required: in fact, there is a high possibility of accidental damage of the protective coatings in case of impact with the cars. Moreover, the possibility of damage becomes elevated when a series of acts of vandalism takes place, for example if the car parks are easily accessible and

not controlled. Because of the uncertainties on the effectiveness of coatings maintenance, in such cases, their use is not recommended.

Therefore, the lack of protective coatings on steel columns and the structural safety during the fire exposure can be evaluated through the application of performance-based approach, which allows to assess, in a more complete and reliable manner, the structural response with reference to the fire scenarios that can realistically occur.

1 FIRE SAFETY ENGINEERING

The performance approach (FSE), as opposed to prescriptive approach, is based on a detailed analysis of the structural behaviour by using advanced analytical models. Therefore, through the engineering method, by following the steps in the layout of Fig. 1, it is possible to evaluate the structural fire safety level. Particularly, it should be defined:

- 1) the ignition fire hazard according to the purpose of the building (type and amount of fire load, type of users) and if there are active and passive fire protection systems;
- 2) the design fire scenarios, fire development and the movement and evacuation of smoke, depending on the geometric characteristics and ventilation conditions of the fire compartment and the type and amount of fire design load.

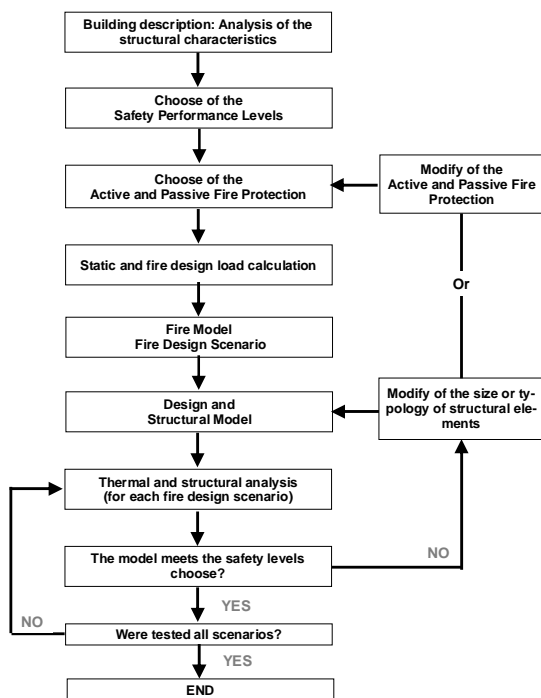


Fig. 1 Fire Safety Engineering: Layout



(a)



(b)

Fig. 2 (a) Typical building of C.A.S.E. Project for L'Aquila, (b) Parking zone

2 CASE STUDY: CAR PARKS

2.1 Building description: analysis of the structural characteristics

Each residential building is built on a seismically isolated plate, with dimensions equal to $21 \times 57 \text{m}^2$ about, capable of supporting a three-storey building with dimensions in plant equal to $12 \times 48 \text{m}^2$ about, in addition to the stairs. The buildings (superstructures) are different for architectural and constructive elements; the structures are built with wood materials, reinforced concrete or steel. Each isolated plate (with height of 50cm) is sustained by steel columns (with height of 260cm) by the isolation system. In this area, below each seismically isolated plate, the parking (Figure 2) for about 34 cars are contained. In order to distribute the actions on the reinforced concrete foundation plate the columns are allocated on a $6\text{m} \times 6\text{m}$ grid. The dimensions in plant of the compartment are

equal to $22 \times 58 \text{ m}^2$; in fact the outside walls, when present, are mismatched 50cm with respect to the vertical projection of the edge of the seismically isolated plate.

The steel columns are a circular hollow steel section with a capital at the top; this latter is useful a) for transferring, through the isolator unit, the load between the column and the seismically isolated plate and b) as a structure of contrast to the operations of substitution of the isolator unit. The parking area can be fully open on the four sides or partially closed on one or more sides. Therefore, among the various examined cases are present both open car parks and almost completely closed, as well as several intermediate cases.

2.2 Choice of the active and passive fire protection systems

In this case study, the objective of fire safety design concerns the mechanical resistance and stability, in fire situation, of the primary structural elements in the zone below the seismically isolated plate. In this case a limited damage after the fire exposure has been required. The damage is quantified in terms of relative vertical displacements between the top of two adjacent columns: in order to limit the finishing damage in the superstructure, the relative vertical displacement must not exceed the limit value, chosen cautiously equals to $L/200$ (5.0 ‰), where L is the distance between two adjacent columns ($L=6000\text{mm}$). Finally, no specific protection systems (active and/or passive) are provided.

2.3 Static and fire design load calculation

The Italian and European codes (NTC, 2008; EN1991-1-2, 2002) classify the fire as an exceptional load, so the fire design load combination is defined by:

$$F_d = A_d + G_{k1} + G_{k2} + \sum_{i=1}^n \psi_{2i} \cdot Q_{ki} \quad (1)$$

where G_{k1} is the characteristic value of permanent structural load; G_{k2} is the characteristic value of permanent non structural load; $\psi_{2i} \cdot Q_{ki}$ is the quasi-permanent value of a variable action i ; A_d is the design value of an exceptional action. Because of the great variability of the superstructure structural type, the fire structural analyses have been carried out, for simplicity and for the benefit of safety, with reference to the maximum combination of exceptional load (maximum axial load on each column equal to 1800 kN).

2.4 Fire model and fire design scenarios.

The fire scenario is significantly affected, among other things, by the geometry and ventilation conditions of the compartment. As regards the evaluation of number of vehicles involved in the fire and the timing of fire initiation by a car to adjacent one, reference is made to the informations from (CEC Agreement, 2001) and the guideline (INERIS, 2001). It is necessary to distinguish the car parks open on all their sides by those partially open (openings limited or absent on one or more sides). The presence of natural ventilation in open car parks does not allow the achievement of the flashover conditions: the phenomenon remains for the entire fire duration of “pre-flashover” type and a limited number of vehicles burn. In partially open car parks, instead, it is possible that the fire involved all of the cars. Therefore, the identification of the more dangerous fire scenarios for the structural stability is to define the position and the number of cars that may be involved in the fire and cause the more dangerous thermal action for the supporting structure building.

By applying the criteria proposed in the aforementioned guidelines to *car parks open on all sides* two localised fire scenarios (L1 and L2) was defined. In this fire scenarios was assumed the presence of cars of category 3, with calorific value equals to 9500 MJ, and only one commercial vehicle (VAN), with total calorific value equals to 19500 MJ (see CEC Agreement 7215-PP/025, 2001). The distribution and number of the cars and the fire propagation times from the VAN (equals to 12 min) are reported in Fig. 3a,b.

For localised fire (Fig. 3a,b), the application of Hasemi’s method (Annex C, EN1991-1-2), with the RHR curve of car of category 3 and VAN (see CEC Agreement 7215-PP/025, 2001), has provide

the heat flux received by steel columns. The heat flux along and around the columns was assumed equal to the heat flux at the top of columns. In Fig. 3c are reported the heat flux on some significant columns.

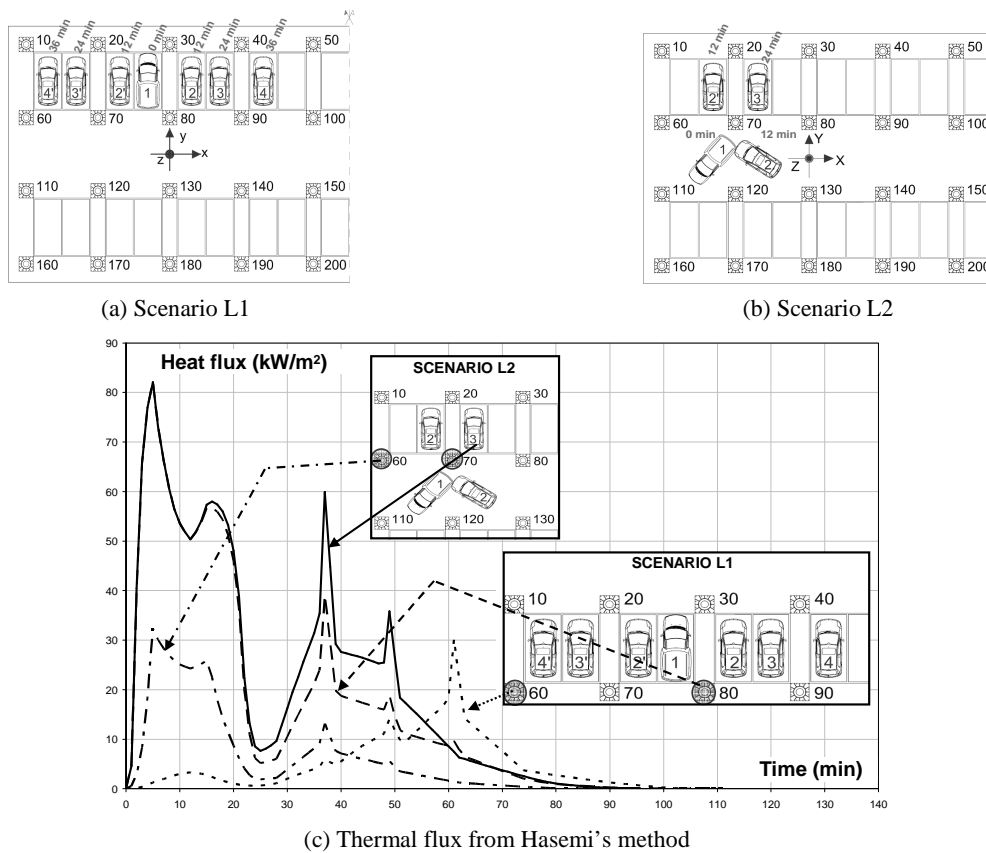


Fig. 3 Fire scenarios

2.5 Structural model and fire safety assessment

In order to limit the analysis time without compromising the accuracy of the results, the thermo-mechanical analyses, for each fire scenario, have been conducted with the reference to the substructure highlighted in Fig. 4 (Nigro et al., 2010). The substructure extension allows assessing in an appropriate way both the thermal field and the hyperstatic effects induced by different thermal expansions of steel columns and bending of the concrete reinforced slab. Along the edge a constraint is introduced for the horizontal movements in the longitudinal direction and for the rotations around transverse axis. This constraint condition, thanks to the structural symmetry, is fully congruent for the analysis in normal temperature conditions and for a generalised fire scenario, while it is on the safe side for the other scenarios (localised fire scenarios), maximizing, thanks to the infinite rotational stiffness, the hyperstatic effects induced on the columns by slab thermal curvature. The steel columns are fixed at the base and linked to the superstructure slab with a hinge. For each fire scenario, the global thermal-mechanical structural analyses of the substructure in Fig. 4 are conducted by using the non linear software SAFIR2007a (Franssen, 2008), developed at the University of Liege (Belgium), which performs the structural analysis under fire situation. The steel columns are modelled with beam elements with circular cross-section, while the reinforced concrete slab is modelled with shell elements.

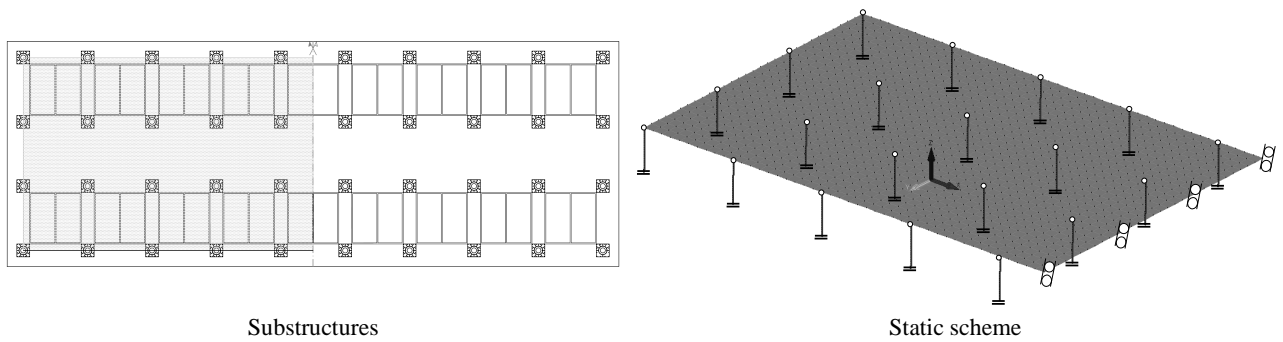


Fig. 4 Thermo-mechanical model of the structure

In addition to the global analysis, for each fire scenario, in order to calculate more accurately the thermal field and stresses distribution in the capitals above the columns and to assess the possible local buckling, a detailed thermo-mechanical analyses has been conducted with reference to the more stressed and heated column. The 3D modelling (Fig. 5) have been developed with the finite element software ABAQUS/standard (2008). The thermal exposure conditions were considered according to the Fig. 3. The axial load corresponds to the axial load obtained by the global structural analyses.

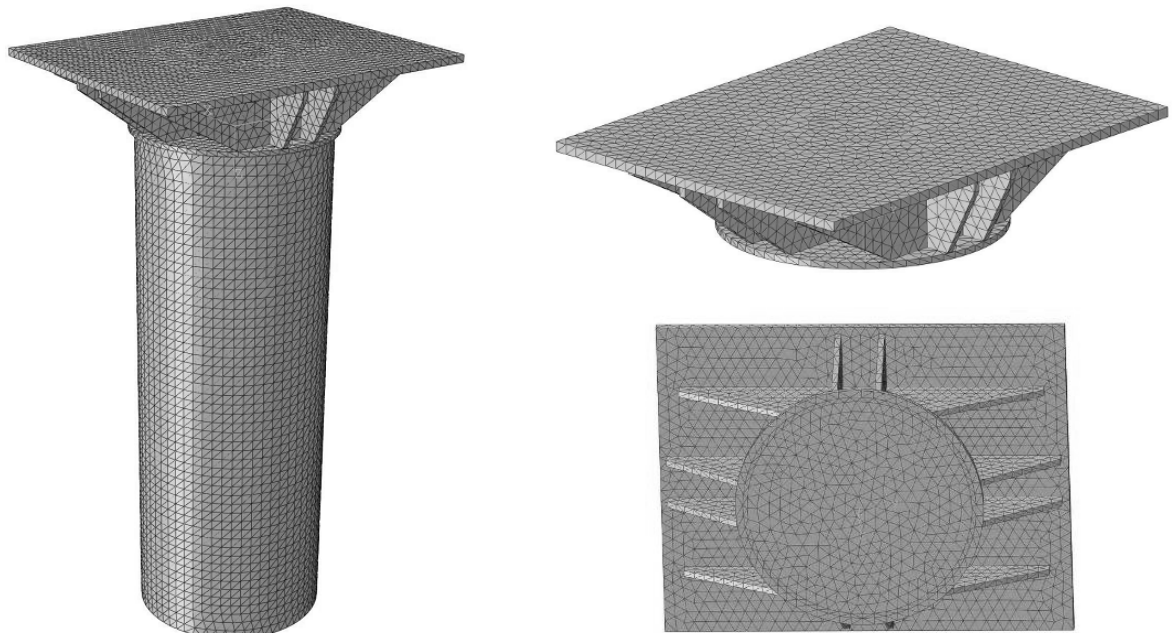


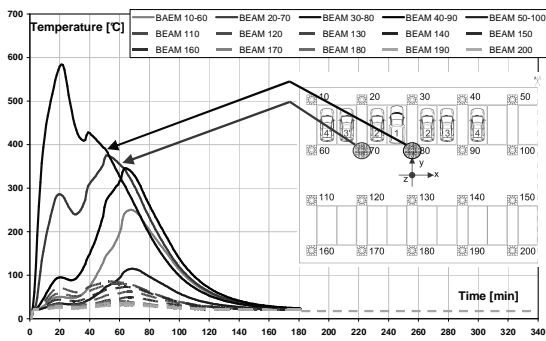
Fig. 5 3D thermo-mechanical model of the column

2.6 Analyses results

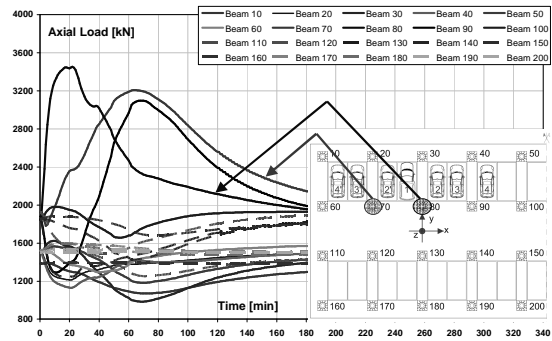
In Fig. 6 and in Fig. 7 are sintetized the main strutural results (tempertaures, axial loads, vertical displacements in function of fire exposure time) for scenario L1 and for Scenario L2, respectively. For sake of brevity, the results of structural response in fire situation are reported only with reference to the fire scenario L2, which appears more unfavourable (Fig. 6).

The maximum temperatures reached in the columns do not exceed 600°C (Fig. 6a). The thermal action produces both in the columns and slabs several thermal expansions. Because of the thermal curvature of the slab the columns axial load increases (Fig. 6b). The axial load is further amplified from the differential thermal elongation (Fig. 6c) of columns, exposed to different thermal conditions, which is constrained from slab shear stiffness. The columns displacement reflects, in general, the temperatures trend. However, the reduction of stiffness that the structural elements suffer, if constrained to high temperatures, may lead to a premature reversal development in

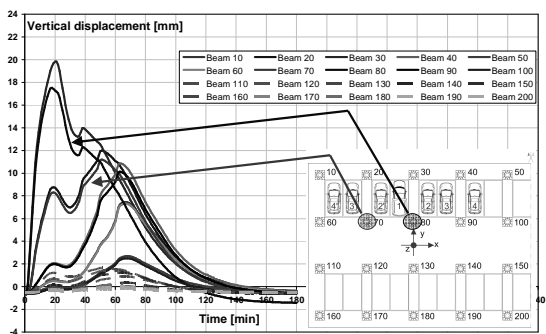
displacement respect to the temperature trend. The maximum differential displacement, during the fire exposure, is about 16mm (between the column 120 and column 130) and this value corresponds to 2.6 ‰ below the limit value of 5.0 ‰. Moreover, in Fig. 6d the axial load resistance of the column, evaluated according to EN1993-1-2, is compared with the axial load during the fire exposure. The final displacement is about 5mm in the central area of capital and about 2mm in the tube head: this is due to the plastic strain which has developed in the tube and in the capital (mainly in the zone of load application) during the fire exposure.



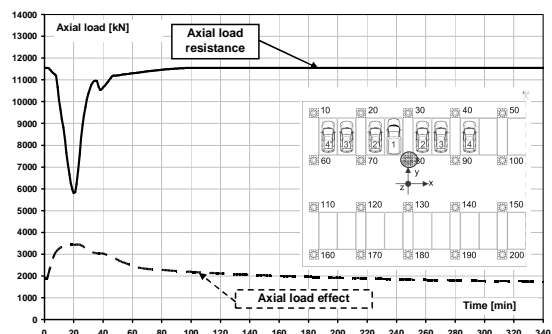
a) Time-temperature curves for the columns



b) Time-axial load curves for the columns

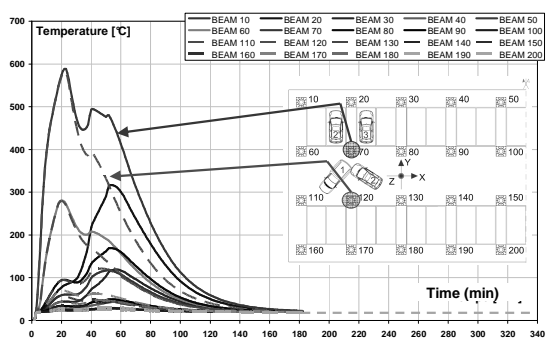


c) Time-displacement curves for the columns' top

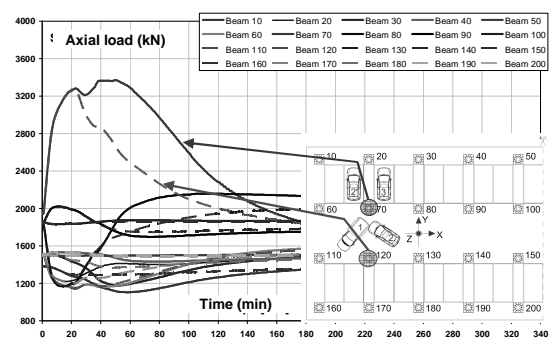


d) Stability check according to EN1993-1-2 (column 70)

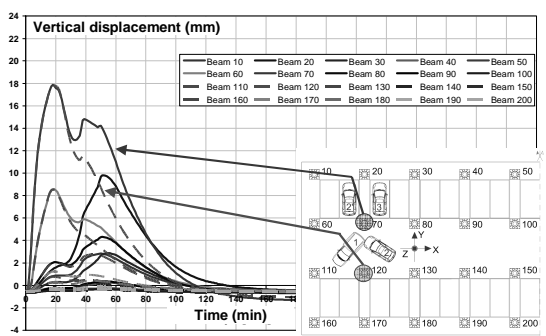
Fig. 6 Fire scenario L1



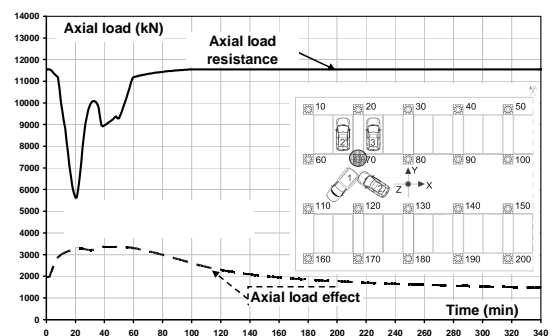
a) Time-temperature curves for the columns



b) Time-axial load curves for the columns



c) Time-displacement curves for the columns' top



d) Stability check according to EN1993-1-2 (column 70)

Fig. 7 Fire scenario L2

As regards the detailed analysis of the column, the displacement at the head of column is very similar to those obtained in the global structural analyses (Fig. 8). The final displacement is about 5mm in the central area of capital and about 2mm in the tube head: this is due to the plastic strain which has developed in the tube and in the capital (mainly in the zone of load application) during the fire exposure.

Similar considerations are also valid for the other fire scenarios. Therefore it can be concluded that the structure, and in particular the columns in the absence of any protection system against fire, during the design fire exposure perform an adequate load-bearing capacity, including the cooling phase.

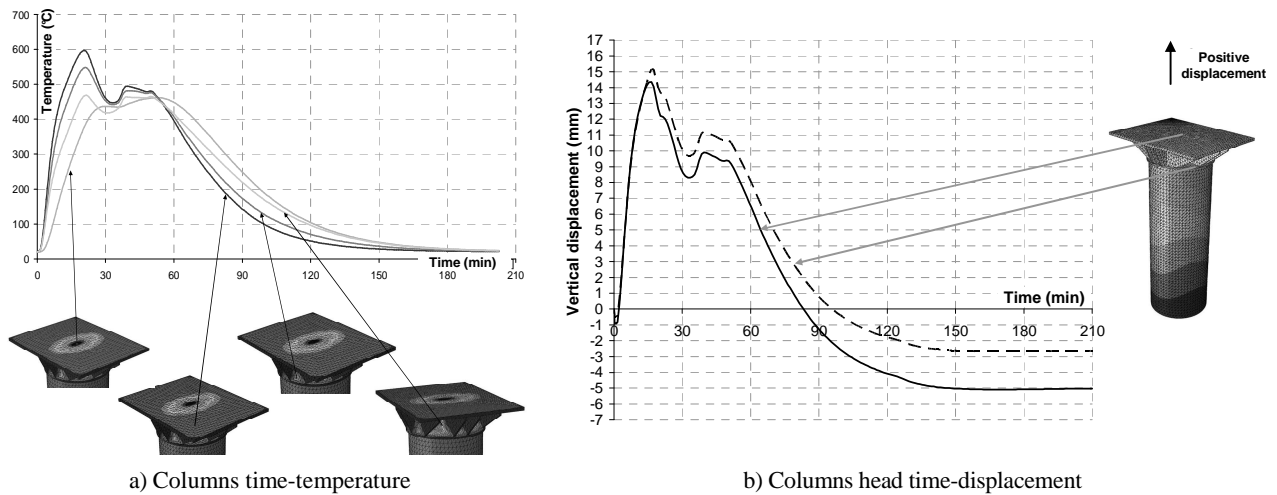


Fig. 8 Scenario L2 – Detailed analysis

3 CONCLUSIONS

The Fire Safety Engineering approach, thanks to advanced calculation models both for fire and for thermo-mechanical analysis of the structure, allows simulating the response behaviour of the structure exposed to “natural” fire scenarios. The FSE application to car parks is facilitated by the informations about the possible fire scenarios provided by the European Research Project CEC agreement 7215-PP/025 (2001).

In the described case study, consisting of the car parks located at the ground floor of buildings of the C.A.S.E. Project - L’Aquila, the application of the Fire Safety Engineering has been developed according to the current National Technical Code and Eurocodes, also utilising the fire scenarios suggested by the quoted European Research.

In order to limit the analysis time without compromising the accuracy of the results, the thermo-mechanical analyses, for each fire scenario, have been conducted with the reference to a significant substructure, for which the steel columns are modelled with beam elements with circular cross-section, while the reinforced concrete slab is modelled with shell elements. The substructure extension has allowed assessing in an appropriate way both the thermal field and the hyperstatic effects induced by different thermal expansions of steel columns and bending of the concrete reinforced slab. In addition to the global analysis, for each fire scenario, in order to calculate more accurately the thermal field and stresses distribution in the capitals above the columns and to assess the possible local buckling, a detailed 3D thermo-mechanical analyses has been conducted with reference to the more stressed and heated column.

Finally, the thermo-mechanical analyses in fire situations for the described case study showed that the structures, and in particular the steel columns, considered unprotected, satisfy the performance level set to the design fire scenarios, also thanks to an overstrength in normal condition design.

REFERENCES

- ABAQUS Standard/explicit User's Manual (2008), Hibbit Karlsson and Soresen, Inc. Vol 1-2-3, Version 6.7, USA 2008.
- CEC Agreement 7215-PP/025, Demonstration of Real Fire Tests in Car Parks and High Buildings, 2001.
- EN 1991-1-2, Eurocode 1. Actions on structures - Part 1-2: General actions - actions on structures exposed to fire, November 2002.
- EN 1993-1-2, Eurocode 3. Design of steel structures - Part 1-2: General rules - Structural fire design, April 2005.
- Franssen J.M., (2008) - User Manual for SAFIR2007a: A Computer Program for Analysis of Structures Submitted to the Fire, University of Liege, Belgium, January.
- INERIS, Parcs de stationnement en superstructure largement ventilés. Avis d'expert sur les scénarios d'incendie, Ottobre 2001.
- Ministry of Infrastructure and Transport (Italian Government) 2008. Technical Code for the Constructions. G.U. n. 29 of 14/02/2008.
- Nigro E., Pustorino S., Cefarelli G., Princi P., Progettazione di strutture in acciaio e composte acciaio-calcestruzzo in caso di incendio (in italian), Ed. Hoepli, Milano, 2009.
- Nigro E., Ferraro A., Cefarelli G., Application of FSE approach to the structural fire safety assessment of steel-concrete composite structures, Proceedings of COST Action C26 Conference, 16-18 September 2010, Naples, Italy.
- Pustorino S., Princi P., Nigro E., Ferraro A., Caciolai M., Cirillo V., Structural design of open car parks in accordance with the fire safety engineering approach (in Italian). Costruzioni Metalliche, n. 6, Nov/Dic 2010, ACAI, pp. 55-66.

CASE STUDIES OF A NEW SIMPLIFIED NATURAL FIRE MODEL AND SAFETY CONCEPT FOR STRUCTURAL FIRE SAFETY DESIGN

Jochen Zehfuss^a

^ahpbberlin fire safety engineers, Hamburg, Germany

INTRODUCTION

The structural fire safety design in most countries is usually carried out on the foundation of the material requirements of the building codes. This prescriptive design bases on the well-known standard temperature-time curve and simplifies the fire exposure to the building elements. Importance such as fire load, ventilation and geometry of the fire compartment are not considered. An alternative design-way is the performance-based design on the basis of natural fires which is especially applied for special complex buildings such as airports, railway stations, big assembly halls etc. The performance based design of construction elements is conducted by Eurocodes and the National Annex. Due to some deficiencies in the methods of the annexes in Eurocode 1-1-2 for the German National Annex a new simplified natural fire model for fully-developed compartment fires was developed.

By means of an example it is shown how to evaluate the relevant fire actions of a natural fire to the structure on the basis of Eurocode 1-1-2 and the German National Annex [DIN, 2010].

1 EUROCODE 1-1-2 ANNEX A

The standard temperature-time curve was developed in the 1930s summarising data from fires in residential, office and commercial buildings. The curve should cover most of the potential courses of fires in common buildings. The standard temperature-time curve is the basis of the prescriptive fire safety design and leads in most cases to an overestimation of the thermal action to the structure. For a performance-based design in Eurocode 1-1-2 natural fire models are available with which the realistic temperature-time development depending on fire load, ventilation conditions and geometry can be obtained.

The simplified natural fire model published in Eurocode 1-1-2, annex A however in some cases provides an unrealistic temperature increase and decrease [Zehfuss and Hosser, 2007]. For this reason the annex A-method was not approved in most CEN-countries. The most critical point is that the annex A-method has no temporal connection with the rate of heat release of Eurocode 1-1-2 annex E. This deficiency will be clarified by comparing the parametric temperature-time curve according to Eurocode 1-1-2 with the test results of [Schleich, 2000] (Fig. 1). Obvious is the discrepancy between the temporal course of the parametric temperature-time curve and the rate of heat release according to Eurocode 1-1-2 annex E. The latter achieves its maximum after 30 minutes and declines after 43 minutes. The temperature-time curve and rate of heat release neither match with each other nor are they temporally congruent.

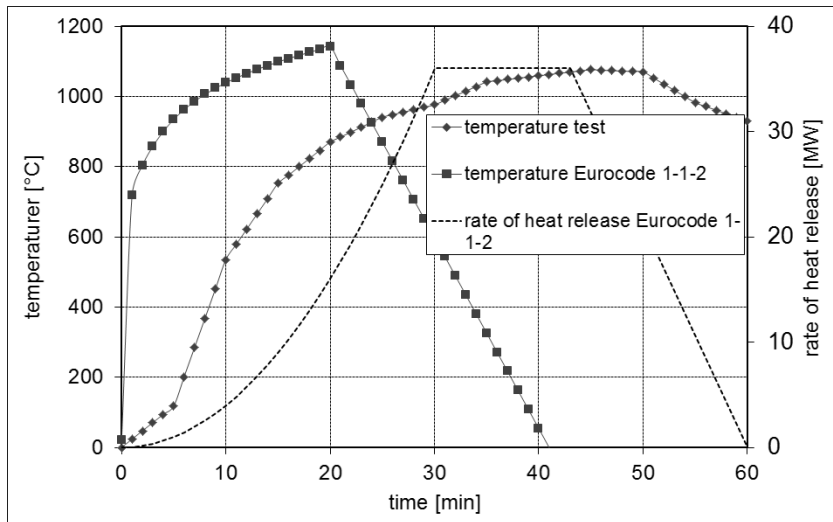


Fig. 1 Temperature-time curve and rate of heat release according to Eurocode 1-1-2

2 NATURAL FIRE MODEL IBMB PARAMETRIC FIRE CURVES

2.1 General

The Eurocode 1-1-2 annex A-method in Germany was not approved by the building authorities due to the mentioned deficiencies. For the reason that in Germany also a simplified natural fire model is provided the new parametric fire curves based on [Zehfuss and Hosser, 2007] were published in the German national annex.

The new simplified natural fire model of the parametric fire curves [Zehfuss and Hosser, 2007], [Zehfuss and Hosser, 2005] is based on the approach of the rate of heat release. The model was derived on simulations with the zone model CFAST for various boundary conditions vs influencing factors. Fig. 2 shows the qualitative shapes of the rate of heat release due to Eurocode 1-1-2 and the simulated temperature-time curve. The temporal link between these curves is evident.

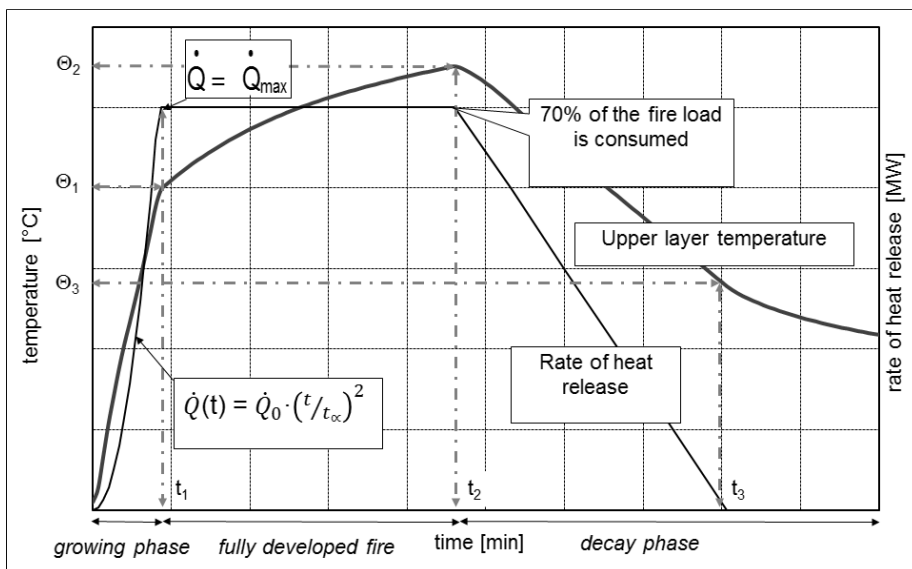


Fig. 2 Approach of heat release and corresponding upper layer temperature (principle)

The parametric fire curves can be divided into three sections (Fig.3). From the beginning of the fire until t_1 the upper layer temperature increases rapidly. At t_1 the maximum of the rate of heat release is achieved and remains constant until t_2 . After t_1 the upper layer temperature enhances increases moderately. As 70 % of the fire load is consumed at t_2 , the rate of heat release drops off linearly and the upper layer temperature declines. At t_3 the complete fire load is consumed and the rate of heat release decreases to 0. At this time the upper layer temperature-time curve bends and declines to a

lesser extent than before. For the total description of the run of the upper layer temperature-time curve the associated temperatures Θ_1 , Θ_2 and Θ_3 have to be ascertained (Fig. 3).

2.2 Rate of heat release

The rate of heat release $\dot{Q}(t)$ is given by

$$\dot{Q}(t) = \dot{m}(t) \cdot \chi \cdot H_{net}$$

Whereby

$\dot{m}(t)$: burning rate [kg/s]

The combustion efficiency χ can be assumed as $\chi = 0.7$ for fire loads in residential and office buildings [DIN, 2010]. The net calorific value can be taken as $H_{net} = 17.3$ MJ/kg for wooden fire loads and furnishings. The rate of heat release strongly depends on the ventilation conditions and a distinction is made between ventilation-controlled fires and fuel-controlled fires.

In ventilation-controlled fires according to Eurocode 1-1-2 the maximum rate of heat release can be assumed as:

$$\dot{m}(t) = 0.1 A_w \sqrt{h_w} \text{ [kg/s].}$$

For residential and office buildings in case of a ventilation-controlled fire can be derived by inserting $\chi = 0.7$ and $H_{net} = 17.3$ MJ/kg:

$$\dot{Q}_{max,v} = 1.21 A_w \sqrt{h_w} \text{ [MW].}$$

According to Eurocode 1-1-2 the maximum rate of heat release of residential and office buildings in case of a fuel-controlled fire can be determined as

$$\dot{Q}_{max,f} = 0.25 \cdot A_f \text{ [MW].}$$

whereby the maximum burning area A_f [m²] is assumed to be limited to the floor area of the fire compartment.

Fig. 2 illustrates the approach for the rate of heat release [DIN, 2010]. The growth phase is described by the t^2 -approach:

$$\dot{Q}(t) = \dot{Q}_0 \cdot \left(\frac{t}{t_\alpha} \right)^2$$

whereby $\dot{Q}_0 = 1.0$ MW and the time of fire growth - with a medium fire growth rate in residential and office buildings - can be assumed as $t_\alpha = 300$ s.

In the fully-developed fire the quadratic increase in the rate of heat release is replaced by a constant value which is taken as the minimum of the two rates of heat release, for fuel-controlled and ventilation-controlled fires [DIN, 2010]:

$$\dot{Q}_{max} = \text{MIN} (\dot{Q}_{max,v}, \dot{Q}_{max,f})$$

When 70 % of the fire load is consumed, the rate of heat release decreases linearly until the fire load is completely burned.

2.3 Parametric fire curves

For a reference fire load density of $q = 1300$ MJ/m² which is taken as an upper value for residential and office buildings, parametric functions for the temperature-time curve were developed which consider the ventilation conditions, thermal properties of the enclosure and geometry of the compartment. For fire load densities less than the maximum temperature is achieved correspondingly earlier. The appropriate time can be ascertained from the rate of heat release function.

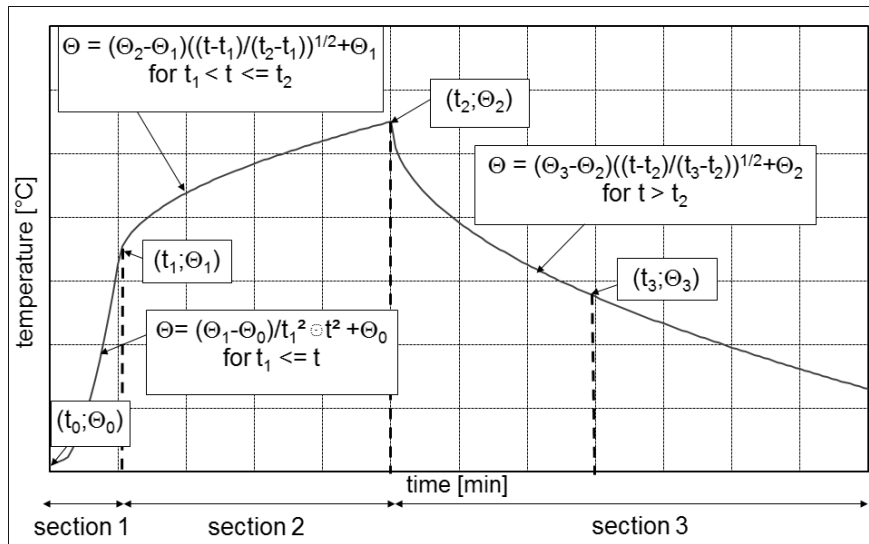


Fig. 3 Mathematical description of the parametric fire curves

A regression analysis for the upper layer temperatures Θ_1 , Θ_2 and Θ_3 of ventilation-controlled fires provides the following functions for the reference fire load density of $q = 1300 \text{ MJ/m}^2$ [Zehfuss and Hosser, 2007]:

$$\Theta_1 = -8.75 \cdot 1/O - 0.1 b + 1175 \text{ [}^\circ\text{C]}$$

$$\Theta_2 = (0.004 b - 17) \cdot 1/O - 0.4 b + 2175 \text{ [}^\circ\text{C]}$$

$$\Theta_3 = -5.0 \cdot 1/O - 0.16 b + 1060 \text{ [}^\circ\text{C]}$$

with

opening factor

$$O = A_w \sqrt{h_w} / A_t [\text{m}^{1/2}],$$

area of ventilation openings

$$A_w [\text{m}^2],$$

averaged height of ventilation openings

$$h_w [\text{m}],$$

total area of enclosing components

$$A_t [\text{m}^2],$$

averaged thermal property of enclosure

$$b [\text{J/m}^2\text{s}^{0.5}\text{K}].$$

For fuel controlled fires the following functions for the reference fire load density of $q = 1300 \text{ MJ/m}^2$ were derived [Zehfuss and Hosser, 2007]:

$$\Theta_1 = 24000 k + 20 \text{ [}^\circ\text{C]} \text{ for } k \leq 0.04 \text{ and } \Theta_1 = 980^\circ\text{C for } k > 0.04,$$

$$\Theta_2 = 33000 k + 20 \text{ [}^\circ\text{C]} \text{ for } k \leq 0.04 \text{ and } \Theta_2 = 1340^\circ\text{C for } k > 0.04,$$

$$\Theta_3 = 16000 k + 20 \text{ [}^\circ\text{C]} \text{ for } k \leq 0.04 \text{ and } \Theta_3 = 660^\circ\text{C for } k > 0.04.$$

with

$$k = \left(\frac{\dot{Q}^2}{A_w \cdot \sqrt{h_w} \cdot (A_t - A_w) \cdot b} \right)^{1/3}$$

maximum rate of heat release \dot{Q} [MW]

The functional form of the parametric fire curves in the three sections is depicted in Fig. 3.

3 EXAMPLE OF APPLICATION

The application of the new simplified natural fire model of German national annex [DIN, 2010] is shown by the example of an office room. The required input data is listed below:

Floor area of fire compartment

$$A_f = 16 \text{ m}^2$$

Height of fire compartment

$$H = 3.00 \text{ m}$$

Ventilation factor

$$A_w \sqrt{h_w} = 12.65 \text{ m}^{3/2}$$

Opening factor

$$O = 0.158 \text{ m}^{1/2}$$

Total area of the enclosing components

$$A_t = 80.0 \text{ m}^2$$

Fire load density $q_x = 511 \text{ MJ/m}^2$

$$Q_{511} = 8176 \text{ MJ}$$

averaged thermal property of enclosure

$$b = 1500 \text{ J/(m}^2\text{s}^{0.5}\text{K)}$$

rate of heat release according to Eurocode 1-1-2 and German national annex:

$$\dot{Q}_{max} = \text{MIN} (\dot{Q}_{max,v}, \dot{Q}_{max,f}) = \text{MIN} (1.21 \cdot A_w \sqrt{h_w}; 0.25 A_f) = \text{MIN} (15.31; 4.0)$$

$$\dot{Q}_{max} = \dot{Q}_{max,f} = 4.0 \text{ MW} \Rightarrow \text{fuel-controlled fire.}$$

Parametric fire curve for reference fire load density of $q = 1300 \text{ MJ/m}^2$:

$$Q = q \cdot A_f = 1300 \cdot 16.0 = 20800 \text{ MJ,}$$

$$t_1 = 600 \text{ s} = 10 \text{ min; } Q_1 = 800 \text{ MJ}$$

$$Q_2 = 13760 \text{ MJ; } t_2 = 4040 \text{ s} \approx 67 \text{ min}$$

$$Q_3 = 6240 \text{ MJ; } t_3 = 7160 \text{ s} \approx 119 \text{ min}$$

for $q_x = 511 \text{ MJ/m}^2$:

$$Q_{2,511} = 4923 \text{ MJ; } t_{2,511} = 1831 \text{ s} \approx 31 \text{ min}$$

$$Q_{3,511} = 2453 \text{ MJ; } t_{3,511} = 3057 \text{ s} \approx 51 \text{ min}$$

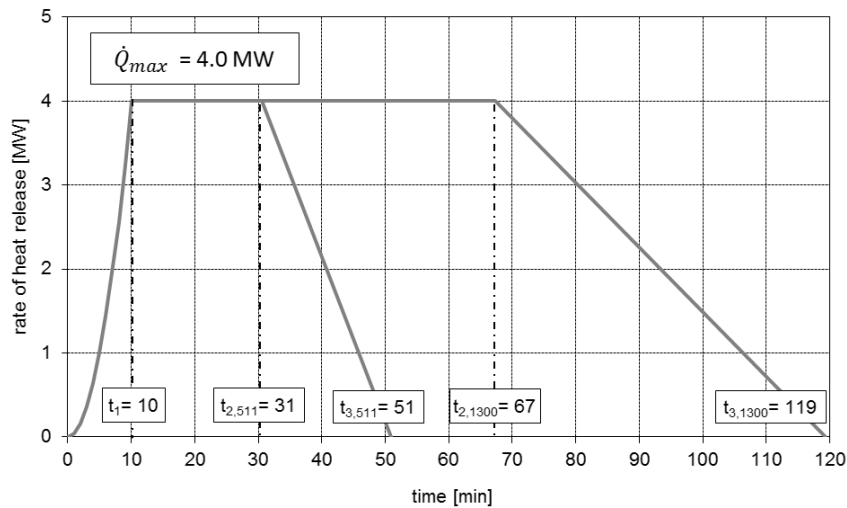


Fig. 4 Rate of heat release example fire in office room

For a fuel-controlled fire it can be derived:

$$k = \left(\frac{\dot{Q}^2}{A_w \cdot \sqrt{h_w} \cdot (A_t - A_w) \cdot b} \right)^{1/3} = 0.0195$$

$$\Theta_1 = 24000 k + 20 = 565^\circ\text{C,}$$

$$\Theta_2 = 33000 k + 20 = 769^\circ\text{C,}$$

$$\Theta_3 = 16000 k + 20 = 383^\circ\text{C.}$$

For the present fire load density $q_x = 511 \text{ MJ/m}^2$ it can be obtained:

$$\Theta_{2,511} = 689^\circ\text{C,}$$

$$\Theta_{3,511} = 316^\circ\text{C.}$$

Fig. 5 shows the parametric fire curve compared to the computed upper layer temperature-time of the advanced natural fire model CFAST and the standard temperature-time curve. The deviation between parametric fire curve and CFAST results are marginal. The new simplified natural fire model of the parametric fire curves can describe the temperature development of a natural fire with a good accuracy.

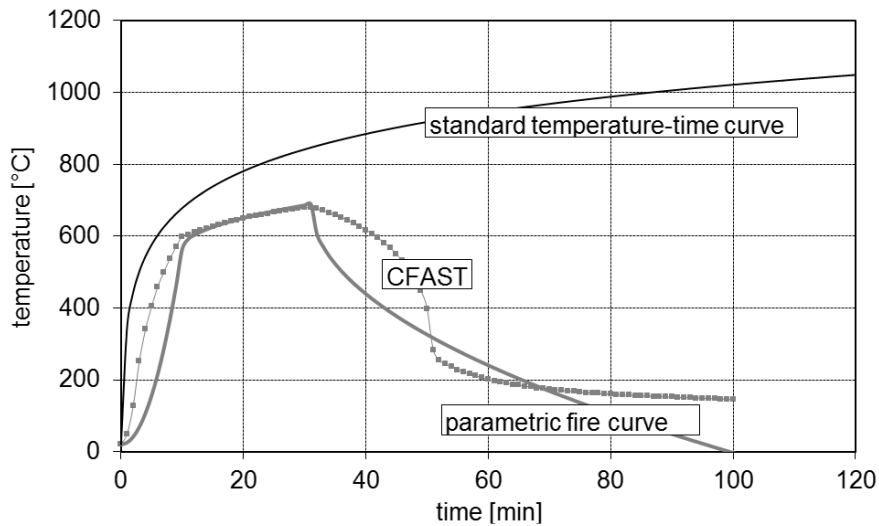


Fig. 5 Comparison of parametric fire curves in German national annex with CFAST results and standard temperature-time curve for an office room

REFERENCES

- DIN EN 1991-1-2/NA: National Annex – National determined parameter -. Eurocode 1: Actions on structures- Part 1-2: General actions – Actions on structures exposed to fire. DIN (German standard association), 2010.
- Schleich J B et al. Natural Fire Safety Concept Full Scale Tests, Implementation in the Eurocodes and Development of a userfriendly design tool. Technical report No. 6 Period from 01.01.2000 - 30.06.2000. CEC Agreement 7210-PA/PB/PC/PD/PE/PF/PR-060. Esch / Alzette, 2000.
- Zehfuss, J, Hosser, D.: A parametric natural fire model for the structural fire design of multi-storey buildings, *Fire Safety Journal* 42 (2007) 115-126, Elsevier.
- Zehfuss, J.; Hosser, D.: Vereinfachtes Naturbrandmodell für die Brandschutzbemessung von Bauteilen und Tragwerken. *Bauphysik* 27 (2005), Heft 2, S. 79-86 (in German)

FIRE RESISTANCE OF CAST IRON COLUMNS IN VINOHRADY BREWERY

František Wald, Mekonnen Dagefa

Czech Technical University in Prague, Czech Republic

INTRODUCTION

The paper presents a procedure for the structural appraisal of old cast-iron columns exposed to fire. Temperature of the gas during the fire is assumed according to nominal standard fire curve. Transfer of heat is modelled by the FE procedure which allows to take into account not only the hollow section particularity but also of the improvement by filling by concrete and to utilise the intumescent coating protection. The buckling resistance is predicted by generalised column curve formulation modified for the cast iron as well as for the elevated temperature. The results are employed on the case study/worked example of the columns used for reconstruction of the Vinohrady brewery in Prague.



Fig. 1 Reused cast iron columns in a show room at ground floor



Fig. 2 Reused cast iron columns in a design office at the first floor

1 VINOHRADY BREWERY

The building of the Vinohrady Brewery has been reconstructed for residential and business purposes, see (Korunní dvůr, 2008). The cast iron columns were redesigned based on the laboratory test results. The recent photographic information, see Figs 3 and 5, corroborate the reuse of columns as they were in the past much in agreement with the authenticity of the existing historical structures. The column geometry is described at Fig. 4. At level $A = 300$ mm were the average values of external diameter 316,4 mm with thickness 316,4 mm, at level $B = 1000$ mm the external diameter 304,0 mm and thickness 31,4 mm; at level $C = 2100$ mm the external diameter 285,8 mm with

thickness 35,4 mm. The height of the column was measured as $D = 2605$ mm and average thickness calculated as 32,0 mm with the average internal diameter 238,1 mm and average external diameter 302,1 mm. From the material test of similar columns were derived the design value of the ultimate compressive strength $f_{u,c} = 213,1$ MPa and the design value of the proof strengths in compression $f_{0,1,c} = 29,9$ MPa and $f_{0,2,c} = 49,1$ MPa. n emerges to be 6,0; see (Degefa, 2008).

2 DESIGN RESISTANCE

2.1 Ambient temperature resistance

The design buckling resistance of cast iron column at elevated temperature was detailed studied by Rondal and Rasmussen (2003). Their proposal is based on the generalized column curve formulation. The design buckling resistance of a compression member is taken

$$N_{b,Rd} = \chi_c A f_{0,2,c} / \gamma_{M1} \quad (1)$$

where $f_{0,2,c}$ is the 0,2 % proof strength of the cast iron in the compression, A is the member area, γ_{M1} is the partial safety factor, and χ_c is the reduction factor, which may be expressed in form

$$\chi_c = \frac{1}{\varphi_c + \sqrt{\varphi_c^2 - \lambda_c^2}} \quad (2)$$

where $\varphi_c = (1 + \eta_c + \lambda_c^2) / 2$; $\lambda_c = \sqrt{f_{0,2,c} / \sigma_{E_0}}$ and $\sigma_{E_0} = \pi^2 E_0 (L/r)^{-2}$. The imperfection parameter, η_c , is given by

$$\eta_c = \alpha ((\lambda_c - \lambda_1)^\beta - \lambda_0) A = \frac{\sqrt{\alpha^2}}{\Omega} \cdot e \quad (3)$$

where α , β , λ_0 and λ_1 are functions of the Ramberg Osgood parameters $n = \ln(2) / \ln(f_{0,2,c} / f_{0,1,c})$ and $e = f_{0,2,c} / E_{0,c}$, see (Ramberg and Osgood, 1943), where $f_{0,1,c}$ is the 0,1% proof strength for compression. Substituting $e = 0,00426$ and $n = 6$, one obtains $\alpha = 0,85$; $\beta = 0,095$; $\lambda_0 = 0,70$; $\lambda_1 = 0,5$; and $\eta_c = -0,0193 > \alpha$ with $\eta_c = \alpha = 0,85$, see (Rondal and Rasmussen, 2003). For cast iron the 0,2 % proof strength may be approximate as a half of the ultimate compressive strength $f_{0,2,c} = f_{u,c} / 2$, see (Blanchard et al, 1997). Cross-section imperfection due to the peculiar eccentricity of the hole to the outer perimeter of a hollow cast iron section is taken into account. It is the result of lifting forces, dislocation and/or deflection of the casting core used for producing the hole of the member during casting.

The eccentricity is given by $g = j d_i^2 / (d_e^2 - d_i^2)$ where $j = (d_e - d_i) / 2 - t_{\min}$, see Fig. 1. The distance g can be estimated based on the proposal $g / d_e \approx 1 / 30$. Cast iron being relatively weak in tension may lead to possibility of tension failure initiated by fracture developed on one side of the column during overall bending. Tension failure becomes critical for slenderness ratio greater than 80. This is very much greater than the slenderness ratio of the columns used for this analysis 56. Hence this study omits the inclusion of tensile stress analysis in the columns.

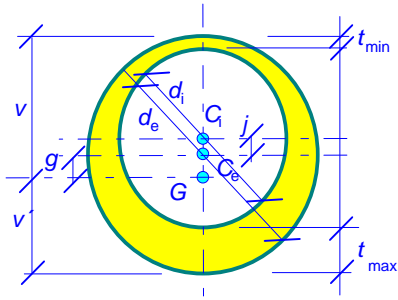


Fig. 5 Cross-section imperfection in hollow cast iron columns, from (Rondal and Rasmussen 2003)

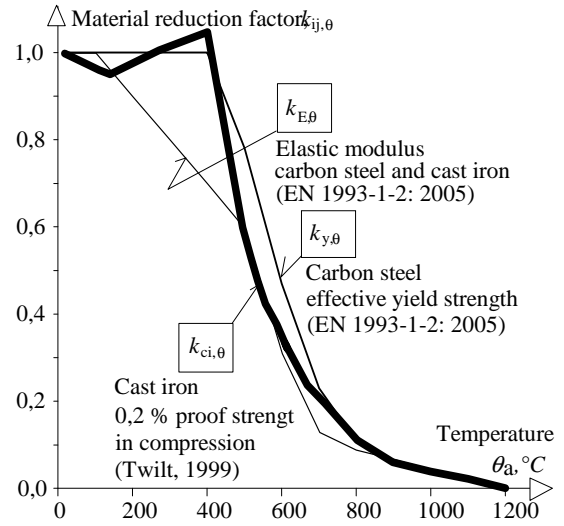


Fig. 6 Reduction factor of 0,2 % proof strength in compression of cast iron $k_{ci,\theta}$ (Twilt, 1999) for effective yield strength steel $k_{y,\theta}$, and for modulus of elasticity $k_{E,\theta}$ (EN 1993-1-2)

1.1 Elevated temperature resistance

The fire design starts with the temperature modelling during the fire. The standard nominal fire curve, see EN 1991-1-2, is the most simple but successful solution for already 120 years. The reduction of material properties was deeply studied in (Twilt, 1999) and Blanchard et al (1997). The results are summarised/compared to EN 1993-1-2: 2005 at Fig. 2.

The integration of Fourier heat transfer equation for non-steady heat conduction inside the member is the general approach to studying the increase of temperature in hollow structural elements exposed to fire. The solution depends on the boundary conditions and in fact numerical solutions, or at least step by step procedure, is necessary. The software SAFIRE (Franssen, 2007), has been used by the idealization of the three dimensional to a two dimensional in those particular model.

As a matter of fact the historical hollow structural cast iron columns have thick cylindrical walls usually falling in the Class 1, see EN 1993-1-1:2005. Hence the design buckling resistance based on the generalized column curve formulation was modified to meet change in properties under elevated temperature

$$N_{b,Rd,\theta} = \frac{\chi_{\theta} k_{ci,\theta} A f_{0,2,c}}{\gamma_{M,\theta}} \quad (4)$$

where χ_{θ} is the reduction factor for flexural buckling in the fire design situation; $k_{ci,\theta}$ is the reduction factor from Fig. 2 for the 0,2 % proof strength of cast iron as the cast iron temperature θ and $\gamma_{M,\theta}$ is the partial factor for fire condition. The value of χ_{θ} for the hollow circular column is the same in any direction given by

$$\chi_{\theta} = \frac{1}{\varphi_{\theta} + \sqrt{\varphi_{\theta}^2 - \lambda_{\theta}^2}} \quad (5)$$

with $\varphi_{\theta} = (1 + \eta_c + \lambda_{\theta}^2)/2$. The imperfection parameter, η_c , is given by $\eta_c = \alpha((\lambda_c - \lambda_1)^{\beta} - \lambda_0)$, neglecting the small variation due to temperature. Where α , β , λ_0 and λ_1 are functions of the parameters n and $e_c = \sigma_{0,2,c}/E_0$. The values are taken from Rasmussen and Rondal (1997) proposal

as $\eta_c = \alpha = 0,85$; $\beta = 0,095$; $\lambda_0 = 0,70$; $\lambda_1 = 0,55$. The non-dimensional slenderness λ_θ for the temperature θ ,

$$\lambda_\theta = \lambda_c \left[k_{ci,\theta} / k_{Eci,\theta} \right]^{0.5} \quad (6)$$

where $k_{ci,\theta}$ is the reduction factor for the yield strength of cast iron at the cast iron temperature θ and $k_{Eci,\theta}$ is the reduction factor for the modulus of elasticity, $E_{ci,\theta} / E_{ci}$ with $E_{ci,\theta}$ as the modulus of elasticity at temperature θ , see (Wouters and Mollaert, 2002).

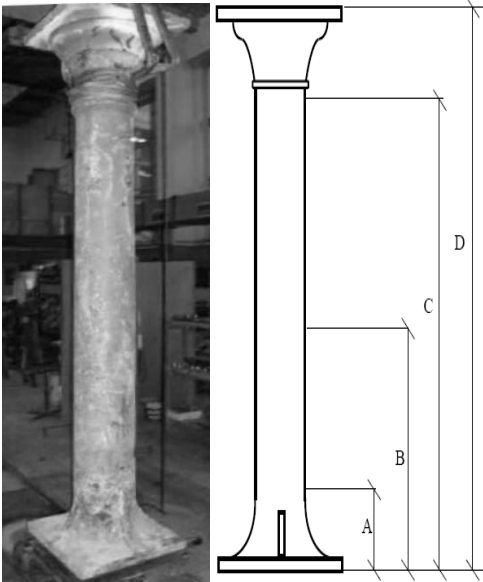


Fig. 5 The laboratory arrangement and geometry of cast iron column



Fig. 6 Failure of base plate during the column test at elevated temperature

3 CASE STUDY

3.1 Ambient temperature verification

The inputs to the procedure described upward are the geometric properties of the column: geometric imperfection $g = 10,07$ mm; distance to extreme fibres $G = 161,12$ mm; sectional area $27153,41$ mm²; area moment of inertia $251094438,07$ mm⁴; radius of gyration $96,16$ mm and slenderness ratio $27,09$. The imperfection parameters may be assumed as $\alpha = 0,85$; $\beta = 0,095$; $\lambda_0 = 0,7$; $\lambda_1 = 0,55$. The parameters to evaluate the reduction factor χ_c are derived for the slenderness $\lambda_c = 0,56$ and $\eta_c = 0,85$; $\varphi_c = 1,08$. The reduction factors $\chi_c = 0,50$ gives the load resistance F_{Rd} of the cast iron column at ambient temperature $4589,5$ kN.

Prototype test on two cast iron hollow cylindrical columns of the Vinohrady Brewery of Prague had been conducted at ambient temperature. These are considered typical for the Brewery building. The columns are anticipated to carry service load $N_{Ed,ser}$ of 1800 kN and load at the ultimate limit state $N_{Ed,ult}$ of 2700 kN at ambient temperature and $N_{Ed,\theta}$ 1500 kN in fire situation. During the test were reached the the design values of the compression force $N_{Ed,ser}$ and $N_{Ed,ult}$. The failure mode was guided by the base plate rupture, see Fig. 5.

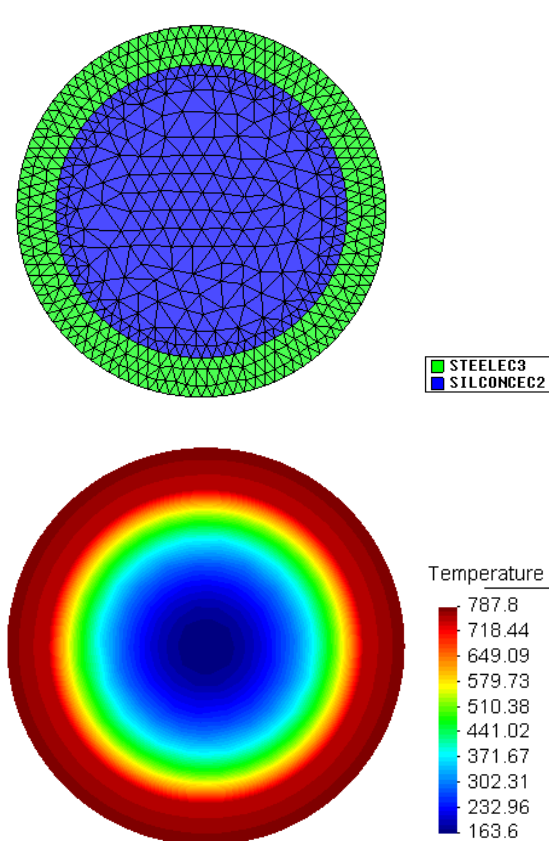


Fig. The meshing and the thermal gradient over the cross section of the concrete infill cast iron column exposed to nominal standard fire curve for 60 min

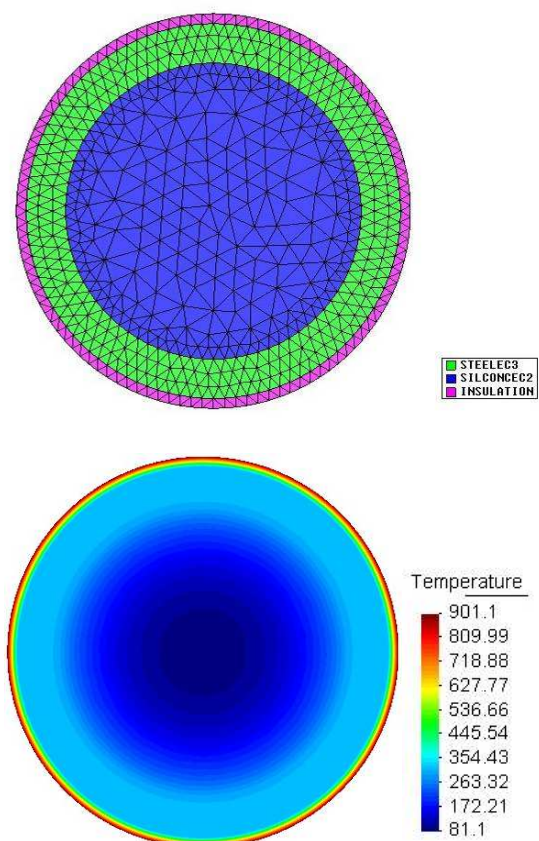


Fig. 8 The meshing and the thermal gradient over the cross section of the concrete infill and intumescent painted cast iron column exposed to nominal standard fire curve for 60 min

3.1 Elevated temperature verification

The transfer of heat was simulated by software SAFIR, see (Franssen, 2007). 2D representation was utilised. The heat induced due to fire is assumed to be uniform around the column meaning it is axis-symmetric like that of the section. Except of fire unprotected column were simulated the column filled by concrete, protected by intumescent coating and filled and protected solution. The geometric properties were taken as: external diameter, $d_e = 301,8$ mm; internal diameter, $d_i = 238,4$ mm; thermal conductivity 55 W/mK; specific heat capacity of cast iron at ambient temperature 460 J/kgK. The thermal properties of intumescent coating PROMAPAIN[®] SC were taken as thermal conductivity 0,2 W/mK; specific heat 1100 J/kgK; specific mass 350 kg/m; relative emissivity 0,8 and the effective thickness 8 mm, see Strejček et al, 2009. The average temperatures of the cast iron wall from the calculation are summarised in Tab. 1. The distribution of the temperature in the column is shown at Fig 7, and 8. The average temperature of the cast iron of the filled unprotected column varies in 60 min of nominal fire from 788 °C till 750 °C, but in case of protection by intumescent coating only from 409 °till 413 °C and with infilling from 354 °C till 274 C. The fire resistance was calculated based on the assumption of the similar imperfection factors as at the ambient temperature, see upward according to Rasmussen and Rondal (1997). The results are summarised at Tab. 1.

Tab. 1 Average temperatures, reduction factors of 0,2 % proof strength in the compression and of modulus elasticity, fire resistance and reduction of resistance for different fire protection of cast-iron column in Vinohrady brewery exposed to 60 min at nominal standard fire

Condition	Temperatures	Factors	R60	Reduction of resistance
Fire unprotected column	864 °C	0,08/0,07	395 kN	8 %
Concrete filled column	769 °C	0,14/0,07	687 kN	15 %
Intumescent coated column	411 °C	1,00/0,67	4530 kN	99 %
Coated plus filled column	314 °C	1,00/0,82	4547 kN	99 %

4 SUMMARY AND ACKNOWLEDGMENT

The procedure of the fire resistance of the columns based on European fire design was completed and applied to a study stay of the reconstruction of Vinohrady brewery. The results of prediction of the fire resistance show a smaller improvement of concrete infilling in R60 as may be expected. The case study recommended applying both protections infilling as well as intumescent coating.

This outcome has been achieved with the financial support of the Czech Ministry of Education, Youth and Sports, project MŠMT CIDEAS No. 1M0579.

REFERENCES

- Blanchard J., Bussell M., Marsden, A. and Lewis, D. (1997), Appraisal of Existing Ferrous Metal Structures Stahlbau 66(6).pp. 333 - 345.
- Degefa M. (2008), Cast Iron Columns under Ambient and Elevated Temperature, with Vinohrady Brewery's Case Study, Master thesis at Czech Technical University in Prague, p. 64.
- Degefa, M., Wald, F., Kolísko, J., Matějka, M., Improvement of Fire Resistance of Cast Iron Columns, v Protection of Historical Buildings PROHITECH 09. London: Taylor & Francis, 2009, vol. 1,2, s. 1378-1391. ISBN 978-0-415-55803-7.
- EN 1991-1-2: 2002., Eurocode 1: Basis of design and actions on structures – Part 2-2: Actions on structures – Actions on structures exposed to fire, CEN, Brussels.
- EN 1993-1-1: 2005, Eurocode 3: Design of steel structures – Part 1-1: General rules and rules for buildings, CEN, Brussels.
- EN 1993-1-2: 2005, Eurocode 3: Design of steel structures – Part 1-2: General Rules – Structural fire design, CEN, Brussels.
- Franssen J. M. (2007), Users Manual for SAFIR 2007. A Computer Program for Analysis of Structures Subjected to Fire. University of Liege.
- Korunní dvůr <http://www.korunnidvur.cz/lokalita-historie.php>.
- Ramberg W. and Osgood, W.R. (1943), Description of Stress Strain Curves by Three Parameters. Technical Note No. 902, National Advisory Committee for Aeronautics, Washington DC.
- Rondal J. and Rasmussen Kim J.R. (2003), On the Strength of Cast Iron Columns. Research Report No R829. The University of Sydney, Department of Civil Engineering, Sydney.
- Strejček M., Cinar R., Stanke V., and Wald F. (2009), Effective parameters of fire protection, in Application for fire engineering, CTU in Prague, pp. 164 - 171, ISBN 987-80-01-04266-3.
- Twilt L. (1999), Urban Heritage and Building Maintenance. Problems and Possibilities, in Urban Heritage Building Maintenance – Iron and Steel, Delft University of Technology, The Netherlands.
- Wouters I. and Mollaert M. (2002), Evaluation of the Fire Resistance of the 19th Century Iron Framed Buildings, Fire technology, 38, Kluwer Academic Publishers. pp. 383 - 390.

SOFTWARE APPLICATIONS FOR ESTIMATION OF FIRE RESISTANCE OF THE BUILDINGS CONSTRUCTION

Kamil Vargovský^a

^aSpecialist and engineer of the fire protection, Self-employed No-G/2008/00958-2, Business license 670-16902

ABSTRACT

The aim of this article/paper is the presentation of the practical experiences with projects and their software's applications by the demonstration of the fire resistance of building's constructions for the need of fire engineering with the use of euro codes.

The main part of this work is the judgement of the fire resistance of the particular realized project of the overhead building construction. This project was accepted by Ministry of Interior of the Slovak Republic – Department of Firemen and Rescuers.

The judgement of the fire resistance presents the software outputs as a part of fire resistance proving, by means of “differential method” and “Finite Elements Method” for calculations and simulation.

1. INTRODUCTION

The main subject of this article is an example of fire resistance proving for the particular realized project of concrete building construction. Software's outputs are integral part of fire resistance proving.

An example is the fire resistance test (REI, REW 120) of the building construction by means of the calculation for the ceiling made of load-bearing reinforced concrete hollow panels, for the inside fire actively cooled by Stable Fire Extinguisher (by Sprinklers) and for the outside fire of the object of furniture storehouse extension.

The estimation of fire resistance is processing theoretical-experiment with help of calculations and simulations and by STN EN series 1363, STN EN 1365 a eurocodes series STN 1990, particularly STN EN 199x-1-2.

In the sense of § 8 ministry regulation MI SR č. 94/2004 Z.z., was estimation of fire protection done for the fire resistance of roof construction:

- REI 120D1 (i → o) –interior fire by STN EN 1991-1-2 (zone model);
- REI 120D1 (o → i) –exterior fire by STN EN 1363-2 (standard exterior fire);
- by limiting states of fire resistance – STN EN 1363-1;
- by differential method of unstationary heat conduction;
- by finite element method (FEM);
- by means of results of the fire resistance test - protocol EMI Ltd. (Hungarian), REI 90 by EN 1363-1 (standard interior fire).

2. METHODOLOGY

2.1 Description of construction

Load-bearing reinforced concrete hollow panel forming rectangular section with longitudinal holes. The panels has diameter of 200/1200mm, and the holes diameter is about 155 mm. The panels are like simple beam.

Material:

Concrete C40, steel cable - Ø 12,5 (EN 138-79) protection thickness is 25 mm.

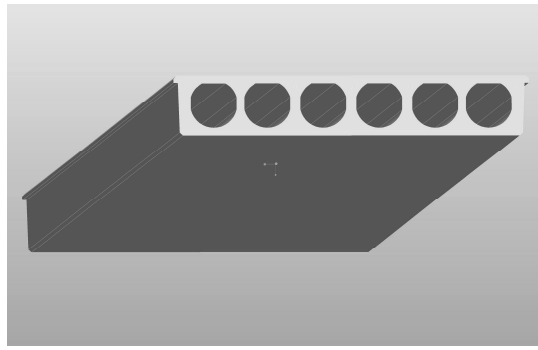


Fig. 2 Loadbearing reinforced concrete hollow panel

2.2 Entrance thermo-technical parameters considered in calculations

In calculations were considered thermo-technical parameters of steel cable by:

Coefficient of the heating conduction	$\lambda = 54 - 0,0003 T$	[W.m ⁻¹ .K ⁻¹],
Volume weight	$\rho = 7850$	[kg.m ⁻³],
Measuring heat	$c = 425 + 0,2 T + 0,00038 T^2$	[J.kg ⁻¹ .K ⁻¹],
Weight humidity	$v = 0$	[%].

In calculations were considered thermo-technical parameters of concrete by:

Coefficient of the heating conduction	$\lambda = 1,6 + 0,002 T + 0,000000833 T^2$	[W.m ⁻¹ .K ⁻¹],
Volume weight	$\rho = 2300$	[kg.m ⁻³],
Measuring heat	$c = 1000 + 0,667 T - 0,000278 T^2$	[J.kg ⁻¹ .K ⁻¹],
Weight humidity	$v = 1,5$	[%].

2.3 Analysis strategy

Selected strategy: Combination 2Zones - 1 Zone Model

Transition criteria from 2 Zones to 1 Zone

Upper Layer Temperature B 500°C

Combustible in Upper Layer + U.L. Temperature B Combustible Ignition Temperature = 300 °C

Interface Height A 0,2 Compartment Height

Fire Area B 0,25 Floor Area

2.3.1 Parameters

Openings	Temperature	% of Total Openings
Radiation Through Closed Openings: 0,8	[°C]	[%]
Bernoulli Coefficient: 0,7	20	10
Physical Characteristics of Compartment	400	50
Initial Temperature: 293 K	500	100
Initial Pressure: 100000 Pa	Linear Variation	
Calculation Parameters	Temperature	% of Total Openings
End of Calculation: 7200 sec	[°C]	[%]
Time Step for Printing Results: 60 sec	20	10
Maximum Time Step for Calculation: 5 s.	400	50
Air Entrained Model: Mc Caffrey	500	100
Temperature Dependent Openings	Time Dependent Openings	
All openings activated at: 400 °C	Time	% of Total Openings
Stepwise Variation	[sec]	[%]
	0	5
	1000	100

2.3.2 Compartment

Form of Compartment:	Rectangular Floor
Height:	3 m
Depth:	43 m
Length:	40 m
Roof Type:	Flat Roof

2.3.3 Parametric Interior Fire - STN EN 1991-1-2 (zone model)

Fire Curve:	NFSC Design Fire			
Maximum Fire Area:	1720	m _c		
Fire Elevation:	0	m		
Fuel Height:	0	m		
Occupancy	Fire Growth Rate	RHRf [kw/m _c]	Fire Load q _{f,k} [MJ/m _c]	Danger of Fire Activation
User Defined	75	6000	6186	1,4
Active Measures				
Description	Active		Value	
Automatic Water Extinguishing System	Yes		δ _{n,1} = 0,61	
Independent Water Supplies	1		δ _{n,2} = 0,87	
Automatic Fire Detection by Heat	Yes			
Automatic Fire Detection by Smoke	Yes		δ _{n,4} = 0,73	
Automatic Alarm Transmission to Fire Brigade	No		δ _{n,5} = 1	
Work Fire Brigade	No			
Off Site Fire Brigade	Yes		δ _{n,7} = 0,78	
Safe Access Routes	Yes		δ _{n,8} = 1	
Staircases Under Overpressure in Fire Alarm	No			
Fire Fighting Devices	Yes		δ _{n,9} = 1	
Smoke Exhaust System	Yes		δ _{n,10} = 1	
Fire Risk Area:	1720	m	δ _{q,1} = 1,83	
Danger of Fire Activation:			δ _{q,2} = 1,4	
		q _{f,d} =	3831,5 MJ/m _c	
Combustion Heat of Fuel:			40 MJ/kg	
Combustion Efficiency Factor:			0,8	
Combustion Model:			Extended fire duration	

2.3.4 Exterior Fire STN EN 1363-2

By the thermal effort of the sample from the outside is the wall afforded according to STN EN 1363 2 ar. 5.2 line of the outside fire (see the equation)

$$T_N = 660(1 - 0,687e^{-0,32t} - 0,313e^{-3,8t}) + 20 \quad (1)$$

where

T_N – is the average temperature in the oven [°C];

t — is the time from the beginning of the exam in minutes

The calculation of the thermal field -

The calculation of thermal fields of the considering composition of that construction comes out from the Fourier partial differential equation of the unstationary heating conduction that has in differential form this version

$$\frac{dT}{dt} = a \cdot \frac{d^2T}{dx^2} \quad (2)$$

where: dT – is the increase of the temperature [$^{\circ}\text{C}$];
 dt – is the increase of the time [s];
 dx – is the thickness of the layer [m];
 a – is the coefficient of the heating conduction [$\text{m}^2 \cdot \text{s}^{-1}$].

We can express the coefficient of the heating conduction by the relation

$$a = \frac{\lambda}{c \cdot \rho} \quad (3)$$

Where: λ – is the coefficient of the heating conduction [$\text{W} \cdot \text{m}^{-1} \cdot \text{K}^{-1}$];
 ρ – is the volume weight [$\text{kg} \cdot \text{m}^{-3}$];
 c – is the measuring heat [$\text{J} \cdot \text{kg}^{-1} \cdot \text{K}^{-1}$].

The calculation of the thermal field runs step by step in time intervals dT .

In each time interval are set temperatures in levels separating individual layers. Time interval of the calculation is necessary to set so that for all the materials will be completed the condition

$$dT \leq \frac{dx_i^2}{2 \cdot a_i} \quad (4)$$

By the instillation of the thermal technical values from (2) to (3) we gain the condition for the maximal time step

$$dT \leq \frac{dx_i^2 \cdot c_i \cdot \rho_i}{2 \cdot \lambda_i} \quad (5)$$

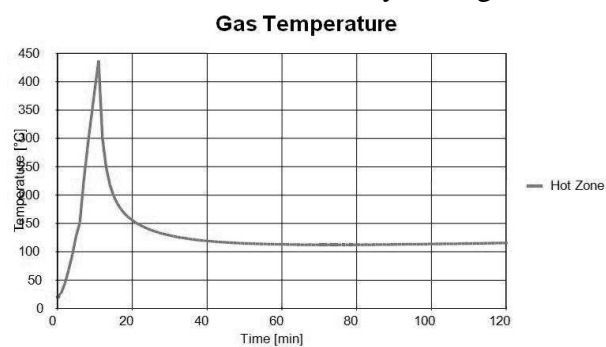
Where: dx – is the thickness of the single layer it's type of the material [m];
 a_i – is the highest value of the coefficient of the heating conduction is type of the material in the examined thermal area of 20°C to 1000°C [$\text{m}^2 \cdot \text{s}^{-1}$].

3. SUMMARY AND ACKNOWLEDGMENT

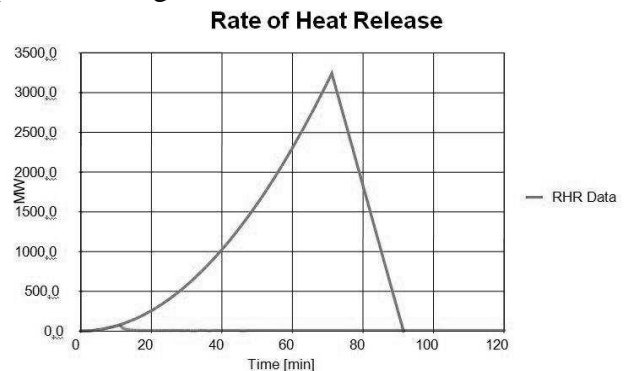
3.1 Results for Interior Fire (zone model)

Fire Area: The maximum fire area (1720.00m_c) is greater than 25% of the floor area (1720.00m_c).
The fire load is uniformly distributed.

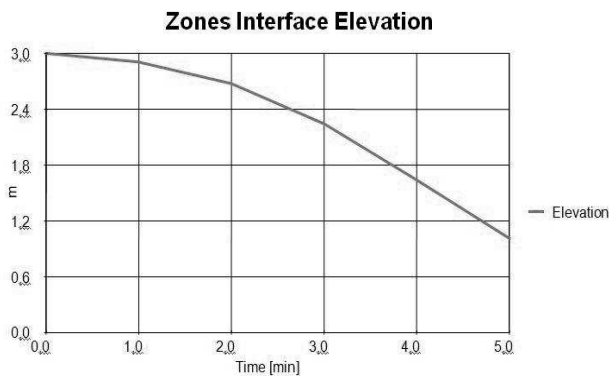
Switch to one zone: Lower layer Height < 20.0% compartment height at time [s] 343.51



Peak: 437°C At: 11 min
Fig. 1 Hot Zone Temperature

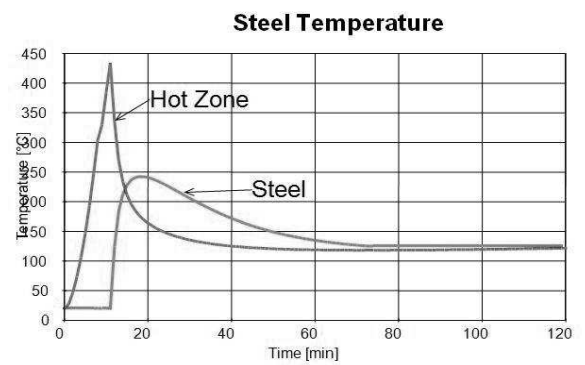


Peak: 3241,41 MW At: 71,2 min
Fig. 2. RHR Data



h = 1,00 m At: 5,00 min

Fig. 3 Zones Interface Elevation



Peak: 434 °C At: 11 min

Fig. 4 Hot Zone and Steel Temperature

STEEL

Protected Section

Catalogue Profile: Steel cable - Ø 12,5 (EN 138-79), coating of steel cable is 25 mm.

Exposed to Fire on: 1 sides

Hollow Encasement

Protection Material: With Constant Values

Protection Thickness: 25 mm

Material Name: Concrete

Unit Mass Specific Heat Thermal Conductivity

[kg/m³] [J/kgK] [W/mK]

2230 900 1,5

HEATING

Profile heated by: Hot Zone Temperature

Convection coefficient: 35 W/m²K

Relative emissivity: 0,8

FIRE RESISTANCE

Element Submitted to Bending

Nominal Steel Grade: S 235

Design effect of actions in fire situation

Plastic Redistribution of the Bending Moment

Loading: Uniform Distributed Load - Simple Beam

$P_{fi, d} = 13,973 \text{ kN/m}^2$

Span = 8,2 m

Adaptation Factors

Non-uniform Temperature Across the Cross-Section: $k_1 = 0,7$

Non-uniform Temperature Along the Beam: $k_2 = 1$

RESULTS

Critical Temperature: 476 °C - by results of the test about fire protection - protocol EMI Ltd. (Hungarian), REI 90 by EN 1363-1 (standard interior fire)

Failure Mode: Flexural Buckling

Class of the Cross Section in Fire: 1

Steel Temperature 242 °C At: 18 min

Fire Resistance: (242,0°C < 476 °C) 120,00 min

REW 120 (i → o)

3.2 Results for standard Exterior Fire

3.2.1 By differential method

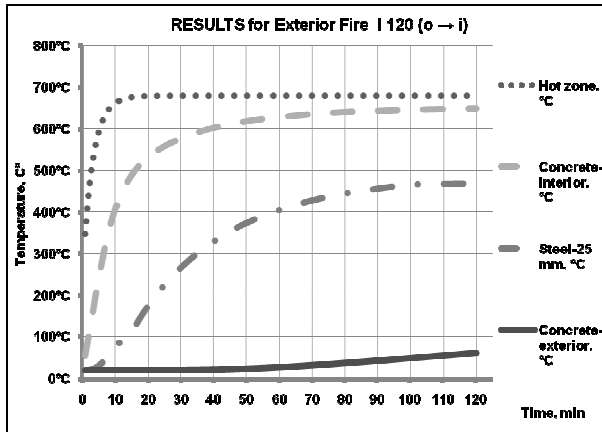


Fig. 5 Graph of the calculation of the unstationary heat conduction

Time, min	Hot zone, °C	Concrete-interior, °C	Steel-25 mm, °C	Concrete-exterior, °C
1	346,1	53,3	20	20
15	676,3	488,6	114,5	20
30	680	577,2	265,3	20,3
45	680	611,4	352,8	22,4
60	680	628,7	405	27,2
90	680	643,9	456,4	42,5
120	680	649,3	469	60,3

Tab. 1 Results of calculation of the unstationary heat conduction

Temperature on interior: 649,3 °C in: 120. minute
 Temperature on exterior: 60,3°C in: 120. minute (E,W 120)
 Temperature of steel cable: 469,0°C in: 120. minute (R 120)
 Critical Temperature: 476 °C
 Fire Resistance: (469,0°C < 476 °C) 120,00 min

REW 120 (o → i)

3.2.3 By finite element method (FEM) for standard Exterior Fire

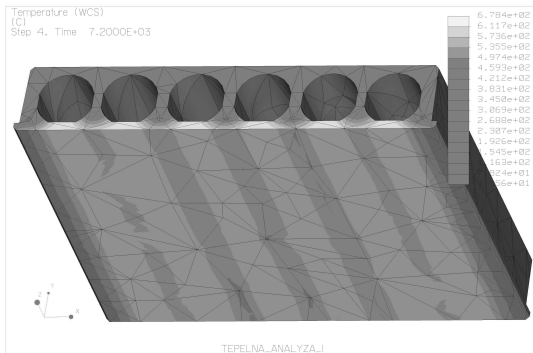


Fig. 6 Results with network analysis by finite element method (FEM) - bottom view.

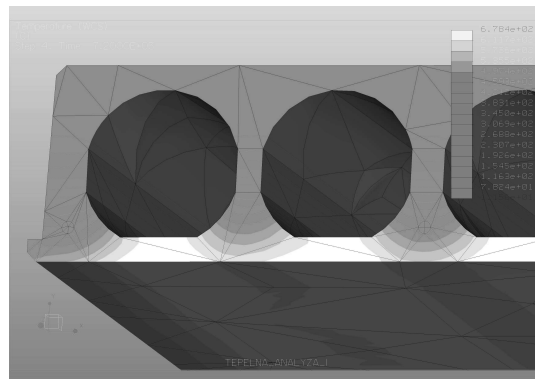


Fig. 7 Results with network analysis by finite element method (FEM) - bottom view.

Temperature on interior: 678 °C in: 120.minute
 Temperature on exterior: 78,2 °C in: 120. minute (E,W 120)
 Temperature of steel cable: 459,3 °C in: 120. minute (R 120)
 Critical Temperature: 476 °C
 Fire Resistance: (459,3°C < 476 °C) 120,00 min

REW 120 (o → i)

3.3 Expert opinion

The subject of this paper was estimation of fire resistance (REI, REW 120) of the building construction by the calculation intended for „load-bearing reinforced concrete hollow panels, roof construction with Sprinkler“, for object storehouse extension.

The judgement was made by theoretical theoretical-experimental with help of calculations and simulations and by STN EN series 1363, STN EN 1365 a eurocodes series STN 1990, particularly STN EN 199X-1-2.

It was proved that: load-bearing reinforced concrete hollow panels, roof construction, for object storehouse extension by the fire exposition from the inside according with Sprinkler to STN EN 1991-1-2 suits to the fire resistance REW 120 (i →o) and from the outside according to STN EN 1363-2 suits to the fire resistance REI 120 (o →i).

REFERENCES

- EN 13501-2 Fire classification of construction products and building elements - Part 2: Classification using data from fire resistance tests, except ventilation services.
- EN 1363-1 Fire resistance tests – Part 1: Essential requirements.
- EN 1363-2 Fire resistance tests – Part 2: Alternative and additional procedures.
- EN 1365-1 Fire resistance tests for load-bearing elements– Part 1: Walls.
- EN 1990 Eurocode: Principles of construction projection (E)(including Attachment A1: Buildings(S)).
- EN 1991-1-2 Eurocode 1: Constructions loading –part 1-2: general loading – construction loading strained by the fire.
- EN 1992-1-2 Eurocode 2: Design of concrete structures – Part 1-2: General – Structural fire design.
- Protocol by over partial researches fire resistance pro requisites statements deuces, published EMI Kft. (EMI Ltd - society pro quality control and innovation in the building industry), Budapest, April 2005.
- Technical and drawing documentation from customer.

THE IMPACT OF FLAME RETARDED TIMBER ON GREEK INDUSTRIES

D.Tsatsoulas ^a

^a Greek Fire service (Kritis 46 & Martiou, 54008, Thessaloniki)

INTRODUCTION

Wood has many good properties as a construction material. It is heavily used in building construction and building because of its ease of processing, physical and mechanical properties, aesthetic, environmental and health aspects[1][2]. Wood is also used in many industrial applications for purposes such as surface lining material, furniture, flooring, roof, shelves, pallets, wooden scaffolding for both offshore and onshore, packing cases etc[3][4]. However with current regulations and standards[5], this is not allowed, as this would significantly add to the fire load within a room in a fire scenario i.e wooden materials in different forms, with the highest percentages, contribute as first ignited materials in fire initiation and spreading and have a major impact in fire losses[3][4][6]. The above clearly signals the importance of controlling the ignition resistance, and flammability of Timber as used in different forms in various constructions. Therefore, it is possible to increase the fire performance of wood, with the application of Flame Retardants (possibly intumescent).

There has been a significant but limited amount of work studying the effect of flame retardants for applied on wooden surfaces. Previous research has shown that flame retardants applied to wood have had a positive affect on the burning behaviour of wood, in terms of ignition and the most important variable to describe fire hazard the heat release rate, HRR[1][7]. Intumescent Flame Retardants have also been the subject of study, in their own right. Birgit et al[2] presented comparative test data with fire retardant treated and untreated wood products. The test results show a significant differences between these two groups. The parameters included in the comparison are t_{ig} , HRR (peak and average values) and total HRR. The wood based products tested in different small-scale national fire tests and in the full-scale room fire tests. Fire retardant wood products achieve an improved classification both in present national systems and in possible new systems based on the cone calorimeter and room fire test. D.Tsatsoulas et al[6] used FTIR to investigate toxic emissions of eight species of wood. 'Significant' acrolein peak values are measured for all samples. At low irradiance (i.e., 35kW/m^2), facing types of timber, e.g., MDF, Chipboard, with melamine or maple increases significantly the ignition resistance of MDF and Chipboard by a factor of 1.5 to 2, due to the flame retarding properties of melamine and maple.

In the present work the effect of typical intumescent flame retardant (latest technology) will be examined on representative types of Timber. Analysis involved thermal behavior, and toxic species analysis of the samples.

1 EXPERIMENTAL

The university of Leeds apparatus[4][8-9] used was: I. a standard Cone Calorimeter manufactured in accordance to ISO 5660 (1993) and ASTM E1354 (1992). The tests were carried out in accordance with the test procedure of ISO 5660, II. a 1.56 m^3 enclosed fire test facility, $1.4\text{m} \times 0.92\text{m} \times 1.22\text{m}$, with separate entrained air inlet at floor level and fire product exit at ceiling level, with online effluent gas analysis equipment (FTIR). A TEMET GASMET CR-Series portable FTIR analyzer was used to experiment with virgin samples that were chosen to be painted with flame retardants and for all flame retarded samples. This has a multi-pass, gold-coated sample cell with a 2m path length and volume of 0.22l . A liquid nitrogen cooled MCT detector was used that scans 10 spectra per second and several scans are used to produce a time-averaged spectrum. The instrument was calibrated by the manufacturers for all the species using reference gas concentrations. The response time of the instrument is 5s to reliability resolve all measured toxic species.

A test time duration of 600s was generally adopted, although, in certain flame retardant samples, the duration was extended up to 1000sec, depending on the thermal behavior of the specimen. The reason for that is that the present work aims at examining the development of fires on wooden samples painted or not with fire-retardant paints during the early stage of fire development, and for a period of time up to 10-15 minutes min. This period in real fire conditions, covers the time needed for the evacuation of the industrial plant by its staff, the potential intervention of the fire-safety staff of the plant, and the arrival of the fire department to extinguish the fire[4][6].

2 EXPERIMENTAL FIRES CONFIGURATION

Tests were conducted in the cone calorimeter (small scale) using : substrates were 100mm square and thickness varied from 19mm to 22mm. Three (3) types of wood intumescent flame retardants were used to represent main classes of commercial products i.e. 'Zero Flame' (water based paint), 'Varnish Zero Flame' (varnish water based) and 'Synto Flame' (solvent based paint). This selection of flame retardant was based on its chemical composition, since each one represents a large homogeneous class of products, and also on the applications for which each one has been designed. The selection of the heat flux is a very important factor when undertaking Cone Calorimeter tests [5]. The current tests were carried out in the horizontal orientation at heat fluxes of 35, 50, 65, 80 kW/m², to represent a possible range of heat fluxes to be encountered in a developing industrial fire[4]. Also, the aim was to examine all bare, flame retarded samples in the same radiation in order to be able to compare them. Fewer tests have been performed at 80kW/m² because of technical difficulties which did not allow to performed further experiments at such a large value of irradiance. Each test was carried out at least three times, to gain some understanding of test repeatability. Based on the above, eight (8) species of wood which constitute common applications in different forms i.e floor, ceiling, shelves, pallets, packing cases, scaffolding, furniture etc., were chosen for experimental investigation [4][6]. In total 96 tests have been performed in total at various irradiances, in order to determine various flammability characteristics of a range of virgin wood species[4][6]. Three typical types of wood i.e. pine, MDF, blockboard were chosen as representative from those used in virgin form, for painting with the typical types of flame retardants that mentioned above (total performed tests 54). The abbreviations are:, Bb 'Blockboard', ZF 'Zero Flame', SF 'Synto Flame', ZFV 'Zero Flame Varnish', .

Tests were conducted in the enclosed Fire Rig (medium scale) using: I. Untreated wooden crib II. Fully flame retarded wooden cribs III. Partial flame retarded wooden crib. From the various types of wood found in different structures in the industry, pine was selected for medium-scale experimental investigation, since it is one of the most commonly used type of wood is "easy-to-use" and produced in large quantities, especially, from the Mediterranean forests [4]. It was chosen to be tested in form of cribs, because, in real fires there are complex wooden geometries and configurations strongly affecting the "spreading of fires" [4][6]. Thus, a wooden crib, which includes a crossed layer of sticks, simulates complex wooden structures, where the confinement of heat and cross-radiation among the surfaces allows for the efficient burning of wooden surfaces, and the rapid development of fires. Analysis involved thermal behavior, and toxic species analysis of the samples. The experiments were run under controlled airflow conditions. The airflow rate used in the experiment was 75 kg/h, i.e., corresponds to well ventilated fire conditions. The reasons for choosing the above-mentioned high ventilation rate were (i) to reasonably simulate the ventilation conditions in the beginning of most real industrial fires [4], (ii) To allow comparisons with small-scale experimental works in cone calorimeter, where the experimental conditions are also well ventilated.

It should be emphasized, that the objective was not to determine or use the best product in the market, but to establish general patterns of behavior of Timber with or without flame retardant.

Wooden cribs with average fire load equal to 45 kg/m²(~765kJ/m²) were chosen to perform medium scale tests. In order for the crib to be easily ignited a small volume of ethanol was used in a dish. The ethanol was placed directly below the center of the crib (as "worst" case position) and was ignited using a blow lamp and the crib placed on top. 'Zero-flame' retarded paint was chosen for coating the wooden crib, since it is water-based and especially designed for interior wooden

surfaces, like those simulating the wooden cribs under experimental testing. The following (% flame-retarded % bare) wooden cribs were tested experimentally in order to examine different cases of fire development at the ventilation rate mentioned above.

- 100% flame retarded, where all their surfaces were painted with ‘Zero-Flame’ retarded paint. Total surface, coated in two (2) layers of flame retarded paint: 0.7 m². Overall, three (3) wooden crib tests were performed with 100% flame retarded surfaces. For their quick ignition, 6g ethanol, 20g ethanol, and 30g ethanol were used, respectively, in the manner, described in the case of ignition of virgin crib.
- 50% flame retarded, 50% bare wood, where the first 5 layers (21 sticks) were treated with ‘Zero Flame’ retarded paint(two(2) coats), and the rest 5 layers (21 sticks) were left untreated. One (1) test was carried out, and 6g ethanol was used as ignition source in the same way described before.
- 60% bare wood, 40% flame retarded wood, where 0.437m² were left untreated, i.e 26 sticks in the first 7 layers, while the remaining 0.268 m², i.e., 16 sticks, were painted with flame retardant paint(two(2) coats), included in the 7th and 10th (last) layer of wooden crib. Two (2) tests were performed with 6g and 20g ethanol as ignition source, respectively.

The reasons for using the above quantities as ignition sources were: to simulate sources of real fires starting, guided by the statistical analysis of industrial fires[4], and show whether they affect the faster spreading of fires or not. All the above tests using various wooden cribs with different strength of ignition sources give an indication whether the application of flame-retardants at different parts of wooden surfaces located near potential ignition sources (as first or second ignited materials) contribute to suppression or to slower fire developing, and show how they may affect the concentrations of the released toxic gases when the wooden surfaces are burned.

3 THERMAL BEHAVIOR- EXPERIMENTAL RESULTS

Fire development results of small scale experimental work(cone calorimeter) cover: i Time to ignition(s), ii HRR(kW/m²). All tests were fairly repeatable in terms of the tig and HRR values i.e 2-4% Std.dev.(expresses the standard deviation as a percentage of the average value). Experimental results represent the mean of a minimum of three (3) tests. In all flame treated samples, the intumescent paint swell into a thick, robust foam upon exposure to heat, thus protecting the underlying material from fire by providing a physical barrier to heat and mass transfer.

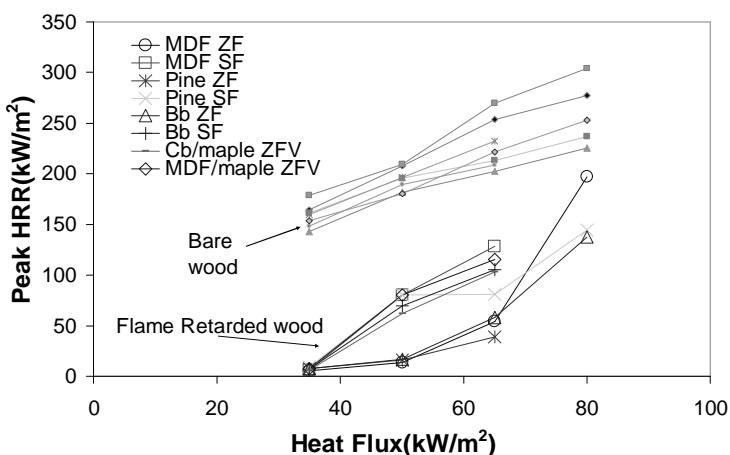


Fig. 1 : Peak HRR(kW/m²) for various flame retarded samples.

As shown in Figure 1, the peak HRR values increase with increasing in irradiance. First of all, in all cases, the irradiance of 35kW/m² did not lead to ignition. At 50 kW/m² irradiance some of the samples ignited, particularly those that had been painted with the solvent based (‘Synto Flame’) retardant. In all cases the ignition delay was very long compared to bare wood data, and this suggests that the ignition process is dominated by the flame retardant coating behavior rather than the substrate. At 65kW/m² all samples ignited, however at remarkably longer ignition times than

those observed in the corresponding virgin wood samples, at the same irradiance. At 80kW/m^2 fewer experiments were performed for the reasons mentioned above the HRR was much higher than at lower irradiances, indicative a fully established flame in agreement with the observation. The most effective behaviors are observed in ‘Zero Flame’, compared to ‘Synto Flame’ samples; this is attributed to their different chemical composition (water-based versus solvent-based).

Fire development results of medium scale experimental work (fire enclosure) cover: i Time to ignition(s), ii HRR(kW/m^2). One untreated sample was tested using 6g of ethanol as ignition source. The corresponding plot in Figure 2 shows that the untreated sample clearly burned faster. The presence of the FR paint clearly suppressed (either partially or totally) the combustion process. ‘No ignition’ of the fully treated (100%) crib was detected even when the ignition source was changed from 6g to 30g of ethanol. The fire mass loss as a percentage of the initial mass is shown as function of time in Figure 3. It is obvious that the fire mass loss of flame retarded samples was slower, especially when the treated surfaces are closer to ignition source. It is reminded that % indicates the fraction of the crib (starting from the bottom) that was either flame retarded or untreated

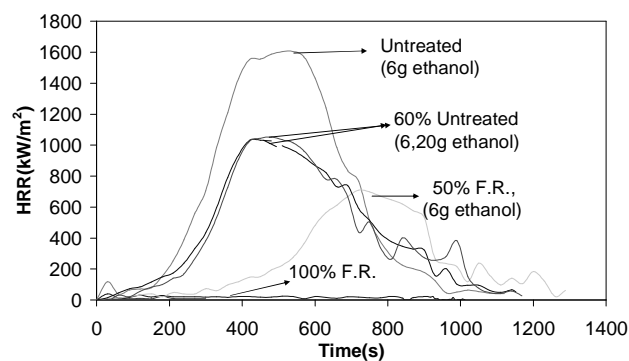


Fig 2: HRR(Kw/m^2) vs time for pine cribs with different FR treatment levels with 75kg/h air flow rate.

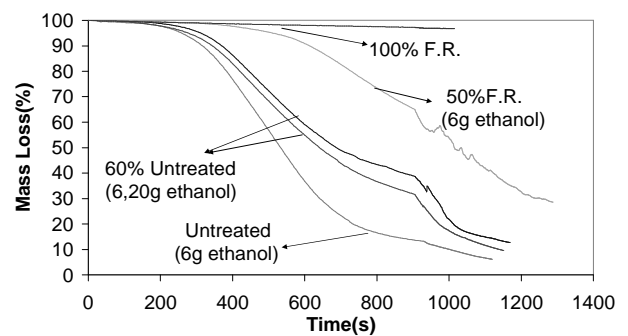


Fig 3: Mass Loss (%) vs time for pine cribs with different FR treatment levels with 75kg/h air flow rate.

An interesting finding evident in Figure 2 is that with regard to the peak HRR the 50% treated test produce about 45% of the untreated peak HRR. However the effectiveness of this partial treatment is in fact far greater when viewed in terms of the ‘300s average HRR’ where it is shown that it is almost as effective as the 100% treated sample (generally less than 15% of the average HRR of the untreated sample). The results clearly show that FR treatment can be very effective and additionally it is not necessary for the whole area to be treated. A partial treatment of the areas nearest to potential ignition sources may be a workable solution which can almost be as effective as the 100% treatment but absolutely much more economical.

4 EMISSIONS - EXPERIMENTAL RESULTS

FTIR analyzer was connected to the Cone Calorimeter for only virgin samples that were chosen to be painted with flame retardants and for all flame retarded samples, at 35, 50, 65 kW/m^2 . Figures (4-5) compares CO emissions (ppm) of treated and untreated samples of MDF at 35 and 50 kW/m^2 . In cases where ‘no ignition’ was achieved (i.e. for both flame retardants at 35 kW/m^2 and for ‘Zero Flame’ at 50 kW/m^2) the CO emissions maximum levels was approximately half of those of bare MDF. However, when the flame retarded samples were ignited the CO emissions were more than doubled (compared with the Bare MDF) results and more over they appeared to increase with higher heat fluxes. Similar behavior occurred for the other kind of timber that have been tested.

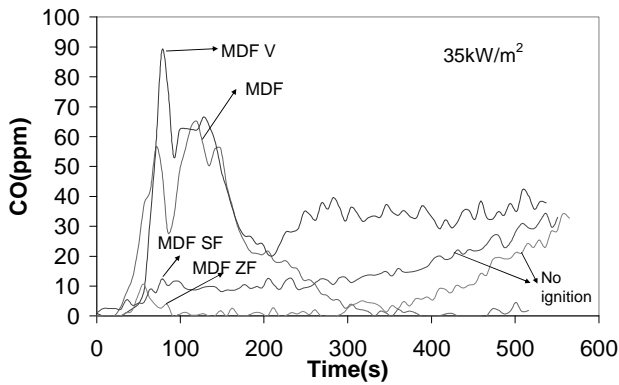


Fig. 4 :CO emissions(ppm) vs time for MDF, varnished MDF, 'Zero Flame' retarded MDF, 'Synto Flame' retarded MDF at 35kW/m²

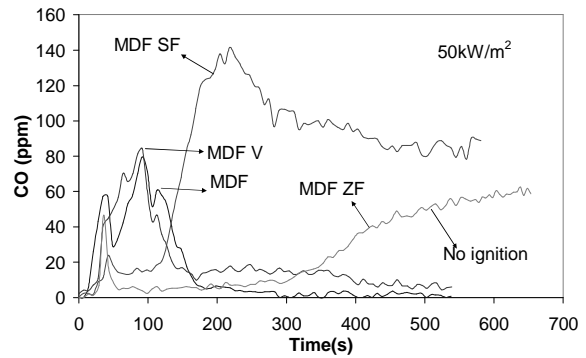


Fig. 5 :CO emissions(ppm) vs time for MDF, varnished MDF, 'Zero Flame' retarded MDF, 'Synto Flame' retarded MDF at 50kW/m²

FTIR analyzer was connected to the enclosed fire rig for all the tests. Only measurements of toxic gases that show “significant” concentrations for life safety based on the maximum exposure levels recommended by COSHH for individual combustion products[10] are reported in this work. Toxic yields of main toxic gases were assessed [4] (see Figures 6 and 7) for better comparison of toxic species of wooden samples, untreated or treated in different parts with typical flame retardant.

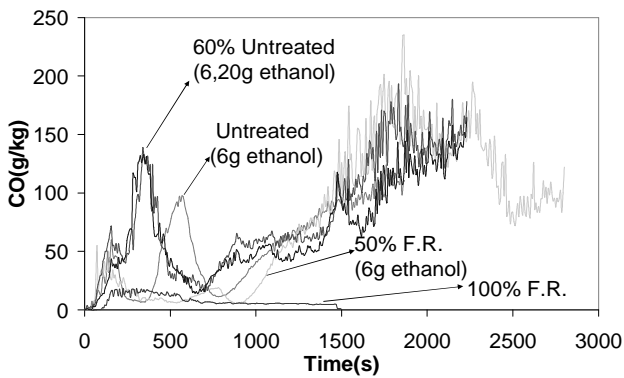


Fig. 6.: CO mass emissions (g/kg) vs time(s) for various (pine) cribs with 75kg/h air flow rate.

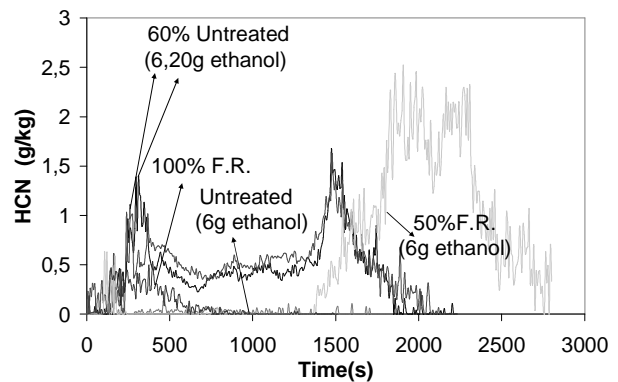


Fig. 7.: HCN mass emissions(g/kg) vs time(s)for various(pine) cribs with 75 kg/h air flow rate.

A direct comparison of the effect of the flame retardant used is achieved by ‘Peak n_(toxic gas) Coefficient Ratio’ ($P.n_{(toxic\ gas)} \cdot R.$) (see Eq. (1) below).

$$‘P.n_{(toxic\ gas)} \cdot R.’ = \frac{P.n_{toxic\ gas} \cdot CoatedSample}{P.n_{toxic\ gas} \cdot BareSample}, \quad (1)$$

where n_{toxic gas} volumetric (ppm). Therefore, the effects of flame retardant treatment on major toxic emissions compared with the bare samples are shown on the following Table 1.

The effect of FR treatments on major toxic emissions in small scale experimental work compared with the bare samples, are shown in Table 1. In the cases of flame retarded samples, where there was ‘no ignition’ of the samples (at 35kW/m² and 50kW/m²), there were similar or less toxic emissions compared to the bare samples. At higher irradiance (65kW/m²) the benefit was reduced or reversed due to more involvement of the flame retarded paint in flaming combustion. It should be noted that irradiances of the order of 40kW/m² or more are generally associated with the receiver being in close proximity (less than one meter) to a large fire (more than 1MW) or actually engulfed by it. So, in these circumstances, the fire is well established and the data shows that the retardands would be ineffective at this stage.

Tab 1 : Comparative effects of flame retardant treatment on major exhaust emissions
(Averaged for all substrates i.e MDF,Blockboard,Pine).

<i>Coated emission</i> <i>Bare emission</i>	35kW/m ² Heat flux		50kW/m ² Heat flux		65kW/m ² Heat flux	
	'Zero Flame'	'Synto Flame'	'Zero Flame'	'Synto Flame'	'Zero Flame'	'Synto Flame'
'Peak CO(ppm) Ratio'	↓	↓	↓	↑	↑	↑
'Peak HCN(ppm) Ratio'	≈	≈	≈	≈	↑	↑
'Peak Acrolein(ppm) Ratio'	↓	↓	↓	≈	≈	↑
'Peak NO (ppm)Ratio'	≈	≈	≈	≈	↑	↑

The effect of FR treatments on major toxic emissions in medium scale experimental work compared with the bare samples, are shown in Table 2. In most fully-treated (100%) cases, even in the half-treated (50%) cases, lower or almost equal to unity emissions were measured compared with the bare samples. This is due to the fact that, in such cases, due to the in-tumescent action, there was either 'no ignition' of the samples (100%-treated cases), or a considerable delay was seen (50%-treated cases). It is worth noting that 50% treatment in some cases was more effective to reduce toxic emissions compared with 100%-treated cases and, of course, much more inexpensive. This may be attributed to the fact that less flame retardant paint was involved in combustion in these cases. Excessive HCN and NO_x occurred in 60% of the untreated cases due to the considerable involvement of the flame retardant paint in flaming combustion, since it contains N in its chemical composition, as mentioned before.

Tab 2 : Comparative effects of flame retardant treatment on major exhaust emissions (during flaming combustion).

<i>Coated emission</i> <i>Bare emission</i>	100%F.R. 6g ethanol	100%F.R. 20g ethanol	100%F.R. 30g ethanol	50%F.R. 6g ethanol	60% Untreated 6g ethanol	60% Untreated 20g ethanol
'Peak CO(ppm) Ratio'	↓↓↓	↓↓↓	↓↓↓	↓↓	≈	≈
'Peak HCN(ppm) Ratio'	↓↓	↓↓	↓	↓	↑↑	↑↑
'Peak Acrolein(ppm) Ratio'	↓	↓	↓	↓	≈	≈
'Peak NO _x (ppm) Ratio'	↓	↓	≈	≈	↑↑	↑↑

≈ almost equal to unity.

Each arrow / ↓ ↑ indicates decreasing/increasing up to a factor of 2-3. Two arrows together is equivalent to a change by a factor of 3-6. Three arrows together is equivalent to a change by a factor for greater than 6.

5 CONCLUSIONS

- The effect of typical intumescent flame retardants (latest technology) on the most common types of Timber in Greek industries was examined in small and medium scale experiments combined with online effluent gas analysis equipment (FTIR).
- Analysis involved thermal behavior and toxic species analysis of the samples.
- No ignition' and lower toxic emissions compared to untreated samples were observed at 35kW/m² (small scale).
- The same behavior was observed in those cases where wooden surfaces located next to ignition source had been treated (medium scale).
- It is proposed that the application of intumescent flame retardants on wooden surfaces located close to ignition sources in the most probable areas for a fire to break out, could be a safe and effective approach in reducing fire losses in industries
- The above experimental data (small and medium scale) are compiled in the form of a database that can be used for validation of mathematical fire models and related software applications.

6 SUGGESTIONS

- Performing of more small- and medium – scale experiments, treated with the updated technology of the intumescent paints (different parts of wooden cribs or some other form of samples), and using various ventilation rates to achieve both establishing and documentation of the contribution of intumescent technology in fire suppression.
- Different coatings should be evaluated in terms of durability, impact resistance, weatherability, etc.;

REFERENCES

- Shields T.J, Silcock G.W.H, Moghaddam A.Z., Azhakesan M.A,Shang.J. 'Acomparison of fire retarded and non-fire retarded wood-bases wall linings exposed to fire in an enclosure'. *Fire and Materials*, vol.23:17-25, 1999.
- Birgit A-L,Ostman, Lazaros D.T. 'Heat release and classification of fire retardant wood products'. *Fire and materials*, vol.19:253-258, 1995.
- Spearpoint M.J. and Quintiere J.G. 'Predicting the piloted ignition of wood in the Cone calorimeter using an integral model-Effect of species, grain orientation and heat flux'. *Fire safety journal*, vol 36:391-415,2001.
- D. Tsatsoulas. 'Industrial fires in Northern Greece. The influence of Flame retardant on Timber Fires'. Ph.D. Thesis, Leeds (UK) 2008.
- D.Drysdale, 'An introduction to fire dynamics',2nd edition. Wiley (1999).
- D.Tsatsoulas, H.N.Phylaktou and G.Andrews. 'Thermal behaviour and toxic emissions of various timbers in Cone Calorimeter tests'. Third international Conference on Safety and Security Engineering, 1-3July 2009, Rome. In the proceedings of 'First International Conference on Disaster Management and Human Health Risk', pp.181-194, 23 -25 September 2009, New Forest, UK.
- Babrauskas V. 'Ten years of heat release research with the cone calorimeter'. *Heat release and hazard*,vol.1, ppIII-1 to III-8,1993.
- D.Tsatsoulas . 'Thermal behaviour and toxic emissions of various timbers in Cone Calorimeter tests' '*International Journal of Safety and Security engineering*',*Vol.1, No1(2011)45-64*.
- D.Tsatsoulas "Thermal behaviour and toxic emissions of flame retarded timber in Fire Enclosure tests",pp 295-306.Seventh International Conference on 'Risk Analysis 2010', 13-15 September, Algarve, Portugal.
- EH 40/2005 workplace exposure limits 'containing the list of workplace exposure limits for use with the Control of Substances Hazardous to Health Regulations 2002 (as amended)', HSE Books, UK Health and Safety Executive.

AUTHOR INDEX

- Ab Kadir M.A., *United Kingdom*..... 87
Abramowicz M., *Poland*..... 31
Ahmed A., *Pakistan* 239
Ali F., *United Kingdom*..... 37
Annerel E., *Belgium* 92, 109, 127
Autio V., *Finland* 400
Balcerzak M., *Poland*..... 37
Baniotopoulos C.C., *Greece*..... 17
Beatty A.A., *United Kingdom* 133
Beneš M., *Czech Republic*..... 139
Bijlaard F., *The Netherlands* 206
Bilotta A., *Italy*..... 23
Bisby L.A., *United Kingdom*..... 133
Björkman J., *Finland*..... 400
Bontempi F., *Italy*..... 251
Bradáčová I., *Czech Republic* 373
Burgess I.W., *United Kingdom* 195, 225, 275, 411
Byström A., *Sweden* 387
Caspelle R., *Belgium* 127
Cayla F., *France*..... 343
Cefarelli G., *Italy*..... 23, 171, 429
Cosenza E., *Italy*..... 23, 429
Couto C., *Portugal* 73
Cvetkovska M., *Macedonia* 149, 299
Čajka R., *Czech Republic*..... 145
Dagefa M., *Czech Republic*..... 443
Davison J.B., *United Kingdom*..... 195, 411
Dong G., *United Kingdom*..... 195
Drosopoulos G.A., *Greece* 219
Dudáček A., *Czech Republic*..... 373
Duma D., *Romania*..... 11
Dwaikat M.M.S., *USA*..... 67
El-Rimawi J., *United Kingdom* 307, 331, 349
Ervine A., *United Kingdom*..... 97
Ferraro A., *Italy*..... 171, 429
Franssen J.M., *Belgium* 11
Gentili F., *Italy* 251, 313
Gernay T., *Belgium* 11
Gillie M., *United Kingdom*..... 43, 87, 97
Giuliani L., *Italy*..... 313
Gkoumas K., *Italy* 287
Gou-qiang L., *China*..... 293
Grönberg P., *Finland*..... 400
Grossi L., *Italy*..... 251
Guo Q., *USA*..... 355
Hadjisophocleous G., *Canada*..... 49
Hager I., *Poland* 103
Han J., *China*..... 393
Haremza C., *Portugal*..... 231
Heinisuo M., *Finland* 400, 405
Hidani Y., *Japan* 61
Hietaniemi J., *Finland*..... 405
Hirashima T., *Japan*..... 61
Hopkin D., *United Kingdom* 307, 331, 349
Hozjan T., *Slovenia*..... 165
Huang Z., *United Kingdom* 275
Huang S-S., *United Kingdom*..... 411
Cheng X., *China*..... 387
Ikuta H., *Japan* 61
Iqbal N., *Sweden*..... 387
Jeffers A.E., *USA*..... 356
Jiang J., *United Kingdom* 122, 319
Jiang Y., *United Kingdom*..... 122, 324
Joyeux D., *France* 343
Kalogeropoulos A., *Greece*..... 219
Kirsch T., *Germany*..... 213
Kisieliński R., *Poland* 31
Klinzmann C., *Germany*..... 281
Kodur V.K.R., *USA*..... 67, 239
Kolstein H., *The Netherlands*..... 206
Kolšek J., *Slovenia* 165

Koltsakis E.K., <i>Greece</i>	17	Saje M., <i>Slovenia</i>	165
Korzen M., <i>Germany</i>	79	Salem O., <i>Canada</i>	49
Kotsovinos P., <i>United Kingdom</i>	122, 263, 319	Sandström J., <i>Sweden</i>	387
Kowalski R., <i>Poland</i>	31	Santiago A., <i>Portugal</i>	231
Król P.A., <i>Poland</i>	361	Shi K., <i>USA</i>	355
Kučera P., <i>Czech Republic</i>	373	Schaumann P., <i>Germany</i>	177, 213
Kwaśniewski L., <i>Poland</i>	37	Schneider R., <i>Germany</i>	55
Laasonen M., <i>Finland</i>	405	Silberschmidt V., <i>United Kingdom</i>	307, 331, 349
Lange J., <i>Germany</i>	55	Simões da Silva L., <i>Portugal</i>	231
Lazarov L., <i>Macedonia</i>	149, 299	Smith H.K.M., <i>United Kingdom</i>	134
Leborgne H., <i>France</i>	343, 367	Sokol Z., <i>Czech Republic</i>	269
Lee J., <i>United Kingdom</i>	43	Sothmann J., <i>Germany</i>	177
Lennon T., <i>United Kingdom</i>	307, 331, 349	Srpčič S., <i>Slovenia</i>	165
Li G-Q., <i>China</i>	393	Stadler M., <i>Germany</i>	177
Lilliu G., <i>The Netherlands</i>	379	Stavroulakis G.E., <i>Greece, Germany</i>	219
Lopes N., <i>Portugal</i>	73, 257	Stern-Gottfried J., <i>United Kingdom</i>	337
Lou G-B., <i>China</i>	393	Stratford T.J., <i>United Kingdom</i>	97, 133
Lu L., <i>Belgium</i>	109	Sun R., <i>United Kingdom</i>	275
Manfredi G., <i>Italy</i>	23, 429	Štefan R., <i>Czech Republic</i>	139
Maślak M., <i>Poland</i>	423	Taerwe L., <i>Belgium</i>	92, 109, 127
Matečková P., <i>Czech Republic</i>	145	Taib M., <i>United Kingdom</i>	225
May I., <i>United Kingdom</i>	122	Tan K.H., <i>Singapore</i>	115, 155, 182
Meda A., <i>Italy</i>	379	Todorov K., <i>Macedonia</i>	149, 299
Mensingher M., <i>Germany</i>	177	Tran H., <i>France</i>	361
Millard A., <i>France</i>	367	Tsalikis C.T., <i>Greece</i>	17
Molkens T., <i>Belgium</i>	417	Tsatsoulas D., <i>Greece</i>	456
Nguyen T.T., <i>Singapore</i>	115, 155	Twilt L., <i>The Netherlands</i>	206
Nigro E., <i>Italy</i>	23, 171, 429	Usmani A.S., <i>United Kingdom</i>	87, 122, 263, 319, 324
Outinen J., <i>Finland</i>	246, 405	Van Coile R., <i>Belgium</i>	127
Pankaj P., <i>United Kingdom</i>	97	Vargovsky K., <i>Slovak Republic</i>	449
Petrini F., <i>Italy</i>	287	Vassart O., <i>Luxembourg</i>	11
Planinc I., <i>Slovenia</i>	165	Veljkovic M., <i>Sweden</i>	387
Procházka J., <i>Czech Republic</i>	139	Vila Real P., <i>Portugal</i>	73, 257
Qiang X., <i>The Netherlands</i>	206	Wald F., <i>Czech Republic</i>	443
Reid E.R.E., <i>United Kingdom</i>	133	Welch S., <i>United Kingdom</i>	324
Rein G., <i>United Kingdom</i>	337	Wickstöm U., <i>Sweden</i>	387
		Ylihärsilä H., <i>Finland</i>	400

Yong D., <i>China</i>	293	Zalok E., <i>Canada</i>	49
Yu H., <i>China</i>	201	Zehfuss J., <i>Germany</i>	437
Yuan Y., <i>China</i>	109	Zhang J., <i>United Kingdom</i>	122, 319
Yuan Z., <i>Singapore</i>	183	Zhao B., <i>France</i>	367
Zaharia R., <i>Romania</i>	11		

SCIENTIFIC COMMITTEE

BURGESS Ian, *United Kingdom*
Chairman
BLOCK Florian, *United Kingdom*
DE LA QUINTANA Jesus, *Spain*
DEHN Frank, *Germany*
FRANSSEN Jean-Marc, *Belgium*
Faris Ali, *United Kingdom*
GAMBAROVA Pietro, *Italy*
KHOURI Gabriel A., *United Kingdom*
KODUR Venkatesh, *USA*
KÖNIG Jürgen, *Germany*
LEJTENA J.M., *The Netherlands*
LI Guo Qiang, *China*
LUO Ming Chun, *China (Hong Kong)*
MAHENDRAN Mahen, *Australia*
MORENTE Fernando Belmez, *Spain*
OKSANEN Tuuli, *Finland*
OUTINEN Jyri, *Finland*
REIN Guillermo, *United Kingdom*
SCHAUMANN Peter, *Germany*
TAERWE Luc, *Belgium*
TAN Kang Hai, *Singapore*
VASSART Olivier, *Luxembourg*
VELJKOVIC Milan, *Sweden*
VILA REAL Paulo, *Portugal*
WANG Yong, *United Kingdom*
ZAHARIA Raul, *Romania*
ZHAO Bin, *France*

ORGANIZING COMMITTEE

DUDÁČEK Aleš, *Czech Republic*
KAISER Rudolf, *Czech Republic*
KREGL František, *Czech Republic*
KUČERA Petr, *Czech Republic*
KUKLÍK Petr, *Czech Republic*
PROCHÁZKA Jaroslav, *Czech Republic*
SOKOL Zdeněk, *Czech Republic*
VAŠKOVÁ Jitka, *Czech Republic*
JÁNA Tomáš, *Czech Republic*
HOROVÁ Kamila, *Czech Republic*
BEDNÁŘ Jan, *Czech Republic*
WALD František, *Czech Republic*
Chairman